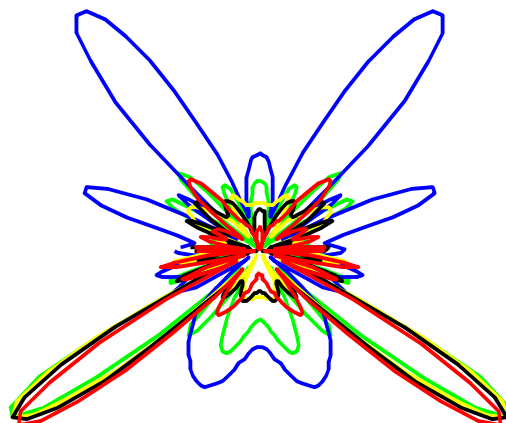




INSTITUTO
SUPERIOR
TÉCNICO

**UNIVERSIDADE TÉCNICA DE LISBOA
INSTITUTO SUPERIOR TÉCNICO**



**Dependencies of Adaptive Beamforming on the
Propagation Channel in Wideband Mobile
Communications**

João Miguel Pissarra Coelho Gil
(Master of Science)

Dissertation submitted for the degree of Doctor in Philosophy
in Electrical and Computer Engineering

Supervisor: Doctor Luís Manuel de Jesus Sousa Correia
President: Rector of the Technical University of Lisbon
Jury: Professor Ernest Bonek
Doctor Henrique José Almeida da Silva
Doctor Carlos António Cardoso Fernandes
Doctor Victor Manuel Alberto Neves Barroso
Doctor Luís Manuel de Jesus Sousa Correia

April 2004

There is something in us which responds to the challenge of this mountain and goes out to meet it...

What we get from this adventure is just sheer joy.

And joy is, after all, the end of life.

— George Mallory (1890 –1924)

To my dear parents.

Acknowledgements

Appreciation is a wonderful thing; it makes what is excellent in others belong to us as well.

—François Marie Arouet (Voltaire) (1694-1778)

During my Ph.D., I have had the chance of working in a remarkably disciplined, demanding and humane environment. I have learnt to aim at achieving quality as well as meeting deadlines and commitments. Besides all of these, the active and wise combination of this work with international projects and undergraduate co-supervision has resulted in a flowing and stimulating working environment. I, therefore, thank my supervisor, professor Luís M. Correia, for generating all of the above conditions, in addition to the most practical ones such as attentive and systematic reviewing and guaranteeing financial support for several activities. I also thank Luís M. Correia for his humane personality, for his trust and patience, and for his choice of right words at the right time.

I thank my colleagues from Lisbon, Gabriela, Filipe, Jorge A., Lúcio and Jorge V. for contributing to the disciplined, demanding, transparent and trustful teamwork that I have been lucky enough to experience. Juan, Tomek and Jacek's acceptance in joining this open and transparent teamwork has also been fundamental. I thank my colleagues from Leiria, Pedro, Luís, Carlos, Telmo, Rafael and Sérgio, for their simple but frequent support.

I am also grateful to my good friends Ricardo, Verdasca, and Lúcia for their presence and good company in the mountains or in the plains, and in joyful meals. These times have been valuable for me to attain a healthy equilibrium between work and rest.

I thank Sónia for her natural, simple but patient and strong support, and my family for their solid backstage backup.

Last but not least, I acknowledge the Instituto Politécnico de Leiria, Escola Superior de Tecnologia e Gestão for providing me with a grant of Leave of Absence and the suitable conditions which allowed me to carry out my research with the necessary peace of mind.

Abstract

This study contributes to understanding what and how fundamental physical wideband and directional properties of the mobile propagation channel constrain adaptive beamforming interference suppression, in broadband mobile communications systems.

A semi-statistical and geometrical wideband propagation directional channel model is used. Multi-user propagation scenarios are generated to statistically approximate real-life situations, varying several parameters, including mobile terminals distribution. An adaptive beamforming algorithm is applied at the base station, in the up-link, for UMTS, but results are not algorithm-dependable, and are extendable to future mobile broadband systems. Close relations to multiple-input-multiple-output issues are also established.

A statistical evaluation of beamforming dependencies on several scenario parameters, for micro- and macro-cells, is closely accompanied by the wideband and directional characterisation of the channel. The defined channel parameters are shown to inherently reflect the channel multipath richness, justifying the channels' or scenarios' impacts on beamforming. Macro-cells involve poorer channels, compared to micro-cells, having important and consistent consequences on the beamforming interference suppression allowed. Among others, grouping of mobile terminals in macro-cells does not lead to signal-to-interference-plus-noise ratio improvements in respect to the single element antenna, for any number of array elements, but to much higher positive improvements in micro-cells, reaching close to 10 dB in those cases.

Keywords

Adaptive beamforming, Propagation scenarios, Propagation channel,
Wideband directional models, Broadband systems.

Resumo

Este estudo contribui para entender quais e como propriedades físicas fundamentais, direccionais e de banda-larga, do canal de propagação restringem o desempenho da formação adaptativa de lobos (ou *formatação de feixe*), na supressão de interferência em sistemas móveis de banda-larga.

É usado um modelo direccional de banda-larga, semi-estatístico e geométrico. Cenários de propagação multi-utilizador são gerados aproximando situações reais, variando vários parâmetros, como a distribuição de terminais móveis. É aplicado um algoritmo adaptativo de formação de lobos, na estação base, no canal ascendente, para UMTS, mas os resultados não são dependentes do algoritmo, e são extensíveis a futuros sistemas móveis de banda-larga. Relações estreitas com sistemas de múltiplas-entradas-múltiplas-saídas são também estabelecidas.

A avaliação estatística das dependências da formação de lobos em função dos parâmetros dos cenários, para micro- e macro-células, é acompanhada da caracterização do canal, direccionalmente e em banda-larga. Os parâmetros de canal definidos reflectem inerentemente a riqueza de multi-percurso do canal, justificando o impacto do canal ou dos cenários na formação de lobos. Macro-células envolvem canais mais pobres, comparando com micro-células, com importantes e consistentes consequências na capacidade de redução de interferência. Dentro de outras, o agrupamento de terminais móveis em macro-células não conduz a melhorias da relação-sinal-ruído-mais-interferência em relação a um único elemento de antena, mas a aumentos consideravelmente maiores em micro-células, nesses casos podendo chegar a 10 dB.

Palavras Chave

Formação adaptativa de lobos, Formatação de feixe, Cenários de propagação, Canal de propagação, Modelos direccionais de banda-larga, Sistemas de banda-larga.

Table of Contents

ACKNOWLEDGEMENTS	I
ABSTRACT	III
RESUMO	IV
TABLE OF CONTENTS	V
LIST OF FIGURES	IX
LIST OF TABLES	XVI
LIST OF ACRONYMS	XVIII
LIST OF SYMBOLS	XXIII
1 INTRODUCTION	1
1.1 MOTIVATION – CONTEXT AND PHILOSOPHY	1
1.2 CONTRIBUTIONS OF THIS STUDY	7
1.3 DISSERTATION OUTLINE.....	10
2 LAYING FOUNDATIONS AND BACKGROUND – CHANNEL MODELS	13
2.1 CLASSICAL VS. SPATIAL CHANNEL MODELS	13
2.2 GENERAL ASSUMPTIONS AND CONSIDERATIONS	16
2.3 REVIEW OF MAIN EXISTING SPATIAL CHANNEL MODELS	18
2.3.1 <i>Statistical Models</i>	18
2.3.2 <i>Measurement-Based Models</i>	28
2.3.3 <i>Geometrically-Based and Semi-Statistical Unifying Models</i>	29
2.3.4 <i>Other Model Types and Methodologies</i>	37
2.4 SUMMARY AND CONCLUSIONS.....	41
3 LAYING FOUNDATIONS AND BACKGROUND – ADAPTIVE BEAMFORMING	43
3.1 BEAMFORMING FOR SMART ANTENNAS.....	43
3.2 BASIC CONCEPTS, PARAMETERS AND STRUCTURES	45
3.2.1 <i>Beamforming Structures</i>	45
3.2.2 <i>Beamformer Response, Steering and Weight Vectors</i>	51
3.3 NON-ADAPTIVE BEAMFORMING PROCESSING	55
3.3.1 <i>Data Independent Beamforming</i>	55

3.3.2	<i>Statistically Optimum Beamforming</i>	57
3.4	ADAPTIVE BEAMFORMING PROCESSING	62
3.4.1	<i>Most Important Beamforming Algorithms</i>	62
3.4.2	<i>Method of Steepest Descent</i>	63
3.4.3	<i>Least-Mean-Square Algorithm</i>	65
3.4.4	<i>Recursive Least Squares</i>	67
3.4.5	<i>Constant Modulus Algorithm</i>	70
3.4.6	<i>Sample Matrix Inversion</i>	71
3.4.7	<i>Conjugate Gradient</i>	73
3.4.8	<i>Neural Networks Implementations</i>	75
3.5	SUMMARY AND CONCLUSIONS.....	77
4	IMPLEMENTATION – THE CHANNEL AND SCENARIOS	79
4.1	SPECIFICATION AND IMPLEMENTATION PERSPECTIVE	79
4.2	SPECIFICATION OF THE SPATIAL CHANNEL MODEL.....	80
4.2.1	<i>Location and Type of Model</i>	80
4.2.2	<i>Selection of the Model</i>	81
4.3	SPATIAL CHANNEL MODEL IMPLEMENTATION	82
4.3.1	<i>General Assumptions and Considerations</i>	82
4.3.2	<i>GBSBEM and CM – the Original and the Modified Variants</i>	83
4.3.3	<i>Physical Interpretation Issues</i>	89
4.4	PROPAGATION SCENARIOS SPECIFICATION	90
4.4.1	<i>Scenarios Perspective</i>	90
4.4.2	<i>Micro-cell Scenarios</i>	92
4.4.3	<i>Macro-cell Scenarios</i>	97
4.4.4	<i>Comparative Micro- and Macro-cell Scenarios</i>	99
4.5	SPATIAL CHANNEL PARAMETERS.....	101
4.5.1	<i>AoA and ToA Spreads</i>	101
4.5.2	<i>Temporal and Angular Densities, and Channel Richness</i>	106
4.6	SUMMARY AND CONCLUSIONS.....	110
5	IMPLEMENTATION – THE ADAPTIVE PROBLEM	113
5.1	SPECIFICATION AND IMPLEMENTATION PERSPECTIVE	113
5.2	SPECIFICATION OF THE BEAMFORMING SCHEME	114
5.2.1	<i>Beamformer Location, Direction and Transmission Mode</i>	114
5.2.2	<i>Stationarity Conditions, Data and Reference Acquisition</i>	116
5.2.3	<i>Type of Smart Antenna, Processing Domain and Adaptivity Coverage</i>	117
5.2.4	<i>Selection of the Adaptive Algorithm</i>	119
5.3	ALGORITHM AND ADAPTIVE PROBLEM IMPLEMENTATION.....	122
5.3.1	<i>General Assumptions and Considerations</i>	122
5.3.2	<i>Reference MT-Specific Codes Specification</i>	123
5.3.3	<i>CG and Adaptive Problem</i>	127
5.3.4	<i>Physical Interpretation Issues</i>	129
5.4	EVALUATION PARAMETERS.....	130
5.5	APPLICATION OF POWER CONTROL.....	133
5.6	MEANS CALCULATIONS AND STATISTICAL ISSUES	136
5.7	SUMMARY AND CONCLUSIONS.....	144
6	SET-UP ANALYSIS	147
6.1	INTRODUCTION	147
6.2	IMPLEMENTATION VS. NARROWBAND AND WIDEBAND	148
6.2.1	<i>Several Definitions</i>	148
6.2.2	<i>Systems and Channel Bandwidths</i>	148
6.2.3	<i>Beamforming and Array Bandwidths</i>	150

6.3	IMPLEMENTATION OF TDD AND FDD MODES.....	153
6.3.1	<i>Dependence on the Propagation Scenarios</i>	153
6.3.2	<i>Correlation Properties of the Reference Codes</i>	156
6.4	MMSE VS. BG OPTIMA DISCREPANCY	161
6.4.1	<i>Initial Considerations</i>	161
6.4.2	<i>The Micro-cell Scenarios Case</i>	163
6.4.3	<i>The Macro-cell Scenarios Case</i>	179
6.4.4	<i>Dealing with the MMSE vs. BG Optima Discrepancy Problem</i>	187
6.5	CG VS. RLS IMPLEMENTATIONS.....	200
6.5.1	<i>RLS Implementation</i>	200
6.5.2	<i>Performance Comparison</i>	202
6.5.3	<i>Complexity Issues</i>	204
6.6	SUMMARY AND CONCLUSIONS.....	209
7	BEAMFORMING IN MICRO- AND MACRO-CELL SCENARIOS.....	211
7.1	INTRODUCTION.....	211
7.2	PERFORMANCE DEPENDENCE ON MIC SCENARIOS PARAMETERS.....	212
7.2.1	<i>MT-BS Distance</i>	212
7.2.2	<i>Number of Array Elements</i>	216
7.2.3	<i>Angular Displacement and Grouping of MTs</i>	218
7.2.4	<i>Linear Displacement and Grouping of MTs</i>	221
7.2.5	<i>Number of Active Links</i>	223
7.2.6	<i>Sectorisation</i>	226
7.2.7	<i>Correlation Matrix Components Dependencies</i>	228
7.3	PERFORMANCE DEPENDENCE ON MAC SCENARIOS PARAMETERS.....	233
7.3.1	<i>MT-BS Distance</i>	233
7.3.2	<i>Scattering Circle Radius</i>	236
7.3.3	<i>Number of Array Elements</i>	240
7.3.4	<i>Angular Displacement and Grouping of MTs</i>	241
7.3.5	<i>Cluster Density and Average Number of Scatterers</i>	244
7.3.6	<i>Number of Active Links</i>	246
7.3.7	<i>Correlation Matrix Components Dependencies</i>	250
7.4	SUMMARY AND CONCLUSIONS.....	253
8	BEAMFORMING PERFORMANCE IN MICRO- VS. MACRO-CELL WDCM SCENARIOS.....	259
8.1	INTRODUCTION.....	259
8.2	COMPARATIVE ANALYSIS RESULTS.....	260
8.2.1	<i>Angular Displacement and Grouping of MTs</i>	260
8.2.2	<i>MT-BS Distance</i>	266
8.2.3	<i>Number of Array Elements</i>	267
8.2.4	<i>Number of Active Links</i>	268
8.2.5	<i>Correlation Matrix Components</i>	270
8.3	RELATIONS TO THE MIMO PERSPECTIVE.....	273
8.4	SUMMARY AND CONCLUSIONS.....	279
9	TOWARDS FUTURE MOBILE BROADBAND SYSTEMS.....	283
9.1	INTRODUCTION – DEFINING PERSPECTIVE AND MOTIVATION.....	283
9.2	FUTURE WIDEBAND MOBILE SYSTEMS FOCUS.....	284
9.2.1	<i>Evolution Trends – A Literature Review</i>	284
9.2.2	<i>Intercepting Scopes from the Present Work</i>	288
9.3	EXTRAPOLATING HYPOTHESES.....	290
9.3.1	<i>Propagation Channel Oriented Hypotheses</i>	290
9.3.2	<i>Scenario Oriented Hypotheses</i>	291

9.3.3	<i>Array Oriented Hypotheses</i>	292
9.3.4	<i>System Oriented Hypotheses</i>	293
9.4	SUMMARY AND CONCLUSIONS.....	294
10	FINAL CONCLUSIONS	297
11	REFERENCES	309
	ANNEX A – SURFACE PLOTS – MICRO-CELL SCENARIOS	329
	ANNEX B – SURFACE PLOTS – MACRO-CELL SCENARIOS	341
	ANNEX C – CG VS. RLS PERFORMANCE PLOTS	357

List of Figures

Figure 2.1 – Circular scatterer distribution, at angle ϕ_{MT} , with ϕ_{n_s} spread over ϕ_{BW} , with radius r , centred at the MT, at distance d_{MT} from the BS.	19
Figure 2.2 – Circular scatterer Uniform density distribution around the MT.	23
Figure 2.3 – Elliptical scatterer Uniform density distribution around the MT.	24
Figure 2.4 – Type of WDCM cluster and scatterer distributions, within the scattering areas defined by BS or MT _{<i>l</i>} , indicating some single-bounce reflections.	34
Figure 2.5 – The general MIMO channel implementation perspective, between M_{Tx} and M_{Rx} element Tx and Rx arrays.	38
Figure 3.1 – A digital adaptive processing network together with an analog beamforming network (based on [LiRa99]).	47
Figure 3.2 – Two signals from the same source in the far field, $u_1(\tau)$ and $u_2(\tau)$, arrive at the ULA $m = 1$ and 2, from angle ϕ	53
Figure 4.1 – Scatterer Uniform distributions, for the GBSBEM and CM.	84
Figure 4.2 – A street, MiC propagation scenario (based on [DGVC03]).	96
Figure 4.3 – City plaza, MiC propagation scenarios, not to scale (based on [DGVC03]).	96
Figure 4.4 – A train, MaC propagation scenario, not to scale (based on [DGVC03]).	99
Figure 4.5 – Average signal intensity for to BS-MT distances, for MiCs, normalised to each maximum (based on [Marq01], with a 3° visualisation resolution).	103
Figure 4.6 – Average signal intensity for 50 and 400 m radii, for $d_{MT} = 1\ 500$ m, for MaCs, normalised to each maximum.	104
Figure 5.1 – The generic adaptive beamforming scheme for l^{th} link (based on [LiLo96]).	123
Figure 5.2 – Code-tree for the generation of the TDD channelisation codes (based on [ETSI02b]).	126
Figure 5.3 – Flow chart of the PC process.	134
Figure 5.4 – An example of SINR progression along the PC iterations, for $L = 4$	135
Figure 5.5 – An example of SINR progression along the PC iterations, for $L = 8$	135
Figure 5.6 – An example of SINR progression along the PC iterations, for $L = 16$	135
Figure 5.7 – SINR among 4 active links, for 20 independent DCIR concretisations.	136

Figure 5.8 – PI DCIR average BG results, for Sc #Lu_mc_Gr_d, function of M , for several d_{MT} and L . Solid lines indicate average results.	138
Figure 5.9 – TI DCIR average BG results, for Sc #Lu_mc_Gr_d, function of the number of antennas, for several values of d_{MT}	139
Figure 5.10 – An example of a BG normal CDF plot, exhibiting its visible linearity, in dB.	141
Figure 5.11 – Comparison of average BG for 20 or 100 concretisations, for Sc #Lu_mc_Gr_5 and Sc #Lu_mc_Sp_5, function of M , for $L=4$ and 16.	142
Figure 5.12 – Comparison of average BG for 20 or 100 concretisations, for Sc #Lu_Mc_Gr_15_200 and Sc #Lu_Mc_Sp_15_200, function of M , for $L=4$ and 16.	143
Figure 6.1 – Representation of the <i>wideband</i> basic beamforming structure.	151
Figure 6.2 – The present adaptive beamforming network, for each of the L active links.	152
Figure 6.3 – Code auto- and cross-correlation, for TDD and FDD, for $L = 4$, for a single code and average interaction.	158
Figure 6.4 – Code auto- and cross-correlation, for TDD and FDD, for $L = 8$, for a single code and average interaction.	159
Figure 6.5 – Code auto- and cross-correlation, for TDD and FDD, for $L = 16$, for a single code and average interaction.	160
Figure 6.6 – Example of the average MSE evolution (and corresponding standard deviations) along optimisation, for Sc #16u_Mc_Gr_15_200, 10 or 20 array elements.	162
Figure 6.7 – MSE along optimisation, for Sc #16u_Mc_Gr_15_200 and all tested values of M	163
Figure 6.8 – Examples of the BG dependence on the iteration number, for Sc #Lu_mc_Gr_d, as function of M , for several values of d_{MT} , at the M^{th} or 4^{th} iterations.	164
Figure 6.9 – Examples of the SINR dependence on the iteration number, for Sc #Lu_mc_Gr_d, as function of M , for several values of d_{MT} , at the M^{th} or 4^{th} iterations.	165
Figure 6.10 – Histograms of the maxima, function of the iteration number, among all links, for the Sc #Lu_mc_Gr_d scenarios.	167
Figure 6.11 – Average BG results and differences along optimisation, as function of M , for several values of d_{MT} , $L = 16$	168
Figure 6.12 – Average P_{DesS} [dBm] and differences along optimisation, as function of M , for several values of d_{MT} , $L = 16$	169
Figure 6.13 – Average $P_{NDesI} + N$ [dBm] and differences along optimisation, as function of M , for several values of d_{MT} , $L = 16$	170
Figure 6.14 – Average P_{DesS} and $P_{NDesI} + N$ contributions to SINR, along iterations, for Sc #16u_mc_Gr_10 and $M = 12$ (normalised to the P_{DesS} maximum).	172
Figure 6.15 – Surface plots of BG, as function of the number of array elements and iteration number, for Sc #16u_mc_Gr_5 and #16u_mc_Sp_5.	173
Figure 6.16 – Surface plots of BG, as function of the number of array elements and iteration number, for Sc #16u_mc_Se_A, for MT ₁ and the MT group.	173
Figure 6.17 – Evolution of the \mathbf{R} condition number, in logarithmic scale, function of scenario and M , for Sc #4u_mc_Gr_d and #16u_mc_Gr_d examples.	174

Figure 6.18 – Array patterns (red, thin line) of one link (MT_1), for $M = 12$, with all the MTs at 0 rad, Sc #16u_mc_Gr_5, for the initial and M^{th} iterations.	175
Figure 6.19 – Array patterns (red, thin line) of another link (MT_{12}), for $M = 12$, with all the MTs at 0 rad, Sc #16u_mc_Gr_5, for the initial and M^{th} iterations.	176
Figure 6.20 – BG, along optimisation, for MT_1 and MT_{12} in Sc #16u_mc_Gr_5, one channel concretisation.	176
Figure 6.21 – Array patterns (red, thin line) for $M = 12$, for MT_4 at $-\pi/5$, in Sc #16u_mc_Se_A, for the initial and M^{th} iterations.	177
Figure 6.22 – Array patterns (red, thin line) for $M = 12$, with the MT_1 at $\pi/4$, Sc #16u_mc_Se_A, for the initial and M^{th} iterations.	178
Figure 6.23 – BG, along optimisation, for MT_1 and MT_4 in Sc #16u_mc_Se_A, one channel concretisation.	178
Figure 6.24 – BG, function of M , for several values of d_{MT} , Sc #Lu_Mc_Gr_d_200, at the 1 st and M^{th} iterations.	180
Figure 6.25 – BG and SINR, function of M , for several values of r , Sc #16u_Mc_Gr_15_r, before any beamforming and at 1 st and M^{th} iterations.	181
Figure 6.26 – BG, function of M , for several values of r , for the MT group in Sc #16u_Mc_Se_A_r, before any beamforming and at the 1 st iteration.	182
Figure 6.27 – Surface plots of BG along optimisation, function of M , for Sc #16u_Mc_Gr_15_200 and #16u_Mc_Sp_r.	183
Figure 6.28 – Surface plots of BG along optimisation, function of M , for Sc #16u_Mc_Se_A_r, MT_1 and MT group.	184
Figure 6.29 – Array patterns (red, thin line) for MT_{16} at $-\pi/5$, in Sc #16u_Mc_Se_A_50, for the initial and M^{th} iterations.	185
Figure 6.30 – Array patterns (red, thin line) for the MT_1 at $\pi/4$, Sc #16u_Mc_Se_A_50, for the initial and M^{th} iterations.	186
Figure 6.31 – BG, along optimisation, for MT_1 and MT_{16} in Sc #16u_Mc_Se_A_50, one channel concretisation.	186
Figure 6.32 – BG, along optimisation, for Sc #4u_Mc_Gr_15_200, with $M = 8$, with the 16-long TDD or 256-long FDD codes, making use of the codes full length or of $N_s = 16$ samples only.	189
Figure 6.33 – BG and SINR, for Sc #4u_Mc_Gr_15_200 and Sc #4u_Mc_Sp_15_200, with $M = 12$, with ND_NN.	190
Figure 6.34 – BG and SINR, for Sc #4u_Mc_Gr_15_200 and Sc #4u_Mc_Sp_15_200, with $M = 12$, with ND_WN.	191
Figure 6.35 – BG and SINR, for Sc #4u_Mc_Gr_15_200 and Sc #4u_Mc_Sp_15_200, with $M = 12$, with WD_NN.	191
Figure 6.36 – BG and SINR, for Sc #4u_Mc_Gr_15_200 and Sc #4u_Mc_Sp_15_200, with $M = 12$, with WD_WN.	192
Figure 6.37 – Power terms due to the composition of \mathbf{R} , for $M = 12$, Sc #4u_Mc_Gr_15_200 and Sc #4u_Mc_Sp_15_200, with ND-NN.	193
Figure 6.38 – Magnitude of the correlation coefficient, for Sc #4u_Mc_Gr_15_200 and Sc #4u_Mc_Sp_15_200, with $M = 12$	194

Figure 6.39 – SINR and BG, function of iterations, for the RLS and CG, for Sc #16u_mc_Gr_05, $M = 12$	204
Figure 6.40 – Number of RLS flops per iteration vs. M , for several values of L , for which beamforming is performed.	205
Figure 6.41 – Number of CG flops per iteration vs. M , for several values of L , for which beamforming is performed.	205
Figure 6.42 – Number of CG flops required for the calculation of \mathbf{R} and \mathbf{d}_l vs. M , for several values of L , for which beamforming is performed.	206
Figure 7.1 – BG, function of M , for several values of d_{MT} , Sc #Lu_mc_Gr_d.	213
Figure 7.2 – SINR, function of M , for several values of d_{MT} , Sc #Lu_mc_Gr_d.	214
Figure 7.3 – BG, function of d_{MT} , for several values of M , Sc #Lu_mc_Gr_d.	215
Figure 7.4 – BG, function of M , for several values of d_{MT} , for Sc #Lu_mc_Sp_d.	216
Figure 7.5 – BG, function of the d_{MT} , for several values of M , Sc #Lu_mc_Gr_d, for larger number of array elements.	217
Figure 7.6 – BG, function of the d_{MT} , for several values of M , Sc #Lu_mc_Sp_d, for larger number of array elements.	218
Figure 7.7 – BG, function of M , for several values of L , Sc #Lu_mc_Se_A.	219
Figure 7.8 – BG, function of M , for several values of L , Sc #Lu_mc_Se_B.	220
Figure 7.9 – BG, function of M , for several values of L , Sc #Lu_mc_Se_C.	220
Figure 7.10 – BG, function of L , for several values of M and d_{MT} , Sc #Lu_mc_Gr_d.	224
Figure 7.11 – BG function of the L , for several values of M and d_{MT} , Sc #Lu_mc_Sp_d.	225
Figure 7.12 – BG, function of the L , for several values of M , Sc #Lu_mc_Se_A, $d_{MT} = 500$ m.	225
Figure 7.13 – SINR, function of the L , for several values of M , including the single element case, Sc #Lu_mc_Sp_5.	226
Figure 7.14 – Average power terms due to the composition of \mathbf{R} , for $M = 12$, Sc #4u_mc_Gr_d.	228
Figure 7.15 – Average P_{DesS} and $P_{S_0}^{other}$ (thicker, dashed lines), for Sc #4u_mc_Gr_d, normalised to their maximum, for $M = 12$	229
Figure 7.16 – Average power terms due to the composition of \mathbf{R} , for $M = 12$, Sc #4u_mc_Sp_d.	230
Figure 7.17 – Average power terms due to the composition of \mathbf{R} , for $M = 12$, Sc #4u_mc_Se_A, MT_1	231
Figure 7.18 – Average power terms due to the composition of \mathbf{R} , for $M = 12$, several sector widths, Sc #4u_mc_Gr_05.....	232
Figure 7.19 – Average power terms due to the composition of \mathbf{R} , for $M = 12$, several sector widths, for Sc #4u_mc_Gr_10.....	233
Figure 7.20 – BG, function of M , for several values of d_{MT} , Sc #Lu_Mc_Gr_d_200.	234
Figure 7.21 – BG, function of M , for several values of d_{MT} , Sc #Lu_Mc_Sp_d_200.	235
Figure 7.22 – BG, function of d_{MT} , for several values of M , Sc #Lu_Mc_Sp_d_200.	236
Figure 7.23 – SINR and BG, functions of M , for several values of r , Sc #16u_Mc_Gr_15_r.	237

Figure 7.24 – SINR and BG, functions of M , for several values of r , for Sc #16u_Mc_Sp_15_r.....	237
Figure 7.25 – BG, function of M , for several values of r , Sc #Lu_Mc_Se_A_r, $L = 4$ and 16.	238
Figure 7.26 – BG, function of M , for several values of r , Sc #Lu_Mc_Se_B_r, for $L = 4$ and 16.	239
Figure 7.27 – BG, function of the M , for several values of d_{MT} , Sc #Lu_Mc_Sp_d_200, for larger number of array elements.	241
Figure 7.28 – BG, function of M , for several values of L , for Sc #Lu_Mc_Se_C_50.	243
Figure 7.29 – BG, function of the MT angular separation, for 4 equally angularly spaced MTs.	243
Figure 7.30 – BG, function of M , for $L = 4$ and 16, Sc #Lu_Mc_Gr_15_200 and Sc #Lu_Mc_Gr_15_200_ld.	244
Figure 7.31 – BG, function of M , for $L = 4$ and 16, MT ₁ in Sc #Lu_Mc_Se_A_50 and Sc #Lu_Mc_Se_A_50_ld.	245
Figure 7.32 – BG, function of M , for $L = 4$ and 16, MT ₁ in Sc #Lu_Mc_Se_A_50 and Sc #Lu_Mc_Se_A_50_ld.	245
Figure 7.33 – BG, function of L , for several values of M , Sc #Lu_Mc_Gr_d_200 and Sc #Lu_Mc_Sp_d_200, for $d_{MT} = 1\ 000$ and $2\ 000$ m.	247
Figure 7.34 – BG, function of L , for several values of M , Sc #Lu_Mc_Sp_d_200, for $d_{MT} = 1\ 000$ and $2\ 000$ m.	247
Figure 7.35 – SINR, function of L , for several values of M , including the single element case, Sc #Lu_Sp_15_200.	248
Figure 7.36 – BG and SINR, function of L , for several values of M , Sc #Lu_Mc_Se_A_200, $d_{MT} = 1\ 500$ m.	249
Figure 7.37 – BG, function of L , for several values of M , Sc #Lu_Mc_Se_A_50, $d_{MT} = 1\ 500$ m.	250
Figure 7.38 – Average power terms due to the composition of \mathbf{R} , for $M = 12$, Sc #4u_Mc_Sp_15_200 and Sc #4u_Mc_Sp_15_50.	251
Figure 7.39 – Average power terms due to the composition of \mathbf{R} , for $M = 12$, Sc #4u_Mc_Gr_15_200 and Sc #4u_Mc_Gr_15_50.	251
Figure 7.40 – Average power terms due to the composition of \mathbf{R} , for $M = 12$, Sc #4u_Mc_Se_A_200 and Sc #4u_Mc_Se_A_50, MT ₁	252
Figure 7.41 – Average power terms due to the composition of \mathbf{R} , for $M = 12$, Sc #4u_Mc_Se_A_200_ld and Sc #4u_Mc_Se_A_50_ld, MT ₁	253
Figure 8.1 – BG, function of M , for several values of d_{MT} , for CSt #Lu_mc_Mc_Gr. Solid lines indicate average results, and error bars indicate respective standard deviations.	261
Figure 8.2 – SINR, function of M , for several values of L , CSt #Lu_mc_Mc_Gr, $d_{MT} = 500$ m and $d_{MT} = 1\ 500$ m, MiC and MaC, respectively.	262
Figure 8.3 – BG, function of M , for several values of d_{MT} , CSt #Lu_mc_Mc_Sp, for $L = 4$ and 16.	263
Figure 8.4 – SINR, function of M , for several values of L , CSt #Lu_mc_Mc_Sp, $d_{MT} = 500$ m and $d_{MT} = 1\ 500$ m, MiCs and MaCs, respectively.	264

Figure 8.5 – BG, function of M , for several values of L , for MT_1 in CSt #Lu_mc_Mc_Se_A.....	265
Figure 8.6 – BG, function of M , for several values of L , for MT_1 in CSt #Lu_mc_Mc_Se_B.....	265
Figure 8.7 – BG, function of L , for several values of M , CSt #Lu_mc_Mc_Gr.....	269
Figure 8.8 – BG, function of L , for several values of M , CSt #Lu_mc_Mc_Sp.....	269
Figure 8.9 – BG, function of L , for several values of M , for MT_1 in CSt #Lu_mc_Mc_Se_A.....	270
Figure 8.10 – Average power terms due to the composition of \mathbf{R} , for CSt #4u_mc_Mc_Gr, $M = 12$, $d_{MT} = 500$ m and 1 500 m, for MiCs and MaCs, respectively.....	271
Figure 8.11 – Average power terms due to the composition of \mathbf{R} , for CSt #4u_mc_Mc_Sp, $M = 12$, $d_{MT} = 500$ and 1 500 m, for MiCs and MaCs, respectively.....	272
Figure 8.12 – Average power terms due to the composition of \mathbf{R} , for CSt #4u_mc_Mc_Se_A, $M = 12$, MT_1	272
Figure 8.13 – The SIMO channel implementation perspective, between MT_l and M_{Rx} element BS array.....	275
Figure 8.14 – The general MIMO channel implementation perspective, between L MTs and M_{Rx} element Rx array.....	275
Figure A.1 – Average BG [dB] and differences (between consecutive iterations) along optimisation, for $L = 4$, function of d_{MT} , for several values of M	330
Figure A.2 – Average P_{DesS} [dBm] and differences along optimisation, for $L = 4$, function of d_{MT} , for several numbers of array elements.....	331
Figure A.3 – Average $P_{NDesI} + N$ [dBm] and differences along optimisation, for $L = 4$, function of d_{MT} , for several numbers of array elements.....	332
Figure A.4 – Average BG [dB] and differences along optimisation, for $L = 8$, function of d_{MT} , for several values of M	333
Figure A.5 – Average P_{DesS} [dBm] and differences along optimisation, for $L = 8$, function of d_{MT} , for several numbers of array elements.....	334
Figure A.6 – Average $P_{NDesI} + N$ [dBm] and differences along optimisation, for $L = 8$, function of d_{MT} , for several numbers of array elements.....	335
Figure A.7 – Average BG [dB] along optimisation, for Sc #Lu_mc_Sp_5, function of L and M , and bar histograms of the maxima, function of the iteration number.....	336
Figure A.8 – Average BG [dB] along optimisation, for Sc #Lu_mc_Se_A, function of L and M , for MT_1 and the MT group.....	337
Figure A.9 – Average BG [dB] along optimisation, for Sc #Lu_mc_Se_B, function of L and M , for MT_1 and the MT group.....	338
Figure A.10 – Average BG [dB] along optimisation, for Sc #Lu_mc_Se_C, function of L and M , for MT_1 and the MT group.....	339
Figure B.1 – Average BG [dB] along optimisation, for Sc #4u_Mc_Gr_d_200, function of d_{MT} and M , and bar histograms of the maxima.....	342
Figure B.2 – Average BG [dB] along optimisation, for Sc #8u_Mc_Gr_d_200, function of d_{MT} and M , and bar histograms of the maxima.....	343
Figure B.3 – Average BG [dB] along optimisation, for Sc #16u_Mc_Gr_d_200, function of d_{MT} and M , and bar histograms of the maxima.....	344
Figure B.4 – Average BG [dB] along optimisation, for Sc #4u_Mc_Sp_d_200, function of d_{MT} and M , and bar histograms of the maxima.....	345

Figure B.5 – Average BG [dB] along optimisation, for Sc #8u_Mc_Sp_d_200, function of d_{MT} and M , and bar histograms of the maxima.....	346
Figure B.6 – Average BG [dB] along optimisation, for Sc #16u_Mc_Sp_d_200, function of d_{MT} and M , and bar histograms of the maxima.....	347
Figure B.7 – Average BG [dB] along optimisation, for Sc #Lu_Mc_Gr_15_50, function of L and M , and bar histograms of the maxima.....	348
Figure B.8 – Average BG [dB] along optimisation, for Sc #Lu_Mc_Sp_15_50, function of L and M , and bar histograms of the maxima.....	349
Figure B.9 – Average BG [dB] along optimisation, for Sc #Lu_Mc_Sp_15_400, function of L and M , and bar histograms of the maxima.....	350
Figure B.10 – Average BG [dB] along optimisation, for Sc #Lu_Mc_Se_A_200, function of L and M , for MT_1 and the MT group.....	351
Figure B.11 – Average BG [dB] along optimisation, for Sc #Lu_Mc_Se_A_50, function of L and M , for MT_1 and the MT group.....	352
Figure B.12 – Average BG [dB] along optimisation, for Sc #Lu_Mc_Se_B_200, function of L and M , for MT_1 and the MT group.....	353
Figure B.13 – Average BG [dB] along optimisation, for Sc #Lu_Mc_Se_B_50, function of L and M , for MT_1 and the MT group.....	354
Figure B.14 – Average BG [dB] along optimisation, for Sc #Lu_Mc_Se_C_50, function of L and M , for MT_1 and the MT group.....	355
Figure C.1 – Average SINR and BG evolution along optimisation, for Sc #4u_mc_Gr_d, for $M = 12$, with the CG or the RLS.....	358
Figure C.2 – Average SINR and BG evolution along optimisation, for Sc #8u_mc_Gr_d, for $M = 12$, with the CG or the RLS.....	359
Figure C.3 – Average SINR and BG evolution along optimisation, for Sc #16u_mc_Gr_d, for $M = 12$, with the CG or the RLS.....	360
Figure C.4 – Average SINR and BG evolution along optimisation, for Sc #4u_Mc_Gr_d_200, for $M = 12$, with the CG or the RLS.....	361
Figure C.5 – Average SINR and BG evolution along optimisation, for Sc #8u_Mc_Gr_d_200, for $M = 12$, with the CG or the RLS.....	362
Figure C.6 – Average SINR and BG evolution along optimisation, for Sc #16u_Mc_Gr_d_200, for $M = 12$, with the CG or the RLS.....	363

List of Tables

Table 4.1 – MGBSBEM optimised input parameters (extracted from [MPKZ01]).	86
Table 4.2 – WDCM MiC scenarios, for all MTs together or all angularly spread, varying BS-MT distance.	92
Table 4.3 – WDCM MiC scenarios, confined to the street, but separating MT_1 from the remaining MTs, grouped together.	94
Table 4.4 – WDCM MiC scenarios, where a single MT is kept angularly separated from the rest, for $d_{MT} = 500$ m.	95
Table 4.5 – WDCM MaC scenarios, for all MTs together or all angularly spread, varying BS-MT distance or scattering circle radius.	97
Table 4.6 – WDCM MaC scenarios, where a single MT is kept angularly separated from the rest, for $d_{MT} = 1\ 500$ m.	98
Table 4.7 – Comparable MiC and MaC propagation CSt scenarios.	100
Table 4.8 – ToA and AoA average spreads, function of d_{MT} , for MiCs.	102
Table 4.9 – ToA and AoA average spreads, function of r and d_{MT} , for MaCs.	104
Table 4.10 – ρ_τ , ρ_ϕ and ω_{DCIR} values involved in several MiCs and MaCs scenarios.	109
Table 6.1 – Average BG results, for MiC and MaC #Gr scenarios ($M = 12$).	203
Table 6.2 – Approximate times involved in some simulations corresponding to 10 times 100 concretisations per scenario, for some examples of MiC scenarios.	208
Table 6.3 – Times involved in some simulations corresponding to 10 times 100 concretisations per scenario, or some examples of MaC scenarios.	208
Table 7.1 – Average BG and SINR, for Sc #Lu_mc_St_Se_A and Sc #Lu_mc_St_Se_B, $M = 12$.	221
Table 7.2 – BG, function of the scenario, without and with the corresponding angular displacement of the BS-MT line.	223
Table 7.3 – BG and SINR, for Sc #4u_mc_Gr_05, with the 12-element array and the single element cases.	226
Table 7.4 – BG and SINR, for Sc #4u_mc_Gr_10, with the 12-element array and the single element cases.	227
Table 7.5 – Average P_{DesS} and $P_{>0}^{other}$ power term values, for several $L = 4$ scenarios, being normalised to the P_{DesS} maximum among all.	231

Table 7.6 – BG, function of L , M and d_{MT} , for Sc #4u_Mc_Gr_d_200 and Sc #16u_Mc_Gr_d_200.....	234
Table 8.1 – BG improvements, between using 20 and 2 array elements, for MiC and MaC Se_A and Se_B scenarios, MT ₁	268
Table 8.2 – Values of the Power Components for MiC and MaC cases, for $M = 12$	273
Table 8.3 – Mean and standard deviation of the 1 st , 2 nd and 3 rd diagonal magnitude values of matrix \mathbf{R}_{Rx} , involved in several MiCs and MaCs scenarios.....	277

List of Acronyms

3GPP	3 rd Generation Partnership Project
ADC	Analog to Digital Converter
AM	Amplitude Modulation
AMPS	Advanced Mobile Phone System
AoA	Angle-of-Arrival
AoD	Angle-of-Departure
AP	Access Point
ARM	Adaptive Resource Management
ARx	Analog Rx
ASILUM	Advanced Signal Processing Schemes for Link Capacity Increase in UMTS
ATM	Asynchronous Transfer Mode
AWGN	Additive White Gaussian Noise
BCE	Before Current Era
BER	Bit Error Rate
BFN	BeamForming Network
BG	Beamforming Gain
BLAST	Bell Labs LAyered Space-Time
BS	Base Station
BU	Bad Urban
CCIR	<i>Comité Consultatif International des Radio-Communications</i>
CDF	Cumulative Density Function
CDMA	Code Division Multiple Access
CE	Current Era
CG	Conjugate Gradient
CGNR	Conjugate Gradient Normal Equation Residual

CIR	Channel Impulse Response
CMA	Constant Modulus Algorithm
COST	<i>COoperation européenne dans le domaine de la recherche Scientifique et Technique</i>
CSt	Comparison Set
DAB	Digital Audio Broadcast
DCIR	Directional Channel Impulse Response
DesS	Desired Signal
DF	Direction Finding
DGS	Directional Gaussian Scattering
DL	Down-Link
DoA	Direction-of-Arrival
DoF	Degrees-of-Freedom
DRx	Digital Rx
DSA	Dynamic Spectrum Allocation
DSP	Digital Signal Processing
DVB	Digital Video Broadcast
FDD	Frequency Division Duplex
FDMA	Frequency Division Multiple Access
FIR	Finite Impulse Response
flops	floating point operations
FLAWS	Flexible Convergence of Wireless Standards and Services
FM	Frequency Modulation
GAA	Gaussian Angle of Arrival
GBSB	Geometrically Based Single Bounce
GBSBCM	Geometrically Based Single Bounce Circular Model
GBSBEM	Geometrically Based Single Bounce Elliptical Model
Gr	Grouped MTs Scenario
GSC	Generalised Sidelobe Canceller
GSCM	Geometry-based Stochastic Channel Model
GSM	Global System for Mobile Communications (former <i>Groupe Spécial Mobile</i>)
GSO	Gram-Schmidt Orthogonalisation
GWSSUS	Gaussian Wide sense Stationary Uncorrelated Scattering
HIPERLAN	High Performance Radio Local Area Network
HPBW	Half Power BeamWidth
HT	Hilly Terrain
IEEE	Institute of Electrical and Electronics Engineers

IF	Intermediate Frequency
IID	Independent and Identically Distributed
IMT-2000	International Mobile Telecommunications after 2000
IP	Internet Protocol
ISI	Inter-Symbol Interference
ITSITM	Institute for Telecommunications Sciences Irregular Terrain Model
ITU	International Telecommunications Union
LCMV	Linearly Constrained Minimum Variance
LMS	Least-Mean-Square
LoS	Line-of-Sight
LP	Local Parameter
LS	Least Squares
LS-CMA	Least Squares Constant Modulus Algorithm
MaC	Macro-Cell
MAC	Medium Access Control
MAI	Multiple Access Interference
MBS	Mobile Broadband System
MC	Multi-Carrier
MCS	Multipath Component Separation
METRA	MultiElement Transmit Receive Antennas
MGBSBCM	Modified Geometrically Based Single Bounce Circular Model
MGBSBEM	Modified Geometrically Based Single Bounce Elliptical Model
MiC	Micro-Cell
MIMO	Multiple-Input-Multiple-Output
MMSE	Minimum Mean Square Error
MSC	Multiple Sidelobe Canceller
MSE	Mean Square Error
MSNR	Maximum Signal-to-Noise
MT	Mobile Terminal
MVDR	Minimum Variance Distortionless Response
NB	NarrowBand
ND_NN	No Delays, No Noise
ND_WN	No Delays, With Noise
NDesI	Non-Desired Interference
NH	Null Hypothesis
NLoS	Non-LoS

NN	Neural Networks
OD	Optima Discrepancy
OFDM	Orthogonal Frequency-Division Multiple Access
OVSF	Orthogonal Variable Spreading Factor
PC	Power Control
PDF	Probability Density Function
PDP	Power Delay Profile
PI	Phase Independent
PN	Pseudo-Random
PSD	Power Spectral Density
QoS	Quality-of-Service
QPSK	Quadrature Phase-Shift-Keying
RA	Rural Area
RADAR	RAdio Detection And Ranging
RE	Radio Environment
RF	Radio-Frequency
RLS	Recursive Least Squares
RNC	Radio Network Controller
RSOB	Reference Signal Optimum Beamformer
Rx	Receiver
SA	Smart Antenna
SATURN	Smart Antenna Technology in Universal bRoadband wireless Networks
SBA	Switched-Beam Array
Sc	Scenario
SCM	Spatial Channel Model
SD	Steepest Descent
SDMA	Spatial Division Multiple Access
SDR	Software-Defined Radio
Se	Separate MTs Scenario
SF	Spreading Factor
SIMO	Single-Input-Multiple-Output
SINR	Signal-to-Interference-plus-Noise Ratio
SIR	Signal-to-Interference Ratio
SISO	Single-Input-Single-Output
SLC	SideLobe Canceller
SMI	Sample Matrix Inversion

SNR	Signal-to-Noise Ratio
SONAR	SOund Navigation And Ranging
Sp	Spread MTs Scenario
TDD	Time Division Duplex
TDMA	Time Division Multiple Access
TI	Totally Independent
TIREM	Terrain Integrated Rough Earth Model
ToA	Time-of-Arrival
TPC	Transmit Power Control
TSUNAMI	Technology in Smart antennas for UNiversal Advanced Mobile Infrastructure
TU	Typical Urban
Tx	Transmitter
UL	Up-Link
ULA	Uniform Linear Antenna
UMTS	Universal Mobile Telecommunications System
VCIR	Vector Channel Impulse Response
WB	WideBand
WD_NN	With Delays, No Noise
WD_WN	With Delays, With Noise
WDCM	Wideband Directional Channel Model
WLAN	Wireless Local Area Network
WMAN	Metropolitan Area Network
WPAN	Wireless Personal Area Network
WWRF	Wireless World Research Forum

List of Symbols

α_p	Complex amplitude of the p^{th} component
α_{p,n_c}	Magnitude of the p^{th} component, within the n_c^{th} cluster
α_{n_s,n_c}	Magnitude of the component from the n_s^{th} scatterer, within the n_c^{th} cluster
$\alpha_{n_s,n_c,l}$	Magnitude of the component from the n_s^{th} scatterer, within the n_c^{th} cluster, l^{th} link
α_{obs}	Obstruction factor exponent
$\alpha_{pc_i,p,l}$	Complex amplitude of the p^{th} path, from the l^{th} link, after the pc_l^{th} PC iteration
$\beta^{(i)}, \beta^{(i,k)}$	Gram-Schmidt constants
δ_{RLS}	Initialising constant, for the RLS
ϕ	Azimuth angle
ϕ_{BW}	Maximum ray azimuth beamwidth due to reflectors around an MT
ϕ_{DesS}	Azimuth AoA, of the DesS
ϕ_{MT}	Azimuth angle of an MT
ϕ_{n_c}	Mean azimuth AoA of the n_c^{th} cluster
$\phi_{n_c,l}$	Mean azimuth AoA of the n_c^{th} cluster, from the l^{th} link
ϕ_{n_s,n_c}	Azimuth AoA of the n_s^{th} scatterer, within the n_c^{th} cluster
$\phi_{n_s,n_c,l}$	Azimuth AoA of the component from the n_s^{th} scatterer, within the n_c^{th} cluster, from the l^{th} link
ϕ_p	Azimuth angle, or AoA of the p^{th} component
$\phi_{p,l}$	Azimuth of the p^{th} path, from the l^{th} link
ϕ_{p,n_c}	Azimuth or AoA of the p^{th} component, from the n_c^{th} cluster
φ	Phase-shift

Φ_{n_s, n_c}	Phase corresponding to the n_s^{th} scatterer, within the n_c^{th} cluster
Φ_{p, n_c}	Phase corresponding to the p^{th} path, from within the n_c^{th} cluster
λ	Wavelength
λ_{EVi}	i^{th} eigenvalue
λ_{EVmax}	Maximum eigenvalue
λ_{LM}	Complex Lagrange multiplier
λ_{RLS}	Exponential weighting factor, for the RLS
μ	Convergence step-size
ν	Doppler-shift
ν_{n_s, n_c}	Doppler-shift of the component from the n_s^{th} scatterer, within the n_c^{th} cluster
θ	Elevation angle to the perpendicular to the ground plane
ρ_τ	Temporal density of arriving signals
ρ_ϕ	Angular density of arriving signals
$\rho_{a,b}$	Correlation coefficient between a and b quantities
$\rho_{i,j}^{\text{Rx}}$	Complex spatial correlation coefficient between i^{th} and j^{th} array elements, at the receiver
$\rho_w^{(l,j)}$	Complex weight vector correlation coefficient between l^{th} and j^{th} beamformers
σ_d	Desired signal standard deviation
σ_n	Noise standard deviation
τ	Time delay or ToA
τ_0	Direct component delay
τ_{FIR}	Relative delay between elements, in a FIR filter
$\tau_{FIR}(\phi)$	Relative delay between neighbour elements, as a function of ϕ , in a FIR filter
$\tau_{FIR}(m)$	Relative delay between neighbour elements, as a function of the element index
$\tau_i(\phi)$	Cumulative i^{th} delay, due relative element delay and element branch delays
τ_{max}	Maximum time delay, or ToA
τ_n	Time delay, or ToA, of the n^{th} temporal bin
τ_{n_c}	Time delay, or ToA, corresponding to the n_c^{th} cluster
$\tau_{n_c, l}$	Time delay corresponding to the n_c^{th} cluster, from the l^{th} link
τ_{n_s, n_c}	Time delay corresponding to the n_s^{th} scatterer, within the n_c^{th} cluster
τ_p	Time delay corresponding to the p^{th} path
$\tau_{p, l}$	Temporal delay of the p^{th} path, from the l^{th} link

τ_{p,n_c}	Time delay or ToA of the p^{th} scatterer, within the n_c^{th} cluster
ω_{DCIR}	DCIR channel richness
$\xi(n)$	Estimation or general error, at the n^{th} instant
$\xi_l(n)$	Estimation error, corresponding to the l^{th} link/beamformer, at the n^{th} instant
Ψ_{p,n_c}	Angle of the p^{th} component of the n_c^{th} reflector, in respect to MT velocity vector
$\sigma_{\phi,NB}$	Narrowband angle-spread
$\sigma_{\phi,WB,=0}$	Wideband angle-spread, corresponding to non-delayed signals
$\sigma_{\phi,WB,>0}$	Wideband angle-spread, corresponding to delayed signals
σ_τ	Delay-spread
Ω	Discrete angular frequency, in radians
Ω_{DesS}	Discrete angular frequency of the desired signal
Γ_{n_s,n_c}	Complex reflection coefficient corresponding to the n_s^{th} scatterer, within the n_c^{th} cluster
$\Gamma_{n_s,n_c,l}$	Complex reflection coefficient corresponding to the n_s^{th} scatterer, within the n_c^{th} cluster, l^{th} link
a (ϕ)	Steering vector
a (ϕ,Ω)	Array response vector, steering vector, function of Ω and ϕ
$a_m(\phi)$	Steering vector m^{th} element, function of the azimuth
a (Ω)	Array response vector, or steering vector, function of Ω
A	Steering vector matrix
A_{scat}	Scattering area
$A_{scat. circle}$	Area of the scattering circle
$A_{scat. ellipse}$	Area of the scattering ellipse
B_c	Coherence bandwidth
B_s	System bandwidth
B_n	Noise-equivalent bandwidth
c	Electromagnetic propagation velocity in free space
C	Constraint matrix for the LCMV
$\mathbf{c}_{code}^{(l)}$	Channelisation code vector, for the l^{th} link
$c_{code,q}^{(l)}$	Channelisation codes q^{th} element, for the l^{th} link

$\mathbf{c}_d^{(l)}$	Desired reference (code) vector, for the l^{th} link/beamformer
$c_d^{(l)}(n)$	Desired reference (code) symbol, for the l^{th} link/beamformer, at the n^{th} instant
C_{n_c}	Set of components within the n_c^{th} cluster
\mathbf{d}	General desired reference vector
$d(n)$	General desired reference signal, at the n^{th} instant/iteration
d_{el}	Distance between antenna array elements
d_i	i^{th} BS distance to the MT
D_i	Subspace span, at the i^{th} algorithm iteration
\mathbf{dir}	Algorithm search direction
\mathbf{d}_l	Desired reference vector, for the l^{th} link/beamformer
d_{MT}	Distance between BS and MT
E_b	Energy per bit
$E_{n_c}(t, \phi)$	Complex antenna radiation pattern contribution, related to the n_c^{th} cluster, as a function of time
$E_p(\phi_{n_c})$	Complex antenna radiation pattern in the direction of the p^{th} component, from the n_c^{th} cluster
\mathbf{err}	Weight estimation error
\mathbf{err}_l	Weight estimation error, for the l^{th} beamformer
$E_{Rx}(\phi)$	Complex antenna radiation pattern at the receiver
$E_{Tx}(\phi)$	Complex antenna radiation pattern at the transmitter
f	Cyclic frequency
f_c	Carrier Frequency
F_{obs}	Obstruction factor
$G_{beamformer, l}$	Beamforming gain, corresponding to the l^{th} beamformer
G_p	CDMA processing gain
\mathbf{H}	Narrowband MIMO channel matrix
$h(\phi)$	Time-invariant AoA impulse response
$h(\tau, \tau_0, \phi)$	Channel impulse response, as a function of ToA, azimuth, at observation time τ_0
$\mathbf{H}(\tau)$	Wideband MIMO channel matrix
$\mathbf{H}(\tau_n)$	Narrowband MIMO channel matrix, at the n^{th} temporal bin
$h(\mathbf{p}, \tau, \phi, \theta)$	Channel impulse response, as a function of the receiver position, ToA, azimuth and elevation
$h(t)$	Time invariant ToA response, or delay-spread function

$h(t, \tau)$	Time variant impulse response, or delay-spread function
$h(t, \tau, \phi)$	Time variant, directional impulse response
$H_{bf}(\phi, \Omega)$	Beamformer directional transfer function
$h_{bf}(n)$	Beamformer impulse response, as a function of discrete time
$h_{BS}(t, \tau, \phi)$	Impulse response component due to scatterers around the BS
$H_{dbf}(\phi, \Omega)$	Desired beamformer transfer function
$\mathbf{H}_{dbf}(\phi, \Omega)$	Desired beamformer transfer function matrix
$h_{distant}(t, \tau, \phi)$	Impulse response component due to major distant scatterers/reflectors
$h_l(\tau)$	Time invariant impulse response, or delay-spread function, for the l^{th} link
$h_{LOS}(t, \tau, \phi)$	Time variant, impulse response component associated with the LoS path
$h_{m_{Tx}, m_{Rx}}$	Channel impulse response between the m_{Tx}^{th} transmitter and m_{Rx}^{th} receiver antenna elements
$h_{MT}(t, \tau, \phi)$	Time variant, impulse response component due to scatterers around an MT
$h_p(\mathbf{p}, \tau, \phi, \theta)$	p^{th} channel impulse response, as a function of the receiver position, ToA, azimuth and elevation
I	Identity matrix
$J(n)$	General cost function, at the n^{th} instant/iteration
$J_l(\mathbf{w}_l)$	Cost function, for the l^{th} beamformer, function of \mathbf{w}_l
k_{Boltz}	Boltzmann constant
$\mathbf{k}(n)$	RLS gain vector
K_{obs}	Obstruction factor gain
l	Link index
L	Number of active MTs
L_{NDesI}	Number of NDesI contributions
L_T	Total number orthogonal arriving signals
m	Antenna element index
M	Number of antenna array elements
m_{Rx}	Array element index at the receiver
M_{Rx}	Number of receiver antenna array elements
m_{Tx}	Array element index at the transmitter
M_{Tx}	Number of transmitter antenna array elements
$N_0(f)$	Noise spectral density
N	Noise power
n_c	Cluster index
N_c	Number of relevant clusters

$N_{flops/iter}^{CG}(M, L)$	Number of flops per iteration, in the CG, as a function of M and L
$N_{flops/\mathbf{R}, \mathbf{d}_l}^{CG}(M, L, N_s)$	Number of flops per calculation of \mathbf{R} and \mathbf{d}_l , in the CG, as a function of M , L and N_s
$N_{flops/iter}^{RLS}(M, L)$	Number of flops per iteration, in the RLS, as a function of M and L
N_{iter}	Number of iterations
N_{mp}	Number of arriving multipaths
$N_{mp,l}$	Number of arriving multipaths, from the l^{th} link
$n_{n,m}$	Complex noise input, at the n^{th} sample and m^{th} array element
n_s	Scatterer index
N_s	Total number of samples
N_{scat}	Total number of scatterers
$N_{scat}(n_c)$	Total number of scatterers, within the n_c^{th} cluster
\mathbf{p}	Location vector
$p_{\tau,\phi}(\tau, \phi)$	Joint probability density function between delay and azimuth
pc_i	PC iteration index
$pc_fact_{pc_i,l}$	PC factor corresponding to the l^{th} link, after the pc_i^{th} PC iteration
P_{DesS}	Desired signal power
$P_{DesS,l}$	Desired signal power, from the l^{th} link
$\mathbf{P}(n)$	Inverse of the correlation matrix of the array input data, for the RLS
$P_{N,l}$	Noise power at the l^{th} beamformer
P_{NDesI}	Non-desired Interference power
$P_{NDesI,l}$	Non-desired Interference power, from the l^{th} link
$P_{>0}^{self}$	Delayed power contribution from each link, averaged among all links
$P_{>0}^{other}$	Delayed power contribution from other than each link, averaged among all links
$P_{l,>0}^{other}$	Delayed power contribution from other than the l^{th} link
$P_{l,>0}^{self}$	Delayed power contribution from the l^{th} link
$P_{=0}^{self}$	Non-delayed power contribution from each link, averaged among all links
$P_{=0}^{other}$	Non-delayed power contribution from other than each link, averaged among all links
$P_{l,=0}^{other}$	Non-delayed power contribution from other than the l^{th} link
$P_{l,=0}^{self}$	Non-delayed power contribution from the l^{th} link
\mathbf{q}_{EVmax}	Maximum eigenvalue

r	Radius of circumference or of circle of scatterers
\mathbf{R}	Correlation matrix of the array input data block
r_0	Path-length, corresponding to the shortest path
$R_c(\boldsymbol{\tau})$	Correlation function, averaged among all codes
$R_c^{(l)}(\boldsymbol{\tau})$	Correlation function, for the l^{th} link code
\mathbf{res}	Residual vector
$\mathbf{res}(n)$	Residual vector, at the n^{th} instant
\mathbf{res}_l	Residual vector, for the l^{th} beamformer
r_p	Path-length, corresponding to the p^{th} path, normalised to the direct component delay
$\mathbf{R}_{l,l=0}$	Non-delayed contribution from matrix \mathbf{R} , corresponding to the l^{th} link
$\mathbf{R}_{l,l>0}$	Delayed contribution from matrix \mathbf{R} , corresponding to the l^{th} link
r_{max}	Path-length, corresponding to maximum delay, normalised to the direct component delay
\mathbf{R}_{MIMO}	MIMO correlation matrix
\mathbf{R}_n	Correlation matrix of the array noise vector
\mathbf{R}_N	Noise contribution from matrix \mathbf{R}
\mathbf{R}_{R_x}	Spatial correlation matrix at the receiver
$\mathbf{R}_{R_x }$	Spatial correlation moduli matrix at the receiver
\mathbf{R}_{T_x}	Spatial correlation matrix at the transmitter
r_w	Effective street width ratio
\mathbf{R}_x	Correlation matrix of the array input data vector
\mathbf{r}_{xd}	Cross-correlation vector of the input vector and the desired signal
$R_{xc}(\boldsymbol{\tau})$	Cross-correlation function, averaged among all cross-combinations of codes
$R_{xc}^{(l)}(\boldsymbol{\tau})$	Cross-correlation function, relative to the l^{th} link code
$s(t)$	Baseband transmitted signal
$\mathbf{s}(t)$	Baseband transmitted signal vector, each vector element corresponding to each antenna element
m^{th}	antenna element
\mathbf{s}_{code}	Complex scrambling code
$s_{\text{code},p}$	Complex scrambling code, p^{th} element
$\mathbf{s}_{\text{comb}}^{(l)}$	p^{th} element of the complex combination of codes vector, for the l^{th} link
$s_{\text{comb},p}^{(l)}$	p^{th} element of the complex combination of codes, for the l^{th} link
SF_l	Spreading factor, for the l^{th} link
SF_{max}	Maximum spreading factor
$SINR_l$	SINR corresponding to the l^{th} link

$SINR_{beamformer,l}$	SINR corresponding to the l^{th} link, with the respective beamformer
$SINR_{single,l}$	SINR corresponding to the l^{th} link, for the single element antenna
$SINR_{pc_i,l}$	SINR of the l^{th} link, after the pc_i^{th} PC iteration
t	Continuous time variable
\mathcal{T}	Noise-equivalent temperature
T_b	Bit duration
T_c	Coherence time
T_{chip}	Chip duration
T_m	Tap-delay within the m^{th} array element
T_{N_s}	Sampling period, corresponding to N_s samples
$T(t,f)$	Time variant transfer function
\mathbf{U}	Signal matrix output by the antenna array
$u(\tau)$	Complex signal envelope output by the antenna array
$\mathbf{u}(n)$	Complex baseband signal output by the antenna array
$\mathbf{u}(t, \tau)$	Complex baseband signal output by the antenna array, function of time and delay
$\mathbf{u}(t, \tau, \phi)$	Complex baseband signal output by the antenna array, function of time, delay and azimuth
$u_0(\tau)$	Complex signal envelope in the reference antenna element
$\mathbf{U}_{l=0}$	Non-delayed contribution from matrix \mathbf{U}
$\mathbf{U}_{l>0}$	Delayed contribution from matrix \mathbf{U}
$u_m(\tau)$	Complex signal envelope in the m^{th} antenna element, as a function of continuous time
$u_m(n)$	Complex signal envelope in the m^{th} antenna element, as a function of discrete time
$u_{n,m}$	Complex signal output by the array, at the n^{th} sample and m^{th} array element
\mathbf{U}_N	Noise contribution from matrix \mathbf{U}
\mathbf{w}	Weight vector
\mathbf{w}_l	Weight vector, for the l^{th} beamformer
\mathbf{w}_{opt}	Optimum weight vector
$\mathbf{w}_{opt,l}$	Optimum weight vector, for the l^{th} beamformer
$w_e(n,i)$	Error square weight, for the RLS
W_{ef}	Effective street width
$x(t), x(n)$	Input signal envelope (baseband), as a function of continuous or discrete time
$\mathbf{x}(n)$	Input signal envelope vector

$\mathbf{x}(\phi, \Omega)$	Input signal envelope vector, as a function of azimuth and discrete frequency
$x_m(n)$	Input envelope signal, at the n^{th} sample and m^{th} array element
$y(t), y(n)$	Output envelope signal, continuous or discrete time
$\mathbf{y}(n)$	Output signal envelope vector
$y_l(n)$	Output signal envelope, for the l^{th} beamformer
$\delta(\bullet)$	Dirac impulse, in the domain of \bullet
$\Delta \bullet$	Variation in the quantity \bullet
$\nabla \bullet$	Gradient vector of function \bullet
$E[\bullet]$	Expectation of the random process \bullet
$\min_{\mathbf{w}}\{\bullet\}$	Minimum of function \bullet , as a function of \mathbf{w}
$x \bmod y$	Modulus operation (signed remainder after division)
$O[\bullet]$	Order of \bullet
$U(a,b)$	Uniform distribution, within the a and b lower and upper limits
$X * Y$	Convolution between X and Y functions
\bullet^*	Conjugate of \bullet
\bullet^+	Pseudoinverse of matrix \bullet
\bullet^H	Hermitian transpose of matrix \bullet
\bullet^T	Transpose of matrix \bullet
\bullet^{-1}	Inverse of matrix \bullet
$\hat{\bullet}$	Estimate of \bullet
$ \bullet $	Magnitude of \bullet

1 Introduction

Every day sees humanity more victorious in the struggle with space and time.

— Guglielmo Marconi (1874-1937)

1.1 Motivation – Context and Philosophy

The duality between exploiting resources and the evolution of civilisation has for long been the drive of human development. In parallel and most frequently, due to the limitation that resources are intrinsically characterised for, civilisation has evolved through maximising the use of all those that are available, even sometimes running the risk of extinguishing many. Take, for example, the most obvious flora, fauna or mineral natural resources that Humankind is strongly dependent on for so many reasons. In some cases, such dependency has been accompanied by the concern to sustain, in others it may lead, or has already led, to exhaustion – crude oil, natural gas, water, forests, productive soil, and so many living species. In Communications, inevitably, the same *laws* of human development apply, since in fact it is one of the fundamental drives of the evolution of our civilisation. Therefore, Communications also reflect which and how physical means are of use, for the sake of such development, as a whole. It is not just the silicon, gold or copper resources that one is resorting to, but Communications especially involve sharing time, frequency, coding and space. In a world with ever increasing population, with connectivity among all users (even in the so-called *3rd World Countries*) having been shortened by evolution, resources such as time, frequency, coding and space are also limited, and their limits have had their own enormous impacts on the recent history of Communications (take, for example, the licensing auctions in which Universal Mobile Telecommunications System (UMTS) has been involved).

With the explosive growth in wireless communications over the last two decades, the need for efficient use of frequency spectrum has expanded in parallel. With the accompanying increasing demand for capacity, the direct traditional solution primarily falls into using more bandwidth and

increasing operation frequency. Nevertheless, as any physical resource, spectrum use is limited by itself, the limits being primarily set by the high infrastructure effort and costs that evolving to other frequency bands entails. If time, frequency or coding/power, i.e., the physical resources that Time, Frequency and Code Division Multiple Access schemes directly rely on, were once resources that sufficed for wireless communications, then another physical resource that is now necessary and still available is *space*. In mobile, wireless communications, where inherently the Mobile Terminal (MT) user can be in one of an infinite number of positions, and where the morphology of the propagation physical medium renders a multitude of conditions, *space* is a resource that seems rich enough to be further explored.

In fact, cellular communication systems have, from the start, inherently explored the spatial domain, through frequency reuse and sectorisation. Nevertheless, the last few years have set the need for further exploration of *space*, through establishing another multiple access scheme – Spatial Division Multiple Access (SDMA). In that way, employing the spatial dimension to separate several links operating in the same time/frequency/code physical channel results in further use of all the directly available physical resources. Such exploitation is not anymore at a large-scale use as cellular and sectorisation structuring is, but deals at a more surgical, smaller scale level. Especially in the case of high-density MT areas, all of the referred time, frequency, code and space fundamental resources require their most efficient use, with SDMA acquiring special significance.

With a propagation channel that is characterised by its variation in time and space, such exploitation of the spatial domain is demanding, requiring flexibility to adapt to a new physical situation. In other words, system *dynamics* or *adaptivity* is required. On the other hand, such adaptivity must be controlled in a self-contained manner, without the intervention of the user or operator; it must accompany the channel conditions and control the physical level electronics at the MT or Base Station (BS); it must involve a measurement means in order to perform such evaluation of the important parameters; and, finally, such adaptivity must also be frequent, according to the correlation time of such channel. In other words, such adaptivity must be *smart, intelligent*, i.e., it must reflect an acknowledgement of the channel, a selection of the important *cost* parameters (in the general sense of the word *cost*), and a subsequent control and change of the adaptive system in order to minimise such *cost*.

In mobile wireless communications, it is in those ways that *smart adaptive* antennas play the role of surgically applying the best array pattern, either at the BS or at the MT, according to their relative location, number, and channel conditions. The ultimate objective of their use is improving system capacity. It is not new that the use of antenna arrays inherently provides processing gain to improve BS range and coverage but, most importantly, such systems render Signal-to-Interference-plus-Noise (SINR) improvement, especially meaningful where user densities and traffic load tend to be large.

Therefore, as it has been understood by the previous paragraphs, Smart Antennas (SAs) allow to *dynamically* and *intelligently* exploit the spatial domain, making use of *space* as the available and exploitable resource. In that sense, such resource requires to be well known, being paramount to understand and model the spatial and wideband properties of the propagation channel, because of its complexity and requirements of the applications at stake.

One then clearly sees two large fields of study, poles of attraction for many research, development and regulating activities – mobile propagation channel characterisation and SAs. The former may involve areas such as measurement and modelling, while the latter may range from baseband signal processing to antenna fabrication. If presently there are numerous measurement campaigns, directly involving array processing and antenna fabrication themselves, it is still not as frequent to find Wideband Directional Channel Models (WDCMs) that have been fully assessed with those measurements. Even less frequent are contributions from linking signal processing together with general channel characterisation. Truly, the current developments and trends towards Multiple-Input-Multiple-Output (MIMO) systems might be able to further draw the attention to the convergence of these areas, and not to their divergence.

Such behaviour of the several intervening parties, being academic or industrial ones, in any of those fields, also follows another most common and natural trend in the evolution of civilisation – specialisation. Such conduct implies that it is by specialising in a field that the results of such work are more efficiency achieved, reaching quality and insight within an area of activity. It may be true that, by specialising, the training, education and directing of people result more effective, therefore reaching results faster. Nevertheless, as the process of field specialisation progresses, the most common tendency is to acquire an excessive abstraction from other fields to which the former does in fact directly relate. For that, for example, much contributive effort is put into adaptive array signal processing making relatively large assumptions, or even none at all, on the wideband directional propagation channel model characteristics. Also, there are many cases of most contributive and important endeavour towards channel modelling and characterisation, though not accounting for the subsequent simulation complexity that such model involves, making further processing-level add-ons even more difficult. As a reflection of that specialisation, many are the scientific contributions within each of those fields alone, but lack of transversal ones. In that way, the current work has intentionally aimed at achieving such transversal coverage, therefore, also establishing a contribution in that sense.

One might say that *engineering* is inherently characterised by involving the combination of fields in a practical view, in manners that allow for the concretisation of a certain application, only made possible through such combination. Nevertheless, one can also view a more complete *scientific contribution* as one that also involves attaining a necessary practical perspective, having something of an *engineering* angle, besides involving the necessary scientific profoundness, specialisation and theoretical background.

Being aware that the transversal combinations of fields are most frequently more *engineering-* than *scientific-oriented* activities, the relative lack of transversal studies within the scientific community can be better understood. On the other hand, if such combination of fields is able to achieve the right scientific profoundness, it will even better contribute to completeness and relevance as a whole. Therefore, in terms of working conduct, a point of equilibrium has been required to develop the present study in a scientific way, nevertheless establishing bridges towards a most practical, engineering-oriented perspective.

The first concern has been to use a sufficiently realistic, but also simple, channel model to evaluate the performance of the antennas, keeping in mind the great variety of channel conditions possible. In that sense, by applying a semi-statistical model, the model is realistic enough in terms of statistical meaning, being sufficiently light in terms of processing to be able to carry out a systematic analysis of the problem. Like so, such model has allowed for its implementation in the form of scenarios, through which also approximate realistic multi-user situations have been considered. In that manner, work has been developed in an UMTS-directed approach, seeking to add further practical perspective and awareness to the scientific contribution. Nevertheless, it is not limited to UMTS, but further extrapolates its results towards future Mobile Broadband Systems (MBSs).

In parallel, concerning the processing side, the concern was to apply an adaptive problem that would not be so complex so as not to introduce function blocks that would involve additional operation factors and sensitivities detracting from the physical level happenings within the propagation channel. It was permanently kept in mind, and this should be clearly understood by the reader, that the objective of the adaptive algorithm was not to verify its function and describe a new algorithm application, but to be able to extract the basic dependencies on the wideband directional properties of the channel. In other words, the algorithm serves as a tool, as a measurement means to reflect the more or less demanding conditions presented by the channel.

As a result of balancing in between the described compromises and adopting such philosophy conduct, the work has attained fundamental and system-independent insight in order to reach most general conclusions. The research, demonstration and evaluation of fundamental physical properties that the wideband directional propagation channel imposes on the operation of SAs, concerning the inherent capabilities for carrying out effective lobe and null positioning for interference suppression, have been possible. After having put forward such reasoning, for either micro- or macro-cellular scenarios separately, the close comparison between macro- and micro-cell performances has also been possible. That comparison has then contributed to the definition and analysis of the physical level channel parameters found to determine the interference mitigation performance allowed through beamforming.

To gain further perspective on the impact of the referred results, again in a system-, practical- or engineering-oriented way, the previously referred conclusions are projected towards future MBSs, according to the forecasted trends, envisaging a relatively strong impact on cellular planning.

It is also important to keep in mind that the whole present contribution is fundamentally based on simulation work, making use of a channel model and making important assumptions. This fact must be pragmatically faced and justified, and is a reflection of another point of equilibrium in the work methodology.

Resorting to simulations may be rough in terms of having to render sufficient confidence in *artificially* generated results, but it is only through simulations that some problems and hypotheses may in fact be put or may be confirmed, in due time. This is the case of this study, where the final conclusions and channel characterisation could only be obtained through analysing many channel concretisations, followed by a statistically controlled analysis, while being subject to a deadline-oriented approach. Undoubtedly, otherwise would mean needing many measurement campaigns with a fully working system, choosing the sites rightly in order to mirror the considered scenarios, and to carry out a full and correct statistical analysis of the results. That approach would involve much larger temporal and work volume scales.

In order to achieve such confidence and to work upon the most solid grounds, while resorting to simulations, all the assumptions must be clearly stated, even any that might be less realistic. As long as the less realistic ones are those of system simplification, always fundamentally respecting the physical level happenings at the required operating scale, it is anyway necessary to resort to several arguments and other parallel simulation means to help to base all conclusions and arguments. If, additionally, such arguments and justifications are based on known fundamental physical level issues, then better physical understanding is delivered, resulting in better confidence. As far as this research is concerned, the involved model use, the considered processes, and the whole beamforming operation do, in fact, deal with fundamental physical level happenings. By simply resorting to these, the logical arguments and justifications for all of the results have been found, related, and are now hereby systematically stated.

Adding to this, if greater simulations complexity may aim at generating an image closer to reality, such reality cannot be ever entirely modelled, and such complexity ends up involving great difficulties in making use of such simulation model. While keeping simplicity and putting forward simplifying assumptions that only concern system implementation issues, the probability of introducing a too great a number of unrealistic factors is kept small and controlled, compared to more complex simulations or adaptive schemes. The constant management of the equilibrium between the advantages and disadvantages that simulating work involves also justifies the reason why a degree of conscientious simplicity has led to more clearly obtained results, almost solely dependent on the most important physical issues and not on additional system blocks.

Finally, one is then able to understand and acknowledge that the context of “smart antennas for broadband mobile communications” is hereby seen to consist of the close intertwining of channel characterisation and modelling, adaptive processing and system-level considerations. By intentionally and consciously evolving within such context, only a pragmatic approach to simplify the problem allows the reach of most general and important conclusions. It is meant to be a contribution towards better understanding the available *space*, as an exploitable resource in mobile communications, establishing the important physical characteristics that affect the adaptive interference reduction operation of smart antennas.

Besides understanding the philosophy ruling the development of this study, it is also important to acknowledge the more specific technical context in which this research fits.

Research contributions such as [LiLi03], [TsAt02], [KuTB02], [CCIC02], [Corr01], [TsAP00], [Petr97] and [Nagu96] are important and good examples of the joint application of several adaptive array solutions together with several types of wideband and directionally characterised propagation scenarios, not being limited to beamforming and already expressing that the problem does extend beyond the algorithms level. Nevertheless, these root from the algorithms, whereas the present research evolves from the channel side. For that, those contributions do not sufficiently qualify the fundamental channel properties that generally affect adaptive array techniques; the way that the type of multi-user environment affects the interference performance, relating such dependence with the channel properties, has not been covered by some; in other cases, the maximum number of mobile users has been set to two, only; finally, a number of those contributions is centred only on micro-cell scenarios, basing their results in specific Ray-Tracing techniques.

Concerning the central applied algorithm, the Conjugate Gradient, a very wide variety of related papers cover its use in antenna array beamforming, e.g., [ChWi00], [ApCB00], [KaBa99], [HeBK99], [Bagh99], [ChLH97], [ChWi95], [ChKi92]. Nevertheless, those references do not address the problem of evaluating performance dependencies on the propagation channel characteristics, by means of a WDCM, nor consider the application of the algorithm in a system-directed way.

Regarding the whole adaptive problem applied, for the set objectives, it is required to be kept simple and effective. Like that, one excludes dependencies on other processes such as Direction Finding (DF) or tracking, as well as their consequently involved physical issues. For example, [CCIC02] and [KuTB02] present how the combination of several processing stages, blind or non-blind, are dependent on certain scenario properties. The functionalities of those stages may be separately evaluated and described, but an array pattern will in fact be a result of several processes, altogether. With a non-blind and simple processing application, solely applying the strict beamforming problem, one exclusively focuses on the overall shaping of the array pattern. Performance results will most directly reflect the fundamental dependencies with the propagation

channel spatial properties, regarding interference reduction and the relative location of lobes and nulls. Like so, one does not detract from this study's objectives and set contributions.

Also, [SÖHM02], [SvWa02], [Svan01], [KMJA00] deal with the notion of *multipath richness*, towards MIMO implementations, reflecting the importance that such characterisation is currently undertaking towards using the channel most efficiently. Anyway, the matter of multipath richness needs not be solely centred on MIMO, this study showing that it is also determinant in constraining beamforming performance.

Lastly, but not least, as already stated, many of the previously referred research inputs do not explicitly or directly infer results in system-wise perspectives, which has been a major concern in this study. Namely, the application is primarily directed towards UMTS, but it is developed and its results are evaluated with the constant objective of conjecturing implications in future MBSs, specifically Code Division Multiple Access (CDMA)-based ones, such as Multi-Carrier (MC)-CDMA.

1.2 Contributions of this Study

It is important to inform the reader of the published outputs with which this work has publicly contributed. Being promptly directed towards such public outputs, the reader not only better understands the study, as a whole, but also grasps the ways in which it has fitted into both the referred scientific- and engineering-directed views. This listing helps in the reader's acknowledgement of this study's substance, covering resulting journal publications, a chapter written for a book, conference papers, given seminar presentations, and summarised project-related activities, not necessarily following the chronological order but that of meaning and content.

The most important and complete contributions, submitted and accepted for publication in scientific journals and a book, correspond to two major workflow steps: the comparison of beamforming performance dependencies between micro- and macro-cells, multi-user scenarios (cases a) and b), listed below), and the evaluation of such main beamforming dependencies on micro-cell ones (case c)). These are listed below:

- a) Gil,J.M. and Correia,L.M., "Comparing Adaptive Beamforming in Micro- and Macro-Cells", submitted to *IEEE Transactions on Vehicular Technology*, June 2003, ([GiCo03d]);
- b) Gil,J.M. and Correia,L.M., "Adaptive Beamforming Performance in Micro- and Macro-Cell Propagation Scenarios", submitted as a contribution to a book entitled *Adaptive Antenna Array Techniques*, being edited by Dr. Sathish Chandran, Springer-Verlag, Heidelberg, Germany, June 2003, ([GiCo03e]);
- c) Gil,J.M. and Correia,L.M., "Impact of Wideband Directional Propagation Channel Characteristics on Adaptive Beamforming", *IEICE Transactions on Communications*, Vol. E85-B, No. 12, Dec. 2002, pp. 1640-7, ([GiCo02b]).

Globally, and starting from the firstly-dated and simplest one, the added value of publication c) resides in the articulation of fields. It combines a channel model in the form of UMTS scenarios and a beamforming algorithm to evaluate the performance dependencies on the micro-cell channel, including the definition, description, and evaluation of the several power components involved in the adaptive problem. In the a) and b) submissions for publication, the most important inputs are the definition and analysis of channel characterisation parameters, such as *channel richness*, *angular* and *temporal densities* of arriving signals, as functions of both the micro- and macro-cell scenarios' characteristics. This has been possible only through the presented comparison between performances in micro- and macro-cell situations. These two contributions mainly differ in the scenarios for which results are explicitly presented; the former includes a thorough evaluation of the significant power components as function of the micro- or macro-cell situations; the latter comprises results on the performance dependence on cluster and scatterer densities.

Concerning the publications in conferences, these have naturally been less profound than the journal ones. Nevertheless, these have contributed with important detailed results, establishing a sort of monitoring control points guiding through a coordinated set of contributing scientific outputs. The successive production of these results is a reflection of the general workflow:

- a) Gil,J.M. and Correia,L.M., “Fundamental Wideband and Directional Channel Parameters Ruling Adaptive Beamforming Performance in Micro- and Macro-Cells”, accepted to *VTC'04 Spring – 59th IEEE Vehicular Technology Conference*, Milan, Italy, May 2004, ([GiCo03f]).
- b) Gil,J.M. and Correia,L.M., “Adaptive Beamforming Dependencies on Wideband and Directional Propagation Characteristics in Micro- and Macro-Cell UMTS Scenarios”, in *Proc. of PIMRC'2003 – 14th IEEE International Symposium on Personal, Indoor and Mobile Radio Communications*, Beijing, China, Sep. 2003, ([GiCo03c]).
- c) Gil,J.M. and Correia,L.M., “Impact of UMTS Macro-Cell Scenarios Directional Characteristics on Adaptive Beamforming Performance”, in *Proc. of IST-MWCS'2003 – IST Mobile and Wireless Communications Summit 2003*, Aveiro, Portugal, June 2003, ([GiCo03a]);
- d) Gil,J.M. and Correia,L.M., “The MMSE vs. Beamforming Gain Optima Discrepancy in Adaptive Beamforming Applied to Directional Channel Scenarios”, in *Proc. of ConfTele 2003 – 4th Conference on Telecommunications*, Aveiro, Portugal, June 2003, ([GiCo03b]);
- e) Gil,J.M. and Correia,L.M., “Dependence of Adaptive Beamforming Performance on Directional Channel Modelled Micro-Cell Scenarios”, in *Proc. of PIMRC'2002 – 13th IEEE International Symposium on Personal, Indoor and Mobile Radio Communications*, Lisbon, Portugal, Sep. 2002, ([GiCo02a]);

- f) Gil,J.M. and Correia,L.M., “Combining Directional Channel Modelling with Beamforming Adaptive Antennas for UMTS”, in *Proc. of PIMRC'2001 – 12th IEEE International Symposium on Personal, Indoor and Mobile Radio Communications*, San Diego, CA, USA, Sep. 2001, ([GiCo01b]);
- g) Gil,J.M., Mendez,J.L. and Correia,L.M., “Comparison of Recursive Least Squares and Conjugate Gradient Applied to Adaptive Beamforming in UMTS”, in *Proc. of IST-MCS2001 – IST Mobile Communications Summit 2001*, Barcelona, Spain, Sep. 2001, ([GiMC01]);
- h) Gil,J.M. and Correia,L.M., “An Implementation of Beamforming Adaptive Algorithms to Particular Mobile Propagation Conditions in UMTS”, in *Proc. of ConfTele 2001 – 3rd Conference on Telecommunications*, Figueira da Foz, Portugal, Apr. 2001, ([GiCo01a]).

The general evolution of the work is grasped through these publications, starting from the latter one to the most recent, in a step-by-step basis. Firstly, h) is the case of the application of an algorithm to a primary wideband directional channel model. Such simplistic model solely consisted in the random generation of clusters of scatterers in space, establishing the corresponding generation of angles- and times-of-arrival. Secondly, already resorting to the hereby described and used WDCM, a comparison between the implementation of two algorithms follows, in g), enabling to set the algorithm with which future work would follow and helping to confirm the correct beamforming operation. Such output has also resulted from comparing the complexity that the algorithms involve, in a multi-user scenario situation. Thirdly, all publications except a), b) and d) were centred on the evaluation of beamforming performance in either micro- or macro-cells, as a function of the respective scenario parameters. The d) output, covering an issue that was addressed well before the date of publication, deals with a processing level optimisation problem that had to be evaluated and solved to the necessary extent. Lastly, the conference paper b) expresses the comparison between micro- and macro-cells beamforming dependency on the most important scenario parameters, and a) describes which/how fundamental channel physical parameters constrain beamforming performance, in those scenarios.

Other sorts of contributions have been output, such as presentations given in seminars (without refereeing) and the production of deliverables and internal documents within projects. Worthy of mention are the presentations within COST 273 (*COoperation européenne dans le domaine de la recherche Scientifique et Technique*) project, and the production of several internal documents and contributions to deliverables within IST-ASILUM (Advanced Signal Processing Schemes for Link Capacity Increase in UMTS) and IST-FLOWS (Flexible Convergence of Wireless Standards and Services) projects. Through these, as means of publicly presenting the work in a frequent basis, it has been possible to have important feedback from the scientific and industrial communities, as well as to keep straight contact with the major trends and visions of those parties. At

the same time, such contact also obliged one to provide work and results, as meaningful as possible in terms of the different possible views that several communities may have of the same subject. For that, the contact with such views has also demanded for mental flexibility and understanding. Lastly, the continuous and joint tracking and output of project and scientific activities has undoubtedly imposed a deadline-directed workflow, very important for the whole progression.

1.3 Dissertation Outline

Having followed the description of the contributions in this Introduction, the reader attains the summarised but fundamental view of the general contribution that is conveyed through this study, as a whole. Understanding the general motivation, context and philosophy views adopted, the reader may verify the reflection of such in the dissertation outline of the hereby-presented study.

The dissertation follows with Chapter 2, Laying Foundations and Background – Channel Models and Chapter 3, Laying Foundations and Background – Adaptive Beamforming. Such chapters summarily describe the most significant approaches to the mentioned two large fields of Propagation Channel Modelling and Adaptive Beamforming Processing, with the objective of introducing the reader to those fields, understanding the several views, presenting their fundamental assumptions and all the reasoning behind these. In that manner, the reader is led to having a widened view of the so-called *state-of-the art* in those fields. Additionally, the involved general issues, quantities, parameters and properties are already introduced, further guiding the reader into the following chapters.

In Chapter 4, Implementation – the Channel and Scenarios, after justifying their choice, the micro- and macro-cell models are presented and characterised in detail. The simulated propagation scenarios are also thoroughly described, following the mentioned practical, system and comparison-directed reasoning. It is in this chapter that the important channel angular and temporal properties and quantities are defined and characterised. After doing so, Chapter 5, Implementation – the Adaptive Problem, systematically presents the justifications for implementing the particular beamforming problem, then describing the algorithm, its implementation, and the physical interpretation of the matter. Additionally, the *cost* parameters that are to be evaluated are presented, being followed by the presentation of the power control method. The chapter ends with an analysis of the simulation and calculations involved.

Having described the whole nature of the application, from the channel model to the applied beamforming algorithms and analysed parameters, Chapter 6, Set-Up Analysis, provides a critical view of the whole simulation workbench created, developing on: its wideband or narrowband nature, according to several notions of this classification of systems, channels, processing and array implementations; the extent to which the present application is or is not dependent on the systems-available signal sources; the somewhat unexpected, but justified and thoroughly characterised, optima

discrepancy problem; on the application of another adapting algorithm for the same evaluation objectives.

Chapter 7, Beamforming in Micro- and Macro-cell Scenarios, is the first core chapter presenting beamforming performance results in detail, dealing with the several dependencies on the propagation channel and scenario parameters at stake. It is divided into two major sections, independently covering the beamforming dependence on the micro-cell scenarios and on the macro-cell ones. Then, Chapter 8, Beamforming Performance in Micro- vs. Macro-cell WDCM Scenarios, provides a detailed comparison between performance dependencies towards micro- and macro-cell situations. It is through this comparison that the relevant channel characterisation parameters are defined and evaluated, establishing the main reasoning behind the wideband and directional constraints that the propagation channel imposes on using beamforming to reduce interference. Therefore, a straight link to Chapter 4 is not only natural, but also very important.

With the aim of gaining perspective and extrapolating the outputs of this work, Chapter 9, Towards Future Mobile Broadband Systems, establishes the links to other most directly related issues and fields, imposed by the trends that are envisaged for mobile wireless communications. These links are presented in the form of hypotheses, also resulting in references to possible paths of future research evolution, as well as important research trends that are currently taking place, closely related to this study.

Finally, Chapter 10, Final Conclusions, presents the overall conclusions reached through this research work.

2 Laying Foundations and Background – Channel Models

- *The world needs not more pictures (...) the world needs models.*

I paint, or try to paint, it's the same, models of the world.

- *He paints models of the world, but it is from the world that he always starts.*

- *That is clear. Nothing can escape from its essence.*

—in *Herta Teresinha Joan ou Memórias de Mateus Maria Guadalupe (Novelas)*,

— Agostinho da Silva (1906-1994)

2.1 Classical vs. Spatial Channel Models

On a general basis, *classical channel models* provide information about path-loss, signal power level distributions (slow- and fast-fading), Doppler-shift, and possibly temporal response, while *spatial channel models* incorporate additional parameters, such as Angle-of-Arrival (AoA), Angle-of-Departure (AoD), or angle-spreads. Furthermore, the need for spatial channel modelling has been in parallel with that of a *WideBand* (WB) implementation, including the characterisation of Time-of-Arrival (ToA) and delay-spread. In a more general sense, larger system bandwidths and larger capacity requirements demand for resorting to WDCMs. Therefore, it is important to keep in mind that a model may be *spatial*, but still *NarrowBand* (NB). For this, the following sections already focus on the spatial model properties, putting forward considerations on their NB or WB nature.

The main models for predicting propagation loss, already established in the past, range from the purely empirical to theoretical and deterministic ones, [Pars96], [Stee96]. The former are based on measurements, whereas the latter use theoretical considerations and approximations. Among these are: the *Okumura*, [OOKF69], the *Hata*, [Hata80], the *CCIR* (*Comité Consultatif International des Radio-Communications*, now ITU-R), [ITUR95], the *Walfisch-Bertoni* and *Ikegami*, [Stub96], their respective COST 231 evolutions, [DaCo99], the *Longley-Rice* (also known as Institute for Telecommunications Sciences Irregular Terrain Model, ITSITM), [LoRi68], [Mill92], [HuLK82] and the *TIREM* (Terrain Integrated Rough Earth Model) model, [Weis82], [Scia90]. These models account

for parameters such as BS and MT antenna heights (above street level and relative to rooftops), frequency of operation, type of surroundings (urban, suburban, or open areas), building density, link distance, building roofs nominal height, building separation, street width, angle of ray incidence (compared to street direction), and so on. By considering these parameters, either directly or indirectly, the propagation path-loss can, therefore, be predicted for different types of environments.

Worth mentioning are also the *Ray-Tracing*-based models, e.g., [TsAt02], [DLPR01], [DaCo99], [SeRa94], [GoCo94], also based on theoretical and empirical approaches, although being site-specific, used for Channel Impulse Response (CIR) analysis and path-loss prediction.

As far as fading is concerned, it has also been widely studied from the early days of mobile communications, establishing two types of fading, depending on the scale of temporal variations – *fast*- and *slow*-fading – and their fading rate Probability Density Functions (PDFs) – Rayleigh or Rice for the former, Log-Normal for the latter case, [Jake74].

The GSM (Rural Area, Typical Urban, and Hilly Terrain) and UMTS (Indoor Office, Outdoor to Indoor and Pedestrian, Vehicular – High Antenna, Rural Area, Hilly Terrain, and Typical Urban) non-spatial propagation models, more recent and widely used, already provide a WB characterisation of the propagation channel, e.g., [ETSI00], [ETSI97], [ETSI96]. These involve tap-delay-line temporal characterisation, while defining Power Delay Profiles (PDPs), delay-spreads, together with fast-fading statistics, according to the scenario at stake. Lastly, High Performance Radio Local Area Network (HIPERLAN) propagation models, still not spatial but WB, also characterise the channel through delay-spread and tapped-delay line parameters, corresponding to specific pico-cell, indoor environments, [MeSc98].

But, besides the means of propagation loss, fading and WB characterisation by themselves, the mobile environment may be described in terms of the combined effects on the radio signal in both the time- and frequency-domains. In this way, further descriptions include channel impulse response and delay-spread function, frequency transfer function, coherence bandwidth, Doppler-spread function, and combined delay-Doppler-spread. As a result, channels may be classified into flat-flat, time-flat, frequency-flat, or dispersive, e.g., [Stee96], these characteristics being possibly assumed for a certain adopted model.

As previously mentioned, these classical models and functions do not include information on AoA, i.e., not developing a spatial characterisation of the channel according to AoA relative to either the MT or the BS. Yet, these former studies are the birth of the new spatial models, since the same channel parameters and their statistics are present, and the same sort of basic reasoning and objectives exist. The effort lies in fitting the angular domain data and the antenna array structure into a new model, while providing characterisation as a whole.

For the current demands, and as a result of the various modelling and measurements put forward, several general conclusions have been reached, [ECSR98], common to most of the reported

spatial channel models: the distribution and physical geometry of scatterers surrounding the MT and BS must be considered, seeing *scatterers* as points that originate specular reflections; there must be a differentiation between spatial response near MT and BS, independent of antenna types; the heights of the antennas determine the number and locations of the scattering objects, assuming that low antennas (in low tier systems) and high antennas (in high tier ones) apply to micro- and macro-cellular mobile structures, respectively – the angle-spread increases as antenna is lowered; the type of environment determines the angle-spread – urban settings experience larger angle-spreads than in suburban cases, and these exhibit larger spread than rural ones; the angle-spread has a major influence on the correlation between pairs of elements in the array – in general, higher angle-spread implies lower correlation; the several spatial models give rise to different angle-spreads, i.e., to different levels of system performance due to different diversity conditions.

Similarly to the classical path-loss models classification, spatial models can be separated into four groups, [ECSR98]: the statistically based, the partially site-specific and based on measurement data, the entirely site-specific, and the geometrically-based and semi-statistical unifying models.

The first type of models is useful for general system simulation and performance analysis, being worth to mention the following: *Lee's Model*, [Lee82], *Discrete Uniform Distribution Model*, [Aszt96], *Uniform Sectored Distribution Model*, [NøAn94], *Gaussian Angle-of-Arrival Model*, [Aszt96], [Otte95], [TrOt95], [AFWP86], [Zett96], *Geometrically Based Single Bounce (GBSB) Statistical Models*, [Jake74], [Petr97], [LiRa99], *Gaussian Wide Sense Stationary Uncorrelated Scattering Model (GWSSUS)*, [ZeEM96], [ZeEs96], [Zett97], *Raleigh's Model (or Time-Varying Vector Channel Model)*, [RaPa95], and the *Modified Saleh-Valenzuela's Model (or Extended Indoor Clustering Model)*, [SaVa87], [SRJJ97]. The *Low-Rank*, NB model, introduced in [Fuhl97] has also been implemented to study channel correlation properties, extensively studying the effects of Gaussian and Uniform distributions of scatterers around the MT.

The second type should yield greater accuracy, but larger dependence on the environment, nevertheless requiring measurement data as input: *Extended Tap Delay-Line Model*, [KIMo96], *Measurement-Based Channel Models*, e.g., [BIKM96], and the *Extended GSM Models* (based on the GSM non-spatial models), e.g., [Zett96], [PeMF97], [MZDE96], [MPFF99].

Ray-Tracing models, or *Ray-Optical* ones, as already mentioned, require accurate description of the physical propagation environment along, being particularly characterised for being site-specific. Their completeness in terms of accounting for many propagation properties is accompanied by inherent low flexibility, e.g., [Corr01].

One must be aware that research is still needed for model validation and enhancement towards a reliable WDCM, along with the necessary corroborating physical measurements. Anyhow, the link between those two important activities has along the years proven not to be as frequent as

intended, in order to establish a fully assessed Spatial Channel Model (SCM)¹. This issue is very clearly raised in, e.g., [MFGH99]. For this, effort has been underway to determine better and unify model philosophies and parameters, also matching measurements among a variety of environments, antenna heights, vehicle speed and bandwidth. Worth mentioning are the *Combined GBSB and GWSSUS Model*, [PiTs99], the *Unified Model*, [FuMB98], [Fuh197], the *Geometry-based Stochastic Channel Model*, [MKLH99], the *Space-Time Channel Model with Stochastic Fading Simulation*, [SJBF99], the *Elliptical Subregions Model*, [LuLL97], the *Modified GBSB Models*, [Marq01], and the *COST 259 SCM*, [Corr01]. [MFGH99] also provides a general insight into some of these models, along with the then *state-of-the-art* in deploying *direction-selective antennas* for cellular mobile communications, at system level.

Most recently, with the birth of MIMO mobile wireless reasoning, MIMO directional and double-directional models have been widely developed and referred to, e.g., [YuOt02], and even established by regulatory parties, [3GPP03]. These reflect the highly expanding trend and need for this new type of models, with different interpretations of MIMO models, physical happenings and model outputs.

Finally, spatial models are also characterised by differing spatial organisation of scatterers, [LiKo99]. Anyway, dividing the models in the previously described way, the following summarised description of the models begins with the simpler models that involve local scattering areas of several shapes, mostly macro-cell, NB models, created to analyse antenna diversity properties. Then, the description of SCMs follows, some involving the clustering effect, more complex scattering area shapes or following geometrical, semi-statistical approaches. Following these, one presents models that combine several features from the previous simpler ones, reflecting several unifying efforts, finally ending up with a short description of the reasoning and objectives behind MIMO and Ray-Tracing channel modelling. In general, these models have been formerly conceived for the 800-900 MHz GSM or IS-54/IS-136 bands, evolving towards 1.8, 2.0 or 5.0 GHz bands, for GSM 1 800, UMTS or HIPERLAN.

2.2 General Assumptions and Considerations

Before acquiring a general view of the reasoning behind the main spatial channel models, it is important to clarify the general and fundamental assumptions and considerations that most spatial channel models consider, and then more specifically characterise those most important models.

The majority of those models use complex envelopes (low-pass equivalents) to represent the signals, where the carrier component $e^{j2\pi f_c t}$ is implicit, f_c being the operating carrier frequency.

¹ Along the text, the SCM and WDCM acronyms are interchangeably used when the SCM at stake is a wideband one. Not all SCMs are WDCMs.

Furthermore, in the case of NB signals, a sufficiently small time delay will solely imply a significant phase-shift of the carrier, with no delay at the envelope itself; oppositely, when considering WB transmission, the envelope delays can no longer be ignored. Channel models, then, may be characterised to be WB or NB (this matter is attentively covered in Section 6.2, Implementation vs. Narrowband and Wideband).

Concerning the spatial dimensions that the model involves, most models not only consider that electromagnetic waves travel in one plane, usually the horizontal one, but also consider planar scatterer distributions at the same plane as that of propagation. Examples of exceptions to this are some Ray-Tracing models. This sort of approximation derives from the fact that the difference between BS and MT antenna heights is usually very small compared to the distance between both antennas in macro-cells, while in micro-cells the BS and MT are reasonably co-planar². Accordingly, any antenna array added to the model is considered to belong to the same plane. Though this approximation is commonly used, it must not be forgotten that the same models may in fact be compared with measurements in which the BS antenna is considerably higher than the MT, as well as may be used to model scenarios with such macro-cell configuration. In many cases, because of its considerable height above streets, the angle-spread at BS has been measured and is modelled to be lower than near the MT, though the applied model is developed in a single propagation plane, still.

Also, as fundamental basis, most models assume that signal sources are dimensionless point sources, these being antennas or scatterers. Though these truly generate spherical propagating waves, any receiving antenna is assumed to be located far away from any source, so that the arriving waves are considered plane. This has implications in both phase and field strength, determining the signal relations among the elements of an array. Additionally, any array is seen to be small enough so that the signal has equal field strength among its elements.

Concerning polarisation, the majority of models does not account for it, considering that the source may radiate in any position, and that diffraction, scattering and reflections will change it in any way. This is to say that only the scalar complex electrical field is observed, with scalar additions. Similarly, diffraction, multiple and diffuse scattering are not included, assuming that these do not contribute with power levels sufficiently relevant for the models' applications.

Viewing the *propagation channel* as the physical medium between, but excluding, Transmitter (Tx) and Receiver (Rx) antennas, or considering that these are isotropic ones, these models assume that antenna elements perfectly transmit or capture the field strength, introducing no linear distortion in the band of interest, with full efficiency, and no mutual coupling in between elements. Additionally, all the involved systems, overall, are seen to be fully linear. The inclusion of any antenna-specific properties of that kind, or not considering isotropic Tx or Rx antennas, implies a

² This may not be so, in pico-, indoor cells.

distinction between the response of the propagation channel and that of the *radio channel*, since the latter introduces those antenna effects. In the case of this study, it is therefore important to focus on the propagation channel, onto which the beamforming is further added. By evaluating beamforming performance, the response of the resulting radio channel is then analysed, and it is done so as a function of the properties of the propagation channel.

Lastly, but very important, for all models, the channel medium is considered to be always homogeneous. It is seen as non-dispersive for each path, making the definitions of an array steering vector, spatial signature, and channel impulse response possible. This is to say that, among all possible paths, the signal will travel at the same speed. Anyhow, considering the whole multipath context, the propagation will still be time- or frequency-dispersive.

2.3 Review of Main Existing Spatial Channel Models

2.3.1 Statistical Models

Lee's Model has been developed to characterise the spatial diversity between a set of antennas due to multipath, within a simplified planar propagation region, [Lee82], [Aszt96]. By considering a certain scatterer distribution, the predicted AoA is used to calculate the signal correlation between two antennas as a function of antenna separation, leading to the *array correlation matrix* at a large array. This, in turn, has been compared with antenna diversity/correlation measurements, giving some indication about the correctness of the scatterer distribution. In general, lower correlation, providing higher diversity gain, will be a result of larger angle-spreads and larger antenna element separation. Correlation measurements have confirmed the existence of small angle-spreads near the BS, if much higher than the MT, and larger angle-spreads at the MT. Also, the same type of measurements at the BS indicates that the majority of effective scatterers exist within 100 to 200 λ around the MT, where λ is the operation wavelength.

This model considers that the N_{scat} scatterers are located on a circumference of radius r around the MT, uniformly spaced as shown in Figure 2.1, at the same plane as that of the BS and MT. Each considered scatterer represents the combined effect of many scatterers in the region, therefore, being called an *effective scatterer*. The description of the model applies to a pair of BS antennas, separated by d_{el} , centred at the origin, at an angle ϕ_{MT} with the line towards the MT, allowing for the calculation of the correlation between two neighbouring array elements, [Aszt96]. The respective AoAs, ϕ_{n_s} , are given by:

$$\phi_{n_s} = \frac{1}{2} \phi_{BW} \sin \frac{2\pi}{N_{scat}} n_s \quad , \quad \text{for } n_s = 0, \dots, N_{scat} - 1 \quad . \quad (2.1)$$

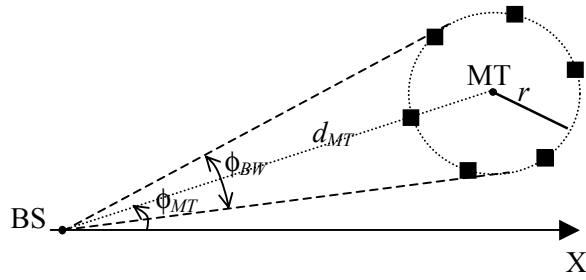


Figure 2.1 – Circular scatterer distribution, at angle ϕ_{MT} , with ϕ_{ns} spread over ϕ_{BW} , with radius r , centred at the MT, at distance d_{MT} from the BS.

Some comments about Lee’s Model may be put forward: it provides information on signal correlation; it considers that the environment is static, where the ring of scatterers has no velocity relative to the MT nor suffers any change, meaning that fast-fading and Doppler-shift are not accounted for; besides being a time-flat channel, it is also assumed to be frequency-flat, with no linear distortion in the band of interest, i.e., it is a NB model; the BS is placed high above any neighbour scatterer, much higher than the MT, which is surrounded by these, or their effective circular placement; being Non-Line-of-Sight (NLoS), with the BS much higher than the MT, the model is adequate for macro-cell urban environments (it was in fact its main application, within the GSM perspective); though the BS and MT are considered at different levels and in NLoS, the propagation is modelled within a planar set of antenna array, rays and scatterers; time-delays are considered small, so that these will only affect signal envelope phase, i.e., only a single cluster of scatterers around the MT is in fact considered; the signal envelope phases are viewed as Independent and Identically Distributed (IID), with Uniform distribution within the $[0, 2\pi[$ interval; the *in phase* and *quadrature* envelope components are independent Gaussian distributed random variables, giving rise to a Rayleigh distributed envelope magnitude; the number of paths is considered large enough so that the *Central Limit Theorem*, e.g., [NIST03], is applied; for the calculation of signal correlations, mathematical approximations are put forward – $r \ll d_{MT}$ and small ϕ_{BW} ; the model indicates that for larger angle-spreads the signal correlation between two elements is lower.

A theoretical model based on that of Lee’s is developed for a moving MT in [StCM94], assuming a discrete number of uniformly spaced scatterers in the ring. With constant scatterer statistical properties, the ring of scatterers is given an angular velocity relative to the MT, while both have the same radial velocity relative to the array. Good agreement is found between statistical and theoretical results. Nevertheless, according to [ECSR98], Lee’s Model fails to provide joint AoA and ToA channel information, leading to a “U-shaped” power profile, in time. In [StCM96] another extension to Lee’s Model is given, making the inclusion of additional scatterer rings to provide different power delay profiles possible. Nevertheless, the most important contribution from such

model presented in [StCM96] is the consideration of movement, either by the MT relative to BS or by vicinity scatterers around the MT.

To conclude, Lee's Model is considered powerful for the calculation of the array correlation matrix, not being particularly well suited for complete spatial channel simulation, involving both AoA and ToA.

Still using the same approximations as those used in Lee's Model, the N_{scat} effective scatterers can be evenly spaced within a narrow angle-spread, ϕ_{BW} , centred about the direction to the MT, resulting in the *Discrete Uniform Distribution Model*, [Aszt96]. The N_{scat} directions of arrival, ϕ_{n_s} , are then given by

$$\phi_{n_s} = \frac{1}{N_{scat} - 1} \phi_{BW} n_s, \text{ for } n_s = -\frac{N_{scat} - 1}{2}, \dots, \frac{N_{scat} - 1}{2}, \quad (2.2)$$

where N_{scat} is considered to be odd. Again, the signal correlation between two antenna array elements can be calculated, obtaining results similar to those of Lee's Model.

A discrete Uniform AoA distribution already had been considered in [Jake74], when specifying the mathematical development for laboratory simulation of multipath interference. The result of such was the excellent match between the simulator results and the theoretical values of envelope probability distribution, fading autocorrelation function, Radio-Frequency (RF) Doppler spectrum, and random Frequency Modulation (FM) spectra. Another study has also considered the Uniform distribution to extract theoretical results on fading correlation in an antenna array, [SaWi94]. Also, in [Nagu96], work is based on this sort of AoA distribution, though admitting that besides [Jake74] and [SaWi94] conclusions, no field measurement data existed, then. This model also fails to relate its outputs with delay-spread and Doppler-spread, it is NB, and once more is aimed at the calculation of the array correlation matrix, not being particularly well suited for complete spatial channel modelling.

The *Uniform Sectored Distribution Model*, [NøAn94], has been firstly devised to study, through simulation, the relationship between angle-spread and spatial diversity, leading to conclusions about beamsteering and beamforming in NLoS, macro-cell conditions. As the name indicates, the model consists of a sector of a defined radial range and angle width, inside which scatterers are assumed uniformly distributed. The magnitude and phase associated have a Uniform distribution within $[0, 1]$ and $[0, 2\pi[$, respectively. It is shown that the envelope statistics tends to a Rayleigh distribution, with Uniform phase. As the previous ones, it is a NB model.

A similar NB SCM, defined as being *Low-Rank*, is proposed in [Fuhl97], with a Uniform distribution of scatterers radially considered around the MT, i.e., resulting in a non-Uniform AoA distribution around the MT azimuth. The envelope correlation is studied for several AoAs and angular-spreads, as well as frequency correlation. Additionally, the model is shown to be implemented

with a moving MT. The model's parameters are tabled to constitute a full SCM to simulate several adaptive antenna algorithms. The study in [Fuhl97], therefore, establishes fading correlation properties as bases to further evolve to the *Unified* SCM (described in sub-Section 2.3.3, Geometrically-Based and Semi-Statistical Unifying Models).

Based on Lee's Model and related approximations, the AoA has also been considered to be Gaussian distributed, relative to the static cluster of effective scatterers around the MT, establishing the *Gaussian AoA Distribution (GAA) Model*. In [Aszt96] the signal correlation between two elements is also evaluated for this case, considering small angle-spreads, as in Lee's Model, showing that the variation in correlation is similar to those obtained with Lee's Model, for small element separation. The same type of approximations, limitations, and conclusions are made as those for Lee's Model.

The GAA model (or similar, with identical correlation function) has been used and tested, [Otte95], [TrOt95], having been validated against experimental data. The field experiments were held with the BS in an urban area (above a 30 m-tall office building), with the MT at suburban and rural scenarios, at a distance d_{MT} near 1 km. These studies have concluded that angle-spreads, for such conditions, vary between 0° and 6° (the array was a 10-element ULA, with 0.4λ spaced elements), at the BS side, which agrees with the applicability of the model (in a macro-cell scenario, where the BS is higher than potential scatterers). The obtained angle-spreads indicate that the scattering area, under such conditions, would have an approximate radius of 50 m, [TrOt95], i.e., near 145λ around the MT (for GSM), as Lee's Model predicts. In [Aszt96], narrower angle-spreads of $[0.5^\circ, 1.1^\circ]$ are also reported, for $d_{MT} = 4$ km, at the BS. Measurements in Aalborg have obtained angle-spreads also lower than 5° , [MPEF97].

The Gaussian distribution is also considered in [AFWP86], where experimental results are presented and compared with their theoretical counterparts. The study covers signals at 900 MHz received by two spatially separated antennas at the BS, for different antenna positions, antenna spacing and angle-spreads, and with moving MT. The experimental values are found to agree reasonably with those based on such scatterer distribution, leading to the same sort of angle-spreads as those indicated in [Otte95], [TrOt95]. Concerning the moving MT, the study does not present important contributions. In [Fuhl97], the Gaussian distribution of scatterers around the MT is also considered, as making part of the proposed *Low-Rank* SCM. As in the case of the Uniform scatterer distribution, the model may account for MT movement.

Also in ACTS-TSUNAMI II (Technology in Smart antennas for UNiversal Advanced Mobile Infrastructure) project, one of the most important with joint and recent contributions to the research on adaptive antennas, a model based on the Gaussian distribution has been obtained and compared with experimental measurements. Specifically, for a Typical Urban (TU) scenario, and for a Bad

Urban (BU) environment (a two-cluster model, with Gaussian distribution at each cluster), Gaussian azimuthal AoAs were obtained, [Zett96], [MZDE96].

Object of some criticism among followers of other models, e.g., [ECSR98] and [LiRa99], is the consideration of a continuous AoA random distribution, after many measurements, such as in [Lee82], having confirmed that the AoA distribution is discrete. Nevertheless, in [Aszt96], where the Gaussian distribution is described and used, it is also stressed that the monotonically decreasing correlation values due to the Gaussian distribution underestimates the correlation values obtained with the discrete distributions (Lee's Model and Discrete Uniform Distribution).

Another issue, seen as a model weakness, is the fact that, as it is the case of Lee's Model, the GAA model gives good results for evaluating antenna correlations, but does not include factors such as delay-spread and Doppler-spread, required for complete spatial channel characterisation.

The *Geometrically Based Single-Bounce Statistical Channel Models* are, as the name indicates, based on pure geometry and probability mathematical relationships, [ECSR98], [Petr97]. Some of the hereby-described models have been established after measurement campaigns had been undertaken, whereas the GBSB models definitely are not. These still require experimental validation campaigns, though they have been fully developed and are being commercialised, [LiRa99]. Related measurements, like those from the same author, e.g., [LiKo99], validate aspects that do not depend on the model, truly giving no indication on its validity. Within the IST-ASILUM project, related versions of the GBSB models, the *Modified GBSB* models, have been assessed with a measurement campaign, though further assessments should be carried out (see sub-Section 2.3.3, Geometrically-Based and Semi-Statistical Unifying Models, for further details).

Following a different approach from that of Lee's, GAA and Discrete Uniform Distribution Models, the GBSB Circular Model (GBSBCM) and the GBSB Elliptical Model (GBSBEM) are based on a scatterer region of circular or elliptical shape, within which the scatterers are placed randomly according to a continuous Uniform scatterer spatial density function. From this function/region shape, one can obtain joint and marginal ToA and AoA PDFs, once more stressing its great importance in the specification and prediction of adaptive antenna performance. In this way, the AoA, ToA and signal complex amplitude can be obtained.

The GBSBCM is applicable to high tier, macro-cellular environments, where the BS is higher than potential scatterers and a circular scatterer area of radius r is centred at the MT, surrounding it; this is why the GBSBCM is also called GBSB Macro-Cellular Model. The GBSBEM is used for low tier, micro-cell systems, where both BS and MT are surrounded by local scatterers (the BS is at the same height as local scatterers), and where it is assumed that scatterers exist between the BS-MT line. Both models have been proposed including the evaluation of how Doppler spectra are affected by MT movement.

In [Jake74], the GBSBCM was already used to derive spatial correlation functions at the BS, indicating some agreement between theoretical and experimental correlation values. More recently, in [Petr97], the GBSBCM was described leading to the PDF of AoAs and generation of theoretical power-delay-angle diagrams (what some call *pda-gram*). The model, purely based on geometrical and probability relationships, puts forward the following assumptions: AoAs are represented in planar form, as a function of azimuth only, and scatterers exist within this plane; scatterers are assumed uniformly distributed inside the circle around the MT, as Figure 2.2 indicates; only one reflection is assumed for each possible path, rejecting other effects such as rough surface scattering, diffraction, and multiple bounce by surfaces and volumes; no scatterers are considered around the BS, in accordance to it being applicable to macro-cell scenarios.

The model must have the scatterer radius and the distance between MT and BS defined, to calculate the AoA PDF, or the joint ToA and AoA PDF, [LiRa99], at both MT and BS sites. Along the study in [Petr97], simulation data and the theoretical conclusions are compared, reaching close agreement. For example, for an MT 10 km away from the BS, and with circle radii of 0.5, 1 and 1.5 km, the AoA PDF would reach near 3°, 5.8° and 8.5°, respectively; for different multipath numbers tested in the simulations, an angle-spread of 5°, for an MT-BS separation of 1 km, would imply a circle radius near 180-200 m, i.e., much larger than Lee's 100-200 λ radius values at 2 GHz. Concerning Line-of-Sight (LoS) conditions, the GBSBCM predicts that there is relatively high probability of multipath components existing with small excess delays close to the LoS, although macro-cell situations do imply NLoS. In [Petr97], the LoS component has in fact been considered to be part of the GBSBCM.

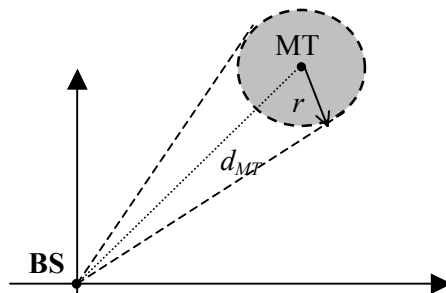


Figure 2.2 – Circular scatterer Uniform density distribution around the MT.

Nevertheless, in both [Petr97] and [LiRa99], it is indicated that the model must still be validated, besides including possible adjustments to the scatterer distribution. Already then, the need for model assessment was clear. Anyhow, the advantages of such model roots from its reasoning, establishing the logical fundamental scattering region, and accounting for the inherent variability through its statistical perspective, while being of simple application. As a consequence, this model is useful for generating sample channels, for systems' simulation purposes.

A detailed description of how the GSBEM has been obtained and is used is presented in [LiRa99]. According to this model, scatterers are uniformly distributed inside an ellipse at which foci the BS and MT are located, as Figure 2.3 shows. As mentioned, the model applies to the case where the BS is surrounded by scatterers that interact directly in the multipath propagation, involving a large amount of power through paths near LoS. The elliptical shape, outside of which no scatterers are considered, implies that absolute delays considered will be less than a maximum, τ_{max} . Its value must be chosen so that the majority of power subject to multipath propagation is within the ellipse. The model itself, then, ignores the longer paths.

As in the case of its circular counterpart, the model does not limit its use to NB, leaving the possibility of being used for WB prediction, since it is purely based on geometric and probabilistic relationships. Furthermore, the results can also be complemented by the path-loss at stake, obtaining a *pda-gram*, and its study has also covered the effects that such model implies concerning Doppler spectrum, [LiRa99].

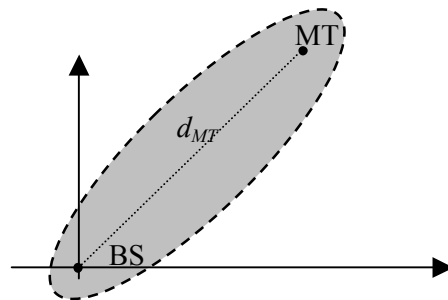


Figure 2.3 – Elliptical scatterer Uniform density distribution around the MT.

The approximations and assumptions that are made to obtain the model are similar to the previous circular model version: AoAs are represented in planar form, as a function of azimuth only, and scatterers exist on this plane; the considered plane is approximately parallel to the ground, so that multipath components appear to arrive from the horizon; LoS exists between BS and MT; scatterers are assumed uniformly distributed inside the ellipse; only one reflection is analysed, rejecting other effects, such as rough surface scattering, diffraction, and multiple bounce by surfaces and volumes.

One must not forget that, although the model is prepared for micro-cell environments, where there is a great probability of a ray suffering more than one reflection, it does make a big approximation assuming one reflection only.

The primary objective of the *Gaussian Wide Sense Stationary Uncorrelated Scattering Model*, [ZeEM96], [ZeEs96], [Zett97], is the characterisation of the signal correlation matrix, as in Lee's Model. The GWSSUS is a generalisation of the GAA model described above, where several N_c clusters are considered, each with a GAA contribution for AoA. As stated before, a cluster is a group of scatterers that imply excess path delays that differ less than the inverse of the system bandwidth. In this way, since more than one cluster is considered, larger channel delay-spread is included in such

model, meaning that the channel bandwidth can be considered smaller than the system's bandwidth, i.e., WB channel propagation modelling and frequency-selective fading can be covered.

In more detail, each n_c^{th} cluster is attributed a constant location and delay during several data bursts, i.e., the channel is assumed *wide sense stationary*, e.g., [Pätz03]³. The received signal will be the sum of several N_c NB versions of the transmitted signal, $s(t)$, delayed by each n_c^{th} cluster delay, τ_{n_c} :

$$\mathbf{u}(t, \tau, \phi) = \sum_{n_c=1}^{N_c} \left[\sum_{n_s=1}^{N_{\text{scat},n_c}} \alpha_{n_s,n_c} e^{j\varphi_{n_s,n_c}} \mathbf{a}(\phi_{1,n_c} - \phi_{n_s,n_c}) \right] s(t - \tau_{n_c}), \quad (2.3)$$

where \mathbf{a} is the *steering vector* (see sub-Section 3.2.2, Beamformer Response, Steering and Weight Vectors, for its definition) function of the azimuth, ϕ_{n_s,n_c} is the azimuth of the n_s^{th} scatterer from within the n_c^{th} cluster, α_{n_s,n_c} and φ_{n_s,n_c} are the corresponding ray magnitude and phase. Each cluster contributes to N_{scat,n_c} multipaths, whose magnitude and phase are statistically characterised: steering vectors are assumed independent among different n_c ; for N_{scat,n_c} sufficiently large, the *Central Limit Theorem* can be applied for each cluster, as it is for Lee's Model, implying that the term in brackets in (2.3) is multivariate Gaussian distributed, with zero mean (if NLoS) and a characteristic antenna correlation matrix (for each n_c); such term is assumed *wide sense stationary*, with delays τ_{n_c} assumed to be constant during data bursts; phases φ_{n_s,n_c} are assumed uniformly distributed in the interval $[0, 2\pi[$. Therefore, the array steering vector will be a function of the mean AoA of each cluster, and the scatterer contributions within each.

A reasonable amount of theoretical work has been developed based on the GWSSUS, specially related with array beamsteering. Nevertheless, no reports about direct practical measurement campaigns have been found, other than those mentioned along with the description of GAA and BU and TU Extended GSM Models.

Being a model set for the calculation of array correlation matrix, it fails to provide the number and location of clusters, possibly being extendable to include such information, though. Such model, being a *cluster model*, is adequate for urban channel characterisation, where measurements have indicated the existence of these groups of scatterers, also rendering a WB characterisation of the channel. Though such model does not define a spatio-temporal analysis of the channel, a related extension has been reported, establishing the *Directional Gaussian Scattering* (DGS) GWSSUS model, [MaGr96].

³ According to [Pätz03], if and only if the gains and frequencies are constant quantities and the phases are random variables, then the sum-of-sinusoids results in a stationary (and ergodic) process. Following the same reasoning, one explicitly distinguishes a *stationary* from a *static* channel, within a certain period. A static channel is stationary, but not all stationary channels are static.

Raleigh's Model or *Time-Varying Vector Channel Model*, [RaPa95], has been developed with the objective of characterising spatial correlation in antenna arrays, analysing fast Rayleigh fading. It is a time-varying Vector CIR (VCIR) model, [ECSR98]:

$$\mathbf{u}(t, \tau, \phi) = \sum_{n_c=1}^{N_c(t)} \mathbf{a}(\phi_{n_c}) \alpha_{n_c}(t, \phi) s(t - \tau_{n_c}) + \mathbf{n}(t) . \quad (2.4)$$

Here, N_c is the number of dominant reflectors, function of time, contributing with impulses arriving at τ_{n_c} , azimuth ϕ_{n_c} , with complex amplitude α_{n_c} , and $\mathbf{n}(t)$ is additive noise. Since the model considers that *dominant reflectors* compose the channel, i.e., bodies that scatter relatively high levels of power, it does account for cluster effect.

The largest contribution seen in Raleigh's Model is the calculation of the complex amplitude $\alpha_{n_c}(t, \phi)$,

$$\alpha_{n_c}(t, \phi) = E_{n_c}(t, \phi) \cdot \alpha(\tau_{n_c}) \sqrt{A_{n_c}} , \quad (2.5)$$

where A_{n_c} accounts for Log-Normal fading, $\alpha(\tau_{n_c})$ introduces the power delay profile, and $E_{n_c}(t, \phi)$ is the complex antenna radiation pattern contribution⁴, function of time and azimuth, following a complex Gaussian distribution in all directions. This last term is seen as a summation of N_{mp, n_c} different signal components, due to each of the n_c^{th} dominant reflecting surfaces. It includes antenna gain and transmitted signal power, A , complex radiation pattern affecting each p^{th} component, $E_p(\phi_{n_c})$, in the direction of the dominant reflector, ϕ_{n_c} , maximum Doppler-shift, v , and angle toward the p^{th} component of the n_c^{th} dominant reflector with respect to the direction of MT motion, ψ_{p, n_c} :

$$E_{n_c}(t, \phi) = A \sum_{p=1}^{N_{mp, n_c}} E_p(\phi_{n_c}) \exp[jv \cos(\psi_{p, n_c})t] . \quad (2.6)$$

The simulation of time and spatial correlation properties are reported to be in accordance with theoretical results. Validation of the model with experimental measurements has not been found, registering that it was developed for Advanced Mobile Phone System (AMPS).

It must be noticed that such model includes cluster effect, antenna array characteristics and Doppler-shift. Contribution about combined AoA and ToA distributions is not clear.

In [SaVa87], an indoor propagation model is presented along with well-known measurements conducted inside buildings, being known as *Modified Saleh-Valenzuela's Model*, arriving to conclusions that some outdoor propagation models share: the signal rays arrive in clusters; the rays have independent Uniform phases within $[0, 2\pi]$; ray magnitudes are independent Rayleigh

⁴ Though it includes the radiation pattern in its definition, it is hereby included as a propagation channel model.

distributed, with variances that decay exponentially with cluster and ray delay; the clusters, and rays within each cluster form Poisson arrival processes.

Summarily, the channel impulse response is modelled according to (2.7), where τ_{n_c} is the time of arrival of the n_c^{th} cluster, τ_{p,n_c} is the time delay of the p^{th} ray within the n_c^{th} cluster and α_{p,n_c} is the normalised magnitude Rayleigh distributed random variable, whose mean square value follows a double-exponential decay function. Similarities are found with the case of (2.3), relative to the GWSSUS model.

$$h(\tau) = \sum_{n_c=0}^{\infty} \sum_{p=0}^{\infty} \alpha_{p,n_c} \delta(\tau - \tau_{n_c} - \tau_{p,n_c}) . \quad (2.7)$$

With the need for relating the AoA with propagation models, this model has been extended, still covering indoor scenarios, [SRJJ97]. Firstly, in such study, an important assumption is made – the ToA and AoA are assumed statistically independent, having found in the experimental data that longer time delays do not necessarily correspond to longer angle-spread. Thereby, though, it is stressed that such assumption would need more consistent foundation. A direct consequence of this important assumption is to separate into ToA and AoA impulse responses, forming the product:

$$h(\tau, \phi) = h(\tau)h(\phi) , \quad (2.8)$$

where the angular impulse response is defined as

$$h(\phi) = \sum_{n_c=0}^{\infty} \sum_{p=0}^{\infty} \alpha_{p,n_c} \delta(\phi - \phi_{n_c} - \phi_{p,n_c}) . \quad (2.9)$$

In this equation, α_{p,n_c} is the normalised magnitude for the p^{th} component from the n_c^{th} cluster, as in (2.7), ϕ_{n_c} is the mean AoA of each cluster and ϕ_{p,n_c} is the ray angle within each cluster. The distributions of the angular variables have been modelled and validated through measurements: ϕ_{n_c} is uniformly distributed within $[0, 2\pi[$, and ϕ_{p,n_c} follows a zero mean Laplacian distribution with a known standard deviation.

Though the model focuses on the indoor propagation channel, many points are common to models described herein, such as the GWSSUS and the Extended GSM TU and BU – it is a cluster model, where Laplacian AoA distributions are considered.

Some of the authors of [SRJJ97] more recently developed a combined temporal-spatial statistical model, for indoor propagation, in [SJJS00]. Such study also roots from the results present by [SaVa87], adding further field spatial wideband measurements. In general, the results support the results of [SaVa87], e.g., Laplacian distribution of AoAs within clusters, exponential temporal decay between and within clusters, and similar ToAs distribution.

2.3.2 Measurement-Based Models

The *Extended Tap-Delay-Line Model* is a WB channel model, being an extension to the statistical tap-delay-line model, [KlMo96]. The extended model includes information on AoA, associating each tap with a certain time delay, τ_p , complex amplitude, α_p and AoA, ϕ_p . The resulting summation of a finite number of taps, corresponding to a finite number of multipaths, N_{mp} , is not at all new:

$$h(t, \tau, \phi) = \sum_{p=1}^{N_{mp}} \alpha_p(t) \delta(\tau - \tau_p) \delta(\tau - \phi_p) . \quad (2.10)$$

As reported in [ECSR98], such study needed that measurements be carried out in order to determine the joint density functions of the model variables, though it has been shown how measurements can be led to provide histograms of the joint distribution of amplitude, time-delay and AoA, as well as how the PDF relate to those histograms.

The model mainly represents the traditional time-variant linear system, adding the angular domain to the well known temporal form. The model primarily states the principle of describing a CIR at the BS side, to which statistics of the model variables are then added, depending on any measurements' outputs. In this way, it fundamentally puts forward a methodology.

As in the case of the GAA and GWSSUS, the *Extended GSM TU* and *BU Models* have been based on Gaussian AoA distributions. However, some of the studies previously referred to have led to more accurate measurements, indicating that for rural and urban scenarios the AoA power distribution follows a Laplacian shape, closer than the Gaussian distribution, [PeMF97], [MPFF99], [PeMF98]. The measurements described in [PeMF97], [PeMF98], cover a rural area, with an average BS-MT distance of 2 km, obtaining angle-spreads near 1.8°, while measurements in urban settings led to 5° (for BS antenna at 32 m) and 10° (for BS antenna height at 20 m).

According to [Zett96], [MZDE96], by means of simulations, the TU model is proposed to be similar to that of GSM 05.05 (GSM-TU), [ETSI93], [ETSI96], in the temporal domain, i.e., implying an exponential PDP, short-term NB Rayleigh fading, and the *classical* Doppler spectrum. It is assumed that the AoA is approximately Gaussian distributed, at the BS. As mentioned, though, later studies have concluded the better match provided by a Laplacian function. Also, a recent field measurement study of Doppler spectra at 5.3 GHz has shown that three spectrum types are most frequently found, *horned*, *narrow* or *flat*, in urban, suburban and rural environments, [ZKVS03]. The authors show how the 3-D spatial characteristics of the channel, namely scattering location, and the used array pattern, strongly condition and determine these.

The BU model consists of the superposition of two Gaussian clusters, each with temporal characteristics as those of GSM-TU, [MZDE96]. One of the clusters is located at the MT, and the other is 45° spatially shifted from the BS-MT line, at the same distance from the BS. This second

cluster would be assigned 5 dB less power than the first one. As far as shadow fading is concerned, between both clusters, it follows independent Log-Normal distributions. The presence of a second cluster will introduce both increased angle and delay-spreads. Such model applies to urban settings with towers, hills and other large obstacles, and it is noticeable that it is totally based on practical measurements (taken place in the city of Stockholm), for which simulations have been carried out. As far as temporal delay-spread shape is concerned, it has been confirmed to follow exponential decaying functions, for both clusters. Again, as for the TU, the Laplacian function has been found to match the AoA distribution best for both clusters.

Finally, it is important to be cautious about the processes used to estimate distributions of azimuth, and the importance of intra-cluster azimuth spectra. In [BeVö01] it is shown that the response of high-resolution DoA estimation towards a highly spatially correlated cluster may lead to erroneous AoA distributions, being critical about the Laplacian case.

2.3.3 Geometrically-Based and Semi-Statistical Unifying Models

Another study has been reported, combining the GBSBCM with the GWSSUS cluster model, establishing the *Combined GBSB and GWSSUS Model*, in order to exploit their advantages and to reduce their limitations, [PiTs99]. The developed model fully considers the temporal dynamics of the channel, also, whereas only the GBSBCM does conclude on Doppler power spectra. In this way, the model analyses the correlation between consecutive channel impulse responses. A further extension has been introduced, which is the consideration that, as the MT moves, the number of multipaths is not kept constant around the MT. In the proposed model, this number is a random process that follows a Poisson distribution.

Though such model has been implemented on a simulation basis only, it is important to mention how it has managed to link the GWSSUS and the GBSBCM, following a concern for extending applicability. Further characteristics can be listed and compared closely, recalling the past descriptions: the GWSSUS is a measurement/stochastic model, whereas the GBSBCM is purely based on a geometry/probability basis; the GWSSUS is a cluster model, where each cluster is defined with a finite number of non-time-resolvable multipaths, and the GBSBCM is not based on cluster propagation, at all; though the GBSBCM is based on uniformly distributed scatterers, the model does not depend on the scatterer density. The proposed model, then, introduces the following assumptions: as the GBSBCM, the scatterers, the MT, the BS, and propagation are considered co-planar, i.e., only the azimuth angular dependency is evaluated; the MT is placed within a circular region of a certain radius, the cluster, as in the GBSBCM, but such cluster is constituted by sub-clusters, each of which satisfy the NB and probabilistic assumptions used in the GWSSUS, being uniformly distributed inside the circular region, similar to the scatterer distribution in the GBSBCM; the MT moves along with the surrounding circular region, the scatterers remaining fixed, i.e., at each moment, the active sub-

clusters are those included in the circular region, implying that new smaller clusters get into the major cluster (contributing to *multipath generation*) while others leave (originating *multipath recombination*); the number of scatterers fluctuates with time, following a Poisson distribution, depending on the density and cluster size; the model has been developed for the simulation of both macro- and micro-cellular scenarios; different environments have been reported and fit the model, according to other studies, establishing the number of sub-clusters and scatterers within each sub-cluster, radius of local cluster, cell range, the existence or not of an additional cluster (as in the BU model), Rician factor (in the case that LoS exists), the reflection coefficient for the scatterers within each cluster, and scatter density.

As a result, this unifying type of model provides discrete data on power delay profile, angle-spread, Doppler-spread and correlation between antenna elements, being able to combine the advantages of two previously defined models, reducing their former limitations. It additionally joins data from both theoretical assumptions and experimental studies, which may reveal to be of advantage. The model simulations presented in [PiTs99], for a BU scenario, exhibit some similarities with other models and measurements.

The model presented in [FuMB98], [Fuhl97], the *Unified Model*, has been explicitly produced in a unifying perspective, being based on the several spatial measurements and theoretical models of the past. The model derives its conclusions either from local scattering models used preferably for macro-cells, e.g., Lee's Model or GAA, or from geometrically based models, e.g., GBSBCM, resulting in a generalised model for macro-, micro- and pico-cell scenarios, with or without LoS, with or without movement of the MT. Such model is applied to simulations, accounting for input data that is also in accordance with the referred measurements, in order to calculate the azimuthal power spectrum (actually, a *spectral density*). Array correlation coefficients are also calculated and compared with other measurements and studies.

Firstly, the study defines two different types of models – *low rank* and *high rank* ones. The former corresponds to the NB case, where also the angle-spread is small compared to the 3 dB beamwidth of the antenna pattern. The latter fits into the WB case, or where the angle-spread is similar or larger than the 3 dB beamwidth of the antenna.

The general modelling considers that the complex channel impulse response will be the sum of four impulse responses – a component associated with the LoS path, $h_{LOS}(t, \tau, \phi)$, the impulse response due to scatterers around the MT, $h_{MT}(t, \tau, \phi)$, the impulse response due to scatterers around the BS, $h_{BS}(t, \tau, \phi)$, and the impulse response caused by major distant scatterers/reflectors, $h_{distant}(t, \tau, \phi)$. Likewise, the directional distributions are characterised, tabled and used in the simulations in a separate manner.

As far as $h_{LOS}(t, \tau, \phi)$ is concerned, a minimum time delay and an AoA are assigned, where its magnitude follows a Log-Normal distribution. Also, according to each simulated case, the Rician

factor is set. Concerning $h_{MT}(t, \tau, \phi)$ and $h_{BS}(t, \tau, \phi)$, a local scatterer model is applied according to Lee's model or to a Gaussian circular spatial distribution around the MT. Also, the AoA power profile is defined uniformly around the BS, though other distributions have been reported in such study (GAA, Uniform and Laplacian). In the case of $h_{distant}(t, \tau, \phi)$, the work considers the cases of discrete reflectors and of clustered scatterers. A particular situation is accounted for, considering the possibility that the BS has LoS to the scatterer, but does not to the MT, e.g., if the wave propagating from the scatterers reaches the MT being guided through a street canyon.

According to each case, i.e., low rank (LoS or NLoS) or high rank macro-cell, micro-cell (LoS or NLoS) and pico-cell (LoS or NLoS), parameters have been tabled. Besides the referred parameters, examples of others are: radius of local scattering circle, number of local scatterers or scatterer discs, cell radii, fading temporal distribution, phase-shift distributions, number of discrete reflectors, and angular distribution between clusters.

The model extends its application to the case of a moving MT, viewing some scatterers as entering the local scatterer region, while others get out of range. No indication is given about the temporal distribution of this process, nor are results presented about Doppler spectra.

Though no explicit experimental validation results have been found in the literature, it must be mentioned that such model not only reveals to be applicable to a wide variety of environments, using some formerly established models in the most appropriate propagation case, but also indicates its possible easy extension to other models. Also, the resulting analysis of the dependence of the correlation coefficients on AoA and angle-spread is consistent with past studies, [FuMB98].

The *Geometry-based Stochastic Channel Model (GSCM)*, [MKLH99], accepts the statistical distribution of scatterers as input. A specific channel instance results from such random distribution, outputting the channel response through a simple ray-tracing algorithm. The model is an evolution from the Unifying Model, introducing the notion of *Nonuniform Scattering Cross-Section* and *equivalent* scatterers to facilitate simulation. The authors address the single-bounce problem, faced as a limitation of the GSCM. It is anyway backed by field measurements, e.g., [KuRB00], showing good agreement with simulation results. Scatterer distributions are suggested, along a local scattering disk around the MT, to account for the street-canyon effect.

A spatio-temporal model is proposed in [LuLL97], named as *Elliptical Subregions Model*, based on the same main assumptions as in the GBSBEM, except that cluster effects and antenna heights issues are accounted for. Anyhow, the base principles behind this model are similar to those of several models described before, characterising the channel by means of a complex baseband impulse response, and assuming scatterers and antennas in the same plane. Some of the specific assumptions that have been put forward also appear in other models, separately, being combined within a single model, in the sense of further generalising its application: each path, except LoS, is considered reflected once, by a single scatterer (as in GBSB models); elliptical regions are set with MT and BS at

their foci (as in GBSBEM); the entire scattering region is constituted by several annular subregions, with the same foci, each corresponding to a particular range of excess delay time due to local scatterers; within each region, a Poisson spatial distributed variable is attributed, according to spatial statistical studies, setting a corresponding Uniform spatial distribution for each subregion; to account for cluster effects (as in the GWSSUS and Extended GSM BU models), for each scatterer considered, whose number is set and distributed within each region, a number of additional reflecting points is set, according to a Poisson distribution, also; to contemplate the possibility of a BS existing at a high location, with no particular scattering objects in its vicinity (as in GBSBCM), the model may include the introduction of a scatterer-free area around the BS, namely a circular area with specific radius; the distribution of excess delay is based on the exponential decay function, through an inter-arrival exponential distribution for each delay interval corresponding to each path from the n_s^{th} scatterer, within each subregion; large-scale fading is included, through traditional power relationships, function of a large-scale parameter, antenna gains, path-loss exponent, scattering coefficients (for each path); the distribution of the large-scale fading parameter is Log-Normal, and so is that of the scattering coefficients, thought of as independent random variables; for simplicity, the scattering coefficient magnitudes have been considered equal and constant, and phases are randomly uniformly distributed over $[0, 2\pi[$; for each cluster, the AoA distribution is seen as Gaussian distributed in azimuth (as in some of the extended GSM TU and BU models).

In [LuLL97], the reason for considering elliptical shaped regions is that scatterers close to the MT-BS LoS are registered to have particular importance in the process (as in GBSBEM). The geometrical optics approximation is seen to be valid, and the model is partially, but not totally, based on geometric relations. It includes the clustering effect, which has been proven to be frequent, and necessarily considered for WB modelling, as well as physical propagation parameters defined by realistic statistical distributions.

The theoretical model also provides the conditional AoA PDF, conditioned by the path ToA, as well as a time-selectivity factor, i.e., a Doppler-shift, dependent on the AoA, for the special case of MT moving towards BS, only.

The impulse channel response of such model, $h(\tau, \tau_0, \phi)$, at observation time τ_0 , results from (2.3) considering the impulse, $\delta(\tau)$, input to such system, [LuLL97]:

$$h(\tau, \tau_0, \phi) = \sum_{n_c=1}^{N_c} E_{TX}(\phi_{n_c}) \left[\sum_{n_s=1}^{N_{\text{scat}, n_c}} \alpha_{n_s, n_c} e^{-j(2\pi v_{n_s, n_c} \tau_0 + \phi_{n_s, n_c})} \delta(\tau - \tau_{n_s, n_c}) E_{RX}(\phi_{n_s, n_c}) \right], \quad (2.11)$$

where, as in (2.3) (referred to the GWSSUS model), N_c is the number of clusters (referred to as *scatterers of a number of reflecting points*), positioned at angle ϕ_{n_c} relative to the transmitter antenna,

whose radiation pattern is given by $E_{Tx}(\phi)$. The receiver antenna, whose radiation pattern⁵ is $E_{Rx}(\phi)$, receives multipath components at angle ϕ_{n_s, n_c} , with a path delay τ_{n_s, n_c} , random uniformly distributed phase φ_{n_s, n_c} , and magnitude α_{n_s, n_c} , from the n_s^{th} scatterer within the n_c^{th} cluster. The Doppler-shifts, ν_{n_s, n_c} , are referred to instant τ_0 , corresponding to each individual path.

As previously mentioned, the model relates several different geometric, statistic and propagation aspects together, which many of the described models have considered separately. This results in greater flexibility and in its application for WB simulations. The model also accounts for back-scattering, affecting the resulting delay-spread, as do the GBSBMs. Its inclusion is not only intuitively understandable but has also been verified, affecting delay-spread especially in the case of a small MT-BS distance.

As far as validation measurements are concerned, it is stated that field experiments have been planned and even undertaken, [LuLL97]. Nevertheless, no report on these has been found. The only comparison with experimental work concerns the delay-spread reduction calculated for different antenna beamwidths, as a function of the MT-BS distance. In the study, a reduction of 21-26 % is theoretically predicted, with respect to an omnidirectional antenna case, using a 60° beamwidth antenna, whereas a measurement campaign achieved 30 %, [SoJD94].

Both the elliptical and the circular versions of the *Modified GBSB Models* are based on the GBSBCM and GSBEM, respectively, having fundamentally added clustering, mobility and gone forward with a measurement campaign to assess the EM model, [Marq01], [MaCo01], [MaCo03]. Additionally, the Modified GSBEM (MGSBEM) and CM (MGSBCM) have been created to support link- and system-level simulation platforms within the IST-ASILUM project, e.g., [Hera00]. In this way, the models reflect the need for their practical implementation for the evaluation of adaptive processing techniques (link-level evaluation), as well as for their inclusion in a more complex multi-cellular simulation platform (system-level evaluation). Simultaneously, the modelling procedure has included the assessment by a measurement campaign.

In order to account for clustering in both the angular and temporal domains, clusters of scatterers have been added to constitute the scattering areas at stake, similarly to the Combined GBSB and GWSSUS Model. For both the EM and CM versions, the clusters are uniformly distributed within the scattering areas. Within each cluster, the scatterers are randomly distributed, following a normal distribution along its cross-section. These are attributed random reflection coefficients, with uniform phases and magnitudes within $[0, 2\pi[$ and $[0, 1]$, correspondingly. The user is able to set the average size of the clusters, and the average number of scatterers within these.

⁵ Though it includes the radiation pattern in its definition, it is hereby included as a propagation channel model.

Additionally, concern has been directed to account for mobility of the MT, through the inclusion or exclusion of clusters within the changing scattering region and including the corresponding Doppler-shifts. In another way, the movements within the propagation environment are introduced through varying the phases of the reflection coefficients of the scatterers. Like this, it is a similar approach as that applied in the COST 259 SCM, [Corr01].

Furthermore, the field measurements that have been carried out in order to assess the model parameters, e.g., [ZoMa00], [MPKZ01], allowed for tuning the statistical physical parameters at stake, e.g., cluster density, cluster mean size, mean number of scatterers within the clusters. The measurements have been most completely held for the micro-cell case, resulting in a better assessment of the elliptical version. Regarding the macro-cell environment, the assessment has been less exhaustive and with too short a BS-MT distances.

By going forth with the referred model adjustment, the resulting path-loss vs. distance, delay-spread vs. distance, delay-spread and angle-spread in fixed positions and signal correlation vs. time delay relations have been adjusted to statistically fit into the measurement results. Anyhow, a much larger number of measurements would be required to be able to tune the model with a complete statistical value, the nature of the model being semi-statistical. Those measurements would be required to be either within a certain environment or in many differing locations, but of the same environment type. Following this, work has been developed within the IST-FLOWS project, [DGVC03], further extending the models, as well as assessing them through primarily analysing and regulating the temporal and angle-spreads obtained from several published references.

Concerning the outputs from the models, a *pda-gram* may be generated, also characterising the AoA and ToA means and spreads. Moreover, it is possible to change the models' parameter values in a very practical way, to support several differing propagation conditions and test the performance of several adaptive processing techniques.

As in the case of the GBSB models, the MGBSBCM and EM versions are applicable to macro- and micro-cell situations, respectively. The layouts have been exemplified by Figure 2.2 and Figure 2.3, but are depicted with the inclusion of the clustering morphology in Figure 2.4.

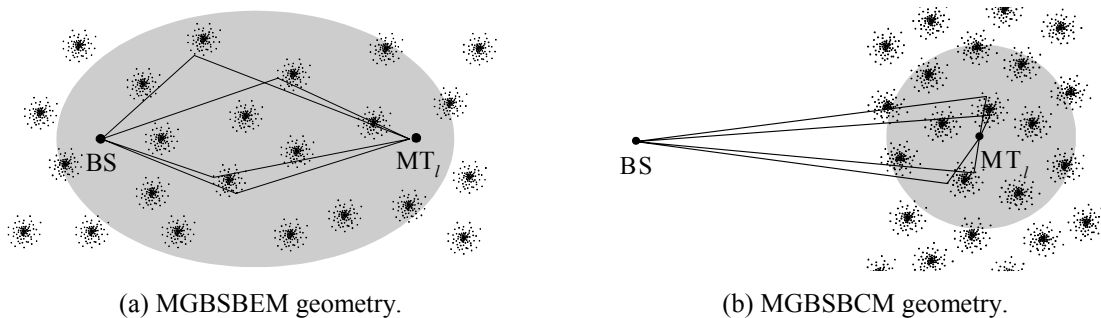


Figure 2.4 – Type of WDCM cluster and scatterer distributions, within the scattering areas defined by BS or MT_i , indicating some single-bounce reflections, for the MGBSB models.

On the other hand, dealing with the micro-cell case, the EM version has been generated to being confined to the street LoS environment, with the BS and MT within the street axis. In the last case, since the model solely accounts for a single reflection, it was concluded that the delay-spreads obtained with a street-wide scattering ellipse would be too small, compared to the measurements. For that, an *effective street width*, W_{ef} , has been introduced, emulating multiple reflections especially present and numerous in the street canyon situation. W_{ef} is larger than the real street width, by a factor of r_w , the *effective street width ratio*.

Lastly, it is important to note that a very useful Discrete Channel Impulse Response (DCIR) generation tool has been created, the user very easily specifying the remaining morphology of the scenario, e.g., MT-BS distances, street widths, and scattering circle radii. Moreover, the easiness of its use renders the potential easy generation of multi-user scenarios.

Establishing the *COST 259 Spatial Channel Model*, within the COST 259 Action, [Corr01], particular concern was directed to establish a WDCM that would account for several definitions, perspectives, and results already provided by previously defined models and contributions, such as the Okumura-Hata, Walfisch-Ikegami, COST 231, [DaCo99], the COST 207 effort towards the definition of GSM models, [Fail89], and ACTS-TSUNAMI II, [MPFF99]. Outputs from other past projects have also been considered, such as RACE-CODIT, [PéJi94], IST-Magic WAND, [HeBF97], and IST-METAMORP, [GrMa99]. Moreover, measurement campaigns have provided extensive data in order to better assess and tune the model.

Additionally, the COST 259 SCM originated from combining different propagation scenario description perspectives. One consists of describing a scenario as a function of the positioning of the BS, MT, and the involved scatterers, while the other describes a scenario by the ToAs, AoAs, and complex amplitudes. The model also addresses the transformation between these two implementation methods. The GSM models had already introduced the scenario perspective, defining the Rural Area (RA), Hilly Terrain (HT), and TU scenario cases, but not in the spatial, or directional points of view.

Therefore, the COST 259 SCM inherently results from the explicit concern of unifying different approaches, past model contributions, with a scenario point of view. In this way, the modular concept behind the model reflects this wide generalisation methodology.

A 3-level structure has been defined, establishing the cell type (macro-, micro- and pico-cell), the *Radio Environment* (RE) and the *Propagation Scenario*. The REs refer to the topographical features of the surrounding in which the system is operating, given by *external parameters*, such as frequency band, average BS and MT heights, MT-BS distance, building heights and separations, LoS or NLoS characteristics. It is within these REs that propagation conditions are statistically characterised, defined through a set of PDFs and/or statistical moments, called *Global Parameters*. The measurement data has been particularly useful in determining these. The propagation scenarios,

differing in *Local Parameters* (LPs), characterise the properties of the waves arriving at the Rx, e.g., their number, complex amplitudes, ToA and AoA, or the location of BS, MT and scatterers.

Concerning the dynamics of the channel, the COST 259 SCM considered that the movement of the MT within a *local area*, not larger than some tens of wavelengths, solely results in variations of the phases of arriving waves, giving rise to *small-scale fluctuations* of the resulting channel response. In this way, variations in propagation delay, attenuation and AoAs are assumed negligible. For larger travelling distances, *large-scale fluctuations* are formed through varying the LPs, the birth and the death of multipath components, defined by transition functions. Variation of RE and transition between these are also accounted for, characterised by a transition function as well.

A DCIR is defined as (2.12), where \mathbf{p} is the location of the Rx antenna, τ is the delay, ϕ is the azimuth, and θ is the elevation angle, considering a total of N_{mp} components arriving at position \mathbf{p} :

$$h(\mathbf{p}, \tau, \phi, \theta) = \sum_{p=1}^{N_{mp}(\mathbf{p})} h_p(\mathbf{p}, \tau, \phi, \theta) . \quad (2.12)$$

Considering a specular wave, each h_p contribution is given by (2.13), with α_i being a complex amplitude, explicitly used for the definition of the local and global parameters based on the delay-angle distribution,

$$h_p(\mathbf{p}, \tau, \phi, \theta) = \alpha_p \delta(\tau - \tau_p) \delta(\phi - \phi_p) \delta(\theta - \theta_p) . \quad (2.13)$$

Therefore, the total response is seen to result from a total of N_{mp} arriving components, each corresponding to an arriving wave. It is noted that the model does not rule out the consideration of the 3 spatial dimensions. Once again, showing how open the model inherently is to the introduction of additional effects, time-variant DCIR, double-directionality and polarisation may be accounted for.

Concerning cluster effects, in either the angular or the temporal domains, (2.12) may be rewritten to express the existence of N_c clusters, each composed by a set of C_{n_c} clustered components, comprising the total of N_{mp} multipaths:

$$h(\mathbf{p}, \tau, \phi, \theta) = \sum_{n_c=1}^{N_c} \sum_{p \in C_{n_c}} h_p(\mathbf{p}, \tau, \phi, \theta) . \quad (2.14)$$

Accordingly, global parameters statistically define the spreading within a cluster and the distribution of the whole set of clusters. Also, statistics that determine the p -indexed local parameters present in (2.13) will also follow different cluster mean values, while each multipath component is seen to be statistically independent from each other.

As already mentioned, besides defining the local and global parameters through delay-angle distributions, the relative position of the BS, MT, and scatterers may also be used. In that case, the Unifying Model, [FuMB98], is used to define the PDF of the location of scatterers. The ToAs and AoAs are obtained by considering simple geometrical optics, each scatterer giving rise to a single

multipath component. Additionally, far scatterer clusters are introduced, to account for groups of tall obstacles. Alternatively, the GSCM may be implemented, [MKLH99].

By using the latter semi-statistic geometric principle, efficient implementation is possible, with the explicit implementation and characterisation of both small- and large-scale phenomena, in the ways already mentioned.

Besides the concern for flexibility, covering a large variety of propagation situations and scenario, the COST 259 SCM has been heavily backed by field measurements. Outdoor campaigns covered macro- and micro-cellular directional measurements at the BS, and directional measurements at the MT side. Indoor measurements have also been held, mainly focusing on office environments.

Finally, as already mentioned, the inputs from several of the past models and the measurement campaigns have led to extensive tables of external and global parameters, explicitly defining REs. Worthy of mention are the general morphological characterisation of the deployment areas, and the operating frequencies, as external parameters. As global ones, particular attention is drawn to path-loss, cluster generation, large- and small-scale fading, number of multipath components, delay/azimuth/elevation dispersion at both the BS and MT, and polarisation.

The COST 259 SCM is, therefore, a strong reflection of the joint action among many parties, with the close relation between past and newer models, with the backing from several measurement campaigns. The modular approach that characterises the model also renders flexibility and wide coverage. Anyhow, due to such, the model has resulted difficult to implement, in link- or system-level evaluation platforms, as a whole. Undoubtedly, anyhow, the validity of the COST 259 SCM roots from that widespread joint action from the many active research and industrial involved parties.

2.3.4 Other Model Types and Methodologies

The use of spatial diversity, both at the Tx and the Rx sides, finally renders larger system capacity, through improving throughput, coverage and spectral use. In the most recent years, the rise of MIMO schemes applied to wireless communications has set a major trend in the *MIMO Channel Modelling* area.

Most important, according to the definition, e.g., [FoGa98], the MIMO propagation channel view, graphically exemplified in Figure 2.5, roots from making use of the possible uncorrelation among all M_{Rx} and M_{Tx} Rx/Tx antenna array elements. By these means, a MIMO channel asymptotically provides $M_{Rx} \cdot M_{Tx}$ diversity, finally leading to $\min\{M_{Tx}, M_{Rx}\}$ independent communication subchannels, for fully uncorrelated antenna elements. In [Fosc96], via the Bell Labs LAYered Space-Time (BLAST) architecture, it was shown that the MIMO channel capacity can potentially increase linearly with that number of spatial subchannels.

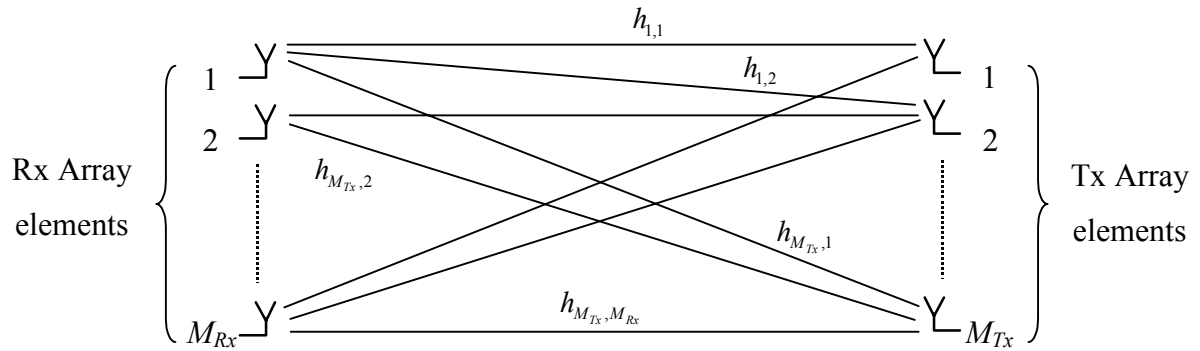


Figure 2.5 – The general MIMO channel implementation perspective, between M_{Tx} and M_{Rx} element Tx and Rx arrays.

For that interpretation of the propagation channel, the baseband output response of the channel, $\mathbf{u}(t, \tau)$, to the transmitted signal, $\mathbf{s}(t)$, vectors corresponding to the M_{Rx} and M_{Tx} array elements, respectively, will be imposed by the $M_{Rx} \times M_{Tx}$ impulse response channel matrix, $\mathbf{H}(\tau)$, through the convolution (represented by ‘*’):

$$\mathbf{u}(t, \tau) = \mathbf{H}(\tau) * \mathbf{s}(t) . \quad (2.15)$$

Therefore, matrix $\mathbf{H}(\tau)$ is constituted by the complex impulse responses between each m_{Tx}^{th} and m_{Rx}^{th} Tx and Rx array elements, $h_{m_{Tx}, m_{Rx}}(\tau)$, (Figure 2.5), hereby assumed in its WB and time-flat form. Alternatively, the channel matrix may be considered to be NB, being represented by \mathbf{H} , and the convolution resulting in a simple multiplication.

Several studies have covered how such correlation depends on the multipath channel richness, angle-spreads and antenna spacing, e.g., [SÖHM02], [XCHV02], [PAKM00], [FoGa98], some in parallel with putting forward a modelling approach. Generally, for a given element separation, in the presence of a richer multipath channel, the uncorrelation within each of the arrays will inherently arise, at least rooting from the AoDs and AoAs of enough planar waves determining a sufficiently large amount of independent phase differences among the elements of each array. Consequently, MIMO channel measurements have also been extensively carried out, e.g., [LeHo03], [WJSJ03], [SvWa02], [SÖHM02], [Pers01], [KMJA00], mostly reaching the conclusion that the channel is rich enough so as to allow for its better MIMO-directed exploitation.

Understandably, allied to the general MIMO philosophy and the subsequent general concern on the directional and WB evaluation and characterisation of the propagation channel, channel modelling has also been a major concern of several parties, having resulted in a relatively large whole family of new models.

According to [YuOt02], [Weic03] or [Saye02], MIMO channel models can be primarily divided into two large groups, as always with differing advantages and disadvantages: the *non-physical* (or *analytical*) and the *physical* models. Non-physical models are those that result from the

statistical characterisation of the involved channel matrix \mathbf{H} , in most cases directly obtained through MIMO measurements. These models have the advantage of being easily implemented, basically through providing the channel matrices. Anyhow, these models tend to be very dependent on the measurement equipment, conditions and scenario, finally strongly limiting their more general application. Physical MIMO models, consider the channel as a physical scattering medium, determining AoAs, AoDs and ToAs, and the resulting channel coefficients. Adding to this most frequent classification, other modelling approaches may be viewed as in-between those two types of models: the virtual channel representation presented in [Saye02], or the evolution to the spatial eigenstructure-based perspective provided in [Weic03]. The latter recent study goes forth with a careful analysis of analytical MIMO models. These are thereby classified and embedded within a framework, helpful for guiding the application of these models. The study involves a comparative analysis among them, regarding their ability to reproduce the channel spatial structure.

Additionally, MIMO models may be considered as being *measurement-* or *scatterer-*based, [YuOt02], meaning that they can directly result from the data obtained through a MIMO field measurement campaign, or through the postulation of a scattering model approximating the essential propagation characteristics (with or without the subsequent assessment via channel measurements). Also, as it has been the case of the many previously described models, MIMO channel models may be NB or WB, i.e., assuming frequency-flat or frequency-selective conditions.

Important contributions worth mentioning are the IST-METRA (MultiElement Transmit Receive Antennas), [ScKM02], and the IST-SATURN (Smart Antenna Technology in Universal bRoadband wireless Networks) project models, [BeYO01], [Lasp02], being non-physical and physical examples. The One-ring and Two-ring models, the Von Mises Angular Distribution model, the Distributed Scattering model, the Extended Saleh-Valenzuela MIMO model, the COST 259 SCM extended to MIMO, the Electromagnetic Scattering model, and the Virtual Channel model are some examples of physical MIMO channel models. These models are summarily described and compared in [YuOt02].

Most recently, the 3rd Generation Partnership Project (3GPP)-3GPP2 SCM for MIMO simulations has been specified, [3GPP03], inherently comprising the interests and views of the many intervening parties. Such contribution develops and specifies the parameters and the methodology involved in system- and link-level evaluation simulations. After going forth with link-level calibration issues, in the sense of comparing results from different implementations of a certain algorithm, the model is systematically presented, directed towards system-level simulations and the subsequent comparison of algorithms.

The whole 3GPP-3GPP2 SCM methodology consists of specifying an environment, then obtaining the respective parameters necessary for the simulations, and finally generating the resulting channel coefficients. The scenarios considered are the suburban macro, urban macro, and urban

micro. For these, several parameters are tabled, following a similar philosophy as that applied in the COST 259 SCM, e.g., the number of paths and subpaths, angle-spread statistics at both BS and MT, relation between AoD and AoA spreads, delays spreads statistics, Log-Normal shadowing statistics, path-loss, mobility parameters. Going into more detail, the procedures to generate *user parameters* are also presented, in a step-wise manner. Finally, the channel coefficients are calculated considering ULAs at the BS and MT sides, organised in a channel matrix for each multipath component, also as a function of time.

As it was already shown with the COST 259 SCM, a model that aims at most generally covering many propagation situations and properties should simultaneously guarantee enough flexibility, in order to facilitate its application. The 3GPP-3GPP2 SCM has been conceived allowing for the flexible inclusion of additional features, from using polarised arrays, considering and characterising far scatter clusters, LoS conditions and the urban canyon situation.

To further complete the system-level application of the model, correlation between channel parameters, inter-cell interference and system-level calibration results are presented.

Concluding about the MIMO 3GPP-3GPP2 SCM, one firstly sees it as aiming at being a standardised modelling methodology, covering the description of the means to apply it for system-level simulations. In this way, the model renders a complete application-directed approach. For its importance, besides such philosophy, it would be very interesting to assess the considered propagation parameters with complete and controlled field measurements.

The model presented in [Moli03b] reflects another recent MIMO channel development, also with the aim of unifying perspectives and encompassing most important phenomena for MIMO. Another important contribution is provided in [WÖHB03], in agreement with the [Weic03] viewpoint. Thereby, the MIMO model is based on the eigenbases at both the Tx and Rx, introducing a coupling matrix to account for the correlation between both ends. Also, these latter studies are accompanied by validating measurement campaigns.

Lastly, but not least, based on geometric optics, including well characterised effects of reflection, diffraction and refraction, *Ray-Tracing Models* tools have been studied widely for outdoor and indoor scenarios, e.g., [ScWi03], [DLPR01], [DaCo99], [SeRa94], [GoCo94]. These are considered strong deterministic prediction tools, whose inputs are site-specific data, such as building or indoor morphological databases, architecture drawings or geographical based information. Computational processing is a concern, involving new evaluation implementation algorithms, e.g., [AFRV00]. Many studies have analysed delay-spread and various propagation effects, frequently comparing with known statistical propagation models and with field measurements. In many situations, simple Ray-Tracing is used to support other models or measurements, e.g., [FSMH02]. Ray-Tracing has also been useful to evaluate the performance of several adaptive antenna algorithms, characterising the channel in the angular domain, e.g., [TsAt02].

The methodology of Ray-Tracing methods differs from the remaining models. Being site-specific, it may still be seen as a modelling technique, but more as an aiding tool than a model itself.

2.4 Summary and Conclusions

This chapter aims at introducing the reader to the several most significant SCMs available in the literature, applicable between 800 MHz and 5.0 GHz. In that manner, both the several perspectives and the fundamental parameters that are involved are conveyed, understanding the main differences between classical and spatial models, and among the statistical-, the measurement-based, and the unifying spatial ones.

Along the SCMs presentation, it also becomes clear how the needs for the generation of such models have changed, along the years, from the initial spatial diversity characterisation to the more complex study and implementation of SAs. It is also seen how their complexity varies, as well as their completeness, the evolution of SCMs reflecting the tendency to join several perspectives, towards unifying ones.

It is also relevant to note that none of these models (except the MIMO or Ray-Tracing-based ones, possibly) include propagation effects such as diffraction, refraction or complex scattering. For beamforming, it is most often assumed that these do not contribute with power levels sufficiently relevant to the analysis of spatial filtering. In a similar way, most SCMs develop within a single plane, based on the fact that most power is conveyed within such plane, i.e., rendering sufficiently valid analyses in most antenna studies of this type.

Additionally, most of the later developed models discern macro- from micro-cell implementations, in that the location of relevant scatterers is limited to the area around the MT or in between the BS and the MT. Expectedly, these model cases tend to be geometrical, in their nature.

MIMO modelling also strongly develops on the spatio-temporal nature of the propagation channel, establishing physical and non-physical models, measurement- or scatterer-based, NB or WB ones. Nevertheless, the involved reasoning extends further from the propagation channel itself, possibly detracting from the focus on plain array beamforming.

Besides grasping the general views about such most relevant SCMs and their perspectives, there are several model characteristics that, already from this point, reveal to be important in the choice of a model used for the study of adaptive beamforming, in a MBSs perspective. These are the following: statistical value, establishing to which degree its application is site-specific, enabling or not some generalisation of results; completeness, in terms of the inclusion of all the major power contributing effects that determine relevant distributions in angle and delay, e.g., the clustering effect; flexibility, concerning their applicability to several environments, being macro-, micro-, or pico-cells, while maintaining the same fundamental modelling nature; implementation practicality and

complexity, enabling or not their practical use together with other simulation blocks such as a beamforming antenna array.

In this way, the track towards arguing for the use of a certain SCM, namely, a WDCM, is set. It is also important to go forth with an equivalent background study on the issue of adaptive beamforming.

3 Laying Foundations and Background – Adaptive Beamforming

*If you have built castles in the air, your work need not be lost.
That is where they should be. Now put the foundation under them.*

— Henry David Thoreau (1817-1862)

3.1 Beamforming for Smart Antennas

The use of SAs for mobile communications has been widely justified by the ultimate capacity gain that such solution inherently provides. For UMTS, applying SAs has been considered from the start of system specification, [ETSI98], and the 3GPP Working Group 1, from the Radio Access Network Technical Specification Group (TSG-RAN), has been submitting documents related to such. In the case of UMTS, and in future MBSs, which will most likely involve MC-CDMA, the use of CDMA allied to the ever increasing demand on the bit/s/Hz/cell capacity, requires more means of reducing intra- and inter-cell interferences. One solution is the use of SAs.

Among several SA techniques, adaptive beamforming may result in interference reduction, multipath and dispersion effects (time and frequency dispersion) reduction and maximisation of the Signal-to-Noise Ratio (SNR). Since this research deals with beamforming, and in particular this chapter, it is at this point most important to keep the concept of *beamforming* clear.

In [VeBu88], a *beamformer* refers to a processor used together with an array of *sensors* to apply some form of *spatial filtering*. In this study, these *sensors* are antenna elements. In communications, by *spatial filtering*, from the Rx point of view, it is meant to separate signals that share the same frequency band, time-slot, and possibly code, but that may originate from sufficiently different spatial locations. From the Tx side, it implies that signals with the same frequency band, time-slot and/or code may be spatially separated, received or transmitted in certain differing directions. Nevertheless, the definition that [VeBu88] provides seems not to be enough, since spatial filtering in SAs may be carried out by many other techniques besides beamforming.

A usual confusion arises from misunderstanding the notion of Direction-of-Arrival (DoA) estimation for that of beamforming⁶. Such is not illogical, since many beamforming schemes work very closely together with some form of DoA estimation scheme. Generally, DoA estimation by itself provides a spatial reference to a beamforming algorithm. Such form of estimation outputs impulses in the angular domain, corresponding to estimated DoAs. By itself, DoA estimation is not responsible for adjusting array elements' weights, shaping the array pattern and directing beams and nulls to provide maximum SINR. Such weight adjustment, shaping the full array pattern with a certain objective, placing lobes and nulls righteously, is what is hereby understood as *beamforming*. It may involve most simply directing one or several well-defined main lobes to the same Desired Signal (DesS). But, most generally, it should be understood as general pattern shaping. The utmost objective that rules this pattern shaping problem is efficiently transmitting/receiving wanted signals through a noisy, correlated and spatially interfering environment. This ultimate objective can be accomplished resorting to the adaptive beamforming algorithm, minimising a certain cost function through some means of interactive convergence. This method will be more or less dependent on the propagation channel or, in other words, on the structure of the signals at stake. It will also provide different complexities and convergence speeds.

Beamforming is used in a wide universe of applications, e.g., Radio Detection And Ranging (RADAR), Sound Navigation And Ranging (SONAR), Communications, Imaging, Geophysical and Astrophysical Exploration and Biomedicine. As the focus of interest of this text is mobile communications, beamforming will hereafter refer to communications applications only, where the array elements will be referred to as *antennas*, instead of general *sensors*.

In general, two types of non-adaptive beamformers can be envisaged, depending on the means of weight calculation: the *data-independent* and *statistically optimum*, [VeBu88]. Adaptive beamformers can be considered as statistically optimum, but with the additional dynamic performance, being capable of optimising their functions towards changing or unknown statistical channel or signal properties. One can therefore understand why many adaptive methods have emerged from the main statistically optimum schemes, in the development of these techniques. Since beamformers may be seen as adaptive or non-adaptive, according to such processing criteria dynamics, one hereby refers to these as being Adaptive or Non-Adaptive Beamforming *Processing Methods*.

Concerning the beamforming structural horizon, one should also apprehend why digital systems are preferable over analog ones, how fixed networks can be used to advantage even together

⁶ In this study, DoA and AoA are interpreted in different ways. DoAs refer to the dominant arriving signals from a identified desired source, implying the involvement of some form of angular estimation, whereas the AoAs refer to all angular contributions of the directional propagation channel, independent of being desired and non-desired ones.

with a fully adaptive array antenna, and why/in which situations are Switched-Beam Arrays (SBAs) preferable to fully adaptive ones. In this sense, one is categorising SBAs and adaptive arrays as making part of the larger universe of SAs, considering that, structure- and pattern-wise, adaptive arrays allow for the generation of a continuous and infinite establishment of lobe and zero locations and relative levels. It is in this sense that one hereby refers to Non-Adaptive or Adaptive Beamforming *Structures*.

With this chapter, then, one objective is to achieve a good grasp of the overall practical and mathematical matters around beamforming structures and processing. The reason for mixing structures with algorithms in this chapter is that these often very closely affect each other directly.

Along the present chapter, the approach to the matter of beamforming will intentionally favour the receiver perspective, also independently from the mobile propagation channel. In fact, beamforming in the reception side has been the major motor of related research, a fact that is reflected by many of the found and referenced related literature sources. Anyhow, it must be realised that beamforming is possible either in the transmitting or receiving sides. Additionally, references to the propagation channel will naturally take place, already in this chapter, though this issue will be dealt with in the following one. Finally, the discussion on beamforming is centred in the discrete time, though many of the descriptions are valid for continuous time.

Important known references, providing grasping views of the issue, are [VeBu88], [Goda97], and [PaPa97]. The latter focuses more directly on wireless communications, providing an excellent systematic view of channel, single- or multi-user issues, in parallel to space-time processing. The former more directly deal with the processing, for several applications, justifying their frequent mention within the chapter. [Fuhl97] presents an excellent and extensive study of smart antenna schemes, besides defining a SCM, applying the referred *Low-* and *High-Rank* SCMs, as in [FuMB98], and analysing several algorithm responses to several channel conditions.

3.2 Basic Concepts, Parameters and Structures

3.2.1 Beamforming Structures

As far as the notion of *aperture*, *interval* or *domain* is concerned, a temporal filter is seen to operate on a time *interval*, temporal *domain* or *aperture*, as a frequency filter also operates in a spectral *aperture*. In the same way, the spatial filter implies a *spatial aperture*, where spatial sampling is discrete.

Two main properties of spatial discrete sampling can be pointed out – spatial discrimination potential depends on the size of the spatial aperture, compared with the working wavelength (the larger the aperture, the better the discrimination); inherent filtering flexibility exists, where the

filtering function may be changed in real time (such is not feasible with a continuous aperture antenna).

As the aperture is to be large enough, remembering that increasing the number of elements will imply larger costs (an RF stage and Analogue-to-Digital Converter (ADC) circuitry can be needed for each element) and severer decalibration, non-uniform element spacing can be a means to achieve lower beamwidths and better side-lobe suppression at considerable low costs, [LiRa99]. Increasing the aperture size through separating the elements further than $\lambda/2$ will contribute to a large number of undesired grating lobes.

The aperture itself being one important factor in the array resolution capability, in the case of being discontinuous, the number of elements will determine the Degrees-of-Freedom (DoFs) available in the design of diverse patterns, [LiRa99], [Vaug88]. Then, spatial filtering will directly and primarily depend on spatial aperture characteristics, such as the number of elements and element separation.

Also as an introductory basis, one can point out a fundamental similarity with a Finite Impulse Response (FIR) filter, in that the beamformer generally linearly combines the spatially sampled temporal sequence, from the several array elements, ending up with a scalar output time sequence, just as a FIR filter. Though the beamformer structure may in itself have feedback chains to calculate the array weights, the overall output is not fed back to any point within the system in order to calculate future overall outputs, therefore, constituting an equivalent FIR⁷. Accordingly, many of the techniques used with FIR filtering are used in beamforming. However, several major differences also exist, especially in the case of mobile communications, indicating that the beamforming matter may be more complex: in antenna array beamforming, the electromagnetic signal samples are characterised by more than one parameter – magnitude (given by attenuation and fading), time-of-arrival, azimuth and elevation angles, polarisation and frequency; if temporal variations are considered, due to channel changes beyond the assumed static or stationarity period, then those parameters can be functions of time; different signals, i.e., characterised by a different set of the referred parameters, can be correlated due to multipath; sampling in the spatial domain may not be uniformly distributed in space, i.e., non-uniform sampling is possible, besides being multidimensional; array element decalibration, as a spatial and responsive uncertainty factor, must often be considered (leading to the development of robust techniques).

The basic analog Intermediate Frequency (IF) and digital complex baseband weighting and combining receiver architectures are well known, e.g., [LiRa99]. Focusing on these, the RF stages are common *down* to the IF level. From that point *downward*, the following divergences occur: the analog

⁷ In fact, in mobile communications, closed-loop control makes use of SINR information being fed-back between the MT and BS, but such is in a larger scale.

Rx (ARx) involves downconversion after the whole weighting and combining, and the digital Rx (DRx) downconverts just after IF filtering, before weighting (noise, Inter-Symbol Interference (ISI), and circuit mismatching problems may be at stake); the ARx has its ADC at the far end, and the DRx immediately converts the IF signal to digital form; in the DRx, weighting exists at baseband level, and in the ARx it does not; the analog weighting is performed by a variable gain amplifier and phase-shifter, whereas, for the DRx, weighting is performed at the digital level, i.e., within the Digital Signal Processing (DSP), differing in the involvement of non-linearities and flexibility problems; the array element outputs in the ARx are at the IF level, whereas in the DRx these are digital and exist in baseband, serving directly as inputs to the weighting algorithms.

The main result of these structural differences is that in a beamforming BS array, with multiple simultaneous Up-Link (UL) beams, the RF/IF analog Rx is much less versatile than the digital Rx – the ARx is capable of forming one beam only, at each instant, requiring several analog weighting structures for several sources, whereas the DRx can create several simultaneous beams.

The analog RF beamforming network stage, *above* IF, can be combined with a digital time-varying spatial processing section, as Figure 3.1 exemplifies. The analog stage is a fixed *BeamForming Network* (BFN), followed by a downconverting stage (either to baseband or IF), ADCs and the digital adaptive array processing section.

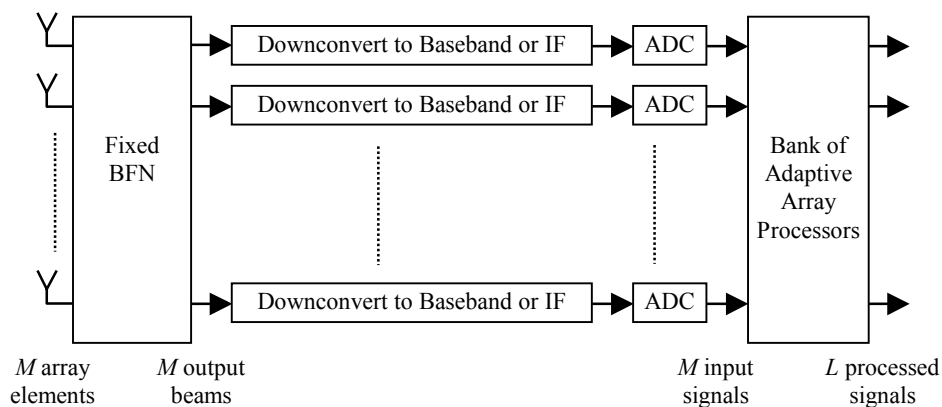


Figure 3.1 – A digital adaptive processing network together with an analog beamforming network (based on [LiRa99]).

With cascaded M inputs BFN and digital spatial processing stages, the whole Rx will be able to discriminate $L \leq M$ sources, if only spatial physical channels exist (case of pure SDMA). In the case that other physical channel domains exist, either time, frequency or code, more than M sources may be separated.

As far as the vectorial domain is concerned, the fixed BFN will be represented by a set of M dimensional weight vectors, each one for each spatial source, forming the $M \times M$ BFN matrix. If the

M vectors are orthogonal, then M spatial sources can be resolved. An example of this matrix is the *Butler* matrix, at the RF stage, [BuLo61].

It can be argued that, if a digital adaptive array already exists after downconversion, the whole Rx would not need a fixed BFN. In fact, if the digital stage is already able to discriminate M sources, then the fixed $M \times M$ BFN will not add any more detectable sources. On the other hand, with a stationary propagation channel, the non-zero determinant (full rank) BFN matrix will not degrade the discrimination response. In fact, the point of using the fixed BFN will then be of a spatial pre-filtering already reducing the Multiple Access Interference (MAI), also reducing the required downconverter and ADC dynamic range, [LiRa99].

Another possibility of using a fixed BFN is using a second RF switched stage, after the BFN – the SBA. The function of such is to select each of the maximum M beams, for a certain source. In that case, for the current beam, when the received Signal-to-Interference Ratio (SIR) lowers beneath a threshold, the receiver changes to the available best beam. Either for reception and transmission, the process is similar. Clearly, to simultaneously resolve the several sources, several of these beam-selection systems would be needed, independently controlling each beam. As it is stated in [HoSA98], the same beam can even be used for both reception and transmission. The switching methods and definition will largely depend on the multiple access technique used.

Anyhow, major SBAs disadvantages can be pointed out: for each SBA, the number of possible beams is discrete, limiting its beamforming dynamic performance; as a result of the latter, the beamforming will not imply best MAI suppression efficiency between close wanted and unwanted steering vectors, because the system will not change its weight vector continuously, allowing for the non-elimination of an angular near interferer; due to the discrete number of beam patterns, the BS received/transmitted power will fluctuate as the MT moves with zero radial velocity respect to the BS, since the used main beam (with varying power along angle) will be kept while the MT crosses the corresponding angular sector (this effect is called *scalloping*); finally, such array is typically not able to perform diversity combining, [LiRa99], [PaPa97].

Nevertheless, at a lower cost, lower technology and engineering demanding complexity, the SBA may achieve the desired delay-spread reduction, MAI and co-channel interference reduction, and ultimately the required capacity increase, compared to an adaptive solution. These do not need complicated combining networks, and can also be designed with well-established technology, which in practice may be a decisive aspect. Furthermore, these systems can be fit into the current existing cellular infrastructures, without great infrastructure changes, [Fuhl97], [HoSA98], [ChSS99], [PaPa97].

In [ChSS99], a good performance and CDMA system complexity comparison is provided between specific types of SBAs and adaptive beamforming arrays, where, for certain conditions (algorithm and interference levels), the SBA overall performance outperforms that of the adaptive

counterpart. In this way, it is shown that the potential provided by both types of beamformers is not that clear, in that it depends on many variables, requiring a careful approach, even if only main beam steering is evaluated. The comparative parameters may be systematised: the beam accuracy obtained by the weight vector, the time taken to define that vector, the interference suppression capability and hardware complexity. As far as accuracy is concerned, two factors are investigated and their implications are described, in such study: sensitivity due to environmental (interference) effects and the phase error in the calculation of the weights.

Concerning the system dependency on the interference levels, keeping in mind that the study in [ChSS99] is applied to CDMA, the algorithm used in the adaptive array largely depends on the processing gain, i.e., the DesS power must be sufficiently higher than that of the interfering signal. The reason for this is that such algorithm is based on choosing the eigenvector corresponding to the largest eigenvalue of the data auto-correlation matrix, knowing that such eigenvector is a good approximation for the needed weight vector. Nevertheless, such approximation will only be in fact valid in the case that the useful signal is sufficiently more powerful than the interference, thereby justifying the performance of the adaptive solution being surpassed by that of the SBA. Anyhow, it is hereby preferred to attribute such performance difference to the algorithm itself, and not the whole beamforming structure. According to [BrUN01], the problem of *eigenbeamforming* roots from the spatial selectivity of the channel. In the case that the channel is spatially selective, the choice of a single eigenvector does not allow for spatial diversity, power from other channel taps is lost, and performance degrades. The space-time *eigenRAKE* presented for the UL avoids this problem.

The other very important factor that highly affects systems' performance is the phase error inevitably existent in the calculation and/or application of the weights. As explained, the mistracking error can be avoided in the SBA case, but not in the adaptive counterpart case⁸. On one hand, the problem is only theoretically solved for the SBA; on the other, as a fundamental comparison factor, independent of the adaptive beamformer potential, this is a major point of performance divergence. The issue of tracking robustness is focused in [KuTB02], anyhow showing that reliability in choosing a pattern that provides best SINR is more important than DoA accuracy by itself. In fact, the adaptive application thereby presented has shown that.

In [ChSS99], it is stated also that the adaptive array performs better in the case that the signal is *very* widely spread, making use of its flexibility and possible further complexity to maximise DesS power, by changing main-lobe beamwidth. Considering this aspect, this could imply that, at the MT and pico-cell low BS antenna array heights, the adaptive solution would be preferable, whereas at macro- and micro-cells BS heights advantages would be less clear.

⁸ For the objective of the current study, this problem is not dealt with, in spite of its importance in conditioning beamforming performance. An applied beamforming scheme may be less prone to these errors, especially in the case of the reference-based beamforming (the case of this study).

The problem of beamforming time has also been addressed, in [ChSS99]. The importance of speed is more severe with adaptive arrays than with SBAs. In the former case, generally, the weight vector needs to be calculated for every snapshot (a set of element outputs collected at a specific instant of time), since the current vector is usually calculated from the past-received signal. Depending on the stationary period, the number of DSP instructions and time taken for each instruction must be evaluated. Thus, the algorithm complexity, though providing much greater flexibility, will strongly affect the overall tracking accuracy.

Anyhow, it is important to note that the complexity of the involved compared structures and algorithms may be very similar. In the referred work, it is also indicated that the SIR improvement is comparable between the defined tracking array and SBA, with the same number of elements, assuming no phase error. Also, the capacity values indicated for a certain Bit-Error-Rate (BER) are not severely worse for the SBA. Still, adaptive solutions render better performance potential. By increasing calculation and hardware complexity, the adaptive beamformer performance can be raised considerably by, for example, placing pre-correlation and post-correlation matrix calculation stages before and after the despreading at reception (inherent to a CDMA application), e.g., [Nagu96].

Conclusively, comparing SBA and adaptive beamformers is not only necessary but requires the analysis of many factors. Anyhow, in 10 years time, or even before that, one envisages the widespread use of SAs in the highly demanding servicing and environments involved in the future mobile systems. Until then, hardware and algorithm evolution will most likely allow for powerful and robust adaptive systems to clearly overtake the SBA solutions, both at BS and MT, judging from the incredible growth in the large electronic integration industry. In this way, one sees that adaptive array solutions will naturally cover UMTS applications, also opening the path to future MBSs.

The expression *degrees-of-freedom* is used along the text referring to its widely understood meaning. However, to fully grasp the concept of partial adaptivity, one should further clarify the concept of a beamformer's DoF. It expresses the number of unconstrained or tuneable weights that can be used for the control of the beams, meaning that that a fully adaptive array will make use of all available weights, with no constraints.

Full control of the array DoFs provides naturally understood advantages: maximum control of the array response, maximum aperture gain (all the aperture elements are used) and consequent maximum spatial resolution. Nevertheless, full adaptivity implies larger computational complexity and the decrease in the convergence rate, knowing that many beamforming algorithms involve a number of products of $O[M]$, $O[M^2]$ or even $O[M^3]$, where M is the full number of unconstrained weights. For this, especially for large arrays, partial adaptivity may be of interest. The expense of this will be an unavoidable optimisation loss, converging to solutions farther from the optimal, compared to the purely adaptive solution, [LiLo96], [VeBu88].

There are several schemes for implementing a partial adaptive structure: selecting a fraction of the total number of array elements for adaptive control (partitioning at the elemental level); grouping the entire array into sub-arrays, using beamforming for these, and adaptively controlling the outputs of the sub-arrays; forming several beams using the entire array, adaptively controlling these. The former strategy is a form of *element-space* processing, whereas the latter is a *beam-space* processing solution. The second scheme may be seen as a form of element-space processing, if one views the sub-arrays as equivalent elements, forming an equivalent aperture, [LiLo96].

As far as digital beamforming types are concerned, beam-space processing (either fully or partially) inherently makes multiple beamforming possible. A beam-space processor implies that the outputs of the array elements are firstly processed by a multi-beam beamformer, forming a group of orthogonal beams. The output of each beam can then be weighted and further combined in order to achieve the desired output, [LiLo96]. Focusing on partially adaptive beam-space processing beamformers, their advantages compared to a fully adaptive case can be pointed out: reduction of overall cost due to the smaller number of DoFs; use of simpler adaptive weight constraints, implying minimum gain degradation at main lobes and sidelobes; reduction of mathematical processing load; faster array response convergence; compatibility with a large number of adaptive algorithms.

Judging by these advantages, one understands how their benefit will be greater for larger arrays. And for this, no clear advantages are expected for mobile communications, reasoning that large arrays will not be the most common ones (even in higher frequency MBSs), and that fast electronics will be easily available. Also, one must not forget that the final error will be larger, and that a large degradation in the SINR is expected, especially when an interference scenario demands for more DoFs. Nevertheless, there is no doubt that partially adaptive beamforming can be of considerable importance from an engineering project point of view.

For details on digital beamforming schemes and on partial adaptivity, [KrVi96], [LiLo96] and [VeBu88] provide good background.

3.2.2 Beamformer Response, Steering and Weight Vectors

Inherently, a beamforming structure samples the propagating wave, since array elements capture the wavefronts from different positions, registering the relative phase difference, directly related to the AoA. Most generally, often depending on how the spatial and temporal apertures are developed, beamforming is classified as being NB or WB. The structural difference between NB and WB is the inclusion of the temporal domain in the case of WB. If NB seldom refers to spatial apertures, WB corresponds to spatio-temporal ones (truly, there are several related interpretations for NB and WB, this matter deserving particular attention and being further developed in Section 6.2, Implementation vs. Narrowband and Wideband). [PaPa97] systematically addresses the issue as *Time-Only*, *Space-Only* and *Space-Time Processing*.

In the NB, spatial aperture, beamforming case, the system output, $y(n)$, for M elements, is given by⁹:

$$y(n) = \sum_{m=1}^M w_m^* x_m(n) , \quad (3.1)$$

where $x_m(n)$ is the input data sequence, function of the discrete time variable¹⁰, n , at the m^{th} antenna element and w_m is the complex weight in the m^{th} branch. The data sequence and the weights are complex numbers, keeping the notation used in the previous chapter. Discrete sampling is assumed, seeing an array element as a complete Rx stage, with A/D conversion, so that digital beamforming may be performed.

In the case of WB, spatio-temporal, beamforming, sampling both in space and time implies a slight change in (3.1), due to the additional DoF, where p is the delay index in each element branch, and P_m is the total number of delays in the m^{th} branch:

$$y(n) = \sum_{m=1}^M \sum_{p=0}^{P_m-1} w_{m,p}^* x_m(n-p) , \quad (3.2)$$

The most practical way to refer to both (3.1) and (3.2) is to use the vector notation:

$$y(n) = \mathbf{w}^H \mathbf{x}(n) , \quad (3.3)$$

where $\mathbf{x}(n)$ and \mathbf{w}^H are $M \cdot P$ dimensional data vectors (P_m is assumed equal to P , among all elements) in the WB case, and $\mathbf{w}^H = [w_1^* \quad w_2^* \quad \cdots \quad w_M^*]$ for NB.

For the NB case, and for a single specific AoA, from (3.1) one may see the beamformer impulse response in the form of a FIR:

$$h_{bf}(n) = \sum_{m=1}^M w_m^* \delta[n - \tau_{FIR}(m-1)] , \quad (3.4)$$

and in the discrete frequency domain, Ω , the frequency response of such case is given by:

$$H_{bf}(\Omega) = \sum_{m=1}^M w_m^* \exp[-j\Omega\tau_{FIR}(m-1)] , \quad (3.5)$$

where τ_{FIR} is the corresponding signal time delay between each antenna element, thought to be equal between each neighbour elements, i.e., the ULA is being considered so that the FIR filter equivalence is possible¹¹ and such frequency response is like (3.5).

⁹ Since large part of the quantities at stake are complex, the covering slash will not be used, i.e., $\bar{y}(n)$ will be represented by $y(n)$, stating along the text that $y(n)$ is complex.

¹⁰ The discrete sample index n corresponds to the t_n sampling instant, using n for simplicity, as usual.

¹¹ According to [VeBu88], such correspondence is best for the ULA and for a single frequency of operation (NB).

Another way to represent the NB beamformer response is by using the *steering vector*,

$$\mathbf{a}(\Omega) = [1 \quad \exp(-j\Omega\tau_{FIR}) \quad \exp(-j2\Omega\tau_{FIR}) \quad \cdots \quad \exp(-j(M-1)\Omega\tau_{FIR})]^T, \quad (3.6)$$

considering $m = 1$ as the phase reference element:

$$H_{bf}(\Omega) = \mathbf{w}^H \mathbf{a}(\Omega). \quad (3.7)$$

$H_{bf}(\Omega)$ is called *beamformer response*, [VeBu88], or *array factor*, [LiRa99], $|H_{bf}(\Omega)|^2$ is the *beam pattern*, and $\mathbf{a}(\Omega)$ may also be called *array response vector*, [VeBu88]. Notice that the indicated delay, τ_{FIR} , will be dependent on the AoA, ϕ , hereby defined as the AoA to the perpendicular of the array, as it is shown in Figure 3.2. If the antenna element spacing is d_{el} and c is the propagation velocity in free space, then $\tau_{FIR}(\phi) = d_{el} \sin \phi / c$. From Figure 3.2, adopting the assumptions provided in Section 2.2, then $u_2(\tau) = u_1(\tau - \tau_{FIR})$.

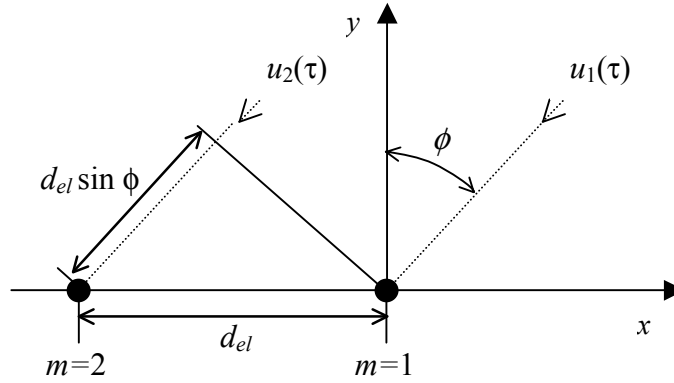


Figure 3.2 –Two signals from the same source in the far field, $u_1(\tau)$ and $u_2(\tau)$, arrive at the ULA $m = 1$ and 2 , from angle ϕ .

The beamformer response is then a function of ϕ , i.e., one has $H_{bf}(\phi, \Omega)$, and so is the steering vector, $\mathbf{a}(\phi, \Omega)$. Therefore, for the NB beamformer, the complete version of (3.7) will be:

$$H_{bf}(\phi, \Omega) = \mathbf{w}^H \mathbf{a}(\phi, \Omega). \quad (3.8)$$

Concerning the WB structure, one can also arrive to the beamformer response:

$$H_{bf}(\phi, \Omega) = \sum_{m=1}^M \sum_{p=0}^{P-1} w_{m,p}^* \exp\{-j\Omega[\tau_{FIR}(\phi) \cdot (m-1) + T_m p]\}, \quad (3.9)$$

where the $\tau_{FIR}(\phi)$ parameter is maintained as the AoA-dependent relative delay between array elements, and T_m is the tap-delay within each m branch (considering equal delay taps, for simplicity).

To understand how the WB response can be represented by (3.8), in an $M \cdot P$ -dimensional vector form, let the total delay due to AoA plus the branch taps be represented by $\tau_i(\phi)$:

$$\tau_i(\phi) = \tau_{FIR}(\phi)(m-1) + T_m p, \quad (3.10)$$

with $1 \leq m \leq M$, $0 \leq p \leq P-1$ and $1 \leq i \leq M \cdot P$. This means that for the $m=1$ reference, $\tau_1(\phi) = \tau_{FIR}(\phi)(1-1) + T_m 0 = 0$, and that $\mathbf{a}(\phi, \Omega)$ is then represented by

$$\mathbf{a}(\phi, \Omega) = [1 \quad \exp(-j\Omega\tau_2) \quad \exp(-j\Omega\tau_3) \quad \cdots \quad \exp(-j\Omega\tau_{M \cdot P})]^T. \quad (3.11)$$

Also, the $M \cdot P$ weight elements need to be placed in the vector form, \mathbf{w}^H . Viewing the matter in this way, one very well understands that the weights vector will therefore affect both the spatial and temporal responses of the system. Furthermore, these weights may be function of frequency, especially in the WB case.

The interesting approach presented in [Vaug88] states that, for the specific case of mobile communications, where the wanted sources and interferers are of more demanding resolving, the array must make use of the signals at the level of each array element branch, i.e., including the temporal domain. In this way only will the array be capable of optimally combining the signals, other than viewing the array as a simple physical mapping of radiation patterns to signals. The array pattern, or array factor, will not be of importance in its own, since it develops on the real array space only. Therefore, the steering vector, or a matrix composed by several of these vectors (called *steering matrix*), with columns corresponding to the several arriving signals, carries *directive* information that should be extracted at the level of each antenna element. In fact, the point that spatio-temporal processing is needed is brought up in [Vaug88], fitting within a WB array concept, thus, making use of the main advantage of a digital beamformer, where a single receiver system (the digital beamformer) will make all data available, both in spatial (between branches) and temporal (within each branch) domains. This very well fits the *element-space processing* concept, as characterised before, and this perspective is fundamental for the algorithm implementation, in this study.

Up to this point, the reasoning has been based on ideal array elements, omnidirectional in the considered plane. Practically, since these will not be omnidirectional, and in the case that these are physically similar and oriented in the same way, the total field pattern will result from the array factor-element radiation pattern product, according to the *principle of pattern multiplication*, e.g., [Coll85]. In other words, the element pattern, function of ϕ , and possibly of m , would be added to (3.8).

The weight and steering vectors make possible the use of orthogonality to establish the possible discrimination between two different AoAs. From (3.7), one understands that, if for a certain (ϕ_i, Ω_i) pair the two vectors are orthogonal, the scalar product of the two vectors will be 0, i.e., the array factor has a corresponding null at such (ϕ_i, Ω_i) pair. On the other hand, the array response will be large if the angle between \mathbf{a} and \mathbf{w} is small. If one source, at (ϕ_i, Ω_i) , is to be discriminated from another undesired source, at (ϕ_j, Ω_j) , it will be important to establish the weight vector so that the angles between \mathbf{w} and both $\mathbf{a}(\phi_i, \Omega_i)$ and $\mathbf{a}(\phi_j, \Omega_j)$ are sufficiently different in the M -dimensional vector space. In that case, the beamformer response may tend to direct a null towards the undesired pair, with

a maximum towards the other. In this way, the ability to perceive two separate DesS sources, at (ϕ_i, Ω_i) and (ϕ_j, Ω_j) , will always depend on the angle between both vectors $\mathbf{a}(\phi_i, \Omega_i)$ and $\mathbf{a}(\phi_j, \Omega_j)$, [VeBu88], [Vaug88].

For a set vector space, there are, therefore, important sources of ambiguity that should be mentioned. As temporal aliasing (ISI) happens in the temporal domain, spatial aliasing can be defined in the spatial domain, i.e., in the NB case, where two AoAs are not discriminated, $\mathbf{a}(\phi_i, \Omega_i) = \mathbf{a}(\phi_j, \Omega_j)$. Another source of uncertainty is the possibility of, in the WB case, two different combinations of (ϕ, Ω) originating two equal steering vectors, $\mathbf{a}(\phi_i, \Omega_i)$ and $\mathbf{a}(\phi_j, \Omega_j)$. From the array vector definition, it can be seen that this situation happens when $\Omega_j \sin \phi_j = \Omega_i \sin \phi_i$.

Though a ULA is being considered in this study, directly paralleling the uniform temporal sampling of a digital signal filter, the beamformer may not have regularly spaced elements and may have another geometry, resulting in that the spatial sampling may not be uniform. The beamformer response, depending on those element relative locations, serves as an additional specification in the array project, where the main aim is to achieve a domain of well-dispersed and unambiguous M -dimensional steering vectors for different sources. The extent of such dispersion and unambiguity will be set by the wideband and directional nature of the propagation channel and propagation scenarios at stake.

3.3 Non-Adaptive Beamforming Processing

3.3.1 Data Independent Beamforming

In a data independent beamformer, the weights are determined independently from the array data, and projected in order to achieve a specified response. Therefore, the beamforming response will be independent of the signal or interference statistics, powers, ToAs and AoAs.

The data independent NB beamforming structure at its simplest is the *linear uniform phased array* or *delay-and-sum beamformer*, where phase-shifters at each array element compensate for the phase difference between arriving plane waves, at an angle with the array axis. In case that the input to the array is given by

$$\mathbf{x}(\phi, \Omega) = [1 \quad \exp(-j\Omega\tau_{FIR}) \quad \exp(-j2\Omega\tau_{FIR}) \quad \cdots \quad \exp(-j(M-1)\Omega\tau_{FIR})]^T, \quad (3.12)$$

(equal to the array steering vector, $\mathbf{a}(\phi, \Omega)$), indicating the relative phases of an electromagnetic wave impinging at a certain time instant, then the phased array directs a main lobe towards the corresponding AoA, i.e., constructively summing up all elements contributions from that direction. By applying the corresponding weight vector with $\mathbf{w}(\phi, \Omega) = \mathbf{x}(\phi_{DesS}, \Omega_{DesS})$, the array output (3.3) leads to M as a result, or to unity by normalising for the number of elements.

Besides the phase *compensation*, the weights can have non-unity moduli, changing the relationship between main-lobe beamwidth and side-lobe suppression. This is called *tapering*. Also, as mentioned before, the WB array will differ from the NB in the inclusion of *steering delay filters* at each tapered element output, developing the system in the temporal domain.

The uniform linear *phased array* can be seen as a Least Squares (LS) estimation problem, [VeBu88], as a deterministic approach, [Hayk96], seeing it based on temporal, not ensemble, averages (which in a mean-ergodic process will not differ, e.g., [Pätz03]). Notice how the array weight response does, in a way, depend on the data, since the optimum will be equal to the input data vector, this system making sense if the AoA is known. That can be the case where AoA is constant, or the array is programmed to change the weights subject to a deterministic phenomenon.

In [WiGa99], a good comparison is put forward between phased and adaptive arrays, evaluating the range increase that the latter can provide compared to the former, with the same number of elements, for both NB and WB. Higher diversity and antenna array gains are registered for the adaptive solutions, for the same number of elements. Also, the phased array does not provide any interference reduction capability, unless the interfering source is stationary and at known direction so as to direct a null towards it.

Phased arrays can, as it has been seen, generate a single main-lobe of unity (normalised to the number of array elements); but, the desired response can be more general, always within a deterministic application. Take the example of generating several unity magnitude main-lobes in specified directions, or the case where several interference sources are known to exist in several directions, towards which nulls in the array factor will be directed.

The general approach is, like the phased array, to find \mathbf{w} in order to near the actual beamformer response, $H_{bf}(\phi_{DesS}, \Omega_{DesS}) = \mathbf{w}^H \mathbf{a}(\phi_{DesS}, \Omega_{DesS})$, to the desired response, $H_{dbf}(\phi_{DesS}, \Omega_{DesS})$. There are several techniques to do so, similar to those used for FIR filter design, but for the current introductory objectives, only the LS estimation logic will be superficially described.

The objective of LS is to minimise the squared error at P points, (ϕ_p, Ω_p) , $1 \leq p \leq P$. Recalling that M is the dimension of the weight vector, i.e., the unknowns vector, if $P > M$ the problem is an *overdetermined* one, whereas if $P < M$ the problem will be *underdetermined*, [Hayk96]. For the former case, the matrix form optimisation function is:

$$\min_{\mathbf{w}} \{\xi\} = \min \left\{ \left| \mathbf{w}^H \mathbf{A} - \mathbf{H}_{dbf}(\phi_{DesS}, \Omega_{DesS}) \right|^2 \right\}, \quad (3.13)$$

where \mathbf{A} is the actual steering vector matrix,

$$\mathbf{A} = [\mathbf{a}(\phi_1, \Omega_1) \quad \mathbf{a}(\phi_2, \Omega_2) \quad \cdots \quad \mathbf{a}(\phi_P, \Omega_P)] , \quad (3.14)$$

and $\mathbf{H}_{dbf}(\phi, \Omega)$ is the desired beamformer responses matrix, for each of the P points,

$$\mathbf{H}_{dbf} = \left[H_{dbf}(\phi_1, \Omega_1) \quad H_{dbf}(\phi_2, \Omega_2) \quad \cdots \quad H_{dbf}(\phi_P, \Omega_P) \right]^T . \quad (3.15)$$

The solution to the problem is given by

$$\mathbf{w}_{opt} = \mathbf{A}^+ \mathbf{H}_{dbf}(\phi_{DesS}, \Omega_{DesS}) = (\mathbf{A}\mathbf{A}^H)^{-1} \mathbf{A}\mathbf{H}_{dbf}(\phi_{DesS}, \Omega_{DesS}) , \quad (3.16)$$

where \mathbf{A}^+ is the *pseudoinverse* of \mathbf{A} , thought to be a *full rank* matrix, [VeBu88], [Hayk96]. Based on this optimisation problem, directions and frequencies can be enhanced in (3.13), for certain sources (ϕ_i, Ω_i) , while others may be reduced.

Finally, it is important to be aware that the norm of \mathbf{w} also affects the white noise contribution, reflected in the *white noise gain* and, therefore, the beamformer's output SNR, [VeBu88].

3.3.2 Statistically Optimum Beamforming

In a statistically optimum beamformer, weights are calculated based on array data statistics, according to a certain optimisation of a cost function. This is the case where, depending on the signal and interfering sources, the main lobe and nulls are placed in order to maximise the SIR, SNR, or SINR.

Another inherent characteristic of statistically optimum beamforming is the fact that the data source is thought to be wide sense stationary, and that its second-order statistics are already known. Therefore, statistically optimum beamforming algorithms do not by themselves account for the channel dynamics, either due to MT mobility or environment movement. Due to such dynamics or if the second-order statistics are not *a priori* known, the algorithms must additionally estimate those statistics, making use of ergodicity. To account for these cases, optimum beamforming algorithms give place to adaptive ones. For example, the Steepest Descent (SD) and Least-Mean-Square (LMS) are examples of adaptive algorithms that derive from the *Wiener* (or MMSE) statistically optimum algorithms.

There are four main optimum beamformers, differing on the optimising criteria and inputs, [VeBu88] – the *Multiple Sidelobe Canceller* (MSC), *Reference Signal Optimum Beamformer* (RSOB), *Maximisation of SNR Beamformer* (MSNR), and the *Linearly Constrained Minimum Variance* (LCMV) *Beamformer*. As it will be seen, the criteria for the calculation of the optimal weights generally cover minimisation of the mean-square error, maximisation of SNR, or minimisation of variance. These lead to the same SNR, corresponding to the common *Wiener* solution, the theoretical steady-state limit for adaptive beamforming, [LiLo96].

In order to work, optimum beamforming methods require that some parameter of the DesS is known – either a specific signal property (in the case of the use of a reference signal, a carrier of an amplitude modulated signal, or a channel code for a CDMA scheme), statistics (also in the case of the

use of a reference signal or in the case of maximisation of SNR, where the signal and noise autocorrelations are required), specific direction (for the MSC, where the highly directive main channel antenna must be directed to the signal direction), or steering vector (in the case of the LCMV). The erroneous knowledge of such needed parameters will imply that the solution will not lead to maximisation of SNR, SIR or SINR. Depending on these algorithms (which accept different inputs), *signal cancellation* may also happen between the DesS and the Non-Desired Interference (NDesI) sources in the case that these are correlated; the result may end up in also reducing the desired signal power, while reducing that of unwanted signals.

Also called *Sidelobe Canceller* (SLC), the MSC system has been developed in the early days of adaptive antenna processing, [Howe76], [Appl76], [ApCh76]. It is considered to be the birth of adaptive beamformers, but not necessarily a fully adaptive one. As far as its array structure is concerned, it has a main beam antenna (a single antenna element or a data independent beamformer) and one or more auxiliary array elements. The main antenna is highly directive and pointed to the DesS AoA. The aim of the canceller is to define the auxiliary antenna element weights so as to make use of the interfering power received by these, using its output to extract interfering power captured by the main antenna.

The MSC requires that the interfering power from the main antenna and from the linear combination of the auxiliary array must be identical, so that interference is reduced to zero. Nevertheless, such optimisation is not possible, or it can lead to a too large a white noise gain, [VeBu88]. In that way, the weights are chosen to balance interference suppression with white noise gain reduction, through minimising the total output power:

$$\min_{\mathbf{w}} \left\{ |y|^2 \right\} = \min_{\mathbf{w}} \left\{ \left| y_{main} - \mathbf{w}_{SLC}^H \mathbf{x}_{aux} \right|^2 \right\}, \quad (3.17)$$

where y is the output, given by $y_{main} - \mathbf{w}_{SLC}^H \mathbf{x}_{aux}$, with \mathbf{x}_{aux} being the auxiliary inputs, \mathbf{w}_{SLC} the weight vector and y_{main} the primary data (from main beam antenna). Considering that the auxiliary inputs correlation matrix is $\mathbf{R}_{aux} = E[\mathbf{x}_{aux} \mathbf{x}_{aux}^H]$, and that the cross-correlation between auxiliary and main inputs is $\mathbf{r}_{am} = E[\mathbf{x}_{aux} y_{main}^*]$, the optimum solution to the problem is given by $\mathbf{w}_{opt} = \mathbf{R}_{aux}^{-1} \mathbf{r}_{am}$, [Hayk96], [VeBu88], [Vaug88].

The result of minimising the total SLC output power, as one well understands, will not be desirable in the case that the wanted signal has high power, relative to the interference. As the DesS power raises, for constant interfering power, the SLC will suppress it. This is why the SLC is used in cases where the DesS power is very low, compared to the interference (in which case the weights will not take into account the small contribution of the desired signal). Another method to use the SLC, if possible, is to adjust the weights if and when the wanted source is not present, and then keeping these constant when the signal appears. In this last case, where the weights are pre-adjusted, the main beam

direction must be known, so that the SIR is maximised. The SIR will not be optimum if the beam is not righteously directed. Finally, for all of this, the SLC will have particular difficulty to efficiently maximise SIR in a dynamic scenario. In this sense, one may see the SLC as not being fully adaptive.

Certain sufficient known properties of the DesS may be conveyed by means of a reference signal in order to adjust the weight vector. The optimising problem of the *Reference Signal Optimum Beamformer* is to minimise the mean squared error between beamformer output and reference, i.e.,

$$\min_{\mathbf{w}} \{ |\xi(n)|^2 \} = \min_{\mathbf{w}} \{ |y(n) - d(n)|^2 \}, \quad (3.18)$$

where y is the output, given by (3.3), with $d(n)$ being the reference *desired* output signal. Considering that the input correlation matrix is $\mathbf{R}_x = E[\mathbf{x}\mathbf{x}^H]$, and that the cross-correlation between desired and main inputs is $\mathbf{r}_{xd} = E[\mathbf{x}d^*]$, the optimum solution to the problem is given by $\mathbf{w} = \mathbf{R}_x^{-1}\mathbf{r}_{xd}$, [VeBu88]. This system, provided the minimum required knowledge of the received signal is possible, e.g., carrier frequency in amplitude modulation, or code in a CDMA system, has the particular advantage of not requiring the specific knowledge of the source AoA. By itself, this method does not account for the dynamics of the channel, anyway easily giving rise to a fully adaptive implementation through repeatedly adjusting the weights to follow the constant desired reference (as it is described in the next sub-Section).

The beamforming system is set to maximise the SNR, as in FIR filters optimisation, in the *Maximisation of SNR Beamformer*. The MSNR is an eigenvalue problem, and the filter is often named *eigenfilter* or *eigenbeamformer*, since the equivalent FIR impulse response coefficients are equal to the elements of an eigenvector, [Hayk96], [LiLo96], [LiRa99], [VeBu88]. The second order statistics that need to be known refer to the DesS, $\mathbf{R}_x = E[\mathbf{x}\mathbf{x}^H]$, and noise, $\mathbf{R}_n = E[\mathbf{n}\mathbf{n}^H]$, correlation matrices. It is assumed that the signal and noise components are not correlated. If the noise contribution, additive white and with zero mean, can be viewed as a single input, then the noise power will be given by $N = \sigma_n^2 \mathbf{w}^H \mathbf{w}$, where σ_n^2 is the variance of the white noise at the input. The output of the system is given by (3.3), and the objective is to find the optimum weight vector, \mathbf{w}_{opt} , that leads to the maximum SNR:

$$SNR_{opt,max} = \frac{\mathbf{w}_{opt}^H \mathbf{R}_x \mathbf{w}_{opt}}{\mathbf{w}_{opt}^H \mathbf{R}_n \mathbf{w}_{opt}}. \quad (3.19)$$

Convergence is subject to the constraint $\mathbf{w}^H \mathbf{w} = 1$. The optimum weight vector will be given by the eigenvector that corresponds to that maximum eigenvalue of matrix \mathbf{R}_x , $\mathbf{w}_{opt} = \mathbf{q}_{EVmax}$, [Hayk96]. In the case of a single DesS AoA, totally uncorrelated to all unwanted contributions, such eigenvector will directly reflect the DesS AoA. Anyhow, in the application to the fading mobile communication

channel, the selection of a single eigenvector by itself may be restrictive, not exploiting diversity, [BrUN01].

In the case of the MSNR, with a NB signal, and DesS signal arriving at a known AoA, ϕ_{DesS} , the optimum weight vector relates to the corresponding steering vector, $\mathbf{a}(\phi_{DesS}, \Omega_{DesS})$ through (3.20), where α is a non-zero complex constant, e.g., [VeBu88],

$$\mathbf{w}_{opt} = \alpha \mathbf{R}_n^{-1} \mathbf{a}(\phi_{DesS}, \Omega_{DesS}) . \quad (3.20)$$

Additionally, if the corresponding interference-plus-noise second order statistics are known, then SINR improvement is also possible, the total undesired contribution being calculated as $\mathbf{w}_{opt}^H \mathbf{R}_n \mathbf{w}_{opt}$, with \mathbf{R}_n including the contribution from NDesI sources. In that case, with the inherent limitation that results from the fact that the number of interfering sources is usually much greater than the number of array elements, M , with powers equivalent to that of the DesS, the solution given by (3.20) also provides SINR improvement, [Wint84].

Again, as with the last optimum combining cases, the MSNR optimising problem does not involve dynamic functioning by itself. Also, especially in the case that DesS, NDesI or noise sources are correlated, its results will not lead to the best SNR or SINR solution, the beams and nulls being wrongly directed. Moreover, if more than one DesS AoA exists, then the corresponding powers may not be fully considered, since all the available DesS power is not captured. Finally, direction estimation may be additionally required, which by itself renders more complexity and the possibility of additional error.

To understand the *Linearly Constrained Minimum Variance Beamformer* problem, it is necessary to keep Linear Optimum theory in mind, starting with the *Wiener* filter. And to do this, one should summarily go through the *method of Lagrange multipliers*, [Hayk96].

With a Wiener filter¹², the mean-square value of an estimation error is minimised, where no constraints limit the optimisation process. Also, the application of such filter requires the knowledge of the desired response. In some applications, the desired response is not available and it is desirable to obey to a specific constraint (involving either one or more variables). Take for example the beamformer response, given by (3.8). Then, the optimum weight vector, \mathbf{w}_{opt} , needs to be calculated so as to minimise the mean-square value at the filter/beamformer output, subject to the following linear constraint:

$$\mathbf{w}^H \mathbf{a}(\phi, \Omega) = g , \quad (3.21)$$

where g is a complex-valued gain. The *linearly constrained* beamformer will be NB if it satisfies the minimisation curve and the constraint at a single frequency, or close to it.

¹² The Wiener filter is also known as *Minimum Mean Square Error* (MMSE) filter. It is seen as *Linear Prediction* in [Hayk96], and as a *Statistically Optimum* technique in [LiRa99].

The LCMV problem is developed using the *method of Lagrange multipliers*. A real-valued function, $f(\mathbf{w})$, is the mean-square value of the beamformer output:

$$f(\mathbf{w}) = \text{E} \left[|y(n)|^2 \right] = \mathbf{w}^H \text{E} \left[\mathbf{x}(n)\mathbf{x}(n)^H \right] \mathbf{w} = \mathbf{w}^H \mathbf{R}_x \mathbf{w} . \quad (3.22)$$

This function is minimised, subject to a complex constraint related to that indicated in (3.21):

$$c(\mathbf{w}) = \mathbf{w}^H \mathbf{a}(\phi, \Omega) - g = 0 + j0 . \quad (3.23)$$

The problem is converted into a non-constrained optimisation of a real-valued function, $J(\mathbf{w})$, which relates both $f(\mathbf{w})$ and $c(\mathbf{w})$:

$$J(\mathbf{w}) = f(\mathbf{w}) + \text{Re}[\lambda_{LM}^* c(\mathbf{w})] , \quad (3.24)$$

the complex parameter λ_{LM} being called the *Lagrange multiplier*. After having defined the cost function $J(\mathbf{w})$, it is minimised through calculating the gradient vector and equalling to zero, in order to determine its minimum. It is easily shown that the optimum weight vector will be a function of λ_{LM} and equal to:

$$\mathbf{w}_{opt} = -\frac{\lambda_{LM}}{2} \mathbf{R}_x^{-1} \mathbf{a}(\phi_{DesS}, \Omega_{DesS}) . \quad (3.25)$$

By using the linear constraint presented in (3.21), the Lagrange multiplier is then determined, leading to the ultimate calculation of the optimum weight vector:

$$\mathbf{w}_{opt} = \frac{g^* \mathbf{R}_x^{-1} \mathbf{a}(\phi_{DesS}, \Omega_{DesS})}{\mathbf{a}^H(\phi_{DesS}, \Omega_{DesS}) \mathbf{R}_x^{-1} \mathbf{a}(\phi_{DesS}, \Omega_{DesS})} . \quad (3.26)$$

For a zero-mean input and output, *minimum variance* is equal to *minimum mean-square value*, i.e., the optimisation leads to minimisation of the beamformer output power, being fundamentally constrained by (3.21).

The *Minimum Variance Distortionless Response* (MVDR) beamformer is a special case of LCMV beamforming, where g is set to unity. This would mean that the beamformer is limited to providing a distortionless response, along the AoA span. The optimum weight is then calculated from (3.26). In practical terms, the system will convey the DesS, with unit response, while minimising the output variance in the angular domain, i.e., interference and noise originating at other angles, other than the DesS AoA, are attenuated. In this way, the beamforming diagram will tend to have sharper peaks and higher resolution. In fact, the MVDR beamformer algorithm is an important type of the *superresolution* algorithms. The function that is minimised can be set as a function of the AoA, ϕ , being seen as a *MVDR spatial power spectrum*:

$$S_{MVDR}(\phi) = \frac{1}{\mathbf{a}^H(\phi) \mathbf{R}_x^{-1} \mathbf{a}(\phi)} . \quad (3.27)$$

Furthermore, though the NB LCMV beamformer has been described by means of a single constraint, as indicated in (3.21), it is possible to use a set of constraints where not only one $\mathbf{a}(\phi_l, \Omega_{DesS})$ is used:

$$[\mathbf{a}(\phi_1, \Omega_{DesS}) \cdots \mathbf{a}(\phi_L, \Omega_{DesS})]^H \mathbf{w} = \mathbf{C}^H \mathbf{w} = \mathbf{g} , \quad (3.28)$$

where the $M \times L$ matrix \mathbf{C} is called the *constraint matrix*, whose L columns are the L constraints, and \mathbf{g} is a vector of dimension L . The *Generalised Sidelobe Canceller* (GSC) is a multi-constraint problem, that can be converted into an unconstrained one, constituting a standard optimum filtering problem, according to the standard Wiener form. The GSC will have a weight vector divided in two – the *quiescent vector* (satisfying the constraints) and an *unconstrained* one (which can be chosen in order to minimise noise and interference at reception, or transmission away from the wanted directions), [Hayk96], [VeBu88].

3.4 Adaptive Beamforming Processing

3.4.1 Most Important Beamforming Algorithms

The adaptive algorithms considered to be the references to base the development of the present beamforming study are the SD, the LMS, *Recursive Least Squares* (RLS), *Constant Modulus Algorithm* (CMA), *Sample Matrix Inversion* (SMI), *Conjugate Gradient algorithm* (CG) and *Neural Networks* (NN) (keeping in mind that NNs are not just *algorithms*, but a whole family of processes). For the current needs, this description focuses on these in a comparative manner, in order to finally argue for the choice of the algorithm and its application. These are listed as being some of the most widely and specifically used for beamforming, even beyond the wireless mobile communications scene, following the definition presented in Section 3.1. This overall view is fundamental to understand the choice/exclusion of an algorithm for this study's aims, in sub-Section 5.2.4.

In general, depending on the type of sampling and estimation, there are two types of data acquisition: *block-sample adaptation* and *sample-by-sample adaptation*. In the former case, weights are calculated based on a temporal sampled data window, whereas the latter implies the calculation of weights as the data is sampled. The block adaptation can be used in a non-stationary application, as long as the weights are reprogrammed periodically and the block lengths are chosen to ensure the pseudostationarity of the input data.

Before going forth with the description of the mentioned adaptive algorithms, it is important to understand the relevance of making use of available referential sources. As it will be seen, as in the case of optimum beamforming methods, some of the described adaptive algorithms consider such information, while others do not. The use of an explicit referential signal, e.g., a training sequence or a signal pilot, may be a requisite, resulting in a *non-blind* method. Alternative techniques have been

developed, being referred as being *blind*. These are able to obtain their own reference, based on *indirect* characteristics of the DesS, e.g., the expectancy of a constant envelope of the DesS, a decision process dependent on the feedback outputs of the adaptive filter/beamformer and cyclostationarity. Examples of these algorithms are the CMA (described further on), the *Decision-Directed Algorithm* and *Cyclostationary Algorithms*, [LiLo96], [PaPa97], [KrVi96].

A reference signal, closely correlated to the DesS, or the *signal-of-interest*, can be of two types: a *spatial* or a *temporal* reference. The former mainly refers to directional information of the DesS, whereas the latter may be a pilot signal, or a known sequence highly correlated in time to the DesS, but with low correlation to the interferences, e.g., a pseudo-random CDMA code. [Laur00] presents a good overview of filtering methods for adaptive antennas, going beyond the strict beamforming concept that is hereby assumed (as described in Section 3.1). Anyhow, along that broader view, the concept of *Semi-Blind* processing algorithms is conveyed. *Semi-blind estimation* defines that which makes use of references that a certain standard already uses for other purposes, e.g., channel estimation, signal separation, estimation and detection.

The type of reference possibly available depends on the overall system within which the beamforming will be working. In the case that an explicit form of a reference signal is available, depending on such system, it should be used to all its possible extent, extracting from it the maximum referential information, [LiLo96]. This will result in lower beamformer overall complexity and cost, simpler adaptive algorithm, higher accuracy, and faster convergence. This is why the training sequence in a GSM burst, or a code in UMTS or in CDMA-based MBSs should be used for such. In [CHSK76], a simple means of reference extracting, a *reference generation loop*, was presented, proving the special suitability of CDMA for beamforming adaptive algorithms. In [KuTB02], a real-time DoA-based SA application is described for GSM 1800, being based on DoA estimation algorithms, nevertheless making use of the available midambles to identify the MTs DoAs, in order to complete tracking and form the final array patterns.

3.4.2 Method of Steepest Descent

The Method of Steepest Descent is the basis for gradient-based algorithms. It is a recursive method, in the sense that it is based on calculating a new weight vector, evolving from the previous one, starting with a specific initialisation vector. It leads to the Wiener solution, while evolving through the surface of the ensemble average of the squared estimation error.

Just as in the Wiener (or MMSE) filter, the SD is based on minimising the ensemble average of estimation error. Considering the beamformer input, $\mathbf{x}(n)$:

$$\mathbf{x}(n) = [x(n) \quad x(n-1) \quad \cdots \quad x(n-M+1)]^T \quad (3.29)$$

as a vector of samples of a stochastic process of zero mean, and the output, $y(n)$, to be related through (3.3), and representing the assumed known desired input by $d(n)$, then the estimation error is defined as:

$$\xi(n) = d(n) - y(n) = d(n) - \mathbf{w}^H \mathbf{x}(n) . \quad (3.30)$$

The $y(n)$ output will be an *estimate* of $d(n)$, corresponding to the input $\mathbf{x}(n)$. Since the problem must now be applicable to a non-stationary channel, the weights vector may vary with n , as well as the estimation error and the function to be minimised, $J(n)$:

$$J(n) = E[\xi(n)\xi^*(n)] = \sigma_d^2 - \mathbf{w}^H(n)\mathbf{r}_{xd} - \mathbf{r}_{xd}^H \mathbf{w}(n) + \mathbf{w}^H(n)\mathbf{R}_x \mathbf{w}(n) , \quad (3.31)$$

where σ_d^2 is the variance of $d(n)$, and \mathbf{r}_{xd} is the cross-correlation, with $\mathbf{r}_{xd} = E[\mathbf{x}(n)d^*(n)]$. The mean-squared error is the minimised cost function of the weights, $J(n)$, which can be expressed in an $(M+1)$ -dimensional surface, with M DoFs¹³, [Hayk96]. Such is called the *error-performance surface*, whose shape is determined by the eigenstructure of \mathbf{R}_x , [VeBu88]. If \mathbf{R}_x is non-singular, such optimum weight vector is unique and it is equal to the Wiener solution:

$$\mathbf{R}_x \mathbf{w}_{opt} = \mathbf{r}_{xd} \Leftrightarrow \mathbf{w}_{opt} = \mathbf{R}_x^{-1} \mathbf{r}_{xd} . \quad (3.32)$$

The left side of (3.32) are called *Wiener-Hopf equations*. The MMSE at that point is found to be:

$$\min_{\mathbf{w}} \{J\} = \sigma_d^2 - \mathbf{r}_{xd}^H \mathbf{w}_{opt} . \quad (3.33)$$

The Wiener optimum can be calculated through solving the Wiener-Hopf equations, e.g., [Hayk96]. The large number of data samples and tap weights will imply a large number of products, though. The SD helps to overcome this problem. It can be well understood through visualising the *bowl-shaped* error-performance surface (in the case of a 2×1 weight vector), and moving in such surface along the direction of higher MMSE difference, i.e., along the gradient at such point. If $\nabla J(n)$ is the gradient vector at discrete instant n , the new weight vector estimate, at time $n+1$ is calculated:

$$\mathbf{w}(n+1) = \mathbf{w}(n) + \frac{1}{2} \mu [-\nabla J(n)] , \quad (3.34)$$

where μ is a positive real-valued constant that determines the convergence step. It can be shown from (3.31) that the gradient is given by:

$$\nabla J(n) = -2\mathbf{r}_{xd} + 2\mathbf{R}_x \mathbf{w}(n) . \quad (3.35)$$

If \mathbf{R}_x and \mathbf{r}_x are known, then the gradient can be used and (3.34) leads to:

¹³ The number of DoFs may be seen as $2M$ if the weights are complex, with information on modulus and phase, [Vaug88].

$$\mathbf{w}(n+1) = \mathbf{w}(n) + \mu[\mathbf{r}_{xd} - \mathbf{R}_x \mathbf{w}(n)] . \quad (3.36)$$

To calculate the optimum and the corresponding MMSE, the method follows as described: the initial value $\mathbf{w}(0)$ is set, usually equal to $\mathbf{0}$; the gradient vector, ∇J , is calculated, where the derivatives are with respect to the real and imaginary parts of the vector $\mathbf{w}(n)$ at discrete instant n , where n is equal to the iteration number; the estimated new weight vector is calculated from the latter one, subtracting the calculated gradient vector; the process is repeated for each newly calculated weight vector, $\mathbf{w}(n+1)$.

To study the SD deeper, covering stability matters and examples, references [Hayk96] and [WiSt95] are suggested.

3.4.3 Least-Mean-Square Algorithm

The Least-Mean-Square Algorithm is a linear adaptive filtering algorithm, widely used for its simplicity and low computational requirements, [Hayk96], [WiSt95], deserving some attention. It does not require the calculation of correlation matrices nor of matrix inversions. It is considered to belong to the *stochastic gradient* algorithm family. As the SD, it develops on the error-performance curve, according to a gradient vector. The main difference is that the LMS does not involve a deterministic gradient, where \mathbf{R}_x and \mathbf{r}_{xd} are known in (3.35), but their instantaneous estimates.

If the input vector, $\mathbf{x}(n)$, and the desired response, $d(n)$, are known, the LMS is generally the best choice in linear adaptive signal processing, [WiSt95]. Though, for mobile communications it does not perform as well as other algorithms due to its slow convergence speed in cases of fast-varying signal/channel characteristics. Additionally, the convergence speed of the LMS is directly dependent on the eigenvalues of \mathbf{R}_x – smaller time constant corresponds to larger eigenvalues. Since the maximum and the minimum eigenvalues normally correspond to the strongest and the weakest sources¹⁴, respectively, the LMS will imply that a strongest source will be cancelled before a weaker one, [Goda97].

The algorithm is made up of three steps, which are repeated through a certain number of n iterations. The discrete time variable will then also refer to the iteration number. The M tap inputs that constitute the input vector, belonging to the M -multidimensional space, are the inputs of the transversal filter (in this case, the ULA beamformer), constituting the first step – the filtering process. The values that build up the weight vector are estimates resulting from the n^{th} iteration, and they will

¹⁴ Each eigenvalue is a ratio of power-related terms, limited by the minimum and maximum Power Spectral Density (PSD) of the corresponding discrete time stochastic process. As M tends to infinity, the maximum λ_{EVi} tends to the PSD maximum, while the minimum λ_{EVi} approaches the minimum PSD. Each steering vector can be represented in the vectorial space defined by an eigenvector orthonormal base. The largest eigenvalue corresponds to the largest eigenvector, which may constitute the largest steering vector, corresponding to the strongest signal.

near the Wiener solution, (3.32), as the number of iterations approaches infinity, for a wide sense stationary channel and independent over time successive input vectors, [WiSt95].

Assuming that the desired signal, $d(n)$, is known, the second stage follows, calculating the estimation error, $\xi(n)$, according to (3.30). Therefore, the filter output is seen as the estimate to $d(n)$. Finally, the *adaptive weight control stage* follows, where the product of $\xi(n)$ and current input data, $\mathbf{x}(n)$ is calculated, providing the weight correction, to the m^{th} tap. By finally using a step-size factor, μ , as in the SD, the next $n+1$ weight iteration is calculated:

$$\mathbf{w}(n+1) = \mathbf{w}(n) + \mu \mathbf{x}(n) \xi^*(n) = \mathbf{w}(n) + \mu \mathbf{x}(n) [d^*(n) - \mathbf{x}^H(n) \mathbf{w}(n)] . \quad (3.37)$$

Comparing with (3.34) and (3.36), one sees that the gradient vector, $\nabla J(n)$, is calculated through $\mathbf{x}(n) \xi^*(n)$, not involving ensemble averages – the m^{th} element of $\nabla J(n)$ is given by $\mathbf{x}(n-m) \xi^*(n)$, without the expectation operator that exists in the SD. Notice also how the estimation error is calculated based on the current weight vector estimated in the previous cycle – the future *instantaneous* estimates are based on past *instantaneous* estimate calculations, not resulting from deterministic corrections to the weight vector.

An important result of not resorting to the calculation of ensemble averages is that the weight calculation is subject to what is called *gradient noise*, [Hayk96], or *perturbation noise*, [Goda97]. As mentioned, in the SD, the calculation of the tap-weights vector involves the deterministic evolution through the error-performance surface, leading to the Wiener optimum solution. The LMS will therefore work differently, due to the gradient noise – the calculated weight vector, $\mathbf{w}(n)$, will not reach the Wiener optimum, though converging towards it, performing a *random motion* around it, [Hayk96], [WiSt95]. The *excess-mean-squared error* will therefore be present, corresponding to the final weight vector, an inherent error that results from the simple nature of LMS.

It must be noted that the step-size factor, μ , affects the overall low-pass filter nature of the LMS. Being a controllable parameter, it defines both the convergence speed and the gradient noise¹⁵. In this way, a suitable μ must be found to maximise performance. In fact, the definition of μ involves two conflictive behaviours: on one hand, larger steps imply reaching the vicinity of the solution faster, but also wandering around it and causing large *misadjustment*¹⁶; on the other, smaller μ will mean lower error, but slower convergence.

The instantaneous values involved in the LMS exhibit large variances, [Hayk96]. Nevertheless, as mentioned before, these are controllable depending on μ , and the feedback nature

¹⁵ It must be kept in mind that slow convergence in a non-stationary environment will imply the estimated weights to lag behind the optimal weights, a phenomenon called *weight vector lag*.

¹⁶ In [WiSt95] *misadjustment* is defined as the ratio of the excess MSE to the MMSE. It is a measure of how close the adaptive process nears the Wiener optimum. With the LMS, this parameter increases linearly with the number of taps, whereas in the SD it increases with the square of such number.

results in a good trade-off between an inherent optimisation error and an effective convergence by means of a simple algorithm. From (3.37), it can be seen that the number of complex products is $2M+1$, the same number for complex summations, for each iteration.

As far as performance comparison is concerned, the LMS is compared with the SD in [WiSt95]. Specifically, it can be mentioned that: for a given μ and number of elements, the LMS will imply smaller misadjustment; the LMS implies a much lower adaptation time than the SD, for the same number of taps. It is further stated that the efficiency of the LMS approaches the theoretical limit for adaptive algorithms when the eigenvalue spread¹⁷ is near or equal to one. On the other hand, if the eigenvalue spread is large, the convergence process can be very slow.

There are other stochastic gradient algorithms closely related to the LMS, having different performances. The LMS hereby described is named *Unconstrained* LMS, but there is also the *Normalised* LMS and the *Constrained* LMS, besides several variable step-size, frequency-domain and other improved LMS versions, [Goda97]. The general point of such improved LMS versions is to lower the weight vector or gradient variance, making the use of the larger step-sizes possible, converging faster while achieving lower misadjustments and not risking algorithm stability.

Algorithm stability issues, step-size factor and performance evaluation are carefully addressed in [Hayk96], [WiSt95], including examples. In [Goda97], implementation matters are addressed, covering finite-precision arithmetic and real/complex implementation. An example of the application of the LMS together with the MVDR beamformer is presented in [Hayk96].

3.4.4 Recursive Least Squares

As the name indicates, the Recursive Least Squares algorithm can be seen as an extension of the LS method in which recursion is included in the process – the new weight vector estimate, at iteration $n+1$, will result from an LS estimate obtained at iteration n , after the arrival of new data, [Hayk96]. The RLS develops on past received data, accounting for the whole data from the initialisation instant onwards.

Let n designate the iteration number, referring to the total iterations from the instant of initialisation. The RLS will base its calculations on the data arrived at instant i , before the iteration number n , i.e., $1 \leq i \leq n$. In the case of the LS, the cost function is the sum of error squares, for a certain time interval (due to the application of *data windowing*), whereas the RLS accounts for the sum of weighed error squares until instant n :

$$J(n) = \sum_{i=1}^n w_e(n,i) |\xi(i)|^2, \quad (3.38)$$

¹⁷ The *eigenvalue spread* is defined as the ratio between the maximum and the minimum eigenvalues of a matrix.

where $w_e(n,i)$ is the i^{th} error square weight, for the n^{th} iteration, and $\xi(i)$ is the estimation error. As in the Wiener filter and in the LMS, $\xi(i)$ is defined as in (3.30). Also, the filter output, $y(i)$, is equal to $\mathbf{w}^H(n)\mathbf{x}(i)$. The $M \times 1$ filter input vector is $\mathbf{x}(i) = [x(i) \ x(i-1) \ \cdots \ x(i-M+1)]^T$, obtained at instant i , and $\mathbf{w}(n)$ is composed by the M tap weights calculated in the n^{th} iteration. The process of calculation of the cost function requires that these tap weights used to calculate $J(n)$ do not change in time during the interval for which $J(n)$ is defined.

The *exponential weighting factor*, λ_{RLS} , is real, positive and lower than 1 (for all n and i), being related to $w_e(n,i)$ as follows:

$$w_e(n,i) = \lambda_{RLS}^{n-i} , \quad (3.39)$$

where λ_{RLS} is lower than, but close to, 1. In this way, for a given n , the cost function sum will have lower contributions from errors with large $n-i$ and larger contributions for smaller $n-i$, i.e., the older errors are gradually *forgotten*. This is why $w_e(n,i)$ is also called *forgetting factor*. By gradually considering less the farthest errors in time, the algorithm does afford to follow statistical variations of a non-stationary channel. The quantity $(1-\lambda_{RLS})^{-1}$ is a measure of the *memory* of the process. In the case of the LS, where $\lambda_{RLS} = 1$, the memory is *infinite*, meaning that all the squared errors have the same weights, being equally considered.

Recalling the *Wiener-Hopf* equations, and in particular noticing how the signal correlation matrix, \mathbf{R}_x , and the cross-correlation between input and desired signals, \mathbf{r}_{xd} , are involved, one sees that with the RLS a similar group of equations is formed, leading to the calculation of a newly estimated value, $\mathbf{w}(n)$, closer to the optimum:

$$\hat{\mathbf{R}}_x(n)\mathbf{w}(n) = \hat{\mathbf{r}}_{xd}(n) , \quad (3.40)$$

where $\hat{\mathbf{R}}_x$ is the correlation matrix and $\hat{\mathbf{r}}_{xd}(n)$ is the cross-correlation vector estimates between inputs and desired response, defined below:

$$\hat{\mathbf{R}}_x(n) = \sum_{i=1}^n \lambda_{RLS}^{n-i} \mathbf{x}(i)\mathbf{x}^H(i) , \quad (3.41)$$

$$\hat{\mathbf{r}}_{xd}(n) = \sum_{i=1}^n \lambda_{RLS}^{n-i} \mathbf{x}(i)d^*(i) . \quad (3.42)$$

The forgetting factor also applies to the calculation of $\hat{\mathbf{R}}_x$ and $\hat{\mathbf{r}}_{xd}(n)$, which are summations of weighted past correlations and cross-correlations, respectively. Besides intuitively understanding that the $\hat{\mathbf{R}}_x$ and $\hat{\mathbf{r}}_{xd}(n)$, resulting from the n^{th} iteration, can be obtained from those of the iteration $n-1$, it can easily be shown that such is so:

$$\hat{\mathbf{R}}_x(n) = \lambda_{RLS} \hat{\mathbf{R}}_x(n-1) + \mathbf{x}(n)\mathbf{x}^H(n) , \quad (3.43)$$

$$\hat{\mathbf{r}}_{xd}(n) = \lambda_{RLS} \hat{\mathbf{r}}_{xd}(n-1) + \mathbf{x}(n)d^*(n) . \quad (3.44)$$

As in other algorithms, the calculation of the tap weight vector estimate in (3.40) can be done through the calculation of the inverse of matrix $\hat{\mathbf{R}}_x$, but such *brute force* method requires too a large computational effort. Another means of calculating $\mathbf{w}(n)$ is recursively, minimising computational effort, in fact building up what is the RLS algorithm. The calculation of $\hat{\mathbf{R}}_x^{-1}$ is possible by applying the *matrix inversion lemma* to (3.43), leading to the recursive equation for $\hat{\mathbf{R}}_x^{-1}$, [Goda97], [Hayk96]:

$$\hat{\mathbf{R}}_x^{-1}(n) = \lambda_{RLS}^{-1} \hat{\mathbf{R}}_x^{-1}(n-1) - \frac{\lambda_{RLS}^{-2} \hat{\mathbf{R}}_x^{-1}(n-1) \mathbf{x}(n) \mathbf{x}^H(n) \hat{\mathbf{R}}_x^{-1}(n-1)}{1 - \lambda_{RLS}^{-1} \mathbf{x}^H(n) \hat{\mathbf{R}}_x^{-1}(n-1) \mathbf{x}(n)} . \quad (3.45)$$

To be able to describe the algorithm itself, some definitions are put forward:

$$\mathbf{P}(n) = \hat{\mathbf{R}}_x^{-1}(n) , \quad (3.46)$$

$$\mathbf{k}(n) = \mathbf{P}(n) \mathbf{x}(n) , \quad (3.47)$$

$\mathbf{P}(n)$ being the *inverse correlation matrix* estimate, and $\mathbf{k}(n)$ the *gain vector*. By dealing with (3.44) to (3.47), one arrives at the equations that constitute the RLS computation:

$$\mathbf{k}(n) = \frac{\lambda_{RLS}^{-1} \mathbf{P}(n-1) \mathbf{x}(n)}{1 + \lambda_{RLS}^{-1} \mathbf{x}^H(n) \mathbf{P}(n-1) \mathbf{x}(n)} , \quad (3.48)$$

$$\xi(n) = d(n) - \mathbf{w}^H(n-1) \mathbf{x}(n) , \quad (3.49)$$

$$\mathbf{w}(n) = \mathbf{w}(n-1) + \mathbf{k}(n) \xi^*(n) , \quad (3.50)$$

$$\mathbf{P}(n) = \lambda_{RLS}^{-1} \mathbf{P}(n-1) - \lambda_{RLS}^{-1} \mathbf{k}(n) \mathbf{x}^H(n) \mathbf{P}(n-1) . \quad (3.51)$$

These are hereby presented in the order that these should be calculated, for each n . The algorithm is initialised by setting $\mathbf{P}(0) = \delta_{RLS}^{-1} \mathbf{I}$, where δ_{RLS} is a small positive constant, and \mathbf{I} is a $M \times M$ identity matrix, and $\mathbf{w}(0) = \mathbf{0}$. Some comments on these follow: the *priori estimation error*, $\xi(n)$, is so called since the estimate of the desired response, i.e., the $\mathbf{w}^H(n-1) \mathbf{x}(n)$ inner product, is based on the previous LS estimate (recall that in the SD and LMS algorithms, the estimation error is a *posteriori estimation error*, where the corresponding inner product involves the *actual* LS estimate); the calculation of the step-size parameter used in the LMS algorithm, μ , is replaced by the calculation of the gain vector, $\mathbf{k}(n)$, which is a simple scalar division involving a fast recursive calculation of $\hat{\mathbf{R}}_x^{-1}(n)$.

As far as the convergence of the RLS is concerned, it is usually one order of magnitude faster than that of the simple LMS, in case the SNR is high, at the expense of larger computation complexity, [Hayk96], [LiLo96]. It is also independent of the eigenvalue distribution of the correlation matrix,

[Goda97], [Hayk96]. Concerning initialisation, convergence and general performance, a detailed analysis is provided in [Hayk96], by means of some examples.

In [WaCr94], the application of RLS to a CDMA mobile environment is presented, evaluating BER performance in the case of existing intra- and inter-cell interferers.

3.4.5 Constant Modulus Algorithm

Also called *Godard algorithm*, the Constant Modulus Algorithm is a particular case of the *Bussgang* algorithms, [Hayk96], [LiLo96], [LiRa99]. These are *blind adaptive techniques*, in the sense that these develop independently from training sequences, adapting by trying to restore a known property of the received signal. Though these have been developed for equalisation, they can apply to adaptive beamforming. In fact, the CMA was initially proposed to compensate for fading of constant envelope signals. In the case of the CMA, the property of low modulus variation is used, meaning that the CMA may be applied to signals with FM, Phase-Shift-Keying, Frequency-Shift-Keying, Quadrature Amplitude Modulation, Gaussian-filtered Minimum Shift-Keying, or M -ary Phase-Shift-Keying. In this sense, the CMA can be used for the UMTS modulation scheme, with Quadrature Phase-Shift-Keying (QPSK).

As previously mentioned, the objective of the CMA is to minimise a cost function, which implies that the beamformer output, $y(n)$, has constant envelope. In this way, the CMA minimises the following non-linear constant function:

$$J(n) = \text{E} \left[(r_p(n) - |y(n)|^p)^2 \right], \quad (3.52)$$

where $r_p(n) = \text{E} \left[|s(n)|^{2p} \right] / \text{E} \left[|s(n)|^p \right]$, p is a positive integer, equal to 2 in the case of the CMA, and $s(n)$ is the transmitted signal.

In order to find the required weight vector, a SD method like the LMS can be used. To do this, one can use (3.34), and calculate the gradient of the cost function at stake. The gradient is found to be given by (3.53), [LiLo96]:

$$\nabla J(n) = -\text{E} \left[(r_p(n) - |y(n)|^p)^2 y(n) \mathbf{x}(n) \right]. \quad (3.53)$$

And, since the gradient cannot be known, the modulus of the arriving signal can be scaled to 1. The cost function, $J(n)$, then provides the measure of the amount that the output deviates from the unity modulus condition. The instantaneous estimate can be used:

$$\nabla J(n) \approx -\left(1 - |y(n)|^p\right)^2 y(n) \mathbf{x}(n). \quad (3.54)$$

Likewise, from (3.34), the new weight vector can be determined:

$$\mathbf{w}(n+1) = \mathbf{w}(n) + \mu \left(1 - |y(n)|^p\right)^2 y(n) \mathbf{x}(n) = \mathbf{w}(n) + \mu \xi^*(n) \mathbf{x}(n), \quad (3.55)$$

where the substitution for $\xi(n)$, $\xi(n) = \left(1 - |y(n)|^p\right)^2 y^*(n)$ has been carried out. The similarity of the right-hand side of (3.55) to the left-hand side of the equation defined for the LMS, (3.37), is clear. The practical result of this is that the hardware used for configuration and programming of the LMS can be directly used for that of CMA, except from using different definitions of the error, $\xi(n)$.

As far as performance is concerned, some notes about the CMA should be pointed out, [LiLo96], [Hayk96]: if the CMA converges, it will converge to the Wiener solution, since the minimisation of $J(n)$ corresponds to the minimisation of the MSE in the output; with the additional magnitude control, generalising the CMA application to other than unity DesS magnitude, the weight vector will require additional scaling, making the converging process more difficult; the convergence of the CMA is not guaranteed, because $J(n)$ is *non-convex*, with possible false minima; the CMA is the most robust of the Bussgang algorithms, since the cost function is dependent on magnitude only, under steady-state conditions reaching a lower MSE and achieving good eye pattern opening in many dispersive channel cases.

Moreover, in its simplest form, the CMA is found not to be particularly adequate for CDMA systems, [Goda97], [WaCr94]. In particular, the Power Control (PC) process, inherent to preventing the near-far effect in CDMA mobile case, will affect the variation of envelopes, either per physical channel (code) or between each slot, in UMTS or CDMA-based MBSs. Therefore, PC must be combined with the CMA, not to eliminate the envelope fluctuations in which the algorithm is based. Otherwise, the CMA by itself will not be able to extract referential information to minimise $J(n)$, extracting the undesired fluctuations.

In [PaPa97], a review of CMA-based solutions is included, presenting the main problems involved with delay-spreads, time-varying channels and multi-user settings; [OSMS93] and [TMCK97] present hardware CMA implementations for mobile communications; [FuKS01] and [YoCh01] are more recent testing/simulation studies of the algorithm for mobile communications, addressing the issue of higher NDesI power relative to DesS, providing solutions for convergence reliability.

3.4.6 Sample Matrix Inversion

The Wiener solution, given by (3.32), can be approximated by using an estimate of the inverse of matrix \mathbf{R}_x . Remembering that the channel suffers frequent changes, the estimated weights can be calculated using block adaptation¹⁸, as mentioned before. Therefore, the estimates of \mathbf{R}_x and \mathbf{r}_{xd} can

¹⁸ In a block adaptation approach, a temporal window of M samples is used to calculate the n^{th} beamformer output. The $n+1$ iteration would be calculated based on the next sampling window. It must be noticed that n will then be a relative integer, independent of both the actual block-sampling period and the actual sample index along the array elements. Along the calculation of the $n+1$ iteration, $\mathbf{x}(n)$ and $d(n)$ are assumed to result from a stationary, or static, channel.

result from a simple arithmetic averaging calculation, an array data block that forms a total of N_s data vectors, [Goda97], [LiLo96], [WuHa95]:

$$\hat{\mathbf{R}}_x = \frac{1}{N_s} \sum_{i=1}^{N_s} \mathbf{x}(i)\mathbf{x}^H(i) , \quad (3.56)$$

$$\hat{\mathbf{r}}_{xd} = \frac{1}{N_s} \sum_{i=1}^{N_s} d^*(i)\mathbf{x}(i) , \quad (3.57)$$

where upper and lower window limits refer to the array *snapshot*. $\hat{\mathbf{R}}_x$ is the *sample covariance matrix* estimate, a maximum likelihood estimate of \mathbf{R}_x , [KrVi96], [ReMB74]. As a consequence, the estimate of the weight vector can be calculated, similarly to the Wiener-Hopf equations:

$$\mathbf{w} = \hat{\mathbf{R}}_x^{-1} \hat{\mathbf{r}}_{xd} . \quad (3.58)$$

As it is understood, as the size of the block or snapshot is raised, the correlation estimates approach their true value, nevertheless requiring more computational effort. The expected average loss in SNR compared to the optimum, due to using N_s data samples, is approximately less than 3 dB if the number of samples is near $2M$, recalling that M is the number of antenna elements. Such power loss reveals to be the trade-off between performance and the number of samples used in the SMI [ReMB74].

It can be said that the SMI is not a truly adaptive algorithm, in the sense that it is an open loop problem. On the whole, though, it is adaptive since it is set to produce a weight vector for each new scenario. Accordingly, it is very important to balance the need for enough N_s data samples, for each correlation matrix estimate, on one hand, and to apply the resulting calculations in time before the channel changes, on the other. Along with the input data being periodically acquired, the correlation estimate must be recomputed, depending on the rate of channel changes, or the *fading-rate* in mobile communications. In order to keep up with the required fast convergence, the calculation of the \mathbf{R}_x^{-1} may follow the matrix inversion lemma introduced with the RLS algorithm, (3.36), leading to a faster matrix calculation. The calculation can be made using a fast recursive algorithm just as with the RLS case, (3.48) – (3.51), [Goda97].

A major advantage of the SMI algorithm is that, in case that the eigenvalue spread of the sample covariance matrix is large, the performance is almost independent of it. This can result in several orders of magnitude faster convergence than the LMS, SLC and the MSNR, [LiLo96], [ReMB74]. The convergence rate will be dependent on the number of weights, being independent of the noise and interferences.

The SMI is an algorithm with a great probability of being used for beamforming in mobile communications, according to [Vaug88]. It relies on its simple conception, its fast weight calculation capabilities and its independence of eigenvalue spread, as long as the number of correlation samples is

sufficient. As far as the number of complex products is concerned, using $2M$ data samples to calculate the matrix estimate will require a number of operations of $O[M^3]$, which is much larger than other algorithms. Furthermore, the SMI will be more accurate the larger the number of input temporal samples is, being preferably larger than $2M$, [ReMB74], [Vaug88].

The SMI algorithm, with small data blocks, is compared to an eigenanalysis-based method, often called *low rank adaptive processing*, in [WuHa95]. The study concludes that the latter achieves a performance (BER as function of SNR, the number of antenna elements and number of block) near that of the optimal and better than that of the SMI case, for small N_s . An SMI-based algorithm is simulated for GSM in [Lind95]. The proposed method uses a *variable* reference signal, avoiding degradation of performance (BER) due to any offset between the symbol sampling instant and the instant for which the reference signal has been designed. The paper presents the SMI not as an innovative algorithm application in itself, but more as a chosen algorithm to work with the reference calculation method. The SMI has been implemented in hardware, using a multi-CPU/DSP system, for a Time Division Multiple Access (TDMA) at 4.096 Mb/s mobile radio system, at a carrier frequency of 3.35 GHz, and a four-element adaptive array, [ToFu00]. Again, the algorithm was chosen for its fast convergence and its particular use for high-speed transmissions. The whole system proved to successfully suppress signals on delayed paths, providing spatial diversity gain on frequency-selective channels, for independent Rayleigh fading.

3.4.7 Conjugate Gradient

The Conjugate Gradient algorithm has been well defined and described in the recent years as an alternative to the widely used LMS and RLS. With the argument of not requiring matrix inversions and avoiding stability problems, the Conjugate Directions type of algorithms, such as the CG, have been conceived for solving linear equation systems, [HeBK99], [Goda97]. The classical paper by Shewchuk [Shew94], and [GoLo96], referenced widely by several other papers, explain the CG thoroughly and in the most direct manner, not focusing on any specific application. For a deep understanding of the algorithm, the reading of these is suggested.

The method is used to solve the $\mathbf{X}\mathbf{w} = \mathbf{d}$ equation system in order to obtain \mathbf{w} . In the case of antenna array processing, the weight vector, \mathbf{w} , needs to be calculated, \mathbf{d} is a vector composed by N_s consecutive desired responses, $\mathbf{X} = \mathbf{U}$ is a matrix whose M columns refer to each of the M antenna array elements¹⁹, and each line corresponds to each sampling period, out of the total N_s sampling periods, [ChKi92], [Goda97]. If the received signal at the antenna array is composed by $u_{n,m} = u_m(n)$ elements, matrix \mathbf{U} is as indicated below:

¹⁹ Along the text, ‘ \mathbf{U} ’ or ‘ u ’ are used to specifically refer to antenna outputs, whilst ‘ \mathbf{X} ’ or ‘ x ’ correspond to more general inputs of a beamforming algorithm, for any application. In the particular case of the CG, ‘ \mathbf{U} ’ or ‘ u ’ are already used, making the bridge to the subsequent chapters.

$$\mathbf{U} = \begin{bmatrix} u_{1,1} & u_{2,1} & \cdots & u_{1,M} \\ u_{1,2} & u_{2,2} & \cdots & \vdots \\ \vdots & \vdots & \ddots & \vdots \\ u_{N_s,1} & u_{N_s,2} & \cdots & u_{N_s,M} \end{bmatrix} . \quad (3.59)$$

Vector \mathbf{w} is composed by M elements, corresponding to each array antenna element. Since, most probably, $N_s \neq M$, an exact solution may not exist, [ChKi92].

The cost function that is involved with such linear equation system solving is given by $J(\mathbf{w})$, called *quadratic form*:

$$J(\mathbf{w}) = \frac{1}{2} \mathbf{w}^T \mathbf{U} \mathbf{w} - \mathbf{w}^T \mathbf{d} . \quad (3.60)$$

The minimum of such quadratic form corresponds to the solution to the system, [Shew94], and also to the minimum of the sum of the squared errors given by $\mathbf{res}^H(n)\mathbf{res}(n)$, where $\mathbf{res}(n) = \mathbf{d} - \mathbf{U} \mathbf{w}$, or by $\|\mathbf{U} \mathbf{w} - \mathbf{d}\|^2$, [PaPa97], [ChKi92].

The CG belongs to the generic family of Conjugate Directions, as mentioned, where the approach is to find a group of orthogonal search directions and to choose one of these in order to minimise the error along one search direction, for every iteration, [Shew94]. The means for obtaining the search direction will define the particular Conjugate Direction method, of which the CG is one example, [HeBK99].

Theoretically, the process will converge to the solution after, at most, M steps, i.e., the CG theoretically provides the fastest convergence of all the iterative algorithms, [Goda97]. In practice, though, the existence of round-off errors implies the convergence after more than M steps, for large M , also depending on how close the initial conditions are set compared to the solution of the system, [HeBK99].

During the iterative process, residual and direction vectors, $\mathbf{res}(n)$ and $\mathbf{dir}(n)$, respectively, are updated in order to calculate the successive weight vector. The recursive equation for the calculation of this vector is similar to that used in the LMS, in (3.37):

$$\mathbf{w}(n) = \mathbf{w}(n-1) + \mu(n) \mathbf{dir}(n) , \quad (3.61)$$

in that $\mu(n)$ is a step-size parameter, here calculated for each repetition of the algorithm cycles. In this way, such step parameter will contribute to minimising the cost function in the $\mathbf{dir}(n)$ direction, in the direction of the steepest descent. Such direction is calculated to be \mathbf{U} -conjugate to the previous search directions, where $\mathbf{dir}(n+1)$ is calculated using a factor $\beta(n)$ that guarantees such orthogonality:

$$\beta(n+1) = \frac{\mathbf{res}^T(n+1)\mathbf{res}(n+1)}{\mathbf{res}^T(n)\mathbf{res}(n)} . \quad (3.62)$$

Other forms of calculation of this parameter exist, including the possibility of resetting during the convergence process, [HeBK99].

For the application of the CG to mobile communications, several versions of the CG have been proposed, e.g., [Bagh99], [ChLH97], [KaBa99]. These have been developed with the objective of reducing the number of processing products and providing sample-by-sample, as opposed to block-, processing. In [ChLH97], the CG is proposed to be calculated as an eigenvalue/vector problem, providing a *Linearised* version of the CG. As a consequence, without worsening accuracy, the number of products is severely reduced from $O[3M^2+12M]$ in the conventional CG case, to $O[16M]$. Another CG based method is suggested in [Bagh99], where sample-by-sample processing is studied, by applying a *Modified* CG, [ChWi95]. A systolic structure for VLSI implementation is also presented, further reducing the processing complexity to $O[M]$.

3.4.8 Neural Networks Implementations

According to [LiLo96], NNs are an ideal tool for use in adaptive signal processing. In fact, since 1960, with the development of the *Perceptron* and the LMS, the NN elements were first generated – Adaptive Linear Element (Adaline) and the Multiple Adaptive Linear Element (Madaline). This evolution was then guided towards adaptive filtering and signal processing, [WiLe90]. The application of NNs can result in very attractive solutions to complex problems, due to the intrinsic interconnected structure, processing efficiency and fast convergence, [SLLL95]. Such structure establishes the direct parallel between biological nervous systems and artificial NNs, consisting of a large number of simple elements with the ability to *learn* and further react according to such *learning* process. Though processing speed limitations always exist, specially during the leaning process, implementations have kept such networks small, having been successfully used to solve difficult tasks, such as those related to beamforming, e.g., [ZoCG98], [ChYC92], [SLLL95], [LiLo96] and [Goda97], and AoA estimation, e.g., [ChLa99].

The basic building blocks of a NN – the Adaline and the Madaline – are in fact the basic structure of any linear beamforming application. The same applies to the type of the parameters at stake. The main structural difference lies within the adaptive block, whose main inputs are the tap inputs, the desired response and the estimation error, and whose outputs are the array weights. This block will be responsible for the core implementation of the NN, generally providing the whole with the ability to *learn* and to *generalise* (except in the Hopfield NN). The former consists of introducing antenna element signal combinations and indicating the desired responses to the linear combiner. An adaptive algorithm then automatically tunes the weights, e.g., a closed loop gradient descent algorithm like the LMS, so that the overall outputs will be as close as desired. If the training patterns are chosen so as to give an indication of a certain statistical regularity, the network may be able of later responding to unknown inputs with small error, i.e., being able to *generalise*.

As it is outlined, then, the general use of NN will involve two major steps – the *training/learning* process and the *performance* phase. The characterisation of the overall NN performance must cover these two processes, since it may happen that the performance phase provides very fast convergence, the training process being very slow and restrictive. This may be very important, considering the application to mobile communications, where the environment variation is very large, the number and position of interfering users will vary greatly, resulting in a possible heavy search for correct training sequences and desired outputs. Periodic, on-line training may be possible, depending on the areas and the time period, so that generalisation may cover as many situations as possible.

As far as application to beamforming problems is concerned, attention is drawn to the application of the *Hopfield*-type neural network, e.g., [SLLL95], [LiLo96], [ChYC92], the Madaline III Rule (MRIII) algorithm, [Goda97], and the *Three-Layer Radial Basis Function Neural Network* (RBFNN), [ZoCG98].

The Hopfield NN described in [SLLL95] is applied to antenna array beamforming (often called *neurobeamformer*) operating with direct sequence spread-spectrum signals, for automatic tracking of the desired signal, while suppressing most of the energy from interference sources. The work involves the simulation of 8-element linear and circular antenna arrays. The system is evaluated for simple but very important cases that commonly happen in mobile communications – DesS and NDesI signals arriving at very near AoA and the existence of multipath. The paper presents the interesting integration between CDMA and a NN algorithm. The Hopfield network is a single layer, fully connected neural network with symmetric interconnections, [LiLo96], [SLLL95]. It does not require a learning phase and its convergence is comparatively fast. The weights are updated so as to minimise the MSE. The expected pseudo-random (PN) sequence is used to derive the referential desired response, similarly to the reference-generating loop presented in [CHSK76], while filtering out most of the energy from interference. In [ChYC92], a Hopfield NN is also applied to beamforming, except that a hardware implementation is put forward and that MVDR optimisation is used. The resulting MVDR-based NN analog circuit exhibits robustness, is independent of signal power level, with a computation time near 0.1 ns (for a 10 element ULA).

The application of the MRIII in beamforming is summarily described in [Goda97], covering convergence and robustness issues. The study presented in [ZoCG98] involves the application of NNs to one- and two-dimensional antenna arrays. Such implementation allows for real-time calculation of the optimum weights, unlike the RLS, LMS and SMI that require optimisation for each change of direction. Though no indications of the dynamic performance or processing time are provided, the performance results have matched the Wiener solution very well.

For further study on NNs, including the full understanding of Madaline Rule I, II and III, the Perceptron, Linear and Non-linear classifiers, Minimum Disturbance Principle and Backpropagation, [WiLe90] provides a good insight, besides the previously referred contributions.

3.5 Summary and Conclusions

A general overview of the beamforming adaptive algorithms has been presented. In order to do so, the basic notions on the vectors, matrices and common relationships involved have been described. The FIR parallel structure has been understood, either in NB or WB systems.

The need for the beamformer to work in the spatio-temporal domain has been conveyed. Some basic structures have been indicated, along with the general description of fixed beamforming networks and switched-beam systems. On this matter, an important conclusion has been drawn – at the current *state-of-the-art*, it is still not clear that adaptive arrays will wholly perform better than a switched counterpart, as far as accuracy, sensitivity to environmental effects, decalibration and weights phase errors are concerned. It is nevertheless foreseen that in 10 years' time the technology will help to resolve these matters, if not before. Partially adaptive structures have been also covered, indicating that these can be of considerable use, reducing the overall cost, computational load at the expense of larger convergence errors. It is reasoned that in mobile communications, partitioning does not result in obvious benefits, since most arrays will not necessarily use a too large a number of elements. Also, element-space beamforming approaches will be required in order to obtain full WB characteristics, needed for UMTS, and future MBSs.

The main types of data independent beamformers were described – phased arrays and generalised data independent beamformer. Also, non-adaptive statistically optimum beamforming algorithms have been superficially covered – the MSC, the RSOB, MSNR and the LCMV (including the MVDR and GSC).

The most important adaptive algorithms used for antenna beamforming are then described – the SD, LMS, RLS, CMA, SMI, CG and NNs implementations. In a first step, it has been clarified that many of these require the acquisition of a spatial and/or temporal reference. At this point, another major conclusion was obtained – there existing an explicit source of referential acquisition, it should be used to its maximum, in order to ultimately achieve the best convergence rate and accuracy. In particular, a CDMA spread-spectrum system will benefit from the inherent availability of a reference signal highly correlated with the DesS, and weakly correlated with NDesI. The conclusion here is that in a UMTS or future MBS environment, CDMA will inherently be favourable to using adaptive techniques, benefiting the most from optimum combining.

In parallel with the learning of the core algorithms, one is able to sense the importance of recursively going forth with the weight vector, or errors, or correlation matrices, or cross-correlations or other parameters' calculation. The recursivity procedure results in less demanding computational

load and faster convergence rates. Particularly, the recursive correlation matrix calculation plays a very important role among the many schemes. Besides the computational load and convergence rates, the several algorithms also vary in stability. The lastly described methods, namely the SMI, the CG and the NNs have been conceived to solve those stability, convergence, and complexity problems.

During the whole description, another problem has been naturally conveyed, regarding the dynamics of the propagation channel and the subsequent adaptation speed and sampling mode. The conclusion here is that any assumptions about static, stationary, or wide sense stationary environments and applications have to be very well evaluated and set, before any algorithm is chosen. For example, the sample-by-sample approaches, requiring low number of products, will best perform in a very dynamic mobile communications environment, but their final errors may be considerably larger than block-sample applications, which on the other hand must be sampled during a maximum allowed period. Stationarity assumptions must, therefore, be put forward, conscientiously accounting for this issue in an approximated manner.

A background on the fundamental antenna beamforming schemes and algorithms has been built, in order to better understand the choice of algorithm and the whole adaptive problem structure that is implemented in this study.

4 Implementation – the Channel and Scenarios

Simplicity is the ultimate sophistication.

— Leonardo da Vinci (1452-1519)

4.1 Specification and Implementation Perspective

This chapter is concentrated on the specification and description of the implemented SCM and related scenarios. The arguments behind the choice of the SCM are firstly presented. Then, the way in which such SCM is implemented is described, covering from the model's main physical parameters to the detailed description of the propagation scenarios, for both Micro-Cells (MiCs) and Macro-Cells (MaCs). These scenarios are individually presented, firstly, but are then directly counterpoised between themselves, through the description of comparative scenarios.

Having done so, the channel is temporally and angularly characterised, resorting to the common definition of spreads, as well as through new parameters that result from viewing the channel in its wideband and directional levels, linking these to the physical constraints behind beamforming.

The current study demands for the right channel modelling and implementation perspectives. For example, the implemented model must allow for the practical implementation of propagation scenarios, which in a whole must render statistical value. It is meant by a *propagation scenario* a morphological set of several or a single BS, and numerous interfering MTs. Therefore, the model and scenarios must involve locating MTs, so as to allow for the simulation of the important propagation cases, in terms of temporal and angular separation of DesSs. Again, this implementation must not fall in the concretisation of site-specific situations, but make use of the statistical potential of a propagation channel model, and the power of a controlled simulation process. It is only by adopting such perspective that the hereby specified and presented simulations definitely result in larger added value, relative to going forth with real-site measurements. Such measurement campaign would have to be not only considerably large, involving a large number of sites of the same morphological type, but

also engage a controlled set of MTs righteously placed within the vicinity of the considered BSs. Moreover, to achieve statistical value, the channel conditions would have to be repeatedly known and also controlled, while guaranteeing statistical independence among differing sites, and acquire enough data from several *in situ* concretisations.

Regarding the consideration of intra- vs. inter-cell interferences, or both, it is viewed that there is no need to consider the latter, keeping the objectives of this study in mind and adopting a *simple-to-complex* approach. Concerning inter-cell analysis, other system-level factors are at stake that would detract from those objectives. For that, the presented scenario approach that is adopted involves a single BS and several intra-cell active MTs. Nevertheless, the model nature and the hereby presented scenario philosophy are also flexible so as to allow the simulation of multi-cell layouts, for either pico-, micro- or macro-cells, making use of the referred statistical value that their application should involve.

4.2 Specification of the Spatial Channel Model

4.2.1 Location and Type of Model

The implementation of a propagation channel model is possible viewed from the BS or MT sides. Depending on which side beamforming is being tested, the model must be applied correspondingly, especially knowing that, according to the mobile environment, the channel may be morphologically different at the BS or MT ends (namely, in MaCs). By *Model Location* one then means in which side of the BS-MT link the model is prepared to be applied, namely characterising the arrival or departure or signals at the BS, at the MT, or both sides.

From Chapter 2, one sees that a few models explicitly consider the specificities of the MT side: Lee's Model accounts for a circle of scatterers around the MT, reflecting a MaC approach, but its perspective is centred on the BS side; the GBSBEM and CM, Elliptical Subregions Model, the Unified Model, the Modified GBSB Models and COST 259 Model explicitly consider either the BS or the MT with significant scatterers in their vicinity, for either MiC or MaC implementations. These are most of the geometrical models, benefiting from the easy distinction of scattering shapes around the BS or MT. Its application must keep in mind the possible later application of beamforming at either or both sides, and for that, it should be flexible enough to go forth with the current study at either of them. Accordingly, the application of a geometrical model will particularly be in favour of such perspective.

Additionally, the SCM must be a wideband one, therefore characterising the temporal response of the channel. The inclusion of clustering, not only in the temporal but also in the angular domains, should also be accounted for. Having these two major characteristics in mind, the decision falls into a more defined set of models.

Another matter is the characteristic of the model being general enough, so as to account for the general happenings that involve the largest power contributions, characterised both temporally and angularly. In this sense, such a model must not be site-specific, and should approximate the enormously variable propagation channel in a statistical way. Nevertheless, it should not be complex so as to imply a difficult subsequent evaluation of how beamforming performance depends on the physical nature and happenings determined by the channel. Also, such model must allow for the easy characterisation of physical level characteristics, besides understanding their relation to beamforming performance.

A SCM that inherently favours a practical perspective is, therefore, advisable. Reasoning that such requirement is justified by the application of different multi-user scenarios, the complexity of the SCM must allow for it, one again not imposing a too great a burden towards the simulations. At the same time, it is desirable that the model is backed by measurement campaigns, resulting in an assessed physical representation of the main wideband and directional channel properties.

Therefore, avoiding excessive complexity, respecting the practical applicability, the generalisation potential, its statistical meaning, and making use of some form of assessment backing are the additional main guidelines determining the choice of a propagation model.

Since the objective does not necessarily imply using MIMO schemes, MIMO modelling is not advisable. Anyhow, in fact, this study is seen as being naturally complementary towards the MIMO perspective, though not having implemented a MIMO channel model. That is possible through characterising the fundamental physical directional and wideband characteristics within the propagation channel that affect the physical constraints involved in the basic shaping of an array pattern. By developing research at the beamforming level, such evaluative contribution is then practically feasible, since one sees beamforming at a lower physical level. It is after better understanding the involved physical phenomena that one envisages a natural evolution to MIMO (see Section 8.3, Relations to the MIMO Perspective). For this, the model to be applied should also allow for its future extension towards a MIMO implementation, in order to better back that evolution.

4.2.2 Selection of the Model

After providing a complete picture of several spatial modelling philosophies in Chapter 2, and establishing the type of model that is required, one is then in the position of understanding the decision to implement a particular model. For that, the central objective of this study is permanently kept in mind – the evaluation of wideband and directional channel physical characteristics that condition beamforming interference reduction performance, analysing several multi-user scenarios in a UMTS and other MBSs-directed approach.

Following the previous reasoning, attention is then drawn towards the models that reflect the combination of several effects, unifying the contributions from other simpler model cases: the

Elliptical Subregions Model, the Unified Model, the Combined GBSB and GWSSUS Model, the Modified GBSB Models, and the COST 259 SCM. By combining several simpler models, these models are more complete in terms of modelled phenomena. All of these explicitly allow for the geometrical distinction of the BS and MT sides, in case of MaCs. Finally, for the present study objectives, either the Elliptical Subregions Model, or the Modified GBSB Models should be applied, for their greater relative simplicity.

For this study, the objective is clearly not generating a new model, but making use of an implementation of one. Therefore, an additional factor that determines the choice of a model is its practical availability. As a direct consequence, in agreement with all the previous arguments, the Modified GBSB Models are used, for both MaC and MiC situations. It is a model that still requires a larger assessment study, though having gone through measurement and statistical tuning campaigns, [MPKZ00], [DGVC03]. Anyhow, it does result from assessment campaign efforts, as is prone to future refinements. Additionally, its implementation allows for the change of several scenario parameters, and is also prone to the practical generation of multi-user propagation scenarios, not only in intra- but also in inter-cell interference frameworks. Besides, such model has proved to be flexible enough to be extendable to MIMO, [DGVC03].

Finally, it is important to understand that through going forth with the implementation of a certain model, if the fundamental conclusions that result from the evaluation of beamforming performance translate the basic physical happenings within the channel, then the same conclusions would necessarily be reached through using another model of similar type. This would be a confirmation of the profoundness and general nature of the conclusions reached in this study.

4.3 Spatial Channel Model Implementation

4.3.1 General Assumptions and Considerations

The assumptions put forward along with the implementation of several SCMs, including the GBSBEM and CM versions, have already been generally pointed out in the beginning of Chapter 2. Anyhow, it is important to go through some of them in more detail, as well as adding any that may be specific of the chosen models.

The GBSBEM and CM, and their Modified variants, involve the generation of complex envelopes that result from the arrival of several f_c carrier components from within the scattering region at stake, travelling between an MT and a BS. The outputs of the model may further be filtered, either angularly or temporally, resulting in low-pass equivalents, according to adjustable resolutions. Being propagation channels, no antenna gains or phases are introduced, confining the channel effects to path-loss and reflections within the medium.

The considered signals are seen as planar waves, independently of the distances involved, either between BS and MT, or among terminals and any of the scatterers. Waves are assumed to travel solely within the horizontal plane, within which all scatterers are distributed as well as the BS and MT are positioned. This sort of approximation is valid, assuming that the difference between BS and MT antenna heights is sufficiently small compared to their separation, leaving to the shaping of the scattering areas the inclusion of significant scatterers.

These models assume that signal sources and destinations are dimensionless points, these being scatterers or the single isotropic terminal antennas.

Polarisation effects are not included, though these can be implemented by considering a random polarisation vector subject to a certain statistical distribution, e.g., [3GPP03]. Therefore, only the scalar complex electrical field is considered, with complex scalar additions.

The channel medium is considered to be homogeneous, non-dispersive, and isotropic, within the scattering area, for each path.

As a ruling principle, more complex propagation phenomena, such as diffraction, diffuse or multiple scattering, absorption, or near-field effects are not included in these models. As their names reflect, solely single-bounce, specular reflections are considered, at every single scatterer in-between MT and BS, meaning that the number of departing signals is equal to that of arriving ones. Each scatterer involves a complex reflection coefficient, with magnitude and phase that do not take into account any specific intrinsic properties of reflecting materials. A scatterer does not absorb or obstruct any signal that geometrically intercepts it (anyhow, to partially compensate for the lack of the consideration of the absorption effect, an *obstruction factor* has been included, as it is described in the next sub-Section). One must not forget that, although the model is prepared for MiC environments, where there is a great probability of a ray suffering more than one reflection (besides the remaining effects being considerably eventful in that case), it does involve relatively large simplifying approximations. In fact, this matter has been dealt with in [StMB01], confirming through measurements that the single-bounce approximation must be carefully considered.

4.3.2 GBSBEM and CM – the Original and the Modified Variants

The GBSBEM and CM are, as the name indicates, based on pure geometry and probability mathematical relationships, being based on a scatterer region of circular or elliptical shape, within which scatterers are randomly placed according to a continuous uniform scatterer spatial density function. From this scattering region shape, one can obtain joint and marginal ToA and AoA PDFs. The AoA, ToA and signal can be obtained for each channel concretisation.

The GBSBCM is applicable to MaC environments, where the BS is higher than potential scatterers and a scatterer area surrounds the MT. The GBSBEM is used for MiC systems, where both BS and MT are surrounded by local scatterers and where it is assumed that scatterers exist near the

BS-MT line. For this, besides the general abiding previously listed assumptions, the circular model considers that scatterers are uniformly distributed inside a circle of radius r centred at the MT, and no scatterers around the BS, whereas for the elliptical model scatterers are uniformly distributed inside an ellipse at which foci the BS and MT are located, as Figure 4.1 depicts. Accordingly, both models assume that a relatively large number of signals travel or are reflected in the vicinity of the LoS, especially in the MiC case. Since no physical obstructions are accounted for, both models do not eliminate the direction-of-travel that coincides with that of LoS, though the macro-cellular environment may in practice not necessarily allow for an existing LoS.

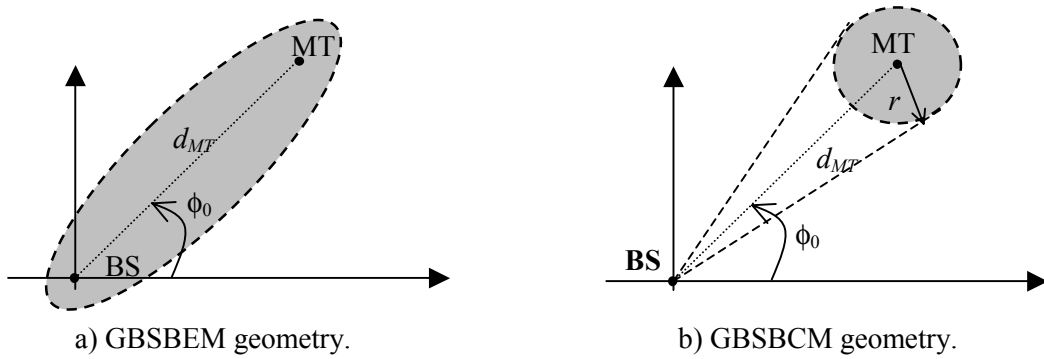


Figure 4.1 – Scatterer Uniform distributions, for the GBSBEM and CM.

The main differences between MiC and MaC models, therefore, root from the differing shape of the scattering areas, due to the relative positioning of terminals: in the case of MiCs, the BS and MT exist at similar heights, both terminals being surrounded by similar densities and areas of scatterers, and in between them a large amount of scatterers participate in the propagation; in the MaCs situation, the BS is considerably higher than the MT, therefore, not being surrounded by neighbouring scatterers, propagation mainly being affected by those around the MT. In this way, at the BS, the models reflect the angle-spreads being much larger in MiCs, compared to MaCs. In terms of MT-BS distances, MiCs naturally involve distances of up to 1 km, whereas MaCs cover over 1 km.

Going forth with a more quantified analysis of the models, [LiRa99], [Marq01], the joint temporal and angular PDFs are given by (4.1) for the MiC case, at either the BS and MT sides:

$$p_{\tau,\phi}(\tau,\phi) = \begin{cases} \frac{(d_{MT}^2 - \tau^2 c^2) [d_{MT}^2 c - 2d_{MT} \tau c^2 \cos(\phi - \phi_0) + \tau^2 c^3]}{\pi \tau c \sqrt{\tau_{max}^2 c^2 - d_{MT}^2} [d_{MT} \cos(\phi - \phi_0) - \tau c]^3}, & \frac{d_{MT}}{c} < \tau < \tau_{max} \\ 0, & \text{elsewhere} \end{cases}, \quad (4.1)$$

where ϕ_0 is the azimuth of the BS-MT line, according to Figure 4.1. For the macro-cellular situation, the joint PDF is given by (4.2), with validity regions given by (4.3) and (4.4) at the BS or at the MT ends, respectively, being zero otherwise:

$$p_{\tau,\phi}(\tau,\phi) = \frac{(d_{MT}^2 - \tau^2 c^2) [d_{MT}^2 c - 2d_{MT} \tau c^2 \cos(\phi - \phi_0) + \tau^2 c^3]}{4\pi r^2 [d_{MT} \cos(\phi - \phi_0) - \tau c]^3}, \quad (4.2)$$

$$\frac{[d_{MT}^2 - 2c\tau \cos(\phi - \phi_0) + \tau^2 c^2]}{\tau c - d_{MT} \cos(\phi - \phi_0)} \leq 2r \wedge \tau > \frac{d_{MT}}{c}, \quad (4.3)$$

$$\frac{d_{MT}^2 - \tau^2 c^2}{d_{MT} \cos(\phi - \phi_0) - \tau c} \leq 2r \wedge \tau > \frac{d_{MT}}{c}. \quad (4.4)$$

Notice that, in these equations, the PDFs are independent of scatterer density, which is not unrealistic, considering that these are probability functions and the scatterer density is assumed constant in the modelling plane at stake.

The Modified GBSBEM and CM are directly based on the GBSBEM and CM, but with scattering areas being constituted by a set of clusters of scatterers, uniformly distributed on a horizontal plane, as Figure 2.4 depicts, [Marq01]. The implemented SCM is therefore constituted by a set of N_c clusters, each composed by an average number of scatterers, N_{scat} , placed within the horizontal plane. Cluster angular positions are randomly generated, being placed at a certain azimuth, ϕ_{n_c} , in respect to the linear array normal. The scatterers are randomly distributed around each cluster central position, following a Gaussian distribution centred at the cluster centre, with a specified spatial standard deviation. An incoming signal with AoA ϕ_{n_s, n_c} , from the n_s^{th} scatterer, in the n_c^{th} cluster, is characterised by a complex reflection coefficient, Γ_{n_s, n_c} , whose modulus and phase follow random Uniform distributions within $[0, 1]$ and $[0, 2\pi[$, respectively. Free-space attenuation is introduced through α_{n_s, n_c} , also defining the magnitude of each ray contribution from each of the n_c^{th} cluster contribution. In the current application, all incoming signals from each cluster are seen as arriving at the same instant, τ_{n_c} , only allowing for relative delays between clusters, i.e., inter-cluster delays (though the WDCM does allow for intra-cluster delays). In this way, the complex channel baseband response, function of the continuous time variable, τ , related to each l^{th} link, independent among links, can be represented by:

$$h_l(\tau, \phi) = \sum_{n_c=1}^{N_c} \left\{ \delta(\tau - \tau_{n_c, l}(\phi_{n_s, n_c, l})) \cdot \sum_{n_s=1}^{N_{scat}(n_c)} (\alpha_{n_s, n_c, l}(\phi_{n_s, n_c, l}) \cdot \Gamma_{n_s, n_c, l}(\phi_{n_s, n_c, l})) \right\}, \quad (4.5)$$

where the l^{th} link index has been added, and the coefficients mentioned and the ToA are explicitly shown to vary with the AoAs. This explicit indication does not mean that such quantities are definite or known functions of the AoAs, but that any value that any of those quantities take will correspond to an incoming signal that arrives from a certain AoA.

The assessment of the model has been centred on MiCs, since most of the referred measurements had been carried out in such type of environment. Anyhow, the fewer and more constrained MaC measurements have anyway allowed the MaC model to be assessed. According to the measurement assessment, the average size of the clusters has been set to be constant, being established by a standard deviation of 1 m radius around each cluster centre, cluster density has been set to 0.001 m^{-2} , and the average number of scatterers per cluster is 10, [MPKZ01]. In the MiC case, the width of the street has been chosen to be 40 m, involving an effective street width ratio, r_w , equal to 12, in order to account for the relative larger delay-spreads that the street waveguide effect involves, [MPKZ01]. The effective street width, W_{ef} , is 480 m in that case, having estimated a maximum of 12 multiple reflections on the street walls.

As another result of the first model assessment, an additional parameter, the *obstruction factor*, F_{obs} , has been added in order to account for the correct attenuation along a moving path, considering the MT radially moving away from the BS. The introduction of such factor can be physically justified with the resulting increasing probability of rays being obstructed by the increasing number of involved clusters. The F_{obs} factor has been calculated according to (4.6), where K_{obs} and α_{obs} are constants denominated *obstruction factor gain* and *obstruction factor exponent*, respectively, and N_{scat} is the number of scatterers contained in the scattering region, [MPKZ01], [MaCo03].

$$F_{obs} = K_{obs}^{\frac{1}{2}} \cdot (N_{scat} + 1)^{\frac{\alpha_{obs}}{2}} . \quad (4.6)$$

Table 4.1 summarises the values that have been obtained for the referred parameters, MiC situation, [MPKZ01]. Except for the effective street width ratio, the remaining parameters have been maintained for the MaC case.

Parameter	Value
Effective street width ratio, r_w	12
Cluster Gaussian standard deviation [m]	1
Cluster density [m^{-2}]	10^{-3}
Average number of scatterers in each cluster	10
Obstruction factor gain, K_{obs}	1/7
Obstruction factor exponent, α_{obs}	1.7

Table 4.1 – MGBSBEM optimised input parameters (extracted from [MPKZ01]).

Average calculations involve results from the L totally independent DCIR instances, with spatial cluster/scatterer placement and corresponding reflection coefficients being independently and randomly generated among these. A *concretisation* is defined as a channel instance, a realisation of

the corresponding stochastic process, maintaining all external parameters, such as random distributions parameters, MT-BS distances and scattering area size. For each concretisation, propagation channels are independent among links. In the case that MTs are grouped, but to account for a few metres' separation among such MTs and the resulting fast-fading, the same DCIR is used, except for the phase of $\Gamma_{n_s, n_c, l}$, random uniformly distributed within $[0, 2\pi[$. In this way, grouped MTs are thought to be making use of the same set of N_c clusters of the same $N_{scat}(n_c)$ scatterers, between themselves and the BS, contributing to the same AoAs, ToAs and each signal power at the BS, except for the phases of each scatterer reflection coefficients. In the case that MTs are angularly spread, the involved DCIRs root from a single common DCIR, the resulting AoAs being shifted by the respective BS-MT angle, besides the independent generation of the reflection coefficients. In this way, the ToAs and the power of each path among angularly spread MTs' DCIRs are considered to be the same. This approximation is intentional, to simplify the simulation procedure. Though it contributes to focusing on the AoA variability, compared to that of ToA and powers, it is anyway seen not to significantly affect the statistical behaviour among the channels. The independent variation in the phase of each path will anyway result in differing temporal profiles among DCIRs, through combining the several paths inside the same angular and temporal resolution bin, within each independent DCIR.

Additionally, still concerning the generation of DCIRs, when a set of DCIRs is output for several MT-BS distances, the whole spatial cluster/scatterer placement setting is considered to be the same among the DCIRs, these naturally differing in the inclusion and exclusion of scatterers depending on the dimensions and areas at stake.

DCIRs are assumed to be stationary on a 10 ms frame basis, well above the sampling and convergence times involved. Moreover, since the involved sampling periods are much lower than the assumed stationary period, the DCIRs are also considered to be static within a slot. These approximations are not seen to be in anyway limitative, since the convergence of the algorithm is relatively fast, due to the nature of the algorithm and to the current electronics development trend. Anyhow, the issue of Doppler-shift or environment movement have intentionally been put aside, in order to solely focus on the wideband directional properties of the channel. For this also, the issues of strict or wide sense stationarity, or ergodicity, e.g., [Pätz03], have not been fully addressed.

In the implementation of the models, as already stated, only inter-cluster delays are accounted for, with relative delays being introduced as integer multiples of the chip duration, 0.26 ms, for a chip rate of 3.84 Mchip/s²⁰, and the WDCM angular resolution used in the simulations has been set to 0.5°. It has been verified that a larger channel angular resolution was necessary for the later assessed WDCM responses, due to the larger angular density of the arriving signals, relatively to the previous

²⁰ Though this timing directly applies to UMTS, the implementation is also directly extendable to other MBSs timings.

version of the WDCM. Since a value as large as $M=114$ array elements would theoretically be needed to place null and lobe maxima at least 0.5° apart (not accounting for the lack of correlation among the elements for such a large an array), such resolution was considered enough in practical terms, keeping the simulation times reasonably practicable and seeing that the resolution effects were no longer important.

The resulting DCIRs characterise each l^{th} link, from a total of L active links. A link is defined as an active MT-BS pair, identified by a code, spatial and temporally independent of any other active MT-BS pair. As it will be explained (Section 5.2, Specification of the Beamforming Scheme), a combination of channelisation and scrambling codes characterises each MT-BS pair, defining the DesS, ideally orthogonal to all NDesI. In respect to the assumed Tx/Rx initial synchronisation, the l^{th} DesS power results only from the non-delayed arriving signal from the l^{th} MT, while the NDesI power is due to the delayed contributions of such link, and to all arriving signals from all the other links, with their non-delayed and delayed contributions. Code synchronisation is assumed for ideal despreading. Furthermore, in order to avoid near-far effect-related dependencies, a PC procedure is applied (which will be described in Section 5.5, Application of Power Control), prior to and independent of the beamforming, their combined convergence problem not having been considered.

A ULA is considered at the BS, oriented with its normal in the direction considered as 0° , on the same horizontal plane as that of the WDCM. Such ULA, with $\lambda/2$ -spaced omnidirectional elements, ideally matched, weighted and calibrated, with no inter-element coupling, is considered having a ground back plane, ideally not receiving any signals from behind, i.e., 180° sectorisation is imposed. Arriving signals are fully correlated among all the ULA elements, and the far-field assumption is put forward. In this sense, each arriving planar wave contributes with M signals that solely differ on the phase-shift that is determined by the AoA. The *narrowband assumption* is put forward, stating that no symbol delays are significant, between any of the array elements, other than the referred phase-shifts.

To show that the use of a ULA is not a limitative option, in respect to the set objectives, it has been demonstrated that the performance of a ULA of 8 elements and a UCA of 12 elements arrays, spaced by $\lambda/2$ and $3/4\lambda$, respectively, do not significantly differ, for some of the tested scenarios, [Olej02], [Szym02]. Such configurations were then set in order to best approximate the respective Half Power Beam-Widths (HPBW), accepting some mismatch regarding sidelobe levels. It is kept in mind that the scenario cases did not include the cases where MTs are spread within the whole 360° domain, in which case the UCA is particularly needed, having restricted the study to placing the MTs within the 1st and 4th quadrants. One could roughly state that three sets of 8-element ULAs, in a triangular triple-antenna structure, would be required to achieve similar 360° coverage, forming a three-sectored cell, while a single set of a 12-element UCA would inherently cover the full 360° , not necessarily implying a three-sectored cell. Anyhow, as it has been shown in [Olej02], [Szym02], the

sidelobe level of the UCA implementation is also higher, in spite of the similar HPBW, whereas the BG and SINR results do not significantly differ among the simulated propagation scenarios.

In order to avoid not being able to account for sectorisation in a simple manner, while building up a set of comparable MaC and MiC scenarios, the ULA has been adopted to deliver the beamforming dependence results. The Frequency Division Duplex (FDD) UCA studies described in [Olej02] and [Szym02], which have been limited in number for the reasons stated in Section 6.3, Implementation of TDD and FDD Modes, are able to anyway provide simple, but important, insight on the use of such array geometry.

4.3.3 Physical Interpretation Issues

It is true that the shapes of the considered scattering areas may be object of criticism, and that measurements do show that other significant scatterer shapes may be involved, [KuRB00]. Anyhow, these are not only geometrically logical, but also reflect the statistical nature of the models. In the MiC case, keeping in mind that the propagation medium is uniform and isotropic, then the rays will suffer the same maximum total path-loss, independent of the direction-of-travel, meaning that outside of a certain area defined by a maximum total path-length the signals will not longer be significant. In statistical terms, such area will be an elliptical one, defined by the positions of the BS and the MT, corresponding to a maximum path-delay, τ_{max} . In the MaC situation, again following the uniform and isotropic assumptions, the significant scatterers will equally surround the MT, being significant up to a certain distance from the MT. This is approximated by a circle at which the MT is centred (truly, fully respecting the maximum attenuation limit and the isotropic assumption, the MT should not be at its centre, and the shape should be a shape between a circle and an end of the corresponding ellipse).

There is confirmed evidence that signals arrive from close propagation routes in the form of temporal and angular groups, or *clusters*, i.e., involving relatively large correlation in those domains, e.g., [Moli03a], [AMSM02]. In an urban setting, these may be contributions incoming from streets, plazas, buildings, specific building shapes, or high-rise obstacles, e.g., [LKTH02], [Kall02]. Therefore, the concentration of energy due to those physical *discontinuities* needs to be accounted for. In the case of the MGBSB models, these are considered in a statistical way, as spatial groups of scatterers, with general circular shapes, in agreement with the model nature. The density of those clusters, their average size and the average number of scatterers per cluster have been adjusted through assessment campaigns, having strong impact on the total angular- and delay-spreads, the deep and directed analysis of the resulting temporal and angular clustering of energy has not been carried out.

The inclusion of the obstruction factor following (4.6) may be object of criticism, since it is introduced as a numerical means of reducing each ray contribution, in a physically *blind* way. Though the obstruction effect is real and its inclusion is justified in a purely physical way, its addition to this

sort of model is not easy, due to the model's nature. For that, the consideration of such effect needs to be carried out in a statistical way, reflecting a tendency to increase with the number of involved. In these senses, (4.6) fulfils the objective in the simplest way. Anyhow, for example, a more complete consideration of such factor should take into account the total path-length, so as to contemplate the average number of clusters that each ray encounters, still in a statistical manner.

Already making a bridge towards the multi-user scenario perspective, in relative and intuitive terms, the sharing of clusters among links should be larger and more probable in MiCs than in MaCs, due to the physical characteristics of the surrounding environment, especially in the case that MTs are close together. And, in fact, the shapes of the respective scattering areas do reflect so, applying the model in the respective propagation scenario embedding. Additionally, if MTs are gradually separated from each other, it is most likely that the relevant clusters in the MiC BS vicinity will keep their contributions in ToA and AoA relatively unchanged, whereas in the MaC situation the involved ToAs and AoAs should more significantly vary, in relative terms. And, again, the location and shape of the involved scattering elliptical and circular areas reflect those changes, in a multi-user scenario perspective.

Lastly, but not least, it is kept in mind that the model and its application does not account for other propagation effects, in order not to divert from the directional and wideband issues at stake. A more complete model including those effects would impose a considerably larger simulation burden, without providing added value towards the confirmation of the hypotheses put forward in this study.

4.4 Propagation Scenarios Specification

4.4.1 Scenarios Perspective

In order to develop work in a practical direction, the objectives of this study demand for the SCM implementation in the form of scenarios. The scenarios that have been defined for both MiC and MaC environments aim to approximate practical situations, concerning the angular distribution of MTs, their grouping and number. Such approximation must be seen as a statistical basis, intentionally never intending to fully reflect reality, following the inherent simplified representation of the channel that the SCM implies. But, additionally, it is important to focus on approximate practical real-life scenario situations that pose particular difficulties towards beamforming, namely, where signals arriving at the array from differing sources are highly temporally and angularly correlated. For example, urban settings may involve streets, cross-roads or plazas, where large numbers of MTs may occupy relatively small spaces, such as train-stations, shopping-centres, bus-stops, entrances or exists, or outdoor cafés. For that, the chosen scenarios must involve the grouping of MTs, making use of the same channel clusters and scatterers to convey signals towards the BS array. In practice, it may be true that no MTs will be exactly co-located, but in a statistical way it can be assumed that being some

metres apart does not imply new obstacles, i.e., no new and differing ToAs and AoAs, but only differing fading envelopes. And if it is important to simulate critically demanding propagation situations, then their added value can only be gained if being counterpoised against the less challenging ones, where MTs may be angularly spread, explicitly separated or at differing distances to the BS. Sub-urban or rural environments may involve much more scattered MTs, in car parks, few shops, small transport stations, isolated parked cars, farms or isolated pedestrian ways. These are the situations where the signals arriving at the BS from several interfering sources present lower angular and temporal correlation, and where beamforming performance is expected to largely improve.

Most of the implemented MiC and MaC scenarios present enough similarities between them, so as to extract logical conclusions from their comparison. In this manner, some parameters are common in order to evaluate the dominant beamforming dependencies. Namely, MaC and MiC scenarios are generated in terms of the angular placement of MTs in respect to the BS, their grouping, the MT-BS distance, d_{MT} , the number of active users, L , and of array elements, M . Other parameters have been varied, more specific to MiCs or MaCs, respectively, as it will be described.

Three major groups of scenarios have, therefore, been generated: the MiCs, the MaCs and the Comparison Sets (CSts) group. The MiCs and MaCs scenario groups are firstly analysed individually, in similar manners, while the final analysis results from the CSts group of scenarios. The latter are sets of both MiC and MaC selected scenarios, required to go forth with the comparison of beamforming performances between those two different environments.

The application of SAs at the BS is most critical in traffic hotspots, and during the traffic busy hour. In the temporal domain, though, the gain of resorting to such technology may not vary, for example if it is located in highly populated areas, with slowly varying user density. Since the matter that is studied does not focus on traffic conditions, the scenarios need not be time-dependent. From another point-of-view, the implementation of multi-user scenarios is considered to be a fundamental requisite, in terms of further rendering the subject with practical meaning, towards UMTS and future MBSs, evaluating the effects of realistic interference conditions, e.g., [PaPa97].

In the spatial domain, the placement of such antennas will most of all be required in micro- and pico-cells, in urban areas. Most likely, then, the BS will be slightly higher than the MT, below rooftops, fitting well with the planar simulation of the problem. This way of thinking is valid for both UMTS and future MBSs, in localised areas. Anyhow, BSs do provide MaC coverage in urban settings, for UMTS. In this case, the covering BS antenna will be much higher than the MTs, being able to cover larger BS-MT distances. It is known that elevation power spectrum is relatively poorer than that in azimuth, especially in the MaC cases (at the BS side), or even in MiCs (at both MT or BS sides). On this matter, the channel measurements in [LKTH02], [KSLK02], [Kall02], [KuRB00], contribute to characterising elevation properties in urban settings. Generally, but depending on

antenna heights and LoS/NLoS conditions, these studies do show clustering in elevation at the BS, differing elevation responses and relatively high elevation spreads at the MT.

Anyhow, the planar modelling of the channel and the whole development of the problem at the planar level are not limiting for this study, on the following related bases: the physical constraints that are at stake are present for both azimuth and elevation; the understanding of the problem in azimuth is extendable to elevation; it is along azimuth that the channel is naturally seen physically richer than in elevation, in both single- and multi-user interference perspectives; in realistic scenarios, the azimuth plane intuitively seems most likely to convey larger variations in beamforming freedom. For these, the azimuth study, by itself, provides significant results from a larger number of scenario variations, before extending to any elevation study.

In practical terms, then, concerning the relevant cell layouts, one firstly pictures the application of SAs in macro-, micro- and pico-cells. In view of this, the implemented scenarios should firstly consider MaC and MiC situations, being anyway extendable to pico-cells.

4.4.2 Micro-cell Scenarios

The simpler MiC scenarios that are considered involve all users grouped together at 50, 500 and 1 000 m. These scenarios, Table 4.2, were named by Sc #Lu_mc_Gr_d, where L is the number of active links, the suffix ‘ d ’ corresponds to d_{MT} , indicating the separation in hundreds of metres, and the term ‘Gr’ refers to the grouped MTs situation.

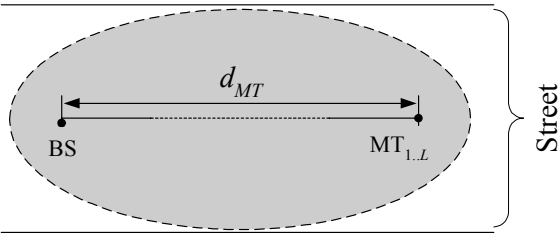
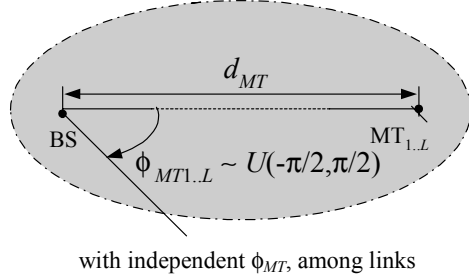
Sc #Lu_mc_	d_{MT} [m]	Scenario (not to scale):
Gr_05	50	
Gr_5	500	
Gr_10	1 000	
Sp_05	50	
Sp_5	500	
Sp_10	1 000	

Table 4.2 – WDCM MiC scenarios, for all MTs together or all angularly spread, varying BS-MT distance.

The street-confined cases not only lead to important results that require attentive analysis, these being exceptionally demanding in terms of spatial and temporal correlation among active links, but also correspond to the practical and realistic situation of MTs existing within a street, MiC environment. Even if the MTs are spread along the street, many AoAs and ToAs are common among links, due to the presence of clusters and scatterers commonly contributing to the reflection of signals from the MT to the BS. In other words, the beamforming potential to differentiate signals from among the active links is being tested in a worse case situation, where the beam pattern directionality capacity of the adaptive array is inherently limited. For this, the implementation of further MiC scenarios is required, maintaining the characteristic elliptical region defined by the MT and BS foci, but freeing its main axis direction, i.e., extending the scenarios to approximate crossroads or plaza situations. The additional MiC scenarios that are implemented consider angularly spread MTs, while BS-MT distance and the number of active links are again varied. In Table 4.2, besides the scenarios where all active MTs are together at the 0° angular reference, additional scenarios are indicated where MTs are placed randomly and uniformly spread within a 180° sector (expressed by $U(a,b)$, where a and b are the lower and upper distribution limits). These are named by Sc #Lu_mc_Sp_d, where ‘Sp’ refers to the angularly spread MTs situation. The case being where statistically all MTs are subject to the same general conditions, these are indicated in the same table, providing results on the beamformer performance dependence on d_{MT} , and grouping of MTs, either altogether or all separate.

Keeping in mind that this study is developed using a ULA, the crossroads or plaza situations that are accounted for consider the ULA beamforming towards angles within the $]-\pi/2, \pi/2[$ interval.

Two more scenarios are considered, still confined to the street, but where different MT groupings exist along it, with a single MT being placed at a distance different from that of the remaining MTs group, Sc #Lu_mc_St_Se_A and #Lu_mc_St_Se_B. The single MT is placed at 50 or 1 000 m, and the group of $L-1$ MTs at 1 000 or 50 m, respectively, as Table 4.3 shows. In these cases, d_{MTl} corresponds to the distance between the l^{th} MT and the BS.

Though not being hereby shown, other scenarios have been generated for specific purposes, e.g., for the comparison of the CG and RLS algorithms’ performances, [GiMC01].

Further extending MiC situations, additional scenarios have been set, involving a single angularly separate MT and the remaining MTs together or angularly spread, again more closely corresponding to the crossroads or the plaza cases. These are depicted in Table 4.4, where the BS-MT distance has been kept constant and equal to 500 m. Sc #Lu_mc_Se_A is the case where MT_1 is placed at $\pi/4$, with the remaining MTs, grouped together, at $-\pi/5$; Sc #Lu_mc_Se_B considers that MT_1 is randomly placed within the 1st quadrant, with the remaining MTs being spread within the 4th; Sc #Lu_mc_Se_C is a similar case, except for the remaining MTs being grouped together, within the 4th quadrant.

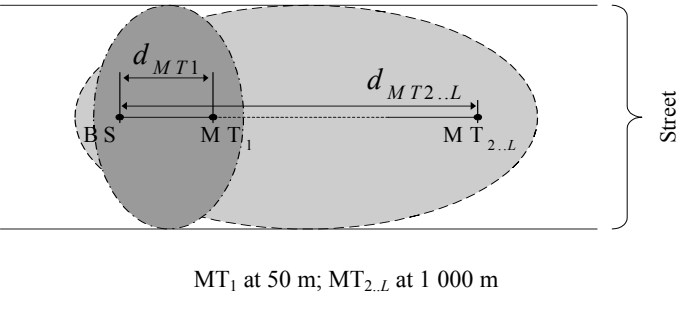
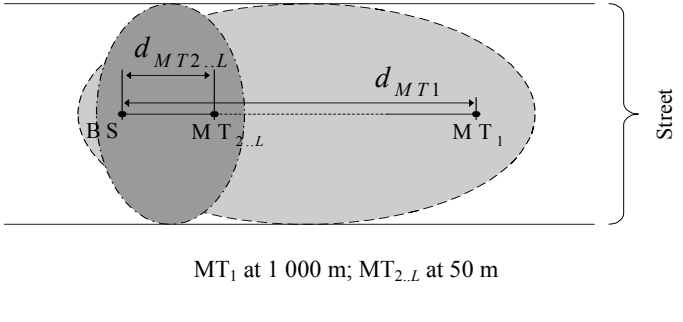
Sc #Lu_mc_St_	d_{MT} [m]	Scenario (not to scale):
Se_A	$d_{MT1} = 50$	 <p style="text-align: center;">MT_1 at 50 m; $MT_{2..L}$ at 1 000 m</p>
	$d_{MT2..L} = 1\ 000$	
Se_B	$d_{MT1} = 1\ 000$	 <p style="text-align: center;">MT_1 at 1 000 m; $MT_{2..L}$ at 50 m</p>
	$d_{MT2..L} = 50$	

Table 4.3 – WDCM MiC scenarios, confined to the street, but separating MT_1 from the remaining MTs, grouped together.

For all of the presented scenarios, the number of MTs, L , is varied, taking the values 4, 8 and 16, posing the worse case usage in the Time Division Duplex (TDD) code tree, per time-slot (these scenarios have also been used for FDD simulations, involving larger values of L per FDD slot, as it is described in Section 6.3, Implementation of TDD and FDD Modes). The number of array elements, M , takes even values from 2 to 20.

The particular sort of scenario implementation, where the direction of the ellipses axis is varied, must be understood in a statistical way. The value of the results resides on such, besides the statistical nature of the WDCM. It can be said that, for example, a certain city centre plaza contributes to large and well-defined clusters, due to the surrounding large buildings or streets, which each WDCM concretisation does not necessarily account for (the model does not consider exceptionally defined clusters outside of the scattering ellipse). However, it is through that statistical nature of the study that its results render their validity. In the scenarios where MTs are angularly distributed, the respective results from considering particular BS-MT angular orientations and distributions must also be viewed in that manner. Additionally, by directing the active links' ellipses, there is an area of ellipses superposition at the BS side, to which the several ellipses contribute with differing scatterers and clusters, but possibly to common AoAs or ToAs. This assumption is kept so, assuming that the validity of the matter naturally roots from the referred statistical nature of the simulations, anyway in agreement with the greater probability of common clusters existing close to the BS.

Sc #Lu_mc_	Scenario (not to scale):
Se_A	<p>Diagram for Se_A scenario: A Base Station (BS) is located on the left. Two Mobile Terminals (MT) are shown. The distance from BS to MT₁ is d_{MT}. The angle between the BS-MT₁ line and the horizontal axis is $\phi_{MT1} = \pi/4$. The angle between the BS-MT_{2..L} line and the horizontal axis is $\phi_{MT2..L} = -\pi/5$.</p>
Se_B	<p>Diagram for Se_B scenario: A Base Station (BS) is located on the left. Multiple Mobile Terminals (MT) are shown. The distance from BS to MT₁ is d_{MT}. The angle between the BS-MT₁ line and the horizontal axis is $\phi_{MT1} \sim U(0, \pi/2)$. The angle between the BS-MT_L line and the horizontal axis is $\phi_{MT_L} \sim U(-\pi/2, 0)$.</p>
Se_C	<p>Diagram for Se_C scenario: A Base Station (BS) is located on the left. Two Mobile Terminals (MT) are shown. The distance from BS to MT₁ is d_{MT}. The angle between the BS-MT₁ line and the horizontal axis is $\phi_{MT1} \sim U(0, \pi/2)$. The angle between the BS-MT_{2..L} line and the horizontal axis is $\phi_{MT2..L} \sim U(-\pi/2, 0)$.</p>

Table 4.4 – WDCM MiC scenarios, where a single MT is kept angularly separated from the rest, for $d_{MT} = 500$ m.

Figure 4.2 and Figure 4.3 are examples of the practical implementation of this scenario philosophy, towards more realistic situations. These have been specified with particular concern to approximate the general geometries of measurement campaign sites, also accounting for several distributions of MTs. These scenarios serve as a common basis to compare several multi-user interference suppression solutions, while applying a newer version of the MGBSB models, [DGVC03].

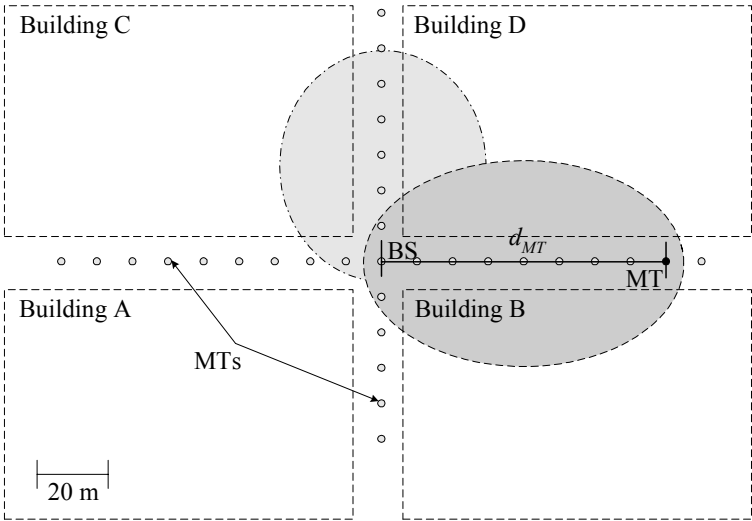
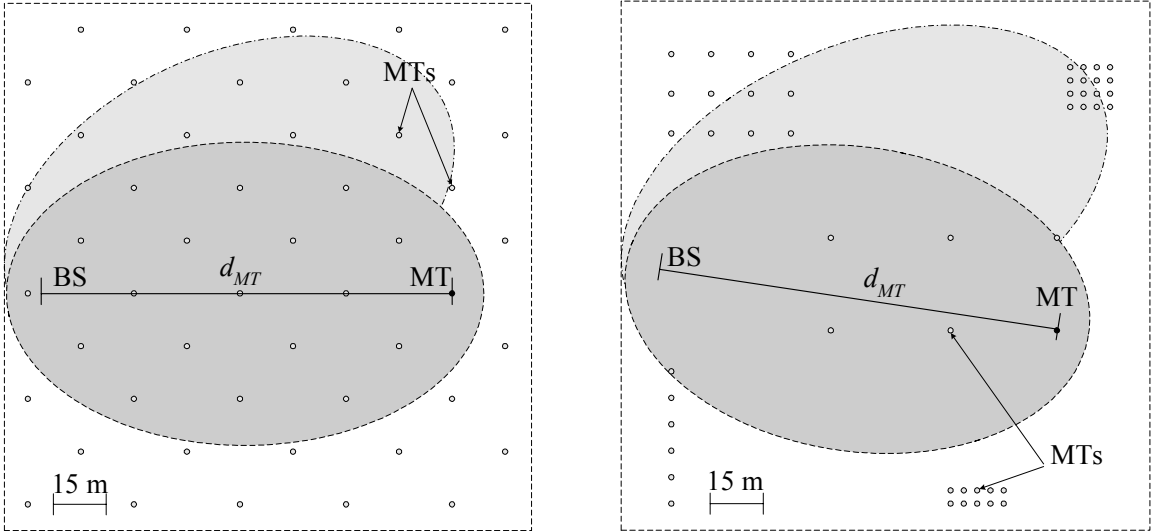


Figure 4.2 – A street, MiC propagation scenario (based on [DGVC03]).



(a) Spread MTs.

(b) Grouped MTs.

Figure 4.3 – City plaza, MiC propagation scenarios, not to scale (based on [DGVC03]).

4.4.3 Macro-cell Scenarios

As its MiC counterpart, the MaC scenarios that are implemented differ in BS-MT distance, number of active links, angular positioning and MT distributions. Additionally, these include scenarios that differ in scattering region radius, r , and scatterer and cluster densities. Table 4.5 presents the scenarios where all active MTs are either together, at the 0° angular reference (Sc #Lu_Mc_Gr_10_200, #Lu_Mc_Gr_15_r or #Lu_Mc_Gr_20_200), or at random and uniformly spread within the 180° sector (Sc #Lu_Mc_Sp_10_200, #Lu_Mc_Sp_15_r or #Lu_Mc_Sp_20_200). These mainly provide results on the beamformer performance dependence on BS-MT distance, scattering circle radius, and grouping of MTs, either together or separate.

Sc #Lu_Mc_	d_{MT} [m]	r [m]	Scenario (not to scale):
Gr_10_200	1 000	200	
Gr_15_r	1 500	50 200 400	
Gr_20_200	2 000	200	
Sp_10_200	1 000	200	
Sp_15_r	1 500	50 200 400	
Sp_20_200	2 000	200	

Table 4.5 – WDCM MaC scenarios, for all MTs together or all angularly spread, varying BS-MT distance or scattering circle radius.

Scenarios for the same 1 500 m BS-MT distance are described in Table 4.6: a single MT is placed at $\pi/4$, with all the others at $-\pi/5$ (Sc #Lu_Mc_Se_A_r); the MT is placed at a random angle within the 1st quadrant, with all the others separately placed at random 4th quadrant angles (Sc #Lu_Mc_Se_B_r); a single MT is similarly placed in the 1st quadrant with the rest grouped together, placed at random angles within the 4th (Sc #Lu_Mc_Se_C_r). As in the MiCs cases, these mainly contribute to evaluating and understanding how the beamformer responds to situations where a separate MT exists, with the other MTs being together or spread, but in other angular positions. Again, the scattering region radius is varied.

Sc #Lu_Mc_	r [m]	Scenario (not to scale):
Se_A_r	50 200	
Se_B_r	50 200	
Se_C_50	50	

Table 4.6 – WDCM MaC scenarios, where a single MT is kept angularly separated from the rest, for $d_{MT} = 1\ 500$ m.

As in the MiCs cases, all the scenarios are implemented and used for $L = 4, 8$ and 16 . The number of array elements, M , also varies in the same manner as for MiCs. Additionally, cluster density is reduced by $1/2$, and average number of scatterers per cluster²¹ by $1/5$, from Sc #Lu_Mc_Gr_15_r, #Lu_Mc_Se_A_r, #Lu_Mc_Se_B_r and #Lu_Mc_Se_C_50, to scenarios referred to as Sc #Lu_Mc_Gr_15_r_ld, #Lu_Mc_Se_A_r_ld, #Lu_Mc_Se_B_r_ld and #Lu_Mc_Se_C_50_ld. In the case of the former scenarios, cluster density is 0.001 m^{-2} , while the average number of scatterers per cluster had been set to 10, [MPKZ00].

Figure 4.4 exemplifies how a MaC propagation scenario may be applied in a more practical point of view, for a sub-urban train environment. The multi-user propagation scenario accounts for a characteristic linear distribution of several MTs along the train coaches, [DGVC03]²².

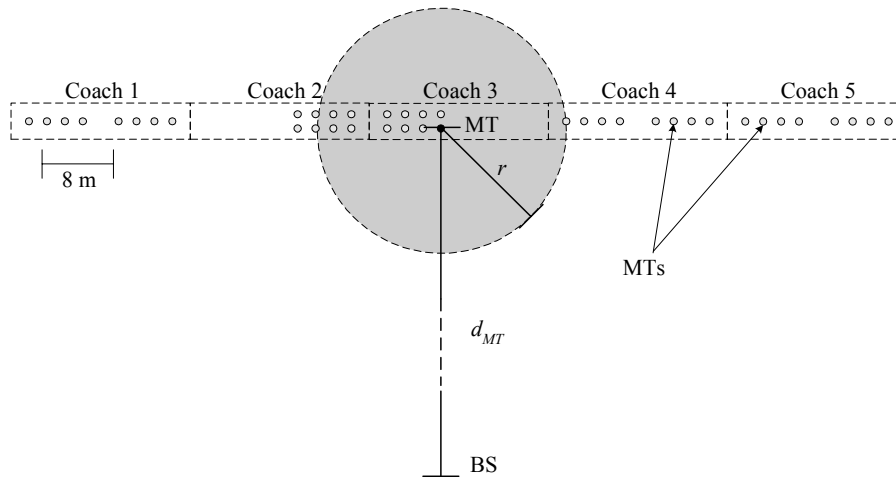


Figure 4.4 – A train, MaC propagation scenario, not to scale (based on [DGVC03]).

4.4.4 Comparative Micro- and Macro-cell Scenarios

As the previous sections have put forward, the MiC and MaC scenarios are numerous, varying many parameters. The point of comparing these two major types of propagation scenarios is not at the level at which their individual characterisation has been made, for specific parameter values, due to the inherently different nature of the scattering area shapes at stake. For that, in order to compare performances in MiCs and MaCs, one also deals with analysing the beamforming dependencies on the variations of the common parameters. Consequently, a study like that must evolve from a set of comparative scenarios that present enough similarities so as to extract logical conclusions. In view of that, most of the MiC and MaC scenarios have been created in order to be comparable with each

²¹ For the current intra-cluster delay assumptions (only inter-cluster delays are included), the number of scatterers per cluster only affects average cluster power. The cluster average size has been maintained.

²² This is a mixed environment, but simpler environments could be envisaged, e.g., an urban plaza, or a park.

other, fundamentally in terms of MTs placement in respect to the BS (very clearly seen by comparing Table 4.2, Table 4.4, Table 4.5 and Table 4.6). The MT displacement and grouping is, therefore, the fundamental comparison parameter that characterises this analysis, resulting in the selected MiC vs. MaC CSSts that are indicated in Table 4.7.

CSt #	MiC Sc #	MaC Sc #	MT Displacement and Grouping
mc_Mc_Gr	mc_Gr_d	Mc_Gr_d_200	
mc_Mc_Sp	mc_Sp_d	Mc_Sp_d_200	
mc_Mc_Se_A	mc_Se_A	Mc_Se_A	
mc_Mc_Se_B	mc_Se_B	Mc_Se_B	

Table 4.7 – Comparable MiC and MaC propagation CSSt scenarios.

The BS-MT distances considered are $d_1 = 50$, $d_2 = 500$ and $d_3 = 1\,000$ m for MiCs, and $d_1 = 1\,000$, $d_2 = 1\,500$ and $d_3 = 2\,000$ m for MaCs, in order to compare the basic BG dependencies on d_{MT} . In a similar manner, the CSts are analysed as functions of the number of active links, L , and of the number of array elements, M . In the case of the MaC scenarios, the scattering circle radius has been set to $r = 200$ m, being the common radius among all of the considered MaC scenarios, and also being the intermediate r value.

In parallel as before, CSt #Gr and #Sp are the scenarios where all active MTs are grouped together, at the 0° angular reference, or at random angles, independently and uniformly spread, respectively. CSt #Se_A and B scenarios involve the same parameters, except that a single MT is placed at $\pi/4$, with all the others at $-\pi/5$ (Se_A), or the MT is placed at a random angle within the 1st quadrant, with all the others separately placed at random 4th quadrant angles (Se_B).

The MiCs Sc #Gr scenarios are closer to the street-confined situation, where MTs may be located near a bus-stop, for example; the MiCs Sc #Sp better approximates the case of a MiC plaza, with the BS at one side of the plaza, at similar height as the MTs; the Se_A and Se_B MiCs scenarios try to depict crossroads situations. Regarding MaCs, the Sc #Gr cases may picture situations where a group of MTs is highly probable, e.g., in a motorway service station or a railway station, within rural or suburban settings; the MaC Sc #Sp situation corresponds to the case that MTs are relatively well spread, below the level of the BS, either in an urban, suburban or rural environment; MaC Se_A and Se_B also approximate the latter situation, but where an MT is explicitly separate from the remaining ones.

It is openly accepted that the comparison of MiC and MaC scenarios involves totally different propagation cases, due to the differing scattering area shapes, the inherently differing parameters, and the different values taken by the common ones. On the other hand, in fact, such comparison does make sense precisely because of such important differences. It is in the way that the comparative scenarios are defined and how the comparison is held that the relevancy of such analysis resides.

4.5 Spatial Channel Parameters

4.5.1 AoA and ToA Spreads

Table 4.8 presents the average ToA spreads, σ_τ , and NB and WB AoA spreads, $\sigma_{\phi,NB}$ and $\sigma_{\phi,WB}$, respectively, for MiCs. The former angle-spread corresponds to the whole of arriving signals, independent of time, whereas the latter is calculated for certain ToA values or intervals. Resorting to the approximate discrete calculation of the central moments, these have been calculated in a similar manner for either τ or ϕ , exemplifying for σ_ϕ in (4.7), e.g., [LiRa99]:

$$\sigma_{\phi} = \sqrt{E[\phi^2] - E^2[\phi]} \approx \sqrt{\frac{\sum_{p=1}^{N_{mp}} \alpha_p^2 \phi_p^2}{\sum_{p=1}^{N_{mp}} \alpha_p^2} - \left(\frac{\sum_{p=1}^{N_{mp}} \alpha_p^2 \phi_p}{\sum_{p=1}^{N_{mp}} \alpha_p^2} \right)^2}, \quad (4.7)$$

where α_p and ϕ_p denote the magnitude and azimuth of the p^{th} path, among a total of N_{mp} paths.

Notice that the spreads are calculated independently of the cluster, for the reason that relatively large numbers of clusters may be at stake, these being randomly placed within the scattering areas, i.e., resulting in varying distances to the BS, varying individual cluster angle-spreads, and common AoAs among differing clusters (in the view of the BS).

d_{MT} [m]	σ_{τ} [μs]	L_T	$\sigma_{\phi,NB}$ [°]		$\sigma_{\phi,WB=0}$ [°]	$\sigma_{\phi,WB>0}$ [°]
			omni.	180° sect.		
50	0.39	$7 \times L$	84	44	25	50
500	0.18	$3 \times L$	46	32	18	39
1 000	0.10	$2 \times L$	28	23	14	30

Table 4.8 – ToA and AoA average spreads, function of d_{MT} , for MiCs.

The $\sigma_{\phi,NB}$ spread has been calculated for no sectorisation, and for the 180° ULA sectorisation. Unless stated otherwise, one will implicitly refer to the 180° case, only. $\sigma_{\phi,WB}$ is given for $\tau = 0$ and $\tau > 0$, being represented by $\sigma_{\phi,WB=0}$ and $\sigma_{\phi,WB>0}$, correspondingly, in order to evaluate the spreads of the non-delayed and delayed arriving signals. The total number of orthogonal (supposing that the ideal orthogonality would be maintained) signals arriving at the BS, L_T , has also been introduced, being calculated by multiplying the number of DCIR chip delays by the number of active users, L .

In the MiCs case, the WDCM presents a larger delay-spread for shorter distances, having a visible impact on L_T , contributing to worsen NDesI reduction capacity. On the other hand, angle-spreads are larger, providing larger angular freedom for more effective location of nulls, thus, tending to improve NDesI reduction. As far as the relation between the different values is concerned, it is seen that: from 50 to 500 and to 1 000 m, σ_{τ} is reduced by a factor of 2.2 and 3.9, respectively; from 50 to 500 and to 1 000 m, $\sigma_{\phi,NB}$ AoA spread is reduced by a factor of 1.4 and 1.9, correspondingly, very close to the variations of $\sigma_{\phi,WB=0}$ and $\sigma_{\phi,WB>0}$; for all distances, $\sigma_{\phi,WB=0}$ and $\sigma_{\phi,WB>0}$ differ by a factor of near 0.5. One then sees that ToA reduction with distance is larger than the corresponding AoA spreads reduction. Also, all the AoA spread definitions vary very similarly with distance, and the relation between respective NB and WB AoA spreads is nearly independent from distance. Moreover, one sees how narrow $\sigma_{\phi,WB=0}$ is in respect to $\sigma_{\phi,WB>0}$, the former being the one that relates to the DesS power contributions.

Figure 4.5 presents average signal amplitude wideband directional diagrams corresponding to MiCs, normalised to each respective maximum, for 50 and 1 000 m. ToA increases from the inner to the outer rings, with integer numbers of chips, and the AoA dimension is also indicated. As one can see, for shorter distances the angular and temporal dispersions are much larger. Power is spread much more in both domains for 50 m, than for 1 000 m. Also, the lobular DCIR characteristic is clear in the 500 and 1 000 m cases, for $\tau > 0$, as it was reported in [MaCo01], also in agreement with [LiRa99]. As it is seen in the example of Figure 4.5 (b), these DCIR lobes, appearing at the edges of the zero-delayed incoming signals, around LoS, contribute to the heavy concentration of NDesI power very near the DesS contribution. Furthermore, the existence of the narrow angular sector with lower NDesI power levels between such lobes, near LoS, may only be of use for larger number of array elements, only then allowing the formation of a useful antenna pattern lobe near the LoS DesS, non-delayed, power. For these reasons, it is expected that the beamformer may present worse interference suppression performance for larger distances.

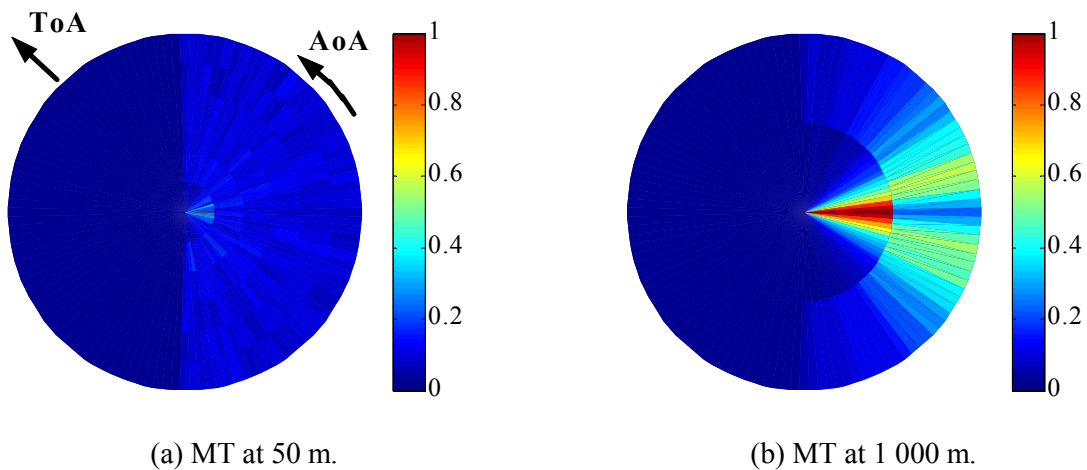


Figure 4.5 – Average signal amplitudes for two BS-MT distances, MiCs, normalised to each maximum (based on [Marq01], with a 3° visualisation resolution).

In parallel to what has been done in the MiCs case, Table 4.9 presents the average σ_τ , L_T , $\sigma_{\phi, NB}$ and $\sigma_{\phi, WB}$, as functions of d_{MT} , and of r , for MaCs.

It is visible how the radius of the scattering region affects all the spreads much more significantly than the BS-MT distance does, as expected. σ_τ does not significantly change with BS-MT distance, but it does with the scattering circle radius, whereas AoA spreads are sensitive to both d_{MT} and r : for 1 500 m separation, from 50 to 200 m and from 200 to 400 m radius, σ_τ increases by a factor of 3.8 and 1.9, respectively, while the $\sigma_{\phi, NB}$ angle-spread rises more than 7.4 and 2 times, $\sigma_{\phi, WB, =0}$ by more than 4 and 1.6 times, and $\sigma_{\phi, WB, >0}$ registers an increase by factors of 8.4 and 2; for the same radius of 200 m, while d_{MT} does not significantly affect ToA spreads, $\sigma_{\phi, WB}$ registers decreases by near 1.5 times, from 1 000 to 1 500 m, or from 1 500 to 2 000 m.

r [m]	d_{MT} [m]	σ_τ [μ s]	L_T	$\sigma_{\phi,NB}$ [°]	$\sigma_{\phi,WB=0}$ [°]	$\sigma_{\phi,WB>0}$ [°]
50	1 500	0.10	$2 \times L$	0.5	<0.5	<0.5
200	1 000	0.36	$6 \times L$	5.6	3.1	6.4
	1 500	0.37	$6 \times L$	3.7	2.0	4.2
	2 000	0.38	$6 \times L$	2.8	1.5	3.1
400	1 500	0.68	$11 \times L$	7.4	3.1	8.4

Table 4.9 – ToA and AoA average spreads, function of r and d_{MT} , for MaCs.

As it was described for the MiC case, higher delay-spreads imply larger delayed NDesI power arriving at the array, but the subsequent larger angle-spreads favour the improvement of NDesI reduction capacity. As it can be understood, the number of reflective scatterers and type of MT grouping will play an important role in the balancing of these two opposite contributions. Following this reasoning, the 50 m radius cases are particularly interesting, these being the situations where delayed NDesI content is lowest, but also where the AoA spreads are much narrower compared to the other scenarios.

The corresponding MaC average signal amplitude wideband directional diagrams are pictured in Figure 4.6, normalised to each respective maximum, for $d_{MT} = 1\,500$ m and 50 and 400 m radii. The previously described differences in angular and delay-spreads are graphically clear. Power is much more concentrated in time and angle for 50 m radius.

Comparing Figure 4.5 and Figure 4.6, for MiCs and MaCs respectively, it is very much visible how the MiC average signal amplitude response is much more spread over the angular domain.

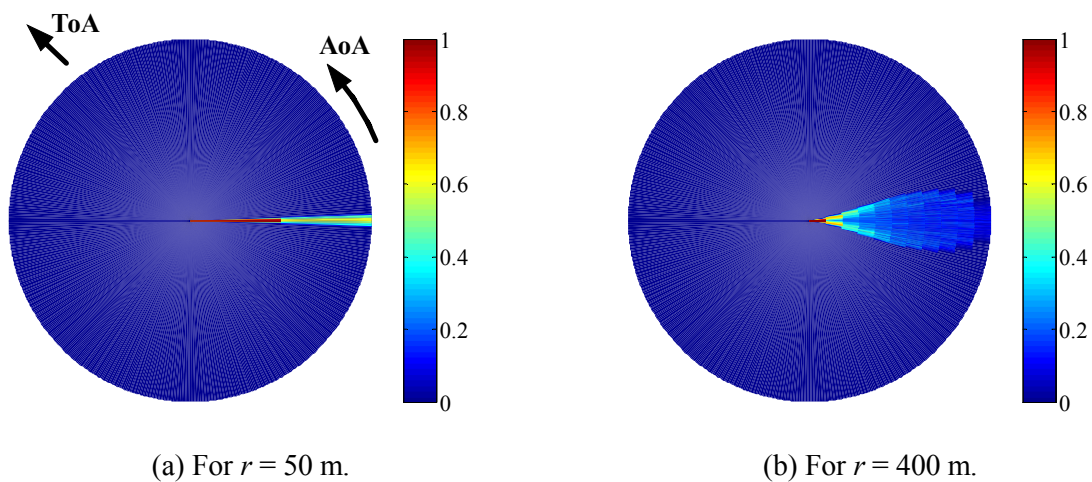


Figure 4.6 – Average signal amplitude for 50 and 400 m radii, for $d_{MT} = 1\,500$ m, MaCs, normalised to each maximum.

For both MiCs and MaCs simulated scenarios, it is clear how all the σ_ϕ spreads decrease with increasing d_{MT} ; among the chosen distances, such relative dependencies are of the same order, independent of the cell type and spread definitions; for MiCs, the involved σ_ϕ values are one order of magnitude larger than those of MaCs, again independently of the spread definitions; for MaCs, the variation of σ_τ with d_{MT} is insignificant, whereas in the case of MiCs σ_τ varies by a factor around 4. One can also understand this by analysing the maximum delays that the scattering areas allow for. In the case of MaCs, the radius of the scattering circle fundamentally determines these delays, whereas for MiCs, such delays are dependent on both the major and the minor axes of the corresponding ellipse. In this way, by increasing d_{MT} the delay-spread will vary more significantly in the case of MiCs. In parallel, regarding σ_ϕ , the circle radius or the ellipse minor axis mainly defines these, for MaCs and MiCs, respectively, i.e., not registering as large dependencies on d_{MT} , and having much larger values in the case of MiCs. Though the delay-spreads involved with the implemented MiC and MaC scenarios may be of similar order (depending on the scattering area shape and its defining parameters), the angle-spreads vary substantially, not only between MiCs and MaCs, but also within each of those cases.

Besides comparing ToA and AoA spreads between MiCs and MaCs, the number of orthogonal codes, L_T , involved in the DCIRs (Table 4.8 and Table 4.9) may also be compared. Though there is a relationship between the ToA spread and L_T , by comparing the corresponding MiC and MaC quantities one sees that the MiC responses involve less arriving orthogonal signals for delay-spreads of similar order, or lower delay-spreads for L_T of similar order, for any of the parameter values that define the corresponding scattering areas. This is a natural verification, multipath delays being more concentrated near its temporal mean in the MaC case, compared to the MiC one. Anyhow, it is important to be aware that even if L_T may be larger, it is the delay-spread that provides indication of the relevant power concentration by its mean, i.e., a large L_T involves many delayed contributions that, however, may be insignificant in terms of power, not being relevant in terms of interference content. For this, the comparison of the several scenarios at the temporal level is centred in the ToA spreads, not dealing with L_T .

Anyhow, following the meaning of L_T helps in understanding that one is not only dealing with the temporal domain. Notice that L_T would only be equal to L if no cluster relative delays were considered, meaning that the temporal correlation among signals would be respected. But, in fact, as Table 4.8 and Table 4.9 show, L_T will be larger than L . Since the adaptive problem develops on an M -dimensional space, viewing the matter solely in the temporal equalisation point-of-view, it is physically understood that if $L_T < M$, then the algorithms will be able to find L weight vector solutions that guarantee the best SINR for each link, due to maximum temporal discrimination made possible through the available full orthogonality. This may be valid for the fundamental temporal equalisation, but in the case of being applied for array beamforming, the angular domain enters the scene. Even in

the case that $L_T = L$ and $L_T < M$, the resulting SINR will also be subject to the degree of coincidence of AoAs, among links. Therefore any of the surrounding NDesI sources and directional propagation channel characteristics will inherently affect the beamforming performance. Moreover, in practice, M will be smaller than L_T , implying the overpassing of the physical limits of the temporal domain problem, but possibly not the limits of the angular domain one.

Finally, then, at a first look one can understand that the differing tendencies of the temporal and angle-spreads, depending on being MiCs or MaCs, have great importance in the way that variation of d_{MT} affects beamforming: higher σ_τ implies more delayed NDesI power arriving at the array, but larger σ_ϕ tends to provide better angular freedom for more effective location of lobes and nulls, helping to improve NDesI reduction capacity. Using these parameters, one realises that it would be interesting to establish a quantitative, yet simple, means to account for both effects regarding beamforming, expressing their opposite nature, resorting to the propagation channel properties and constraints imposed by it. One is therefore dealing with both the temporal and angular domains, inherently combined through beamforming within a wideband directional propagation channel model.

4.5.2 Temporal and Angular Densities, and Channel Richness

Besides the ToA and AoA spreads, the MiC and MaC DCIRs strongly differ in the total number of arriving signals. For MiCs, the major axis of the scattering ellipse renders much larger scattering areas, involving richer multipath, with differing ToAs and AoAs among arriving signals. Since the densities of clusters and scatterers are considered constant, MiCs involve much more scattering than MaCs due to the larger areas involved, leading to a larger number of arriving signals. To understand such in a more quantitative manner, one must keep in mind that the areas of the circle and ellipse are given by (4.8) and (4.9), respectively. In this way, firstly one sees that the largest contribution to the ellipse area comes from d_{MT} , which in MiC may take values up to 1 000 m. Secondly, $W_{ef}/2$ is similar to or much larger than r , since W_{ef} is several times greater than the real street width. According to Table 4.1, the MiC measurement assessment has concluded that $W_{ef} = 480$ m for a street width of 40 m.

$$A_{scat. circle} = \pi \cdot r^2 \quad (4.8)$$

$$A_{scat. ellipse} = \pi \cdot \frac{W_{ef}}{2} \cdot \sqrt{\left(\frac{W_{ef}}{2}\right)^2 + \left(\frac{d_{MT}}{2}\right)^2} \quad (4.9)$$

Quantifying further, for the MiC and MaC scenarios presented in Table 4.2 to Table 4.6, the total scattering areas range from near 0.182 to 0.418 km² for MiCs, whereas for the shown MaC cases, those vary from near 0.008 to 0.503 km² for $r = 50$ and 400 m.

This major divergence between MiC and MaC situations means that, for the same cluster and scattering spatial densities, the larger number of MiC scatterers implies a larger number of

independent variables defining the magnitudes and phases of the signals arriving at the BS. Even with common AoAs among the active links, such a larger number contributes to more independency among the present DCIRs, i.e., to a richer variety of uncorrelated arriving signals among the active links.

Following this reasoning, having shown how the average temporal and angle-spreads and the number of arriving signals vary with the scenario, one thinks about the *temporal* and *angular densities* of arriving signals as indicators of the temporal and angular *closeness* of the incoming signals, i.e., as means of expressing the correlation richness that the channel involves, in terms of ToA and AoA: the more a number of arriving signals is concentrated close to the temporal mean, related to the temporal density of arriving signals, the better the correlation properties among all links' signals tends to be, contributing to beamforming improvement (this is better understood seeing that the *on-the-air* delayed NDesI power term that primarily derives from the other links' delayed contributions is the main interference component that rules the resulting SINR, as it is described in sub-Sections 7.2.7 and 7.3.7, Correlation Matrix Components Dependencies, for MiCs and MaCs, and that larger temporal density will lower its relative level); larger angular density of incoming signals, involving both DesS and NDesI powers, renders worse angular discrimination among these, in that case tending to worsen performance.

Since the WDCMs involve a Uniform distribution of clusters, and the average number of scatterers per cluster is constant, such densities are proportional to the total scattering areas at stake. One then defines the *equivalent temporal* and *angular densities*, ρ_τ and ρ_ϕ , respectively, as the ratios between the MiC or MaC scattering total area and the involved NB angular and delay-spreads, where the elliptical or circular areas at stake, A_{scat} , are proportional to the total number of scatterers, N_{scat} :

$$\rho_\tau \text{ [km}^2 \text{ / } \mu\text{s]} = \frac{A_{scat} \text{ [km}^2\text{]}}{\sigma_\tau \text{ [\mu s]}} \propto \frac{N_{scat}}{\sigma_\tau \text{ [\mu s]}} , \quad (4.10)$$

$$\rho_\phi \text{ [km}^2 \text{ / rad]} = \frac{A_{scat} \text{ [km}^2\text{]}}{\sigma_{\phi,NB} \text{ [rad]}} \propto \frac{N_{scat}}{\sigma_{\phi,NB} \text{ [rad]}} . \quad (4.11)$$

Since ρ_τ and ρ_ϕ have opposite and independent influences, an additional parameter is considered, accounting for their combined effect, hereby named as DCIR *channel richness*, ω_{DCIR} , calculated according to (4.12). In this way, larger values of ω_{DCIR} will imply a richer variety of uncorrelated signals, due to their either angular or temporal dispersions, in accordance to the previously presented reasoning: lower σ_τ lead to higher ω_{DCIR} , for the same σ_ϕ , or larger σ_ϕ lead to higher ω_{DCIR} , for the same σ_τ .

$$\omega_{DCIR} \text{ [rad/\mu s]} = \frac{\rho_\tau}{\rho_\phi} = \frac{\sigma_{\phi,NB} \text{ [rad]}}{\sigma_\tau \text{ [\mu s]}} \quad (4.12)$$

Note that these definitions cover both DesS and NDesI contributions, and that ω_{DCIR} combines the effect in both domains, as a quantitative account for the multipath richness of the wideband and directional channel. Furthermore, it relies on the physical wideband and directional characterisation of the channel, accounting for the cluster contribution as a whole.

It is important to further understand the physical meaning of the hereby-defined *channel richness* parameter, which is expressed by units of angular frequency, [rad/ μ s]. Notice that, larger multipath richness usually implies having larger delay-spreads, i.e., larger number of uncorrelated multipath components in delay, whereas the (4.12) definition seems to behave in the opposite way. In fact, the hereby-presented definition does not contradict the usual meaning, seeing such parameter as an indication of the quantity of different incoming signals' AoAs per time unit. For a certain ω_{DCIR} , seen as an average quantity per time unit, higher delay-spreads imply relevant angular components along more time units, reflecting the larger multipath richness, on the whole, solely in the temporal sense. But, if those same significant angular components arrive in a smaller time period, i.e., if the delay-spread is lower, then ω_{DCIR} value increases, reflecting the higher multipath richness, in both the angular and temporal senses, together. Thus, larger ω_{DCIR} values mean that a greater variety of signals from different angles arrive, per time unit, reflecting larger multipath richness in both domains.

The principle hereby put forward has close relationship to the notion of *Multipath Component Separation* (MCS), defined in [SÖHM02], both rooting in the physical matter of multipath dispersion: higher angular MCS means that multipath components are more angularly separated, which would also mean lower ρ_ϕ , i.e., both in the sense of larger multipath richness; nevertheless, lower temporal MCS would imply higher ρ_τ , which then apparently render opposite tendencies. But, in the manner explained in the previous paragraphs, the current ω_{DCIR} definition must be seen as a mean quantity, per time unit, and having more units with a certain value of ω_{DCIR} , i.e., larger delay-spreads, does imply larger multipath richness. Also, if the notion of MCS has the advantage of being extendable and applicable to other domains, such as the Doppler one, the ω_{DCIR} definition more directly reflects the opposite dependencies and constraints that the angular and temporal domains introduce. Conclusively, the notions of MCS or ω_{DCIR} are not opposite, but related and complementary²³.

Additionally, the presented definitions not only strongly relate to angular diversity, but also involve the temporal domain. The issue of the achieved diversity gain, directly affecting beamforming performance, has been addressed in [KuTB02], for LoS or NLoS conditions, where such available gain has been explained to root from the decorrelation of signal amplitudes, low resulting DesS levels being improbable.

²³ For this, it may be argued that ω_{DCIR} should not be termed as *channel richness*, this involving a vaster notion. Other terms would be applicable, such as *multipath content*, or *multipath frequency*.

For the several MiCs and MaCs situations shown in Table 4.8 and Table 4.9, Table 4.10 presents the corresponding ρ_τ , ρ_ϕ and ω_{DCIR} values, calculated according to (4.10)-(4.12): in the MaC case, incoming signals are more concentrated in angle, but generally less in time, compared to MiCs; within the presented MaC cases, the effect of r in the densities is more evident than that of d_{MT} , whereas ω_{DCIR} varies more significantly with d_{MT} than with r ; for the MiC cases, the variations of densities with d_{MT} are much larger, compared to those of MaCs. But, most important is the fact that the values of ω_{DCIR} are one order of magnitude greater in MiCs than MaCs, and the variations of ω_{DCIR} as functions of d_{MT} are inverse of the MaCs ones. As it will be seen, these divergences will have a visible impact on the beamforming performance.

Note that these are fundamental wideband and directional channel features, which will render very general final conclusions. In this way, a good degree of independency from the applied beamforming method as well as from the system application may be reached. By analysing the response of the beamformer towards the several scenarios, one will then be able to understand how and which fundamental channel characteristics condition the physical process of locating lobes and nulls in their best positions, in the sense of minimising interference.

Cell Type	Physical Parameters		Scattering Area [km ²]	ρ_τ [km ² /μs]	ρ_ϕ [km ² /rad]	ω_{DCIR} [rad/μs]
	d_{MT} [m]	r [m]				
MiC	50	-	0.182	0.47	0.24	1.94
	500		0.261	1.48	0.47	3.15
	1 000		0.418	4.18	1.10	3.82
MaC	1 500	50	0.126	0.09	0.56	0.15
	1 000	200		0.35	1.29	0.28
	1 500	200		0.36	1.95	0.19
	2 000	200		0.36	2.57	0.14
	1 500	400		0.503	0.80	3.90

Table 4.10 – ρ_τ , ρ_ϕ and ω_{DCIR} values involved in several MiCs and MaCs scenarios.

Realising that each scatterer entails a number of reflected signals that is directly proportional to the number of active links, L , the ω_{DCIR} parameter will anyway be independent of such, since L affects both densities in equal manner in (4.12). For this, ω_{DCIR} does not account for the propagation channel multi-user usage, in terms of the number of active users. Anyhow, the meaning of such densities demand for careful use of such parameter: in the case that MTs are grouped, L would directly multiply by ρ_ϕ or ρ_τ , giving indication that the total number of signals per angular or delay unit are larger; in that case, the higher temporal density does not mean that each link's signals are

more concentrated in time, but that all links' DesS and NDesI are closer together in time, involving other MTs powers; the quantity of NDesI signals is larger, due to L , and the performance should in fact be worse, in contradiction with the indication that the corresponding density is meant to entail. Additionally, depending on MTs being grouped or spread, the beamforming dependencies are also different, additionally confirming that the consideration of L is a more complex issue. By involving several links, the code nature and properties also strongly condition performance, resulting in that the influence of the density values may be less visible. Judging on this, for the current study, it is for a given L that such densities give the information for which they have been created, i.e., for the analysis of the wideband and directional physical properties of the propagation channel. Anyhow, the prospect of defining similar density and richness parameters that additionally account for a *whole*-DCIR, i.e., for all of the L DCIR contributions, the whole covered scattering area and the scenario at stake, is not only realistic but also figures as a prospect for future work development.

It is important to be aware that no diversity scheme is being considered in this study, assuming that all arriving signals are correlated among each array elements. In this way, though the *channel richness* expresses the degree of independency among the arriving signals at each element, being directly related to the angular and delay-spreads as in the case of diversity, the sense for the presented meaning of *channel richness* is independent from any such diversity scheme, and even of any specific beamforming, depending solely on the propagation channel itself. By resorting to such definition, one is relating the whole independency of arriving signals, at any of the array elements, to the beamforming performance, before any diversity method is applied between those array elements.

Later in this study, the matter of channel richness and correlation will be further developed, establishing relations of this study to other multi-antenna perspectives.

4.6 Summary and Conclusions

The WDCM to be implemented in this study has been defined, from among the several models that have been previously presented. A pragmatic approach has been adopted, favouring a wideband cluster model, statistical in its nature, not too demanding in terms of processing burden, backed by measurement campaigns, and flexible enough for future extensions and use within propagation scenarios. Furthermore, such model versions also apply to both micro- and macro-cellular situations, maintaining its fundamental nature. In these senses, and for the availability factor, the MGBSBEM and CM versions are used.

Secondly, the way that such model is applied has been conveyed, describing how the physical composition of the channel is modelled, the DCIRs involved in a multi-user perspective, and the fundamental model implementation assumptions.

Having done so, the propagation scenarios are described in detail, primarily conveying their practical perspective importance and statistical value. These have been thought of to satisfy two

important study demands: the simulation of both approximate practical real-life situations (generally approximating streets, cross-roads and plazas), and those that pose highly or low demanding beamforming conditions (grouping or spreading of MTs, contributing or not with temporally or angularly correlated signals). Their designations as well as their pictorial description have been provided, as function of the several parameters. This is done for MiCs and MaCs, independently. However, the intentional parallelism in the MiCs vs. MaCs characterisation has been fundamental to generate the comparative set scenarios, important for the later comparison of performances.

Then, the wideband and directional propagation characteristics of the involved channels are characterised, in terms of AoA and ToA spreads, the number of orthogonal arriving signals, as well as defining temporal and angular densities, and DCIR channel richness parameters. Their physical interpretation and values have been presented, already understanding their expected importance in expressing the beamforming interference suppression – larger ToA spreads imply larger NDesI powers, whilst larger AoA spreads are expected to lead to higher beamforming freedom in the location of lobes and nulls; larger temporal densities of arriving signals imply better correlation properties among all links' signals, tending to improve beamforming performance, whereas larger angular densities entail worse angular separation from among DesS and NDesI, rendering worse performance; the defined DCIR channel richness reflects these opposite effects in the temporal and angular domains.

Among MiCs and MaCs, a direct link between those channel parameters and the scattering areas and shapes at stake has then been established, therefore, rendering a physical level characterisation. It is most relevant to conclude that: σ_ϕ spreads decrease with increasing d_{MT} and such relative dependencies are of the same order, independent of the angle-spread definitions; for MiCs, the involved σ_ϕ values are one order of magnitude larger than those of MaCs, again independently of the spread definitions; for MaCs, the variation of σ_τ with d_{MT} is insignificant, whereas in the case of MiCs σ_τ varies by a factor around 4, for that expecting larger implications in the sensitivity to temporal discrimination in MiCs; though the delay-spreads involved with the implemented MiC and MaC scenarios may be of similar order, the angular ones vary substantially, not only between MiCs and MaCs, but also within each of those cases; compared to MaCs, the larger number of MiC scatterers implies a larger independency among the present DCIRs, resulting in a richer variety of uncorrelated arriving signals among the active links, i.e., larger multipath richness; the values of ω_{DCIR} are one order of magnitude greater in MiCs than for MaCs, and the variations of ω_{DCIR} as functions of d_{MT} are inverse of the MaCs ones; in the MaC case, incoming signals are more concentrated in angle, but generally less in time, compared to MiCs; within the presented MaC cases, the effect of r in the densities is more evident than that of d_{MT} , whereas ω_{DCIR} varies more significantly with d_{MT} than with r ; for the MiC cases, the variations of densities with d_{MT} are much larger, compared to those of MaCs.

Conclusively, the studied directional and wideband properties of the involved MiC or MaC channels/scenarios have not only been registered to differ in several ways, but also to imply differing beamforming performance divergences. In both temporal and angular domains, the ways that the physical channel properties affect performance strongly root from the beamforming freedom that the channel or scenario allow for, i.e., from the involved multipath richness. It is now important to specify and characterise the beamforming problem, applied together with the defined model and scenarios, before the analysis of results and the confirmation of the hereby-placed hypotheses take place.

5 Implementation – the Adaptive Problem

The wisdom of life consists in the elimination of nonessentials.

— Lin Yutang (1895-1976)

5.1 Specification and Implementation Perspective

It is now important to specify and describe the application of the adaptive problem and algorithm. This involves defining and characterising the algorithm itself, its inputs, the adaptive problem within which the algorithm is implemented, and the performance parameters that require to be evaluated. This chapter also includes the definition of the performance evaluation parameters, the several involved power components, as well as the PC process that must be applied. To finalise, calculation and statistical issues are presented, covering the type of averaging and statistics of the obtained results.

First of all, the whole beamforming problem needs to be fully specified. Besides selecting an adaptive algorithm to be studied and developed within an initial UMTS perspective, with the aim of further extrapolating results to future MBSs, one must deal with the following aspects: location of beamformer, at the BS and/or MT; communication way, in Down- (DL) or UL; transmission mode, FDD and/or TDD; stationarity conditions and data acquisition type, block-sample or sample-by-sample; reference acquisition method, using a temporal or spatial reference; type of SA, switched-beam or adaptive; spatial processing domain, either element- or beam-space processing; degree of adaptivity, full or partial; adaptivity coverage, intra- and /or inter-algorithm. The definitions of these possibilities have been presented in Chapter 3, already conveying a general analysis of the main antenna beamforming algorithms and perspectives, providing an initial critical view on the application at stake. But, it is in the present chapter that its full specification is provided and justified.

The following analysis will also aim at relating and weighting the whole beamforming problem to a communications system perspective. Though it is most directly focused on UMTS, it is seen in that way only as a primary basis, defining general conditions and assumptions. These considerations are most important for the current study, hereby establishing decisions and specifications, building upon the background provided in Chapter 3. Nevertheless, one summons for a particularly important and whole objective that rules the present study, at the level of the adaptive problem/algorithm and of the system directed approach – it is fundamental to present and view these specifications as not limiting the final conclusions to a specific algorithm or system. The decisions on these, most directly presented in this chapter, must not be set to be restrictive in that sense. It is only by adopting such reasoning that the results of this study acquire the desired sufficient generalisation. Accordingly, the final beamforming dependency on the fundamental physical properties of the channel must be shown to be independent of such algorithm and system implementations specificities.

5.2 Specification of the Beamforming Scheme

5.2.1 Beamformer Location, Direction and Transmission Mode

Though it can be forecasted that in mature UMTS implementations, and most certainly in future MBSs, beamforming structures will exist at both BS and MT ends, e.g., [MAC03], due to the ever demanding services provision, this study should firstly evolve from the BS side. The main reason for such is that, inherently, the BS has the function of effectively directing centralised information to or from various MT users. This means that more interference power must be more efficiently dealt with at the BS, for all established links. Also, as far as cost and system implementation complexity are concerned, the application of such beamforming systems is easier at the BS side. It is probably because of that, in parallel to stating that UMTS standards are favourable to using SAs, that the reference to their usage is primarily directed towards the BS implementation, [ETSI98].

On the other hand, the variability of the type, shape, location relative to user, scenario, AoA and ToA at the MT side are so much greater than those of a BS that the dynamics at the MT side will render larger and more important SINR variations. Thus, adaptivity should inherently provide greater SINR gain, at the MT level. Besides the forecasted operational-oriented nature of MBSs, e.g., [PrEU99], with configurable baseband processing and software reconfiguration techniques, the use of adaptive antennas at the MT may also prove to contribute to the mandatory power consumption reduction. These are important enough reasons in favour of developing from the MT side. For UMTS, the MT would have to be ready to provide more than one simple beam (for UL and DL), to guarantee the existence of soft handover. One can reason that with future MBSs, for even more demanding situations than those expected for UMTS, the several types of handover will also require more than one beam. This is even more important in another way, being predicted that future MTs will integrate

several standards, being highly reconfigurable in terms of software, depending on the communicating supporting network, e.g., [PrEU99], [Evan03].

The choice of beamforming location for this study could cover either the MT or BS sides, or their combined operation. Nevertheless, those are seen as more complex situations, which should be preceded by considering the simpler case of beamforming at one side only. Additionally, the variety of situations that the MT side involves also implies larger complexity in terms of propagation scenarios, compared to the BS side. And, again, this supports the decision that the simpler BS situation should be firstly covered. This *simple-to-complex* approach allows future research to be later led towards covering the MT side, making use of the conclusions extracted from the simpler BS end, on the fundamental interactions between beamforming and the WDCM. Respecting the *simple-to-complex* approach, the present study considers adaptive beamforming at the BS side.

Concerning beamforming direction, it is important to be aware that standardisation and extensive research have focused on SA technologies for both UL and DL. Anyhow, for the current research, in the practical sense, attention must be drawn towards either UL or DL. This must not be understood as a limitation, but as a step towards enabling the reach of the main objectives. The issue is not deciding on the basis of whether the system is UL- or DL-limited: firstly, because one envisages that future MBSs will include beamforming at both the UL and DL; secondly, UL and DL beamforming processes are anyway related, at least due to the channel's symmetric directional nature, and feedback control loops are to be implemented, e.g., [Hugl02], [HoTW03]; also, in a MaC, rural environment, the system may be coverage- and UL-limited, whereas in a MiC, urban setting, it may be capacity- and DL-limited, depending on the traffic loads, e.g., [MAC03]; finally, a system may be UL-limited, and another may be DL-limited, e.g., [Laih02].

At the physical radio propagation level, the effects of interference at the BS are generally more critical in the UL than in the DL, especially reasoning upon how the propagation channel and possible scenarios affect the resulting signal correlations, AoAs and ToAs. Additionally, the large number of interfering signals that arrive at the BS, constituting both intra- and inter-cell interferences, may be near in terms of AoAs, ToAs, and powers. Therefore, at the BS, UL beamforming will naturally reflect the propagation channel conditions detected, directly fitting into the aim of the current study, along with not accounting for the more complex situation of including inter-cell interference.

Anyhow, DL beamforming may be a reflection of the established UL beamforming at the BS, either directly (in the case of TDD implementations) or indirectly (in FDD). In [Hugl02], particular concern is directed towards the UL-DL correlation issue. The author has confirmed that the UL and DL channels at differing frequencies are mainly uncorrelated due to fast-fading (besides the array response). It has been also shown that the directional responses in UL and DL at differing frequencies maintain close relation in respect to dominant AoAs and the whole angular response. These results

further support the idea that studying the directional constraints present in the UL are extendable to an equivalent study in the DL.

Concerning UMTS, the TDD mode will most probably be characterised by data rates much higher in the DL than in the UL, being highly asymmetrical. However, the simplifying condition of existing propagation channel symmetry reduces the apparent greater importance that DL beamforming then acquires. On the other hand, for FDD, the establishment of DL beamforming will result from the involvement of other techniques that surpass the problem of beamforming itself, e.g., [Hugl02]. For this, again, working in the UL is closely centred in the aim of the present study.

Making use of the symmetric nature of the propagation channel, for TDD, is possible if there is enough correlation in the temporal domain. Such assumption makes sense, considering stationary conditions during the 10 ms frame or, in a more demanding way, during a certain number of slots within a frame. Again, the measurements in [Hugl02] show that, for both TDD and FDD, the channel uncorrelates quickly, relatively to the time required for feeding back channel information from MT to the BS. Such uncorrelation is again shown to be due to fast-fading. In that study, the space-selective fading was found still being correlated along the 10 ms frame, with speeds of up to 50 km/h.

The stationarity hypothesis must further consider the flexibility involved in the dynamic and unbalanced nature of the slot allocation process of the TDD mode. This physically justifies why the study is firstly centred on TDD, anyway reporting some analysis results corresponding to the application to FDD. Since the algorithm performance should be evaluated independent of the mode, especially knowing that one is dealing with fundamental physical restrictions that rule the generation of the necessary array patterns, the FDD results are precisely useful to verify that it is so. An additional factor supporting the TDD application, for the objectives of this study, is the involved simulation burden. As it will be seen (Section 6.3, Implementation of TDD and FDD Modes), the TDD implementation involves much less complex computational effort in the generation of the channel for UMTS, in respect to the FDD one.

Another issue is connected to power, in that the power source at the BS is inherently less limited than at the MT. This means that there is a higher probability that the DesS powers received at BS will be lower than that received at the MTs from the servicing BS. In this sense, UL beamforming at the BS is already important to improve SNR.

Concluding, the present study is focused on UL beamforming to most pragmatically go forth with the analysis and extract the meaningful results, not diverting from the objectives.

5.2.2 Stationarity Conditions, Data and Reference Acquisition

Even though stationarity may be easily accepted during an UMTS frame or even slot (666 μ s long), for the higher mobility and data rates covered by future MBSs, such approximation is expected

to be more critical. Besides the higher frequencies and bandwidths, this should be so also due to the much lower wavelength, movements by terminals and by scatterers implying larger fading rates.

In ten years' time, realising the rhythm by which technology has been growing, e.g., [Kurz01], [ITRS02], real-time sample-by-sample data acquisition will most probably not present a problem, not implying higher costs or power consumption increase for either UMTS or future MBSs implementations. It is forecasted that around 2010 a DSP processor may well deliver around 3 trillion instructions per second, [TI00]. Weight vectors may well be output highly above the rate of each input data sample.

Anyhow, it is also important to view the application of an algorithm in the light of the aims of the current research. In fact, as it will be seen, the block-sampling will allow for the better characterisation of the mean channel and scenario responses, compared to a sample-by-sample approach. For this, block-sampling is not only effective, but also renders conclusions that are anyway valid for sample-by-sample approaches. As a consequence, the stationary or static assumptions must allow for the sampling of the full block with no critical channel changes, or none at all, in order to simplify the adaptive problem. The block size must, therefore, not be sufficiently large so as to extend beyond the stationary or static period.

In the case of UMTS, one directly states that the inherently available CDMA codes that may identify a source should be used in order to extract the maximum temporal referential information from the total received signal. The code will be highly correlated to the DesS, and with very low correlation with other signals, making it a good means of extracting the needed reference. Also, for future MBSs, access schemes have yet to be established, the possibilities being Frequency Division Multiple Access (FDMA), TDMA, CDMA, among others, e.g., [SFBP00]. Anyhow, along the line of the possible evolution-oriented nature of future mobile systems, in respect to UMTS, CDMA-based multiple access schemes are foreseen, such as MC-CDMA, e.g., [Lu02]. Therefore, both the resulting greater algorithm efficiency, and the future perspective for MBSs strongly support the use of identifying reference codes, based on the CDMA scheme. In this sense, the use of such standard-available temporal references falls into the *semi-blind* concept provided in [Laur00].

5.2.3 Type of Smart Antenna, Processing Domain and Adaptivity Coverage

Since this study aims at extrapolating its conclusions towards future MBSs, roughly forecasting their implementation to be working within the next ten years, and in light of the mentioned enormous advances in electronics, one envisages that by that time technology will easily cope for sufficiently fast processing for powerful beamforming, as already mentioned. In this way, the complexity and cost related arguments against the use of adaptive solutions, and for the switched-beam counterpart, will most probably no longer make sense. Also, there will be enough processing

throughput to deal with other more complex matters, such as multidimensional arrays, antenna calibration methods or polarisation issues, making part of the core beamforming system.

In a similar manner, the arguments against full adaptivity of the beamformer do not prevail against the enormous hardware development that has already characterised the past, needless to mention, that will characterise the future. Anyway, the problem of partial adaptivity is more of a resource management one, an issue that does not make part of the present study.

Concerning the implementation domains, there is no intention of answering the question as to what extent these NB or WB adaptive structures must be applied, at the link- and system-levels, either for UMTS or for future MBSs. As discussed, full WB performance will be possible through an element-space scheme, where spatio-temporal processing will be applied. Once more, the technology trend will most probably allow for the easy and powerful implementation of WB schemes. Additionally, respecting the objectives set, a spatio-temporal application must be implemented, in order to primarily evaluate which and how fundamental propagation channel spatial and temporal characteristics affect beamforming.

Finally, the previous arguments backup the decision on developing the present work within a fully adaptive antenna, WB or spatio-temporal platform.

Inter-algorithm adaptivity makes sense if the beamforming structure will be subject to very different traffic and/or propagation conditions, during its operation. Take, for example, the case of a BS placed near a railway, prepared to cover an MT in a very fast moving train, but in other times covering a much lower velocity and lower data rate demanding MaC encompassing that station. The antenna may be ready to switch fast between a passive to an adaptive operation, and return back to the passive BS coverage. Or, possibly changing from a single very fast converging WB algorithm scheme to a group of much less demanding NB sub-structures, depending on those scenarios. As mentioned earlier in the text, another example concerns that of existing large traffic fluctuations during the day, at the same BS coverage location. The antenna may also be required to change algorithms depending on the required SINR, for the demanding traffic. Another possible example, from the MT point of view, is that of a user that moves from a low MT density area, with low density of buildings, to another area with high traffic and high building density. Furthermore, if the user is demanding for high data rates, it may be useful for the MT antenna to switch to an algorithm that performs more efficiently (with the possible temporary cost of the heavier processing involving large power consumption).

It may be true that *inter-algorithm* capability and advanced software radio schemes should not be put aside, especially being aware of the strong trend that software radio is gaining in the establishment of future mobile systems. Nevertheless, before intaking more complex schemes, at the system and network levels, the problems raised in the present research must be resolved. The issue is

solely dealt with in an *intra-algorithm* basis, in order to study the combined relations between the wideband and directional nature of the propagation channel and beamformer performance.

5.2.4 Selection of the Adaptive Algorithm

This is the final major decision that must be undertaken, to go forth with the proposed objectives. Though undoubtedly many adaptive algorithms may be used for adaptive beamforming, their inputs, assumptions and performance differ considerably. Most of all, the selection of the adaptive algorithm requires a pragmatic approach, most directly dealing with those differences. This procedure follows from the descriptions provided in Section 3.4. As it will be seen, these are important even in the case of an algorithm/process that is ruled out.

The CMA, as emphasised, is not particularly adequate for the use with PC, which inherently makes part of a CDMA-based system specification. Also, if CDMA-based schemes are being, and going to be, used, then PC will be always required. Furthermore, it is kept in mind that these PC procedures will inevitably be combined with beamforming, meaning that CMA applications will anyway inherently account for the PC process, in a combined manner. Therefore, such approach results in unnecessary complexity, for the current objectives.

As far as NNs are concerned, their great possibilities may deliver very good performance results, but the study of these would imply a knowledge path that is seen to diverge from the interests for the current research. Such sort of decisive reasoning is as valid and as important as any other technical based argument, in any practical work development. Also, the practical application of a complete and high computational load involved with the learning process may not be compensated by the fast generalisation procedure. Nevertheless, a very fast converging Hopfield network, using a systolic analog network, has been implemented, [ChYC92]. Generally, the Hopfield solution outperforms the classical LMS convergence rate, [SLLL95]. Additionally, NNs allow for real-time weights production, [ZoCG98]. A particular use of NNs has also made possible the compensation of decalibration errors and inter-element coupling, minimising the effects of these in the array performance, [ChLa99].

The remaining algorithms, the LMS, RLS, SMI and CG, along with their related versions, need a closer and more careful look. Following the futuristic reasoning already conveyed along this text, the different convergence speeds obtained with these algorithms will not be a major decisive argument. In this way, decisive parameters may be final error performance, dependence on the correlation matrix eigenvalue spread, and resulting SINR and BER.

Concerning the LMS, its convergence speed performance not only depends on the propagation conditions, eigenvalue spreads strongly determining the convergence speed, but also the inherent gradient noise and large variances in the instantaneous values explicitly affect the final error. Its dynamic range is relatively limited, requiring the use of PC, [LiLo96], [ChYC92]. In fact, the

normalised LMS has been conceived to solve this, and the system may already inherently include PC, e.g., in CDMA systems. Nevertheless, even with PC, it is not totally clear if the dynamic range limitations of the LMS may affect, or not, the final SINR. In spite of its limitations, or due to them, the LMS and the gradient-based methods may be limited to mobile pedestrian or indoor applications, [Vaug88], due to the low MT mobility. But, since processing speed will not be a decisive factor, such algorithms may be applicable to other environments. Additionally, many faster versions of the LMS have been conceived, introducing constraints to ensure that the DesS contributions are not filtered out together with the interference. Anyway, considering that the chosen algorithm performance should not depend greatly on propagation conditions nor itself introduce any excess SINR loss, then the LMS (its unconstrained version, best adapted for the case where a temporal reference exists) should be put aside.

Concerning the SMI, its most valuable asset is the fact that its performance is almost independent of the eigenspread of the correlation matrix. Consequently, it should converge faster than the LMS. The SMI, nevertheless requires that enough correlation data is averaged together, colliding with the need of fast calculating the new weight vector in a dynamic environment. Practical implementation issues can be pointed out, also – the computational complexity may be large and finite-precision issues may affect the matrix calculations and errors, [LiLo96], [WaCr94]. An inherent drawback of the SMI is the inevitable error, and consequent SINR loss, resulting from the use of correlation estimates. In the case that the number of estimates is not enough, the SINR performance will be severely affected. An eigenanalysis-based method has been referred to as a better solution, in that case, [WuHa95].

The RLS algorithm does not depend on eigenvalue spread. Its performance does not depend on propagation conditions, as does the LMS. The most important characteristic of the RLS algorithm is that the calculation of the correlation matrix inverse is substituted by a recursive scalar calculation. As a consequence, it will typically converge an order of magnitude faster than the LMS, as long as the SNR is high, [LiLo96]. According to [HeBK99] and [Bagh99], the RLS still requires high computational complexity and heavy matrix calculation, exhibiting numerical instabilities. It has been widely used for adaptive filtering, but its complexity has also been the reason for many researchers to choose other methods, such as the CG.

Regarding the CG, the algorithm does not pose any specific reason not to be applied, due to its simplicity and very fast convergence. A very wide variety of related papers exists, covering the use of the CG in beamforming, e.g., [ChWi00], [ApCB00], [KaBa99], [HeBK99], [Bagh99], [ChLH97], [ChWi95], [ChKi92]. Several sample-by-sample CG algorithms have been conceived, making real-time convergence possible, with the need for very little number of products, $O[M]$, meaning that potentially low computational complexity may be required, [Bagh99]. In fact, the CG is seen to be the fastest of the iterative algorithms mentioned, [Chry00], also being of simple implementation.

Moreover, those studies do not treat the problem of evaluating how the propagation channel characteristics affect CG's performance, by means of a WDCM, nor consider the application of the algorithm in a system-directed way. Therefore an area of required contribution has also been identified.

Due to the lack of concrete data on the relative SNIR performance for the case of UMTS or future MBSs, and for different propagation conditions, the final decision is of a conservative nature, not selecting a particular unique algorithm for any clear advantages. The other reason for not being able to be so assertive is the fact that convergence speed and algorithms complexity are thought not to be relevant. In the literature, these factors have indeed been indicated as the reasons for selecting a particular algorithm.

For all of these arguments and the elimination of the remaining algorithms, the CG algorithm has therefore been chosen for the present study, in order to pursue the set objectives, being simulated and applied to specific propagation scenario conditions, within a UMTS perspective, bridging towards future MBSs. Anyhow, the application of the RLS is also added, though involving a less profound study. Comparing both algorithms not only results in verifying their mutual convergence, but also in evaluating their main application differences. As it will be described, the two algorithms provide comparable complexities but significantly different performances due to their different sampling.

It is argued that by dealing with the same propagation channel constraints, at the fundamental physical level, any beamforming algorithm would theoretically lead to the same results, concerning the performance dependencies on these channel characteristics. Therefore, the choice of the algorithm is more of a practical one, most of all being required to effectively render results that solely and clearly reflect the channel constraints that limit beamforming operation. Also, in [LiLo96], it has been shown that all criteria for the calculation of optimal weights tend towards the same SINR, provided the conditions are ideal for their use. This comes from the fact that these problems tend to the same optima, which is the Wiener solution, the Wiener-Hopf equations establishing the main steady-state performance limits. For this, the use that adaptive methods make of the optima calculation schemes will always be referenced to the Wiener solution, regardless of the method.

Finally, adaptivity has been presented and discussed in the sense that a beamformer will function using a single chosen algorithm to calculate the necessary weights for a dynamic and not completely uncertain environment. Since all the covered algorithms have their own limitations, one can say that the ideal adaptive beamformer would be able to change between several adaptive algorithms, besides working within each. Truly, that would be an *adaptive selection of adaptive algorithms*. It would be capable of adaptively changing from more to less complex, from faster to slower, from partially to fully adaptive alternatives, depending on the interference scenario and dynamic spatio-temporal changes.

5.3 Algorithm and Adaptive Problem Implementation

5.3.1 General Assumptions and Considerations

The used array geometry, far-field reception conditions, narrowband transmission/reception array, and the general antenna properties assumptions and considerations have already been presented in Section 2.2 and sub-Section 4.3.1. Additional ones that particularly concern the implemented algorithm and array are hereby systematically listed:

- the array is constituted by isotropic, ideally matched antenna elements, ideally weighted and calibrated, with no inter-element coupling;
- the array is a ULA, with element spacing of $\lambda/2$, placed on the same horizontal plane as that of the WDCM;
- MT and BS are considered to be perfectly synchronised so as to achieve ideal despreading and dechannelisation;
- for each l^{th} link, the desired code is already known at the BS, having been previously determined by the Radio Network Controller (RNC);
- the front-end, demodulation and down-conversion stages are also thought of as ideal, except for the noise figure (used to determine the noise power level);
- for simplifying reasons, the signals considered to be transmitted are the codes, only, not including any information data. It is believed that, for the established objectives, the introduction of additional data and symbol shaping would not be a necessary added value, in fact contributing to larger complexity in the reaching of the most general conclusions.

Upon these assumptions, the implemented beamforming processing is set to work at the baseband level, as Figure 5.1 shows, meaning that $\mathbf{x}(n) = \mathbf{u}(n)$ will represent the signal vector at the beamformer input, at sampling instant n , whose M elements represent the received, downconverted and analogue-to-digital converted signals. The weighted sum of these constitute the beamformer output, $y_l(n)$, calculated through (3.3) in Section 3.2, containing minimal contribution from interference and noise, subject to an adaptive process whose objective is to approximate $y_l(n)$ to the desired code $c_d^{(l)}(n)$, known to the system. The structure hereby represented for MS-BS link l applies to each of the L active links, so that each link has a dedicated beamformer array pattern, where a $M \times L$ weight matrix can be processed within the same digital signal processor.

The $N_s \times M$ signal matrix $\mathbf{U}(n)$ is then obtained from a block of N_s baseband signal samples, taken at chip-rate, at discrete instant n , from each of the M array elements, including thermal Additive White-Gaussian Noise (AWGN) and summing up all links' contributions. Resulting from the baseband model described before, for each m^{th} array element and instant τ_n , each element of \mathbf{U} ,

$u_{n,m} = u_m(n)$ ²⁴, is given by (5.1). $a_m(\phi_{n_s, n_c, l}) = e^{j\frac{2\pi}{\lambda}d_{el}(m-1)\sin(\phi_{n_s, n_c, l})}$ is the corresponding steering vector element, d_{el} is the element spacing and λ is the wavelength; similarly to (4.5), $\Gamma_{n_s, n_c, l}$ is the complex reflection coefficient corresponding to the n_s^{th} scatterer, within the n_c^{th} cluster, l^{th} link; $\alpha_{n_s, n_c, l}$ is the magnitude of the corresponding ray accounting for path-loss; $c_d^{(l)}(n)$ is the transmitted referential signal. A total of N_c clusters is assumed, as well as $N_{scat}(n_c)$ scatterers within each cluster.

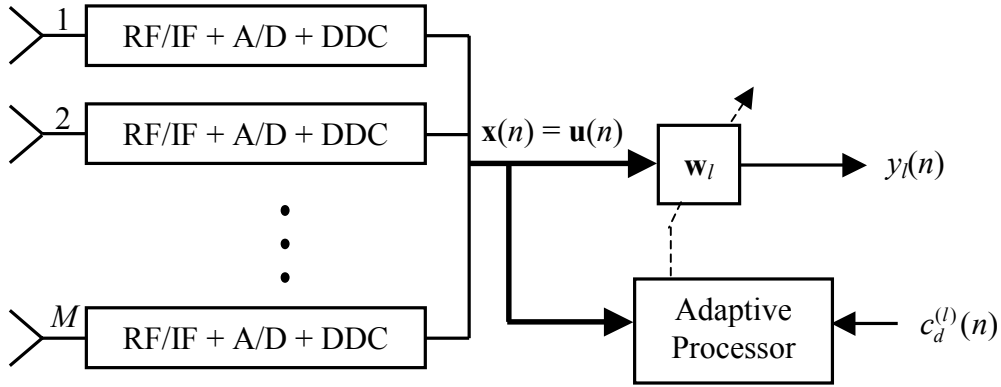


Figure 5.1 – The generic adaptive beamforming scheme for l^{th} link (based on [LiLo96]).

$$u_{n,m} = \sum_{l=1}^L u_{l,n,m} = \sum_{l=1}^L \sum_{n_c=1}^{N_c} \left\{ c_d^{(l)}(\tau_n - \tau_{n_c, l}) \cdot \sum_{n_s=1}^{N_{scat}(n_c)} \alpha_{n_s, n_c, l} \cdot \Gamma_{n_s, n_c, l} \cdot a_m(\phi_{n_s, n_c, l}) \right\} + n_{n,m} \quad (5.1)$$

5.3.2 Reference MT-Specific Codes Specification

CDMA is especially favourable for providing a signal reference closely correlated to the DesS, but weakly correlated to the interfering sources – a code. It is known that such a referential source existing, it should be used to its maximum extent, providing best convergence and final error performance, e.g., [LiLo96]. Also, such method poses less problems regarding antenna element decalibration, since knowing about a reference signal will help counteract such.

In case of UMTS, for either TDD or FDD mode, the signal sample data can be obtained at the beginning of the first data block, within each slot. For TDD, this means that the formation of beams is completed before the reception of the midamble, therefore also rendering the best conditions to capture and make best use of the midamble.

²⁴ The index n refers to the sampling instant, being used interchangeably referring to the signal matrix at instant n , $\mathbf{U}(n)$, or each of the N_s temporal samples that constitute that matrix.

Following UTRA specifications, e.g., [ETSI01c], [ETSI01d] or [HoTo00], different families of codes are used, to separate channels, cells or MTs, depending on the duplex mode, and transmission direction:

- for both the FDD or TDD, DL or UL, channelisation codes separate physical channels from the same source, being derived from the respective code tree structures;
- in the UL or DL, TDD mode, different MTs are separated by Orthogonal Variable Spreading Factor (OVSF) channelisation codes, 16 chips long, and midamble sequences of different length depending on the environment;
- in the UL or DL, TDD mode, different cells are separated by scrambling codes with the length of 16;
- for the UL FDD, different MTs are separated by long Gold scrambling codes (38 400 chips long), or alternatively short S(2) family scrambling codes (256 chips long), depending if a RAKE receiver or more advanced multi-user interference suppression techniques are used at the BS, respectively;
- for the DL FDD, different MTs are separated by OVSF channelisation codes (256 or 512 chips long), within one cell;
- for the DL FDD, different cells (or sectors) are separated by long Gold scrambling codes, as in the UL (38 400 chips long).

Judging on this, interpreting the *separation* of cells or terminals in both the temporal and spatial domains, the channelisation and scrambling codes have been chosen as the most adequate reference sources for the following reasons:

- they can be used for either TDD and FDD, with a simple change in the code used;
- midambles exist within the TDD time-slot, after the first data symbols, requiring that the reference acquisition be made at that block only, whereas the channelisation and scrambling codes are present during the whole slot;
- midambles are not included within the FDD slot;
- the use of channelisation and scrambling codes allows for easier integration of the suggested beamformer with a RAKE Rx structure.

Therefore, the use of the referred codes not only results in flexibility, by applying the same beamforming structure for both TDD and FDD modes; in simplicity, by solely requiring a change in the reference code; in the maximisation of the available resources, since the beamforming is performed during all the slots, at any point within such slot, in particular allowing for the convergence from the start of the slot. For the current study objectives, these factors are fundamental in order to be able to present a solid and co-ordinated set of assumptions, hypothesis and conclusions.

The use of the midamble to identify the MT has been explicitly specified for beamforming, [ETSI02a], in the TDD mode. Among the three types of bursts, burst 1 supports the largest number of

training sequences, which can be used to estimate the different channels for different MTs in UL and, in case of beamforming, also in the DL. When DL beamforming is used, at least that user to which beamforming is applied, with its dedicated channel, shall be attributed an individual midamble. Nevertheless, as mentioned, the use of such reference would not only involve a different approach to that applied for FDD, but also require synchronisation and midamble detection within the TDD time-slot.

It is also important to understand that, for a future application of the presented beamforming problem, the identification of cells is also relevant, since MTs will make use of the same channelisation code tree. Therefore, already putting forth the future consideration of neighbour cells and the analysis of inter-cell interference, the identification of cell scrambling codes avoids beamforming to take a NDesI signal for a DesS one from the wrong cell, allowing to look at other cells' signals as NDesI. In this manner, for both TDD and FDD modes, a combination of channelisation and scrambling codes is required.

In [Olej02] and [Szym02], the beamforming has been centred in the FDD mode implementation. The implementation of the TDD mode is hereby more thoroughly described, the adaptive problem being anyway very similar on this subject (refer to Section 6.3, Implementation of TDD and FDD Modes, for a comparison of both implementations).

Channelisation codes allow different channels to be mixed into the same time-slot, with different spreading factors, while preserving the orthogonality, [ETSI02b]. In the TDD mode, these are constituted by elements $c_{\text{code},q}^{(l)}$, for $l=1,\dots,L$ and $q=1,\dots,SF_l$, taking values within $\{-1, 1\}$, building up OVFSF codes of size equal to SF_l , $\mathbf{c}_{\text{code}}^{(l)} = [c_{\text{code},1}^{(l)} \quad c_{\text{code},2}^{(l)} \quad \dots \quad c_{\text{code},SF_l}^{(l)}]^T$. They are chosen from the code tree presented in Figure 5.2, following fundamental simple rules: each level in the code tree defines a certain Spreading Factor (SF); not all codes within the code tree can be used simultaneously in a given time-slot; a code can be used in a time-slot if, and only if, no other code on the path from the specific code to the root of the tree, or in the sub-tree below the specific code, is used in this time-slot.

In this manner, the number of available codes in a slot is variable, depending on the rate and spreading factor of each physical channel, i.e., on the number of active links, L . Considering that the maximum spreading factor is 16, for UTRA-TDD, then a maximum of $SF_{\text{max}} = 16$ MTs per-time-slot is possible. The allowed spreading factors are $\{1, 2, 4, 8, 16\}$, being equal to the maximum number of active MTs at each level.

Besides spreading the data by the real valued channelisation code $\mathbf{c}_{\text{code}}^{(l)}$ of length SF_l , a cell-specific complex scrambling sequence of length 16, $\mathbf{s}_{\text{code}} = [s_{\text{code},1} \quad s_{\text{code},2} \quad \dots \quad s_{\text{code},16}]^T$ is generated. The elements $s_{\text{code},p}$, for $p=1,\dots,16$ are complex values, taken from the complex set $\{1, j, -1, -j\}$,

where j is the imaginary unit. A certain scrambling code \mathbf{s}_{code} is then generated from specified binary scrambling codes, $\mathbf{s}_{\text{bincode}} = [s_{\text{bincode},1} \ s_{\text{bincode},2} \ \cdots \ s_{\text{bincode},16}]^T$, according to $s_{\text{code},p} = (j)^p \cdot s_{\text{bincode},p}$, with $s_{\text{bincode},p}$ being taken from set $\{-1, 1\}$.

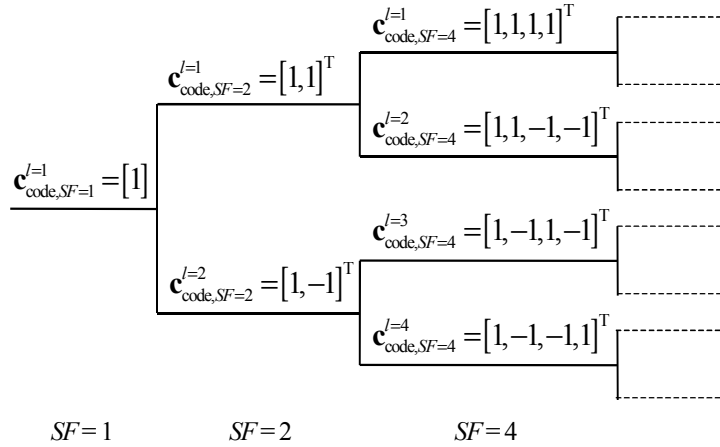


Figure 5.2 – Code-tree for the generation of the TDD channelisation codes (based on [ETSI02b]).

Therefore, after spreading the data symbols with the channelisation codes, the scrambling code is multiplied by each chip, chip-by-chip, with length matching by concatenating SF_{max}/SF_l spread words before the scrambling.

Finally, the combination of the l^{th} user specific channelisation and cell specific scrambling codes can be seen as a user *and* cell specific spreading code $\mathbf{s}_{\text{comb}}^{(l)} = [s_{\text{comb},1}^{(l)} \ s_{\text{comb},2}^{(l)} \ \cdots \ s_{\text{comb},N_{\text{data}} \cdot SF_l}^{(l)}]^T$, where N_{data} the length of the data sequence. This final code is calculated from (5.2), with $l = 1, \dots, L$, $p = 1, \dots, N_{\text{data}} \cdot SF_l$, and $x \bmod y$ referring to the remainder after integer division of x by y .

$$s_{\text{comb},p}^{(l)} = c_{\text{code},1+[(p-1) \bmod SF_l]}^{(l)} \cdot s_{\text{code},1+[(p-1) \bmod SF_{\text{max}}]} \quad (5.2)$$

Finally, for the objective of the current work, the data symbols have been set to be equal to ‘1’, i.e., carrying no information, with a maximum length equal to the smallest length of the first data block inside the TDD time-slot. In fact, under those simplifying conditions, the length of the data block need not be larger than the SF_{max} , since the resulting combination code will have a final period of $SF_{\text{max}} = 16$.

3GPP specification changes have been subsequently introduced after the hereby-described algorithm implementation, e.g., the introduction of a channelisation code specific multiplier, [ETSI00]. A possible consequence of adding this multiplier is to improve the resulting orthogonality properties that the $s_{\text{comb},p}^{(l)}$ codes exhibit (whose correlation characteristics are described in sub-Section

6.3.2, Correlation Properties of the Reference Codes). Nevertheless, such is not seen as a problem, whatsoever. The fundamental codes and calculation method have not only been kept, but truly the present adaptive implementation anyway allows for very straightforward changes in the reference codes, even if these are radically changed. It is only through the openness conveyed by the hereby-presented implementation that this study is able to render sufficiently algorithm- and system-independent results, namely not fundamentally depending on the specificities of the involved UMTS codes, and leaving the path directly open towards MBSs.

5.3.3 CG and Adaptive Problem

As it has been described in sub-Section 3.4.7, the CG is a known iterative method used for solving large systems of linear equations, [Shew94], [GoLo96]. The cost function is the quadratic form, given by (3.60). At discrete instant n , for the M -dimension unknown weight vector $\mathbf{w}(n)$, known $M \times M$ symmetric and positive-definite signal matrix $\mathbf{U}(n)$ and a general known $M \times 1$ vector $\mathbf{d}(n)$, the CG solves the system $\mathbf{U}(n)\mathbf{w}(n) = \mathbf{d}(n)$ by minimising the quadratic form, requiring at most M steps to converge. To calculate the weight vector for instant n , the iterative process develops by calculating new vector estimates, from iteration i to iteration $i+1$, $\mathbf{w}_{(i+1)}(n)$, in a *search direction*, $\mathbf{dir}_{(i)}$ ²⁵, according to:

$$\mathbf{w}_{(i+1)} = \mathbf{w}_{(i)} + \mu_{(i)} \mathbf{dir}_{(i)} , \quad (5.3)$$

where the *convergence step gain magnitude* at the i^{th} iteration, $\mu_{(i)}$, is calculated according to:

$$\mu_{(i)} = \frac{\mathbf{res}_{(i)}^H \mathbf{res}_{(i)}}{\mathbf{dir}_{(i)}^H \mathbf{U} \mathbf{dir}_{(i)}} , \quad (5.4)$$

and \mathbf{res} is the *residual error*, giving the direction of *steepest descent*, directly related to the *distance* to the reference vector, \mathbf{d} :

$$\mathbf{res}_{(i+1)} = \mathbf{d} - \mathbf{U} \mathbf{w}_{(i+1)} = \mathbf{res}_{(i)} - \mu_{(i)} \mathbf{U} \mathbf{dir}_{(i)} . \quad (5.5)$$

The search directions are *U-orthogonal* (or *conjugate*) to the new weight estimation error vector, $\mathbf{err}_{(i+1)}$, which provides the distance of the actual solution to the optimum, \mathbf{w}_{opt} , given by:

$$\mathbf{err}_{(i+1)} = \mathbf{w}_{(i+1)} - \mathbf{w}_{opt} = \mathbf{err}_{(i)} + \mu_{(i)} \mathbf{dir}_{(i)} , \quad (5.6)$$

useful for the convergence analysis, but not being known in practice. After each step, the search subspace span expands by one dimension, where the current subspace span, D_i , given by $\{\mathbf{dir}_{(0)}, \mathbf{dir}_{(1)}, \dots, \mathbf{dir}_{(i-1)}\}$ or $\{\mathbf{res}_{(0)}, \mathbf{res}_{(1)}, \dots, \mathbf{res}_{(i-1)}\}$ is added a new subspace $\mathbf{U}D_i$, to provide D_{i+1} ,

²⁵ The representation of $value_{(i)}(n)$ or $\mathbf{vector}_{(i)}(n)$ is simplified to $value_{(i)}$ or $\mathbf{vector}_{(i)}$, respectively, where n is implicitly assumed. Several i sub-iterations exist for each n^{th} sampling instant, for which the n^{th} weight vector is calculated.

characterising the CG as a *Krylov subspace* method, e.g., [Shew94]. Furthermore, for every step, the best solution is found within the bounds of the subspace it has been previously allowed to search, where the new error and residual are evermore U-orthogonal and orthogonal to the old search directions, respectively, whilst it allows for stepping in a new search direction never taken before. The new search direction, $\mathbf{dir}_{(i+1)}$, is found by:

$$\mathbf{dir}_{(i+1)} = \mathbf{res}_{(i+1)} + \beta_{(i+1)} \mathbf{dir}_{(i)} , \quad (5.7)$$

where the Gram-Schmidt constants $\beta_{(i+1)}$ are given by (3.62), guaranteeing the generation of the U-orthogonal search directions $\{\mathbf{dir}_{(i)}\}$.

From (3.59), with $N_s > M$ (which is most probable), \mathbf{U} is not square, nor symmetric, $\mathbf{U}\mathbf{w}_l = \mathbf{c}_d^{(l)}$ is overdetermined (or *overconstrained*). As a consequence, the new equation problem,

$$\mathbf{U}^H \mathbf{U} \mathbf{w}_l = \mathbf{U}^H \mathbf{c}_d^{(l)} , \quad (5.8)$$

often called CG Normal Equation Residual (CGNR) method, is applied, leading to a solution \mathbf{w}_l that minimises the residual $\|\mathbf{U}\mathbf{w}_l - \mathbf{c}_d^{(l)}\|$, [Shew94], [GoLo96]. Therefore, for the specific beamforming application at stake, the CG is applied to minimise the function:

$$J_l(\mathbf{w}_l) = \frac{1}{2} \mathbf{w}_l^H \mathbf{R} \mathbf{w}_l - \mathbf{d}_l^H \mathbf{w}_l , \quad (5.9)$$

where $\mathbf{R} = \mathbf{U}^H \mathbf{U}$ ($M \times M$), \mathbf{w}_l is the $M \times 1$ unknown antenna weight vector, for the MT-BS link l , and $\mathbf{d}_l = \mathbf{U}^H \mathbf{c}_d^{(l)}$ ($M \times 1$). Vector $\mathbf{c}_d^{(l)}$ ($N_s \times 1$) is the link DesS code ($1 < l < L$), whose elements correspond to each code symbol. In the TDD case, as it has been described in Section 5.2, $\mathbf{c}_d^{(l)} = \mathbf{s}_{comb}^{(l)}$.

With the inclusion of AWGN, \mathbf{R} is of rank M and satisfies the conditions to apply the CG. Though \mathbf{R} may be ill-conditioned, anyway, the CG guarantees the convergence within the maximum of M iterations, as mentioned before.

For this study, the CG problem has been applied following these definitions and applying each of these steps, all calculations being held with double precision. According to [Shew94], $\mathbf{w}_{(0)}$ is set to $\mathbf{0}$, but has been hereby set with element values equal to 10^{-20} , to facilitate the calculation of the initial SINR.

Concerning other implementations of the CG, the sample-by-sample implementation of the CG, may be object of the future study, reducing the overall algorithm processing complexity considerably, e.g., [ChWi00], [KaBa99]; the use of the Polak-Ribière method [Shew94] to calculate the Gram-Schmidt constants has not been proven to be necessary for this application case, where linear block-sampling is used; for the cases of the sample-by-sample CG beamforming applications, either such method or algorithm resetting have proven to improve performance considerably, e.g.,

[ChWi00], [KaBa99]. Anyhow, in order to guarantee the best algorithm convergence, the Gram-Schmidt Orthogonalisation (GSO) has been implemented, at the expense of more multiplications, (5.7) giving side to (5.10), and the Gram-Schmidt constants being calculated through (5.11), [HeBK99], [Shew94]:

$$\mathbf{dir}_{(i+1)} = \mathbf{res}_{(i+1)} + \sum_{k=0}^i \beta_{(i+1,k)} \mathbf{dir}_{(k)} , \quad (5.10)$$

$$\beta_{(i+1,k)} = - \frac{\mathbf{res}_{(i+1)}^T \mathbf{R} \mathbf{dir}_{(k)}}{\mathbf{dir}_{(k)}^T \mathbf{R} \mathbf{dir}_{(k)}} . \quad (5.11)$$

5.3.4 Physical Interpretation Issues

The CG develops on primarily minimising an error norm, the norm of $\mathbf{err}_{(i+1)}$ given by (5.6). In this way, such algorithm does not directly guarantee that SINR monotonically decreases during convergence. Anyhow, it is shown that it develops in the *sense* of SINR minimisation. To understand such, it must be firstly seen that, at the optimum, the CG cost function for link l , given by (5.9), leads to a function minimum equal to:

$$J_l(\mathbf{w}_{opt,l}) = -\frac{1}{2} \mathbf{w}_{opt,l}^H \mathbf{R} \mathbf{w}_{opt,l} . \quad (5.12)$$

Since this result is a minimised value, the algorithm then guarantees that the maximum total power is achieved, given by $\mathbf{w}_{opt,l}^H \mathbf{R} \mathbf{w}_{opt,l}$, for link l . Also, since $\mathbf{w}_l^H \mathbf{R} \mathbf{w}_l \rightarrow \mathbf{w}_l^H \mathbf{U}^H \mathbf{c}_d^{(l)}$ along iterations and $\mathbf{w}_{opt,l}^H \mathbf{R} \mathbf{w}_{opt,l} = \mathbf{w}_{opt,l}^H \mathbf{U}^H \mathbf{c}_d^{(l)}$, such real valued quantities are maximised during the algorithm evolution, meaning that the power that is maximised is the one that is best correlated to the DesS code, $\mathbf{c}_d^{(l)}$. In parallel, the power $\mathbf{w}_{opt,l}^H \mathbf{U}^H \mathbf{c}_d^{(i)}$, where $i \neq l$, corresponding to the i^{th} NDesI captured by the same l^{th} beamformer, develops in the sense of being reduced, due to the orthogonality between the considered codes. If the number of NDesI signals is lower than M , and if sources are sufficiently angularly uncorrelated, this quantity may be zeroed since the problem has enough DoFs available. In this way, the NDesI power gradually lowers, as the algorithm converges, resulting in a final SINR improvement for link l . In other words, minimising the cost function $J_l(\mathbf{w}_l)$, for any code and link l , implies increasing the same cost function for all other $L-1$ codes i , for $i \neq l$. It is stressed that the main primary objective is minimising $J_l(\mathbf{w}_l)$, for any code l , and only then does this result in the maximum possible $J_l(\mathbf{w}_l)$ for the other codes, due to orthogonality, under the possible propagation and interference conditions. Such implication does not work in the opposite sense:

$$\min_{\mathbf{w}_l, \mathbf{c}_d^{(l)}} \{J_l(\mathbf{w}_l)\} \Rightarrow \max_{\mathbf{w}_l, \mathbf{c}_d^{(l)}} \left\{ J_l(\mathbf{w}_l) / \min_{\mathbf{w}_l, \mathbf{c}_d^{(l)}} \{J_l(\mathbf{w}_l)\} \right\} . \quad (5.13)$$

Furthermore, this SINR increase explanation for link l is valid for all the L links, where L cost functions are minimised in parallel, independently (to the extent that the sub-space of existing desired and undesired codes is common).

Resorting to a geometrical visualisation, each cost function $J_l(\mathbf{w}_l)$, for all l , defines a *shape* given by the term $\mathbf{w}^H \mathbf{R} \mathbf{w}$, function of \mathbf{w} . Since matrix \mathbf{R} is symmetric positive-definite, the minimising solution is unique, for any l , therefore not presenting any local-minima, [GoLo96], [Shew94]. If $M = 2$, such shape corresponds to a paraboloid, equal between all l functions, but located at different positions in the weight vector subspace, defined by $\mathbf{U}^H \mathbf{c}_d^{(l)}$. Each paraboloid provides the minimum l^{th} cost function, and the referred maximum possible NDesI cost functions.

By implementing beamforming independently among L links, the reach of this study's objectives is once more safeguarded, intentionally not introducing combined multi-user detection methods. Anyhow, it must be kept present that the joint detection of multiple spread signals is known to be superior to decoupled detection of individual ones, e.g., [Verd86].

5.4 Evaluation Parameters

Several error norms can be used to evaluate algorithms' performance. From (5.5), applying the *Frobenius* norm definition, the residual error norm $\|\mathbf{res}_l\| = \|\mathbf{U} \mathbf{w}_l - \mathbf{c}_d^{(l)}\|$ (or its square) at each iteration helps to insure the convergence, [GiCo01a], [ReMa01]. In Section 6.4, MMSE vs. BG Optima Discrepancy, the convergence in terms of the respective CG MSE, leading to the MMSE, is further described, the quantification of such error definition being considered most significant. Note that, in a sample-by-sample implementation, as it is the case of the RLS (whose application in described in Section 6.5), the residual norm is useful to define algorithm convergence, but in this calculation it must be assumed that the sample matrix \mathbf{U} is in a whole *a priori* known, in a way not consistent with the sample-by-sample approach. Anyway, in the comparison of the block-sampling or sample-by-sample CG or RLS implementations, [GiMC01], [Mend01], the dimension N_s of the matrix has been considered similar between implementations, to make the best comparison of residual error possible.

From (5.6), the weight estimation error norm, $\|\mathbf{err}_l\| = \|\mathbf{w}_l - \mathbf{w}_{opt,l}\|$, [Hayk96], for each l^{th} beamformer (calculating the optimum *Wiener* solution vector, $\mathbf{w}_{opt,l}$, through directly obtaining the correlation matrix inverse) has been useful for initial evaluation purposes only. An *error energy norm*, defined as $\sqrt{\mathbf{err}^H \mathbf{R} \mathbf{err}}$, [Shew94], has also aided in that process.

The SINR calculation for the l^{th} link follows (5.14), after despreading, where G_p is the CDMA processing gain, $P_{DesS,l}$ and $P_{NDesI,j}$ are the DesS and NDesI powers, respectively, N is the total noise power, and L_{NDesI} is the total number of NDesI contributions.

$$SINR_l = P_{DesS,l} \cdot G_p \cdot \left(\sum_{j=1}^{L_{NDesI}} P_{NDesI,j} + N \right)^{-1} . \quad (5.14)$$

The l^{th} BG, $G_{beamformer,l}$, is then defined as the gain in SINR relative to the one achieved with a single omnidirectional antenna at BS, having been subject to the same PC:

$$G_{beamformer,l} [\text{dB}] = SINR_{beamformer,l} [\text{dB}] - SINR_{single,l} [\text{dB}] . \quad (5.15)$$

In [KuTB02], *Carrier-to-Interference Ratio (C/I)* and *beamforming gains* have also been defined and used to characterise beamforming performance (in the wide sense), for LoS or NLoS conditions: *beamforming gain* is thereby viewed as an SNR gain by using more than one array element, i.e., as an array gain; the definition of *C/I gain* is closer to that of BG hereby defined. Nevertheless, both gains are thereby interpreted as SNR differences at the output of the whole adaptive beamformer (in the wider sense), in respect to the input at each single array element (apart from considering interference as noise and accounting for the PDFs involved). For the present work, *beamforming* is interpreted in its strict sense, by itself rendering SINR improvement (not only SNR), as it is described and justified in Chapter 3. In [KuTB02], those gains result from the whole adaptive antenna array processor, also including DoA estimation and tracking.

Finally, the L values of $SINR_l$ and of $G_{beamformer,l}$ that result from each l^{th} DCIR are averaged among the present MTs that are in similar situations, i.e., all those that are grouped, or those that are spread, or being limited to the one that is isolated.

The calculation of the BER for QPSK, may also be calculated using the known relationship (5.16), resorting to the Q -function, [Carl86]:

$$BER = Q \left(\sqrt{\frac{2E_b}{N_0}} \right) , \quad (5.16)$$

where E_b is the energy per bit, and N_0 is the total noise power density. Considering that the noise equivalent bandwidth is close to $1/T_b$, where T_b is the bit duration, and applying the *Gaussian Approximation* to consider the NDesI signal contribution as a Gaussian random variable, it is easily shown that $SINR = E_b/N_0$, [LiRa99]. Therefore, the BER may be calculated using:

$$BER = Q(\sqrt{2SINR}) . \quad (5.17)$$

For the set objectives, the fundamental evaluation parameters are the plain SINR and BG values, leaving the BER values for the comparison of the CG and RLS algorithms performance, [ReMa01].

Regarding the noise power calculation, a matched circuit is assumed for each antenna. For noise-equivalent temperature $\mathcal{T} = 290$ K, the maximum available noise spectral density from a matched load is given by [Carl86]:

$$N_0(f) = k_{Boltz} \times T \text{ [W/Hz]} , \quad (5.18)$$

k_{Boltz} being the Boltzmann constant. The total noise available power for a noise-equivalent bandwidth, B_n , of 5 MHz, will then be equal to -107.02 dBm. Additionally, if each low-noise amplifier at each antenna element has a noise factor of 3 dB, the resulting additive noise power at each element will be -104.02 dBm. According to [Carl86], such noise power characterises both in-phase and quadrature components, being added to the whole beamformer input signal matrix/vector and subject to the beamformer weight vector. Furthermore, through despreading, the noise contribution to the SINR will be reduced by the SF (near 12 dB, with a spreading factor of 16), as does the total NDesI power.

Besides evaluating BG and SINR, it has been important to analyse the DesS, NDesI and noise power components, individually. For that, the signal matrix, \mathbf{U} , and its resulting correlation matrix, \mathbf{R} , have been decomposed into several components, separated in time and by their originating sources.

Focusing on the non-delayed, $\mathbf{U}_{l,l=0}$, and delayed, $\mathbf{U}_{l,l>0}$, wideband contributions to \mathbf{U} , also discriminating each l^{th} link component, matrix \mathbf{R} will have the following components, contributing to real powers, among many other cross-correlation components:

$$\mathbf{R}_{l,l=0} = \mathbf{U}_{l,l=0}^H \mathbf{U}_{l,l=0} , \quad (5.19)$$

$$\mathbf{R}_{l,l>0} = \mathbf{U}_{l,l>0}^H \mathbf{U}_{l,l>0} , \quad (5.20)$$

$$\mathbf{R}_N = \mathbf{U}_N^H \mathbf{U}_N , \quad (5.21)$$

where \mathbf{U}_N is the AWGN matrix.

In this way, one can analyse power components, in respect to each of the L beamformers:

$$P_{l,l=0}^{self} = \mathbf{w}_l^H \mathbf{R}_{l,l=0} \mathbf{w}_l , \quad (5.22)$$

$$P_{l,l>0}^{self} = \mathbf{w}_l^H \mathbf{R}_{l,l>0} \mathbf{w}_l , \quad (5.23)$$

$$P_{l,l=0}^{other} = \sum_{j=1, l \neq j}^L \mathbf{w}_l^H \mathbf{R}_{j,j=0} \mathbf{w}_l , \quad (5.24)$$

$$P_{l,l>0}^{other} = \sum_{j=1, l \neq j}^L \mathbf{w}_l^H \mathbf{R}_{j,j>0} \mathbf{w}_l , \quad (5.25)$$

$$P_{N,l} = \mathbf{w}_l^H \mathbf{R}_N \mathbf{w}_l . \quad (5.26)$$

These powers, specific of each link, have been averaged over all links and scenario concretisations:

- powers $P_{l,l=0}^{self}$, which is $P_{DesS,l}$, lead to the average calculation of P_{DesS} ;
- powers $P_{l,l>0}^{self}$ lead to the calculation of the average self-interference due to multipath, $P_{>0}^{self}$, present in P_{NDesI} ;

- also present in P_{NDesI} , powers $P_{l=0}^{other}$ and $P_{l>0}^{other}$ lead to the delayed and non-delayed average interference contributions, $P_{=0}^{other}$ and $P_{>0}^{other}$, respectively, from all the other interfering MTs other than the l^{th} , affected by its \mathbf{w}_l weight vector;
- $P_{N,l}$ allows the noise power, N , to be calculated.

Having obtained these quantities, besides the ones related to all the other cross-correlation components within the whole \mathbf{R} , it has been possible to analyse their relative contributions. These were also compared to the average of $\mathbf{w}_l^H \mathbf{R} \mathbf{w}_l$ term in the CG cost function, such term being the sum of all those components.

5.5 Application of Power Control

A simple but effective PC process is implemented, in order to avoid near-far effects, that would additionally influence the dependencies that need to be analysed, and to render a more robust beamforming implementation, being less sensitive to the SINRs imposed by the scenarios. Also, any fast-fading deep nulls are compensated for, among all active links. Through simply regulating all links' powers for a single element antenna, i.e., independent from beamforming, it is guaranteed that all links achieve similar single element SINR in the UL, for each propagation scenario case, being aware that the subsequent convergence depends on such SINRs. Therefore, the problem is more confined to measuring only how the directional and wideband characteristics of the channel affect the performance of beamforming, knowing that the PC procedure does not change these.

An iterative process is held, where the magnitude of each incoming ray is affected by a factor that depends on the respective link SINR. The SINR due to each respective link's DCIR concretisation is firstly calculated, considering a single receiving antenna element only, before any beamforming action takes place. The SINR is calculated for each link in the same way as it is calculated for the optimised beamformer (Section 5.4), taking into account the DesS power, P_{DesS} , the NDesI powers, P_{NDesI} , and thermal noise, N . After such calculation, for each iteration pc_i , a real power control factor is found for each l^{th} link's SINR, $SINR_{pc_i,l}$:

$$pc_fact_{pc_i,l} = \frac{\text{Constant}}{SINR_{pc_i,l}} . \quad (5.27)$$

At each array element, m , from user l , a sequence of $N_{mp,l}$ impulses will arrive, each p^{th} path at $\tau = \tau_{p,l}$, with complex amplitude $\alpha_{pc_i,p,l}$ and azimuth $\phi_{p,l}$. An impulse response vector, $\mathbf{h}_l(\tau)$, due to transmitter l , can be considered in its general form:

$$\mathbf{h}_l(\tau) = \sum_{p=1}^{N_{mp,l}} \mathbf{a}(\phi_{p,l}) \alpha_{pc_i,p,l} \delta(\tau - \tau_{p,l}) , \quad (5.28)$$

where $\mathbf{a}(\phi_{p,l})$ is the steering vector corresponding to each p^{th} path from the l^{th} link. After calculating $pc_fact_{pc_i,l}$, then each incoming ray complex amplitude, $\alpha_{pc_i,p,l}$, is affected by the corresponding PC factor, calculating the next iteration value:

$$\alpha_{pc_i+1,p,l} = \alpha_{pc_i,p,l} \times \sqrt{pc_fact_{pc_i,l}} \quad (5.29)$$

which corresponds to affecting $\mathbf{h}_l(\boldsymbol{\tau})$ by such PC factor. Afterwards, the resulting $SINR_{pc_i+1,l}$ is calculated, and the process is repeated, for all links. In Figure 5.3, a flow chart summarily describes the PC algorithm that has been applied.

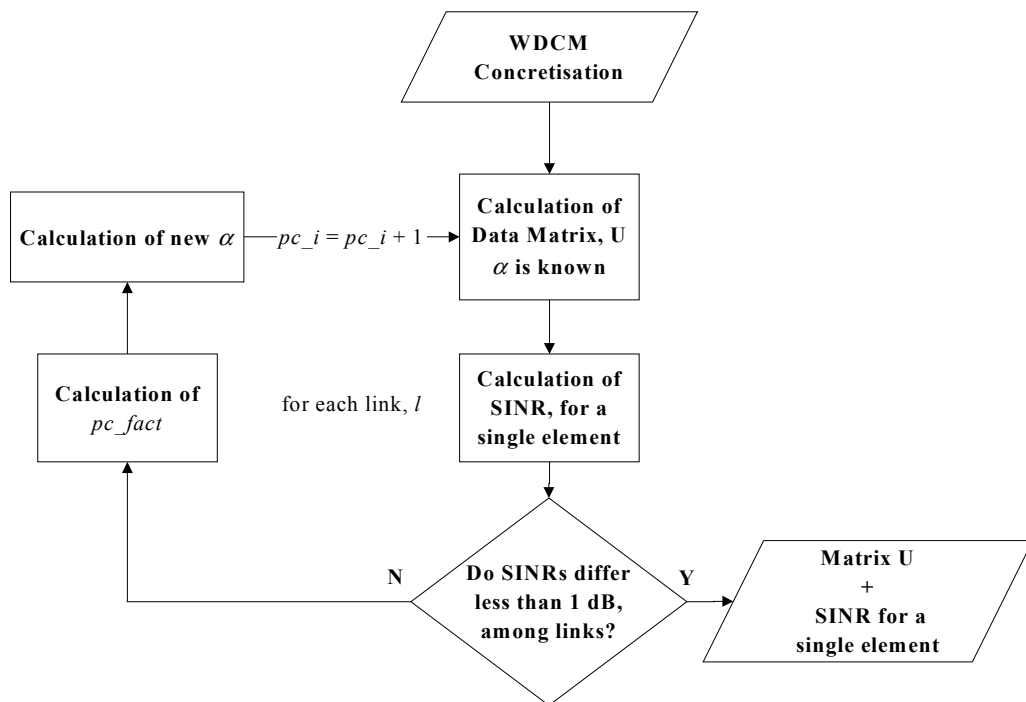


Figure 5.3 – Flow chart of the PC process.

In Figure 5.4 to Figure 5.6, it is seen how SINR values, for all active links, get closer, along iterations (these figures are just for showing the performance of the implemented PC algorithm, and the values of SINR are not under analysis). As expected, for the case of 16 users, the values' spread is larger than for less users. Nevertheless, even for such case, the total SINR interval is reduced from near 4 dB to less than 1 dB at the second iteration. For such reason, no more than two iterations have been needed for all simulations.

Figure 5.7 presents the SINR values before or after PC, as a function of each channel concretisation and corresponding PC simulation number, for 4 active MTs, all at 50 m from the BS, considering the single antenna. It is again visible in Figure 5.7 (b) how close all links' SINR values are after two iterations of the PC, where all active links' results are visually superimposed. The SINR range also decreases due to PC, from more than 3 dB to 2 dB.

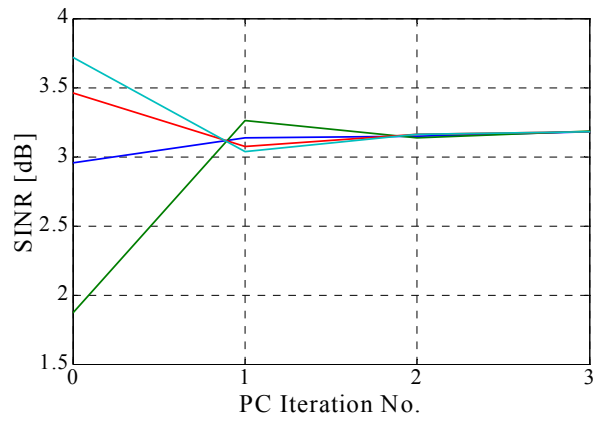


Figure 5.4 – An example of SINR progression along the PC iterations, for $L = 4$.

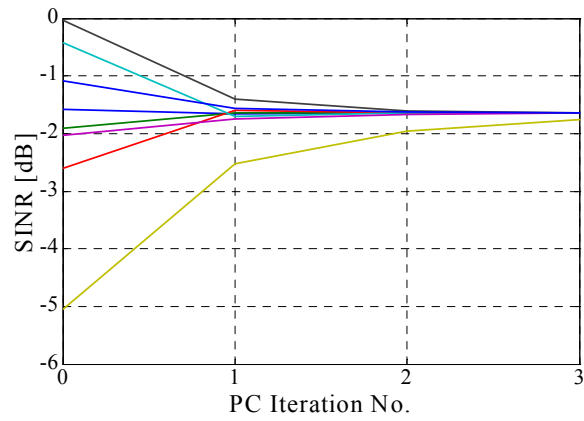


Figure 5.5 – An example of SINR progression along the PC iterations, for $L = 8$.

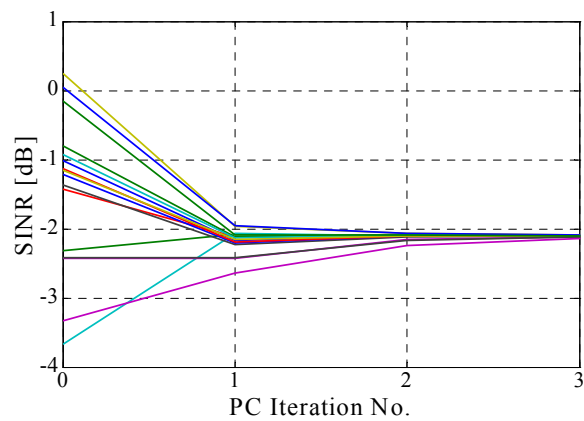


Figure 5.6 – An example of SINR progression along the PC iterations, for $L = 16$.

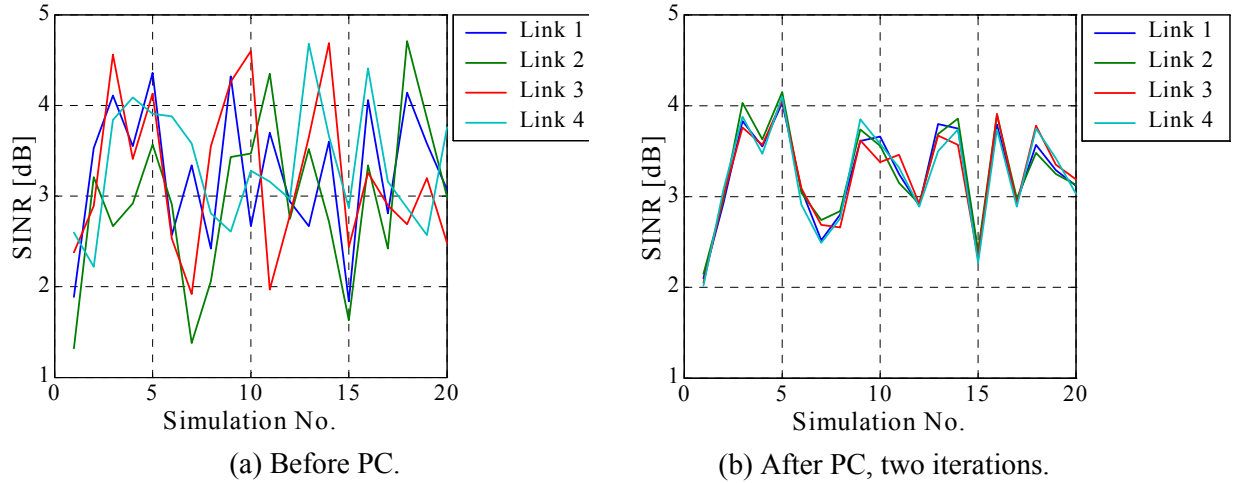


Figure 5.7 – SINR among 4 active links, for 20 independent DCIR concretisations.

The method hereby applied approximates a closed-loop PC in the UL, where each MT would respond to a Transmit Power Control (TPC) command sent by the BS, here being independent from any outer loop PC. In fact, for the UTRA-TDD UL 3.84 Mcps option, the PC is open-loop, based on the path-loss measurements taken from the DL, values being determined by higher level layers and a path-loss weighting factor, [ETSI01c], [ETSI01a]. An inner loop (closed-loop) PC is used for the DL, based on SIR measurements at the MT receiver and an UL TPC command sent by the MT, [ETSI01c], [ETSI01b]. For the UTRA-TDD UL 1.28 Mcps option, the UL PC may also be closed-loop, the MT regulating its transmitting power in response to one or more TPC commands received in the DL.

It must be noticed that the implemented PC process is totally independent from the beamformer operation, meaning that the process does not lead to an optimum final solution in the sense of minimum transmitted power together with the optimum beamformer. For a reference on joint PC and beamforming algorithms see, e.g., [RaRL99]. In [BoSc03], the joint PC and beamforming optimisation issue is covered, for the DL, also exploiting the duality between the UL and DL channel, in a multi-user scenario. In fact, the importance and performance dependence on the angular distribution of MTs, i.e., on the propagation scenarios, is stressed in [BoSc03].

Lastly, the implemented PC is not directly system-dependent, its application being extendable to MBSs, fitting within the current research perspective, also in that way.

5.6 Means Calculations and Statistical Issues

In terms of the calculation of mean values and of their statistical value, it is important to understand which and how these have been calculated, as well as verifying the degree of independency involved.

Concerning the type of averages that have been calculated, the calculations have involved the following type of averaging results, for a WDCM angular resolution of 0.5°:

- beamformer optimisation for each of the Phase-Independent (PI) DCIR concretisations, followed by SINR and BG averaging; the PI DCIRs differ only on the phase of each of the considered signal arriving at a certain AoA and ToA, these phases being randomly generated, uniformly distributed within $[0, 2\pi[$; the cluster and scatterer positions are, therefore, maintained, calculating a first single DCIR from which all the DCIRs are generated for the PI averaging, for the corresponding scenario; this situation corresponds to that where several repetitive beamformer solutions are calculated for a static MT within a time-varying channel environment, with fast-fading variations only; thus, the SINR and BG average variations due to AoA spread variations, function of the scenario, are not evaluated. For this, apart from noise, each PI averaging fulfils the necessary and sufficient conditions for a channel model based on the sum-of-sinusoids to be stationary and ergodic, [Pätz03], evaluating issues related to fast-fading;
- beamformer optimisation for each of the Totally-Independent (TI) DCIR concretisations, followed by SINR and BG averaging; the TI DCIRs differ on all parameters, i.e., modulus, phase, ToA and AoA; these parameters have been randomly generated, according to the distributions described in, e.g., [MaCo01] and [Marq01], meaning that the cluster and scatterer positions are changed between concretisations, for each link; this situation, though truly not fully translating a practical situation, since no continuity care has been taken between each TI DCIR, does contribute to the average beamformer performance evaluation, as a whole; therefore, the SINR and BG TI average variations due to AoA variations, function of the scenario, are also evaluated.

A common spatial cluster and scatterer distribution concretisation is used among each of the scenarios, in the sense that the first cluster/scatterer distribution for Sc #4u_mc_Gr_05 is the same as the first considered for Sc #8u_mc_Gr_5, or Sc #16u_mc_Gr_10. In this way, since each of the TI averages accounts for 100 TI DCIRs, a total of 100 cluster/scatterer spatial distributions have been generated, for each type of scenario, independent of the number of active links, L , and the MT-BS distances, d_{MT} .

As it is seen in Figure 5.8 and Figure 5.9, corresponding to Sc #Lu_mc_Gr_d where all MTs are grouped together, the type of averaging does not affect results considerably in their general variations as function of the number of array elements. Nevertheless, as far as values are concerned, there are considerable differences, comparing TI averages to the PI ones. Such changes reach 5 dB, involving BG relative variations of near 50 %, between TI and PI values, but most important is the fact that the PI relationships to the scenario characteristics are also not as clear. Following from the more complete nature of such mean, the TI results exhibit smoother SINR and BG plots and better consistency among the different scenarios.

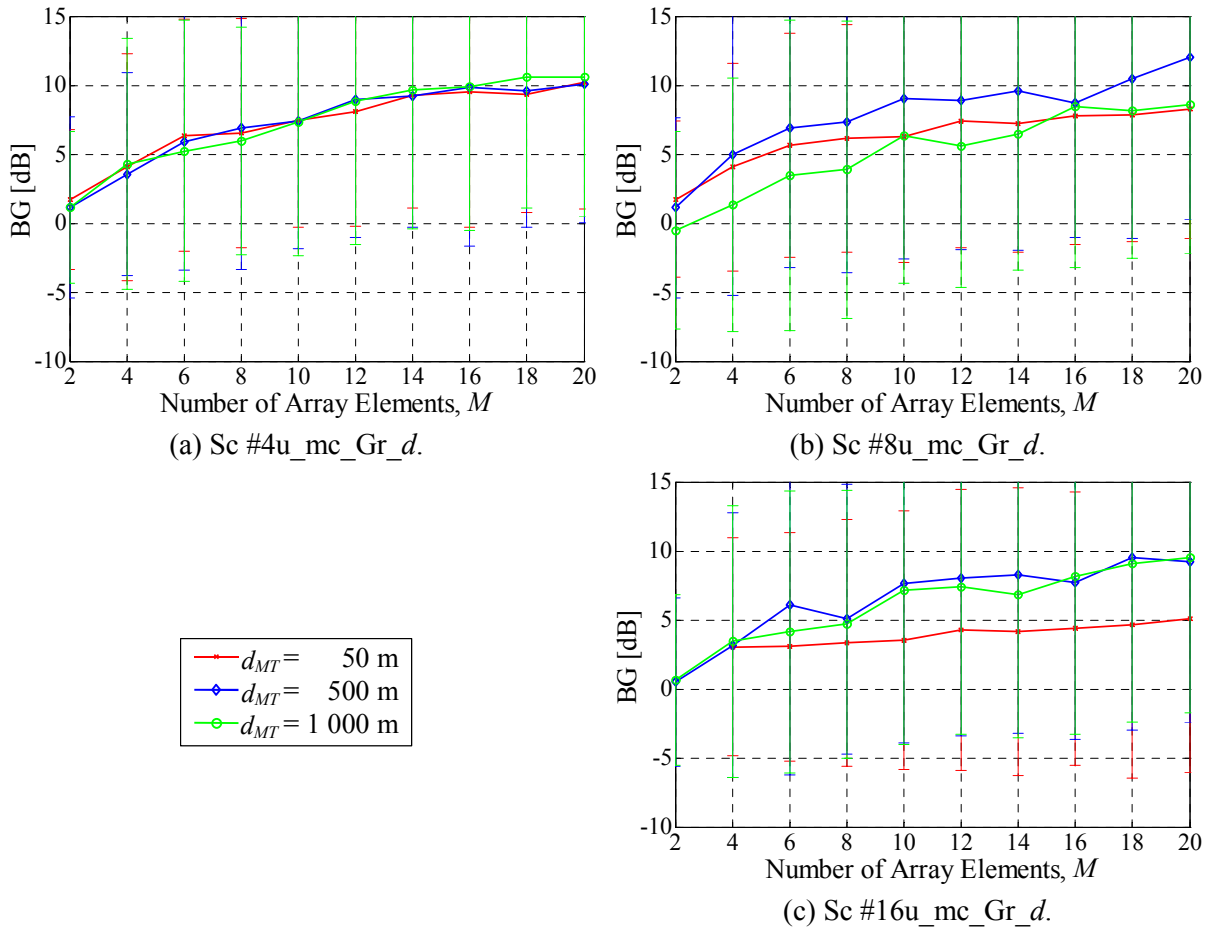


Figure 5.8 – PI DCIR average BG results, for Sc #Lu_mc_Gr_d, function of M , for several d_{MT} and L . Solid lines indicate average results, and error bars indicate respective standard deviation.

As mentioned, different BG results were expected between the TI and PI averages, the variations in the AoA domain being accounted for, in the former case. The calculation of the PI averages only contributes to evaluating how the beamformer performs towards a variable fast-fading propagation channel, for exactly the same cluster/scatterer positions. These results are based on a specific temporal and angular response, a given spatial set of clusters and scatterers, which may show a certain channel dependency that could be totally different from that of another temporal/angularly different channel response, another spatial concretisation, for the same MT-BS distance. In order not to depend on such possibly misleading bias, for the current purposes, only the TI averages are considered valid. The PI calculations should be most useful when dealing with how fast-fading effects affect the beamformer's performance. For this, and since the TI provide most complete information, the results presented in this work cover TI averages, developing the statistical study in both the angular and the temporal domains. Unless otherwise stated, one will hereby implicitly refer to the BG values as being the TI ones.

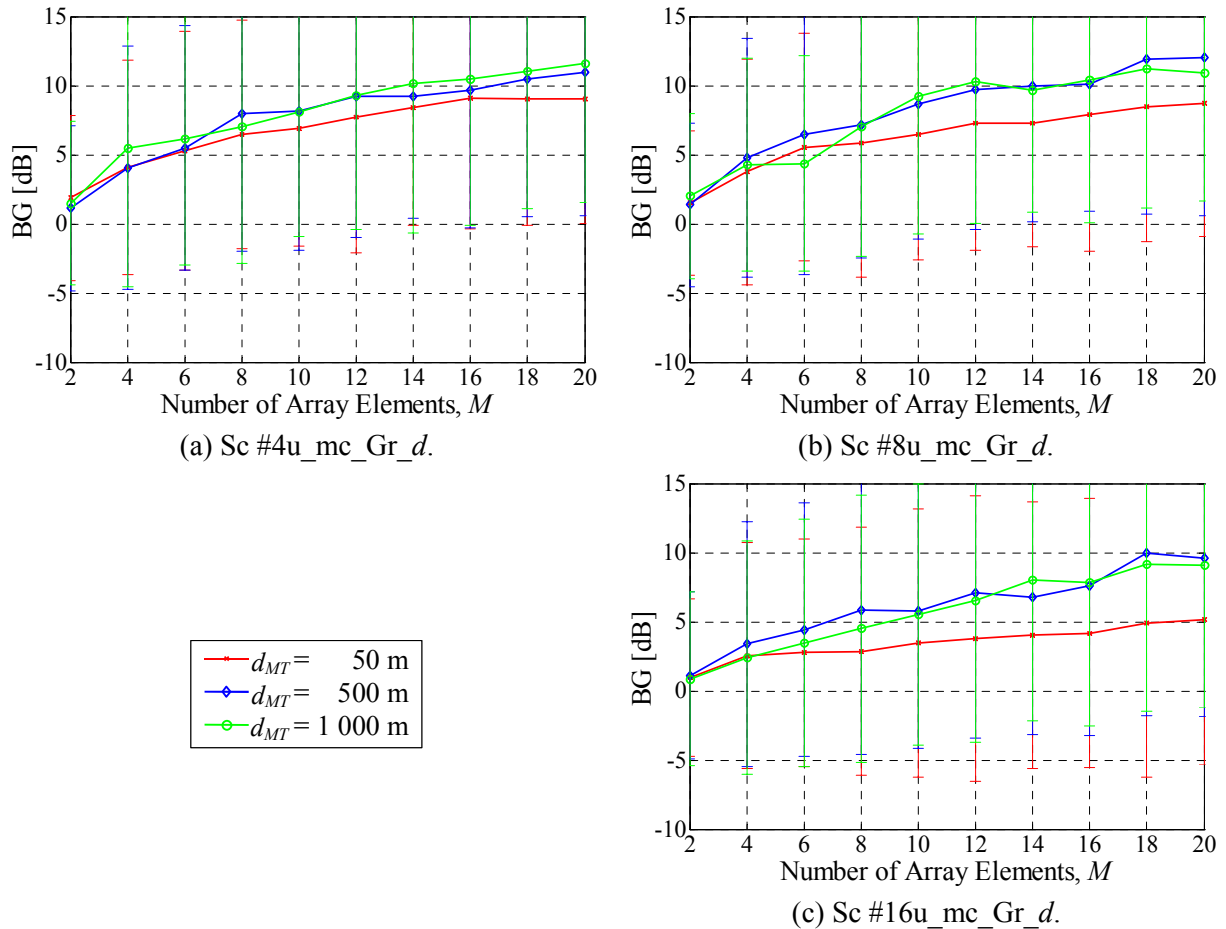


Figure 5.9 – TI DCIR average BG results, for Sc #Lu_mc_Gr_d, function of the number of antennas, for several values of d_{MT} . Solid lines indicate average results, and error bars indicate respective standard deviations.

Also important, and in fact it is one of the first general verifications before focusing on the parameter dependence, is that the standard deviations may be large enough (reaching more than 10 dB) so as to indicate relatively frequent negative BGs. That is, indicating a relative large number of negative improvements, after or during optimisation, i.e., the beamformer in fact worsening the SINR in respect to the single element antenna. This fact is worse the worse interference content is, either due to more active links or due to larger delay-spread, for both types of averages. Other characteristics that strike the eye are the relatively large values for those standard deviation results and the non-smooth average BG and SINR plots, for any distance, any number of users and array elements. These effects take place for either TI or PI averages, and will be brought up further along the text.

On the other hand, a *whole*-DCIR, in the sense that it includes all the active links' contributions (excluding thermal noise), can be defined. Therefore, one will refer to the former DCIR, corresponding to each l^{th} link, independent of the number of links and array elements, as DCIR, simply. Better than a picture to describe it, each *whole*-DCIR is described by a signal vector or by a

signal matrix, U , for a certain number of array elements. In this sense, for the MiC scenarios, PI or TI averages, something of the order of 3 300 (number of MiC scenarios, 33, times 100 DCIRs) *whole*-DCIRs have been accounted for, for each number of array elements, M . For MaCs, 4 500 *whole*-DCIRs have been calculated. By these numbers, the advantage of resorting to simulations, using a SCM, in respect to unrealistically measuring all of these in real sites, becomes clear. Besides being able to generate numerous multi-user *whole*-DCIRs through measurements, also achieving the required degree of independency would be very difficult, if not impossible, resulting in a defective extraction of any statistical trend.

As far as the TI average calculations themselves are concerned, it has been important to evaluate the independency of the samples and how the resulting SINR and BG are distributed. To corroborate the hypothesis that the results follow a Log-Normal distribution – the *Null Hypothesis* (NH) – a Kolmogorov-Smirnov test, e.g., [NIST03], has been applied to compare the obtained SINR and BG distributions to the corresponding normal ones, using MATLAB[®], [Math03]. In parallel, for the scenarios where the observation and expected frequencies permit, the Chi-Squared Goodness-of fit test, e.g., [NIST03], has also been used to further verify the NH.

In the NH test, the *sensitivity*, *alpha-value* or *significance* level of a statistical test is the pre-selected probability of incorrectly rejecting the NH when it is in fact true. A significance level of $X\%$ means that more than $X\%$ of all the results, not satisfying the hypothesis, would be needed to lead to the effective NH rejection, wrongly. In other words, if X is small, the risk of rejecting the null hypothesis, when it is in fact true, is small. Therefore, larger X indicates that the NH is more strongly maintained. Another parameter, the *p-value*, is the probability of observing a test statistic at least as extreme as the value actually observed, while maintaining the NH, indicating how unusual a test statistic is compared with what would be expected under the NH. A p -value of $Y\%$ means that $Y\%$ is the probability of obtaining a result more extreme than the expected, but still not affecting the statistics of the population. Larger Y also corresponds to larger confidence in the NH acceptance. Concerning this study, it has been verified that for most of the MiC scenarios, accounting for 10 to 100 concretisations, the tests lead to the acceptance of the NH, with a significance level of 5% . And in fact, in most cases, the obtained *p-values* are much greater than 5% (and the NH would be accepted with larger significance levels), providing even better confidence in the independency of the results, [MoRu94].

Still for the case of MiCs, but for larger numbers of concretisations, up to 100, the independency of the results diminishes, which is understandable since the same major channel conditions are being applied, also depending on the number of involved array elements, active links and scenario. In some of these cases, the NH is in fact rejected (also confirmed by the Chi-squared process). Among 20 concretisations, mean *p-values* of 74.3% , 14.8% and 15.4% were obtained for scenarios Sc #4u_mc_Gr_05, 4u_mc_Gr_5 and 4u_mc_Gr_10, with $M = 10$, respectively; for $M = 2$,

19.1 %, 17.1 % and 19.7 % were obtained; for $M = 20$, the average p -values are 68.8 %, 85.3 % and 50.4 %. The worst cases are those of 16 MTs, for 20 concretisations: for Sc #16u_mc_Gr_05, 16u_mc_Gr_5 and 16u_mc_Gr_10, $M = 10$, 3.7 %, 3.2 % and 30.5 %; whereas for 10 concretisations the p -values rise up to 17.3 %, 13.2 % and 43.8 %, thus, better providing better confidence in the NH and in the independency of results.

In very few cases the NH has been rejected, as mentioned. Namely, for all MiC or MaC scenarios where MTs are grouped together, the independency of BG results is reduced, which is as expected, since these are the situations where all MTs contribute with the same ToAs and AoAs. Keeping that in mind, it has been assumed with good confidence that for all the scenarios, for any number of antennas, links and any algorithm's iteration number, the SINRs and BGs are log-normally distributed, the dB values being normally distributed around a certain average, μ_{dB} , with a certain standard deviation, σ_{dB} . Also, though this confidence analysis has mostly centred on MiC situations, similar conclusions have been reached for the MaCs cases, further allowing for the generalisation of the NH acceptance.

Normal probability plots visually provide information on the empirical Cumulative Density Function (CDF) from the histogram corresponding to their empirical distributions. In Figure 5.10, the BG sample data is displayed with the blue symbol '+', with a linear fit red line joining the first and third quartiles of the data, for Sc #4u_mc_Gr_05, $M = 10$, and 100 concretisations. For this case, the obtained p -value is 10.5 %, i.e., showing a good fit. In green, the interval corresponding to the 15.9 and 84.1 % percentiles is indicated, verifying that 68.2 % of the data visually fits into the linear normal plot.

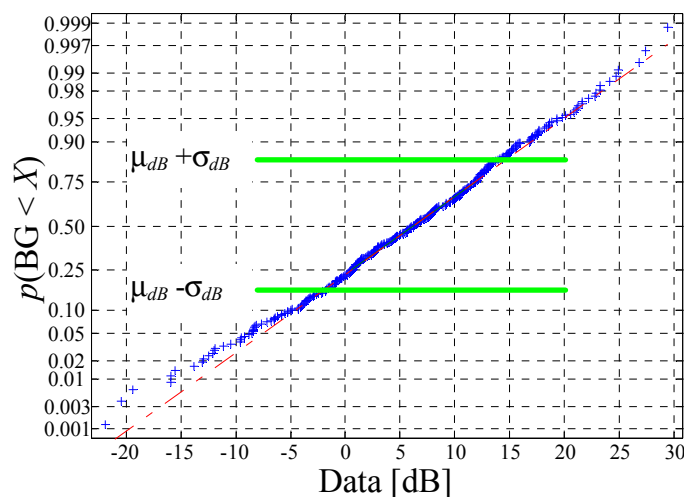


Figure 5.10 – An example of a BG normal CDF plot, exhibiting its visible linearity, in dB.

Judging on the verifications, the averages and standard deviations have been directly calculated from the dB values. Apart from affecting this calculation, these data confidence results also

indicate that the number of DCIRs and their independence are in agreement with the application of the *Central Limit Theorem*, e.g., [NIST03], following the most natural power-related distribution among simulations, thus, providing good confidence on the results.

Another issue is the direct consequences of varying the number of simulations required to achieve confidence. Due to the relatively large standard deviations, such is very important. It is important to evaluate how the number of simulations affects results, comparing the average values for 20 or 100 concretisations, seeing if the BG variations are within the corresponding standard deviations. As Figure 5.11 shows, exemplifying for MiC scenarios Sc #Lu_mc_Gr_5 and Sc #Lu_mc_Sp_5, for $L=4$ and 16, the fluctuations that result from only considering 20 concretisations may be considerable (up to 3 dB), resulting in difficult final characterisation and analysis, in the light of the set objectives. In general, the results using 100 concretisations lead to average BGs values that are more adequate for the characterisation of the beamforming performance, with the expense of involving much larger simulation times. In terms of significance, 20 simulations would anyhow lead to valid means, those variations being well within the found standard variations. This is anyway in agreement with the previously described NH confirmation analysis.

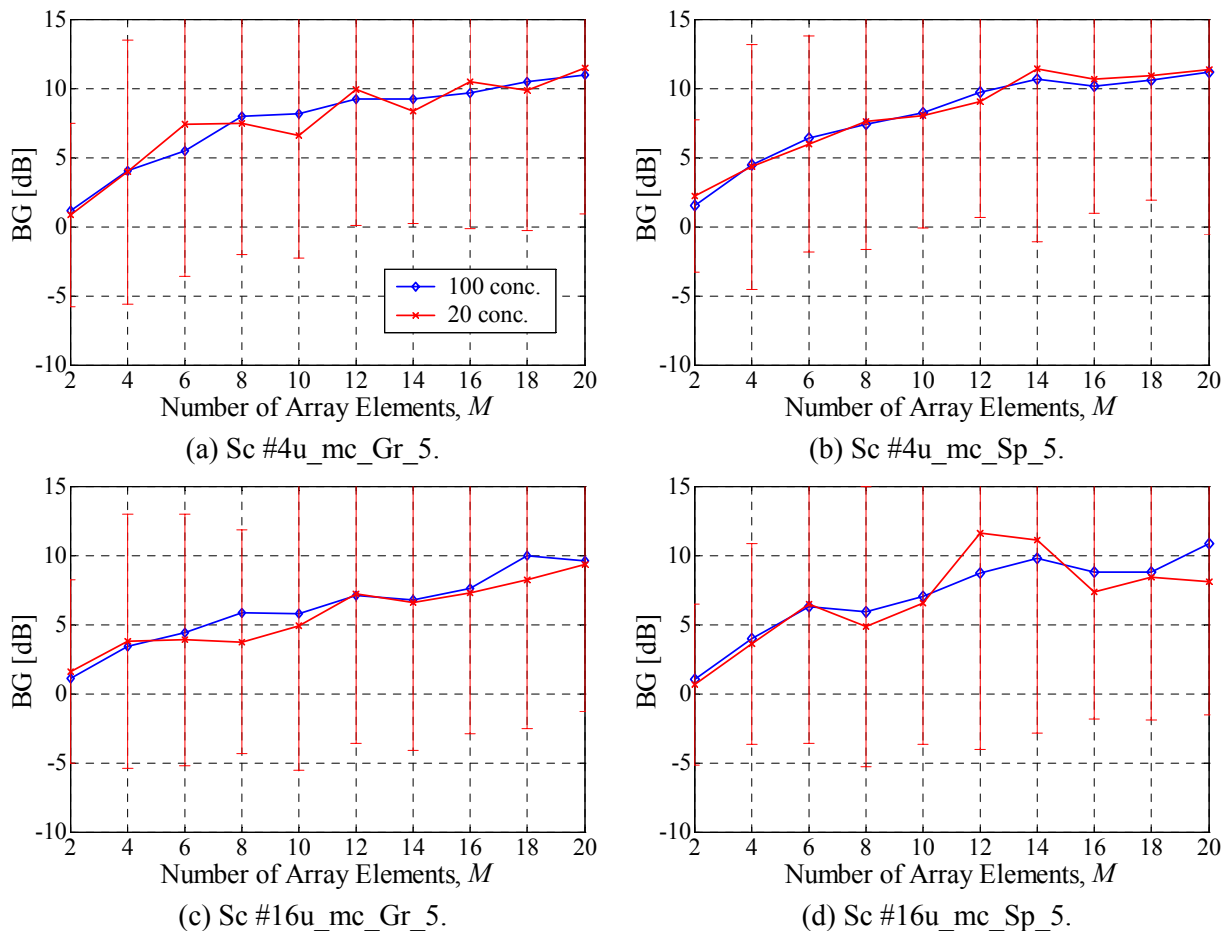


Figure 5.11 – Comparison of average BG for 20 or 100 concretisations, for Sc #Lu_mc_Gr_5 and Sc #Lu_mc_Sp_5, function of M , for $L=4$ and 16.

In a similar manner, the verification of how the number of samples affects the calculation of means has been carried out for MaC cases. For such, mean BGs corresponding to Sc #Lu_Mc_Gr_15_200 and Sc #Lu_Mc_Sp_15_200 have been compared, again accounting for 20 or 100 concretisations; the average BG and corresponding standard deviation results are plot in Figure 5.12, for $L=4$ and 16, where one can verify that averages may differ by at most 2 dB, still within the corresponding standard deviation, but with important fluctuations that make the performance characterisation more difficult, just as in the MiCs case. Since this type of behaviour has been found for other scenarios, in spite of the large simulation times at stake, it has been decided that 100 concretisations should be applied, especially in the cases where angular displacement of MTs is random. In Figure 5.12, it is visible how using 100 concretisations reduces BG fluctuations, especially for Sc #Lu_Mc_Sp_15_200.

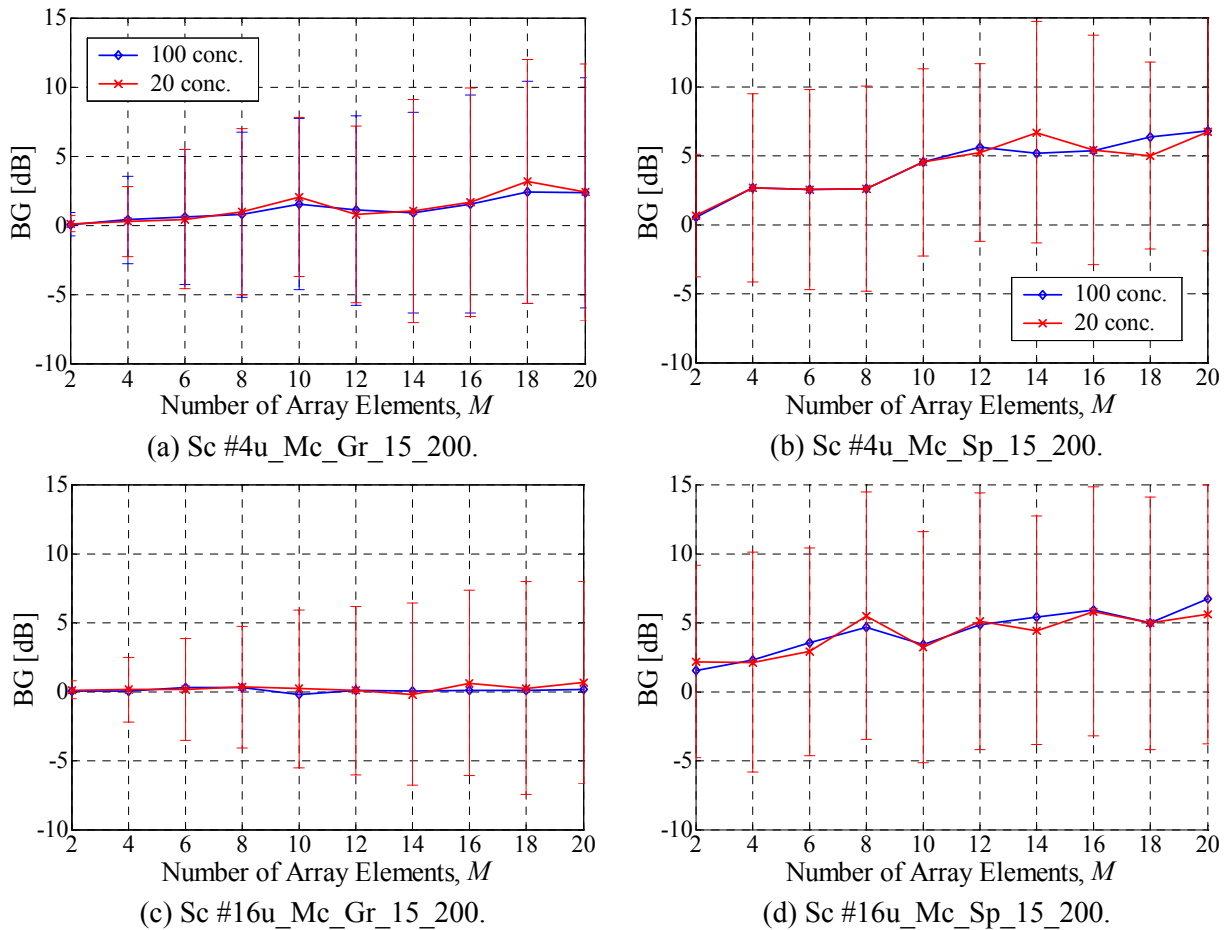


Figure 5.12 – Comparison of average BG for 20 or 100 concretisations, for Sc #Lu_Mc_Gr_15_200 and Sc #Lu_Mc_Sp_15_200, function of M , for $L=4$ and 16.

5.7 Summary and Conclusions

This chapter has dealt with the specification of the beamforming problem, in the wider sense, i.e., not only covering the algorithm, but also all the embedding that its application involves. In this way, adaptive reference-base beamforming is chosen to function at the BS side, making use of the available system resources. For the specific case of UMTS, the specifications on channelisation and scrambling codes are used. Anyhow, one must keep aware that using these specific codes, more directly focusing on UMTS, is neither system- or algorithm-restrictive, since the conclusions hereby drawn deal with physical fundamental and general aspects that involve the channel properties and the formation of an array pattern that minimises the relative level of NDesI power. For this, the major channel/scenario dependency conclusions drawn from this study should not only apply to other reference-based algorithms, but also to other reference sources, or even blind applications. Seeing the matter in the simplest way, even in the case that other beamforming algorithms may reach better SINR or BG values, such dependencies on the channel/scenario properties are seen to prevail, i.e., the sense and relative importance of the variation of SINR or BG due to changes in the array patterns (concerning lobe levels, positions and widths) result from changes in the channel conditions in a certain consistent sense, independent of the algorithm and its type of inputs. Having chosen the CG algorithm, for its simplicity and efficiency, its inputs and outputs are well defined, as well as the quantities that need to be measured in order to characterise beamforming performance – SINR and BG.

This chapter also contributes to understanding that several NDesI power components are involved in the optimisation process, besides noise and the DesS powers. The corresponding definition of those components develops on multi-user and wideband perspectives, since the *self* and *other* MTs powers are differentiated from each other, as well as the non-delayed and delayed contributions become explicitly clear.

Additionally, the applied PC process is described, showing its efficiency, though being applied independently from beamforming. For all the scenarios at stake, the implemented PC requires a maximum of 2 iterations in order to keep all links' SINRs within the same 1 dB interval.

From the two possible types of averaging, PI and TI, the latter ones are the most important, involving the independent generation of DCIRs in both the temporal and angular domains. Though, in fact, PI averaging allows for concluding that the beamforming is not particularly robust against fast-fading. As a sign of that, BG standard deviations may reach more than 10 dB. Concerning the number of simulations required, 100 independent concretisations render sufficiently coherent means results, not having considerable impact on the standard deviations, but enabling the evaluation of results that is necessary in this study.

Still on the subject of calculations and simulations, a statistical analysis of the obtained BGs confirms the general acceptance of the NH, i.e., reflecting the general independency among the involved concretisations, and confirming the Log-Normal distribution of the involved BG average

values. Therefore, the relatively large standard deviations due to the particular sensitivity of the process to fast-fading do not reflect any threat to the independency of the obtained data, the study rendering statistical value.

Finally, the beamforming problem is fully specified, understanding the fundamental parameters at stake. Along with the previously defined WDCM scenarios, it is now possible to analyse the whole beamforming-WDCM-scenarios set-up, in a critical way. The issue of the mathematical burden that such problem involves will also be dealt with in the next chapter.

6 Set-Up Analysis

And a man should not abandon his work, even if he cannot achieve it in full perfection; because in all work there may be imperfection, even as in all fire there is smoke.

— in *Mahabharata*, The Bhagavad Gita 18:48 (500 BCE-500 CE)

6.1 Introduction

This chapter presents an analytical view on the implementation at stake. In this way, the several wideband vs. narrowband notions are evaluated, in the perspectives of the system, propagation channel, model, beamforming and array factor calculation. Particular concern is directed towards keeping ideas clear on this subject, at the several levels at stake.

Then, the issue of implementing the problem in either the TDD or the FDD UMTS modes is also dealt with, comparing their implementations, simulation practicalities, their general results, and the properties of the involved codes. In this way, the study is led to conclude on the independency of the overall analysis from the implemented duplex mode.

The additional matter that is hereby presented and analysed, most important in this research study, is the optima discrepancy problem. Having previously verified the convergence of the CG algorithm, the study verifies that the MMSE and SINR (or BG) optima may in fact not coincide. For its importance, this issue deserves particularly detailed examination, in this chapter. This is put forward for the several possible MiC or MaC scenarios, analysing SINR, BG, the several power components at stake and the involved array patterns. After understanding the matter, through that analysis, the justification for its happening is conveyed, finally being possible to propose solutions to avoid, or attenuate it, in the perspective of this study and of practical system-directed applications. Therefore, it is also shown how such problem does not root from the specific implementation.

To further base the present research work, the CG application is compared to using the RLS. For that, the RLS is problem is defined, following its former summarised description in Chapter 3, also being applied for the same scenarios as the CG. Their performance is compared, in terms of SINR and BG maxima, their evolutions along optimisation, and the involved processing complexity.

Finally, this major chapter, at several levels, aims at creating a solid ground on which the subsequent chapters may be based upon.

6.2 Implementation vs. Narrowband and Wideband

6.2.1 Several Definitions

This study makes use of a *Wideband* Directional Channel Model, evaluating the performance of a beamforming adaptive algorithm implementation, which will be verified to be *wideband*, having considered the ULA with the *narrowband assumption*. Furthermore, the research is directed towards *broadband* mobile communications systems. From this, it is very clear that the use of *narrowband* and *wideband* terms involves different meanings, according to their context, all of those making sense. Four contexts are involved, leading to different meanings – the perspective of the system, the propagation channel characterisation, the adaptive processing scheme, and the way the antenna array factor is calculated. As it will be seen, some of these meanings may in fact not be so disparate, being very important to be clear about them. In a work that involves such varied contexts, this clarification only becomes more important. Such is the aim of this section, also verifying the agreement with adaptive beamformer implementation.

In the perspective of the system, it is important to compare the system and channel coherence bandwidths, where the symbol duration and the channel delay-spread are at stake. On the other hand, the involvement of uncorrelated multipath components provided by the model characterise the bandwidth of the used channel model, in the sense of involving independent components in the temporal delay domain. Also, the temporal acquisition of such multipath components (within a certain finite sampling rate), compensating for the temporal dispersion and also making use of several delayed samples to discern DesS from NDesI power among links, must also be related to the temporal dispersion of the channel, i.e., to the wideband characteristics of the channel. Lastly, the relation between array element separation and the involved symbol duration must also be dealt with, verifying that the envelope delay among array elements is not relatively significant.

6.2.2 Systems and Channel Bandwidths

The transmission system bandwidth and its relation to the channel bandwidth is the key issue. In any communications system, the symbol duration is inversely proportional to the transmission bandwidth. For a DS-CDMA system, e.g., [LeMi98], as an example, the null-to-null bandwidth, B_s , of rectangular chip waveform signals is related to the chip duration, T_{chip} , by $B_s = 2/T_{chip}$. On the other hand, the *power delay-spread*, σ_τ , is related to the *coherence bandwidth*, B_c , so that $B_c \approx 1/2\pi\sigma_\tau$, this bandwidth being defined as the frequency separation between two frequencies, when their envelope correlation is 0.5, [Jake74], [Stee96]. Another definition for the coherence bandwidth roots from the

Bello function transforms, being defined as the frequency at which $|T(t, f)|^2$ lowers to half of its maximum, [LeMi98], where the *Time Variant Transfer Function*, $T(t, f)$, is the Fourier transform of the time variant *Delay-Spread Function*, $h(t, \tau)$, with respect to the time delay variable, τ , as it is described in Chapter 2. Independently of the two definitions, σ_τ is inversely related to the coherence bandwidth, and the coherence bandwidth indicates the maximum frequency separation for which propagation conditions are strongly correlated.

Then, for the DS-CDMA example, the ratio between the σ_τ and T_{chip} is of the sort given by (6.1), relating the system bandwidth to the channel coherence correlation bandwidth:

$$\frac{\sigma_\tau}{T_{chip}} \propto \frac{B_s}{B_c} \quad (6.1)$$

If the symbol duration is small compared to the delay-spread, $\sigma_\tau > T_{chip}$, then the system is *wideband* relative to the channel, i.e., $B_s > B_c$ (apart from the constant). For that, the channel is said to be *frequency selective*, relative to the system bandwidth, since the system involves spectrum components that are out of the channel coherence band, therefore exhibiting independent fading. Due to the high relative delay-spread, such channel is *time dispersive*, contributing with several multipath components that are uncorrelated in delay, e.g., [LiRa99], [Jake74], and so the channel is said to be *wideband*. For the opposite situation, where $\sigma_\tau < T_{chip}$, or $B_s < B_c$, the channel is *frequency-flat, non-dispersive*, and the channel is said to be *narrowband*. Notice that where there are apparently contradictory designations, a system being *wideband* relative to the channel, while the channel is also called *wideband*, the meanings are different, but equally valid – the comparison to the coherence bandwidth is at stake in one case, and the multipath components constituting the channel temporal response, concern the other.

Since the delay-spreads at stake range from 0.10 to 0.68 μs (Section 4.3), among the modelled MaC and MiC scenarios, then the coherence bandwidth is between 234.1 and 1 592.5 kHz. For the case of UMTS, TDD bands are allocated within [1900, 1920] or [2010, 2025] MHz, the bandwidth being 5 MHz for the high chip rate (3.84 Mcps, $T_{chip} = 0.26 \mu\text{s}$), and 1.6 MHz for the low chip rate option (1.28 Mcps, $T_{chip} = 0.78 \mu\text{s}$); for UL- and DL-FDD, the 5 MHz paired bands are within [1920, 1980] and [2110, 2170] MHz, respectively. It is clear, then, that UMTS is a *wideband* system, when the coherence bandwidth is compared with the width of the radio channel. On the other hand, with a T_{chip} of 0.26 μs for both TDD and FDD, each system operation channel is *wideband* in the case of some MiC and MaC scenarios (where the delay-spreads reach 0.39 or 0.68 μs , respectively), but cannot be said to be either *wideband* or *narrowband* in other MiC or MaC cases (with delay-spreads as low as 0.10 μs).

On the other hand, the *wideband channel model* designation is seldom used as being relative to the system bandwidth to which such channel model is applied; in fact, such is not right,

propagation channel characteristics being independent of any system. By *wideband* it is meant that such modelling of the propagation channel involves the characterisation of the temporal response of the signals, discerning among uncorrelated multipath components, as opposed to the classical models that provide information on power levels and Doppler-shift only (Chapter 2). Following the same reasoning, as it was described previously, a channel that is time dispersive is referred to as being a *wideband* channel, since uncorrelated multipath components exist within the arriving signal envelope. Since the WDCM, as it is described in [Marq01], generates several multipath independent components, originating from the reflections of spatially distributed scatterers, the resulting DCIRs inherently account for uncorrelated multipath, thus, constituting a *wideband* model, in that sense.

In another way, the role of the propagation model can be seen as that of a measurement means, including the analysis of the delay behaviour of the impulse response of the channel. In that sense, if such measurement is capable of discerning from among uncorrelated multipaths, in delay, therefore, such means is *wideband*, in the same way that such equivalent model is seen to be.

6.2.3 Beamforming and Array Bandwidths

As it was already defined in Chapter 3, a wideband combining beamforming network is constituted by a spatio-temporal set of optimising weights, e.g., [LiRa99], [PaPa97], [VeBu88]. Nevertheless, the issue goes further than just that, seeing that the temporal set of optimising weights may function with three distinct objectives, involving different time scales – delay taps may be used to reduce ISI, at the symbol duration level, or to help compensating for the temporal variations of the channel, at the frame duration level, respectively. In another manner, if such makes sense in a single-user scenario, exploiting the temporal domain has the additional objective of reducing interference among links in the multi-user case, thus, acting in the symbol duration level, if such symbol information is required for differentiating DesSs from NDesI.

Firstly, at the frame duration level, it is important to call upon the definition of *coherence time*, T_c , being the time interval along which the propagation channel characteristics are correlated in time. Thus, the temporal variations of the channel are at stake, defining the coherence time as the maximum time interval within which the correlation among signals is higher than 0.5, e.g., [Rapp02]. The time dynamics of the channel, responsible for Doppler-shift, is at stake in the frame duration level. If, in this case, the beamforming system requires N_s input data samples, covering a total time of T_{N_s} , and the coherence time is larger than such, then, there is no need for making use of the temporal domain to account for channel variations. In fact, as it is the case of the presented beamforming application, the channel is assumed stationary on a 10 ms frame basis and static at the slot level. Additionally, since $N_s = 16$ or 256 chip samples are considered, covering from 4.16 to 66.6 μ s, then the total sampling duration is much lower than the coherence time, and the static channel assumption it further added. From this point of view, the beamformer will largely satisfy this

condition, not requiring a *wideband* implementation, in that sense. In [MaCo02], coherence time results are presented, based on MaC scenario measurements, showing that the stationarity assumption hereby put forward is very realistic, for a static MT.

Secondly, at the chip symbol level, with the use of a wideband channel model, one understands that such beamformer requires that all signal samples cover the temporal dispersion of the channel, especially being the case where interference mitigation is developed on a chip symbol basis. Accordingly, the sampling period involved by the beamformer, T_{N_s} , is then required to be at least as large as such delay-spreads, and the implementation does require being *wideband*, in such sense. As it is shown in Figure 6.1, in light of has been stated in Chapter 3, and again resorting to FIR filter representation, the inputs to a wideband beamforming application can be seen as N_s consecutive channel delay samples, from M array elements. In this way, the beamformer makes use of a signal matrix, \mathbf{U} , ($N_s \times M$), exploring the temporal domain at the symbol level, i.e., being considered to be *wideband*, in that sense.

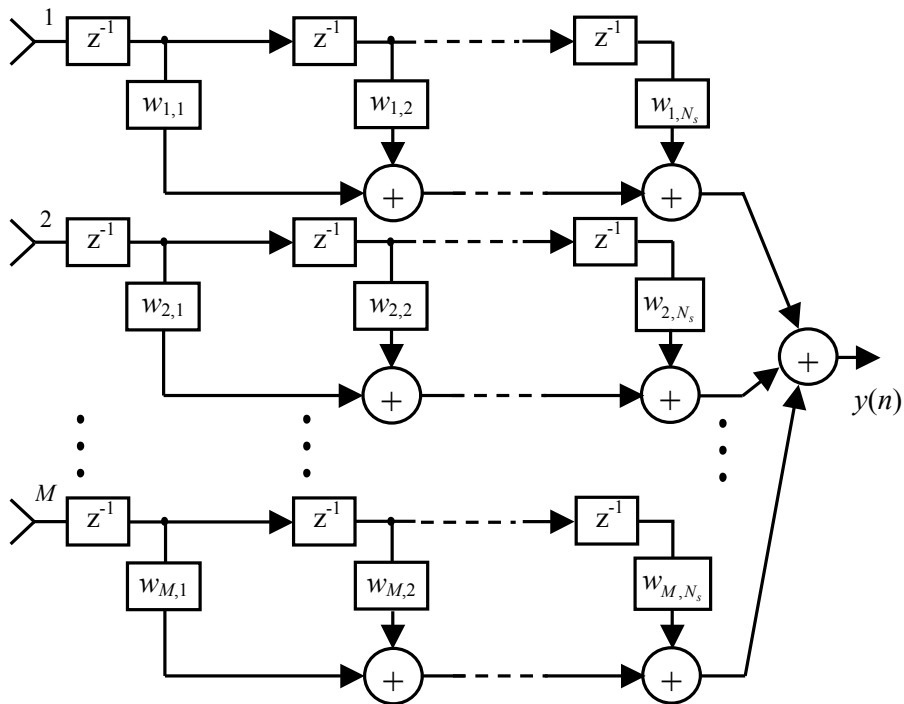


Figure 6.1 – Representation of the *wideband* basic beamforming structure.

In the studied application, for each l^{th} link, a beamforming vector, \mathbf{w}_l ($M \times 1$) is obtained, as opposed to the beamforming matrix case, \mathbf{W}_l ($M \times N_s$), of the structure provided in Figure 6.1. Accordingly, each of the actual L beamformers finds the best weight vector, taking into account all N_s temporal samples from each of the M array elements, adding the outputs from all M elements at each discrete instant, n , as it is depicted in Figure 6.2. The output of the beamformer is not a single sample, as in Figure 6.1 case, but a set of N_s symbols, represented by $\mathbf{y}(n)$, with elements $y(n)$ to $y(n-N_s+1)$.

Keeping in mind that the optimum weight vector is found from a set of temporally delayed samples, at the chip symbol level, accounting for the temporal dispersion of the medium, i.e., for the independent uncorrelated multipath components, one sees that the present adaptive solution is *wideband*, satisfying the previously mentioned requirements, i.e., $T_{N_s} \gg \sigma_\tau$. Anyhow, in a situation where the channel response is equal for all tap-delays, the N_s weight vectors do not differ in the delay domain, along the sampling period, T_{N_s} .

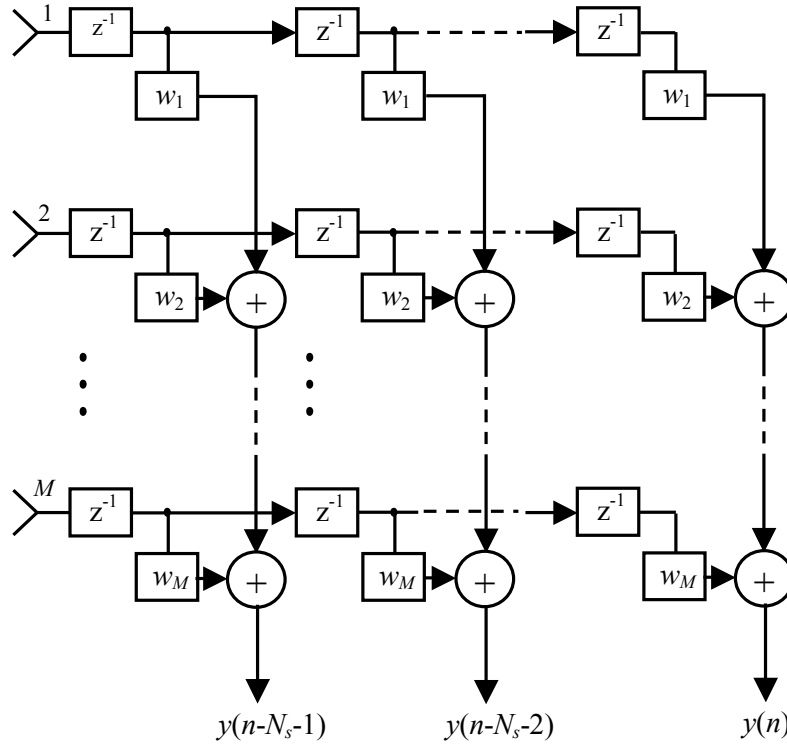


Figure 6.2 – The present adaptive beamforming network, for each of the L active links.

Yet another important issue is the sampling rate at which signals are input or output from the beamformer. It must be noticed that, keeping the sampling rate equal to the $0.26 \mu\text{s}$ chip rate, Figure 6.1 implementation involves tap delays that are lower than such chip duration, the beamformer outputting samples at that same rate. On the other hand, the implemented structure (Figure 6.2) outputs a block of size N_s , taking $T_{N_s} = 0.26 \cdot N_s \mu\text{s}$ to be output, with tap-delays equal to the chip duration. Thus, the former structure works at the intra-symbol level, whilst the latter, the implemented one, processes at the inter-symbol level, as stated before. Both applications have definite time domain objectives, at different levels. The implemented one deals with both temporal dispersion and interference mitigation.

The ULA array factor is formed by considering that there is only a relative phase-shift between antenna elements, due to the arrival of each planar wave to the array at a certain AoA, thus,

not involving symbol envelope delays. For this matter, the signal delays that are at stake are those among array elements, only affecting signal phase. As it has been superficially mentioned in Section 2.2, according to, e.g., [PaPa97], [KrVi96], such is called the *narrowband assumption*, and once more, it is relevant to be aware of its meaning, as well as to verify its validity in the case of this study. A *wideband* implementation, in such sense, is of the sort depicted in Figure 6.1, processing at intra-symbol level.

For the implementation described in this work, the signals are sampled at the 3.84 Mchip/s UMTS rate, meaning that the symbol duration, T_{chip} , is 0.26 μ s. The maximum propagation delay between each $\lambda/2$ -separated element is $1/2f_c$ (in the end-fire direction), where f_c is the operating carrier frequency. For $f_c \cong 2$ GHz, the maximum delay is 0.25 ns, which is approximately 1 000 times smaller than T_{chip} . In this way, the *narrowband* array assumption makes sense, and its meaning is understood, comparing the maximum delays within the array elements to the symbol duration. The implemented array system is *narrowband* relative to the array physical size and elements' separation.

Another point that must be mentioned concerns the relative bandwidth, B . Its usual definition, the ratio between the system bandwidth and the centre operating frequency, determines how *narrow-* or *wideband* any electronic equipment is considered, in terms of RF hardware implementation (having direct impact on ISI, on circuit matching and linearity). For the hereby-studied application, for TDD, B is at most 6.4 %, and a maximum of 12.2 % for FDD, covering both paired UL and DL bands, along all UMTS bands. Naturally, for the FDD mode, the array is *wideband* in such sense. Anyway, though such perspective is not forgotten, it is not dealt with at the level of this work. As an example, in [Comp88], the importance of the inter-element temporal delay is treated, further analysing the impact on interference reduction, as function of B , the number of taps, their temporal separation and AoA. It is thereby shown how the SINR degradation due to not considering delay taps for each antenna element may not be negligible, depending on B . Based on such work, one may reason that such delay taps would lead to better SINR suppression, even in the case of TDD mode. Nevertheless, as mentioned, such band widening concerns the RF level, being relative to the operating frequency and involving delay taps of the order of a quarter wavelength. In this way, such concern is beyond the scope of this work, hereby dealing with baseband signals and with tap delays of the order of the chip duration.

6.3 Implementation of TDD and FDD Modes

6.3.1 Dependence on the Propagation Scenarios

As it is mentioned in the previous chapter, beamforming performance dependence on the directional and wideband characteristics of propagation scenarios has been analysed for both TDD and FDD modes, though with much more detail in the former case, for several reasons. It is important

to present the reasons for such study to be focused on TDD, anyway evaluating the main performance issues in common, or in divergence, between both of these modes, independent of the type of cell.

The main operational properties that differ between TDD and FDD modes concern spectrum allocation, management between transmit directions, interference sources, capacity allocation and channel properties, according to transmit directions, [HoTo00]. More specifically, though specification issues have been presented in Section 5.2, focus is directed towards those properties dealing with the propagation and the beamforming conditions, in general: FDD involves two paired bands, while a single unpaired is required for TDD; in TDD, due to the sharing of frequency bands, the UL and DL interference may happen between MTs and BSs, within the cell or among neighbouring cells; the UL and DL channel is reciprocal, in TDD, the fast-fading being uncorrelated between UL and DL FDD; the possible spreading factors differ between TDD and FDD, the latter involving many more users, per slot, i.e., possibly presenting the beamformer with much larger NDesI powers.

Since this work deals with UL beamforming, at the BS, the UL and DL correlation issues are not of direct concern. Also, as a single cell is considered, only intra-cell interference is accounted for, the interference present being due to the all the active MS-BS radio links. In this way, for the most direct concern of the present study, the TDD and FDD implementations differ on the references used in the beamforming. Adding to what was presented in Section 5.2, the SFs vary between 1 to 16, or 4 to 256, in TDD- or FDD-UL, respectively. As a result, the beamforming involves references that differ in nature and length, and the number of MTs engaged can be much larger in FDD, per slot, i.e., for each beamforming weight solution and subsequent analysis. Finally, such differences have in fact had impact on the held simulations, involving much lower variety of simulation scenarios and lower number of averaged concretisations, for FDD, [Olej02], [Szym02].

It is important to keep in mind that the burden put into the simulations primarily roots from the generation of the whole channel DCIR matrix, accounting for the number of reference code symbols (at least 16 times larger in the case of FDD, compared to TDD), besides all L users, M elements and DCIR components.

In order to have a quantitative notion of the differences in the involved computational effort, the following example is presented: the scenario Sc #8u_Mc_Sp, $r = 200$ m, for the total of the three distances d_1 , d_2 , and d_3 , and for the whole M span from 2 to 20, with 100 concretisations each, has taken close to 7.9 hours, for TDD; the same scenario, but only for d_2 , only $M = 12$, and FDD, and the same number of concretisations, has taken close to 4.9 hours.

Anyhow, though less profound, the FDD implementations have helped to analyse the behaviour of the beamformer in respect to the nature of the codes, as it is described in Section 6.4, MMSE vs. BG Optima Discrepancy. But most important, the FDD simulations have helped to

consistently confirm the major dependencies of beamforming performance on the propagation channel conditions, in both directional and wideband perspectives, independently of the duplex mode.

In order to go forth with the comparison between all TDD and FDD results, a qualitative analysis is presented, primarily dealing with the dependency tendencies registered. Such conclusions are based on the [Olej02], [Szym02] studies.

In a more general overview, all FDD results have led to higher BG values than the corresponding TDD ones, for either MiCs and MaCs, a fact that is understood by the longer involved codes and the differing BG evolution along optimisation (as presented in Section 6.4, MMSE vs. BG Optima Discrepancy).

For the MiC scenarios, the BG variations with the number of active links, L , are of similar relative magnitude, between 4, 8 and 16 MTs, for any of the scenarios; unlike the TDD results, the FDD BGs do not register degradations for $L = 4$, for any of the grouped MTs scenarios (described in sub-Section 7.2.5, Number of Active Links); for the situations where MTs are grouped together along the street axis, the dependency with distance is very much similar between both modes, the BG suffering visible degradation for $d_{MT} = 50$ m MT-BS distance, with neither significant nor well defined differences from 500 to 1 000 m (sub-Section 7.2.1, MT-BS Distance); in the case that a single MT exists, separate from the remaining MTs grouped together, in both TDD and FDD, the grouped MTs show a tendency to lead to lower BGs, especially for higher L , with no significant differences for smaller values of L (sub-Section 7.2.3, Angular Displacement and Grouping of MTs).

Regarding the MaCs study, the match between TDD and FDD has also resulted very good, regarding the dependencies on the scenarios' parameters. The dependencies with the MT grouping and displacement are of the same type, the grouped MTs leading to critically degraded BGs, with values near 0 dB, and the spreading of MTs leading to very similar BG values, as opposed to the corresponding TDD ones (sub-Section 7.3.4, Angular Displacement and Grouping of MTs); regarding the dependency on the number of active MTs, L , the FDD results do not present the degradation found for TDD $L = 4$, comparing to 8 MTs, also affecting BGs more strongly, in the grouped MTs situation (sub-Section 7.3.6, Number of Active Links); a divergence exists, though not significant, concerning the dependency with d_{MT} , also in the case that the MTs are grouped, where the FDD results do show more explicit lowering of BGs with increasing MT-BS distance (in the case of TDD, the values do not present any dependencies with d_{MT} , as presented in sub-Section 7.3.1, MT-BS Distance); in the case of spread MTs, the dependence with L and d_{MT} are very close to those regarding the TDD situation, also involving very similar values; as far as the cases of the single MT, angularly separate from the remaining ones, are concerned, the FDD results show that BGs increase with increasing L , for MT_1 , unlike the TDD results, which decrease with L , from 8 to 16 MTs; the sensitivity to the variation of the scattering circle radius are in the same sense, for TDD or FDD, if the MTs are angularly spread,

though involving larger variations in the latter case; another divergence is that the FDD BGs may increase with circle radius, for grouped MTs, while the TDD results do not present variations.

Therefore, the same general dependencies on the channel and scenario parameter have been found, among MiC and MaC situations, independent of the duplex mode, being further indications of the fundamental constraining effects imposed by the scattering areas and positioning, and not of the codes. Anyway, it must be noticed that the registered divergences, between the two modes implementation, root from the higher BG values achieved in the FDD case due to the better correlation properties of the codes involved. Similar justification is found for the BG degradation found in the TDD $L = 4$ case, compared to $L = 8$, the correlation nature of the involved codes having an impact on the beamforming performance. In Section 6.4, MMSE vs. BG Optima Discrepancy, the importance of the reference code length is conveyed, viewing the impact on the BG results. In the next sub-Section, the correlation properties of these codes are also analysed.

The main outcome of these verifications is not limited to the specific dependencies on a particular parameter, having expressed the general agreement among the results from both modes. Furthermore, it is by verifying the fundamental explanations for such dependencies, for both TDD and FDD, that the full comparative analysis between both modes' implementations is concluded: between MiCs and MaCs, TDD or FDD results, the grouping of MTs leads to critically degraded performances in the MaC case, due to the lower channel richness that characterise MaC DCIRs; the dependency with BS-MT distance, between MiCs and MaCs, for both TDD or FDD modes, also reflect the role of the DCIR channel richness, angular and temporal densities of arriving signals.

The importance of the FDD study is primarily viewed as an aid to understanding the effects of the different codes involved, as well as confirming the implications of involving higher numbers of users. It is believed that the deepness of the analysis has reached the desired point, not aiming at pursuing further into the FDD case. Anyhow, there is no doubt that certain points on the FDD studies can be further followed, leading to constructive contributions, for both MiCs and MaCs. Finally, the general agreement between FDD and TDD results, in terms of dependency on the scenarios characteristics, makes the MiCs vs. MaCs analysis possible in parallel to that of the performance dependence on the fundamental channel parameters, at a level that is more independent from the mode. In this way, the most complete characterisation that has been put forward for TDD provides the necessary data and means to achieve so, in an efficient and practical way.

6.3.2 Correlation Properties of the Reference Codes

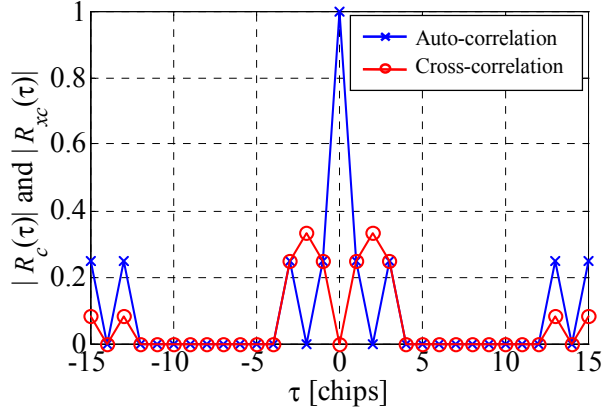
As expected, the length of the reference code determines the evolution and values of the BG and SINR along optimisation. In the TDD MaC case, the BG evolution presents initial peaks, severely degrading to negative values in the following iterations, whereas for the FDD MaC case, the BG increases in a positive step-like manner, reaching a plateau, at a level close to the maximum value,

still exhibiting an initial peak. The definition of significant iteration must be applied to both TDD and FDD results, its application being equally important for both modes (for TDD see Section 6.4, MMSE vs. BG Optima Discrepancy, for FDD see [Szym02]), in order to establish the SINRs and BGs that are relevant for analysis.

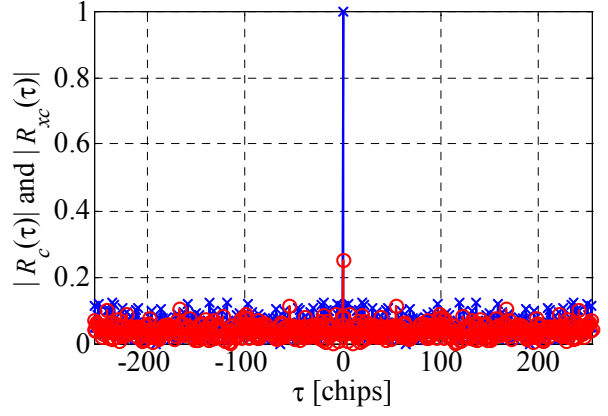
In light of the described sensitivity to the reference codes used, studying the implications on beamforming performance of using TDD or the FDD codes, with varying lengths, also depending on the scenario, is relevant, and work could follow in such direction. Nevertheless, it is kept in mind that the main focus is on the dependency of beamforming operation on the several scenarios, being able to compare MiCs and MaCs results. However, the implications of the dependency on the code properties need to be addressed, not only concerning length but their correlation properties.

As it has been detailed in Section 5.2, for the TDD case, the reference codes used are user-specific combinations of channelisation and scrambling codes. The channelisation codes have their length changed, according to the number of users and the data rates, but the additional combination of the scrambling code, in order to identify the respective cell, lead to a final code with a fixed length of 16. In this way, the variation of data rates or number of users does not affect the length of the algorithm reference, therefore, not influencing beamforming performance by means of changing the code length. Similarly, for the FDD UL case, the SFs of the channelisation codes vary from 4 to 256, further being combined with scrambling codes with 38 400 or 256 chips. Therefore, the final MT-specific codes are either 38 400 chips, if a RAKE receiver is used at the BS, or 256 chips long, if advanced multi-user detection or interference cancellation schemes are used at the BS, [HoTo00], i.e., for the present application the MT-specific code will have a fixed length of 256. Again, as it happens with the TDD mode implementation, it is not due to any change in the code length that the present beamforming operation will be affected by the variation of data rates or number of users.

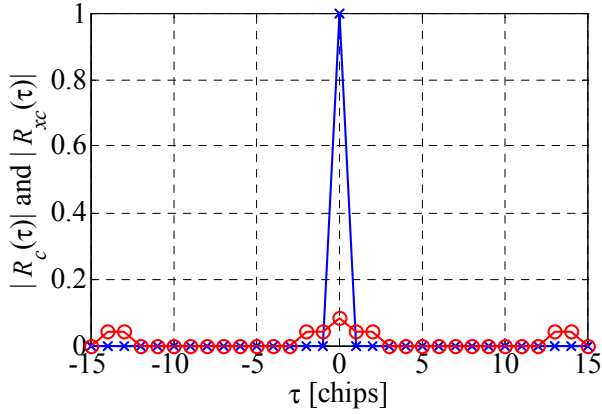
However, keeping the combination of channelisation and scrambling codes length constant as the number of MTs varies does not mean that the correlation properties of such codes do not vary. It is most important to keep in mind that the final MT-specific combinations of channelisation and scrambling codes are not orthogonal, in spite of the used channelisation OVSF codes, the MTs still being identified by the beamformer, making use of still convenient correlation properties. In Figure 6.3 the auto- and cross-correlation sequences of the TDD and FDD MT-specific codes are depicted, for $L = 4$, either in the perspective of a single code, (a) and (b), or averaged among the several involved codes, (c) and (d). In Figure 6.4 and Figure 6.5, similar results are shown for $L = 8$ and 16 MTs, respectively.



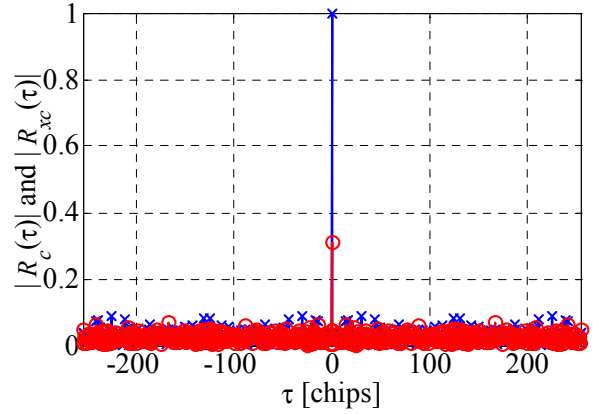
(a) For TDD, $N_s = 16$, in respect to Code 1.



(b) For FDD, $N_s = 256$, in respect to Code 1.



(c) For TDD, $N_s = 16$, averaged.



(d) For FDD, $N_s = 256$, averaged.

Figure 6.3 – Code auto- and cross-correlation, for TDD and FDD, for $L = 4$, for a single code and average interaction.

The auto-correlation has been calculated according to (6.2) and (6.3), for the single l^{th} code, $R_c^{(l)}(\tau)$, or the averaged code, $R_c(\tau)$, contributions²⁶, e.g., [OpSc75]:

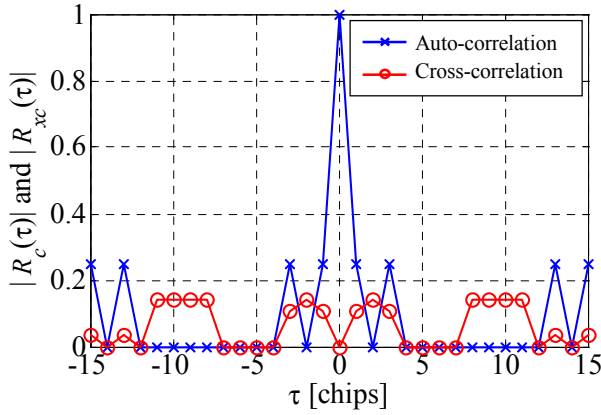
$$R_c^{(l)}(\tau) = \frac{1}{N_s} \sum_{n=1}^{N_s} c_d^{(l)}(n) \cdot c_d^{(l)}(n-\tau), \text{ for } \tau \in]-N_s, N_s[, \quad (6.2)$$

$$R_c(\tau) = \frac{1}{L \cdot N_s} \sum_{l=1}^L \sum_{n=1}^{N_s} c_d^{(l)}(n) \cdot c_d^{(l)}(n-\tau), \text{ for } \tau \in]-N_s, N_s[, \quad (6.3)$$

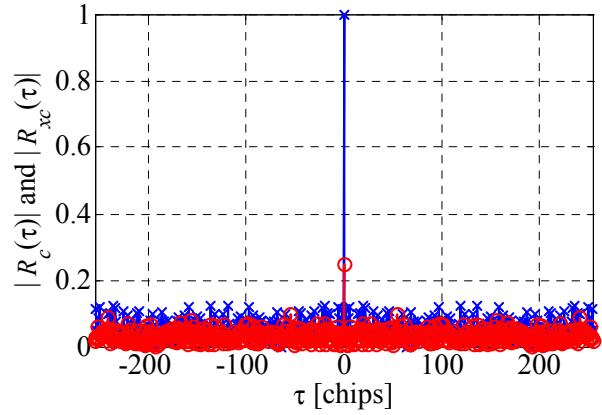
where L is the number of active users, N_s is the number of samples (equal to the code length), $c_d^{(l)}(n)$ is the n^{th} chip of the desired code for the l^{th} link. As it is seen, the average has been taken among all possible active links. In a similar manner, for a single code or averaged contributions, the cross-correlations have been calculated by:

$$R_{xc}^{(l)}(\tau) = \frac{1}{(L-1) \cdot N_s} \sum_{j=1, j \neq l}^L \sum_{n=1}^{N_s} c_d^{(l)}(n) \cdot c_d^{(j)}(n-\tau), \text{ for } \tau \in]-N_s, N_s[, \quad (6.4)$$

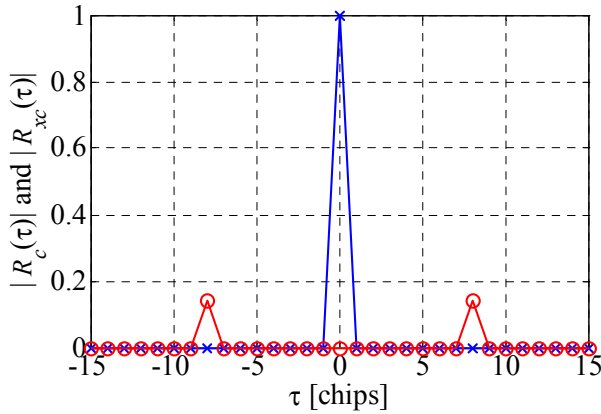
$$R_{xc}(\tau) = \frac{1}{L \cdot (L-1) \cdot N_s} \sum_{l=1}^L \left(\sum_{j=1, j \neq l}^L \sum_{n=1}^{N_s} c_d^{(l)}(n) \cdot c_d^{(j)}(n-\tau) \right), \text{ for } \tau \in]-N_s, N_s[. \quad (6.5)$$



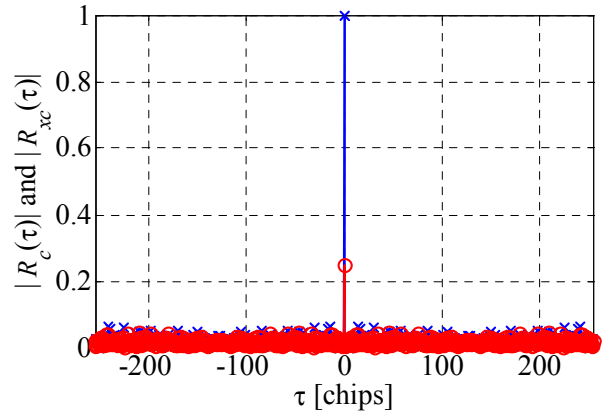
(a) For TDD, $N_s = 16$, in respect to Code 1.



(b) For FDD, $N_s = 256$, in respect to Code 1.



(c) For TDD, $N_s = 16$, averaged.



(d) For FDD, $N_s = 256$, averaged.

Figure 6.4 – Code auto- and cross-correlation, for TDD and FDD, for $L = 8$, for a single code and average interaction.

From these, concerning TDD, one sees that: the average cross-correlation properties of the involved code combinations for $L = 8$ and 16 are better than those relative to $L = 4$, where within the $|\tau| < 3$ interval the correlation is not zero, being 0.08 maximum; besides such interval, the cross-correlation may achieve absolute values very close to 0 ; the auto-correlation is also 0 , or very close to 0 , for $|\tau| > 0$, and 1 for $\tau = 0$, in all L cases. Among all the averaged FDD results, the cross-correlation is maximum at $\tau = 0$, being 0.31 for $L = 4$, and 0.25 for $L = 8$ or 16 ; the remaining cross-correlation values are lower, but still above zero, as it is the case of TDD; for $|\tau| > 0$, the cross-correlation absolute values are below 0.07 , 0.04 and 0.05 , for $L = 4$, 8 and 16 , respectively; the auto-correlation

²⁶ These are discrete correlations, where τ is hereby used to refer to the discrete sample shift.

values for $|\tau| > 0$ are not zero either, as the TDD are; for $|\tau| > 0$, the auto-correlation average absolute values are below 0.09, for $L = 4$, being lower than 0.06, for $L = 8$ and 16.

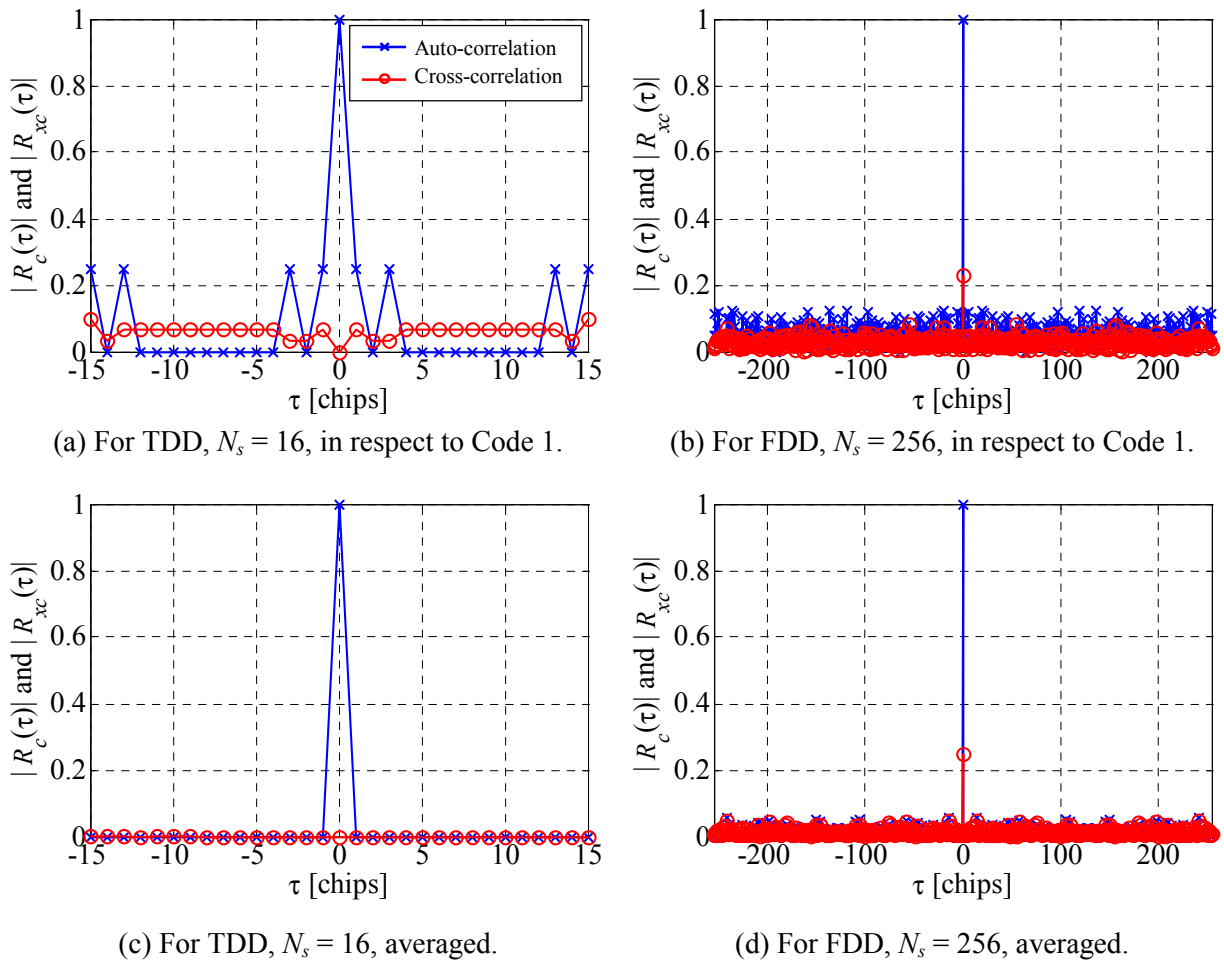


Figure 6.5 – Code auto- and cross-correlation, for TDD and FDD, for $L = 16$, for a single code and average interaction.

In this way, one can generally state that: the TDD reference codes present better correlation properties than the FDD ones, for the presented average calculation; for both modes, such average correlation properties tend to improve with increasing L , noticing a particularly larger degradation for $L = 4$; for $L = 4$, TDD, the cross-correlation presents a relatively wide interval, around $\tau = 0$, with non-zero absolute values.

On the other hand, the correlation properties that Figure 6.3, Figure 6.4 and Figure 6.5 show, relative to Code 1, are generally much worse than the corresponding averaged calculations; for $L = 4$, TDD, the degradation of the Code 1 correlation properties is most evident, relative to the higher L values; these properties are much worse for TDD, than for FDD. Therefore, the TDD code properties show to be largely dependent on the combination of the involved codes and delays, since the corresponding averaged calculations lead to considerably different values (as opposed to the case of

FDD codes). Since the formerly described averaged correlation properties assume equal weighting among all links contributions to the average, which is not the case when being subject to the respective propagation channels (even with the application of PC), and since the channel also introduces non-uniformly delayed contributions from the other links, one then expects that the TDD implementation should lead to worse SINRs and BGs, compared to FDD. In fact, this last property is believed to be the cause for the degradation of SINRs and BGs, for TDD, compared to FDD, also contributing to the larger optima discrepancy registered in the former case (see Section 6.4, MMSE vs. BG Optima Discrepancy). Such also justifies why SINRs and BGs are worse for $L = 4$, relative to the $L = 8$ TDD scenarios. Simultaneously, the longer codes involved in FDD, implying the use of a much larger number of samples, counteract their worse average correlation properties, making the convergence more robust, thus, also leading to average SINRs and BGs that are better than those obtained for TDD, for the generality of propagation scenarios.

6.4 MMSE vs. BG Optima Discrepancy

6.4.1 Initial Considerations

This section presents how the MMSE and BG (or SINR) optima may not coincide, depending on the MaC or MiC scenarios. It is shown how such discrepancy depends on the scenarios, how array patterns are affected, in order to justify its occurrence. By doing so, it is shown that it does not depend on the use of the CG (in fact explicitly verifying that it is present in the RLS similar application), but on the way that the code references are made use of, resorting to the MMSE criterion, and being subject to particularly demanding channel/scenario conditions.

Such issue is not a problem of convergence, the CG leading to the best solution in terms of MMSE or other error norms, relative to the reference codes used. Nevertheless, the high number of arriving correlated and closely correlated signals, added to being a multi-target implementation, and the composed nature of the correlation matrix in the algorithm's cost function, result in that the MMSE solutions do not necessarily lead to the best interference suppression. In terms of physical and practical meaning, though the implemented adaptive optimisation conduces towards a beamformer output that is as *close*, or correlated, as possible to the corresponding DesS code, such *closer* solution may not correspond to the best BG and SINR one, i.e., *farther* solutions, in the sense of not being as correlated to the DesS as possible, may lead to better SINR and BG results.

Since the central contribution of the work deals with the beamforming performance dependence on MiC and MaC scenarios, modelled by a WDCM, the optima definition issue has required an attentive study, with the fundamental aim to decide the iteration number at which SINR and BG should be considered, i.e., the significant SINR and BG optima. It is stressed that it is not the aim of this section to describe the relationships between scenario properties and the beamforming

performance, though inevitably the analysis is based on the same results, some of these being called upon. Another part of the overall study, described in sub-Sections 7.2.7 and 7.3.7, Correlation Matrix Components Dependencies, inherently presents and exposes the optima discrepancy problem, though mainly focusing on the several correlation matrix components, involved in the optimisation process.

In Section 5.4, the parameters required to confirm the convergence the MMSE of the CG implementation have been described – the residual error norm (directly relating to the MSE), the weight estimation error norm, and an error energy norm. In terms of all of these, the CG implementation converges, for either simpler directional scenarios, e.g., [GiMC01] and [GiCo01a], or for the subsequent more complex WDCM scenario implementations, e.g., [GiCo02b] and [GiCo03b]. The MMSE has confirmed to decrease monotonically, along iterations, in any scenario concretisation case, requiring a number of iterations close to M , after which no further significant changes in MMSE are registered. Figure 6.6 exemplifies how the MSE monotonically decreases along the CG optimisation, for 10 and 20 array elements, for the particularly beamforming limitative case of Sc #16u_Mc_Gr_15_200, averaging from 100 concretisations. It is also clearly exemplified how for larger M the final MSE is naturally lower. Figure 6.7 shows those expected MSE dependencies on iteration number and M , for the same scenario.

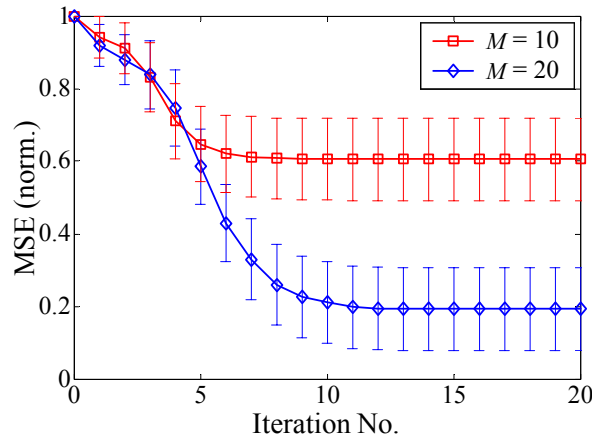


Figure 6.6 – Example of the average MSE evolution (and corresponding standard deviations) along optimisation, for Sc #16u_Mc_Gr_15_200, 10 or 20 array elements.

It is known that MMSE approaches lead to the best SINR results, but such only happens under certain conditions, much simpler compared to the hereby used multi-target WDCM conditions, [LiRa99]. On the one hand, for most of the tested scenarios, one is in the presence of an overloaded array, in the sense that more significant interfering L_T signals exist, compared to the number of array elements, M ; furthermore, each of these L_T signals arrive from a multitude of AoAs, which may load the beamformer even further. On the other, due to multipath, the correlation properties of the codes transmitted by each MT are broken. On the whole, the situation of receiving a large number of

correlated and closely correlated signals from many, including common and correlated, AoAs and ToAs, limit the actual capacity of the beamformer to place the possible nulls, [LiRa99], and also leads to MMSE optima not coinciding with the SINR, or BG, ones. Such is hereby referred as *Optima Discrepancy* (OD), and is the object of study in this section.

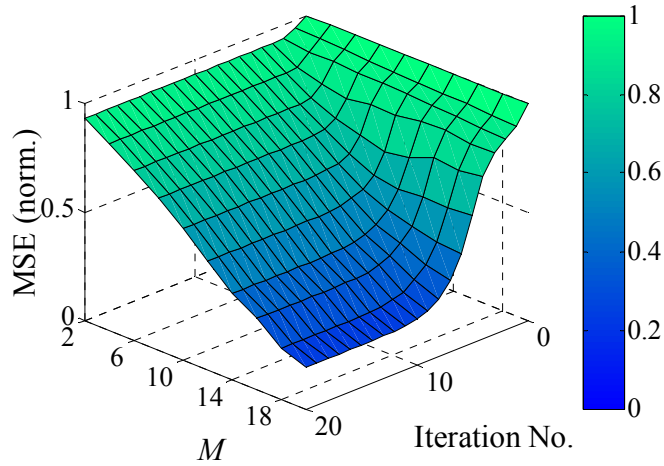


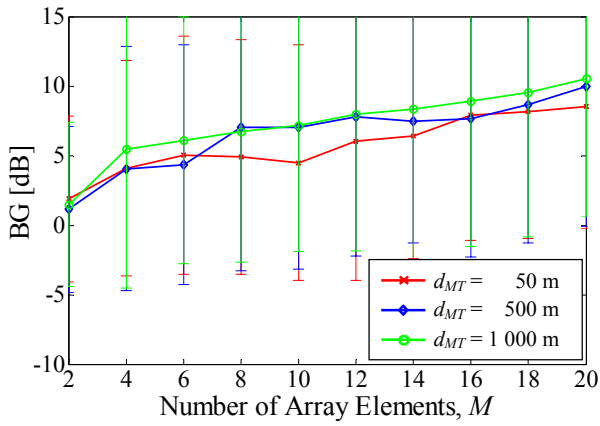
Figure 6.7 – MSE along optimisation, for Sc #16u_Mc_Gr_15_200 and all tested values of M .

Nevertheless, after confirming the general convergence of the algorithm, concerning MMSE, the parameters that require attention are the BG and SINR, to then focus on their dependence on the propagation scenario characteristics. Accordingly, the text follows with the description of the SINR or BG evolutions, along optimisation, for the implemented WDCM MiC and MaC scenarios.

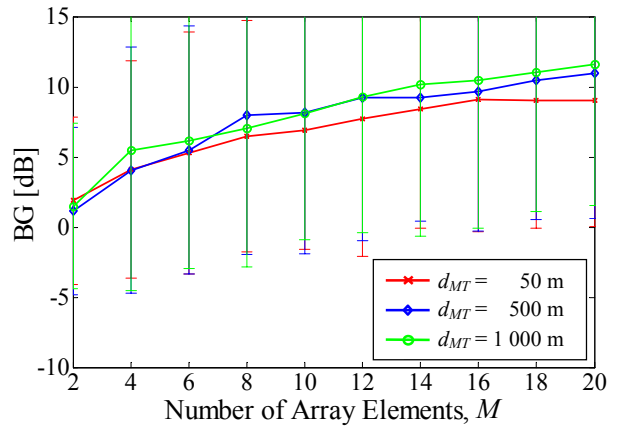
6.4.2 The Micro-cell Scenarios Case

6.4.2.1 MMSE versus SINR and BG Evolutions

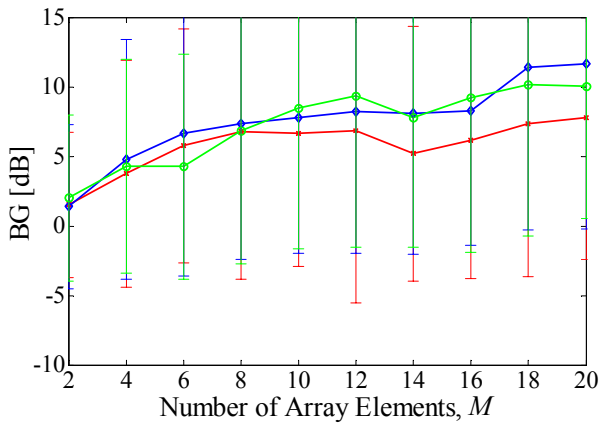
In Figure 6.8, an example is given to show how the average BG values may evolve differently as a function of M and of BS-MT distance, d_{MT} , depending on the iteration number, corresponding to Sc #Lu_mc_Gr_d scenarios, for $L = 4, 8$ or 16 . As it is exemplified, BGs reach different values, the M^{th} iteration not leading to the largest; the BG presents degradations near 14 or 16 array antennas, at the M^{th} iteration, where BGs should in fact show monotonic increases with increasing M , due to the inherent increase in the spatial beamforming resolution. Alternatively, the results generally reveal that the values of the BG and SINR near the 4th iteration, function of the number of links, MT-BS distance and number of array elements, lead to the most logical and consistent dependencies on the scenario parameters, thus, being of importance for the characterisation of the MiC WDCM-performance connection. For these scenarios, though the MMSE convergence is guaranteed close to the M^{th} iteration, it is close to the 4th that most BG maxima occur.



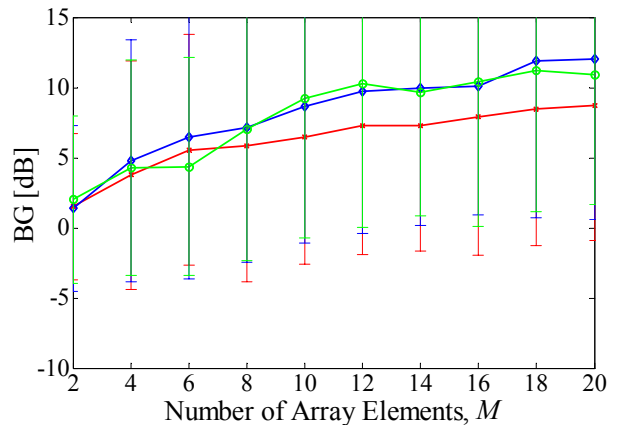
(a) Sc #4u_mc_Gr_d, iteration M .



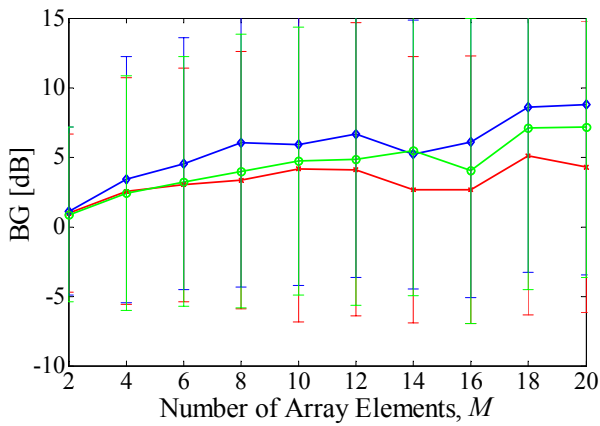
(b) Sc #4u_mc_Gr_d, iteration 4.



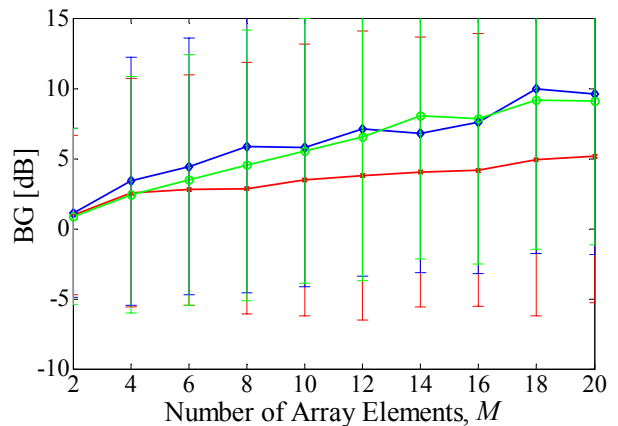
(c) Sc #8u_mc_Gr_d, iteration M .



(d) Sc #8u_mc_Gr_d, iteration 4.



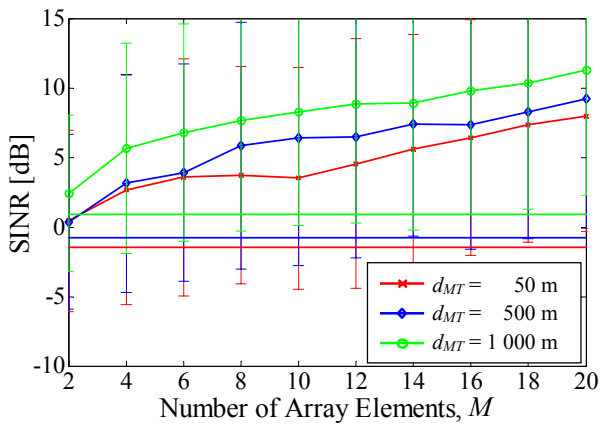
(e) Sc #16u_mc_Gr_d, iteration M .



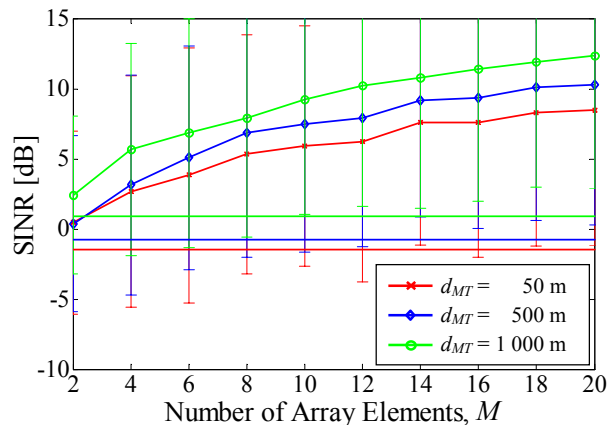
(f) Sc #16u_mc_Gr_d, iteration 4.

Figure 6.8 – Examples of the BG dependence on the iteration number, for Sc # L u_mc_Gr_d, as function of M , for several values of d_{MT} , at the M^{th} or 4th iterations. Solid lines indicate average results, and error bars indicate respective standard deviation.

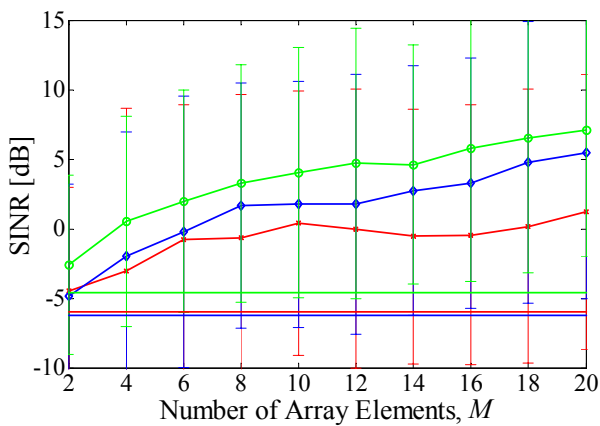
Additionally, as Figure 6.8 once again exemplifies, standard deviations are large. In this way, the SINR or BG standard deviations also reflect that optimisation in the MMSE sense does not necessarily lead to optimisation of SINR and BG. In Figure 6.9, the corresponding average SINR values are presented, once more showing how *better behaved* the 4th iteration results are. The straight horizontal lines correspond to the single element average SINRs, also seeing how these vary with d_{MT} .



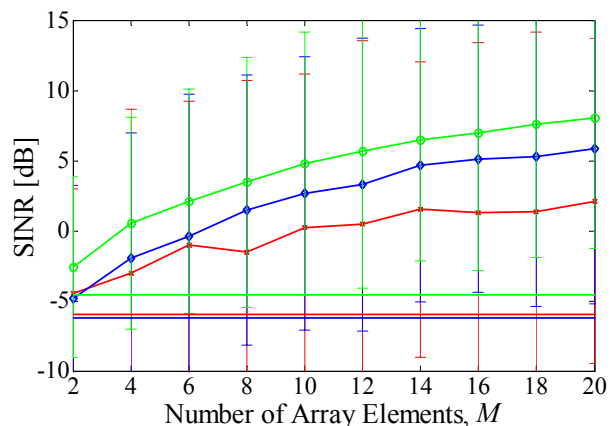
(a) Sc #4u_mc_Gr_d, iteration M .



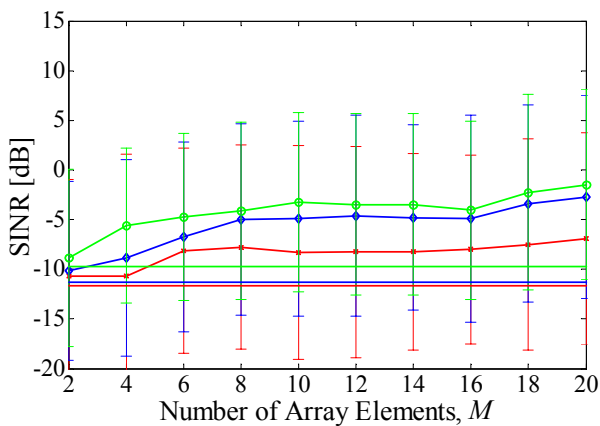
(b) Sc #4u_mc_Gr_d, iteration 4.



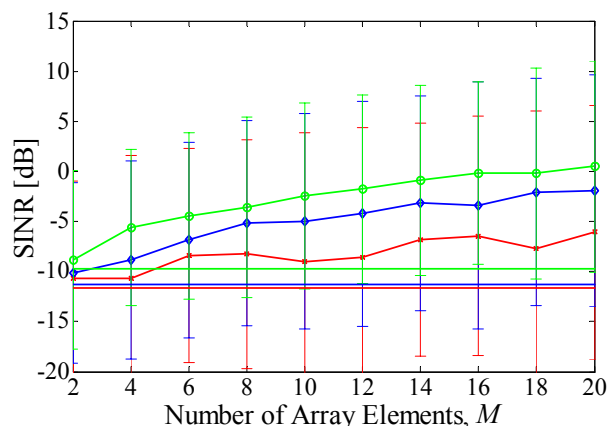
(c) Sc #8u_mc_Gr_d, iteration M .



(d) Sc #8u_mc_Gr_d, iteration 4.



(e) Sc #16u_mc_Gr_d, iteration M .



(f) Sc #16u_mc_Gr_d, iteration 4.

Figure 6.9 – Examples of the SINR dependence on the iteration number, for Sc #Lu_mc_Gr_d, as function of M , for several values of d_{MT} , at the M^{th} or 4th iterations. Single element average SINRs are also shown, as horizontal solid lines.

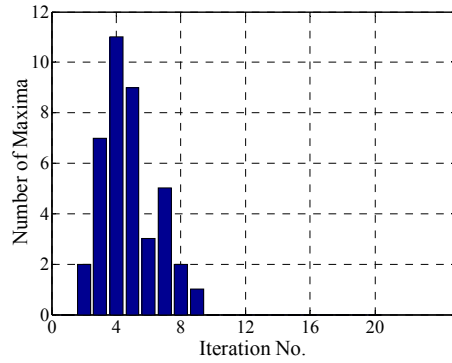
In Figure 6.10, histograms of the number of BG maxima are provided, function of the iteration number, for all Sc #Lu_mc_Gr_d MiC scenarios, being clear how the BG maxima are concentrated between the 3rd and 8th iterations. Additionally, Figure 6.10 shows how maxima are more concentrated for larger BS-MT distances, i.e., for the cases where ToA and AoA spreads are lower.

6.4.2.2 Evolution of Signal, Interference-plus-Noise Powers

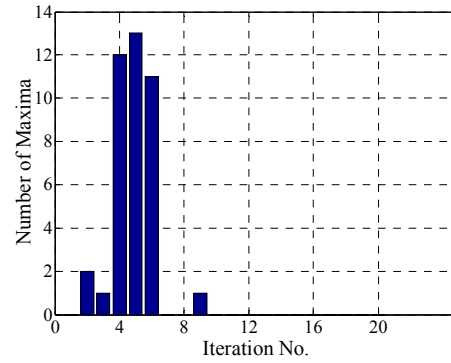
The better and more logical results obtained around the 4th iteration require the whole evolution, even beyond the M^{th} iteration, to be well verified and known. For this reason, the way the BG values, the DesS power, P_{DesS} , and the NDesI, P_{NDesI} , plus noise, N , powers vary helps in this study. In Figure 6.11 to Figure 6.13, surface plots provide these results for 16 active users, varying the number of array elements, M , from 2 to 20, viewing the average BG evolutions along optimisation. The plots for 4 and 8 users are presented in Annex A – Surface Plots – Micro-Cell Scenarios. All plots, except for the BG ones, start on the second iteration, since the values relative to the first iteration are comparatively large, scaling out all the subsequent much lower BG differences. The BG plots start on the first iteration. Common colour axes and representation axes have been set, in order to better compare the results.

From Figure 6.11, one sees how the BG results can be in fact better near the 4th or 5th iterations, for any number of array elements, decreasing as the algorithm progresses. For example, for Sc #16u_mc_Gr_10, the maxima are at most 3.3 dB above the M^{th} iteration values. The existence of this peak consistently happens for any value of M , though the values after the decrease do show some dependence on it. Such is also seen for the 4 and 8 users cases, though the peak is relatively larger for larger L and larger MT-BS distances. It is, therefore, again seen how having more array elements may or may not lead to better BG results, depending on the iteration number. Also, from the BG difference plots, it is exemplified how, until the 3rd or 4th iterations, the BG presents large increases (positive large differences), relative to the relative low subsequent decreases (negative differences). The major contribution to the BG increase happens near the 3rd or 4th iterations, in the cases of Sc #4u, #8u and #16u, MiC scenarios.

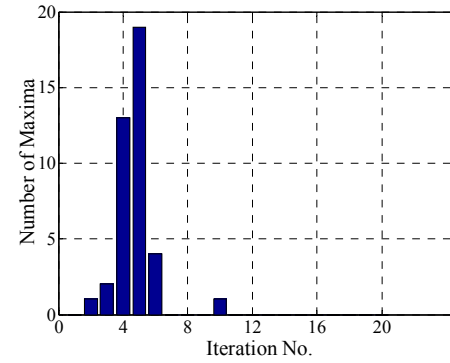
Regarding the P_{DesS} evolution, one sees in Figure 6.12 that the values always increase with the number of antennas and along the optimisation. As the optimisation progresses, the P_{DesS} values reach a near-plateau after near the 4th iteration (better seen in the difference plots). This evolution becomes clearer for lower number of users (Annex A – Surface Plots – Micro-Cell Scenarios). It is also verified that the P_{DesS} reaches similar values for $L = 4, 8$ or 16, independent of distance, and that P_{DesS} clearly decreases as the number of links, L , increases. This latter outcome can be viewed as directly resulting from the limited discrimination capacity of the beamformer. Consequently, the results obtained for the P_{DesS} evolution present no surprises in its dependence on the number of array elements, number of iterations, number of MTs and MT-BS distance. The interference plus noise powers, $P_{NDesI} + N$, should be the components that are responsible for the less expected BG variations, further helping to understand why the SINR and BG values do not simply increase with M , for any iteration number, nor simply increase along the optimisation, for any M .



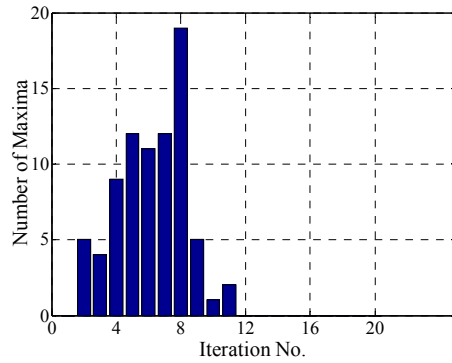
(a) Sc #4u_mc_Gr_05



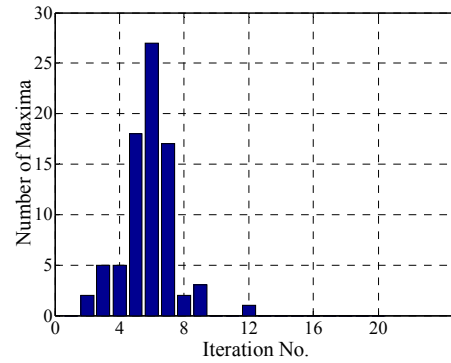
(d) Sc #4u_mc_Gr_5



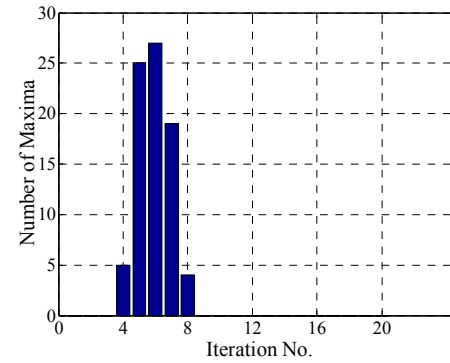
(g) Sc #4u_mc_Gr_10



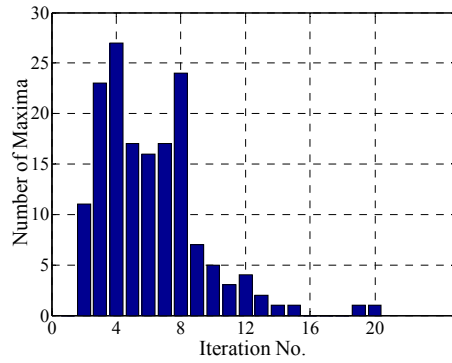
(b) Sc #8u_mc_Gr_05



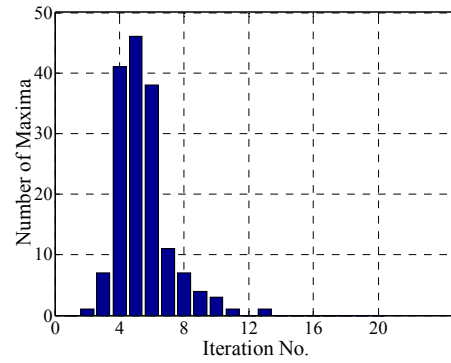
(e) Sc #8u_mc_Gr_5



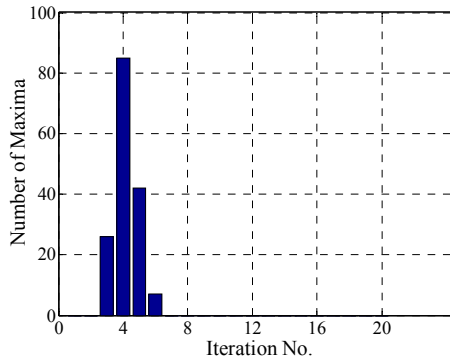
(h) Sc #8u_mc_Gr_10



(c) Sc #16u_mc_Gr_05

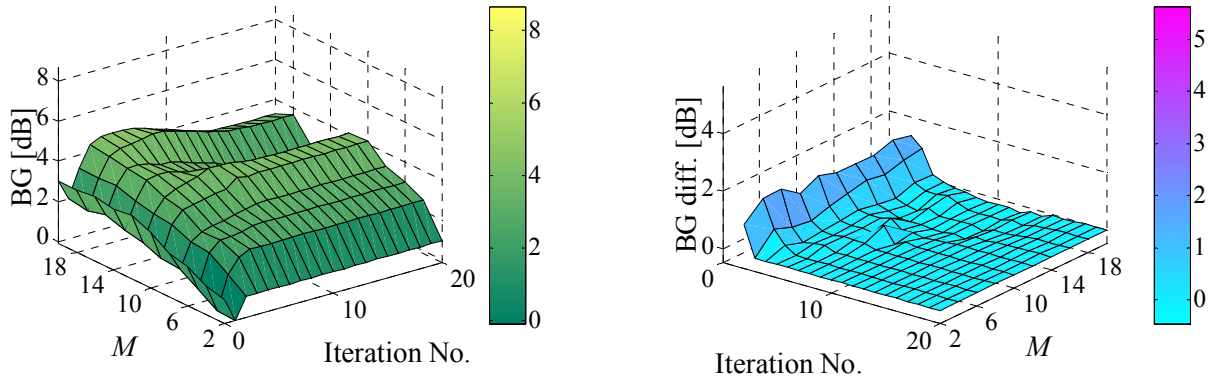


(f) Sc #16u_mc_Gr_5

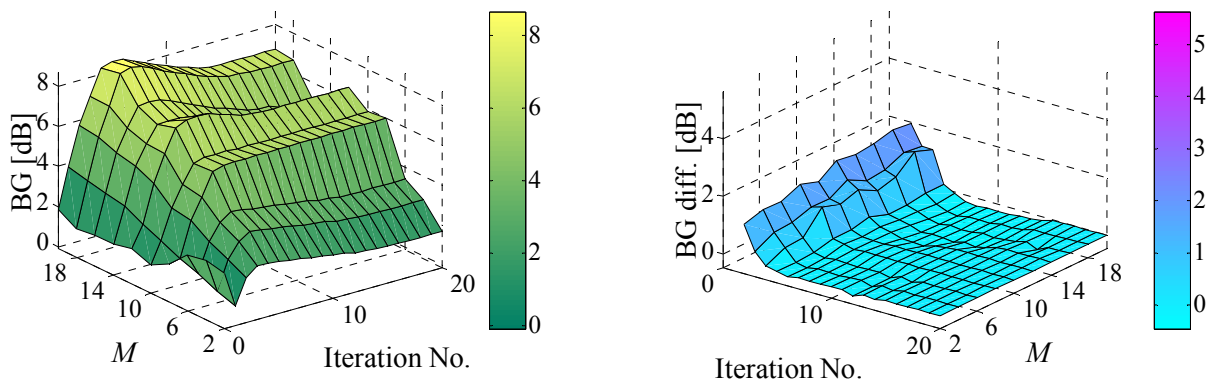


(i) Sc #16u_mc_Gr_10

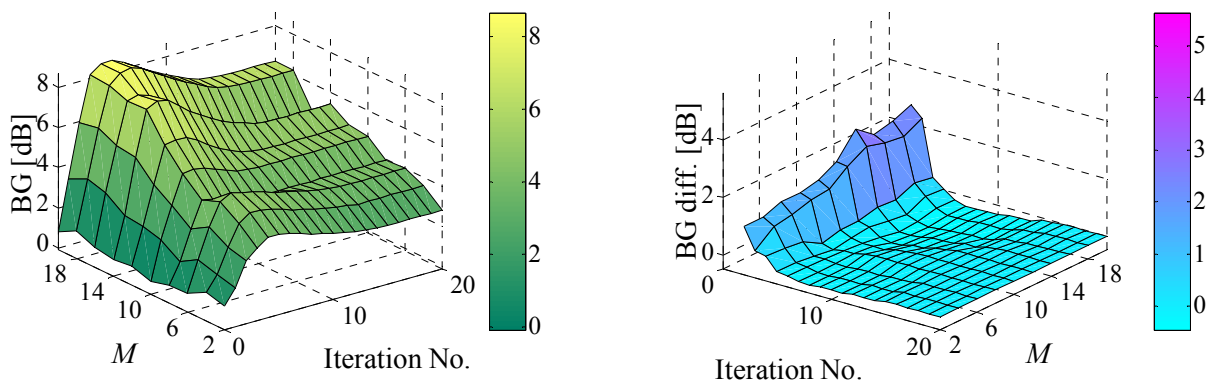
Figure 6.10 – Histograms of the maxima, function of the iteration number, among all links, for the Sc #Lu_mc_Gr_d scenarios.



(a) Sc #16u_mc_Gr_05.

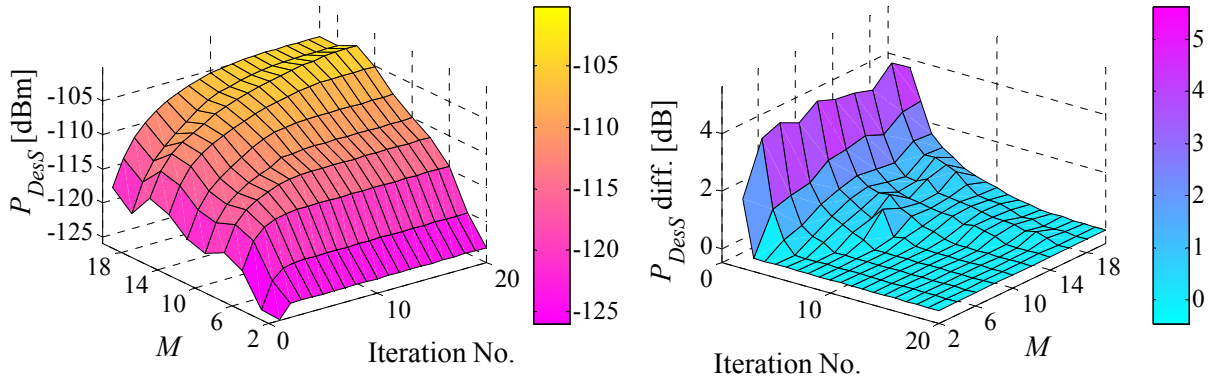


(b) Sc #16u_mc_Gr_5.

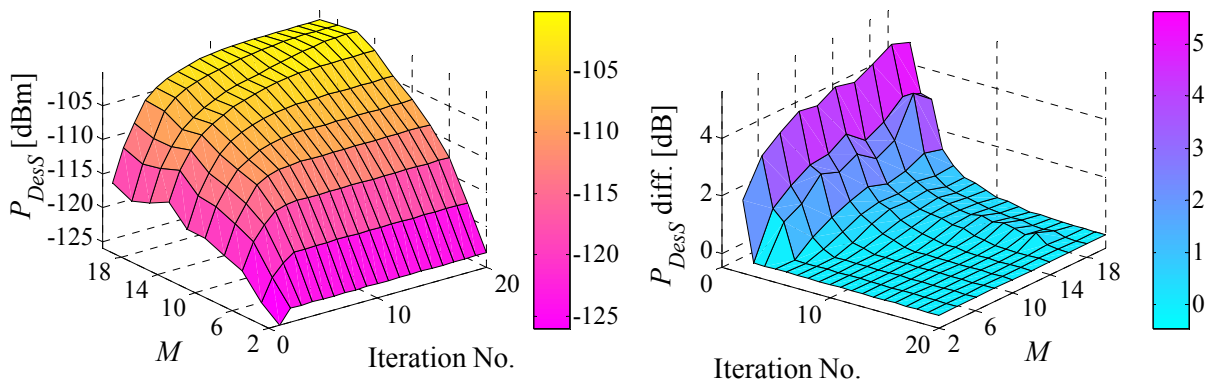


(c) Sc #16u_mc_Gr_10.

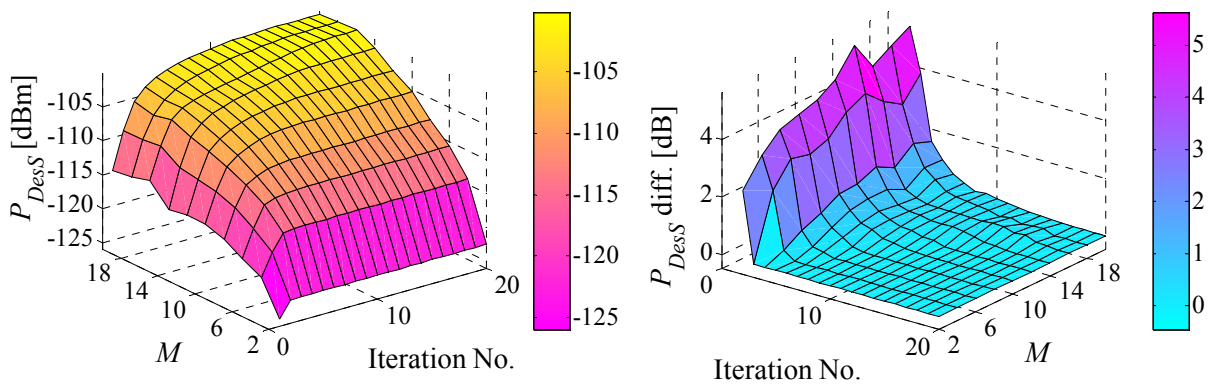
Figure 6.11 – Average BG results and differences along optimisation, as function of M , for several values of d_{MT} , $L = 16$.



(a) Sc #16u_mc_Gr_05.

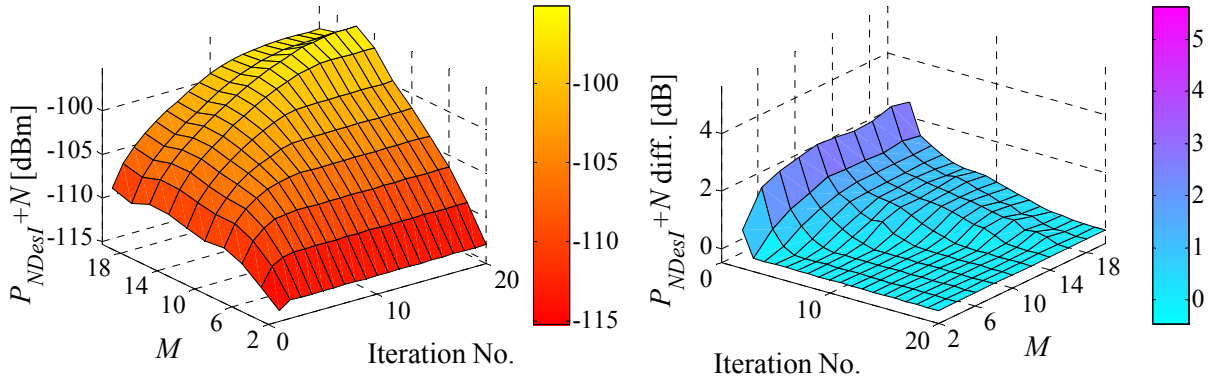


(b) Sc #16u_mc_Gr_5.

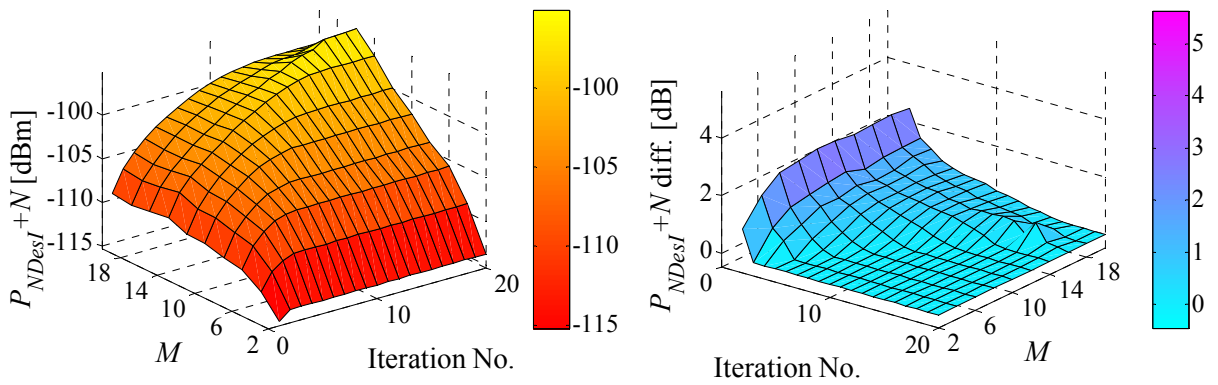


(c) Sc #16u_mc_Gr_10.

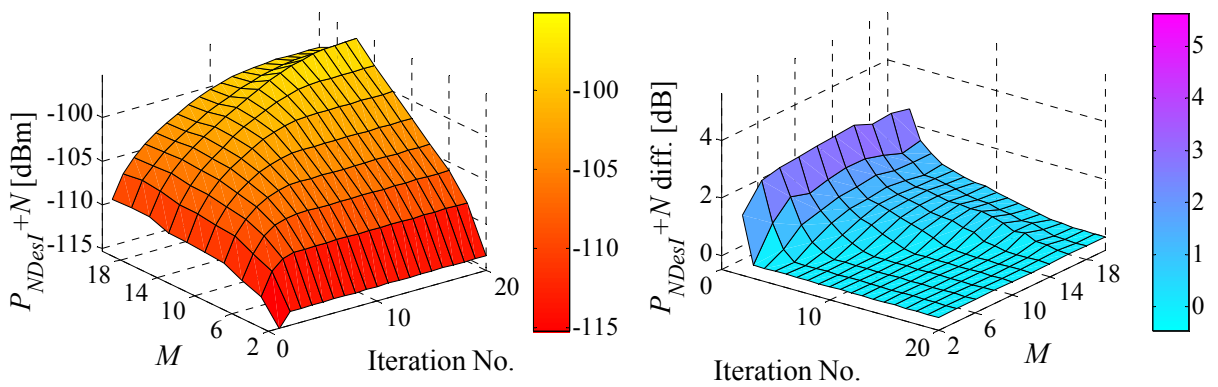
Figure 6.12 – Average P_{DesS} [dBm] and differences along optimisation, as function of M , for several values of d_{MT} , $L = 16$.



(a) Sc #16u_mc_Gr_05.



(b) Sc #16u_mc_Gr_5.



(c) Sc #16u_mc_Gr_10.

Figure 6.13 – Average $P_{NDesI+N}$ [dBm] and differences along optimisation, as function of M , for several values of d_{MT} , $L = 16$.

In Figure 6.13, the $P_{NDesI} + N$ results for 16 users do not show any power decrease along the optimisation, independent of the number of array elements (also for 4 and 8 MTs). Further related to this, two important areas exist in the surface plots – for $M > \text{Iteration No.}$ and for $M < \text{Iteration No.}$. In the former area, $P_{NDesI} + N$ power levels do not increase with the number of array elements for all scenarios, in fact decreasing with M only in the case of the less interference demanding scenarios. On the other hand, in the latter area, where $M < \text{Iteration No.}$, for the same Iteration No., the power levels increase with M , reaching a well defined peak, further decreasing for larger values of M . These power increases tend to be larger and better defined the larger the number of active MTs or the shorter the BS-MT distance, i.e., for larger L_T , which follows an expected trend. In the cases where such peak is larger, the effects are clearly identified in the BG surface plots. Such peaks, in the $M < \text{Iteration No.}$ area, can happen near $M = 4, 10, 12$ or 16 . Especially for Sc #16u, the peak is present for $M = 16$, for any BS-MT distance, having major destructive effects on the BG in such surface plot area.

For the described results, one then concludes that BG is more dependent on the $P_{NDesI} + N$ power variation than that of P_{DesS} powers, due to distance or number of links. The P_{DesS} powers increase very slightly tending to a plateau, in the cases where the number of links is larger, or do not register any improvement after very quickly reaching a well-defined plateau. Judging from the relatively *well behaved* P_{DesS} results, it has been verified that the referred $P_{NDesI} + N$ peaks and their undesired increases, function of M and Iteration No., are responsible for the unexpected BG *worse behaviour* in the $M < \text{Iteration No.}$ surface area. The behaviour of the P_{DesS} values depends much less on the scenario characteristics, while the $P_{NDesI} + N$ values do present large dependencies. Accordingly, for all cases, near the 4th iteration, the $P_{NDesI} + N$ values show tendencies that lead to the most expected BG values dependencies. Thus, the area defined by $M > \text{Iteration No.}$ confirms to be that at which the most logical dependencies on the scenario apply. As it will be seen further in the text, for larger numbers of M , the condition of \mathbf{R} strongly degrades, showing a relation to the *bad behaviour*, near $M = 16$. Also, since the CG algorithm develops along a maximum of M possible search directions, defined by the rank of the correlation matrix, the $M > \text{Iteration No.}$ area does not truly contribute to effective optimisation, e.g., [Shew94]. Furthermore, it is verified that it may contribute to degradation of BG results.

As it is exemplified in Figure 6.14, for a specific number of array elements, as the algorithm evolves, the increase in the $P_{NDesI} + N$ values until $M \cong \text{Iteration No.}$ is much more gradual than those that P_{DesS} values present (the latter faster reaching a plateau). The reason for the P_{DesS} and $P_{NDesI} + N$ values behaving in the described way, along the optimisation, requires further insight into the CG cost function, studying what and how the different internal products and power components vary. As it is described in sub-Section 5.3.3 and Section 5.4, due to the decomposition of \mathbf{R} , the $\mathbf{w}_l^H \mathbf{R} \mathbf{w}_l$ term in the CG cost function involves not only P_{DesS} , several P_{NDesI} components, and N powers, but also cross-correlation terms that do not contribute to the SINR calculation. These results are presented in

Chapter 7, Beamforming in Micro- and Macro-cell Scenarios, confirming the differing relative levels and behaviour of such components. Seeing that, it is then better understood that the MMSE solution may not necessarily lead to the best SINR and BG.

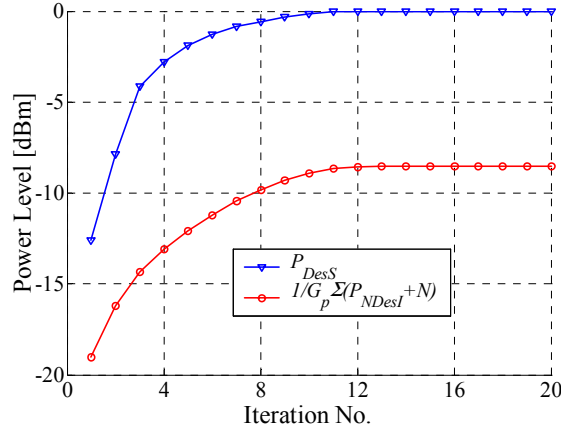


Figure 6.14 – Average P_{DesS} and $P_{NDesI} + N$ contributions to SINR, along iterations, for Sc #16u_mc_Gr_10 and $M = 12$ (normalised to the P_{DesS} maximum).

The MiC scenarios with MT angular displacement also show the same type of response, compared to the street-confined MiC situations. In Figure 6.15, the BG average results are presented, as a function of the number of array elements and iteration number, concerning Sc #16u_mc_Gr_5 (hereby repeated for comparison, with the same scale) and Sc #16u_mc_Sp_5. The responses do not significantly differ in terms of the peak, or of the subsequent BG degradation, for higher iteration numbers. Also, as it is seen in Annex A – Surface Plots – Micro-Cell Scenarios, the histograms of the maxima again indicate that these are also most frequent at the 4th or 5th iterations. There are in fact differences in the BG improvement before the 4th or 5th iterations, increases being much larger in the Sc #16u_mc_Sp_5 case. This behaviour can be explained by the MTs no longer being illuminated by the main lobe of the initial broadside array pattern, as it did happen in the Sc #Lu_mc_Gr_d scenario cases.

In the case that a single MT is angularly separate from the remaining grouped ones, e.g., for Sc #16u_mc_Se_A with results shown in Figure 6.16, the BG progression has an even less pronounced (nearly not present, at all) peak for MT₁ link, while the grouped MTs result in an evolution very similar to all the other group results, with the relatively small, but present, peak near the 4th or 5th iterations.

Judging from the several results, for all MiC scenarios, from which some examples have been taken to picture the general tendencies, the issue of defining a *significant iteration* number is, again, relatively critical, very important to guarantee study consistency. The presented average results and whole subsequent analysis are, therefore, based on the iteration number considered as the significant iteration, at which the corresponding scenario most often leads to BG maxima.

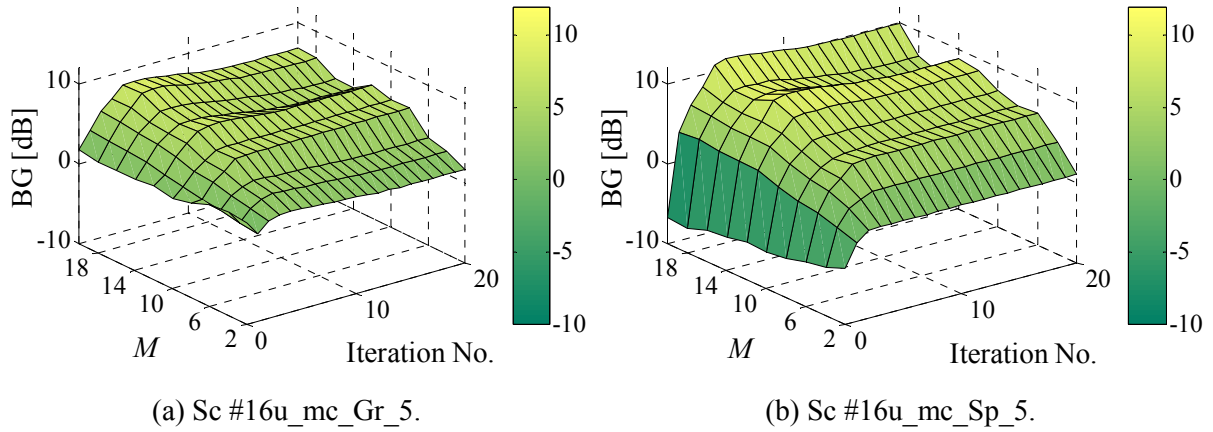


Figure 6.15 – Surface plots of BG, as function of the number of array elements and iteration number, for Sc #16u_mc_Gr_5 and #16u_mc_Sp_5.

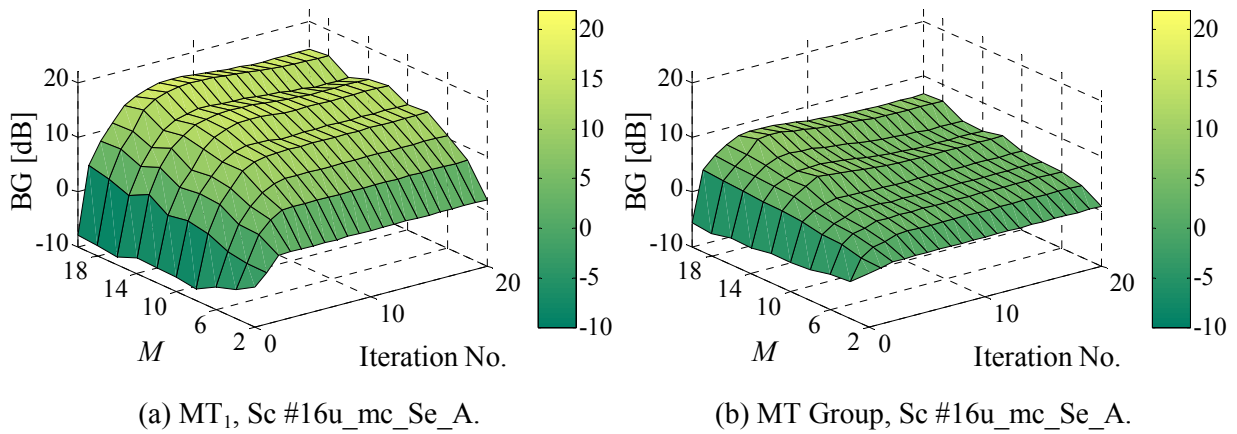


Figure 6.16 – Surface plots of BG, as function of the number of array elements and iteration number, for Sc #16u_mc_Se_A, for MT₁ and the MT group.

6.4.2.3 Numerical Issues

As it has been described in sub-Section 5.3.3, GSO is applied within the CG algorithm, in order to guarantee the R-orthogonality among search directions. GSO tends to prevent lowering of the BG for $M < \text{Iteration No.}$ due to round off errors, [GiMC01]. Though its application is not critical, with the expense of demanding for much greater complexity, in the case of the current DCIRs better values are in fact obtained through applying it, especially for a larger number of array elements.

Regarding the condition of the correlation matrix, \mathbf{R} ($M \times M$), it has been confirmed that it is severely degraded as the number of array elements increases, as Figure 6.17 shows. The major relative increase in the condition number in the case of having 16 or more array elements is visible. Such should be the reason for the major BG decrease and for the $P_{NDesI} + N$ power peaks to exist near

$M = 14$ or 16 , in the $M < \text{Iteration No.}$ area, though, beyond $M = 16$ the levels of these may also rise. This happens since the size of the used TDD sample block, N_s , is 16, i.e., 16 being the maximum possible rank of the signal and correlation matrices. Nevertheless, this fact does not affect any of the results near the significant iteration, nor prevent the problem from anyway converging in terms of MMSE.

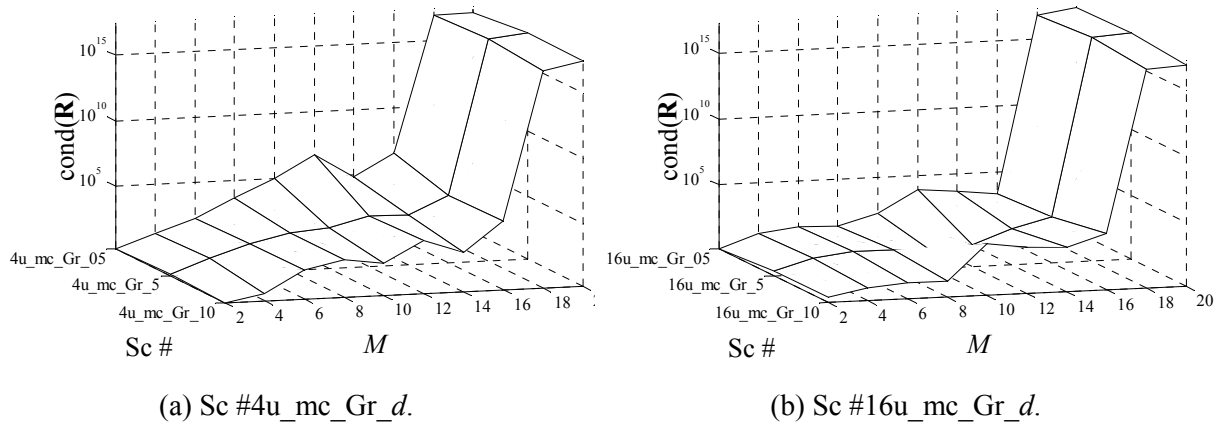


Figure 6.17 – Evolution of the \mathbf{R} condition number, in logarithmic scale, function of scenario and M , for Sc #4u_mc_Gr_d and #16u_mc_Gr_d examples.

6.4.2.4 Array Pattern Analysis

Regarding the array patterns obtained at the 4th or M^{th} iterations, with some acuteness, one can see that the former cases naturally result in patterns that are better correlated to the AoAs than those corresponding to the latter ones. Nevertheless, the ULA inherent limitations and the WDCM demanding characteristics, mainly in the MiC scenarios limited by the street, affect the resulting pattern in the sense that the visual analysis can only be superficial, e.g., placing major lobes at angles that do not have any apparent relation to the desired link, but still leading to better BG or SINR results. In [GiCo02b], an example is presented, for $L = 4$, $d_{MT} = 50$ m, and also $M = 12$, such pattern still presenting some visual correlation to the corresponding DCIR AoAs. Additional patterns are hereby provided, as function of the iteration number. These are depicted in Figure 6.18 and Figure 6.19, for two links within the same group, corresponding to the 1st to 3rd, and M^{th} weight vectors. Expectedly, and as it happens to other cases with MTs being grouped together, the patterns do not visibly correlate to the DCIR, being difficult to relate to the corresponding BG evolution, as plot in Figure 6.20. Anyhow, one sees that it is in the sector within which most DCIR contributions arrive, that the lobes are narrower and most frequent (in angle), i.e., where the pattern varies more significantly with the azimuth angle.

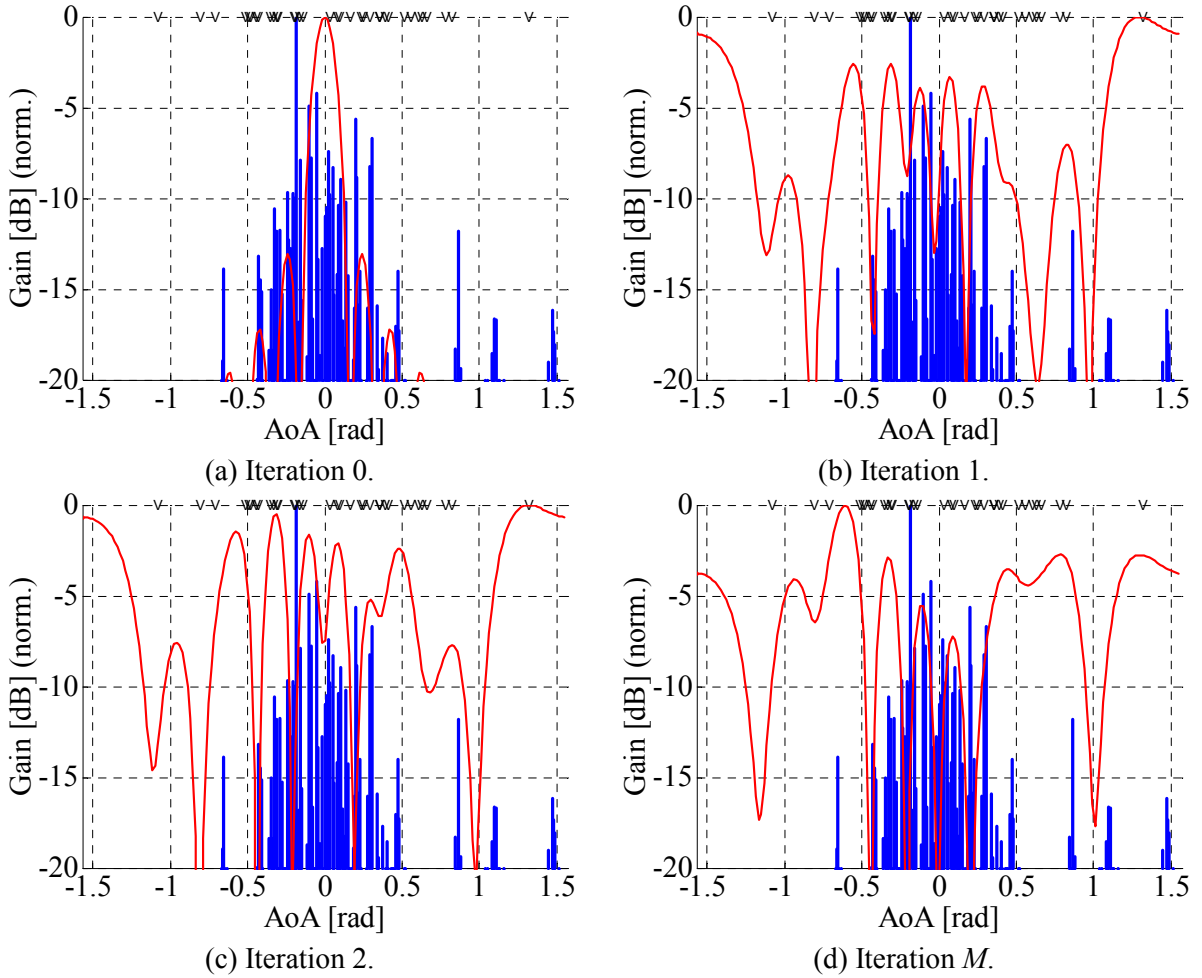


Figure 6.18 – Array patterns (red, thin line) of one link (MT_1), for $M = 12$, with all the MTs at 0 rad, Sc #16u_mc_Gr_5, for the initial and M^{th} iterations, where the AoA of the DesS (blue, thicker lines) and of delayed NDesI from the other MTs (indicated by ‘V’) are shown.

Certainly more informative are the patterns for the MiC scenario cases where MTs are angularly spread, as in a crossroads, plaza or large avenue, the pattern evolution along optimisation being clearer, as a function of the MT positioning and grouping. As it is exemplified in Figure 6.21, for Sc #16u_mc_Se_A, the array patterns for MT_4 are shown, for the 1st, 3rd and M^{th} vectors. At the first iteration, this MT, pertaining to the MT group, has its corresponding pattern changed from broadside to pointing at the region where such MT group exists, towards $-\pi/5$ (-0.63) radians. After the 3rd iteration, the pattern continues changing, and at the M^{th} iteration, a sharp null is formed close to $\pi/4$, towards MT_1 , while a main lobe and reasonably important secondary ones are directed towards very near such undesired MT contributions. Also, the lobe towards $-\pi/5$ is no longer the largest one, additionally contributing to lower BG. For the single MT_1 , placed at $\pi/4$, the same scenario and WDCM concretisation, the pattern keeps its main-lobe shape with more consistence and better side-lobe suppression, along optimisation, as it is seen in Figure 6.22, along with well defined deep nulls around the $-\pi/5$ direction.

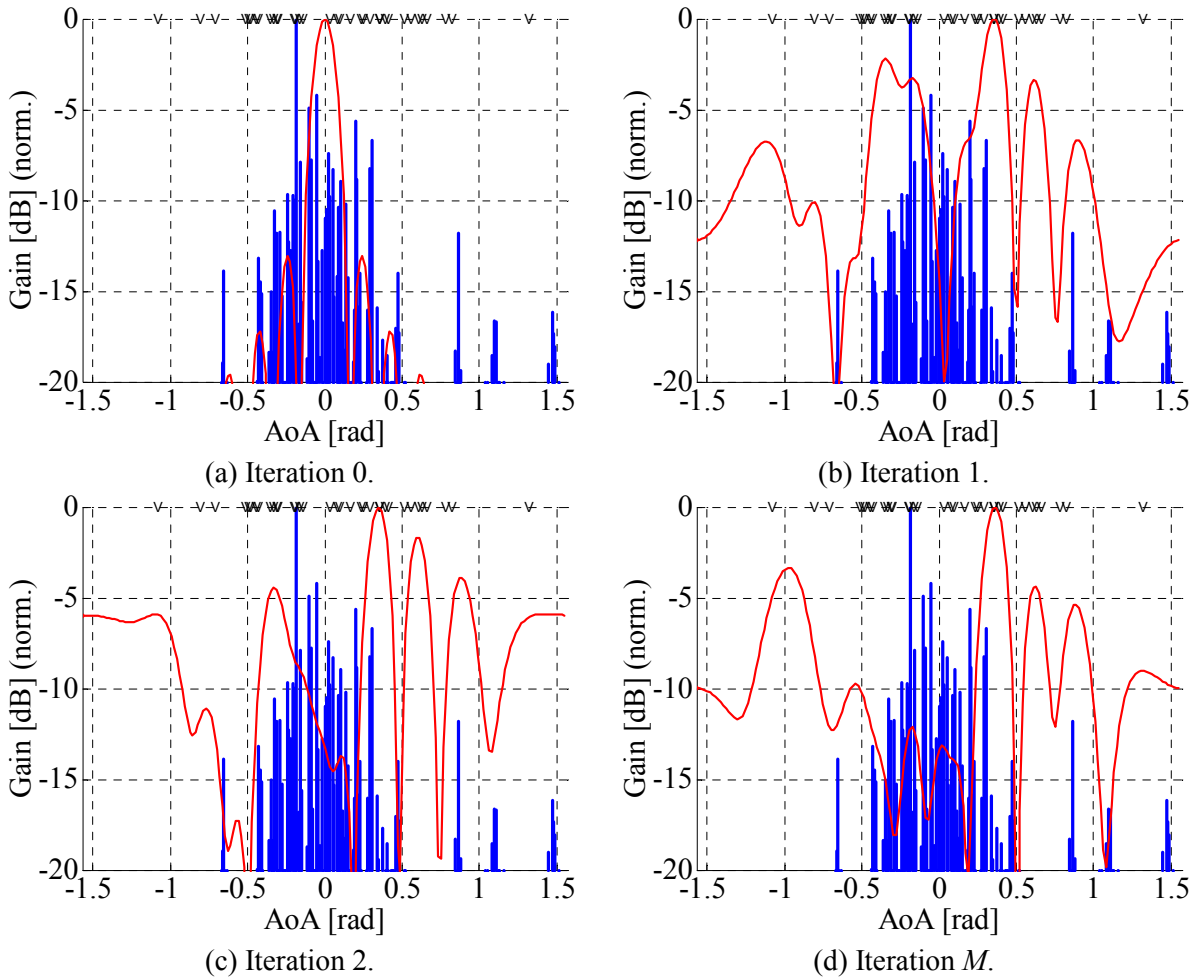


Figure 6.19 – Array patterns (red, thin line) of another link (MT_{12}), for $M = 12$, with all the MTs at 0 rad, Sc #16u_mc_Gr_5, for the initial and M^{th} iterations, where the AoA of the DesS (blue, thicker lines) and of delayed NDesI from the other MTs (indicated by ‘V’) are shown.

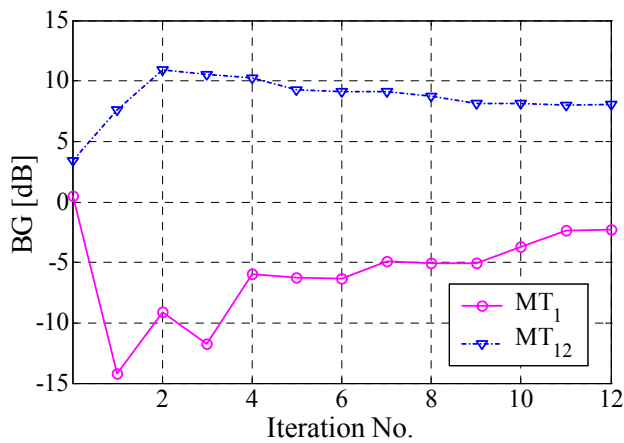


Figure 6.20 – BG, along optimisation, for MT_1 and MT_{12} in Sc #16u_mc_Gr_5, one channel concretisation.

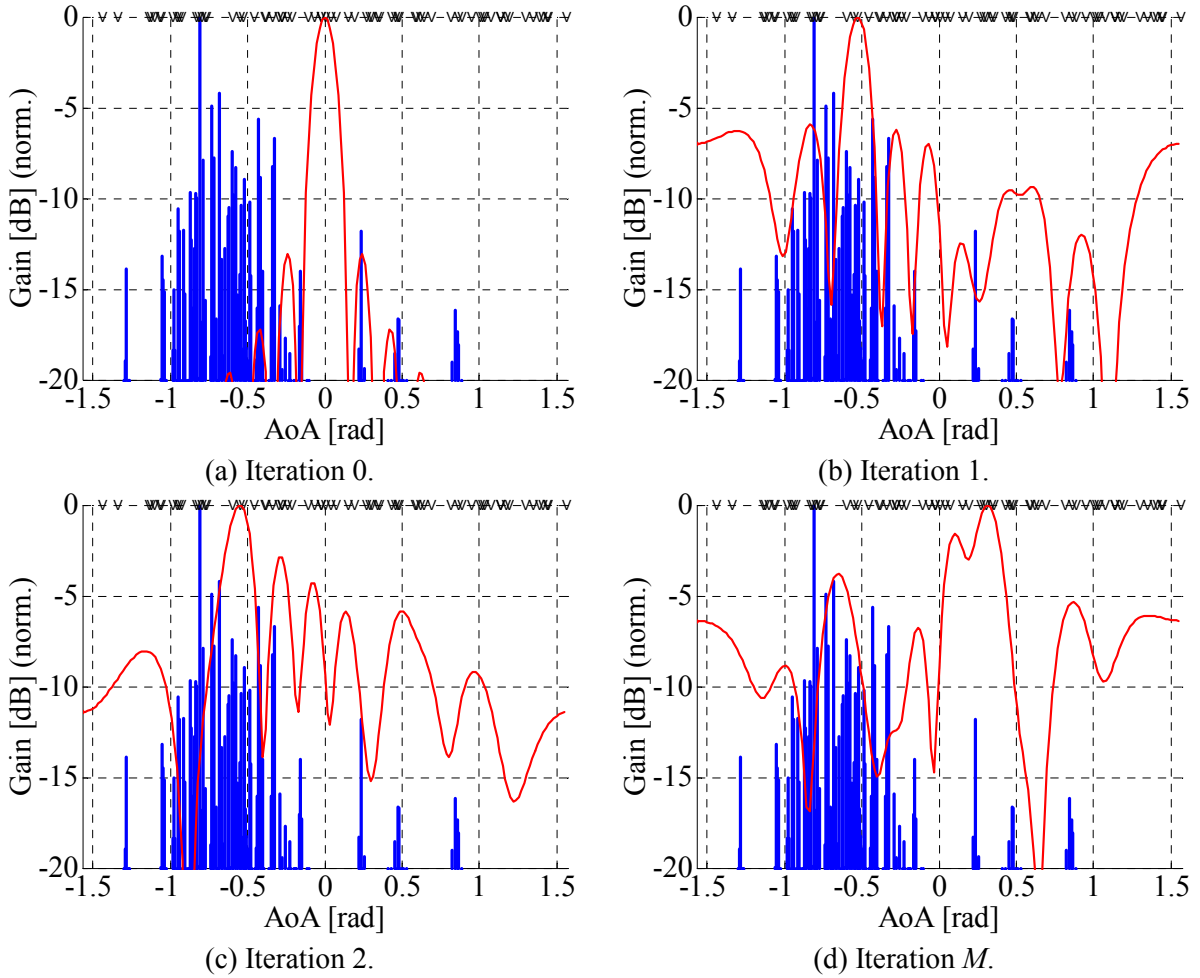


Figure 6.21 – Array patterns (red, thin line) for $M=12$, for MT_4 at $-\pi/5$, in Sc #16u_mc_Se_A, for the initial and M^{th} iterations, where the AoA of the DesS (blue, thicker lines) and of delayed NDesI from the other MTs at $-\pi/5$ and $\pi/4$ (indicated by ‘V’) are shown.

The example of the MT_4 has been chosen, as one of the worst ones, for this WDCM concretisation, either in respect to patterns or BG evolution. The respective BG evolutions are visible in Figure 6.23, along optimisation, BGs of MT_1 and MT_4 evolving differently, either establishing a plateau with an insignificant relative peak, or with a peak and following considerable degradation, respectively. Their differences in BG levels are also in close relationship to the relative lobe level differences in their array patterns. This sort of BG responses is, therefore, in consistence with the respective intuitively clear array patterns, again keeping in mind the limited intuitive analysis that the patterns are able to provide.

The MiC array patterns explicitly show that the channel at stake is complex, especially in the cases that the MTs are grouped together. As it was seen before, among MiC scenarios, it is also for these cases that the MMSE vs. BG OD is more evident, also resulting in lower BG optima values, in some accordance to the resulting patterns.

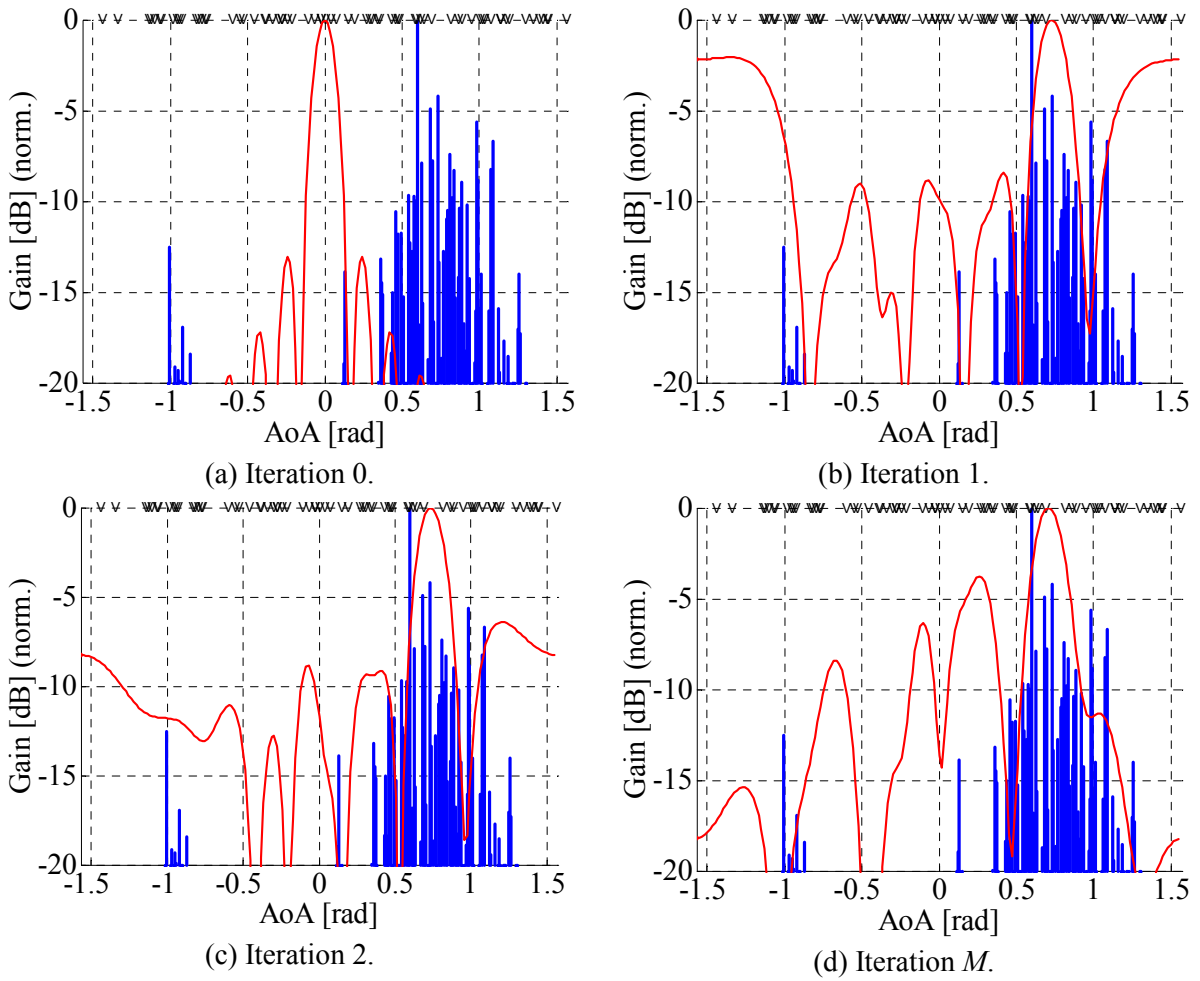


Figure 6.22 – Array patterns (red, thin line) for $M = 12$, with the MT_1 at $\pi/4$, Sc #16u_mc_Se_A, for the initial and M^{th} iterations, where the AoA of the DesS (blue, thicker lines) and of delayed NDesI from the other MTs at $-\pi/5$ (indicated by ‘V’) are shown.

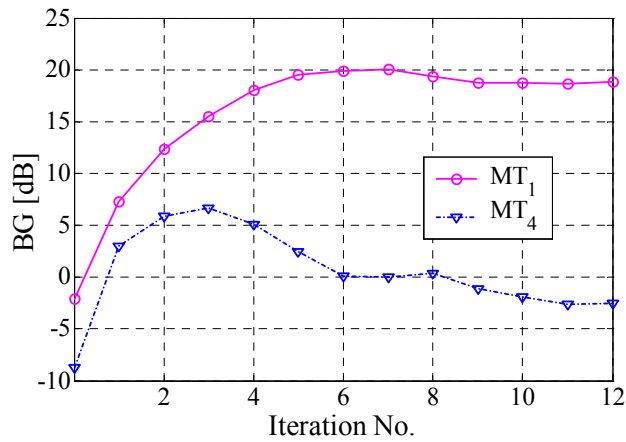


Figure 6.23 – BG, along optimisation, for MT_1 and MT_4 in Sc #16u_mc_Se_A, one channel concretisation.

6.4.3 The Macro-cell Scenarios Case

6.4.3.1 MMSE versus SINR and BG Evolutions

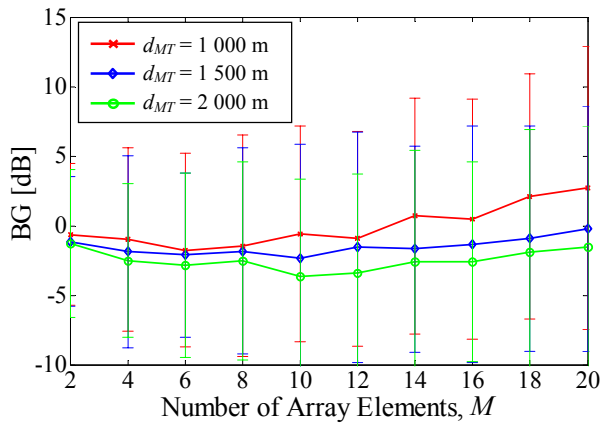
As in the case of MiCs, the evolution of SINR and BG along iterations presents characteristics that affect the beamforming dependence on MaC scenarios characteristics. In fact, for the MaC cases, such evolution may change radically, according to the scenario, making the definition of the *significant iteration* most critical. As a first example, Figure 6.24 presents the average BG results for Sc #Lu_Mc_Gr_d_200, where all active MTs are grouped together. This example shows the relatively large difference among the BGs corresponding to the *significant iteration* and the M^{th} one, the latter ones reaching particularly low negative values. It is also interesting to notice that M^{th} iteration BGs show a tendency to increase with M , but only in the case that M is larger than 12 or 14, for 4 (or 8) active links. This sort of less logical behaviour has again helped in the establishment of the *significant iteration* as being that at which BG optima are most frequent. Additionally, Figure 6.24 very clearly shows that the BG dependency on the BS-MT distance, d_{MT} , changes considerably according to the iteration number, expressing the importance of the definition of the *significant iteration*.

It is also verified, as plot in the corresponding Annex B – Surface Plots – Macro-Cell Scenarios, that BG values are less sensitive to the iteration number in the scenario cases where MTs are angularly spread over the 1st and 4th quadrants, further confirming that the MMSE vs. BG OD is particularly present when MTs are grouped together.

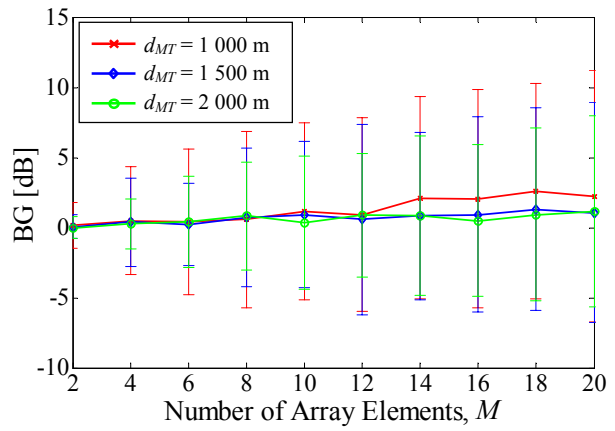
Also, concerning the dependence on the scattering circle radius, the iteration number proves its relevance, once more. In Figure 6.25, the corresponding BG and SINR results are presented, for scenarios Sc #16u_Mc_Gr_15_r, with 50, 200 and 400 m radii, for iteration 0, 1 and M . The initial broadside solution, where all L weights are 0, right away leads to positive BGs, which even increase with the number of array elements, M , for 200 or 400 m radius²⁷. For the case of 50 m, BGs are close to 0 dB, not registering any dependence with M , at iterations 0 and 1, though at the M^{th} iteration BG again varies with M . Though SINRs are negative, the BGs do not indicate SINR degradation in comparison to the single antenna case, for the two initial weights, at iterations 0 and 1.

For these scenarios, where MTs are making use of a common set of scatterers to convey signals towards the BS, it is therefore understood that a definite characterisation results difficult, regarding the performance-scenario properties relationships, since there may exist no iteration where most BG maxima occur, except for iteration 0, i.e., before any optimisation takes place, meaning that, in truth, such does not characterise any beamforming performance. In this way, the values at iteration 1 reveal consistency of results, as being the most significant for the study of MaC scenarios where MTs are grouped together.

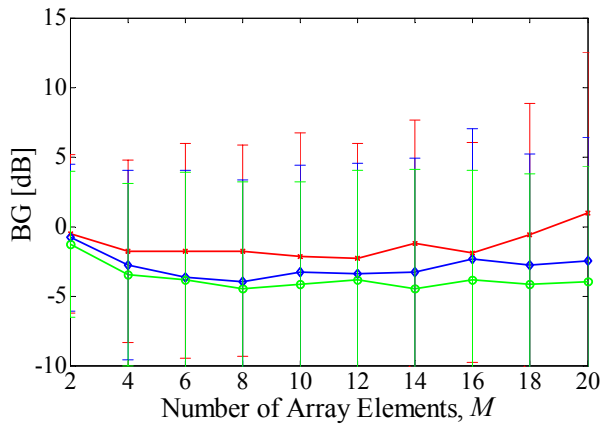
²⁷ This is a very important indication that there can be solutions that result in better BGs and SINRs, other than the MMSE ones, and even the ones that are hereby considered as *significant*.



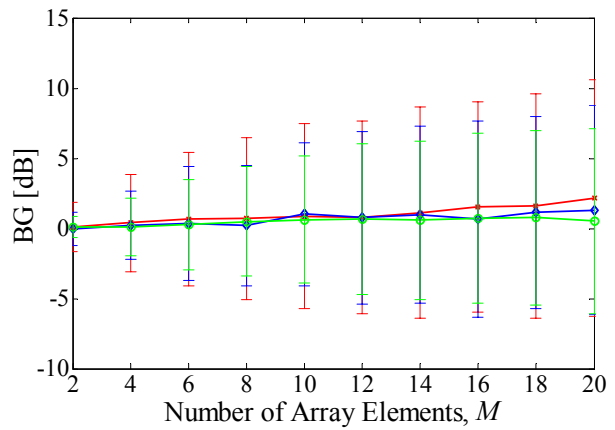
(a) Sc #4u_Mc_Gr_d_200, iteration M .



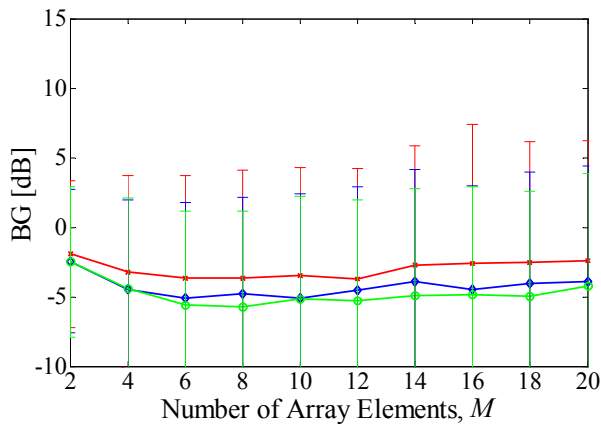
(b) Sc #4u_Mc_Gr_d_200, iteration 1.



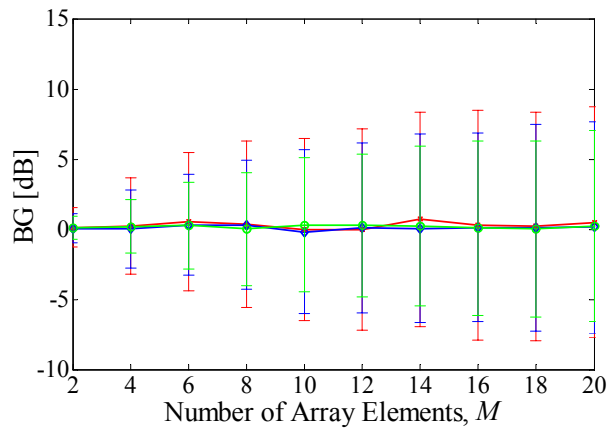
(c) Sc #8u_Mc_Gr_d_200, iteration M .



(d) Sc #8u_Mc_Gr_d_200, iteration 1.

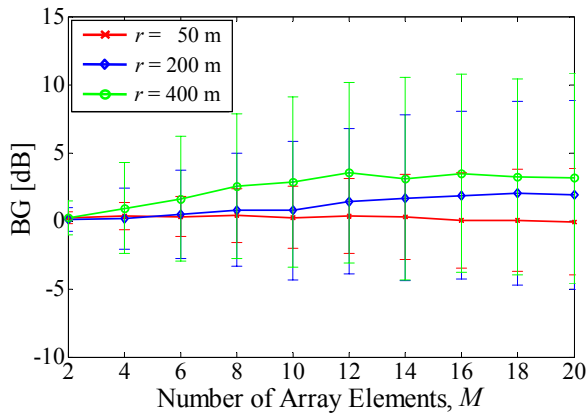


(e) Sc #16u_Mc_Gr_d_200, iteration M .

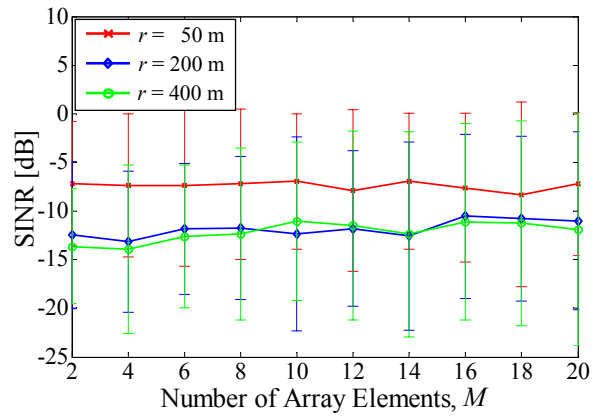


(f) Sc #16u_Mc_Gr_d_200, iteration 1.

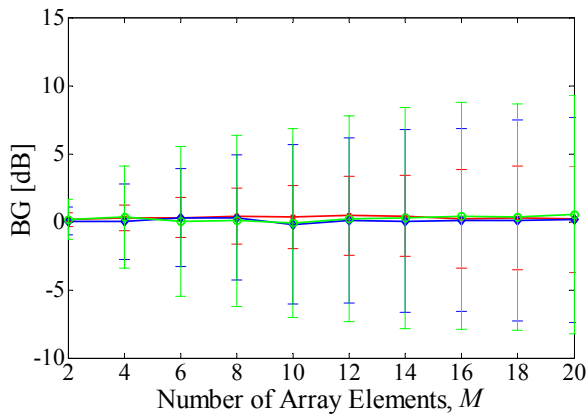
Figure 6.24 – BG, function of M , for several values of d_{MT} , Sc #Lu_Mc_Gr_d_200, at the 1st and M^{th} iterations. Solid lines indicate average results, and error bars indicate respective standard deviations.



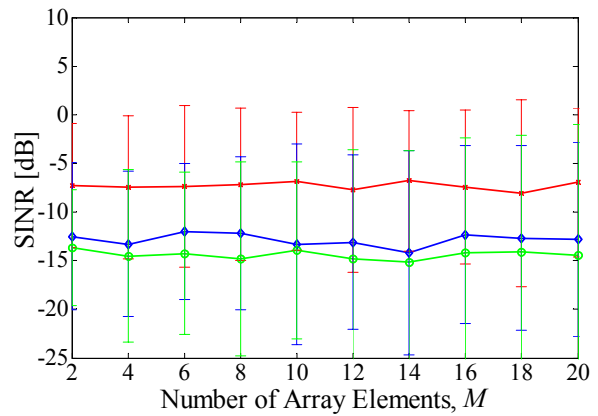
(a) BG, Sc #16u_Mc_Gr_15_r, Iteration 0.



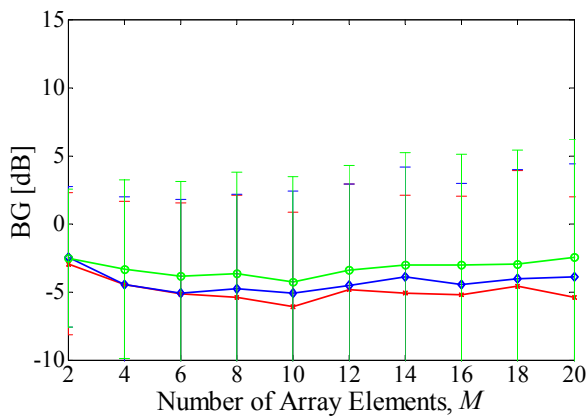
(b) SINR, Sc #16u_Mc_Gr_15_r, Iteration 0.



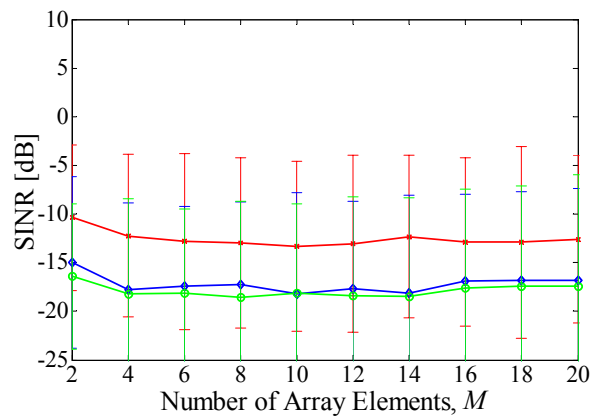
(c) BG, Sc #16u_Mc_Gr_15_r, Iteration 1.



(d) SINR, Sc #16u_Mc_Gr_15_r, Iteration 1.



(e) BG, Sc #16u_Mc_Gr_15_r, Iteration M .



(e) SINR, Sc #16u_Mc_Gr_15_r, Iteration M .

Figure 6.25 – BG and SINR, function of M , for several values of r , Sc #16u_Mc_Gr_15_r, before any beamforming and at 1st and M^{th} iterations.

In order to make sure that the existence of such BG peak is due to the MT grouping, and not to the initial beamforming weights, which correspond to the broadside pattern, therefore illuminating the MT group at 0 radians, Scs #Lu_Mc_Se_A_r provide other angular situations, still involving a group of MTs. In this way, at iteration 0 the average BG results are poor, with several negative values, while at the iteration 1 the BGs reach values close to 0 dB, for any M , to then degrade as optimisation progresses. Figure 6.26 exemplifies so, again indicating the importance of iteration 1 and its independence on the initial MT group illumination, in the cases where MTs are grouped.

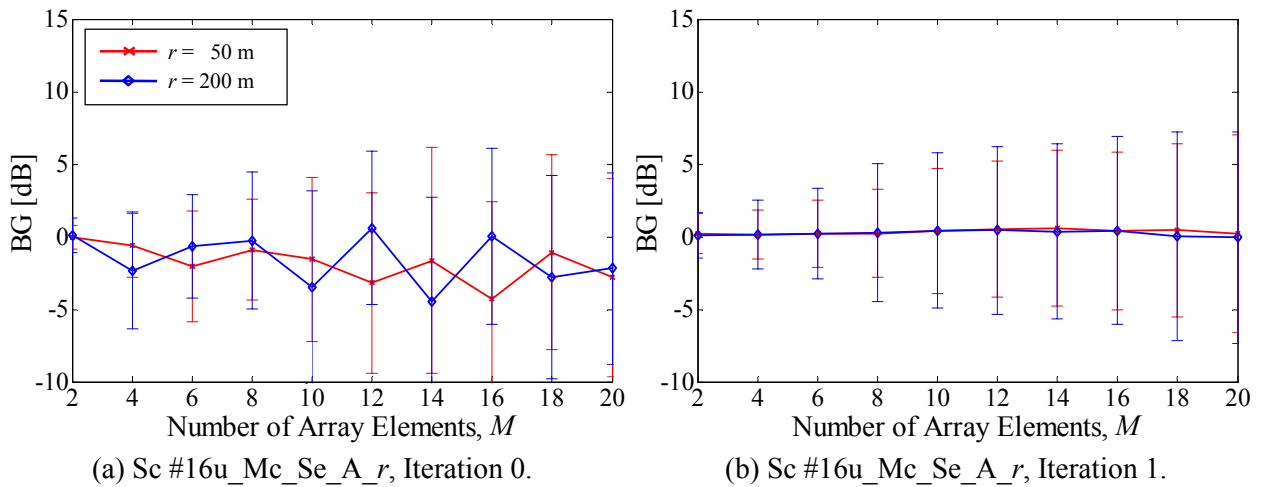


Figure 6.26 – BG, function of M , for several values of r , for the MT group in Sc #16u_Mc_Se_A_r, before any beamforming and at the 1st iteration.

As previously mentioned, the MaC scenarios where there is sharing of scattering areas, lead to BG degradation along optimisation, being the most critical cases of MMSE vs. BG OD, over all MiC and MaC scenarios. Using the most elucidative examples, Figure 6.27 (b)-(d) shows how the spreading of MTs leads to BG values that exhibit a quick increase after the 1st iteration, then decreasing only slightly along iterations (besides the clear positive values achieved), for any number of array elements. It is also seen that scattering circle radius also affects the BG evolution, lower radii leading to a more brisk BG step-like increase. Once more, the severe BG degradation is clear, along optimisation, in the case that MTs are grouped together, in Figure 6.27 (a). Accordingly, Figure 6.28 shows how the BGs evolve for scenario Sc #Lu_Mc_Se_A_r, again presenting the referred degradation in case of grouped MTs.

Though this matter is further complemented by the analysis of the several \mathbf{U} matrix and power components and their dependencies for both MiC and MaC scenarios in sub-Sections 7.2.7 and 7.3.7, Correlation Matrix Components Dependencies, sub-Section 6.4.4, Dealing with the MMSE vs. BG Optima Discrepancy Problem, presents a detailed discussion and solutions regarding the OD problem.

In terms of the procedure to go forth with the most important aim of this work, which is the establishment of the relationships between beamforming performance and the characteristics of the wideband directional propagation scenarios, the same approach as that applied for MiCs has been adopted in order to analyse the dependencies on the MaC scenarios characteristics. In this way, the BG values taken as significant are those at which most maxima occur, establishing the corresponding *significant iteration number*.

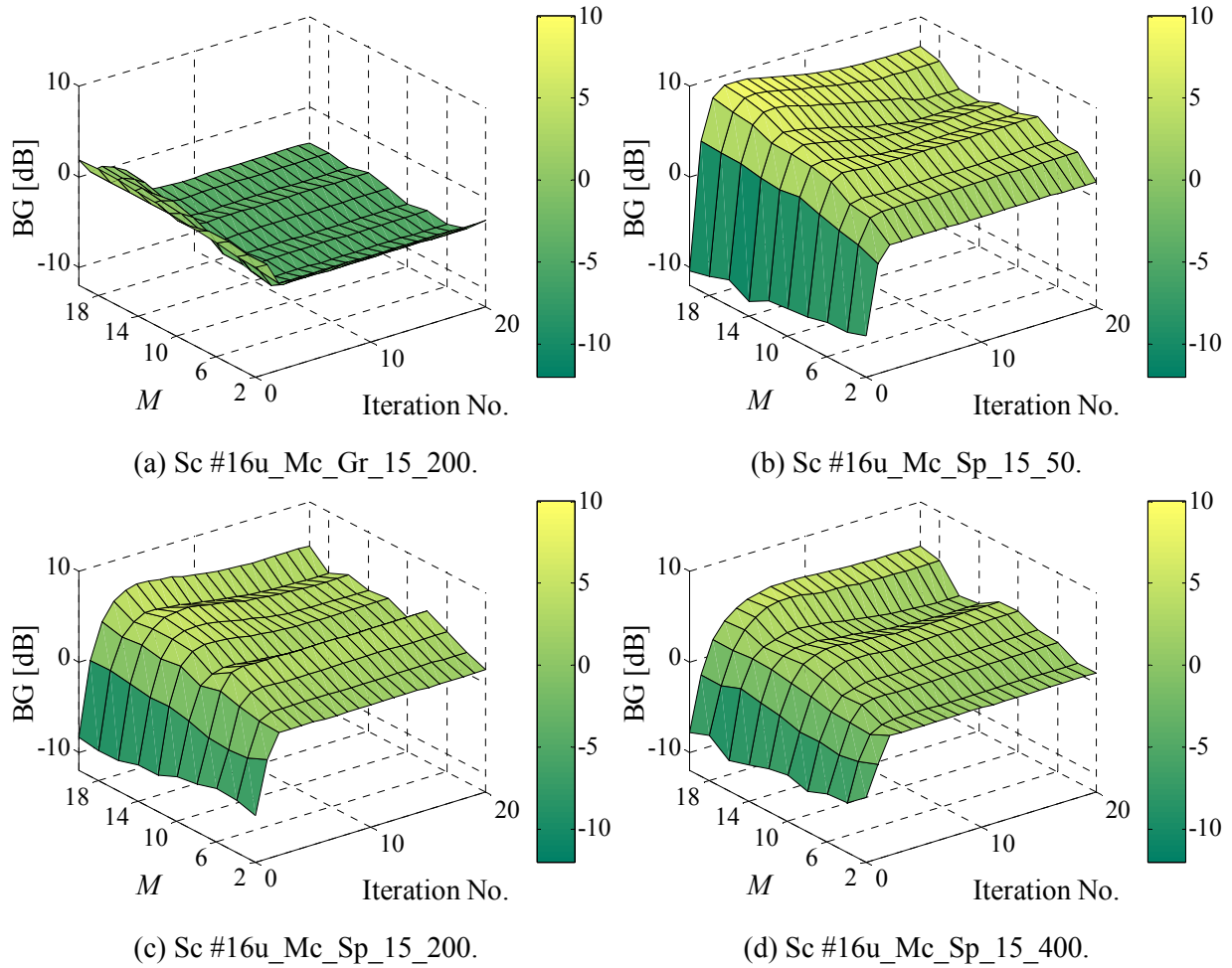


Figure 6.27 – Surface plots of BG along optimisation, function of M , for Sc #16u_Mc_Gr_15_200 and #16u_Mc_Sp_r.

6.4.3.2 Array Pattern Analysis

As already seen for MaCs, the cases where MTs are grouped together, after the first iterations, lead to BGs decreasing to negative values, indicating that the present beamformer application does not improve SINR in respect to a single element antenna, in fact degrading it considerably. As in the MiCs situations, it has been verified that the problem does not relate to using $\mathbf{w} = \mathbf{0}$ (corresponding to the broadside array) as the seed for the CG algorithm. Though the Sc #Lu_Mc_Gr_d_r scenarios do involve MT groups placed in such direction, a similar group of MTs exists at $-\pi/5$ in scenario Sc

#Lu_Mc_Se_A_r, still leading to the same type of BG results, as Figure 6.28 (b) and (d) shows. As Figure 6.29 exemplifies, for the case of an array of 12 elements, the pattern corresponding to MT₁₆, within the MT group, changes from broadside to pointing at the angle where the MT group exists, at the first iteration, corresponding to the BG maxima close to 4 dB. After such, the pattern loses its main lobe, in fact placing a sharp null near $-\pi/5$, corresponding to a BG degradation, reaching just above 0 dB. Also, very close to $\pi/4$ a large lobe and a sharp null are gradually formed, i.e., towards the direction of the MT₁ NDesI source. The DesS and NDesI sources that are indicated through ‘V’ correspond to signals at most 12 dB below the maximum DesS power. For the single MT₁ placed at $\pi/4$, the same scenario and WDCM concretisation, the pattern does keep its main-lobe shape much more consistently, along optimisation, as it is seen in Figure 6.30, along with a well defined deep null near the $-\pi/5$ direction. The respective BG evolutions are visible in Figure 6.31, along optimisation, BG of MT₁₆ reaching a peak at iteration 1, and that of MT₁ at iteration 3.

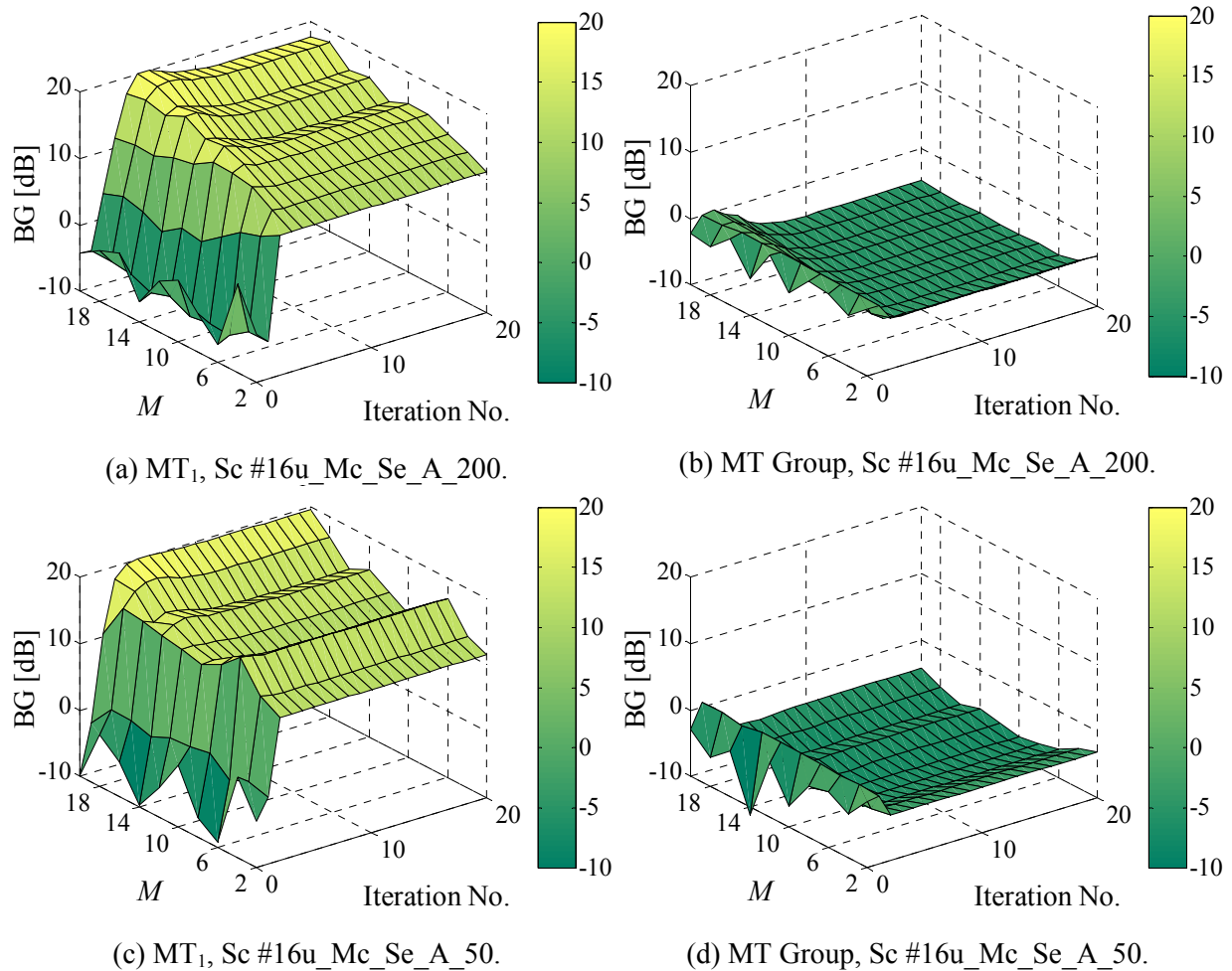


Figure 6.28 – Surface plots of BG along optimisation, function of M , for Sc #16u_Mc_Se_A_r, MT₁ and MT group.

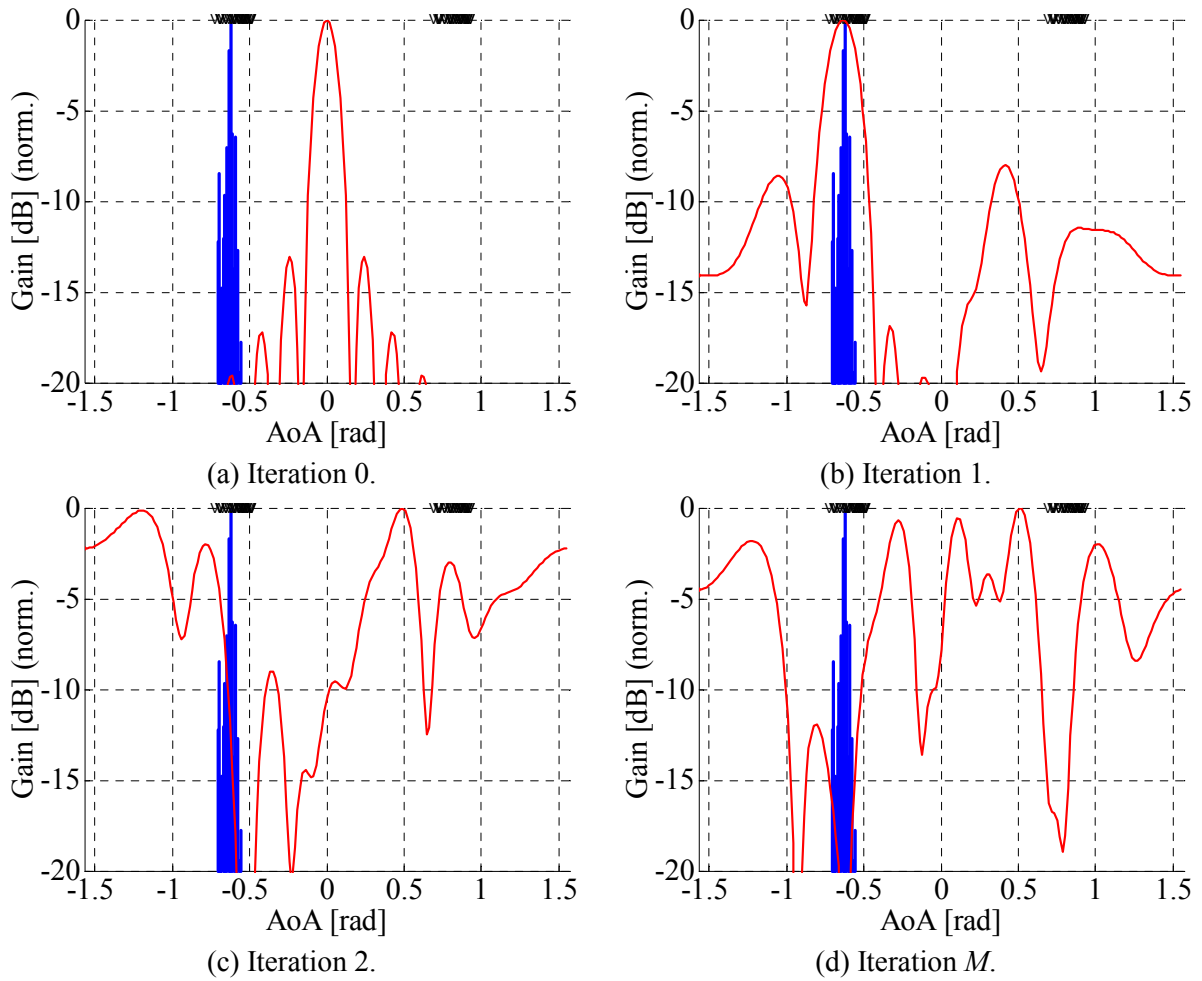


Figure 6.29 – Array patterns (red, thin line) for MT_{16} at $-\pi/5$, in Sc #16u_Mc_Se_A_50, for the initial and M^{th} iterations.

Such type of pattern behaviour has been verified to apply to all the grouped MTs, whilst being viewed as a merely qualitative analysis procedure, and understanding that less obvious pattern evolutions are particularly present in the cases of grouped MTs. In fact, as it is described in sub-Sections 7.2.7 and 7.3.7, Correlation Matrix Components Dependencies, beamforming is particularly noise-limited in the case that MTs are grouped together, the array pattern being further related to MT directions in less obvious ways. For the single MT example, the SINR and BG do expectedly reach high values just after iteration 1, gradually leading to a deeper pattern null near the NDesI dominant AoAs, at $-\pi/5$, then decreasing, matching the slight apparent pattern degradation, towards the M^{th} iteration (Figure 6.30 and Figure 6.31).

In terms of mean behaviour and performance, for the separate MT, the presented types of pattern results apply, in accordance to the OD found. The array patterns also reflect how the MaC cases with grouped MTs are most critical, making use of the same scatterers and clusters, contributing to a relatively narrow AoA spread.

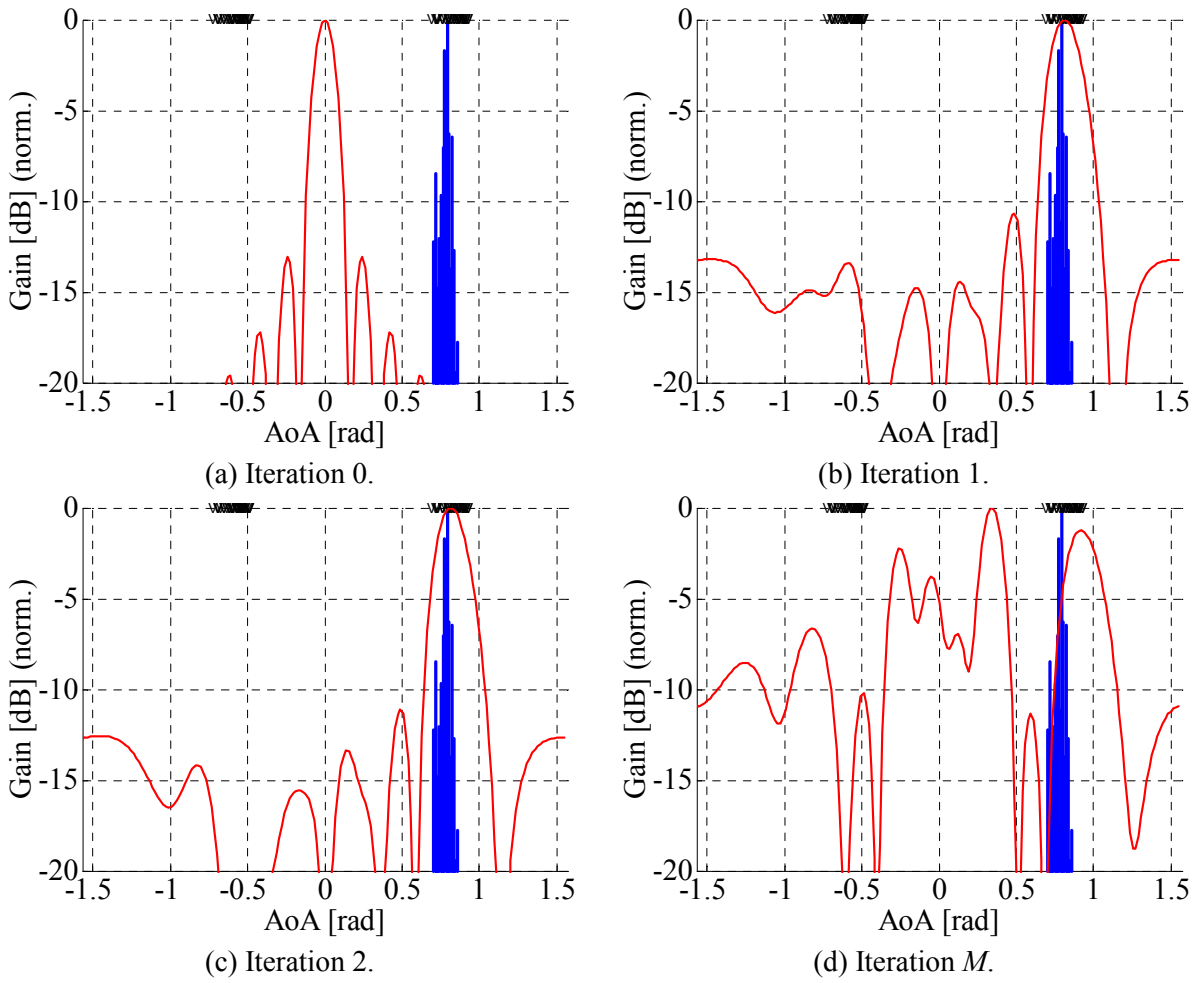


Figure 6.30 – Array patterns (red, thin line) for the MT_1 at $\pi/4$, Sc #16u_Mc_Se_A_50, for the initial and M^{th} iterations.

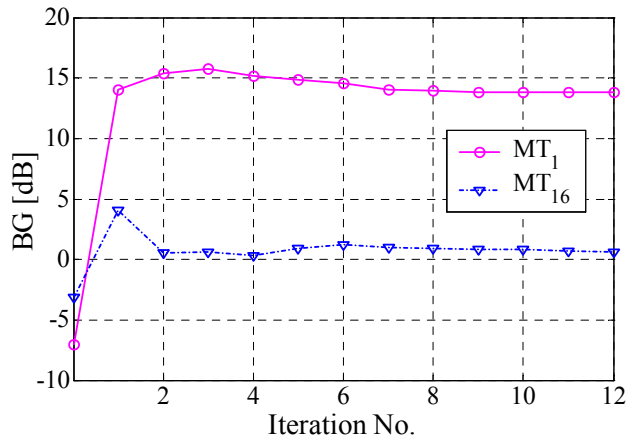


Figure 6.31 – BG, along optimisation, for MT_1 and MT_{16} in Sc #16u_Mc_Se_A_50, one channel concretisation.

6.4.4 Dealing with the MMSE vs. BG Optima Discrepancy Problem

6.4.4.1 Considerations

In an overall view of the presently described problem, judging from the several results, from which some examples have been taken to picture the general tendencies, one can say that the OD problem is much less critical for the MiC than for the MaC cases studied. The MiC BG and SINR evolutions along optimisation do not exhibit peaks as large as the ones found to exist in the MaC cases, these also leading to severely degraded, negative BG averages. On the whole, also independent of the duplex mode, grouping of MTs leads to the worse beamforming performance in MaC scenarios, where iteration-significant BG maxima are barely above 0 dB, unlike in the MiC grouped MT cases (this issue is attentively presented in Chapter 7, Beamforming in Micro- and Macro-cell Scenarios).

Viewing the matter in a simple way, one has concluded that there is a solution, other than the MMSE one, that leads to better orthogonality between the l^{th} beamformer output and the remaining NDesI, comprising all delayed and all other signals' contributions. The MMSE solution corresponds to the maximum orthogonality among all original, non-delayed, codes, but these codes are no longer separately present at the channel output, nor are they orthogonal towards the remaining NDesI. Such MMSE solution, by definition, establishes a theoretical limit that assumes that the original codes are the only NDesI contributions present. In realistic terms, each of the original, non-delayed, codes arriving at the beamformer cannot be separated from the remaining NDesI power contributions, delayed and non-delayed ones, especially having seen (as it is described in sub-Sections 7.2.7 and 7.3.7, Correlation Matrix Components Dependencies) that the delayed components from the remaining links are the strongest NDesI contributions to SINR and BG degradation. Consequently, due to the definite loss of correlation properties among a certain l DesS and all NDesI powers, the corresponding l^{th} beamformer output may be best correlated to such DesS original code, while not being as uncorrelated as possible, i.e., orthogonal, with all arriving NDesI powers. This can be easily understood by considering a simple 2-dimensional example, with two originally orthogonal vectors being subject to the propagation channel. Due to the loss of orthogonality among these, at the channel output, an estimate of each DesS code can be found, which maximises the orthogonality towards the other NDesI one, while not corresponding to the minimum error between the original and output DesS vector. If the estimate of the DesS would be equal to the corresponding original code, its correlation to the other arriving NDesI vector may be too high, i.e., corresponding to lower SINR.

The practical and realistic solution must be based on the available arriving signals, directly relating to the SINR and BG quantities, though also weighed against each of the original known codes. In this way, it is well understood why MMSE evaluation does not necessarily reflect the tendency for the beamformer to increment SINR and BG. Furthermore, such matter does not only involve the temporal dependency, but also the angular one. If it were for the temporal dependency

only, the angularly spread MTs, at the same distance and with the similar scattering area size, would lead to the same type of BG peaks and subsequent degradation along the convergence.

Among several referential bibliographical sources, [TsAP00] and [TsAt02] provide BG results, corresponding to small- to medium-sized cells, with the propagation channel inherently contributing with clusters, by way of site-specific Ray-Tracing methods. The performance of several SA algorithms is tested. In [TsAt02], the SINR gain is evaluated depending on propagation characteristics, such as clusters and LoS, the respective propagation channel involving a smaller set of clusters, varying the number of users from 1 to 2, in a TDMA GSM perspective. In [TsAP00], the algorithms performances are evaluated, depending on some interference and multipath conditions, the number of array elements ($M = 4, 8, \text{ or } 12$), weight magnitude and phase mismatches, as well as on the number and data-rates of interfering users, in an UTRA-FDD embedding. In this way, the related but different views with which such studies have been developed, even involving different propagation situations, serve as a relevant reference source. Besides the whole important scientific contribution of such papers, though being applied with different conditions and methods, more specifically, the BGs thereby obtained are of the same order as those described in this study. Moreover, negative SINRs have also been obtained, in the case of eigenvector-based optimum combining for two MTs (depending on the power window used to discern the number of relevant eigendirections), or temporal-reference beamforming optimum combining (thereby not described in detail), further providing confidence in the hereby obtained values.

It could be argued that the reasons for MMSE not coinciding with BG optima may root from the codes used not being orthogonal (as it is stated in Section 6.3), but it has been verified that such still happens if pure OVFS codes would only be used to identify the MTs. Additionally, it should be clear that the justifications of the OD do not root from the CG application itself, but on the way that the references are accounted for, this matter gaining importance due to being sufficiently general.

Furthermore, for several of the presented TDD scenarios, the size of the sample block, N_s , has also been varied, taking the values 64 and 128. With the heavy cost of conducting to even longer simulations, these tests have helped to verify to what extent the interference suppression, measured by an SINR or BG, is dependent on the number of samples. The tests have demonstrated that the number of samples does not lead to significant or consistent changes in BG. In fact, such is a plausible verification, keeping in mind that the channel does not change (assumed to be static in an interval much larger than the sample block duration), but also realising that any additional number of equations multiple of 16, the length of the used codes, does not introduce any new data to the problem, apart from the noise component which varies among samples. Likewise, the size of the involved block does not have any noteworthy impact on the evolution of the BG and SINR, along optimisation, namely regarding the OD.

In addition, it is important to evaluate how the code length, not just the number of samples, affects beamforming performance. This analysis has been extended from UTRA-TDD to the UTRA-

FDD case, presented in [Olej02] and [Szym02], involving non-orthogonal S(2) family pseudorandom scrambling codes, with length 256, to differentiate MTs in the UL, [HoTo00]. It is predicted and logical that, for the same channel characteristics, with temporal delays of the order of some chips, longer codes result in lower sensitivity to delays and to subsequent better correlation and decorrelation properties. For this, though the MT identifying FDD codes are non-orthogonal, these may still provide better correlation and decorrelation properties, meaning that better SINR and BG results may be obtained due to their longer length.

In [Szym02], it is already visible that the BG and SINR evolutions along optimisation are in fact different, comparing the same type of scenario and array, with the same number of array elements and MT users. In particular, the MMSE vs. BG OD is strongly reduced, the scenarios of grouped MTs presenting much lower BG degradations along the optimisation, and larger BG values also being obtained with the longer FDD codes. As an exemplifying case, Figure 6.32 presents such type of differences very clearly, referring to Sc #4u_Mc_Gr_15_200, with $M = 8$. On the other hand, if only 16 samples of the 256-long FDD code are used, the resulting BG evolution approximates very closely that of the former TDD case, using 16 samples of the 16-long code.

Regarding the differences among the TDD and FDD implementations for the scenarios where MTs are angularly spread along the 1st and 4th quadrants, FDD results again present no BG peaks, also leading to final BGs that are within 1 to 2 dB higher than the TDD ones.

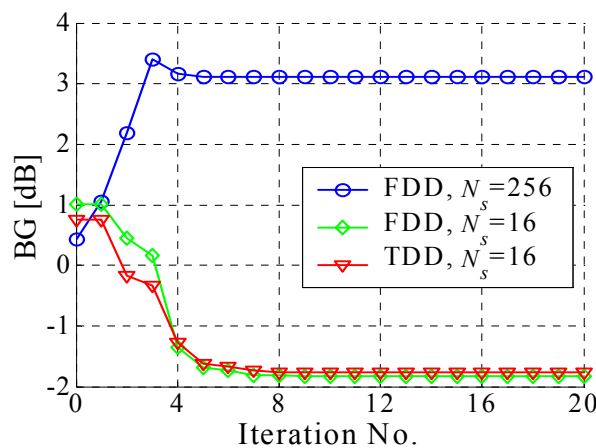


Figure 6.32 – BG, along optimisation, for Sc #4u_Mc_Gr_15_200, with $M = 8$, with the 16-long TDD or 256-long FDD codes, making use of the codes full length or of $N_s = 16$ samples only.

Very important conclusions are then put forward: the nature of the MT identifying codes, namely their length, strongly affects the beamforming performance; such implications are most severe in the case that MTs are grouped together, making use of the same scatterers to convey signals towards the BS; the impact on the MMSE vs. BG OD is also large, longer codes leading to lower, or even non-existing, BG degradations along optimisation.

It may be argued that the presented SINR gains in applying an optimised array, of many elements, are not as large as expected, compared with using a single element antenna, even for the cases where MTs are separate. Since, for some readers, this may seem as a surprising conclusion, it is important to evaluate the effects of scattering area superposition, delayed NDesI and noise contributions. One hereby directly evaluates how eliminating or including delays and/or noise influences the SINR and BG. In practice, such has been possible by nulling out these components before building up the signal matrix, \mathbf{U} .

The situations that are of importance are the following: No Delays, No Noise (ND_NN); No Delays, With Noise (ND_WN); With Delays, No Noise (WD_NN); With Delays, With Noise (WD_WN). This analysis has covered the case of an $M = 12$ element array, $L = 4$ active MTs, with distribution and distances as in Sc #4u_Mc_Gr_15_200 and #4u_Mc_Sp_15_200, whose respective results are provided in Figure 6.33, Figure 6.34 and Figure 6.35. In Figure 6.36, the results are provided with Delays, With Noise (WD_WN), for comparison.

In the case that all DCIR delayed contributions and noise are nulled out, where the initial orthogonality among arriving signals is maintained, meaning that the beamformer can discern all signals, among all links, BGs reach exceptionally high values, whatever is the distribution of MTs. By comparing Figure 6.33 (a) and (b), one sees that: the grouped MTs situation leads to BGs that are approximately 20 dB lower, in respect to the dispersed MTs, which is anyway only close to 7 % of the maximum; in the perspective of each link, the only NDesI component that is present is the non-delayed power from all the other remaining links, leading to very close BG and SINR values; the BG evolutions present a peak, near the 7th or 5th iterations, in a situation where no delays are present.

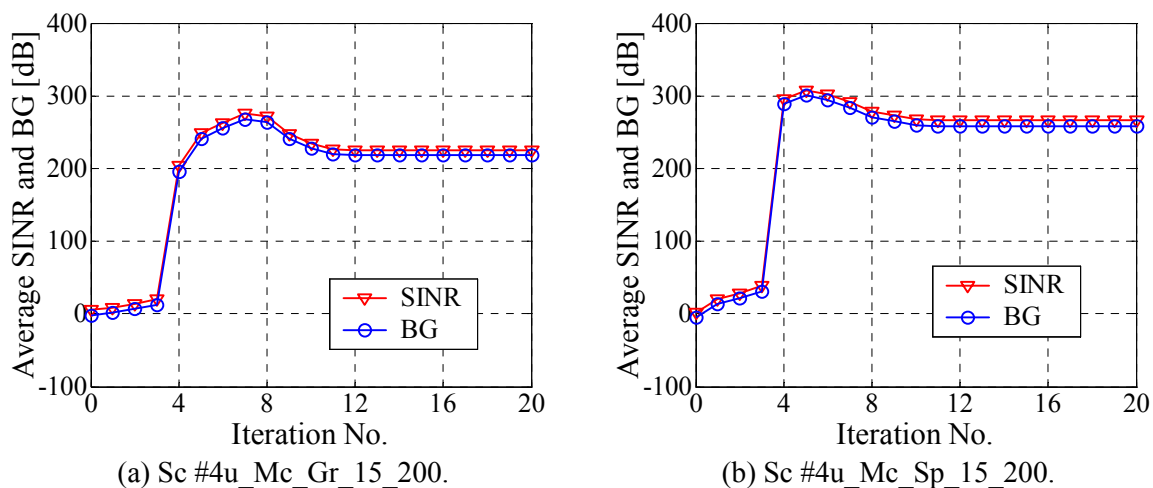
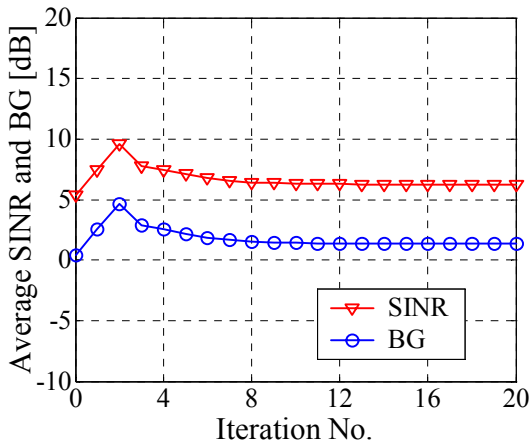
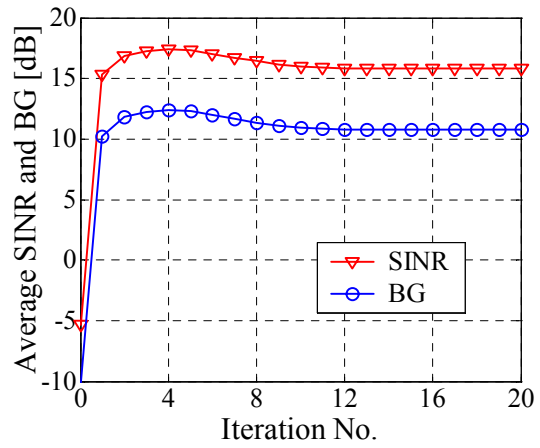


Figure 6.33 – BG and SINR, for Sc #4u_Mc_Gr_15_200 and Sc #4u_Mc_Sp_15_200, with $M = 12$, with ND_NN.



(a) Sc #4u_Mc_Gr_15_200.

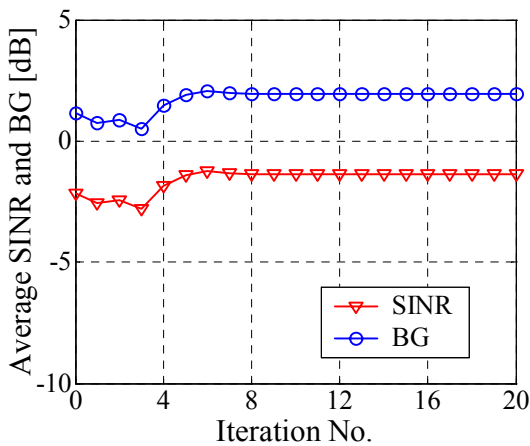


(b) Sc #4u_Mc_Sp_15_200.

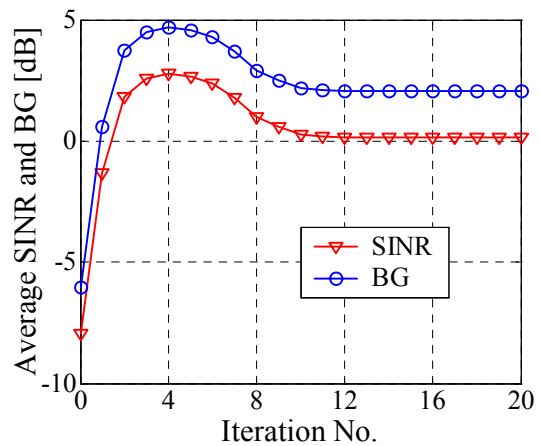
Figure 6.34 – BG and SINR, for Sc #4u_Mc_Gr_15_200 and Sc #4u_Mc_Sp_15_200, with $M = 12$, with ND_WN.

Just by adding noise, the resulting degradation in BG is clear, seen in Figure 6.34: the effect of the distribution becomes relatively larger, grouped and spread MTs leading to maximum BG values close to 5 or 12 dB, respectively; the evolutions along iterations also differ, the BG peak being followed by a degradation to values lower than 50 % of the respective peak value, in the case of grouped MTs; again, this peak exists, in this situation where no delayed components are being included.

By only adding DCIR delays, BGs again suffer large degradations, compared to the ND_NN situation, as Figure 6.35 illustrates: values are even lower than in the ND_WN case; evolutions again differ, depending on the MT positioning, with a relatively large overshoot in the spread MTs case; maximum values differ, between Figure 6.35 (a) and (b), BGs being very similar after the 12th iteration; BGs are above the SINR values, unlike in the previous two cases, meaning that the single element SINRs are negative; the BG peak is present in the distributed MTs case, only.



(a) Sc #4u_Mc_Gr_15_200.



(b) Sc #4u_Mc_Sp_15_200.

Figure 6.35 – BG and SINR, for Sc #4u_Mc_Gr_15_200 and Sc #4u_Mc_Sp_15_200, with $M = 12$, with WD_NN.

By adding the delayed and noise contributions, corresponding to Figure 6.36, BGs again change: in the case of grouped MTs, BGs reach the already mentioned negative values, always with a decreasing tendency, along optimisation; these values are the lowest among all the previous situations, but in the case of the spread MTs, average BGs are even larger than those of the WD_NN case. With these comparisons, one then confirms that both delayed NDesI and noise are equivalently influent in grouped MTs case, whereas, for the spread MTs situation, the noise impact is less important than that of the delayed NDesI power.

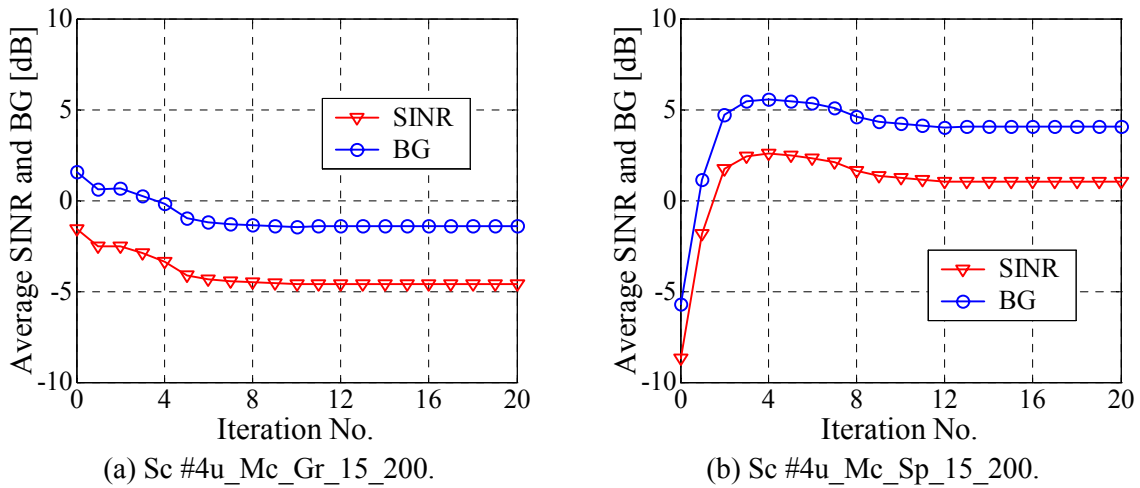


Figure 6.36 – BG and SINR, for Sc #4u_Mc_Gr_15_200 and Sc #4u_Mc_Sp_15_200, with $M = 12$, with WD_WN.

The decomposition of \mathbf{R} is useful in further understanding the formation of the OD BG peak. Namely, in the NN_ND test situation, one then verifies to what extent the only NDesI term, $P_{=0}^{other}$, evolves in relation to P_{DesS} . In Figure 6.37 (a) and (b) the corresponding results are presented for Sc #4u_Mc_Gr_15_200 and Sc #4u_Mc_Sp_15_200, clearly seeing that those are the only two power components present, and that the global term, $\mathbf{w}^H \mathbf{R} \mathbf{w}$, does reach the ideal value of 16 (the code length and number of samples, N_s). By comparing both graphs, the visibly significant evolution of terms happens until the 4th iteration, the rank of matrix \mathbf{R} , which in this ideal case is equal to the total number of present codes/links, $L = 4$, even for $M = 12$ array elements. The components' evolutions (including those after the 4th iteration, with smaller but still significant variations, not visible in these plots) differ according to the scenario, showing the importance of the distribution of AoA, apart from the delay-spread and noise influences.

Concluding, by jointly analysing these test cases, one verifies that the type of MT distribution, i.e., the whole AoA spreading, plays a fundamental part in not only determining the performance, but also in establishing how strong the effects of noise and delay are, affecting the evolution of SINR and BG. The BG peaks do not only root from ToA dispersion, seeing that the ND_NN and ND_WN situations do present such type of peaks, solely resulting from the non-delayed NDesI contributions

from the remaining MTs. Also, it must be kept in mind that, even without any delayed NDesI, the length of the involved codes directly affects the orthogonality properties between all the DesS from the several links, as well as the relationship of DesS powers to noise.

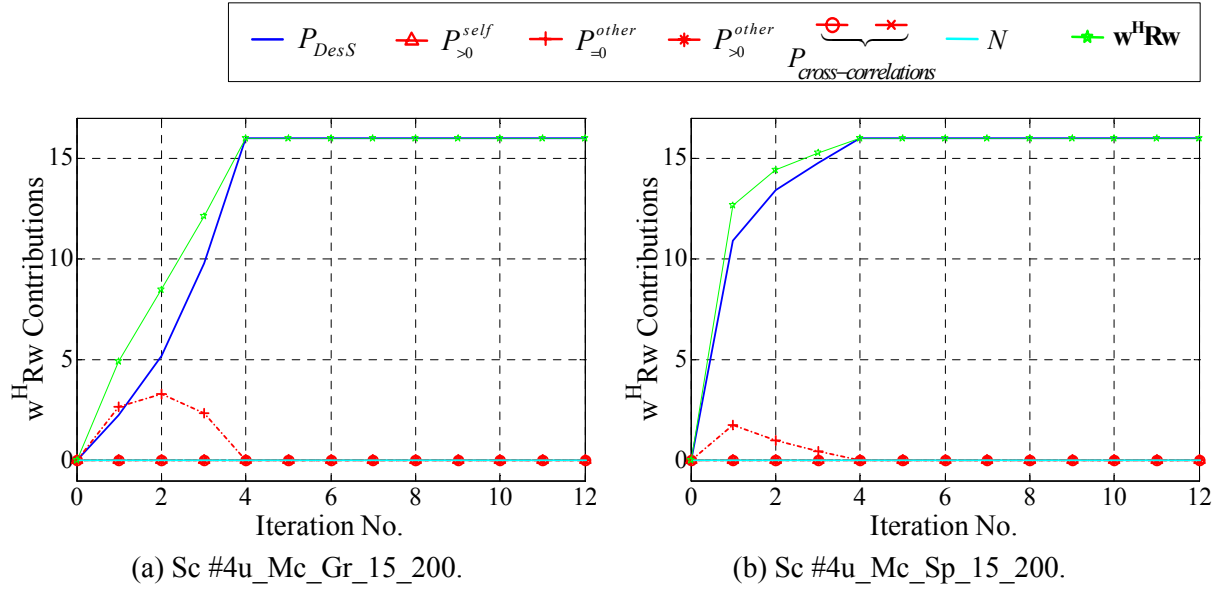


Figure 6.37 – Power terms due to the composition of \mathbf{R} , for $M=12$, Sc #4u_Mc_Gr_15_200 and Sc #4u_Mc_Sp_15_200, with ND-NN.

It is also important to be aware of how the independently generated weight vectors are related along optimisation, as regards mutual orthogonality. For that, the *weight vector correlation coefficient*, [LiRa99]:

$$\rho_w^{(l,j)} \triangleq \frac{\mathbf{w}_l^H \mathbf{w}_j}{\|\mathbf{w}_l\| \|\mathbf{w}_j\|}, \quad (6.6)$$

for each pair of different active l and j links, provides indication of the relative orthogonality among the obtained weight vectors. Thus, along optimisation in the sense of MMSE, it would be likely that the $\rho_w^{(l,j)}$ coefficients would monotonically lower, for $l \neq j$, indicating the progressive generation of orthogonal solutions, even with the optimisation being independent among all L beamformers. In fact, not only does the progression of $\rho_w^{(l,j)}$ coefficients not monotonically decrease along iterations, but it also indicates some correlation with the progression of BG or SINR, again depending on the scenario case. Therefore, the OD reveals itself by another means, indicating that though the MSE may be lower, the orthogonality among weight vectors may be higher. Figure 6.38 exemplifies so, for Sc #4u_Mc_Gr_15_200 and Sc #4u_Mc_Sp_15_200, with $M=12$, plotting the corresponding absolute value of the average correlation coefficient and the corresponding standard deviation. Though the standard deviations are relatively small, one sees the disagreement with the BG and SINR evolutions shown in Figure 6.36, for Sc #4u_Mc_Gr_15_200. Also, though for this scenario the final (at the M^{th}

iteration) BGs and SINRs are lower than those of Sc #4u_Mc_Sp_15_200, the corresponding correlation coefficient is lower in the former case. On the other hand, for Sc #4u_Mc_Sp_15_200, the agreement is very good, the average coefficient nearing 0 at the 4th iteration, where the average BG and SINR are maximum, where also these are most frequent.

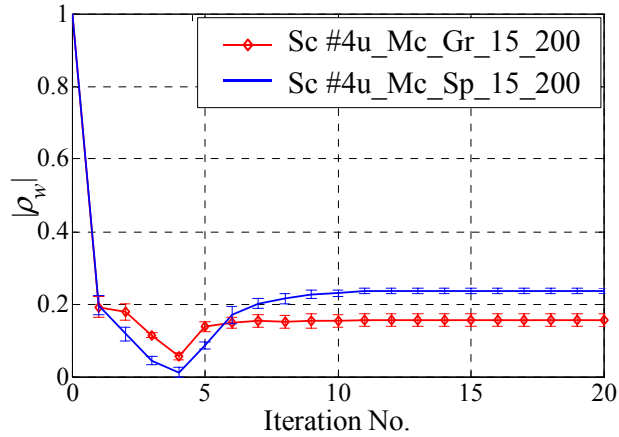


Figure 6.38 – Magnitude of the correlation coefficient, for Sc #4u_Mc_Gr_15_200 and Sc #4u_Mc_Sp_15_200, with $M = 12$.

These results, again, not only show how the directional properties of the multi-target propagation situation significantly affect the relationships among the involved parameters, in this case affecting the orthogonality among the beamforming weight vectors; additionally, it is shown that, contrarily to much simpler propagation cases where such orthogonality leads to best SINRs, [LiRa99], in this more complex case, an OD again arises, concerning the weight vector correlation coefficient, MMSE and SINR (or BG) optima; finally, it is seen that, for the less critical scenario cases, in terms of directional spreading of MTs, where AoAs from different MTs are less superimposed, there is a large coincidence between SINR (or BG) and correlation coefficient optima.

6.4.4.2 Solutions to the Optima Discrepancy Problem

Besides analysing, verifying and justifying the MMSE vs. BG OD matter, it calls for solutions, which can be viewed in two ways. Firstly, in the perspective of the analysis study hereby presented, with the aim of characterising the beamforming behaviour towards differing propagation scenarios properties, it is required that results are consistent with the most fundamental logic ruling the beamforming operation. In that sense, the iteration identified as the *significant iteration* has been found to lead to such results, by several means, presenting better *behaved*, coherent and physically well justified BG values, as function of the various parameters. But besides the view of the analysis study by itself, as it has been frequently brought up in the text, direct or indirectly, it is not the objective of the overall study to be confined to abstract issues, away from the system-wise reality that is established by the present, and future, mobile communication systems. Accordingly, the optima

definition problem inevitably puts forward the practical issue of allowing the beamformer to find the weights for best SINR or BG. Also, it must be kept in mind that the results exhibit relatively large standard deviations, meaning that very often (in a relative way) the beamforming may not be advantageous at all, compared to the single antenna case, even for large number of array elements, in some scenario cases, i.e., not being particularly robust.

In order to cover the practical problem of beamforming implementation, it is important to call upon a verification provided by the presented simulation work – by maintaining the spatial distribution of scatterers and clusters, solely varying the scattering coefficients' phases, the resulting BGs considerably vary, also exhibiting large standard deviations, even with the application of PC. In this way, assuming such variations to be resulting from the local movement of the MT, or from the general movement of the radio environment, in the order of the wavelength, λ , the repeated convergence will lead to other possibly different SINRs, and BGs, after the stationarity period (this is why the PI BG and SINR averages calculations, presented in Section 5.6, are still of importance). Thus, the PI BG and SINR average results will in fact generally reflect the repeated operation of the beamformer, for an MT in a particular fixed location. Keeping in mind that the stationary period hereby assumed is the frame duration (10 ms, for UMTS), also assuming a static channel during a slot (666 μ s, in UMTS), and if the algorithm is applied once for each slot and link, even in the case of successive slots corresponding to the same MT-BS UL pair, then, very quickly (relative to the data rates at stake) the averaging effect will take place. Nevertheless, such averaging effect, even leading to positive averages, does not guarantee that BGs are always positive, which is a major robustness problem. The PI averages, therefore, already indicate that fast-fading achieves particular relevance in the definition of the beamforming performance. For these points, the important relation between fast-fading effects, and the wideband and directional properties of the propagation channel naturally arises, e.g., [CaCo03], as well as the definition of stationarity and ergodicity, e.g., [Pätz03], in fast-fading channels.

With the aim of guaranteeing the best BGs possible, there are several practical solutions that can be suggested:

- a) A control process to limit the optimisation up to the point where SINR ceases to increase, or where the best weight vector from among the several obtained is chosen, for each beamformer. Such a solution does not imply a change in the algorithm nor criterion, tending to reduce the number of iterations, lowering complexity, and guaranteeing to lead to the best SINR obtained with this solution, for each beamformer.
- b) Dealing with the orthogonality properties of the weight vectors, a complementary criterion is suggested. Likewise, the CG application, independent among all the L beamformers, could be complemented by the control of the correlation coefficient, among links. A similar method is suggested for the Least Squares Constant Modulus

Algorithm (LS-CMA) application, complementing it with the application of GSO among all weight vectors, in order to guarantee orthogonality, [LiRa99].

- c) Application of the longer code references, possibly using the midamble for TDD. Such is a direct consequence of the presented analysis, where the use of longer codes, in particular FDD codes, has been shown to lead to better BGs and less critical MMSE vs. BG ODs.
- d) Extending the present CG application to including delayed versions of the reference codes as references, i.e., allowing the beamformer to converge towards the MSEs relative to the non-delayed and delayed codes; Like so, for each link, the beamforming will make use of the same signal matrix, \mathbf{U} , but ideally requiring as many CG cost functions as the number of delays considered.
- e) Complementary use of a DF, DoA estimation-based algorithm to aid in the best SINR or BG optimisation, together with the proposed CG application, in order to make use of the available system referential information; Additionally, the use of pilot signalling, allowing for wideband channel estimation should also contribute to minimisation of the OD, and the reach of the optima.
- f) Adding a spatial diversity-combining scheme to the present beamforming application. In that manner, the verified performance sensitivity to fast-fading would be reduced, possibly also contributing to the reduction of the OD.
- g) Joint application of the beamforming at the BS with a beamforming array at the MT. Especially in the case of handheld terminals, and seeing that adaptive beamforming is very sensitive to the propagation channel, such solution is a complex one due to the size of terminal and to the closeness of the user head or hands. Anyhow, such solution would tend to reduce the importance of fast-fading, i.e., rendering larger robustness against it.
- h) Joint application of the beamforming at the BS with manual directing of the antenna elements at the MT, prior to adaptive beamforming and to communication, so as to optimise initial SINR, especially in the case of laptop, quasi-static terminals. Such is a form of archaic physical configuration of the array, a form of array reconfigurability, being complemented by electronic adaptive beamforming. Naturally, such solution at the MT level would lead to other issues, such as lack of correlation among elements and MIMO channel modelling, besides the operational awkwardness.

Solutions a) to f) are applied at the BS, while the g) and h) are forms of beamforming at the MT side. Some are not only seen with the objective of minimising the OD problem, but also with that of improving overall beamforming performance. As for the issue of extrapolating the current application to 4G systems, the mentioned solutions maintain their validity, with differing degrees and

perspectives, as long as referential sources such as the spreading codes are made of use by the beamformer. This matter is addressed in Chapter 9, Towards Future Mobile Broadband Systems.

The a) solution is important and, yet, simple to implement at the level of the algorithm. Truly, it is the practical means to finding the *significant iteration*, possibly being that after which SINR registers a reduction, for each concretisation. Through this, for each link, the weight vector would only take the following iteration value only if the corresponding link SINR would be higher. This would mean that, for each iteration vector, the corresponding link's SINR would require to be measured. By linking such method to the closed-loop PC, together proceeding with PC and the non-decreasing BG controlled beamforming, the beamforming can in fact rely on the measurement of SIR already involved in closed-loop PC. In fact, for FDD, closed-loop PC operates with 1.5 kHz command rate, the BS measuring the SIR in the UL every 0.67 ms, i.e., 15 times within the 10 ms frame, and for TDD, in the UL, it is 100 or 200 Hz, 1 to 2 times within the frame, [HoTo00]. On the one hand, this means that for each closed-loop PC cycle, a completely new beamforming solution would need to be established. On the other, with the expense of possibly retarding the optimisation, but guaranteeing the best SIR or SINR for most of the slot duration, each CG iteration could be made to coincide with each PC SIR measurement, like that making use of the already available system functionalities. Anyhow, such additional delay in the definition of each weight vector is counterbalanced by less than M iterations being required to effectively find the best SINR solution. Truly, that would also be a form of combining PC with beamforming, aiding in improving efficiency and robustness against fast-fading. Additionally, since there is no need for weight vectors to be repeatedly calculated starting from the $\mathbf{w} = \mathbf{0}$ seed, making use of the previously obtained optimum weight vector, the number of iterations required to reach the SIR or SINR maximum can be further reduced. In view of the described BG and SINR evolution results, in the worse scenario case, e.g., MaC with grouped MTs, this would mean that the optimum vector would be initially found at the 1st or 2nd iterations, even possibly settling close to such vector for the subsequent slots (depending on the effective channel correlation time). For the less critical scenario case, e.g., a separate MT in the MaC situation, high values of BG would most likely be achieved during the initial slot, to then further improve BG and SINR in the following slots (again, depending on the effective correlation time).

Besides not introducing additional complexity to the system, as its readily available resources are being used, with such method the significant BGs inherently tend to be most frequently positive, leading to better average results. Furthermore, linking beamforming with PC would additionally provide optimisation in the sense of minimising transmitted power, important for DL TDD in-band interference reduction from the neighbour MTs and for terminal power consumption reduction. Finally, this procedure would further warrant that the noise power would not reach too high a value, being aware of the particularly negative role it plays in the case of grouped MTs, MaC scenarios (Sub-Sections 7.2.7 and 7.3.7, Correlation Matrix Components Dependencies).

Prospective work has been developed, applying such method to the several scenarios: SINRs and BGs do significantly improve in the MaC, grouped MTs scenarios cases; for the case of an angularly separate MT, the corresponding SINRs or BGs are significantly degraded, since there are SINR reductions prior to the large SINR increase during optimisation (as it is described in Section 7.3, Performance Dependence on MaC Scenarios Parameters), some reductions being relatively significant; for the remaining scenarios, no significant changes in the means are registered; for all cases, the SINR or BG standard deviations are severely reduced.

In light of these results, though superficial, it is concluded that such method has a positive impact but would require improvements, so as to effectively lead to SINR and BG maxima for all scenarios, e.g., the algorithm may evaluate the SINRs from a set of sequential obtained weights, and then select that which leads to the best SINR among all. Also, having seen that the prospective application of process a) leads to the same fundamental beamforming dependencies on the scenario characteristics as those deeply described in this study, further confidence applies to this and the applied method.

Solution b) is more of an upgrade of the CG application, suggesting a wholly implemented multi-target beamformer, where all L beamformers are optimised jointly, calculating the weights with the described CG, but in parallel controlling the orthogonality among all weights. Having shown that best orthogonality not necessarily leads to the best SINR, in the case of the L beamformers converging independently, the weights can be calculated through jointly applying the CG and the GSO among the weights. As mentioned, such has been suggested for the multi-target LS-CMA algorithm application, implying larger number of iterations for full optimisation, in [LiRa99], but possibly involving lower OD and leading to higher SINRs.

Solution c) is also of simple implementation, keeping the 256-long terminal identifying codes for FDD, but using the terminal specific midamble for TDD, with a minimum length of 256 chips, [ETSI02a]. In this way, in the light of the study described in sub-Section 6.3.2, by using longer codes for either TDD or FDD, better BG averages would be obtained, thus providing the beamforming with lower dependence on the grouping of MTs. Anyhow, such solution c) would entail the application of a), due to the anyway present large SINR standard deviations. Also, such implementation has the inconvenience of involving much larger number of multiplications, worsening the effect of the number of MTs on complexity (as it is explained in sub-Section 6.5.3, Complexity Issues).

Concerning other algorithm implementations maintaining the MMSE criteria, such as the case of the RLS algorithm application to similar directional scenarios, it has also been verified that MSE reduction does not necessarily imply SINR improvement (as it is described in Section 6.5, CG vs. RLS Implementations). Furthermore, the application of the RLS does imply relatively much larger SINR (or BG) fluctuations along optimisation, compared to the ones resulting from the CG application, [GiMC01], [Mend01]. As a result, it can be argued that some sort of solution to the OD problem is likely to be anyway needed for other MMSE-based algorithms, besides the CG one,

therefore not necessarily justifying their alternative use. From the exposed, though, where the justification for the OD has been presented as rooting from the (non)orthogonality properties among realistically available and non-available signals, an hypothesis can be generated – at reception, as orthogonality among received signals must not be based on the no longer present known original codes, the best reference signals that lead to the best SINR should not be limited to such original codes, but other also reflecting the delays imposed by the channel, establishing the solution d). In other words, extending the present beamforming implementation further towards the *wideband* sense, as it is described in Section 6.2.

As opposed to the optimum combining applied, subject to the MMSE criterion while making use of reference signals, the possibility of making use of other optimisation criteria, such as the MSNR, arises. Truly, such methods would not eliminate the OD problem, because it does exist independent of the method and because it is a direct result of the propagation channel conditions. But, for example, it could be the case that the algorithm would be applied to directly maximise BG and SINR, possibly leading to better values compared to those hereby obtained. Nevertheless, such is not guaranteed since, as mentioned in Chapter 5, blind solutions effectively lead to larger convergence errors, especially in the multi-target and overloaded cases, where arriving signals are correlated to a great extent. In this way, it is reasoned that the OD problem does not justify resorting to exclusive use of blind solutions, not making use of readily available references. For that, e) proposal comes about naturally. In fact, there are several examples of complementary application of several methods, e.g., [LiLi03], [KuTB02], and [CCIC02].

Solution f) brings upon the issue of spatial diversity, implying the use of two arrays, spaced by several λ s in order to compensate for the harmful effects that fast-fading has on each link's beamforming operation. In that way, independent diversity and beamforming combining would be performed among all links, making use of the different contributions from scatterers and clusters, maximising the throughput for each link. It is important to point out that beamforming and spatial diversity may be seen as conflicting processes, if array antenna gain is an objective, [Weis82]. For this, it is stressed that *beamforming* is hereby firstly seen as a means to spatially filter interference, and not necessarily improve array antenna gain. This beamforming perspective and spatial diversity are, therefore, not disagreeing.

In the perspective of a more terminal dependent adaptive beamforming application, the g) and h) possibilities are more of add-ons to the BS beamforming adaptive process, not really being solutions to the OD but methods to improve overall BG performance. Also, these are larger problems by themselves, only being hereby referred for completeness. Either by adaptively g) or physically h) changing the array elements' positions, in order to achieve the best SINR, the beamforming procedure at the BS may then lead to best SINR and BG, therefore gaining more independence on the scenario characteristics. Namely, in the prejudicial case of the grouping of MTs, array element positioning (either electrical or physical) may decide, with natural physical differentiation, on the actual scatterers

and clusters that a link is making use to convey signals towards the BS (and vice-versa). Truly, this is beamforming in the terminal, with the objective of mitigating interference among MTs and towards other cells, but also to differentiate from among the whole set of illuminated clusters and scatterers, allowing for BS beamforming to disjointly select these from among each link as possible.

After all this elucidation and problem analysis, two practical, very simple questions may still be put forward: how can an array, with its array factor with lobes and nulls at any direction, at any beamforming iteration, lead to worse SINRs than those obtained with a single antenna, omnidirectional in the same plane, while MSEs are lower? How can such happen even if the delay and noise contributions are nulled out? Trying to answer to such questions in a definite manner, it is argued that the real solution, the answer that definitively resolves this issue, only passes from understanding that it relies in the inclusion of the angular domain in the optimisation process, either in more or less direct ways. In Chapter 7, Beamforming in Micro- and Macro-cell Scenarios, by characterising how the beamforming performance depends on the propagation scenario, the several results help in understanding the importance that both the temporal and angular domains have on the establishment of the SINRs and BGs. In this way, while it is advisable to guarantee convergence to be based on temporal references, the use of angular references such as array manifold or signature matrices can be envisaged, not in an exclusive (as in blind DF beamforming) but in a complementary way, jointly accounting for both domains.

6.5 CG vs. RLS Implementations

6.5.1 RLS Implementation

Predicting that processor speed will not be a problem in the near future, above all, it will be necessary to achieve the largest SINR gain, for critical traffic areas and high data rate services provision. Many algorithms differ largely in complexity and convergence speed, contrasting in the correlation matrix eigenvalue spread dependence, inherent gradient noise, limited dynamic range and number of samples used, as mentioned in sub-Section 3.4.4. For that, and within the scope of this study, applying other algorithms towards the same problem may contribute to further understand how such channel affects their operation.

Since the objectives of this work naturally imply a correctly functioning application, the CG should be compared and verified against at least another non-blind algorithm.

Some beamforming RLS implementations are present in the literature, e.g., [WaCr94], [Hayk96], [Goda97], being very much used for general adaptive filtering. It has been shown that it can converge sufficiently fast, depending on the correlation matrix and stationary conditions at stake. The algorithm's speed dependence on the correlation matrix eigenspread, transient response and final error can be pointed out to be the major factors, which should be evaluated together with the application of a WDCM, within a *hostile* interference scenario.

In this way, the additional application of the RLS to the same type of WDCM and scenarios is hereby presented, weighing the relative algorithm performance, its dependence on the propagation channel, as well as relative complexity.

Concerning the RLS algorithm itself, its fundamentals have already been presented in sub-Section 3.4.4. The application to the present problem, as in the CG case, involves L independent beamformers, minimising each l^{th} cost function and the corresponding l^{th} estimation error. Concerning reference signals, in (3.49), these have been set to be the sequential $c_d^{(l)}(n)$ code chips. The RLS implementation is therefore a sample-by-sample implementation, accepting an input symbol sample and outputting a weight vector at each discrete instant n , as opposed to the implemented CG application.

For this study, λ_{RLS} has been set to 1, as in [WaCr94], $\hat{\mathbf{w}}(0) = \mathbf{0}$ and δ_{RLS} has been set equal to 0.0001. Variations of the latter have been compared without finding large dependency in terms of convergence, [Mend01], being very important in the transient phase of the RLS algorithm, finding approximately the same steady-state after the algorithm convergence, [Mous97].

Through (3.48)-(3.51), the RLS is then used to update the weights after each input vector $\mathbf{x}(n) = \mathbf{u}(n)$ at instant n . It minimises (3.38), where in each iteration (3.49) is being taken into account to achieve the steady-state that takes place when the algorithm converges and (3.38) is minimum. According to (3.49),

$$\xi_l(n) = d_l(n) - \hat{\mathbf{w}}_l^H(n-1)\mathbf{u}(n) = c_d^{(l)}(n) - \hat{c}_d^{(l)}(n), \quad (6.7)$$

where $\hat{c}_d^{(l)}(n)$ is the beamformer output estimate corresponding to $\mathbf{u}(n)$, from link l . Therefore, for a user l , RLS implicitly solves the following problem:

$$\mathbf{w}_l = (\mathbf{U}^H \mathbf{U})^{-1} \mathbf{U}^H \mathbf{c}_d^{(l)}. \quad (6.8)$$

RLS then estimates \mathbf{R}_x^{-1} ($M \times M$) by a sample-by-sample recursive process, through the calculations of the matrix \mathbf{P} , as defined in (3.46). Compared to the described CG application, the RLS does not require knowing the whole matrix \mathbf{U} , at each instant, because the weight vector updating is made sample-by-sample, meaning that to achieve its steady-state the algorithm needs the same number of samples as the number of iterations. Alternatively, through (3.38) the RLS does account for the previously input estimation errors.

The physical interpretation for the RLS algorithm application can be understood together with the interpretation of the LS one in its geometrically meaning. There are many interpretations for LS, but one very useful and easy to understand is the projection operation to find the direction of the desired signal, in this case, the code. Using (6.8) the whole estimated code vector will be:

$$\hat{\mathbf{c}}_d^{(l)} = \mathbf{U} \hat{\mathbf{w}}_l = \mathbf{U} (\mathbf{U}^H \mathbf{U})^{-1} \mathbf{U}^H \mathbf{c}_d^{(l)}. \quad (6.9)$$

According to [Hayk96], the multiple matrix products $\mathbf{U}(\mathbf{U}^H\mathbf{U})^{-1}\mathbf{U}^H$ can be seen as a *projection operator* onto the linear space spanned by the columns of the data matrix \mathbf{U} . The matrix difference $\mathbf{I} - \mathbf{U}(\mathbf{U}^H\mathbf{U})^{-1}\mathbf{U}^H$ is the *orthogonal complement projector*, and it is equal to the minimum residual error $\mathbf{res} = \hat{\mathbf{c}}_d^{(l)} - \mathbf{c}_d^{(l)}$. Note that both the projection operator and its complement are uniquely determined by the signal matrix \mathbf{U} . Vectors \mathbf{res} and $\hat{\mathbf{c}}_d^{(l)}$ will be orthogonal, \mathbf{res} being ideally $\mathbf{0}$.

The norm of vector \mathbf{res} is then minimised, minimising the subspace contribution in the “*direction*” of each of the considered desired signal, minimising the difference between them. This aspect must be well understood, because of the importance of the loss of the orthogonality between signals or the presence of correlated signals. These can worsen the properties of convergence, lead to an inadequate final solution, or make the OD more critical. Also, when the number of codes is higher than the number weights/antennas, the loss of orthogonality will be more severe, since the dimension of the arriving codes subspace is higher than that of the subspace of weights. This results in the loss of orthogonality between the solution/weights and interfering codes, driving to a final higher error.

The existence or not of more solutions or local minima is explained by the own LS problem at stake. The LS estimate $\hat{\mathbf{w}}_l$ is unique if, and only if, the *nullity*²⁸ of the data matrix \mathbf{U} equals zero, [Hayk96]. For the problem at stake, at least the presence of AWGN in the data matrix assures that the matrix \mathbf{U} will have full rank, therefore, resulting in a unique solution for each beamformer. Additionally, the richness of the channel inherently results in decorrelation among all array elements, further contributing to such solution uniqueness.

6.5.2 Performance Comparison

For that comparative analysis, the number of array elements as been set to 12, and the average calculations of the TI type were obtained from 100 DCIR concretisations. The simulations have been limited to the TDD case, where N_s has been set to 16. The corresponding SINR and BG results are presented in Table 6.1, for MiCs and MaCs, #Gr scenarios, varying L and d_{MT} .

In Table 6.1 one firstly sees that the RLS achieves considerably lower SINRs and BGs, compared to the CG. Additionally, as in the CG application, it is clear how the BGs obtained with the RLS are also significantly degraded in MaCs, compared to the MiCs results. The MiC results generally reflect the same tendencies as the CG, whereas the MaC negative BG results do not follow those of the CG, as a function of L and of d_{MT} . In this way, the sample-by-sample nature of the RLS application reveals to be particularly sensitive to the channel/scenario demanding conditions, compared to the larger robustness of the CG one. Additionally, it is seen how the different simulation conditions have significant impact on the SINR and BG results, comparing to those reported in

²⁸ The *null space* of a matrix \mathbf{A} is the space of all vectors \mathbf{x} such that $\mathbf{Ax} = \mathbf{0}$. The *nullity* of \mathbf{A} is the dimension of that null space, [Hayk96].

[GiMC01]. Such is especially due to the higher angular resolution, the involvement of different cluster and scatterers densities that the later model version has implied.

Cell Type	Physical Parameters		BG [dB]	
	d_{MT} [m]	L	CG	RLS
MiC	50	4	7.91	4.60
		8	7.28	3.25
		16	4.00	2.64
	500	4	9.25	8.14
		8	10.37	6.19
		16	7.34	3.89
	1 000	4	9.42	8.39
		8	10.74	5.80
		16	6.51	3.37
MaC	1 000	4	0.97	-1.08
		8	0.80	-1.23
		16	-0.03	-0.89
	1 500	4	1.11	-0.26
		8	0.76	-0.44
		16	0.10	-0.60
	2 000	4	0.89	-0.14
		8	0.65	0.15
		16	0.26	-0.13

Table 6.1 – Average BG results, for MiC and MaC #Gr scenarios ($M = 12$).

The evolution of average SINR and BG values along the optimisation also differs between both algorithms, for the same type of scenario. Figure 6.39 exemplifies so, for Sc #16u_mc_Gr_05, and other examples are provided in Annex C – CG vs. RLS Performance Plots.

Therefore, it has been verified that both algorithms' optimisation evolves in the sense of improving SINR or BG, nevertheless not in a monotonic manner, meaning that the OD problem is present in both applications. Additionally, for the several cases, the evolution of RLS generally involves greater SINR and BG variances and greater oscillations along optimisation. This can also be seen in the various plots of Annex C – CG vs. RLS Performance Plots, for other scenarios, MiC and MaC ones. Such differing behaviour, also resulting in that CG SINRs and BGs may be significantly better than the RLS ones, while the CG requires a lower number of iterations to converge, are hereby

justified by the block-sample nature of the CG application, whereas the RLS does not have as much input data available at a certain instant.

From these verifications, one directly and practically concludes that the sample-by-sample nature of the RLS implementation negatively affects reaching the utmost objective of this study, analysing beamforming performance as a function of the physical channel constraints. Anyhow, the RLS implementation and comparative analyses help in the overall verification of convergence, but most important, helps in verifying that the general dependencies of both the CG or RLS on the channel follow similar trends.

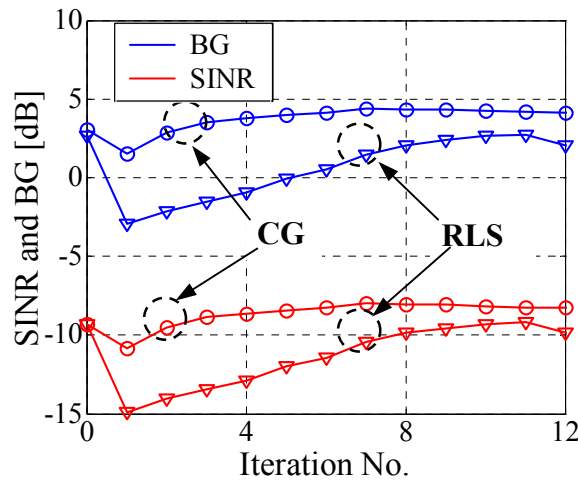


Figure 6.39 – SINR and BG, function of iterations, for the RLS and CG, for Sc #16u_mc_Gr_05, $M = 12$.

6.5.3 Complexity Issues

Besides performance, the complexity involved in the RLS and CG implementations has been evaluated. For that, the number of floating point operations (flops) has been calculated, using MATLAB[®], accounting for the number of calculations involved in each iteration, for both the CG and RLS algorithm application. For the CG (described in sub-Sections 5.3.2 and 5.3.3), the additional flops required to calculate the correlation matrix, \mathbf{R} , and the desired signal vector for each link, \mathbf{d}_l , for all L active links, are also presented. All the results are plot as function of M and L . In Figure 6.40, the evolution of the number of flops for the sample-by-sample RLS is shown, where it can be seen that the increase of L implies a proportional increase in the number of operations. This increase is small, since only a small change in the source code is necessary, in order to include an additional user.

An estimate to the number of flops per iteration, function of M and L , is given by:

$$N_{flops/iter}^{RLS}(M, L) \approx 24M^2 + [30 + 16(L - 1)]M + 1 = 16ML + (24M^2 + 14M + 1). \quad (6.10)$$

One verifies, then, that the increase in the number of flops, due to the number of users, varies by a factor of $16M$, only. The major contribution, only dependent on the number of antennas, follows a second order polynomial on M .

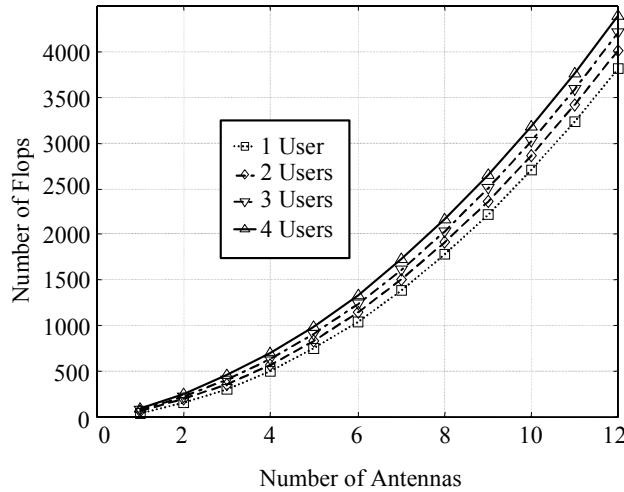


Figure 6.40 – Number of RLS flops per iteration vs. M , for several values of L , for which beamforming is performed.

In Figure 6.41, the same type of results is plot for the CG block-sample implementation.

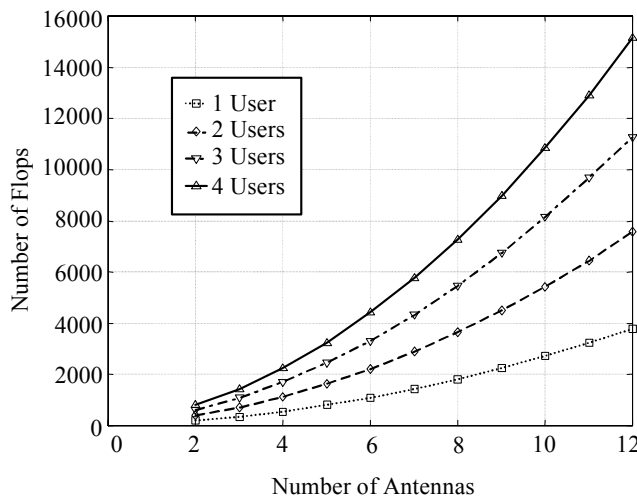


Figure 6.41 – Number of CG flops per iteration vs. M , for several values of L , for which beamforming is performed.

As it is seen, the number of involved flops per CG iteration is much greater than the corresponding number for the RLS implementation. The main reason for such is the larger contribution of array elements, revealing increases that are again proportional to the number of active links, but more dependent on M . For one user, the number of flops required for the CG is relatively close to those needed for the RLS, but increasing L has a much larger impact on the number of flops,

especially if M is larger. The justification lies on the completely independent CG calculation of each weight solution, where the search directions and residuals have to be calculated for each cost function. An estimate to the number of flops per iteration, now for the CG, follows:

$$N_{flops/iter}^{CG}(M, L) \approx (22L)M^2 + (51L + 2)M + (13L - 8) = (22M^2 + 51M + 13)L + (2M - 8) \quad (6.11)$$

The number of flops can be approximated by a second order polynomial on M and, in contrast with the RLS case, the contribution of the number of users is affected by a second order polynomial on M , reflecting the larger increases, still proportional to L .

In Figure 6.42, the additional flops required to calculate \mathbf{R} and \mathbf{d}_l for the CG block-sample implementation are plot, also as function of the number of antennas and of users, for $N_s = 64$.

As it is seen for this case, the number of additional flops is of the $O[10^4]$, increasing with the number of antennas. The number of users, not affecting the number of flops in the calculation of \mathbf{R} , affects the calculation of \mathbf{d}_l , with an increase that is also proportional to the number of active users, L .

An estimate to the number of flops required for the calculation of \mathbf{R} and of \mathbf{d}_l , function of M , L , and the number of block samples, N_s , is given by:

$$\begin{aligned} N_{flops/\mathbf{R},\mathbf{d}_l}^{CG}(M, L, N_s) &\approx (8N_s)M^2 + (8N_sL)M + L = \\ &= (8N_sM + 1)L + (8N_sM^2) = 8(M^2 + LM)N_s + L \end{aligned} \quad (6.12)$$

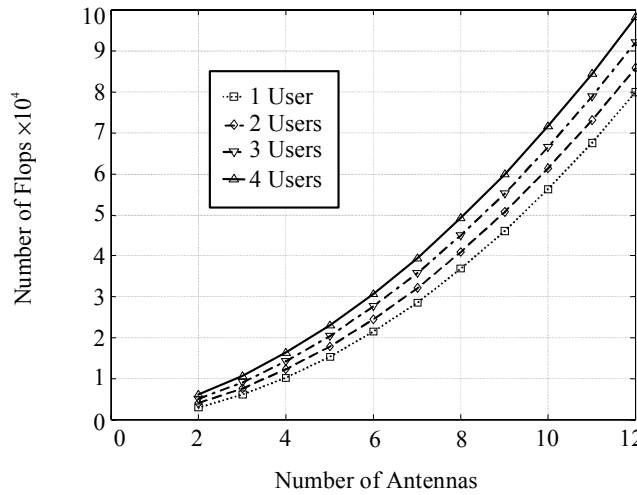


Figure 6.42 – Number of CG flops required for the calculation of \mathbf{R} and \mathbf{d}_l vs. M , for several values of L , for which beamforming is performed.

Again, the number of flops follows a second order polynomial on M . But in this case only the order one and zero coefficients depend on the number of active links. This means that the greater contribution to the number of flops is the number of block samples required to calculate \mathbf{R} and of \mathbf{d}_l , if L is small. Nevertheless, the first order term on M has a coefficient both dependent on N_s and L . For a large number of active links, it must be noted that, since the number of samples may be at least 16,

close to a realistic number of antennas, L will be another great contributor the number of flops, and not only the number of block samples, anymore. In that case,

$$N_{flops/\mathbf{R},\mathbf{d}_l}^{CG}(M, L, N_s) > 8(N_s + L)M^2 + L = (M^2 + 1)L + (8M^2 N_s) , \quad (6.13)$$

where the contributions become clearer.

Finally, it must be kept in mind that the RLS implementation is a sample-by-sample one, in fact requiring a certain number of iterations, N_{iter} , in its case equal to N_s , involving a total of $N_s \cdot N_{flops/iteration}^{RLS}$ flops to converge, at the end. In the block-sample CG case, $N_{iter} \cdot N_{flops/iter}^{CG} + N_{flops/\mathbf{R},\mathbf{d}_l}^{CG}$ flops are involved, after N_{iter} iterations. For this, (6.10) must be accompanied by the additional multiplying N_s factor in order to truly compare the total number of flops between the CG and the RLS, for N_s samples and iterations. Consequently, the total complexity differences registered between both algorithms are in fact not as large. It can be easily seen that for larger number of N_s , and small L , the CG may in fact involve lower total number of flops than the RLS, and that for N_s close to L , the numbers of flops are not significantly different. Moreover, the CG requires as much as M iterations to converge, whilst the RLS may require much more, further reducing complexity differences. Consequently, though a full complexity comparison of both algorithms would require the consideration of the propagation scenario at stake (since both algorithms require different N_{iter} values to reach similar SINR and BG values, as seen in sub-Section 6.5.2), it can be stated that both algorithms to not significantly differ in complexity, on the whole.

Besides understanding how the algorithm complexity, in terms of flops, varies with the implementation parameters, it is important to show how the overall simulation times themselves highly depend on those. In order to do so, one should keep aware that the significant time consuming effort is not related to the CG (or RLS) itself, but is dedicated to the calculation of the signal matrix, \mathbf{U} , whose elements result from the summation of all DCIR components, from each AoA and ToA, for each of the L active MTs, for each array element. Since most of the presented results cover $10M$ values, taking even numbers from 2 to 20, using 100 DCIR concretisations for each scenario, it is easily understood that 1 000 calculations of \mathbf{U} have resulted in large evaluation times. Furthermore, these take longer times for larger number of users, larger AoA or ToA spreads, and the larger number of signals involved by the MiC DCIRs, compared to the MaC case further contribute to longer simulations. Table 6.2 and Table 6.3 provide actual times corresponding to some MiC and MaC scenario examples, TDD mode, in order to quantitatively grasp the actual involved effort, using an Intel P4 CPU, 1.5 GHz, 260 MB RAM. Both the number of active users and the MT-BS distances have a strong impact on the time required for the signal matrix calculation: comparing MiCs and MaCs times, the former are generally much larger for the same L , which is a direct result from the much larger number of multipaths present in MiCs; in the case of MiCs, it is particularly visible how increasing L results in increasing simulation times, approximately in the same proportion as L changes; it is for the lowest d_{MT} values, for which the involved delay and angle-spreads are largest,

that the MiCs simulations take the longest; for MaCs, the simulation time dependency on L is again close to proportional to L ; it is for the largest r that, in MaCs, the simulation times also result longer, again due to the larger delay and angle-spreads.

Sc #	Simulation Time [h]
4u_mc_Sp_05	7.0
4u_mc_Sp_5	6.8
4u_mc_Sp_10	4.5
8u_mc_Sp_05	14.5
8u_mc_Sp_5	11.4
8u_mc_Sp_10	8.9
16u_mc_Sp_05	29.7
16u_mc_Sp_5	26.5
16u_mc_Sp_10	17.4

Table 6.2 – Approximate times involved in some simulations corresponding to 10 times 100 concretisations per scenario, for some examples of MiC scenarios.

Sc #	Simulation Time [h]
4u_Mc_Sp_15_50	0.2
4u_Mc_Sp_d_200	3.9
4u_Mc_Sp_15_400	4.3
8u_Mc_Sp_15_50	0.4
8u_Mc_Sp_d_200	7.9
8u_Mc_Sp_15_400	9.0
16u_Mc_Sp_15_50	0.8
16u_Mc_Sp_d_200	15.6
16u_Mc_Sp_15_400	17.2

Table 6.3 – Times involved in some simulations corresponding to 10 times 100 concretisations per scenario, or some examples of MaC scenarios.

Since these are only some among the total of implemented scenarios, it is easily seen how much the simulations have demanded in terms of effective evaluation effort and time. In the MiC case (Table 6.2), it is clear how the \mathbf{U} matrix implies longer times as d_{MT} decreases, due to the richer DCIR angular and temporal response. The same reason justifies the increases as the MaC scattering circle radius rises (Table 6.3). In both the MiC and MaC cases, it is especially clear how the number of active users affects the time required to calculate the \mathbf{U} matrix.

6.6 Summary and Conclusions

Some of the contexts that involve the NB and WB meanings have been clearly presented, and related – the propagation channel characterisation, the system perspective, the adaptive processing scheme, and the antenna array factor calculation. The several situations, some characterised as *narrowband* and others as *wideband*, are not in contradiction, for the beamforming application described in this work. Their meanings are different, according to the context. It has been verified that the system application is *wideband*, the channel model is *wideband*, the beamforming process is *wideband*, and that the array *narrowband* assumption is very valid.

Concerning the application towards the TDD or the FDD mode, it is verified that the nature and correlation properties of the involved reference codes do vary between the two modes, and that these do not present ideal correlation properties. Like that, it is justified why the beamforming implementation may lead to SINR and BG values that are better for FDD than for TDD, also leading to different evolutions along optimisation. Anyhow, most important, the beamforming performance dependencies on the implemented scenarios do not significantly vary with the duplex mode.

The MMSE and BG OD problem is described, understood and dealt with, so that the subsequent chapters may describe other issues most clearly and independently. Besides expressing the problem, its analysis has been presented as function of the several MiC and MaC scenarios, providing examples of the most critical situations. Through its justification, it is shown that the OD does not root from the applied algorithm(s) themselves, but from the nature of the reference codes vs. the channel and the way that those references are input. Also, other related topics have been naturally mentioned in the text, these being described in other chapters or sections, for clarity purposes, again. Though these topics will inevitably bring about the OD issue, such matter is only addressed explicitly in this chapter.

For the purpose of the analysis of the beamforming performance dependence on the multi-target scenarios directional and temporal characteristics, it has been found that the *significant iteration* is defined as that at which SINR or BG maxima are most frequent, for each scenario, independent of being either MiC or MaC situations. The reasons for such root from the overall consistence in the obtained results, respecting logical fundamental relationships, also being founded on other issues described in other chapters or sections. In this way, in Chapter 7, Beamforming in Micro- and Macro-cell Scenarios and subsequent ones, the iteration number to which the results correspond will not be mentioned, its importance being limited to this section.

Anyhow, in order to extend the OD problem from the abstract point of view towards a system-directed perspective, the practical solutions presented apply at either BS or at MT levels. These cover the improvement of the algorithm application by: including a simple SINR control procedure; jointly linking all L independent beamformers through controlling orthogonality among the L weight vectors; making use of longer references, involving longer code lengths; extending the code references to their

delayed versions; adding spatial diversity schemes; or considering beamforming at the MT, to selectively convey signals through AoA disjoint directions towards the BS. These methods have also been presented in the light of improving overall interference suppression capacity.

From the extended analysis of the optima issue, the extreme importance of the angular domain already comes about, seeing that it is another factor strongly affecting SINR and BG evolutions, besides the temporal one.

Concerning the RLS and the CG implementations, both algorithms lead to agreeing beamforming dependencies on the WDCM characteristics, though the sample-by-sample RLS implementation leads to lower SINR and BG values, compared to the block-sample CG. Regarding the OD, the RLS also exhibits non-monotonic evolutions in SINR or BG, in agreement to having justified such problem with the loss of arriving signals' orthogonality, i.e., independently of the applied algorithm. These results provide a reasonable degree of confidence so as to extract the way how the WDCM affects beamforming performance. Both algorithms' general dependency on MiC or MaC scenarios is also clear, the RLS implementation being particularly sensitive in the grouped MT MaC case. Along iterations, the RLS and CG implementations do differ, the former exhibiting larger variations along iterations and among links' respective results. In this way, the CG converges to final values much faster than the RLS, in most cases. It is also for these reasons that the CG shows to be comparatively more suitable for the analysis purposes carried out in this study.

Concerning complexity, the number of flops required by the RLS and block-sample CG implementations has been analysed and found to be approximated by second order polynomials, function of the number of antennas. The number of operations involved in each iteration is proportional to the number of active links, for both the CG or RLS applications. The RLS, being inherently sample-by-sample, requires much less flops per iteration than the CG block-sample counterpart. Anyhow, the fact that the CG requires the calculation of a correlation matrix and a desired vector is partially counteracted by the need for several RLS iterations, ending up with complexities that do not significantly differ, in a whole, in a multi-user realistic mobile environment.

Finally, regarding the choice of particular algorithm to go forth with the proposed analysis, there is no doubt that many other algorithms could/should be applied and compared, further analysing how their behaviour would depend on the channel characteristics. Contributions [TsAP00], [TsAt02], [CCIC02] and [LiLi03] are some examples of studies that focus on the comparison of algorithms, for certain channel conditions. It must be kept in mind that the aim of this study is not analysing algorithms, but using algorithm(s) to analyse how channel properties affect general beamforming. Making use of an algorithm that is capable of rendering fast and stable convergences in terms of SINR and BG, the choice of the CG proves to be more adequate than the RLS. The block-sample nature of the former better reflects the dependencies on the channel, making simultaneous use of several acquired channel output samples, while also not involving significantly larger mathematical complexity.

7 Beamforming in Micro- and Macro-cell Scenarios

In every job that must be done, there is an element of fun.

You find the fun and - SNAP - the job's a game!

—Pamela Lyndon Travers (1899-1996)

7.1 Introduction

It is now time to present and evaluate the resulting BGs and relevant SINRs, as functions of several MiC and MaC scenarios. The involved correlation matrix components and the resulting power components are also analysed, playing an important part in the further understanding of the interference suppression process.

The scenarios and the relevant wideband, directional and spatial characteristics have been put forward in Chapter 4, in parallel to defining important parameters that characterise MiC and MaC channels – the angular and temporal densities of arriving signals, DCIR channel richness, besides AoA and ToA spreads. It is within such context that particular concern is hereby directed towards relating the performance results to the physical meaning that those channel characteristics involve, so that the important and physically fundamental hypotheses and relations are correctly extracted and argued for. In particular, the fundamental issues of the available beamforming freedom and the inherent physical constraints that determine it naturally arise, finally justifying the importance of defining such parameters.

In terms of description methodology, this chapter deals with the separate analysis of the MiCs and MaCs results, in similar ways, so as to prepare the development of the overall comparison of performances between MiCs and MaCs, following in the next chapter. It is in that chapter that the quantitative relations between the defined channel parameters and the results are presented, corroborating the conclusions from the present chapter. This chapter is based on the primary

settlement of the mentioned fundamental physical happenings as functions of the scenarios' parameters.

In order to follow the present chapter in the most efficient way, it is important to keep track of the propagation scenarios presented in Chapter 4, in parallel. The hereby-conveyed results are more solidly apprehended and understood, by physically visualising the scenario cases, e.g., the grouping or spreading several MTs, or the separation of a single MT from remaining ones, the scattering areas at stake, and by keeping present what and how parameters have been varied.

7.2 Performance Dependence on MiC Scenarios Parameters

7.2.1 MT-BS Distance

From Figure 7.1 and Figure 7.2, it is seen how BG and SINR vary with d_{MT} , for various numbers of antennas, M , and of MTs, L , for scenarios Sc #Lu_mc_Gr_ d^{29} . As far as SINR values are concerned, there is a clear tendency for these to increase as the BS-MT distance increases (Figure 7.2). These results are understood, seeing that the NDesI content is in fact lower, due to the decreasing ToA spread, σ_τ (Table 4.8). One also sees that, although the SINR of the single element also varies in the same sense as a function of d_{MT} , its dependencies with BS-MT distance are not as large as those achieved with the beamformer. Such is inherent of the beamformer operation, naturally showing that other factors are at stake, rooting from the exploitation of the angular domain, depending on distance, number of active users, and even on the number of array elements. In fact, one then sees that BG is dependent on those parameters, as it is already evident in Figure 7.1. It shows how BGs decrease with increasing L is more severe in the Sc #Lu_mc_Gr_05 case, which presents the largest ToA spread. Thus, the effect of the increasing number of arriving orthogonal codes, L_T , comes about more or less evidently depending on either L or on σ_τ .

In Figure 7.3 these relationships are presented as direct functions of BS-MT distances. In the case of grouped MTs, and confined to the street axis, the most relevant analysis results are the following: there is a tendency for BG to increase with distance, taking the MT from 50 to 500 or to 1 000 m; from 500 to 1 000 m, for any of the #Lu_mc_Gr scenarios, BGs do not differ significantly, indicating a particularly worse situation for 50 m; among all of these scenarios, for any number of array elements, M , the Sc #Lu_mc_Gr_05 case leads to the most degraded BGs; such degradation is clearer as the number of MTs increases; SINR and BG sensitivities to the distance differ, the latter being naturally lower.

²⁹ It must be noticed that negative average SINR values obtained after beamforming still correspond to positive BGs, i.e., indicating a definite average gain in applying the beamformer.

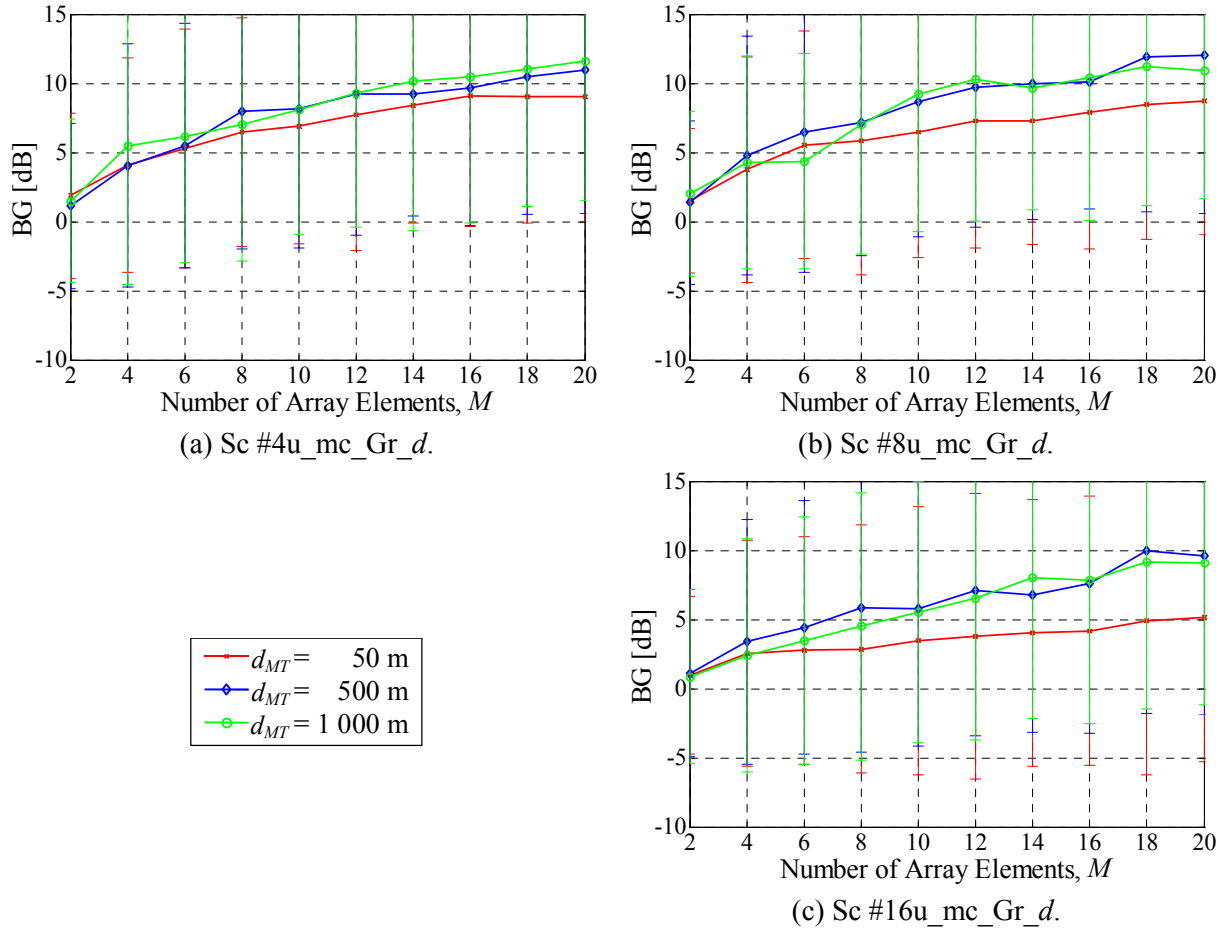


Figure 7.1 – BG, function of M , for several values of d_{MT} , Sc #Lu_mc_Gr_d. Solid lines indicate average results, and error bars indicate respective standard deviations.

These results are expected and justified: by increasing d_{MT} , one is actually reducing AoA and ToA spreads, as it is seen in Table 4.8; also, by lowering L , the *on-the-air* interference content is lowered (as it is seen through the L_T parameter). On the one hand, an AoA spread reduction will tend to increase the minimum possible P_{NDesI} at the output of the weighted array, due to the limited angular capacity to place closer nulls in response to higher angular density of the incoming rays; on the other, the ToA spread reduction leads to higher achievable SINRs. Furthermore, the NDesI power content presented to the beamformer is naturally sensitive to L (again, reflected by L_T). It is then verified that, for Sc #Lu_mc_Gr_05, characterised by the largest temporal and angle-spreads, the effect of ToA spread, allied to L , overrides that of the referred opposing AoA influence.

Another point about which one must be aware of is that, though SINRs may be the best, the corresponding BG may not be so. Keeping in mind that BGs and SINRs are solely related by an SINR obtained with a single omnidirectional antenna, it all depends on the latter quantity, which also varies with d_{MT} , not due to the near-far effect, hereby compensated for through PC, but due to the varying

NDesI power. The average SINR results obtained with a single-element, as those provided in Figure 7.2, confirm this among all scenarios. For the single antenna, the effects of the BS-MT distance are solely due to the total interference content with no spatial processing, since no AoA discrimination is at stake. This effect is visible through the different offsets among 50, 500 and 1 000 m horizontal lines, for any number of users.

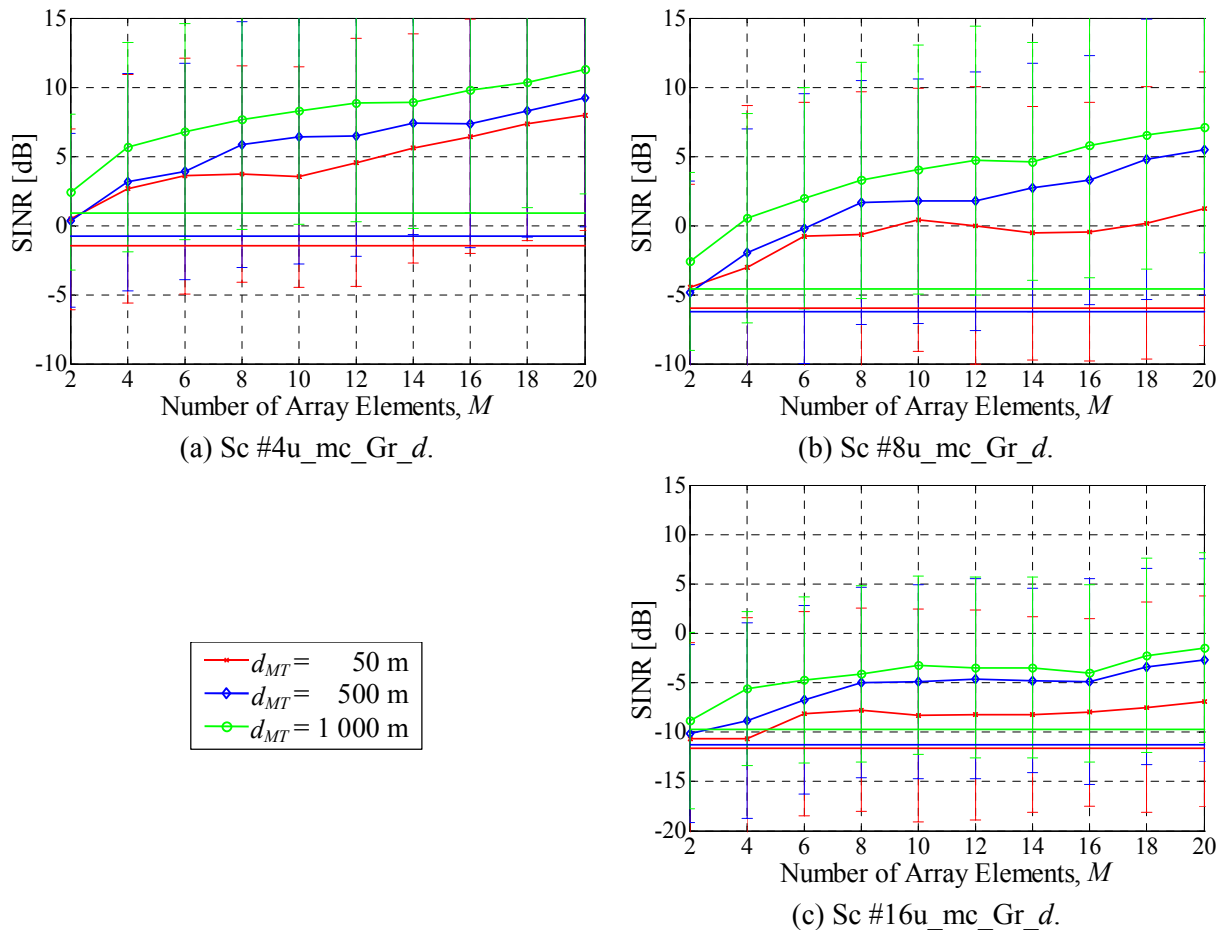


Figure 7.2 – SINR, function of M , for several values of d_{MT} , Sc #Lu_mc_Gr_d. Solid lines indicate average results, and error bars indicate respective standard deviations. Horizontal lines indicate single-element SINR values.

It is also important to extend the same type of study towards the case where the same numbers of MTs are angularly spread. In Figure 7.4, BG results are presented for scenarios Sc#Lu_mc_Sp_d. Besides the averages and standard deviations being very similar to the previous scenario cases, there is a natural tendency for the average values to be higher in the latter case, the dependencies with BS-MT distance also becoming more evident among the 500 and 1 000 m situations. Such can be justified by realising that, while the MTs are angularly spread, it is for the narrowest angle-spread case, i.e., for $d_{MT} = 1000$ m, that the beamformer most gains from such MT angular separation, since AoAs are less probably shared among links. For that, the sensitivity to d_{MT} is not as significant for the lower number

of MTs, as it happens in the grouped cases. Also, as before, the 50 m separation reveals to lead to particularly degraded BGs, for the reasons mentioned.

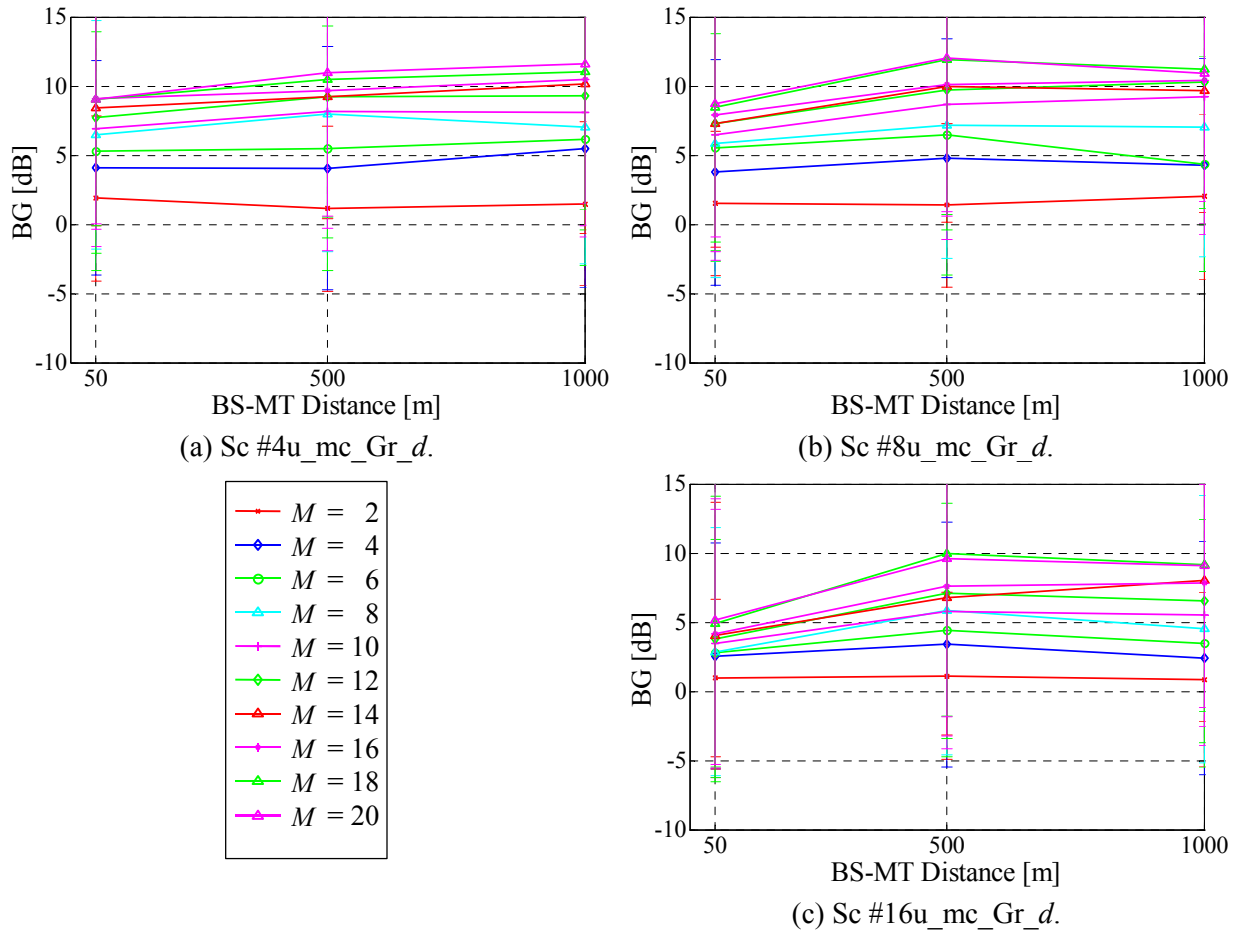


Figure 7.3 – BG, function of d_{MT} , for several values of M , Sc #Lu_mc_Gr_d.

As mentioned before, besides the mean BG and SINR values, their standard deviations are of importance, having obtained relative large values. Anyhow, these do not present significant variations with any of the varied parameters, nor with the number of independent concretisations, from 10 to 20, or to 100. Concretisations leading to negative BGs have been obtained for all scenarios, shown by the large standard deviations, as mentioned, though the average results are positive. Keeping in mind that all MTs are grouped together in scenarios Sc #Lu_mc_Gr_d, making use of common scatterers to convey signals to the BS with the same ToAs and AoAs, results of this sort are of relatively easy acceptance (in addition to the justifications presented in Chapter 6, Set-Up Analysis and the following ones).

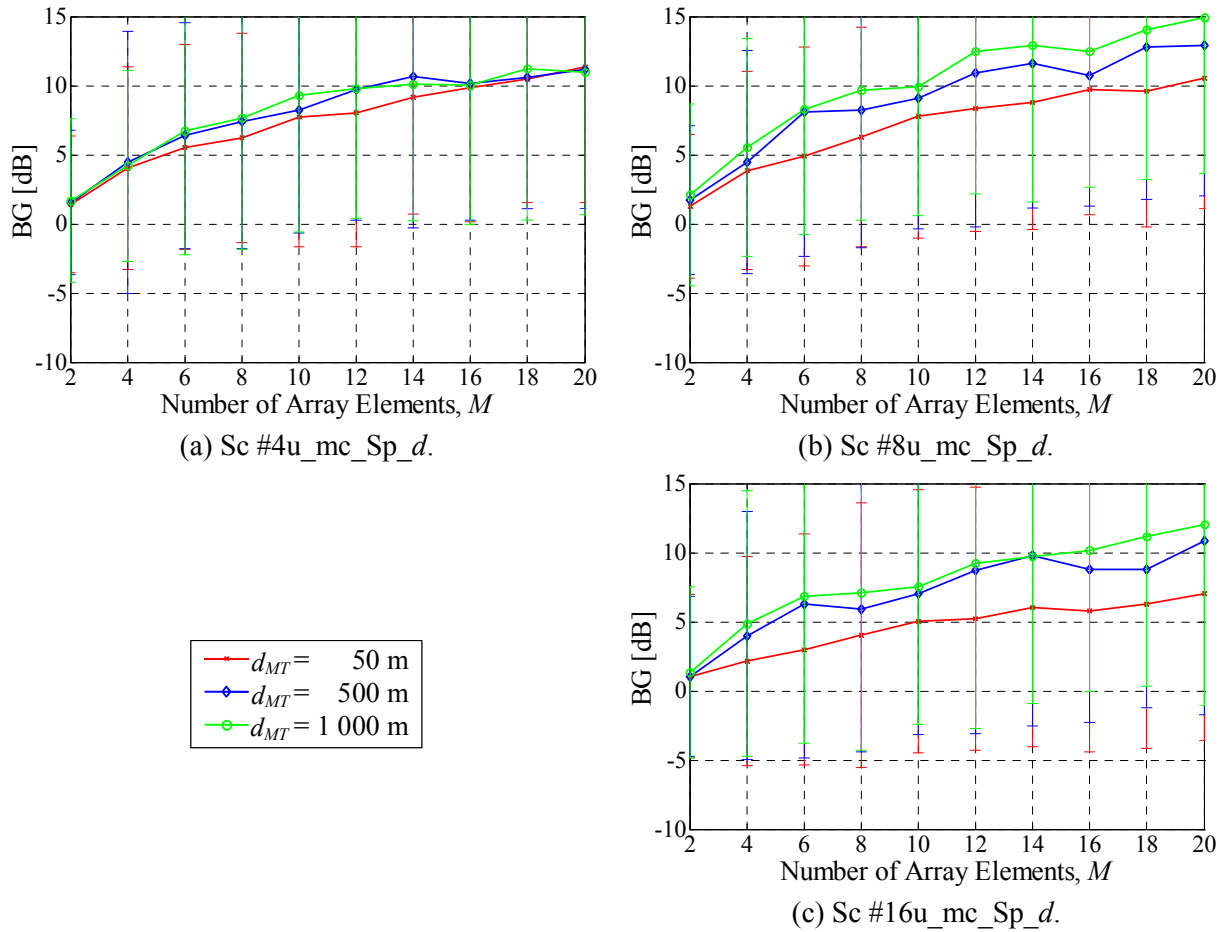


Figure 7.4 – BG, function of M , for several values of d_{MT} , for Sc # $Lu_{mc}Sp_d$.

7.2.2 Number of Array Elements

In general, SINR and BG values increase as the number of antennas increases, as it is seen in the Sc # $Lu_{mc}Gr_d$ and Sc # $Lu_{mc}Sp_d$ scenario plots of Figure 7.1 and Figure 7.4. Such is an expected verification, since having more antennas means that the incoming DesS and NDesI signals can be better discriminated, leading to better interference suppression. In Figure 7.5 and Figure 7.6, though being aware that the numbers may be unrealistic and assuming that the signals among array elements are always correlated independently of the number of elements, and therefore viewing these results in a conceptual way, additional average BGs are presented for larger number of array elements³⁰. For these, 10 concretisations have been used for the averaging, due to the exceptionally long simulation times (simulation times have reached close to 14 h, in the MiC case, $L = 16$, $M = 60$, for 10 concretisations), owing to the large signal matrix, thus, revealing larger fluctuations as a function of M .

³⁰ For higher frequency MBSs, covering bands as high as millimetre-wave, some of these numbers are not so absurd, even in the case of a ULA.

Besides confirming the previously described sensitivities to BS-MT distances, BGs are seen to increase with M , where a general asymptotical progression becomes visible. That is thought to be because of two factors, one at the level of inherent physical array properties, and the other related to simulation limitations: the larger the antenna array, the less correlated the signals among elements are, (the matter of spatial correlation coefficients is pursued in Section 8.3, Relations to the MIMO Perspective), meaning that the optimality of a certain array pattern will be reduced on the whole, since such pattern inherently assumes total correlation of signals among all elements; the finite WDCM angular resolution also imposes a limit to the analysis, the resulting *saturation* effects being more noticeable for higher number of array elements. Anyhow, due to the former physical-level limitation, these interesting results reveal that the increase of M is in fact not followed by unlimited increase in the array angular resolution, and on BG³¹.

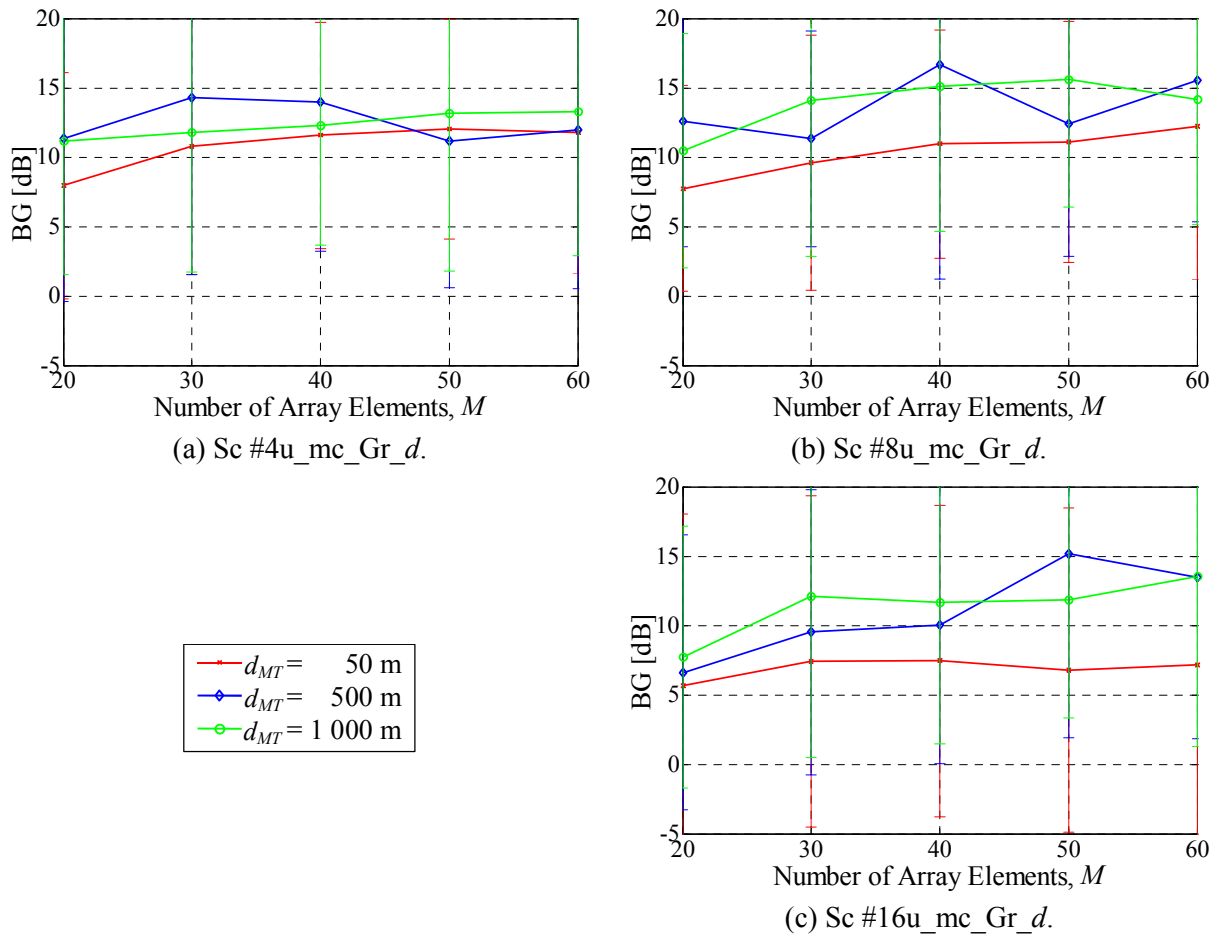


Figure 7.5 – BG, function of the d_{MT} , for several values of M , Sc #Lu_mc_Gr_d, for larger number of array elements.

³¹ In a practical perspective, the increase in BG does not compensate for the increase in M , with all that such involves, e.g., cost, mathematical burden, power consumed, decalibration and non-linearities.

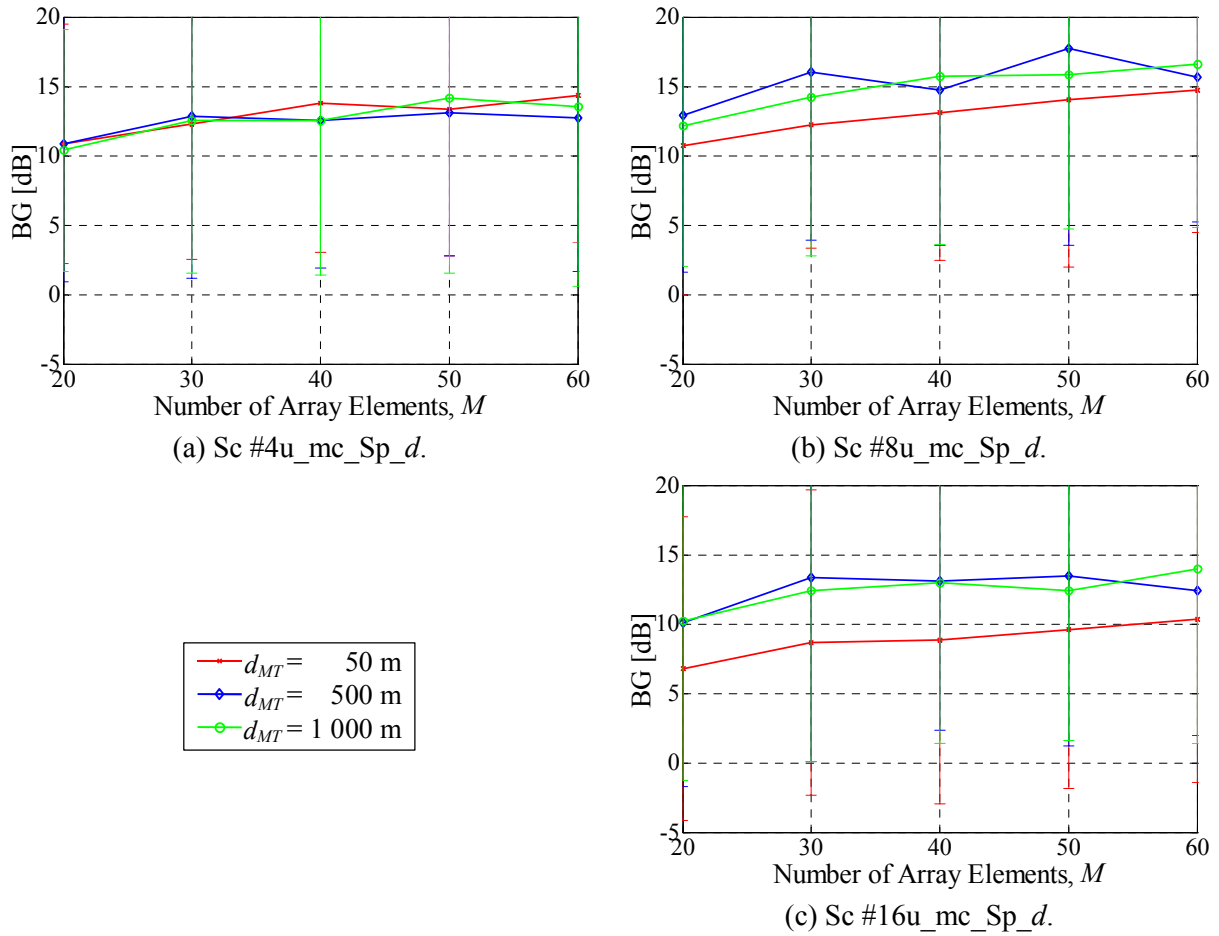


Figure 7.6 – BG, function of the d_{MT} , for several values of M , Sc #Lu_mc_Sp_d, for larger number of array elements.

It is also verified that the turning point where the BGs could be expected to substantially increase, when the number of array elements is larger than the number of arriving orthogonal signals, $M > L_T$, does not exist. This is another indication of another factor, related to the AoA spread and density of arriving signals, regulating the major beamforming dependence on the propagation channel, not confining its performance dependence to the temporal domain.

7.2.3 Angular Displacement and Grouping of MTs

With the previously described MiC scenarios, Sc #Lu_mc_Gp_d and Sc #Lu_mc_Sp_d, one is already in the presence of two opposite situations in terms of grouping of MTs – in the former case, all ToAs and AoAs are common among all active links, the DCIRs only differing in the signals' phases among links, while in the latter case, within some probability some AoAs are not shared, and within a common AoA each link contributes with differing ToAs and signal strengths. In this way, the beamformer better angularly discriminates the DesS from the NDesI from the remaining MTs, therefore, leading to higher SINRs and BGs. As mentioned before, that tendency is visible while comparing Figure 7.1 and Figure 7.4. By going forth with the corresponding analysis, one realises

that, for all L , the situations where MTs are 1 000 m from the BS are those that present the largest sensitivity. As mentioned before, the 1 000 m situation is that at which DCIRs have narrower angle-spreads (Table 4.8), meaning that by spreading the MTs, AoAs are less probably superimposed as compared to the wider angle-spread case. For such distances, BGs may increase up to 4 dB, by spreading the terminals. Anyhow, with MTs at 50 m from the BS, with angle-spreads that are much wider, meaning that the spreading of terminals does not contribute to particularly less probable superposition of AoAs, the results show improvements of up to 2.3 dB, only.

Adding the remaining scenarios to the analysis, one sees that several situations are at stake, concerning the angular positioning of active MTs. There are situations where there is a group of MTs in the same location (in Sc #Lu_mc_Gr_d, #Lu_mc_Se_A and #Lu_mc_Se_C), and others where MTs are angularly spread (Sc #Lu_mc_Sp_d and #Lu_mc_Se_B). Secondly, the Se_A, B and C are also the cases where an angularly isolated MT is present, making use of scatterers different from those affecting the remaining MTs. For the MiC case, as it is understood from the angle-spreads involved, such isolated MT does not benefit so much from AoAs being totally disjoint from those of the remaining MTs, nevertheless posing the situation where such AoAs are the least common. As expected, such MT should lead to the best corresponding SINRs and BGs, among all MiC scenarios.

In Figure 7.7, average BGs are presented³², corresponding to Sc #Lu_mc_Se_A. As expected, the group of MTs, for all L and M , presents results that are very close to the Sc #Lu_mc_Gr_d cases, the effect of involving one less MT not being noticeable. On the other hand, the single MT leads to much better performances, BGs reaching up to 5.6, 9.0 or 8.1 dB higher than that of the grouped MTs, for 4, 8 or 16 active users, respectively.

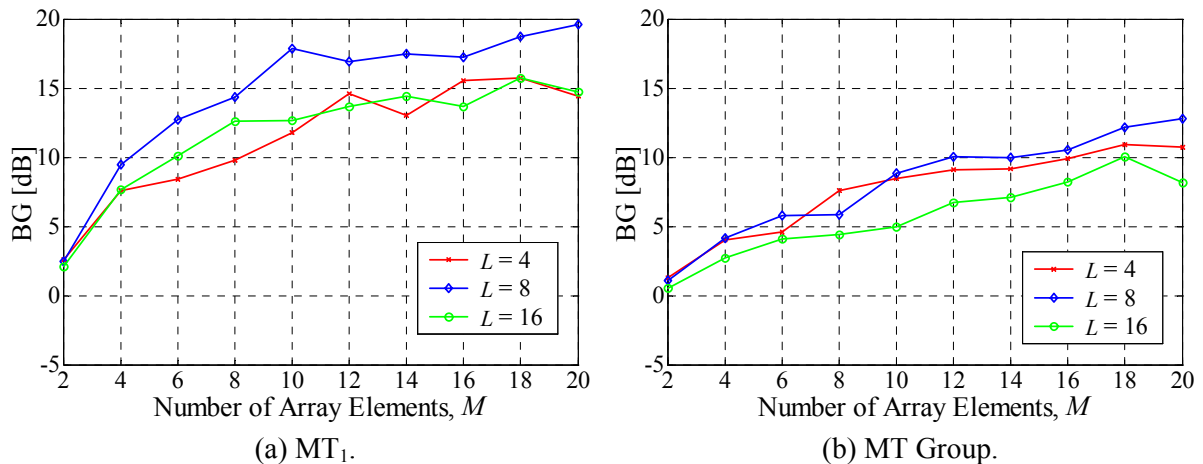


Figure 7.7 – BG, function of M , for several values of L , Sc #Lu_mc_Se_A.

³² For clarity, the standard deviations are not shown in some plots.

As it is seen in Figure 7.8 and Figure 7.9, comparing to the Sc #Lu_mc_Se_A case, Sc #Lu_mc_Se_B and Sc #Lu_mc_Se_C scenarios present very close BG results, very lightly reflecting the spreading or grouping of the 4th quadrant MTs or the random positioning of the 1st quadrant MT: in Sc #Lu_mc_Se_B, the single MT leads to lower average BGs, while the spread 4th quadrant MTs tend to higher values, compared to Sc #Lu_mc_Se_A; the results from Sc #Lu_mc_Se_C are closer to the Sc #Lu_mc_Se_A ones, also expectedly.

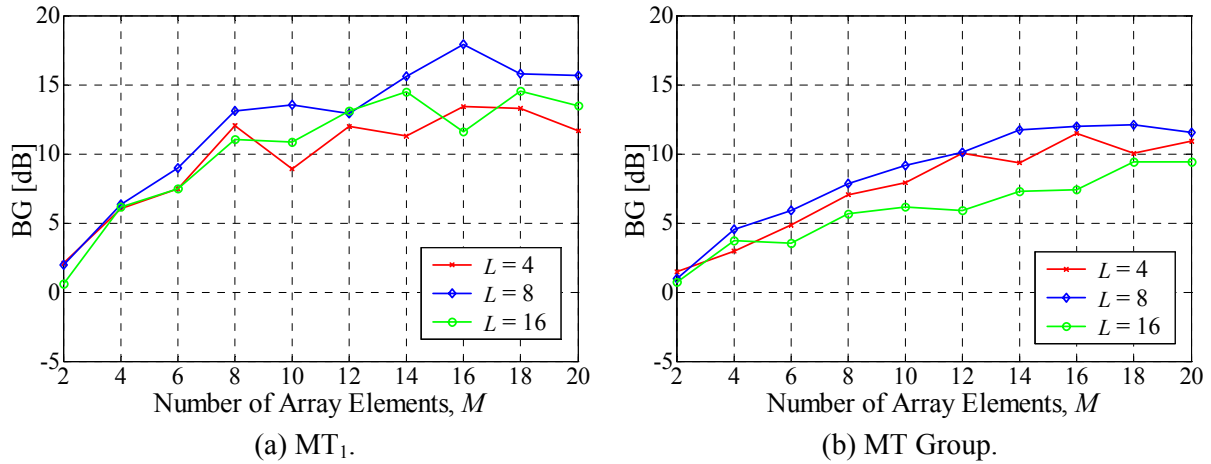


Figure 7.8 – BG, function of M , for several values of L , Sc #Lu_mc_Se_B.

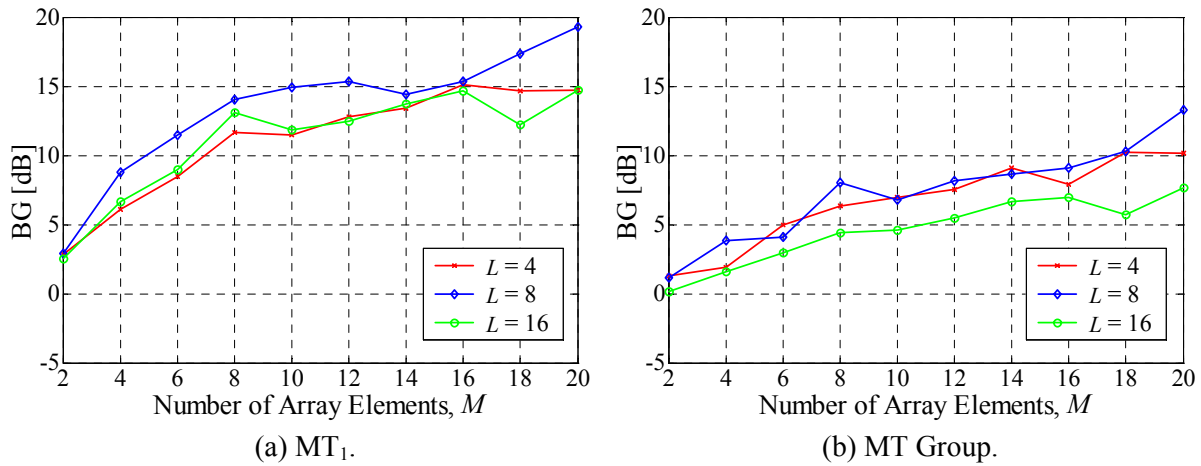


Figure 7.9 – BG, function of M , for several values of L , Sc #Lu_mc_Se_C.

In this way, from the Table 4.4 Se_A, B and C scenarios, where an MT is clearly angularly separate from the remaining ones, meaning that the corresponding DCIR AoAs are the least shared among those MTs, one confirms the expected better interference suppression performance. But additionally, one can say that the beamforming corresponding to such single MT is not sensitive to the sort of displacement of the remaining MTs, anyhow showing tendencies, though relatively minimal. This latter result is also natural, since the MiC propagation situations involve relatively wide angle-spreads, not only of the DesS, but also of the delayed NDesI. It is the delayed NDesI that most

strongly contributes to the interference content, conditioning the beamforming most (as it is presented in sub-Sections 7.2.7 and 7.3.7, Correlation Matrix Components Dependencies).

7.2.4 Linear Displacement and Grouping of MTs

Besides the angular displacement of MTs, it is of importance to sense how the displacement of MTs along the street axis affects beamforming operation. For that, scenarios Sc #Lu_mc_St_Se_A and #Lu_mc_St_Se_B, where a single MT is placed at 50 or 1 000 m, and the group of $L-1$ MTs at 1 000 or 50 m, respectively (presented in Table 4.3), are important in helping to confirm several of the already mentioned hypothesis, further providing confidence in the results. These scenarios are also examples of realistic situations, where a group of MTs, either close or far from the BS, may act as interference clutter towards any single separate MT in the same MiC street site.

Again, it is expected that BGs of the group of MTs are lower than those of the single MT, since the former share all AoAs among each other, anticipating the BGs of the grouped MTs to be similar to those of the previously analysed cases. Moreover, between Sc #Lu_mc_St_Se_A and Sc #Lu_mc_St_Se_B, having a group of interfering MTs closer to the BS should lead to lower BGs, overall, contributing to larger NDesI power and covering more that the AoA spread region that corresponds to the single MT.

The analysis of these scenarios has been set for $M = 12$ only, evaluating SINR and BG, and the number of users, L , has been set to 4, 8 and 16, as before. Results are presented in Table 7.1. It is seen that Sc #Lu_mc_St_Se_A BG results are generally higher than those of Sc #Lu_mc_St_Se_B scenarios, as expected, due to the farther positioning of the group of MTs, confirming that such group has a stronger impact on the beamformer performance if closer to the BS, for the stated reasons. Additionally, for nearly all scenarios, the group of MTs leads to SINRs and BGs lower that the values of the single MT. Anyhow, such differences strongly depend on L , where an increasing L leads to BGs that differ more among the single and grouped MTs. As a result, the difference between single and grouped MTs is larger for Sc #Lu_mc_St_Se_B than for the respective Sc #Lu_mc_St_Se_A one, since the group of MTs has its respective beamforming operation more degraded with the decreasing distance, more visible as L increases.

Sc #	MT ₁ BG [dB]	MT _{2..L} BG [dB]	MT ₁ SINR [dB]	MT _{2..L} SINR [dB]
4u_mc_St_Se_A	11.5	12.2	10.9	11.5
4u_mc_St_Se_B	10.6	8.5	10.6	8.6
8u_mc_St_Se_A	11.4	10.0	2.8	2.1
8u_mc_St_Se_B	9.8	6.8	5.3	2.9
16u_mc_St_Se_A	9.1	5.7	2.6	-1.8
16u_mc_St_Se_B	7.9	3.9	-3.7	-7.1

Table 7.1 – Average BG and SINR, for Sc #Lu_mc_St_Se_A and Sc #Lu_mc_St_Se_B, $M = 12$.

Still concerning the street-confined scenarios, another matter that has been studied is the evaluation of to what extent the assumption that all MTs are together along the street axis is affecting the achieved SINR and BG, as opposed to MT angular shifts existing across the same street, where each MT-BS link would contribute to some AoAs uncommon to those of any other link. By randomly shifting each l^{th} link ellipse axis, still within the maximum angular limits imposed by the street width and d_{MT} , approximating a transversal MT offset from the street axis, the average SINR and BG results are in fact expected to vary, depending on the BS-MT distance. For such test, the same source DCIR was used, meaning that the same moduli, AoA and ToA have been considered for all the MTs at a certain distance from the BS, only varying signal phases and adding the angular shift to all original DCIR AoAs. Due to the statistical nature of the evaluation, added to the effect of varying each scatterer reflection coefficient between each DCIR, the referred assumption is thought not to be misleading. Anyway, it is realistic to think that the main set of clusters and scatterers remains the same, even among links across the street, their relative angular positions changing and resulting AoAs changing within the same order of magnitude.

The test is therefore primarily based on scenarios Sc #Lu_mc_Gr_d, but are similar to Sc #Lu_mc_Se_d, the angular spreading of MTs being correspondingly confined to the street width of 40 m. In Table 7.2 the obtained BGs are given, for the referred scenarios, where the number of elements has been set to $M = 12$, for this study. Naturally, the BG rises relatively more in the cases of 50 m separation, since the angular displacements of mobiles are larger, being closer to the BS. For 500 m, BGs do not suffer relevant changes, and for 1 000 m BGs show a slight decrease by considering the angular displacement. The fact that BGs would not vary for larger distances is an expected result, since the smaller angular displacement tends to loose importance. For this, though the results for 1 000 m seem to contradict the expected tendency, the corresponding BG degradation is seen as not significant. The reason found for such tendency roots in the relationship between sector width, 180° , and the angular shift. For the 50 m case, the angular shifts allied to the subsequent sectorisation cut off imply a considerable reduction in the delayed NDesI power, whereas for 1 000 m this reduction is not considerable, due to the corresponding narrow angle-spread of the DCIRs. Additionally, due to the average lobe-like nature of the corresponding channel responses (shown in Figure 4.5), the small angular shifts tend to keep the NDesI power levels while further superimposing the delayed NDesI significant lobe-like contributions over the AoAs of the DesS ones. At this point, it is worth keeping in mind that the SINR and BG increase has been previously confirmed for the cases where MTs are more widely spread, independent of any street confinement.

Judging from the indicated results, assuming that the same sort of tendencies are present for other values of M , it is concluded that the 50 m results in fact only apply to the MTs being close together, near the street axis, not across the street. On the other hand, for 500 and even 1 000 m one can assume that the results obtained can still be generalised for the cases where MTs are either together or across the street.

Sc #	BG [dB]	
	Without Angular Shift	With Angular Shift
4u_mc_Gr_05	7.7	9.5
8u_mc_Gr_05	7.3	9.2
16u_mc_Gr_05	3.8	6.1
4u_mc_Gr_5	9.2	9.6
8u_mc_Gr_5	9.7	9.7
16u_mc_Gr_5	7.1	6.8
4u_mc_Gr_10	9.3	8.9
8u_mc_Gr_10	10.3	9.1
16u_mc_Gr_10	6.5	6.2

Table 7.2 –BG, function of the scenario, without and with the corresponding angular displacement of the BS-MT line.

7.2.5 Number of Active Links

For all scenario cases, for the same distance, i.e., the same AoA and ToA spreads, increasing L involves increasing the angular and temporal densities of arriving signals, L_T increasing due to L only. In this way, the corresponding SINRs and BGs are expected to decrease with increasing L . It is also clear that the SINR values should be more sensitive to L , compared to BGs, this being a reflection of the inherent beamformer operation (Figure 7.1 and Figure 7.2).

Relative to scenarios Sc #Lu_mc_Gr_d and Sc #Lu_mc_Sp_d, Figure 7.10 and Figure 7.11 show that BG variations from 4 to 16 MTs are in generally very small, being clearer for the shorter BS-MT distances, i.e., when the temporal and angle-spreads are the largest. Anyhow, the BG decrease from 4 to 8 users is virtually non-existent, for any of these 50 m distance cases. Also, for the 500 and 1 000 m cases of these scenarios, an improvement from 4 to 8 MTs is even registered. Furthermore, the same sort of improvement is presented by MT₁ in Sc #Lu_Mc_Se_A, whose results are plot in Figure 7.12, but in this case BGs increasing by several dB from 4 to 8 MTs.

These rather unexpected results are justified by the SINRs dependencies on L , either referring to the SINRs obtained with the whole array, with M elements, or to the SINR obtained with the single array element: by increasing the number of users, spread over the 1st and 4th quadrants, the single antenna element SINR is reduced, following a $\log(1/x)$ trend³³, naturally not depending on the angular characteristics of the scenario; the SINR obtained with the beamformer is also reduced, but following the trend set by the beamformer performance, dependent on the scenario; as the number of

³³ From the calculation of SINR, in (5.14).

users increases, the single element SINR presents a negative derivative that tends to 0, meaning that the SINR decreases less from 8 to 16 MTs, compared to the reduction from 4 to 8 users; so happening, while the beamformer SINR shows a constant or even gradually larger decrease as L increases, the BG then presents values that can be larger in-between the extreme values of L , 4 and 16. In fact, such has been confirmed to happen in all the presented cases, justifying the apparently unexpected results.

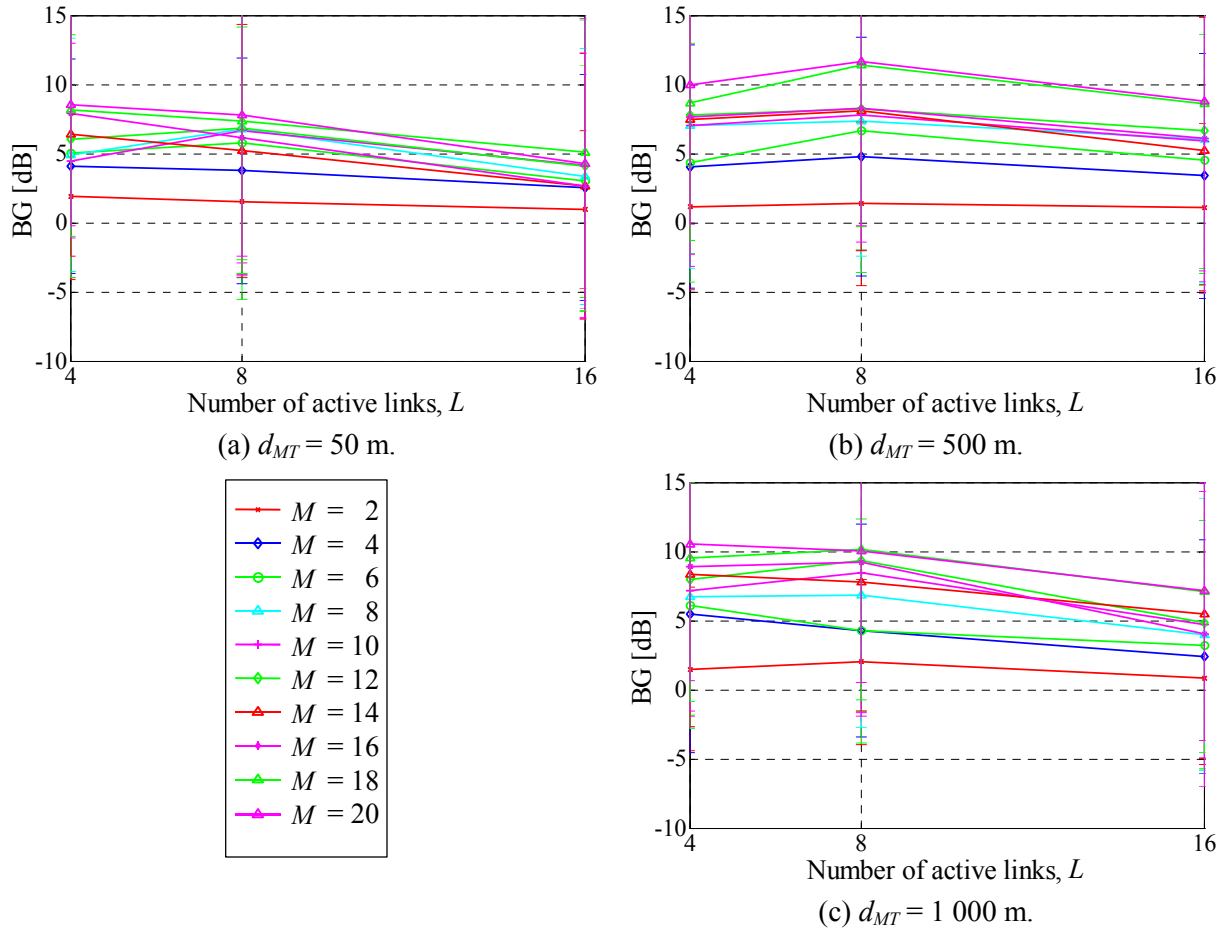


Figure 7.10 – BG, function of L , for several values of M and d_{MT} , Sc #Lu_mc_Gr_d.

In Figure 7.13, the corresponding SINR values are shown, relative to scenario Sc #Lu_mc_Sp_5, exemplifying how the SINR dependence with L does vary with L , for both array and single element cases. It must be noticed that the single element SINR shown has been averaged among all concretisations, among all M values. In fact, the 1st derivatives of these, function of L , have opposite sign, thus, ending up with the BG peak at $L = 8$.

Finally, one sees that for the TDD case, where a maximum of 16 MTs may be present per time-slot, the dependence of the BG with L is relatively small, keeping in mind that BG is the SINR gain obtained with the array over that of the single element. Additionally, though the beamformer is reasonably able to compensate for the variation of the number of MTs, in terms of interference suppression over the single element situation, the corresponding SINRs do significantly still degrade with L , revealing dependencies with L which are anyway similar to those of the single element case.

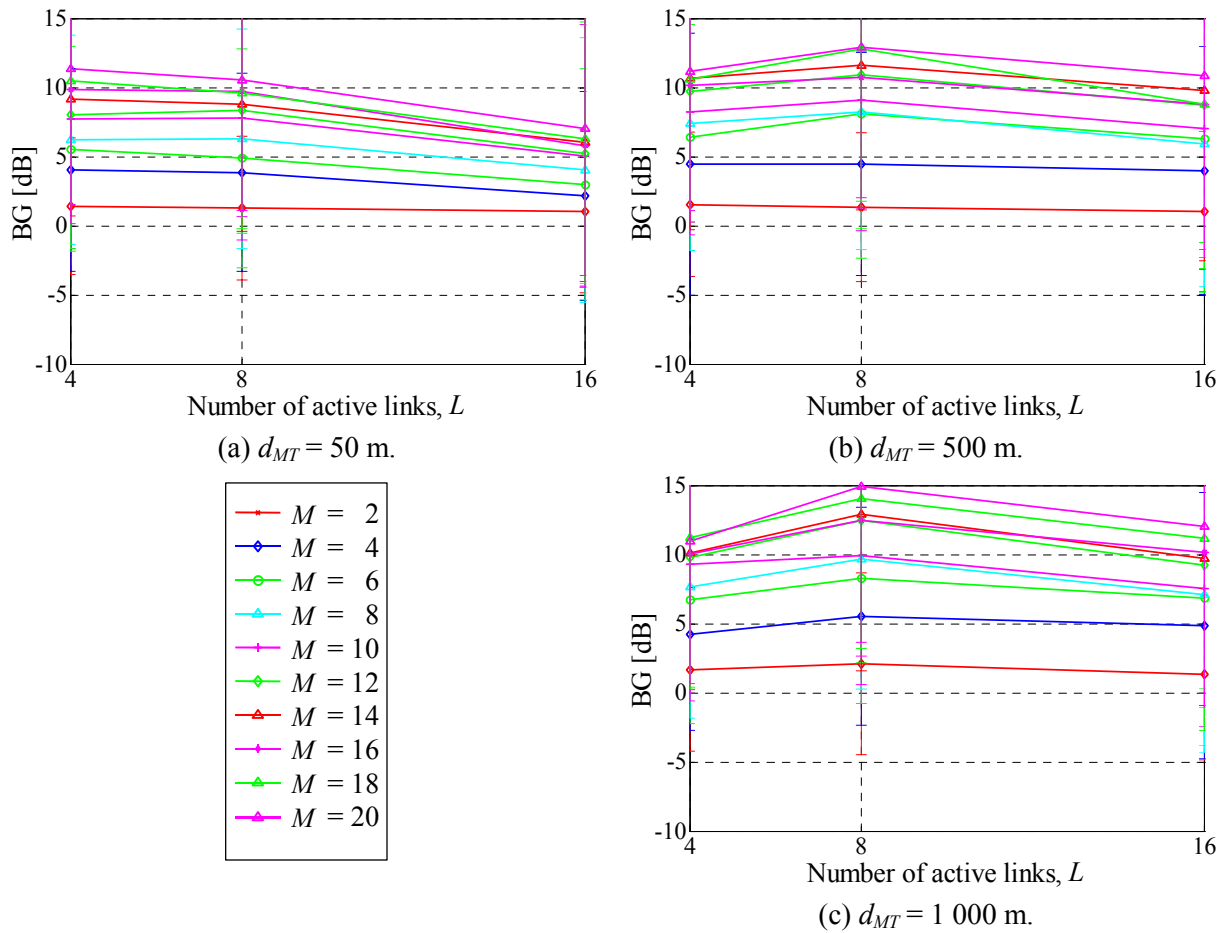


Figure 7.11 – BG function of the L , for several values of M and d_{MT} , Sc #Lu_mc_Sp_d.

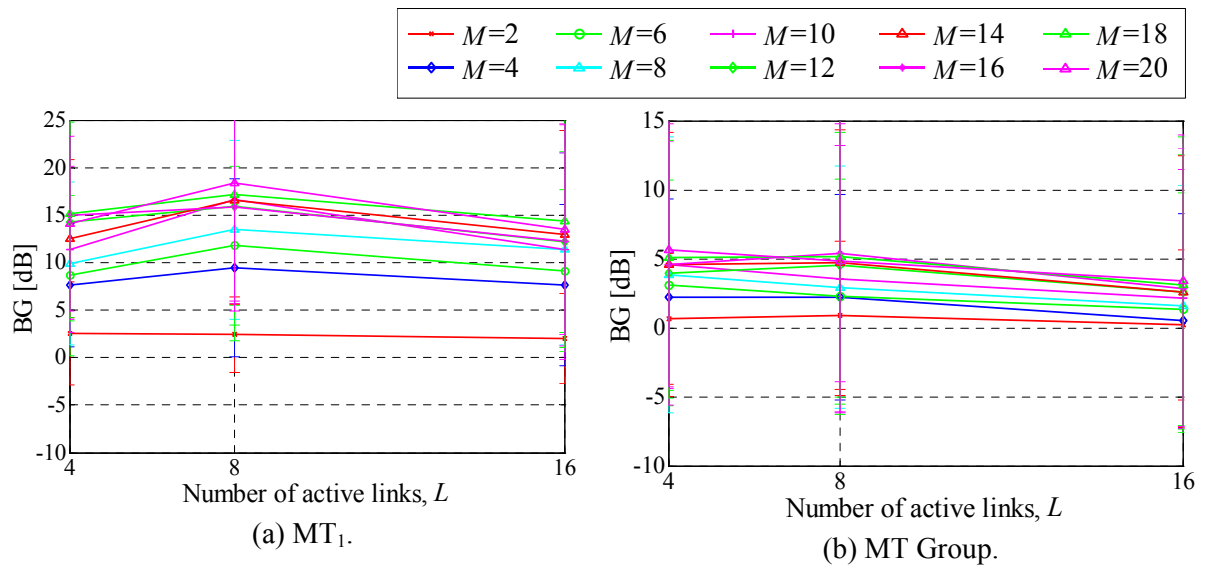


Figure 7.12 – BG, function of the L , for several values of M , Sc #Lu_mc_Se_A, $d_{MT} = 500$ m.

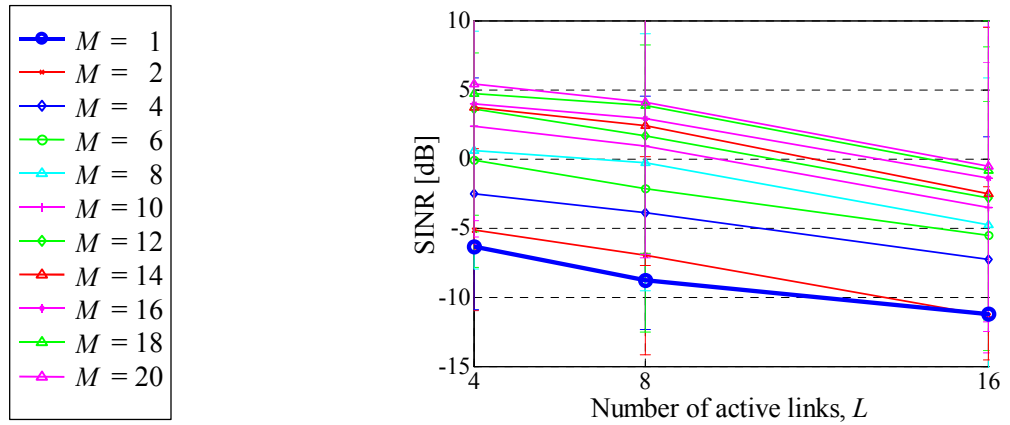


Figure 7.13 – SINR, function of the L , for several values of M , including the single element case, Sc #Lu_mc_Sp_5.

7.2.6 Sectorisation

The effects of changing the array *equivalent* sectorisation angle have also been evaluated. The aim of these tests is to further work as another confirmation and better settling of former results, regarding the dependencies on the propagation scenarios. The sectorisation is referred to as being *equivalent*, since it is reproduced by eliminating the DCIR contributions from outside the respective angular sector, considering an ideal truncation of signals. The sectors considered are 180° (the generally described results), 120° , 90° and 60° .

As Table 7.3 and Table 7.4 show, respectively for 50 and 1 000 m MT-BS separation, SINR and BG values have different behaviour, as function of the sectorisation. In the 50 m case, the beamformer leads to SINR and BG values that vary within near 2.1 dB, depending on the sector width, BGs decreasing as the sector width decreases. For the 1 000 m case, the sensitivities of both SINR and BG values are not as clear, BG even showing improvements from 180° to 90° . Again, the single element SINRs must not be forgotten in the analysis of these results: for 50 m, it is clear how its values decrease with widening sector, while this effect is less clear in the 1 000 m case.

Sector Width [°]	BG [dB] for $M = 12$	SINR [dB] for $M = 12$	SINR [dB] for $M = 1$
180	7.9	6.4	-1.5
120	8.2	8.0	-0.3
90	6.3	6.9	0.6
60	6.1	7.0	0.9

Table 7.3 – BG and SINR, for Sc #4u_mc_Gr_05, with the 12-element array and the single element cases.

Sector Width [°]	BG [dB] for $M = 12$	SINR [dB] for $M = 12$	SINR [dB] for $M = 1$
180	9.4	10.3	0.9
120	9.5	10.3	0.8
90	10.1	10.8	0.8
60	8.8	10.4	1.6

Table 7.4 – BG and SINR, for Sc #4u_mc_Gr_10, with the 12-element array and the single element cases.

On the whole, these are expected results, remembering that WB AoA spreads, $\sigma_{\phi, WB, =0}$ and $\sigma_{\phi, WB, >0}$, are 25° and 50° for 50 m, but 14° and 30° in the 1 000 m case, respectively (Table 4.8). The sector width is therefore affecting the channel response most when the BS-MT distance is shorter, understanding that the sector width reduction primarily leads to the reduction of the delayed NDesI power, much more widely spread than the DesS one. For this, as distances shorten, accompanied by wider angle-spreads, narrower sector widths lead to larger single element SINR.

Centring the analysis on the BG results, one sees that in the 50 m case, from 180° to 120° BG shows an increase, though relatively small (0.3 dB), whereas from 120° to 90° or 60° BG shows a larger degradation (1.9 or 2.1 dB); in the 1 000 m case, as mentioned, the tendencies are more difficult to characterise, nevertheless involving less significant variations. The cause for the BG to decrease with the sector width reduction is of simple understanding, reasoning that the angular density of DesS and NDesI powers with common AoAs increases, as the sectors narrow, an effect which is more visible for the shorter BS-MT distances due to the larger AoA spreads and larger delayed NDesI power. The limited beamformer capacity to place zeros and nulls close together, for the same number of array elements, becomes more evident in this way, since these have to be placed closer to each other, within a narrower angular sector. On the other hand, for both 50 and 1 000 m cases, the varying behaviour of the BGs, lowering after exhibiting a BG rise as the sector width decreases from 180°, is thought to root from the differing wideband angle-spreads of the DesS and delayed NDesI powers, reasoning that the sectorisation affects these in diverse manners.

Concluding, for larger MT-BS distances one verifies that the BG and SINR obtained with the beamformer are less sensitive to sectorisation, unlike for shorter distances. In the latter case, due to the wider AoA spreads involved, SINRs and BGs are largely affected. In this way, and by also sensing the effects of AoA density for particularly short sector widths and small BS-MT distances, the influence of AoA spread characteristics in the beamforming performance again arises.

7.2.7 Correlation Matrix Components Dependencies

Following the definitions put forward in Section 5.4, the evolution of the several \mathbf{R} components average contributions is presented in Figure 7.14, for the Sc #4u_mc_Gr_d, $M = 12$ examples, where the cross-correlation components are hereby only summarily pointed out. This type of results was obtained for all scenarios and values of M . The most important idea to convey is not the evolutions themselves, but the relative values among all contributions. The $\mathbf{w}^H \mathbf{R} \mathbf{w}$ term in the (5.9) CG cost function tends to N_s , along the optimisation. As it is also seen, for all distances, the $P_{>0}^{other}$ power, i.e., the component of the delayed signals from all the other MTs, is the main NDesI contributor. It is followed by $P_{=0}^{other}$ and then by $P_{>0}^{self}$, with the noise having relatively a relatively small contribution. Only for larger distances does the N power acquire more significance. Again, it is visible how all components evolve differently from the DesS power.

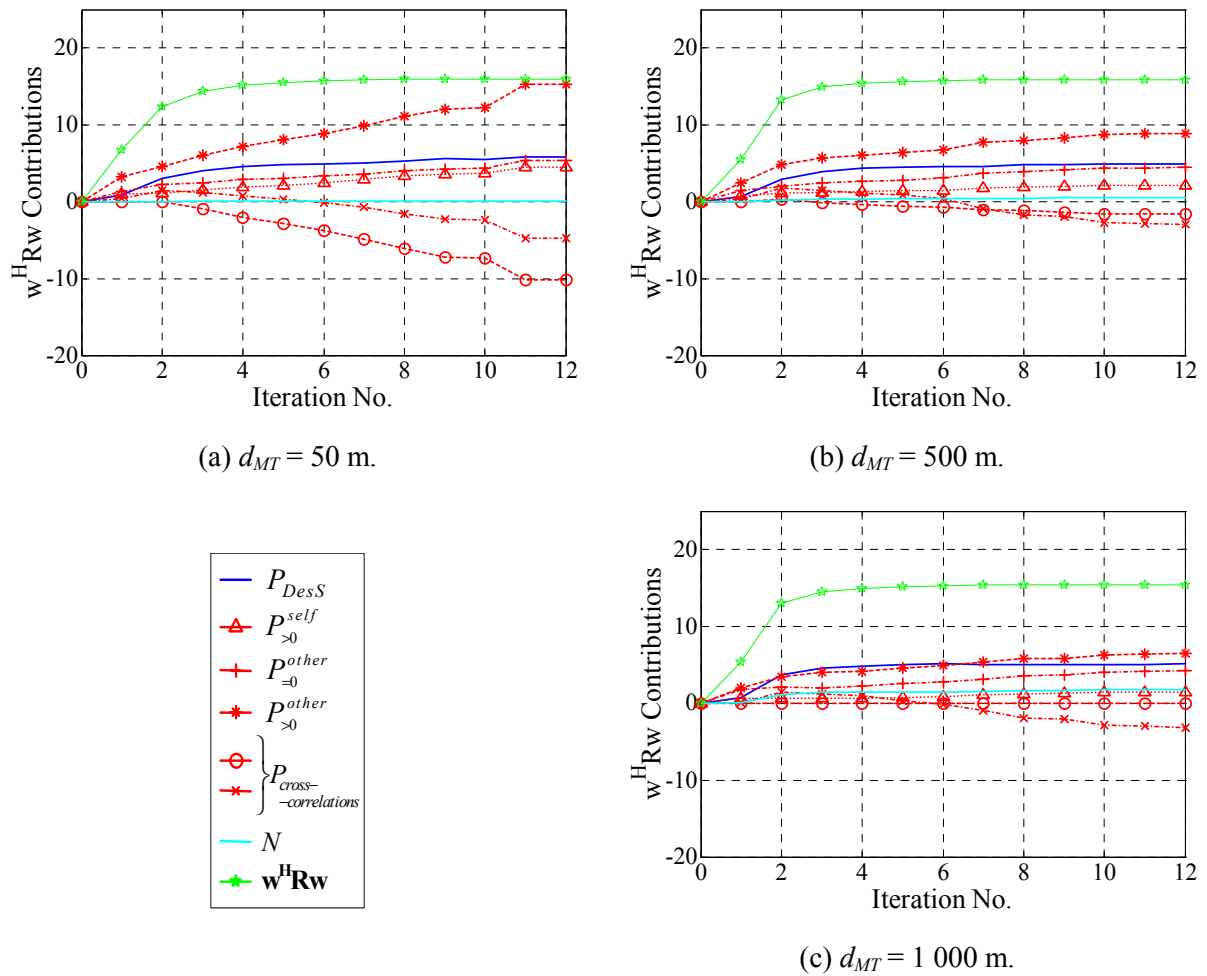


Figure 7.14 – Average power terms due to the composition of \mathbf{R} , for $M = 12$, Sc #4u_mc_Gr_d.

In Figure 7.15, the average P_{DesS} and $P_{>0}^{other}$ power terms are shown, along optimisation, again for $M = 12$, for the several Sc #4u_mc_Gr_d scenarios. It has been described before that the DesS power varies much less with distance compared to the $P_{NDesI} + N$ one, again verifying such by only accounting for the $P_{>0}^{other}$ component. Again, Figure 7.15 shows how DesS powers much faster reach a plateau, compared to $P_{>0}^{other}$. But most important, one sees that the relative component values involved are in consonance with the previously described SINR dependency on distance (Figure 7.2), seeing that for lower separations the delayed NDesI powers from all the other $L-1$ users are particularly higher, the achieved DesS powers not revealing any sensitivity to such.

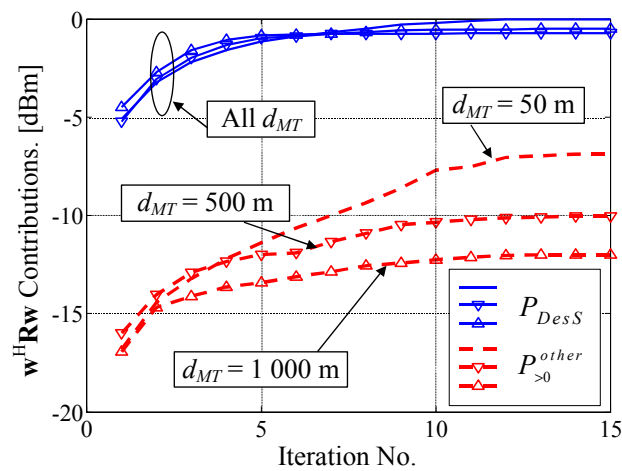


Figure 7.15 – Average P_{DesS} and $P_{>0}^{other}$ (thicker, dashed lines), for Sc #4u_mc_Gr_d, normalised to their maximum, for $M = 12$.

In a similar manner, for Sc #4u_mc_Sp_d, $M = 12$, the average evolution of the several \mathbf{R} components is given in Figure 7.16, for the several BS-MT distances. One again sees how the relative weight of the $P_{>0}^{other}$ component varies relative to the DesS power. Though this is the most important interference component among all, as seen before, the remaining interference components also lower with increasing distance. Again, it is seen that the DesS power does not show any significant variation with distance, as stated before, and noise only registers a rise, though minimal, for the 1 000 m situation. As in the case of the previous scenarios, these results are in agreement with the corresponding SINR and BG dependencies, described before, also showing that the component most responsible for the definition of the beamforming performance is the $P_{>0}^{other}$ term.

In the previous section, the involved power terms corresponding to two major different grouping situations have already been presented. In sub-Section 7.2.3, where the beamforming performance has been described as a function of the MT displacement and grouping, it has been

shown that the differences between the BGs relative to Sc #4u_mc_Gr_d and Sc #4u_mc_Sp_d are not substantial, though showing a tendency for the latter case to lead to better values. Through Figure 7.14 and Figure 7.16, one mainly sees differences in P_{DesS} and $P_{>0}^{other}$ components, which are anyway minimal as the differences in BGs are, between the results relative to the same BS-MT distance. P_{DesS} levels are higher, and $P_{>0}^{other}$ powers are lower, in the Sc #4u_mc_Sp_d case, keeping in mind that, according to the extensive description of the problem in Section 6.4, this analysis concerns the iteration numbers near the 5th iteration (not the M^h , where it is most clear that the interference content is larger). The fact that P_{DesS} is larger, while $P_{>0}^{other}$ power is lower, is an expected result for the case that the MTs are randomly spread, being a consequence of the better capacity for the beamformer to angularly discern DesS from NDesI.

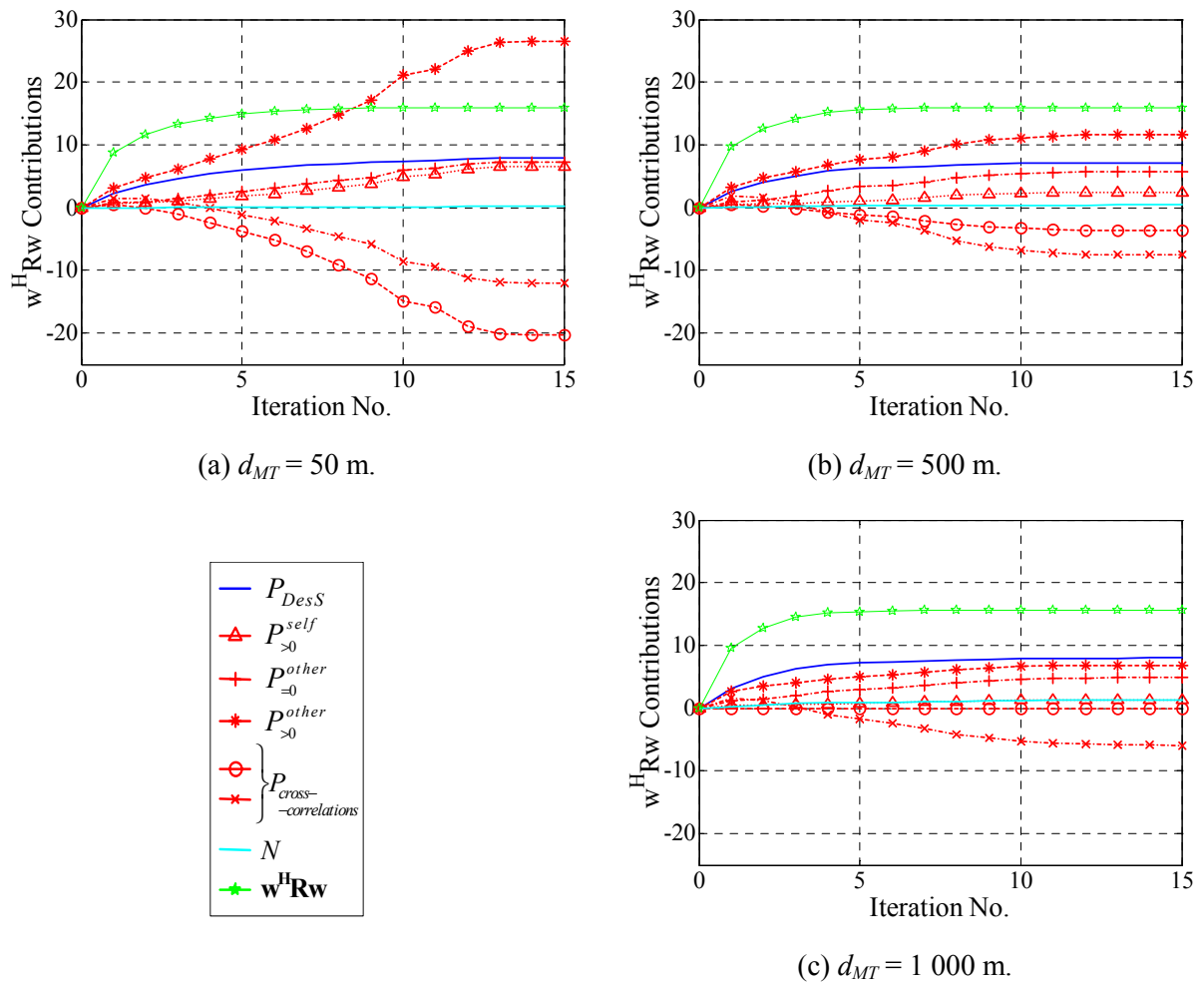


Figure 7.16 – Average power terms due to the composition of \mathbf{R} , for $M = 12$, Sc #4u_mc_Sp_d.

Concerning the case of MT_1 in Sc #4u_mc_Se_A, one expects higher P_{DesS} levels, accompanied by even lower NDesI ones, comparing to the previous cases, since the positioning of

MTs allows for the particularly favourable suppression of the latter, while not having any relevant interference opposing the acquisition of the DesSs, in the angular domain. Once again, keeping in mind that the significant iteration is near the 5th iteration, in Figure 7.17 the involved components in fact show those tendencies, which can be compared to the results plot in Figure 7.14 (b) and Figure 7.16 (b), for MTs at 500 m from the BS. In Table 7.5, the corresponding term values are indicated, for these scenarios, better helping in the observation of the stated results.

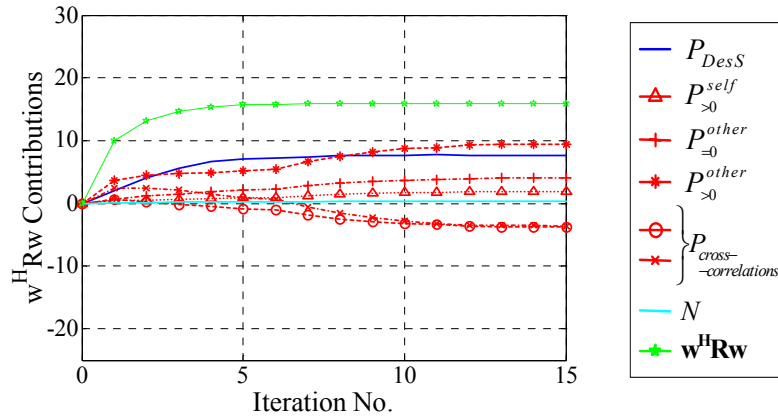


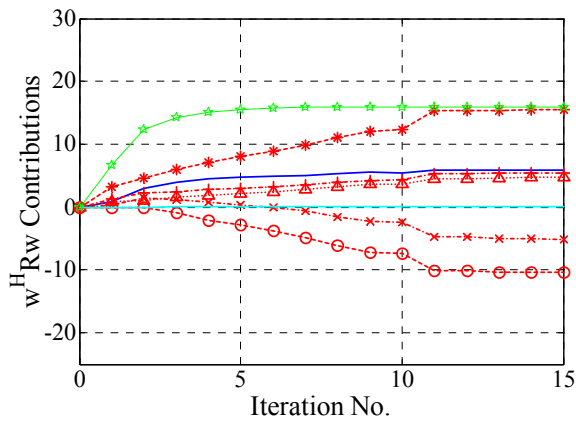
Figure 7.17 – Average power terms due to the composition of \mathbf{R} , for $M = 12$, Sc #4u_mc_Se_A, MT₁.

Scenario #	P_{DesS} [dBm]	$P_{>0}^{other}$ [dBm]	$P_{DesS} - P_{>0}^{other}$ [dB]
Sc #4u_mc_Gr_05	-0.81	-10.89	10.08
Sc #4u_mc_Gr_5	-0.87	-11.35	10.48
Sc #4u_mc_Gr_10	-0.33	-12.82	12.49
Sc #4u_mc_Sp_05	-0.88	-11.01	10.13
Sc #4u_mc_Sp_5	-0.48	-11.14	10.66
Sc #4u_mc_Sp_10	-0.02	-13.40	13.38
Sc #4u_mc_Se_A, MT ₁	0	-13.46	13.46

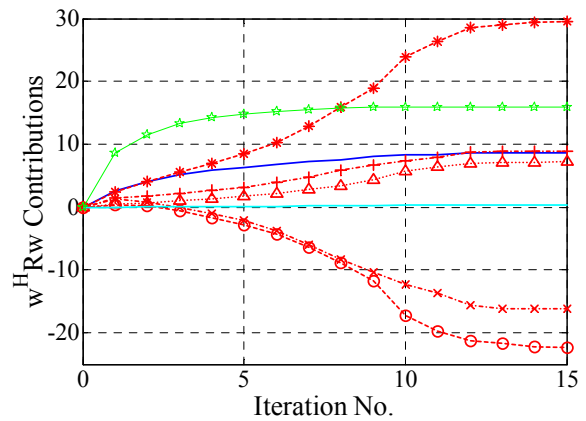
Table 7.5 – Average P_{DesS} and $P_{>0}^{other}$ power term values, for several $L = 4$ scenarios, being normalised to the P_{DesS} maximum among all.

As far as the dependence with sectorisation is concerned, it is also important to analyse the relative values of the involved power components, as function of the various sector widths. The same components are presented in Figure 7.18 and Figure 7.19, for 50 and 1 000 m, respectively, and sector widths of 180°, 120° and 60°.

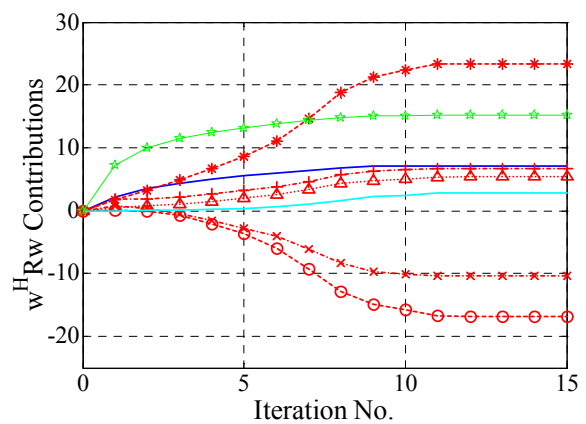
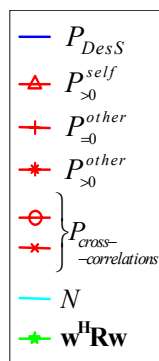
As before, the same relations among the several terms are present, the delayed NDesI from the remaining MTs, in the perspective of each MT, being the largest interference contributor. Additionally, among 50 and 1 000 m, it is clear that the components' variations as a function of the sector width are much more significant for 50 m, with the exception of the DesS term, which again reveals larger independence with such parameters, among all terms. Anyhow, such term shows an increase from 180° to 120° sector width, in agreement with the respective SINR evolution given in Table 7.3. Concerning the noise power component, it is seen that it increases, though with relatively small importance, as the angle-spreads narrow, i.e., for the lower sector widths with $d_{MT} = 50$ m, or for all $d_{MT} = 1\,000$ m cases. As it is described in sub-Section 7.3.7, such noise power behaviour is particularly present in the MaC scenario cases, in the case that MTs are also grouped, making use of narrower AoA spreads.



(a) 180° sector width.

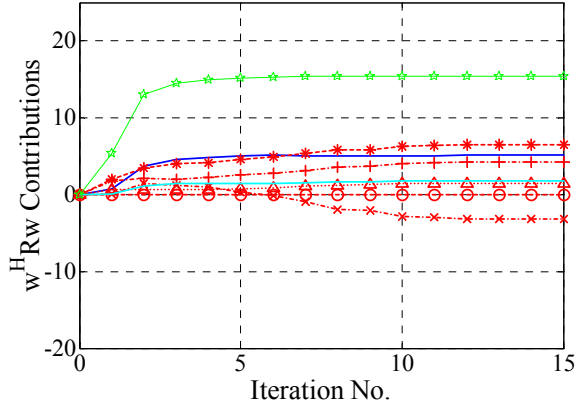


(b) 120° sector width.

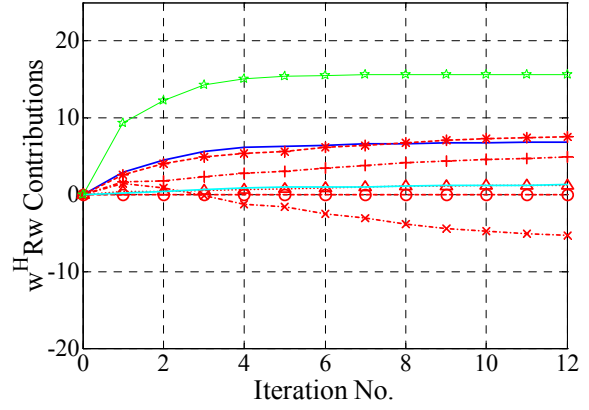


(c) 60° sector width.

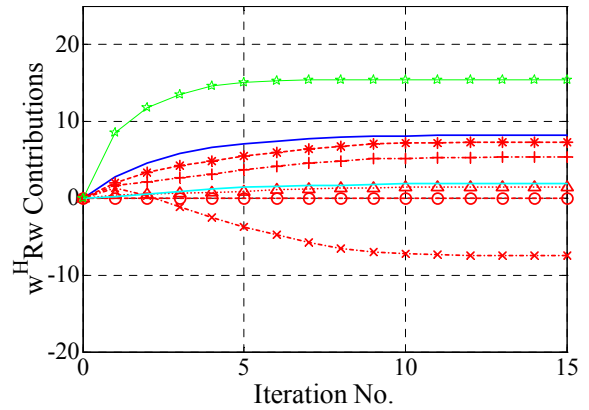
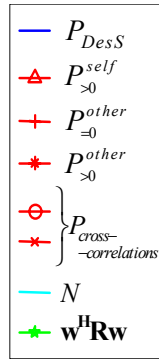
Figure 7.18 – Average power terms due to the composition of \mathbf{R} , for $M = 12$, several sector widths, Sc #4u_mc_Gr_05.



(a) 180° sector width.



(b) 120° sector width.



(c) 60° sector width.

Figure 7.19 – Average power terms due to the composition of \mathbf{R} , for $M = 12$, several sector widths, for Sc #4u_mc_Gr_10.

7.3 Performance Dependence on MaC Scenarios Parameters

7.3.1 MT-BS Distance

From Figure 7.20, corresponding to scenarios Sc #Lu_Mc_Gr_d_200, it is clear that BG does not show a significant dependence with distance. Such is a general result, also for any number of array elements. Keeping in mind that these scenarios are those in which all MTs are making use of the same scatterers to convey signals towards the BS, contributing to common ToAs and AoAs, and fundamentally limiting the advantageous positioning of lobes and nulls, one then understands that the change in distance, with the consequent variation in temporal and angle-spread, does not strongly determine beamforming performance. Furthermore, as it is also seen in Figure 7.20, for lower L , there is a slight tendency for BG to be lower for larger BS-MT distances; by increasing the number of active MTs, this already small BG sensitivity to distance tends to decrease even more. This is also an expected behaviour, since the more severe the channel is, in terms of the number of active users or of orthogonal and non-orthogonal codes involved, the more the DCIRs are commonly shared by each

link, with the NDesI power increasing for the same channel characteristics, at the same AoAs and ToAs as those of the DesS contributions.

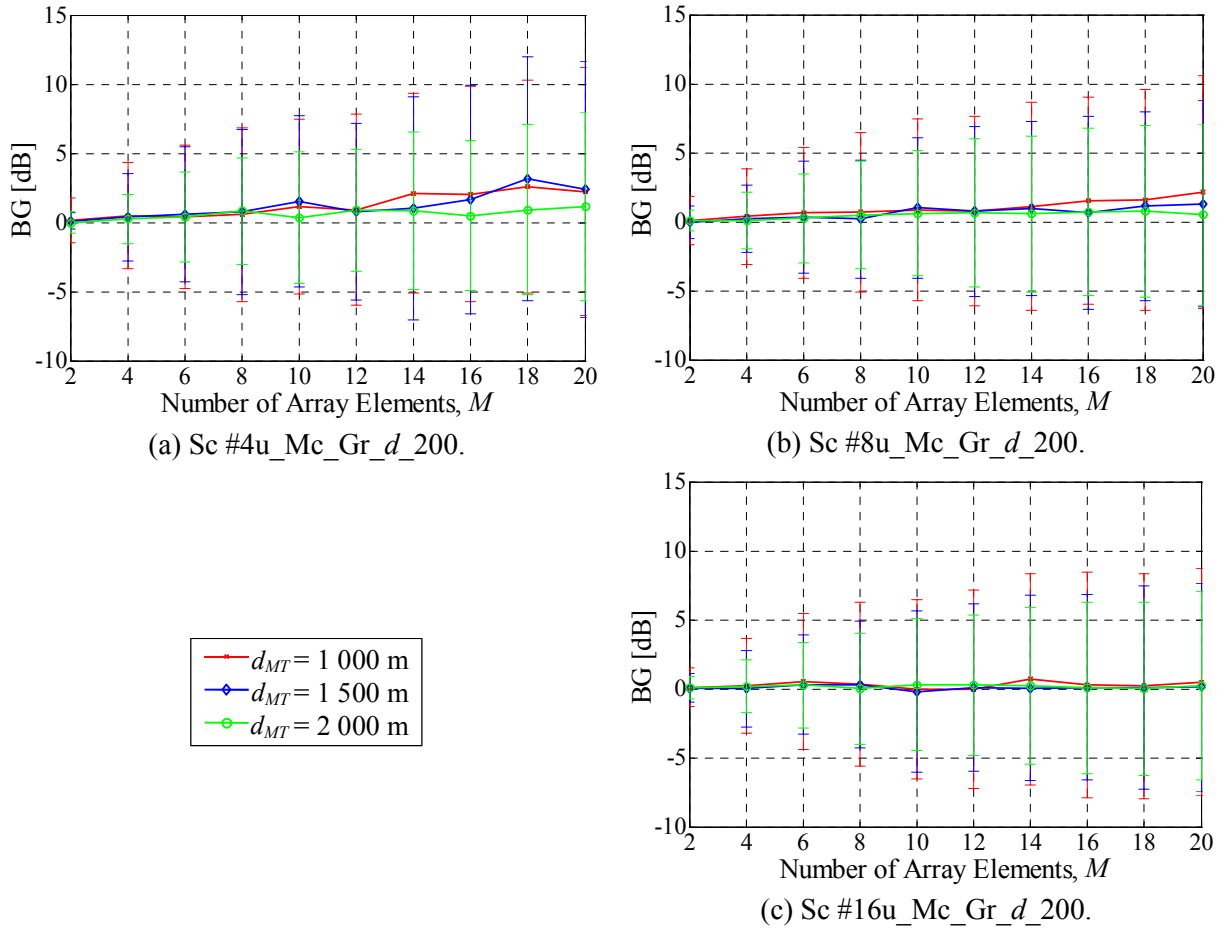


Figure 7.20 – BG, function of M , for several values of d_{MT} , Sc #Lu_Mc_Gr_d_200.

Table 7.6 provides some average BG values for Sc #4u_Mc_Gr_d_200 and Sc #16u_Mc_Gr_d_200, for $d_{MT} = 1\ 000$ and $2\ 000$ m, more quantitatively verifying the described results.

L	M	d_{MT} [m]	BG [dB]
4	4	1 000	0.49
		2 000	0.26
4	20	1 000	2.24
		2 000	1.14
16	20	1 000	0.48
		2 000	0.22

Table 7.6 – BG, function of L , M and d_{MT} , for Sc #4u_Mc_Gr_d_200 and Sc #16u_Mc_Gr_d_200.

Regarding the other MaC scenarios presented in Table 4.5, Sc #Lu_Mc_Sp_d_200, where the same MTs are angularly randomly spread within the 180° sector, Figure 7.21 and Figure 7.22 provide the obtained results. From these, it is seen that the distance relationship is slightly more significant, though still small, results also presenting larger fluctuations due to the additional random parameter. For 4 or 8 active links, a tendency for BGs to be lower for larger BS-MT distances is more visible, one seeing that BGs tend to depend less on d_{MT} as L increases. Such behaviour roots from the fact that MTs are angularly spread, uniformly distributed; for larger number of MTs, AoAs tend to differ less among links, and BG's dependence on their respective AoAs is less defined; the probability of AoAs not being shared lowers as L increases, meaning that the angle-spread of each DCIR also loses its importance.

From the several MaC scenarios' results, it is then concluded that, for any number of active links, the MT-BS distance does not have a significant impact on BG, from among the tested scenarios. Anyhow, it is understandable that the beamformer may show a tendency to lower SINRs and BGs for larger distances, since a nearly invariable delay-spread is accompanied by an angle-spread reduction (Table 4.9), leading to higher minimum achievable NDesI powers due to the closer vicinity of arriving signals.

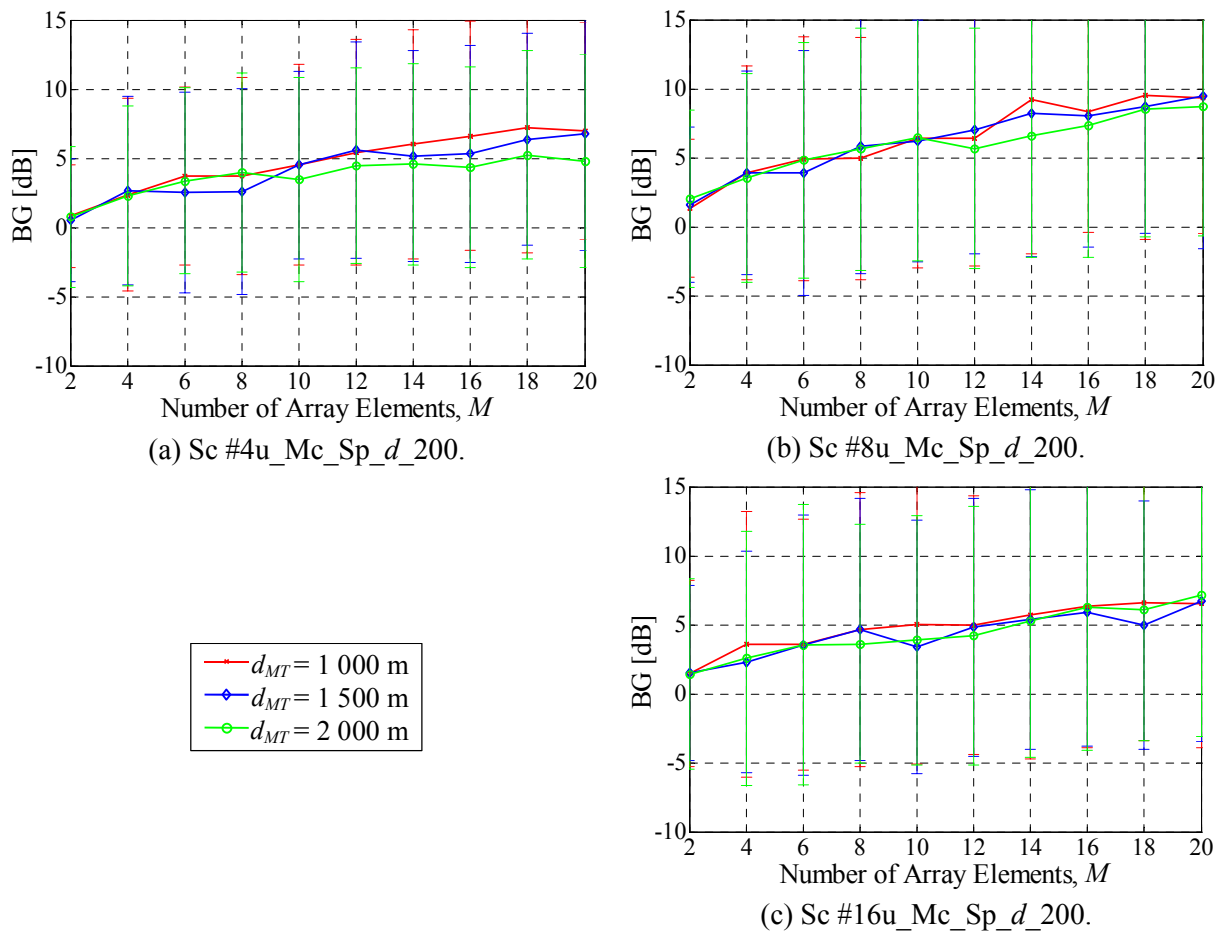


Figure 7.21 – BG, function of M , for several values of d_{MT} , Sc #Lu_Mc_Sp_d_200.

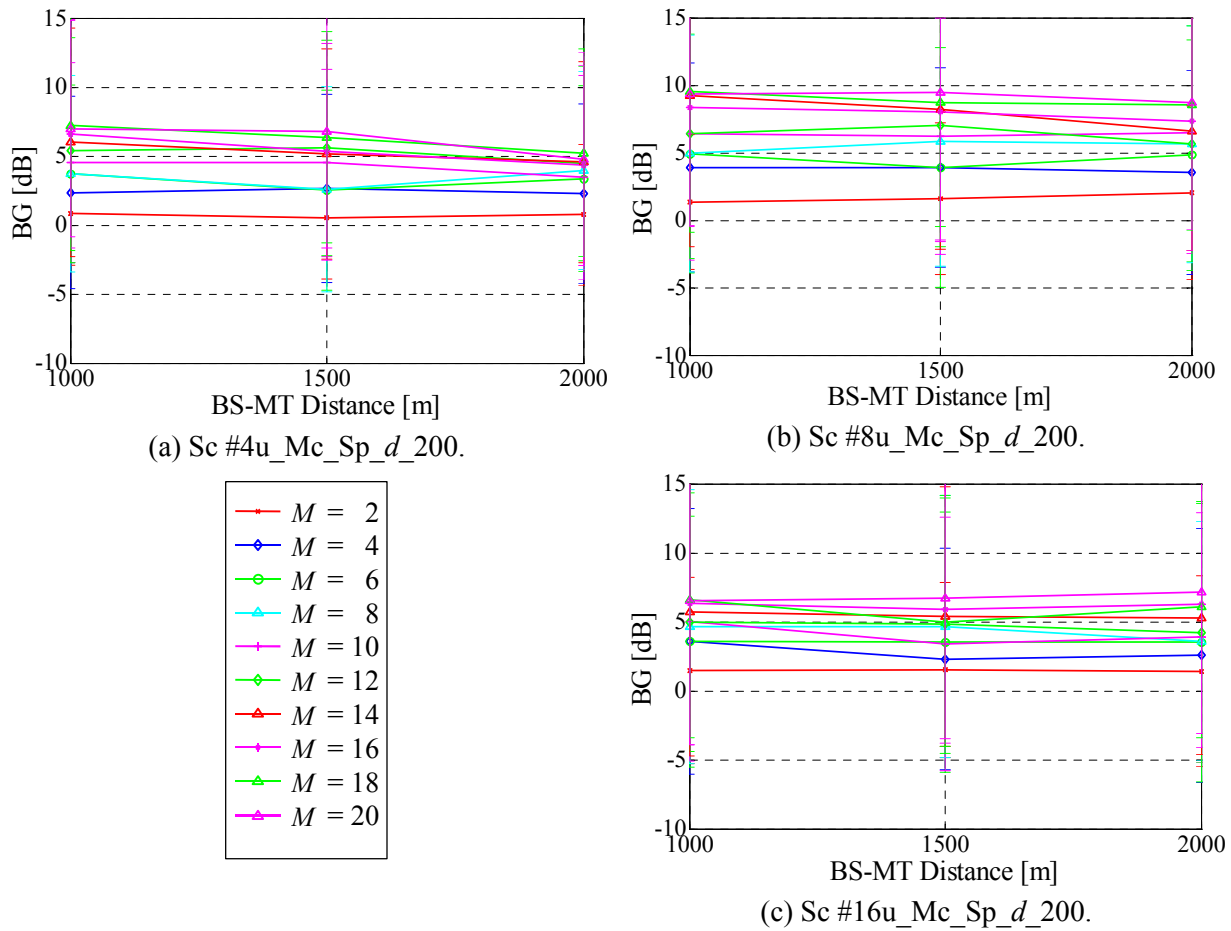


Figure 7.22 – BG, function of d_{MT} , for several values of M , Sc #Lu_Mc_Sp_d_200.

7.3.2 Scattering Circle Radius

In the cases of grouped MTs, like Sc #Lu_Mc_Gr_15_r, BG results are consistent with those previously described as a function of MT-BS distances, i.e., beamforming is highly limited, leading to BGs close to 0 dB. This is so, independently of the scattering circle radius, or the closely related delay-spread (Table 4.9). Figure 7.23 shows exemplifying results. Though SINRs are negative and significantly decrease with increasing r , BGs do not indicate final SINR degradation, or improvement, in comparison to the single antenna case. Also, it is visible how SINRs are considerably affected by the delay-spread variation, while BGs are not. Such is an indication that, though the NDesI increases due to the increase of the delayed contributions (with the increase in r), the beamformer is still able to compensate for these, though doing so to the 0 dB BG ceiling.

As for the scenarios where the MTs are angularly spread, the dependency with the scattering circle radius presents different tendencies. Taking the example of Sc #16u_Mc_Sp_15_r, in Figure 7.24, both BGs and SINRs result lower as the radius increases.

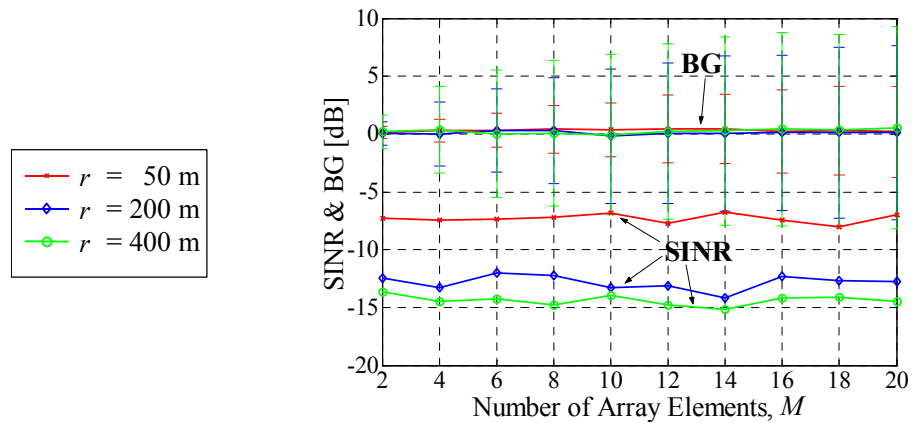


Figure 7.23 – SINR and BG, functions of M , for several values of r , Sc #16u_Mc_Gr_15_r.

The SINR tendency is a natural result, as it was stated before. Regarding BGs, also as expected and as before, its sensitivity is much lower than that of SINR, as function of r . Nevertheless, such variations may reach 4.6 or 3.6 dB, from 50 to 400 m, or to 200 m, respectively, decreasing as the angle-spread increases. This happens since, by angularly spreading MTs, there will be neighbouring cluster and scatterer contributions to ToAs and AoAs that are not shared among links, meaning that with higher probability the beamformer may better angularly discern DesS from NDesI; as the scattering area radius increases, the probability for AoAs overlapping increases, the beamforming potential being reduced, leading to lower BGs; also, with larger AoA sectors, the array is presented with large sectors of DesS, but also of NDesI, meaning that more difficultly the beamformer is able to place as many zeros as possible within such NDesI sector, inevitably involving undesired lobes near such directions.

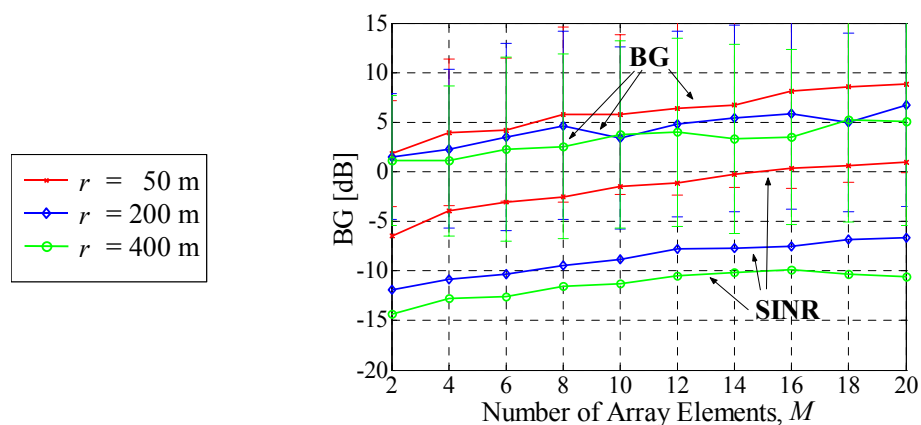


Figure 7.24 – SINR and BG, functions of M , for several values of r , for Sc #16u_Mc_Sp_15_r.

Scs #Lu_Mc_Se_A_r, with 50 or 200 m radii, also contribute to the analysis of the influence of the scattering radius, again involving a group of MTs, but also an isolated MT, at $\pi/4$. In the case of the grouped MTs, at $-\pi/5$, the BGs reach values close to 0 dB, as before, mostly independent from L ,

M or also r , as Figure 7.25 exemplifies. On the other hand, results relative to the single MT in scenarios like Sc #Lu_Mc_Se_A_r may show a larger dependency on r , with a radius of 50 m leading to BGs that can be at most 8.6 dB higher than those of 200 m radius, especially for lower L . The reason for this behaviour to be clearer is thought to root from the single and grouped MTs existing at fixed angles, with no random positioning, rendering the r effects to being most visible. The superimposition of angular sectors is naturally less important than in Sc #Lu_Mc_Sp_15_r, but the additional effect of placing lobes and nulls within the explicitly different AoA sectors has larger implications: by keeping MTs fixed, though being separate by much more than the involved AoA spreads (Table 4.9), larger NDesI sectors oblige the beamformer array pattern to place more lobes within them, delivering lower BGs. As for the way that L affects this dependence, one sees that for 16 MTs the r dependency is non-existent for the single MT, whereas for 4 MTs the grouped MTs show improvement with increasing r . In the former case, the independency with r shows a large disparity compared to the dependencies for the two lower L cases. Due to such, similar tests have been put forward for $L=8, 10, 12$ and 14 (though not shown), indicating the gradual tendency for the 50 and 200 m curves to fuse, as L increases.

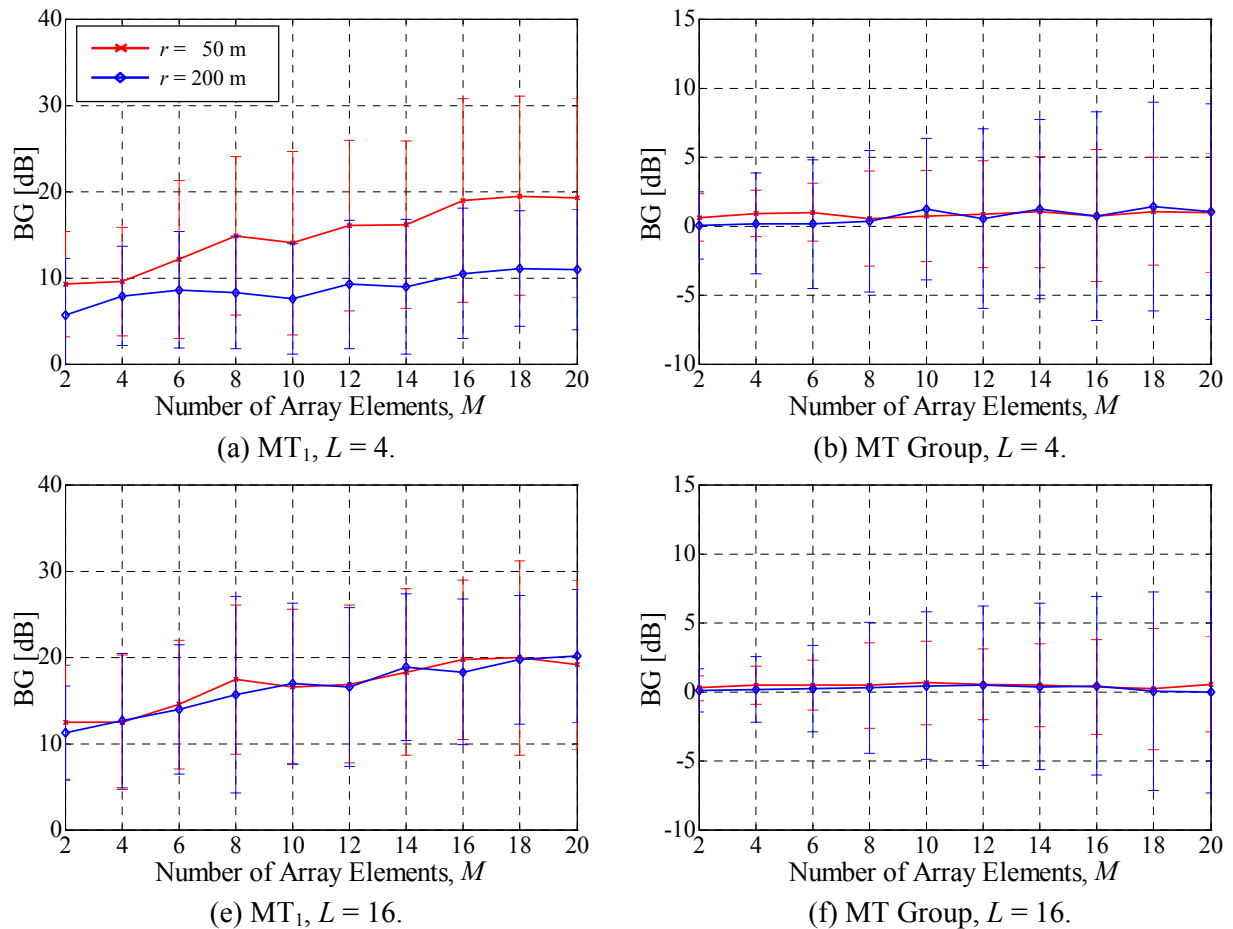


Figure 7.25 – BG, function of M , for several values of r , Sc #Lu_Mc_Se_A_r, $L = 4$ and 16 .

Scs #Lu_Mc_Se_B_r, with 50 or 200 m radii, again help in the analysis of the scattering radius influence on beamforming, where a single and the remaining MTs are angularly spread within the 1st and 4th quadrants, respectively. In Figure 7.26, Sc #16u_Mc_Se_B_r results are plot, where it is seen that the scattered MTs' ones are similar to those of Sc #16u_Mc_Sp_15_r (Figure 7.24). The Sc #16u_Mc_Sp_15_r ones are slightly better, since MTs are angularly spread over both the 1st and 4th quadrants, whether in the Sc #16u_Mc_Se_B_r case, the MTs are placed over the 4th only. Regarding both the single or grouped MTs, it is seen that larger r leads to a BG degradation, which increases with M , as happens with the previous cases. As in the Sc #Lu_Mc_Sp_15_r cases, such is justified, on the one hand, by the higher probability for AoAs to be superimposed as the radius of the scattering circle increases, and on the other, by the increase in NDesI power as the radius increases, as stated before. In the case of the MT in the 1st quadrant, the effect of the radius is also evident, registering differences above 3 dB, between 50 and 200 m. These differences are less evident than those in Se_A case, due to the random positioning.

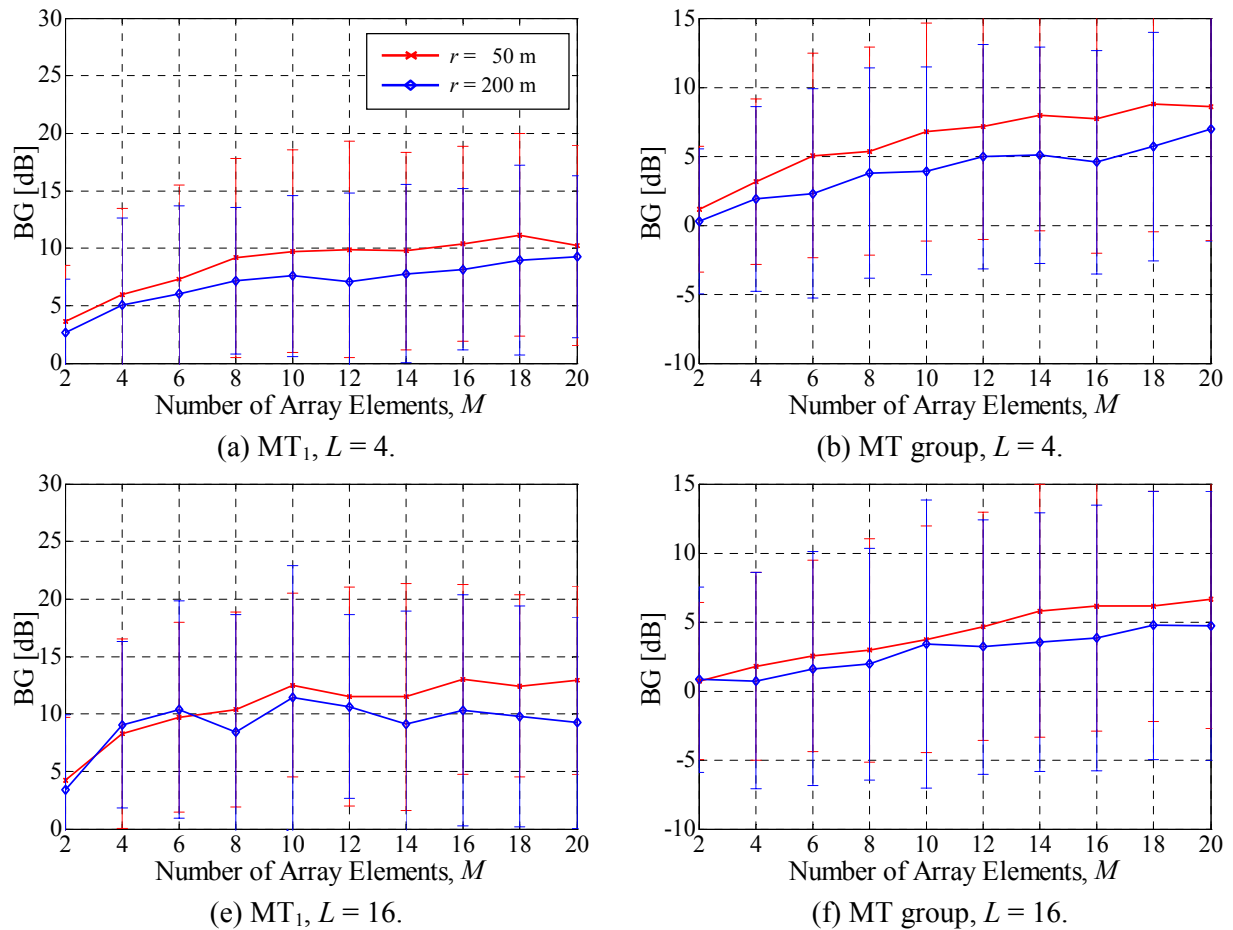


Figure 7.26 – BG, function of M , for several values of r , Sc #Lu_Mc_Se_B_r, for $L = 4$ and 16.

Regarding the beamforming behaviour towards the variation of the MaC scattering circle radius, concerning the scenarios simulated, the results show that: there is no dependency on r , if MTs

are grouped together, BGs being kept very close to 0 dB; in the case that MTs are spread, larger radius implies worse beamforming performance, BGs varying up to 5 or 3.8 dB, from 50 to 400 or 200 m, respectively, among the tested scenarios; if a single MT is explicitly angularly separate from the others, then the influence of r on its corresponding beamforming is in the same sense depending on how that and the other MTs are distributed; an MT that is in a well defined, separate angular sector, leads to corresponding BGs up to 8.6 dB lower, with scattering circle radius varying from 50 to 200 m, as long as the remaining MTs are sufficiently separate from it, so as not to significantly share AoAs; in the case that a single MT may be located closer to the remaining MTs, sharing more AoAs, then the increase in the radius leads to the narrowing of exclusive sectors, with BGs being reduced, by more than 3 dB from 50 to 200 m; generally, the presented dependencies show to be larger for larger M or lower L .

7.3.3 Number of Array Elements

In the previous analysis description, though not directly covered, it has been seen that the effects of the number of array elements strongly depend on the type of MT grouping and displacement present: in the cases where MTs are closely located, making use of the same scatterers to reflect signals towards the BS, the higher number of array elements does not involve any BG or SINR increases (Figure 7.20, Figure 7.23, and Figure 7.25, for several scenarios); a group of several MTs that are angularly spread over sectors relatively larger than each corresponding DCIR angle-spread lead to BGs that increase with M (Figure 7.21, Figure 7.24, and Figure 7.26); these variations range from near 4 to 7 dB, M varying from 2 to 20 (depending on the MT-BS distances and the scattering circle radius), and the second order derivative, function of M , is close to 0; in the case that a single MT is separate from the remaining MTs, but with a high probability of sharing AoAs, then BGs register increases of up to 10 dB, with a first order derivative that stronger varies with M , BGs reaching a well defined plateau (Figure 7.26); if such MT is more clearly separate from the remaining ones, then BGs may increase by at most 15 dB, approximately (Figure 7.25).

For the separate MT₁, in the Se_A case, where all MTs are fixed, contributing to very well defined AoAs towards which lobes and nulls can be most efficiently directed, the increase in the number of M leads to BGs increasing close to linearly. For Se_B, with higher probability of the single MT AoAs being shared among all links, such MT involves a fast rise from 2 to 4 elements, presenting a plateau near 10 dB. In fact, for larger scattering circle radius, comparing 200 to 50 m, the probability of sharing AoAs is even larger, leading to a more defined BG plateau, as function of M (Figure 7.26).

From these results, as it happens in the MiC scenario situations, it is seen that SINR and BG do not register any particular improvement in the case that L_T (provided in Table 4.9) is lower than M . Where a significant improvement would be expected while increasing M , the array presenting enough DoFs to discern all L_T codes, in fact BG may exhibit a plateau. In light of the portrayed performance

dependencies on the scenarios, the angular domain again shows its importance in this way. Another indication of that is provided by the BG results for MT_1 , in Sc #16u_Mc_Se_A_r and #16u_Mc_Se_B_r, the BG variation with M being a function of the angular distribution of all MTs present.

To further help on this analysis, the number of array elements has been taken to higher values. Figure 7.27 shows the results, for the Sc #Lu_Mc_Sp_15_200 case, for M up to 60, in steps of 10. Besides the dependency with MT-BS distance becoming more evident, compared to the cases of Figure 7.21, the limited BG increases with M are more clearly seen. These further confirm that the temporal domain dependency on the number of orthogonal arriving codes is not the only limiting parameter, once more.

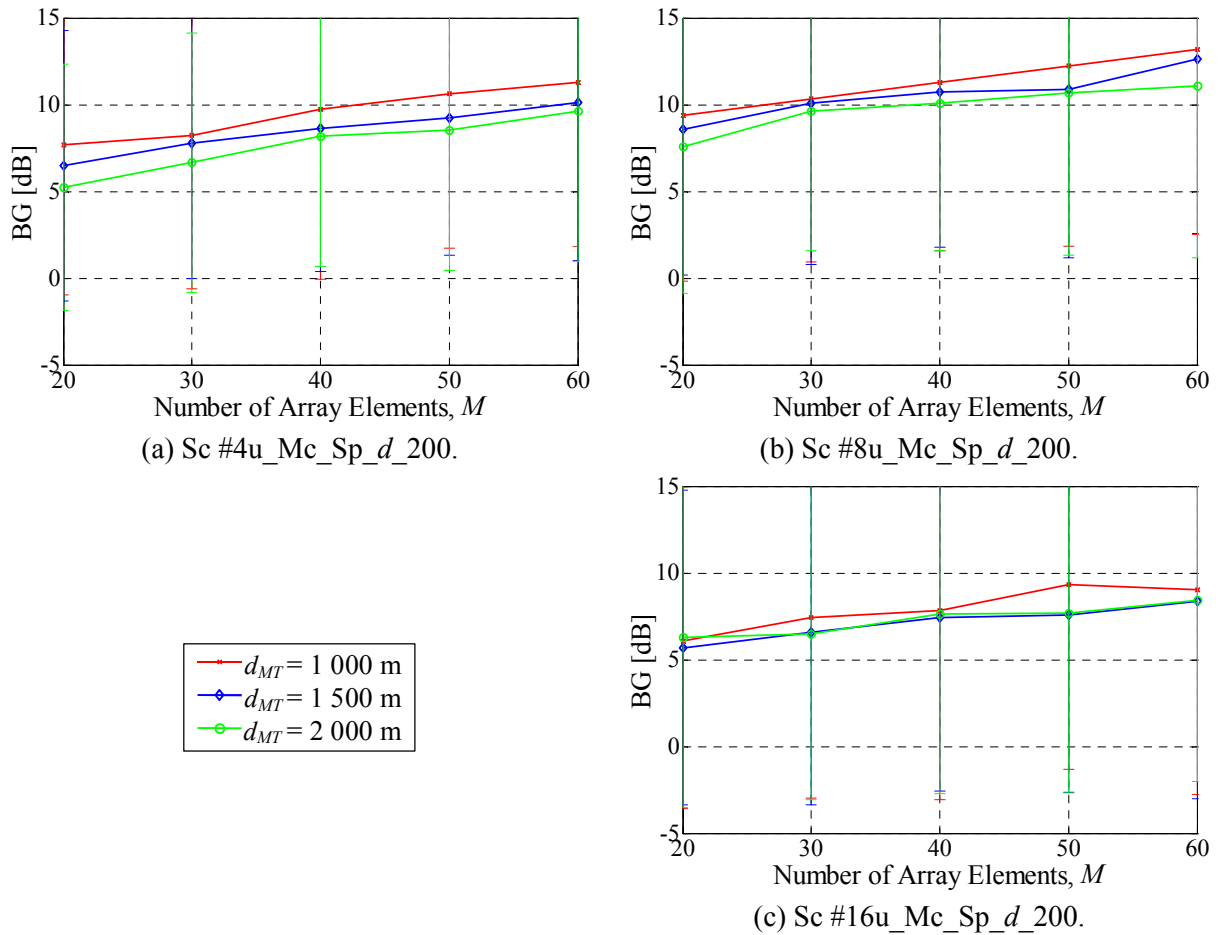


Figure 7.27 – BG, function of the M , for several values of d_{MT} , Sc #Lu_Mc_Sp_d_200, for larger number of array elements.

7.3.4 Angular Displacement and Grouping of MTs

In the same way that the importance of the angular positioning and grouping of MTs has already, and will further, come about in other sections, this matter again requires specific attention in the MaCs case. Several points are at stake, concerning the angular positioning of the active MTs.

Firstly, there are situations where there is a group of MTs in the same location (in Sc #Lu_Mc_Gr_d_r, #Lu_Mc_Se_A_r and #Lu_Mc_Se_C_50), and others where the MTs are angularly spread (Sc #Lu_Mc_Sp_d_r and #Lu_Mc_Se_B_r). Secondly, the cases where an isolated MT is present, making use of scatterers different from those reflecting signals from the remaining MTs, are not only realistic practical situations but are also important contributions to the analysis.

As it has already been described, the grouping of MTs at the same location is inherently limiting due to the usage of common scatterers to convey the signals to the BS. Furthermore, such happens independently of the number of active users, array elements, BS-MT distance and scattering circle radius, resulting in BGs close to 0 dB. For the same scenario parameters, grouped MTs lead to lower BGs compared to the same, but angularly spread, MTs. For example, if $r = 50$ m and $M = 8$, 4 active users achieve average BGs of 1.2 or 6.7 dB in Sc #4u_Mc_Gr_15_50 and Sc #4u_Mc_Sp_15_50, respectively. Graphically, Figure 7.20 and Figure 7.21 have already shown the type of behaviour, for $r = 200$ m.

Focusing only on the Se_A, B and C scenarios of Table 4.6, the expected results are that the single BS-MT link should always achieve best BG, compared to the remaining MTs of the same scenario. These are the situations where, in the perspective of MT₁, interference arrives from a very well defined and limited angular position, i.e., being relatively easy for the beamformer to place a sharp null towards such directions, without greatly affecting the DesS power from MT₁. For Sc #Lu_Mc_Se_A_r and #Lu_Mc_Se_C_50, the best results among all scenarios have been obtained for the single MT, as expected; BGs of the grouped MTs are similar to those of the grouped MTs in Table 4.5 scenarios, for the same number of MTs, BS-MT distance, region radius; the single MT ones are slightly lower in the Sc #Lu_Mc_Se_B_r and #Lu_Mc_Se_C_50 cases, compared to Sc #Lu_Mc_Se_A_r, due to the random positioning. Sc #Lu_Mc_Se_C_50 results are shown in Figure 7.28.

In Figure 7.25 and Figure 7.28, Sc #16u_Mc_Se_A_r and Sc #16u_Mc_Se_C_50 results already made clear how BGs may differ by 10 to 35 dB, between the single and grouped MTs, depending on the number of array elements. As for Sc #16u_Mc_Se_B_r, Figure 7.26 also shows large differences, though, for the reasons mentioned, these are lower. Its results are closer to those of Sc #Lu_Mc_Sp_15_r, further indicating that, limiting the $L-1$ MTs to the 90° sector in Sc #Lu_Mc_Se_B_r, statistically tends to the case of Sc #Lu_Mc_Sp_15_r, where several MTs are randomly placed within the 180° sector. Furthermore, as it was seen, the performance relative to the single MT highly depends on the grouping of the remaining ones, possibly reaching a BG plateau as function of M .

Additional scenarios have been introduced, based on the Sc #Lu_Mc_Sp_15_200, but placing MTs at fixed, not random, angles, being equally separated by gradually larger angles, i.e., varying the superposition of involved scattering circle areas. This case has been applied for $L = 4$, with scattering radius of 200 m, at 1 500 m from the BS, separating the MTs from 0° to $\pm 25.3^\circ$, having kept in mind

that the incoming signals cover a an angular sector of 15.2° maximum, approximately (Table 4.9). MTs have been separated by multiples of $1/12$ of the angle covered by each (1.27°). The results have been evaluated in terms of BG, for a ULA of $M = 12$ elements, as function of the angular separation multiple of 1.27° , referred to as index x , and are shown in Figure 7.29, being approximated by a 5th degree polynomial fit curve (with a residual norm of 1.88, for the shown angular separation index span). The figure confirms several relevant points, in accordance to many of the past descriptions. Expectedly, BGs rise as the angular separation increases, reaching above 95 % of its maximum, from the 12th index upwards, the limit at which the angular sectors are fully disjoint. The full superposition of scattering areas, as it has been seen, leads to BGs close to 0 dB, quickly leading to positive results as the number of uncommon scatterers increases.

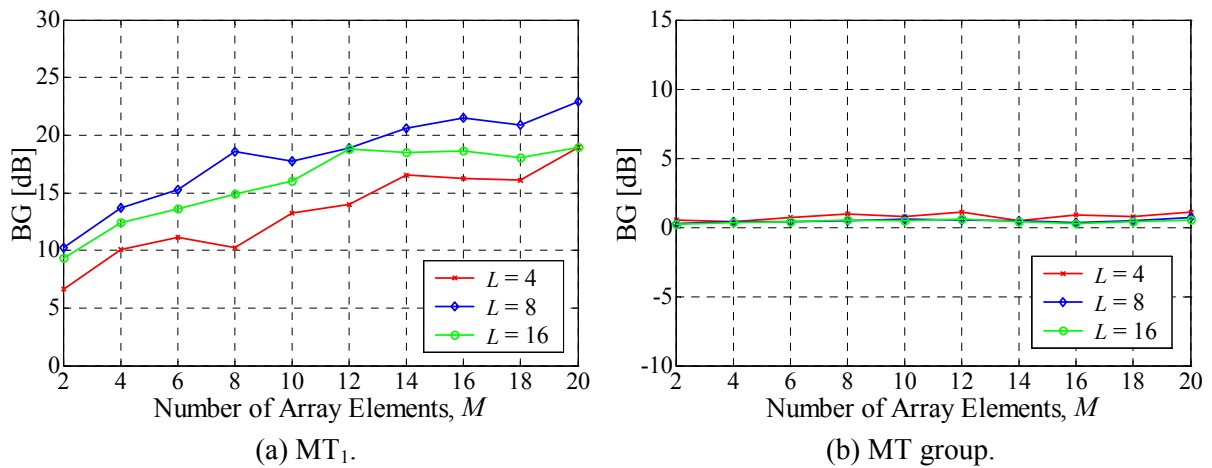


Figure 7.28 – BG, function of M , for several values of L , for Sc #Lu_Mc_Se_C_50.

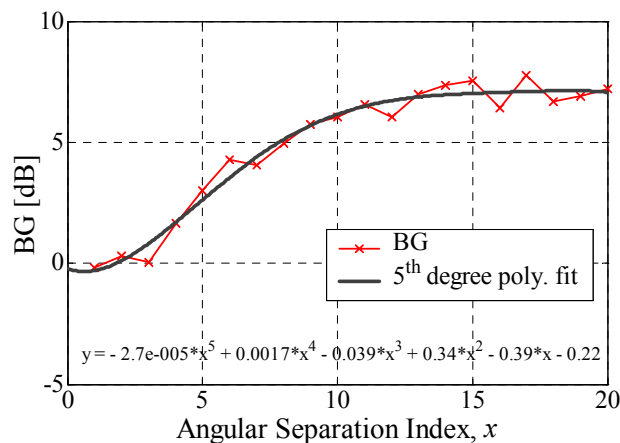


Figure 7.29 – BG, function of the MT angular separation, for 4 equally angularly spaced MTs.

To conclude, the several scenarios have made clear how important the grouping of MTs is to the beamforming performance, critical limitations being registered if MTs are in the very close

vicinity, being subject to the same set of scatterers around them; angularly spread MTs lead to positive BGs, being very dependent on the other parameters; MTs that are clearly separate from the remaining ones lead to BGs of up to 35 dB, depending on the number of array elements and placement of the remaining MTs. The displacement and grouping of MTs result in the largest variations in BG, among all the varied parameters.

7.3.5 Cluster Density and Average Number of Scatterers

One of the main issues at stake is the number of reflections from MT to BS, i.e., the number of signals, N_{mp} , arriving at the BS from each of the scattering circles, for the same radius.

The scenarios where MTs are grouped together, Sc #Lu_Mc_Gr_15_r and Sc #Lu_Mc_Gr_15_r_ld, present tendencies for lower N_{mp} to lead to lower BGs, for the same scattering circle radius. Figure 7.30 exemplifies BG differences, for $r = 200$ m, $L = 4$ and 16, anyway revealing a relatively small and not very well defined dependence on N_{mp} . For 50 m radius or for $L = 4$, the registered dependencies are relatively larger, though still of the same order and difficult to define. The same applies for the MT groups in Sc #Lu_Mc_Se_A_r and #Lu_Mc_Se_C_r. These are also expected results, being the cases of all MTs contributing to common ToAs and AoAs, at BS, where the inherently limited beamforming should not depend significantly on the number of incoming rays. Anyway, by reducing the number of incoming rays, even sharing common ToAs and AoAs, leads to even lower signal richness and larger DCIR correlation among links, justifying the lowering of BGs.

Comparing the cases where MTs are angularly spread, the 4th quadrant MTs in Sc #Lu_Mc_Se_B_r with those in Sc #Lu_Mc_Se_B_r_ld, the BG variations that have been registered are even less significant, indicating that such parameters do not have impact on the BG while MTs do not share ToAs or AoAs.

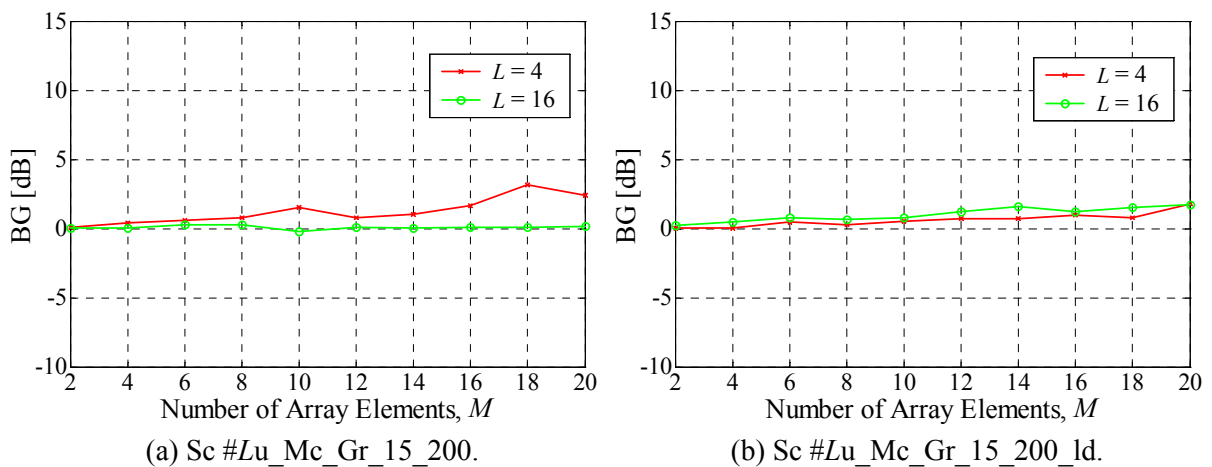


Figure 7.30 – BG, function of M , for $L = 4$ and 16, Sc #Lu_Mc_Gr_15_200 and Sc #Lu_Mc_Gr_15_200_ld.

The separate MT link in Sc #Lu_Mc_Se_A_r and #Lu_Mc_Se_C_r does present a significant change, BG rising as N_{mp} decreases, with more consistent and relatively larger relative changes for a scattering radius of $r = 50$ m, for lower values of L . In Figure 7.31 and Figure 7.32, BGs results as a function of M are shown for Se_A and Se_C scenarios, for $r = 50$ m, $L = 4$ and 16. For example, in the case of Se_A scenarios, with $r = 50$ m, $L = 4$, and $M = 12$, the single MT leads to average 13.7 and 18.9 dB, for higher and lower N_{mp} , respectively; for $r = 50$ m, $L = 16$, and $M = 12$, BGs vary from 16.8 to 18.2 dB. For $r = 200$ m, the dependency on these parameters is not as clear.

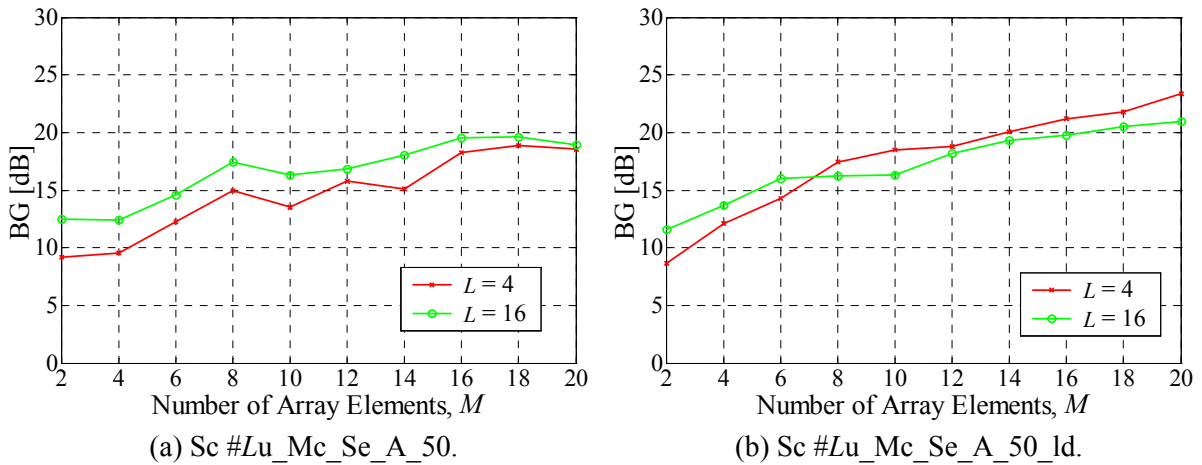


Figure 7.31 – BG, function of M , for $L = 4$ and 16, MT₁ in Sc #Lu_Mc_Se_A_50 and Sc #Lu_Mc_Se_A_50_ld.

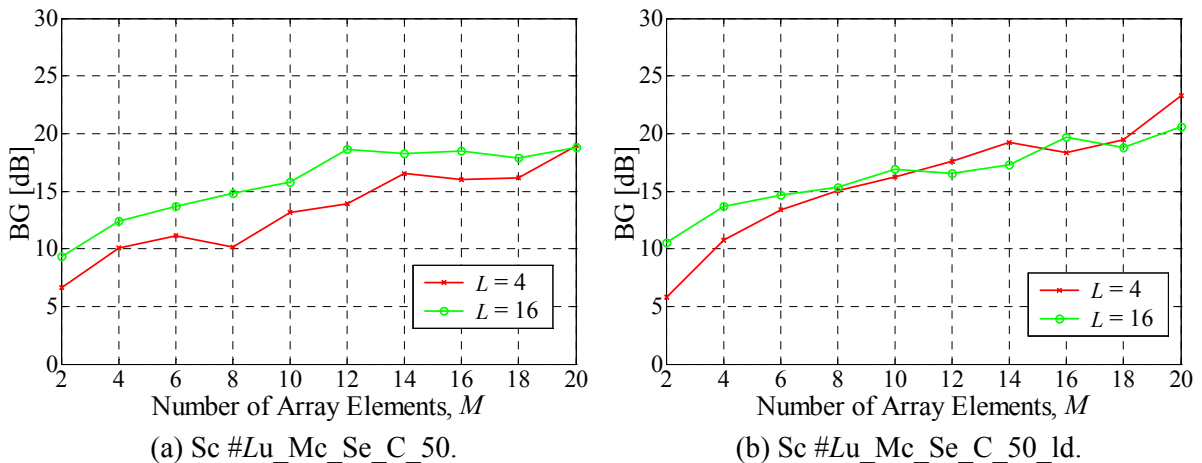


Figure 7.32 – BG, function of M , for $L = 4$ and 16, MT₁ in Sc #Lu_Mc_Se_A_50 and Sc #Lu_Mc_Se_A_50_ld.

Judging from the described results, one again must consider two situations that lead to different dependencies on the number of clusters and scatterers, for the same scattering circle radius: the situation of a group of MTs, together, and that of a separate MT. As N_{mp} increases, in the former case, the BGs inherently show relatively small degradations, whereas in the latter situation, BGs may

significantly increase. Furthermore, the BG sensitivity shows to be larger for lower L and r . In light of this, one then verifies that cluster density and scatterer number have impact on beamforming if the number of orthogonal codes, L_T , is sufficiently low. Then, lowering N_{mp} results either in lower independent beamforming freedom if MTs are grouped together, or in larger freedom in the case of a single MT. For this case, as it will be shown, for lower N_{mp} and the same angle-spread, the single MT involves higher achieved P_{DesS} power, and lower $P_{NDesI} + N$ powers. Again, the coherence of this resides in reasoning that higher angular density of DesS and NDesI leads to lower angular freedom in placing lobes and nulls, i.e., worse interference capacity and lower BG, not only due to the self-interference from MT_1 but also from the remaining ones.

7.3.6 Number of Active Links

As far as the number of active links is concerned, it is expected that BG and SINR decrease with increasing L , due to the NDesI power increase and the decreasing capability for the beamformer to discriminate signals, for the same propagation channel characteristics. As it can be well understood from the previous expositions, one fundamentally needs to distinguish three scenario cases: all MTs grouped together, all MTs spread along the 180° sector (1st and 4th sectors), and MTs which are grouped or close together leaving a single remaining separate one. Being already familiar with the characteristics of the corresponding results, this analysis is centred in the scenarios cases where $r = 200$ m, e.g., Sc #Lu_Mc_Gr_d_200, #Lu_Mc_Sp_d_200 and #Lu_Mc_Se_A_200.

In the case of Sc #Lu_Mc_Gr_d_200, as Figure 7.33 (a) and (b) exemplify, the results are naturally independent of the number of users, since BGs are limited to being close to 0 dB. The beamformer performance is inherently limited to the point that there is no significant dependency on L . On the other hand, for Sc #Lu_Mc_Sp_d_200, the results should reflect the referred tendency, for the BG to degrade with increasing L . In Figure 7.33 (c) and (d), the outcome of the Sc #Lu_Mc_Sp_d_200 example is provided. It is generally seen that, in fact, BG presents improvement from 4 to 8 active users, degradation from 8 to 16, and even a slight improvement from 4 to 16 users, i.e., the sensitivity of BG on L does not follow the anticipated trend. Moreover, by randomly spreading MTs within the 180° sector, it is more likely that 16 users have their incoming signals superimposed, at the BS, compared to the 4 users case, being expected to lead to further degradation. Even for larger number of array elements, from 10 to 60, the same sort of results have been obtained, with larger BGs for 8 active users, as it is depicted in Figure 7.34.

As in the MiCs case, described in sub-Section 7.2.5, Number of Active Links, these somewhat unpredicted results are justified by the differing and varying derivatives of the single element and beamformer's SINRs, as functions of L . Figure 7.35 shows such single element and beamformer SINR behaviour, for Sc #Lu_Sp_15_200, and various M values. Such type of results has also been obtained for the MiC scenarios case (sub-Section 7.2.5).

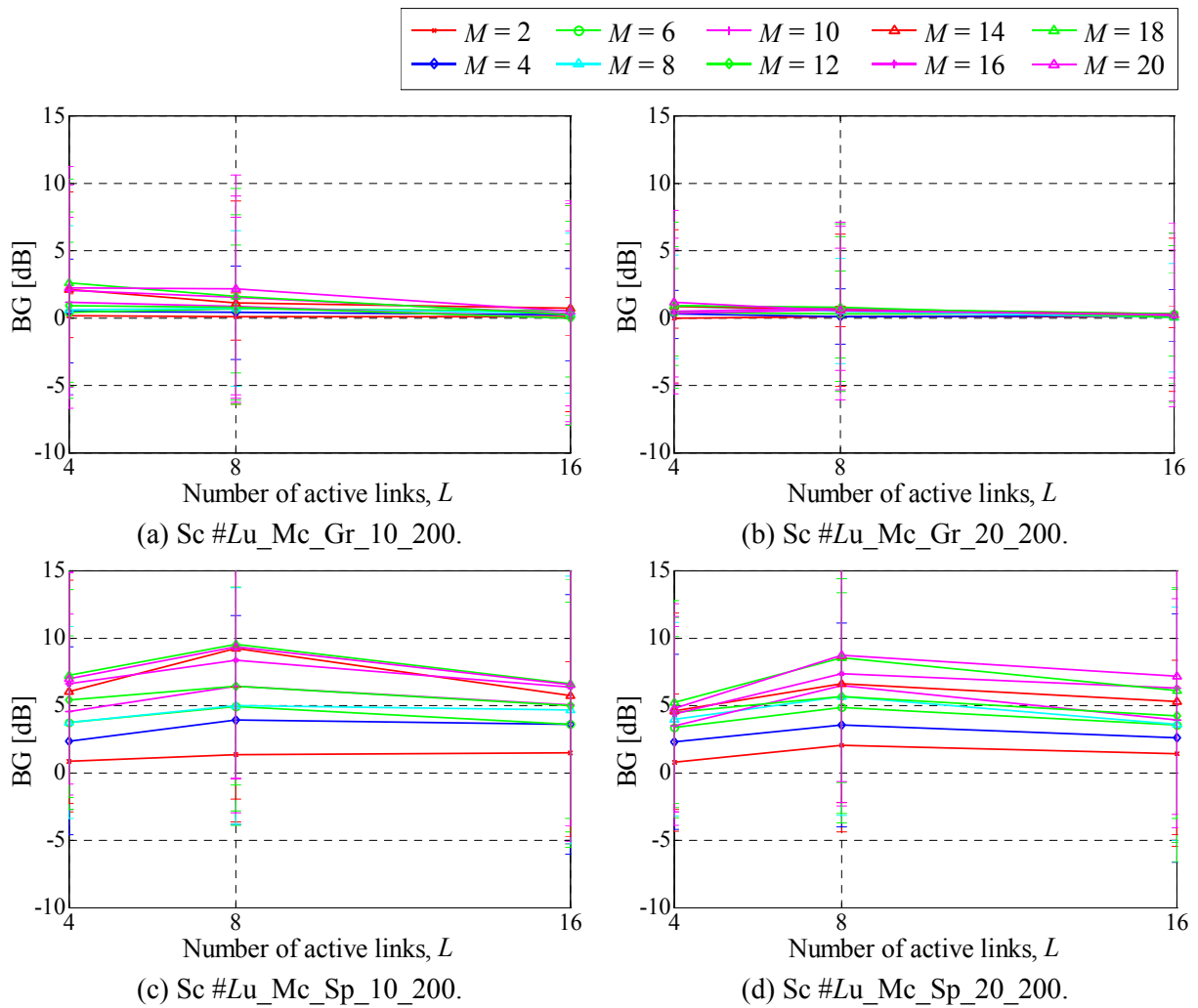


Figure 7.33 – BG, function of L , for several values of M , Sc #Lu_Mc_Gr_d_200 and Sc #Lu_Mc_Sp_d_200, for $d_{MT} = 1\ 000$ and $2\ 000$ m.

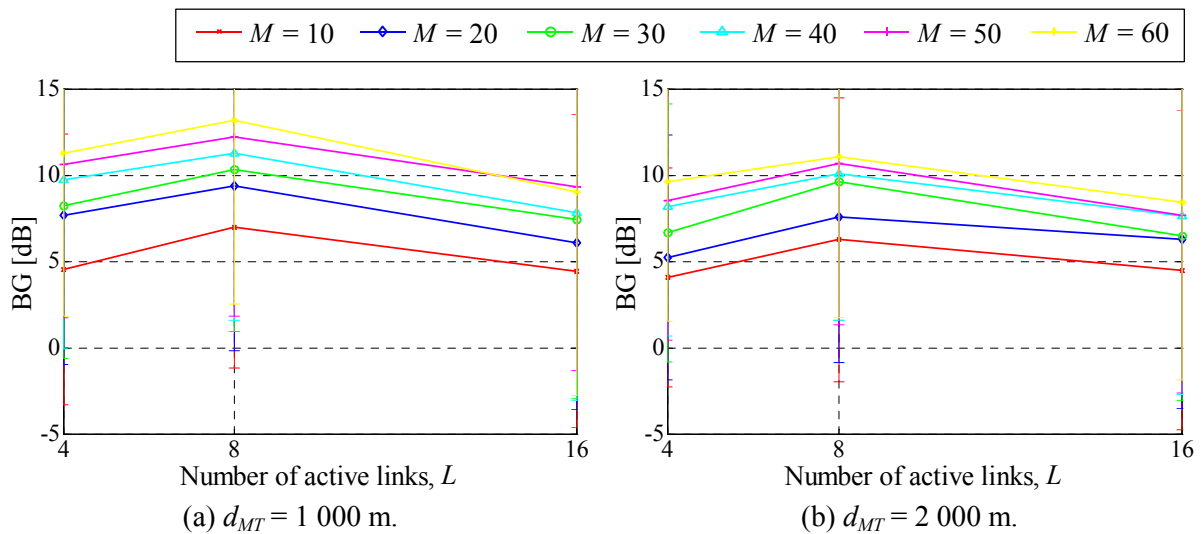


Figure 7.34 – BG, function of L , for several values of M , Sc #Lu_Mc_Sp_d_200, for $d_{MT} = 1\ 000$ and $2\ 000$ m.

Concerning the cases where a single MT is present, separate from a group of MTs, Figure 7.36 (a) and (b) illustrate the obtained results for Sc #Lu_Mc_Se_A_200. As regards the single MT, the BG again improves from 4 to 8 users, for any M , and then decreases from 8 to 16 MTs. For each M case, BGs for $L = 16$ are higher than those for $L = 4$, for the reasons stated. For the MT group, the values evolve closer to 0 dB, as described before, but still being able to reveal better BG values at $L = 8$.

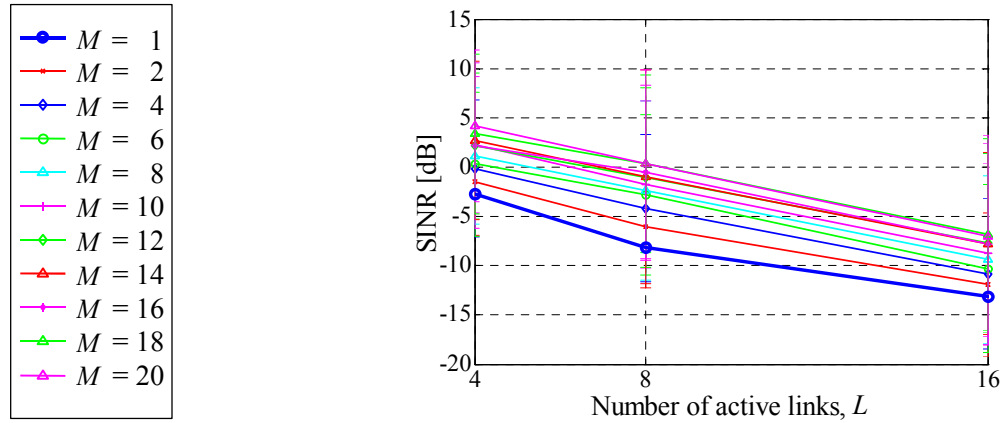


Figure 7.35 – SINR, function of L , for several values of M , including the single element case, Sc #Lu_Sp_15_200.

In Figure 7.36 (c) and (d), the corresponding SINR dependence with L is shown for the same scenario, Sc #Lu_Mc_Se_A_200, $d_{MT} = 1500$ m. SINR values are also higher for $L = 8$, in the case of the single MT, with the lowest values for 16 MTs; for the grouped MTs, SINRs may be better for $L = 8$, depending on M , while 16 MTs lead to considerably lower values. Unlike the Sc #Lu_Mc_Sp_d_200 results, where SINRs monotonically decrease with increasing L (Figure 7.35), it is not only the BG but also the SINR that presents best values for 8 MTs.

As for results for Sc #Lu_Mc_Se_A_50, shown in Figure 7.37, the single MT tendencies are enhanced, BGs improving by 11 to near 17.5 dB, from 4 to 8 MTs, further decreasing for 16 MTs, to values that are again close to the $L = 4$ results. For the group case, as it was previously described, the BGs are even closer to 0 dB, compared to the $r = 200$ m case.

Though not shown for this scenario, the SINR dependence on L is of the same sort as those of Sc #Lu_Mc_Gr_d_200 and Sc #Lu_Mc_Se_A_200, for the grouped MTs and single MT, respectively.

The justification for the latter, in some way less expectable, SINR dependence on L resides in another phenomenon: it is the $P_{NDesI} + N$ suppression, in the MT_1 case, that is considerably better when $L = 8$, among the tested values of L , having a different behaviour, compared to all the remaining situations; instead of $P_{NDesI} + N$ power increasing and reaching a constant level with increasing M , as in most cases (as it is described in Section 6.4), in fact it considerably decreases in these specific ones; furthermore, it has been verified that such also happens for Se_C and Se_B scenarios, except

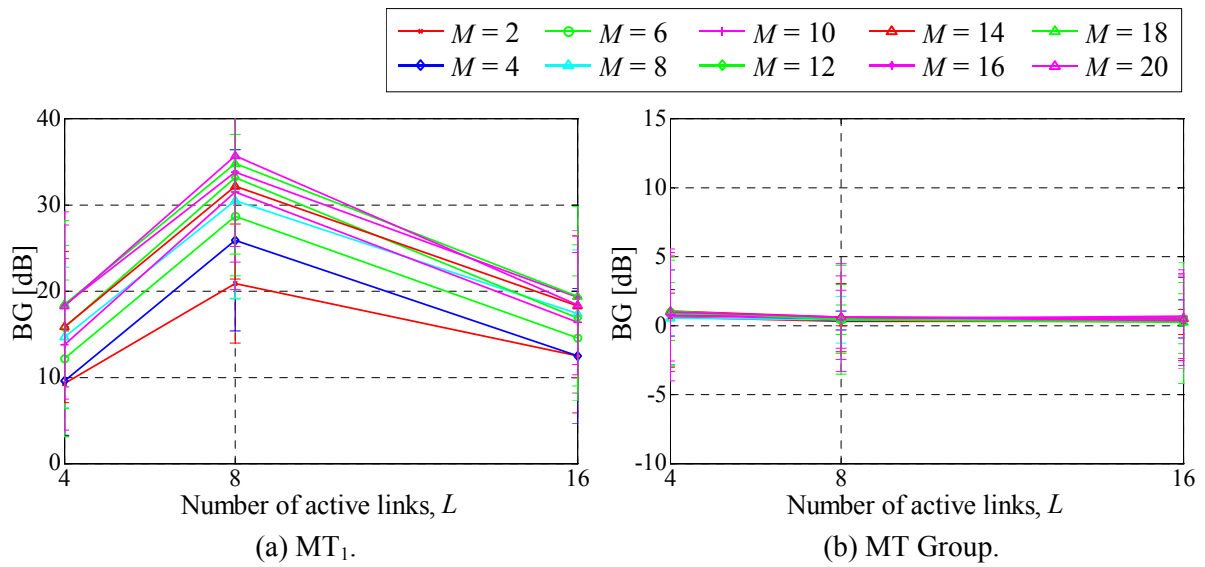


Figure 7.37 – BG, function of L , for several values of M , Sc #Lu_Mc_Se_A_50, $d_{MT} = 1\ 500$ m.

7.3.7 Correlation Matrix Components Dependencies

As in the MiC case, it is also important to evaluate how the different involved powers relate to each other for MaCs. The several power components have been calculated for several scenarios with $L = 4$, for $M = 12$, with MTs 1 500 m from the BS, with 200 or 50 m scattering circle radii. By comparing the Sc #4u_Mc_Sp_15_200 and 4u_Mc_Sp_15_50 cases, depicted in Figure 7.38 (a) and (b), it is clear how the delayed NDesI component once again achieves predominance in the 200 m case, compared to the 50 m, and to the DesS power in any case. Also, it is seen how the beamformer is able to obtain higher DesS power for 50 m, besides NDesI and Noise powers being relatively lower, indications of better interference and noise suppression, relative to the DesS. Regarding noise, for these examples, its relevance is equivalent to that of some of the involved NDesI powers.

The importance of noise is shown, for example for Sc #4u_Mc_Gr_15_200 and Sc #4u_Mc_Gr_15_50, whose results are presented in Figure 7.39 (a) and (b), correspondingly. On the one hand, for 200 m, the delayed NDesI component is large along iterations, comparable to the noise one, while on the other, for 50 m, it is the noise that is limiting performance most. The cases where MTs share the same scattering region, that have shown to lead to heavy SINR degradation along the optimisation, leading to negative BGs, reveal to be strongly noise-limited as the algorithm progresses. Such is another fundamental difference among the scenarios with spread or grouped MTs, added to the clear weakened capacity for the beamformer to optimise SINR in the latter case (notice that the latter graphs have half the scale as the former ones, respectively).

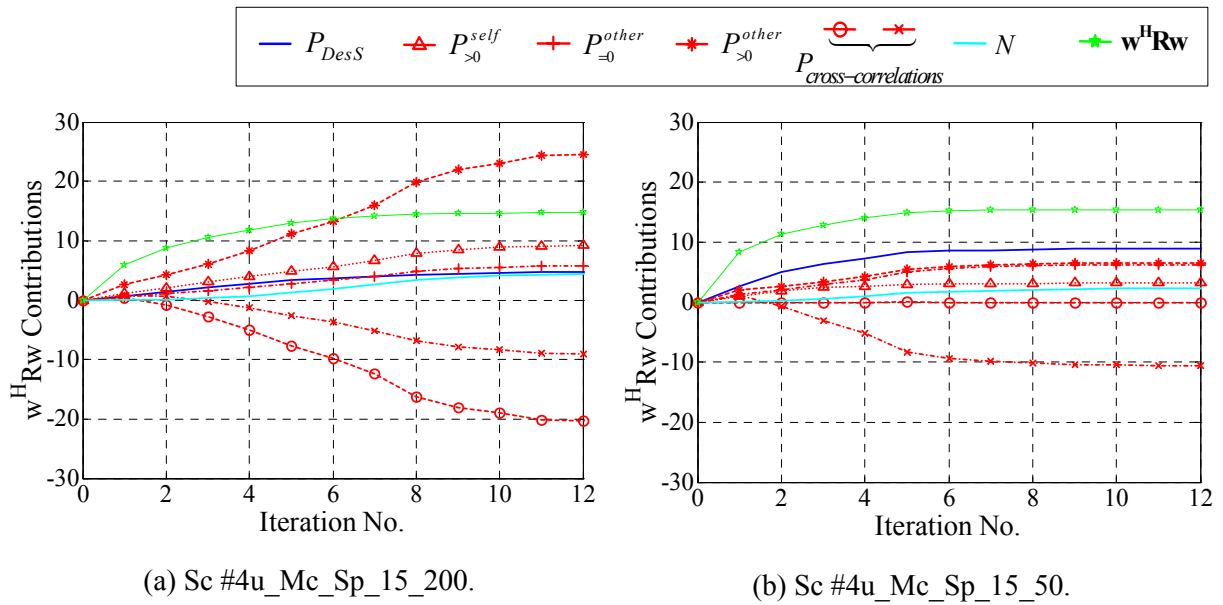


Figure 7.38 – Average power terms due to the composition of \mathbf{R} , for $M = 12$, Sc #4u_Mc_Sp_15_200 and Sc #4u_Mc_Sp_15_50.

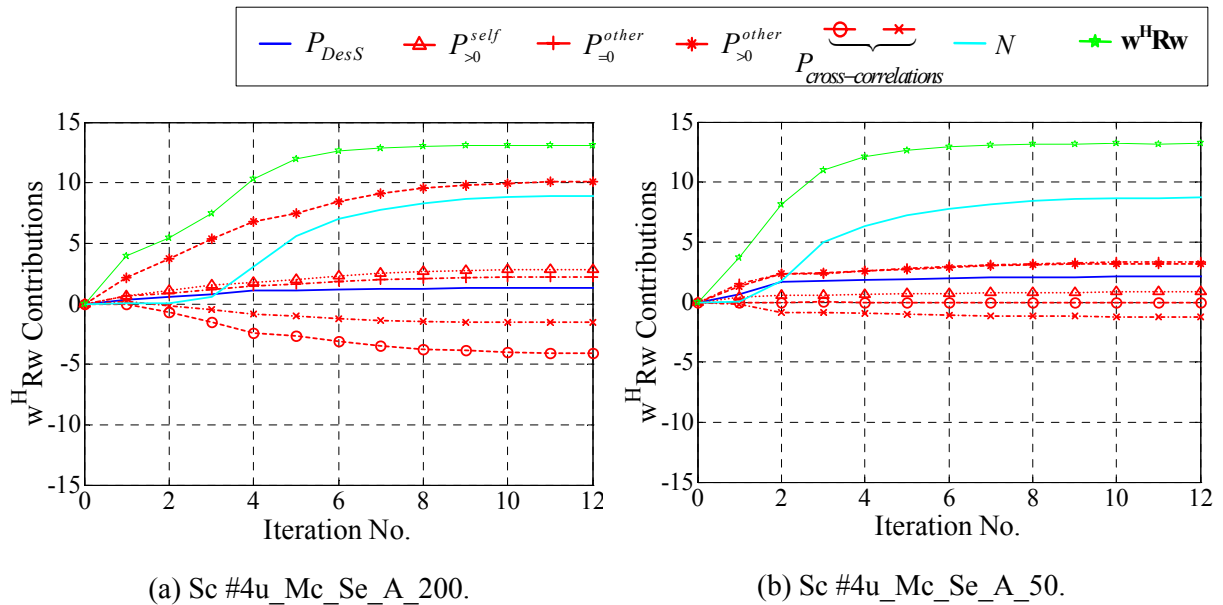
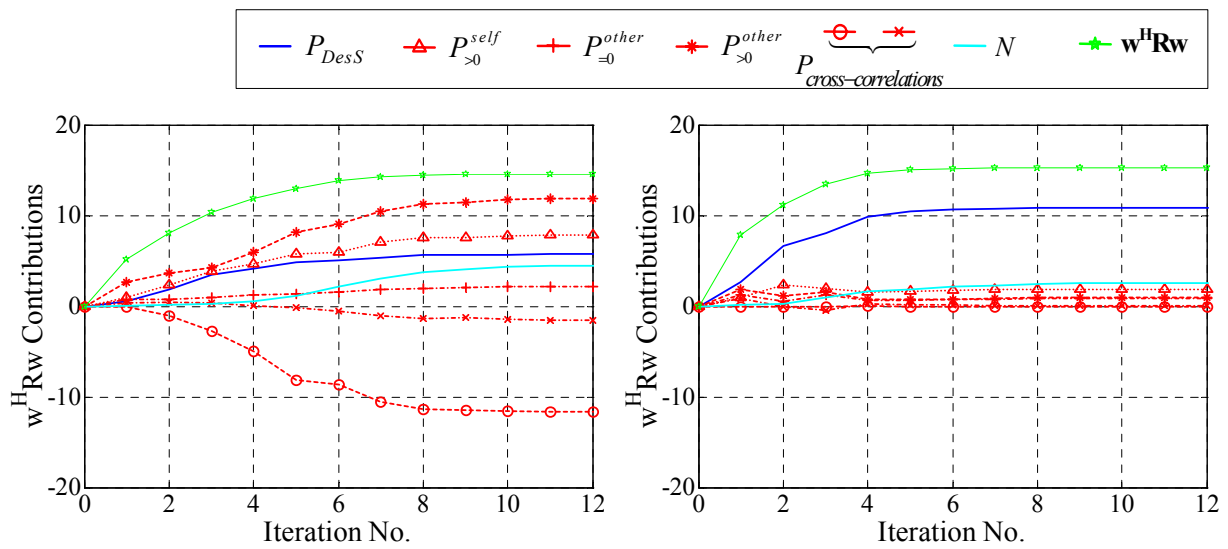


Figure 7.39 – Average power terms due to the composition of \mathbf{R} , for $M = 12$, Sc #4u_Mc_Gr_15_200 and Sc #4u_Mc_Gr_15_50.

As for the scenario cases where a single, angularly separate MT is present, it is also important to analyse how the several components behave. For Sc #4u_Mc_Se_A_200 and #4u_Mc_Se_A_50 cases, the results are plot in Figure 7.40 (a) and (b), corresponding to the single MT perspective. Thus, in the view of MT_1 , the beamformer again reveals the differing importance of the two delayed

NDesI power components, $P_{>0}^{self}$ and $P_{>0}^{other}$, depending on the circle radius. Also, in the case of 200 m, the noise term again presents important relative significance, in contrast to the DesS power for 50 m, with the largest relative importance, among all the hereby-presented scenario cases. Such is the scenario case where the beamformer is presented a particularly comfortable interference reduction situation.



(a) Sc #4u_Mc_Se_A_200.

(b) Sc #4u_Mc_Se_A_50.

Figure 7.40 – Average power terms due to the composition of \mathbf{R} , for $M = 12$, Sc #4u_Mc_Se_A_200 and Sc #4u_Mc_Se_A_50, MT₁.

Concerning the effects of cluster density and average number of scatterers, it is also important to evaluate how the several components, again, relate. As described before, it is only for the cases where the single MT is present, with 50 m scattering circle radius, that significant changes in BG have been registered, such being reflected in the power components. In Figure 7.41 (a) and (b), the evolutions are shown for Sc #4u_Mc_Se_A_200_ld and Sc #4u_Mc_Se_A_50_ld. As mentioned before, the 50 m case involves lower $P_{NDesI} + N$ and higher P_{DesS} values, comparing to the case of higher N_{mp} , leading to higher SINR and BG. As for the 200 m case, though similar changes in the several components happen, the effects on BG and SINR are not as large.

Finally, by analysing the several power components involved, along optimisation, it has become again visible how strongly the displacement of MTs and scattering circle radius affect performance, how the noise power term may play a very significant part in the process, in the particular case of MaCs, and how the different evolution of terms helps to understand the OD problem.

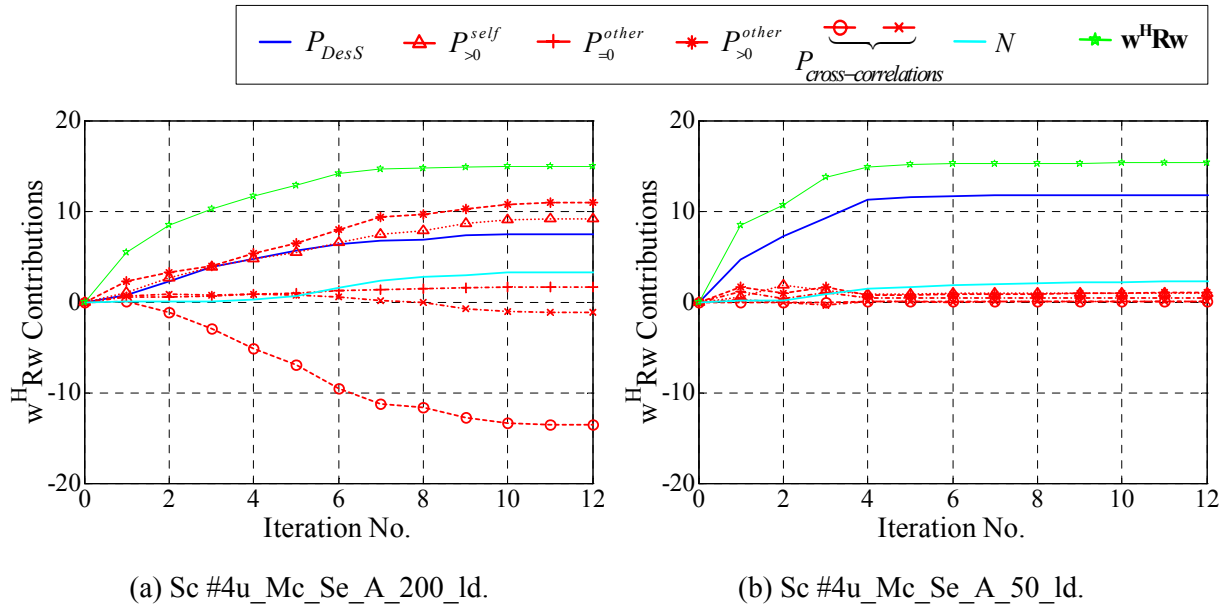


Figure 7.41 – Average power terms due to the composition of \mathbf{R} , for $M = 12$, Sc #4u_Mc_Se_A_200_ld and Sc #4u_Mc_Se_A_50_ld, MT₁.

7.4 Summary and Conclusions

From the presented application to MiC and MaC scenarios, several important conclusions are drawn. For both MiCs and MaCs, the WDCM multi-user scenarios are characterised by a large number of correlated and closely correlated arriving signals, due to multipath and several interfering sources, having important impact on the beamforming performance dependencies on channel/scenario parameters.

For the simulated MiC scenarios, it is both their AoA and ToA spreads that strongly affect beamforming gain, ToA spreads conditioning the BG much strongly over the former, leading to BG degradation for shorter BS-MT distances. From 50 to 1 000 m, BG may degrade by up to 5 dB, among the tested grouped MT scenarios, being particularly worse for 50 m BS-MT distance. On the one hand, the corresponding SINR sensitivity to d_{MT} is much clearer, being mainly justified by the significant variations in ToA spread. On the other, BG's lower sensitivity reflects the beamformer's operation, the angular domain already having a visible influence in determining dependencies.

Since the effect of AoA spread and the corresponding angular density of arriving signals, for a certain number of array elements, may not be particularly visible in the cases of the scenarios where MTs are grouped together and confined to the street, freeing the ellipses axis from the street has further helped in confirming the relationships at stake. By spreading MTs, the BG dependency with d_{MT} becomes more visible, for lower number of array elements, especially in the case of larger distances, for which the sharing of AoAs among links is more reduced.

To aid in the analysis, higher number of elements has helped to confirm the dependencies with BS-MT distance, also verifying that the increase in M leads to an asymptotical evolution of BG.

This *saturation* effect is justified by the increasingly uncorrelated signals that higher M implies, among array elements. Due to the various arriving signals with differing AoAs, such higher decorrelation adds on to a larger pattern mismatch, since the calculation of the array pattern considers total correlation. Additionally, the WDCM implementation introduces a finite angular resolution, which for larger M may become gradually insufficient. These tests also show that for $M > L_T$, i.e., with apparently enough DoF to angularly discriminate the several temporally orthogonal sources, BG does not show any particular increase, therefore, reflecting the importance of the angular domain issues that are involved in the multi-user WDCM scenarios.

In the case that MTs are angularly spread, BGs show increases relative to the cases where those are grouped, but these improvements are very limited by the relatively wide angle-spreads. Such is an expected tendency, since large AoA spreads imply large sharing of AoAs even if MTs are angularly scattered. For 1 000 m BS-MT distance, BG improvements reach 4 dB, whereas for 50 m, these are up to 2.3 dB.

In the scenario cases where a single MT is placed angularly separate from the remaining ones, such MT renders BGs of up to at least 5.6 to 9.0 dB above the BG values of the grouped cases. The way that the remaining MTs are located is not significantly relevant to the definition of any of the beamformers' performances, again due to the wide angle-spreads at stake. Anyhow, all BG variations with MT spreading follow the expected logic, in the sense of sharing more or less AoAs among DesS and NDesI.

Besides the displacement in angle, the scenarios where a single MT is separate from the remaining grouped ones along the same street-confined axis have further confirmed the reasoning behind hypotheses and analyses. As expected, a group of MT closer to the BS functions as clutter to a farther MT, due to both larger AoA and ToA spreads, leading to the subsequent degradation of BGs among all active MTs. Again, BGs corresponding to MTs within such group lead to lower values, relative to the single MT, for almost all of the tested scenarios.

Still within the street environment, it has been important to analyse to what extent the approximating assumption that MTs are only along the street central axis significantly affects results. By spreading MTs within the possible physical dimensions of the street scenario, it is verified that it is only for the lower BS-MT distances that MTs must definitely be considered at its centre. For larger distances, the corresponding possible ellipse angular shift that MTs across the street imply does not considerably affect BGs.

Regarding the dependence with the number of active MTs, having 16 MTs leads to worse performances, as expected. Nevertheless, from having 4 to 8 MTs, BGs do not substantially vary, in fact even increasing in some cases. This is justified by the differing trends that single element and array SINRs follow. Anyhow, BGs show relatively small sensitivity, among the tested scenarios, to the number of active MTs.

The variation of the sector width also brings up the importance of the AoA spread, seeing that DesS and NDesI powers are affected in different manners, depending on the sector widths and on the type of WB angle-spreads. But most important, it is generally confirmed that lowering sector widths implies lowering of beamforming freedom to place lobes and nulls in closer vicinity, towards DesS or NDesI signals. In this sense, narrower sectors contribute to reducing the available AoA spreads that MiC environments involve, therefore, leading to lower BG.

Finishing the MiC analysis, the evaluation of the relative values of DesS, NDesI and noise powers have confirmed all of the previously gathered conclusions. Additionally, it is seen that the delayed power from remaining MTs, $P_{>0}^{other}$, in the perspective of each single MT, is the most important NDesI component, taking larger relative values and being the most sensitive one to the scenario conditions. On the other hand, DesS power, P_{DesS} , shows to be much less sensitive to those. Most important is that these most significant power components follow the tendencies determined by the larger or lower freedom that the scenario presents to the beamformer.

In the MaCs case, it is the AoA spreads that play the most important part in determining beamforming performance. For all scenario implementations, the general MT distribution has a very strong impact on the beamforming performance, also ruling the effects of all the remaining varied parameters: grouped MTs suffer from the limiting situation where all AoAs and ToAs are shared, leading to BGs close to 0 dB, independent of the number of array elements or any other scenario parameter; angularly spread MTs lead to BG that vary with the remaining parameters, always leading to positive values; the single separate MT lead to the highest BG values, possibly reaching 35 dB.

The dependence with MT-BS distance is not significant, among the tested MaC scenarios, though a tendency for BGs to decrease with increasing MT-BS distance has been registered. Anyhow, these are only significant in the case that MTs are spread, for larger number of array elements, M . From 1 000 to 2 000 m, values may vary by 4 dB. Since the variation of distance only involves significant angle-spread changes, the results already indicate how the beamforming may depend on such. By increasing the AoA spread, for the same ToA one, the beamformer may make use of more angular freedom in order to place lobes and nulls more effectively.

As regards scattering circle radius, the general tendency is for BGs to degrade for larger radii. Again, it does not have any effect in the case that MTs are grouped together, unlike in the spread or in the separate MTs cases. The variations at stake vary from 3.8 to 8.6 dB, depending on the scenario situation, the highest variations corresponding to the single MT case, very clearly separate from the remaining ones. The effect of involving a larger scattering area is two fold: if MTs are spread, the larger are the chances of AoAs from differing MTs for superimposing, leading to lower BGs, for larger radii; on the other hand, the larger radii involve larger delayed NDesI power components, also incoming from a wider angular sector, meaning that most probably more undesired lobes will be directed towards such NDesI sources.

The dependence on the number of array elements is also a strong function of the distributing of MTs, in MaCs, the sharing of AoAs determining the way that BGs evolve with M . BGs increase with M in a manner very close to linear, but again showing an asymptotical evolution, justified by spatial correlation and finite angular resolution issues. The relation of the number of orthogonal arriving codes to the number of array elements does not, by itself, determine the beamforming capabilities, as in the MiC case. Once more, the importance of the angular domain scenario characteristics again shows to be playing a very important part, in this way.

Regarding the dependence on the density of clusters and the average number of scatterers, again the effects vary according to MT positioning, in MaCs³⁴: no relevant changes are registered for grouped or spread MTs, unlike the single MT case, where larger number of incoming rays lead to lower BGs; the effects of these are more significant, as the scattering circle radius is reduced.

With reference to the dependence on the number of active links, in MaCs, once more it is determined by how MTs are distributed: grouped together MTs do not exhibit particular dependencies, due to the inherently limited beamforming capacity, as already mentioned; if MTs are angularly spread, BG results have shown to be best for 8 MTs, having clarified that such is due to the asymptotical reduction in the single antenna SINR, compared to the almost linear reduction of the beamformer's output SINR, from 4 to 16 users; in the case of the single separate MT, especially in the case of a well localised group of MTs at a different angle, its BGs and SINRs in fact increase from 4 to 8 MTs, while 16 terminals may not necessarily lead to lower BG or SINR results compared to the 4 MTs case. Such situation results from the cross-correlation nature of the reference codes involved, being worse in the case of 4 MTs (sub-Section 6.3.2).

As in the MiC case, the involved power components reflect how the scenario favours more or less beamforming performance, confirming the reasoning behind the justification of performance trends. The $P_{>0}^{other}$ power confirms to be the most significant one, but P_{DesS} and N powers also show to considerably vary with the scenario. In the cases where a single MT is angularly separate from remaining ones, P_{DesS} values reach considerably high values in respect to the remaining components.

Conclusively, several scenario types and variation of the several parameters, along with the decomposition of the several involved powers, have helped to characterise the response of the beamformer, in a whole, for both MiCs and MaCs. The fact that the MT positioning and distribution most strongly affect the beamforming performance, in MaCs, and the several dependencies on the varied parameters very clearly show the importance of not only considering a directional model by itself, both the MiCs or MaCs cases, but also of applying such model in a multi-target implementation scenario perspective. The role of the angular domain not only plays a part among each active link, but

³⁴ This analysis has not been additionally put forward for MiCs due to the much lower sensitivity that MiC scenarios have shown to all remaining parameters. Nevertheless, there is no doubt that it would be important in further corroborating the presented hypotheses and conclusions.

also mostly determines how the multi-target scenarios affect beamforming performance, strongly establishing the available freedom that the channel presents to the beamformer. Having gone forth with the MiC and MaC analyses, independently, it is now time to closely compare the two situations, altogether.

8 Beamforming Performance in Micro- vs. Macro-cell WDCM Scenarios

Nature does nothing uselessly.

—Aristotle (384 - 322 BCE)

8.1 Introduction

It is important to compare the performance between MiC and MaC scenarios, with the objective of better basing the study of the fundamental channel constraints behind beamforming performance. In order to do so, the comparative scenarios defined in Chapter 4 are particularly required to be kept in mind.

The previous analyses have covered both TDD and FDD modes, with more detail in the former case, for the reasons already put forward. Their major resemblances and differences in the way performance is affected have been described in Section 6.3. In this way, hereby at a higher level, the study follows more independently of the duplex mode, to the extent expressed in such section. The analysis is centred in the BG values, thus, evaluating the effective interference reduction capacity of the beamformer rather independently from the single antenna SINRs.

Truly, the comparison of MiCs and MaCs results has already started with a comparison of the DCIRs, in terms of their temporal and angular characteristics, being directly related to the differing scattering areas (Chapter 4). Then, new parameters were introduced, such as the *temporal* and *angular densities* of arriving signals, and the DCIR *channel richness*. Along the description of the comparative analysis results, focus is drawn towards these DCIR temporal and angular characteristics, in this chapter. As in the cases of the beamforming performance analyses towards MiCs or MaCs, in Chapter 7, these relationships will arise naturally, being fundamental channel parameters ruling the beamforming behaviour.

In this chapter, as before, the study primarily covers the dependencies of BG and SINR on the channel and scenarios characteristics, comparing their main similarities and differences between the MiC and MaC cases. The overall performance is analysed, covering the dependencies on the MT grouping and angular displacement, the number of array elements, the number of active MTs, and BS-MT distances. A comparison of the involved power components also provides important insight on this comparative analysis, from the previously presented in sub-Sections 7.2.7 and 7.3.7.

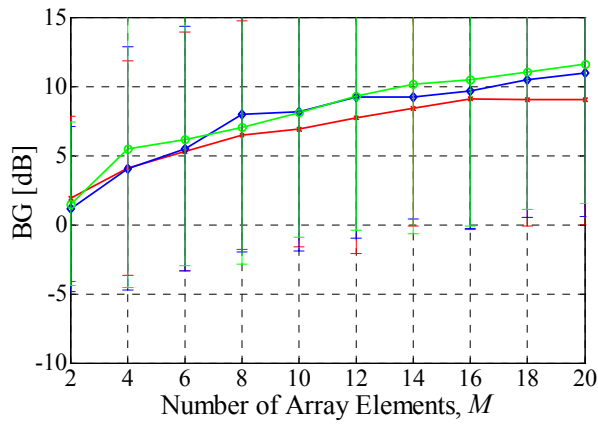
Finally, from the conclusions that are drawn, covering matters that are naturally in convergence towards the characterisation of the channel matrix in a multiple antenna point of view, their relations to the MIMO perspective are naturally presented along the text, but also explicitly covered at the end of the chapter. In this way, the fundamental physical features that are brought up while characterising the scenarios, determining a *better* or *worse* multipath channel that fundamentally constrains beamforming performance, show to also relate to other issues besides the presented beamforming application.

8.2 Comparative Analysis Results

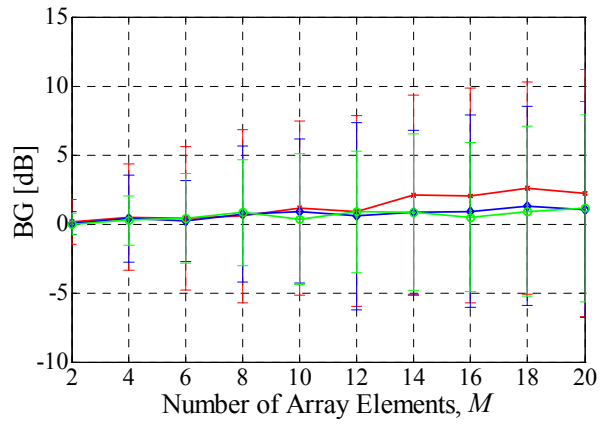
8.2.1 Angular Displacement and Grouping of MTs

At this point, one calls upon the analyses presented in Chapter 7, for MiCs or MaCs, separately. In general, among all CSts, the MiC and MaC situations at stake decide to which degree the AoAs are shared among the active links. In this way, for both the elliptical and the circular scattering areas, CSt #Lu_mc_Mc_Gr is the case where the superposition of AoAs is total. In Figure 8.1 and Figure 8.2, CSt #Lu_mc_Mc_Gr BG and SINR, MiC and MaC results are put side-by-side, hereby repeating the plots in order to better compare the results.

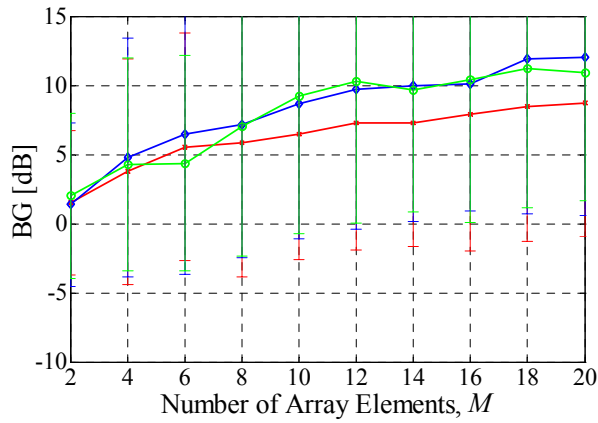
The first striking difference that is registered among the CSt #Lu_mc_Mc_Gr cases is that BGs are kept very close to 0 dB in the MaC case, mostly independent of the BS-MT distance and number of array elements. One reason for such is the much greater richness of independent signals in the MiC case, due to the larger areas involved, therefore leading to larger independent freedom to placing lobes and nulls among links. Related to that, its importance has been brought up in Chapter 7, having seen the much narrower AoA spreads that the MaC scenarios involve, for much more comparable delay-spreads. Even with the number of scatterers being lower for MaCs than for MiCs, the ρ_ϕ values are greater in the former case (Table 4.10). With larger angular densities, DesS and NDesI powers are in closer vicinities, making the angular differentiation between these more difficult, while the temporal density varies much less, at the end implying lower beamforming capabilities. Additionally, larger values of ρ_τ are involved among the MiC scenarios, also rendering better correlation properties. In this way, the values for both angular and temporal densities reflect the general differences, being ultimately expressed by the disparity in the ω_{DCIR} parameter values, between MiCs and MaCs, differing by one order of magnitude (Table 4.10).



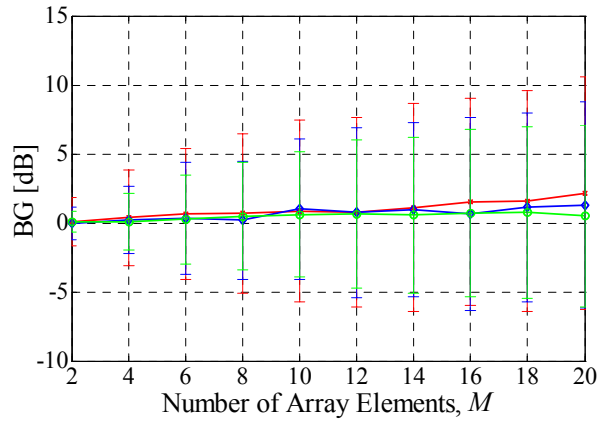
(a) Sc #4u_mc_Gr_d.



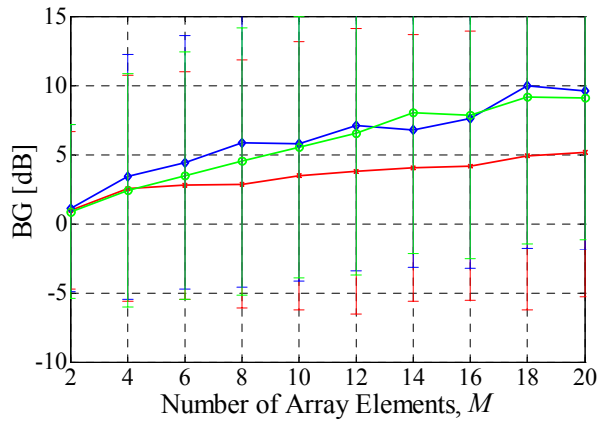
(b) Sc #4u_Mc_Gr_d_200.



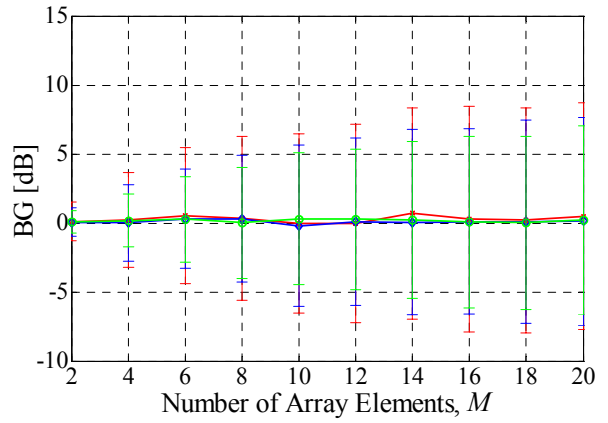
(c) Sc #8u_mc_Gr_d.



(d) Sc #8u_Mc_Gr_d_200.



(e) Sc #16u_mc_Gr_d.



(f) Sc #16u_Mc_Gr_d_200.

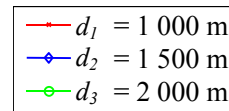
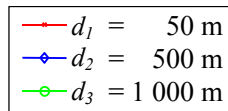


Figure 8.1 – BG, function of M , for several values of d_{MT} , for CSt #Lu_mc_Mc_Gr. Solid lines indicate average results, and error bars indicate respective standard deviations.

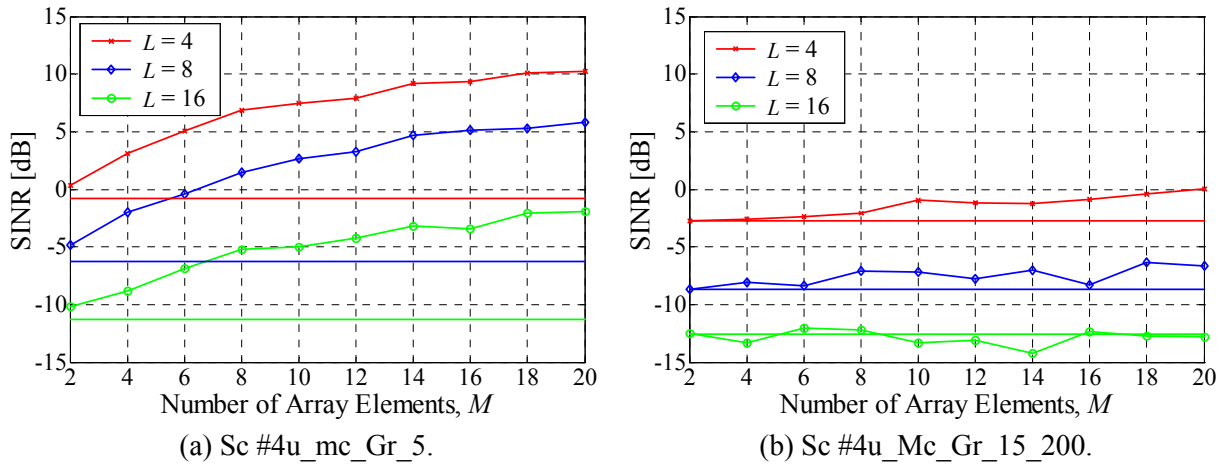


Figure 8.2 – SINR, function of M , for several values of L , CSt #Lu_mc_Mc_Gr, $d_{MT} = 500$ m and $d_{MT} = 1\,500$ m, MiC and MaC, respectively.

The SINR results provided in Figure 8.2 show how the single element SINR values do not significantly differ between MiC and MaC scenarios (indicated by the horizontal straight lines). On the other hand, the beamforming SINRs show how much greater the interference suppression capacity is for the case of MiCs, compared to MaCs.

It should be noted that the presented SINR results show relatively small differences relative to the respective BG ones (comparing Figure 8.1 and Figure 8.2). This results from the average single element SINRs also exhibiting fluctuations among each group of the 100 concretisations, for each M , due to the statistical nature of the process. In Figure 8.2, the shown single element SINR, indicated by the horizontal straight line, corresponds to the case of $M = 2$, averaging among the corresponding 100 concretisations, in order to simplify visualisation. Anyhow, the values still indicate the order of magnitude of the respective SINRs, dependent solely on the scenario.

Concerning the CSt #Lu_mc_Mc_Sp cases, where all MTs are randomly spread within the 1st and 4th quadrants, similar effects again condition MiC and MaC BG values' relation, as the results in Figure 8.3 show³⁵. Two most important effects take place in these latter scenario situations: since MTs are angularly spread, the narrower angle-spreads involved with MaCs imply that AoAs are less superimposed among links, compared to MiCs; at the same time, the higher channel richness, ω_{DCIR} , of each of the MiC links provide the beamformer with larger freedom to more independently and efficiently direct lobes and nulls, being able to better endure the present superposition of signals, keeping in mind the relatively wide angle-spreads involved.

³⁵ To aid in the reading, in the next figures of the same type, the results for $L = 8$ will not be shown, since the results have already been presented, these are in-between those for $L = 4$ and 16. For the same reasons, standard deviations are not plot.

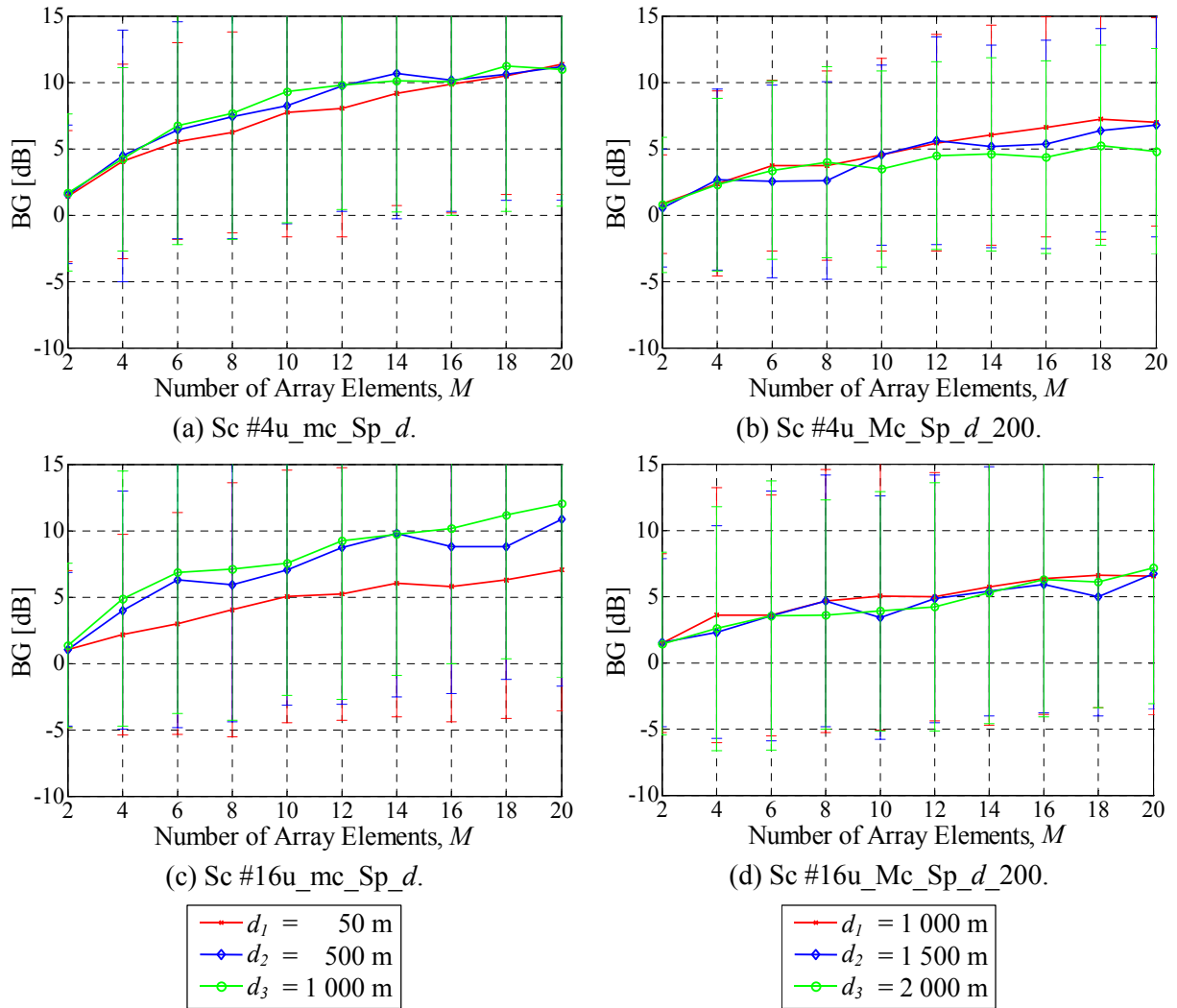


Figure 8.3 – BG, function of M , for several values of d_{MT} , CSt #Lu_mc_Mc_Sp, for $L = 4$ and 16.

The simulation results therefore show that the beamformer renders relatively small BG improvements in the MiC case, but a much larger BG rise for MaCs, when changing from scenario CSt #Lu_mc_Mc_Gr to CSt #Lu_mc_Mc_Sp. As with the previously presented CSt #Lu_mc_Mc_Gr results, where the MTs totally share ToAs and AoAs and where the channel richness most evidently proves to render larger freedom and better suppression in the MiC circumstances. Such property again shows its strength in the latter scenario case. In the MiC case, where MTs are angularly spread within two quadrants, even if the larger AoA spreads imply that signals are more superimposed among active links, the inherent channel richness results in larger robustness towards variations in the grouping and angular displacement of MTs. On the other hand, since MaCs involve much narrower AoA spreads, spreading the MTs leads to a significant rise in BG, i.e., presenting larger sensitivity towards MT grouping, compared to MiCs.

Similarly as before, the single element and beamformer's SINRs are shown for scenarios Sc #Lu_mc_Sp_5 and Sc #Lu_Mc_Sp_15_200, in Figure 8.4, in order to keep track of the corresponding

values. Except for the $L = 4$ case, the single element SINRs do not substantially differ between MiCs and MaCs, again more clearly showing the better performance that is possible with the former case.

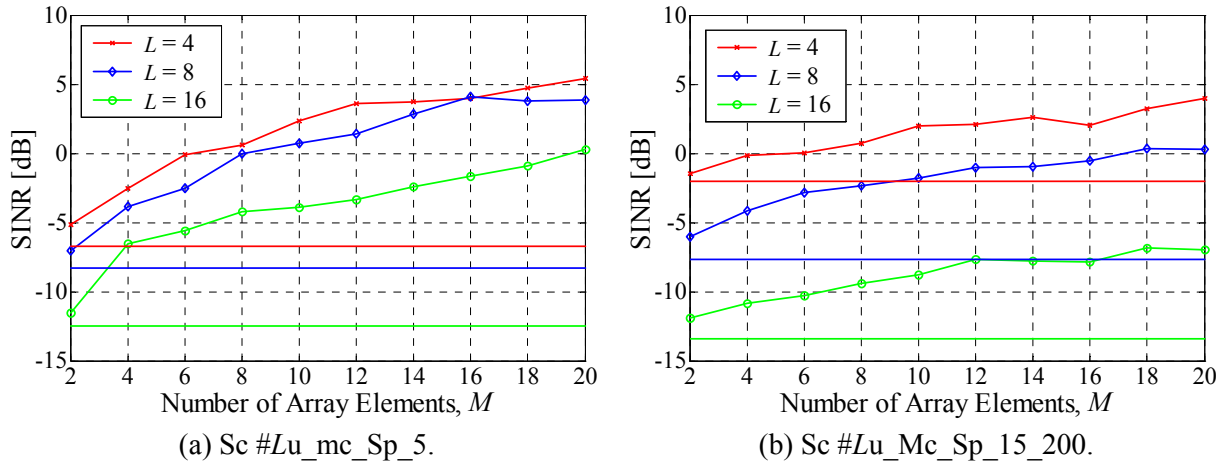
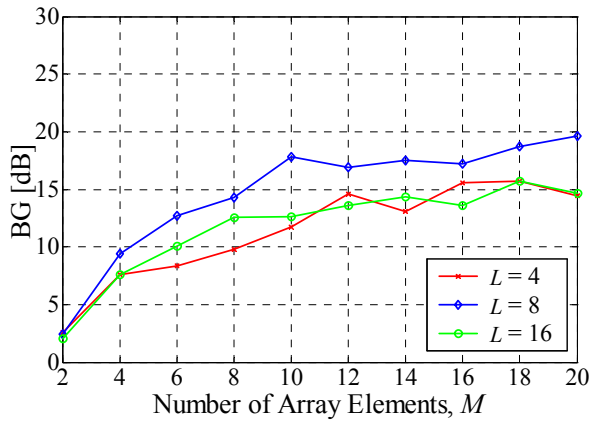
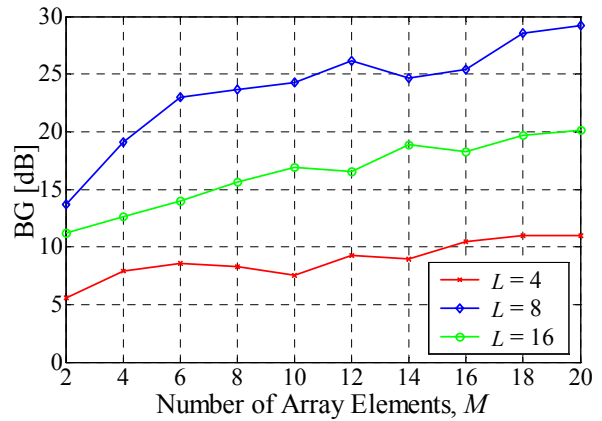


Figure 8.4 – SINR, function of M , for several values of L , CSt #Lu_mc_Mc_Sp, $d_{MT} = 500$ m and $d_{MT} = 1500$ m, MiCs and MaCs, respectively.

Regarding the scenarios where a single MT is placed angularly separated from the remaining ones, it has been previously verified that their added value concerns the analysis of such MT, since the remaining ones result in BGs which are very similar to those of the simply grouped, or randomly spread, MTs scenarios (CSts #Lu_mc_Mc_Gr and #Lu_mc_Mc_Sp). Figure 8.5 presents the BGs corresponding to the single MT, in the case that the remaining MTs are grouped together, all located at $-\pi/5$, for both MiCs and MaCs. For that scenario situation, it would be reasonable to expect the MaC cases to lead to higher BGs, reasoning that the main NDesI sources are located within a well restricted angular sector, involving AoA spreads that are much narrower than those of MiCs, therefore, posing more favourable interference suppression conditions. In fact, among CSt #Lu_mc_Mc_Se_A scenarios, such happens, and is gradually clearer as the number of active users increases, which is a direct consequence of the following: as the number of MTs increases, the single element SINR decreases; in the MaCs case, due to the narrow angular sectors involved, for either DesS and NDesI, the beamformer can still guarantee interference suppression in a very efficient manner, thus, leading to reasonably invariant beamforming SINRs; concerning the MiC situations, it is natural to expect beamforming SINRs to degrade more with increasing L , for MT_1 , due to the much wider angle-spreads involved by both DesS and NDesI powers; finally, as a consequence, the BGs of the angularly separate MT, while the remaining MTs are grouped together, turn out to being lower in the MiC cases, compared to the MaC ones, for larger L .



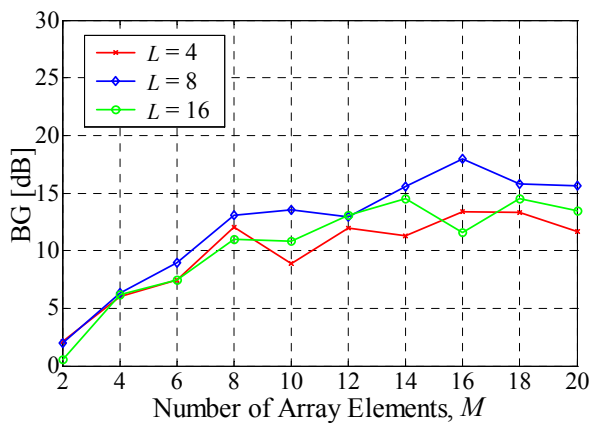
(a) Sc #Lu_mc_Se_A.



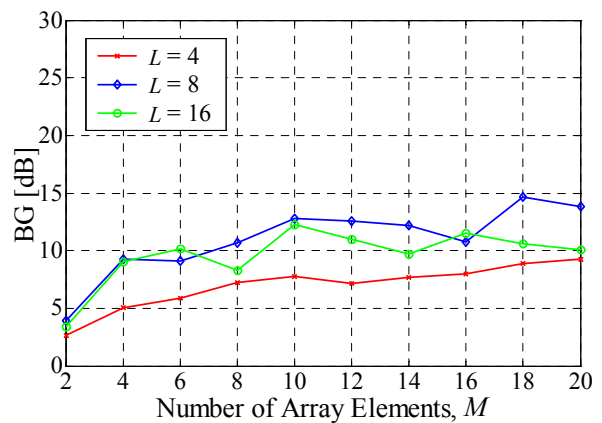
(b) Sc #Lu_Mc_Se_A.

Figure 8.5 – BG, function of M , for several values of L , for MT_1 in CSt #Lu_mc_Mc_Se_A.

Concerning CSt #Lu_mc_Mc_Se_B scenarios, where the $L-1$ MTs are spread over the 4th quadrant, the formerly described effect present in the CSt #Lu_mc_Mc_Se_B MaC scenarios will not be as important due to the following: the spreading of remaining MTs and of respective AoAs result in less favourable interference reduction conditions, even if MT_1 is separately placed, at $\pi/4$; in the perspective of such MT, the main NDesI sources are no longer located at a specific angle, meaning that the array SINRs more strongly follow the single element SINR degradation, as the number of active MTs increases. As Figure 8.6 does show for this scenario, the MiC BG values turn out being greater than the MaC ones, for all of the tested L values, the importance of the channel richness becoming once again visible, in this situation.



(a) Sc #4u_mc_Se_B.



(b) Sc #4u_Mc_Se_B.

Figure 8.6 – BG, function of M , for several values of L , for MT_1 in CSt #Lu_mc_Mc_Se_B.

Concluding, beamforming performance significantly differs between MiC and MaC scenarios, as a function of the MT grouping or angular displacement of the active MTs. In general, the larger channel richness that characterises the MiC situation shows its importance most strongly when MTs are grouped together, in the sense that the beamformer achieves comparatively higher performance in

such situation, even with the total sharing of ToAs and AoAs among links. This means that, by spreading the active MTs, though the resulting BGs are larger for both MiCs and MaCs compared to the respective grouped situation, those BG improvements are much lower in the former case, the MiCs situations rendering larger robustness towards MT grouping. Among the tested scenarios, MiCs in general render better interference suppression. It is only for the extreme case where all $L-1$ interferers are grouped together, angularly separate from a single MT, that such MT leads to better BGs in the MaC situation, and such happens for larger L , due to the particularly favourable role that the much narrower angle-spreads involved play, in that specific scenario situation.

8.2.2 MT-BS Distance

The performance dependence on the BS-MT distance, as it is seen in Figure 8.1 and Figure 8.3, for scenarios CSt #Lu_mc_Mc_Gr and CSt #Lu_mc_Mc_Sp, is highly determined by the angular displacement and grouping of MTs. In general, among all of these scenarios, the dependence with the distance is much lower for MaCs, as the figures show. Again, the justification roots from the channel richness. Due to the much more restrictive nature of each BS-MT MaC channel, the dependencies on other factors, such as distance, do not achieve significant expression.

Being more specific, for CSt #Lu_mc_Mc_Gr MaC cases, if some trend is to be registered, especially for lower L , and higher M , one sees a small tendency for BGs to be higher as distances lower. On the other hand, the corresponding MiC situations show BGs that tend to decrease with decreasing distance. As far as the CSt #Lu_mc_Mc_Sp MiC scenarios are concerned, BGs exhibit the same type of dependency with d_{MT} (for 8 or 16 MTs), as compared to the MiC grouped situations. As for the CSt #Lu_mc_Mc_Sp MaC, where the beamformer is able to achieve positive average BGs, the dependence with d_{MT} is not clear, but a slight tendency can be seen in the sense of BGs decreasing with increasing distance, i.e., opposite to that of the comparable MiC cases. Relating these results with the angular and temporal densities and DCIR channel richness, Table 4.10 illustrates how ω_{DCIR} in fact increases with increasing BS-MT distance, in the MiC case, whereas it decreases in the MaC situation. Notice that among the MaC channel responses, it is the angular density of signals that increases with rising distance, while the temporal density shows no significant changes.

By this, one sees that the analysis of the channel richness is particularly useful for the comparison of MiCs vs. MaCs scenarios, in order to base the justification for the obtained relationships. It may not be valid by itself within some of the MaC scenario cases, specifically when comparing performance between scenarios with angularly spread MTs, due to the additional effect of scattering area superposition among all active links, as the radius increases.

8.2.3 Number of Array Elements

Regarding the BG dependence with M , the previously presented results clearly and naturally show how it also strongly depends on the MT grouping, also differing between MiCs and MaCs.

By comparing Figure 8.1 and Figure 8.3 MiC BG results, it is seen that the improvements with increasing number of array elements are larger when MTs are angularly spread. This has already been indirectly justified, the larger M implying more efficient use of the angular dispersion of the signals, while the *whole*-DCIR allows for such better exploitation of the angular domain. In the case that MTs are angularly spread, it is expectable that such efficiency improvement will be larger, compared to the case where all AoAs are totally shared among links. In a similar manner, due to the lower channel richness that characterises the MiC cases with MTs closer to the BS, the *whole*-DCIR allows for weaker exploitation of the angular domain, BGs therefore not being as sensitive to the increase of M as for larger distances. For example, Sc #16u_mc_Gr_d, for $d_{MT} = 50, 500$ or $1\ 000$ m, from $M = 2$ to 20 , BGs improve by $4.2, 8.8$ and 8.3 dB, respectively, whereas for Sc #16u_mc_Sp_d, average BGs increase by $6.0, 9.8$ and 10.7 dB.

Naturally, for the MaC case, the change in the dependence of M is even more evident, as a function of the grouping, since the grouped MT situation leads to BGs near 0 dB, independent of the number of array elements, while for spread MTs the *whole*-DCIR does allow for BGs to rise with increasing M . For example, regarding Sc #16u_Mc_Sp_d, for $d_{MT} = 1\ 000, 1\ 500$ or $2\ 000$ m, from $M = 2$ to 20 , BGs improve by $4.7, 4.9$ and 5.1 dB, i.e., up to 5.6 dB lower than the comparable Sc #16u_mc_Sp_d scenarios.

Also expectedly, the angularly separate MT_1 , in scenarios CSt #Lu_mc_Mc_Se_A or B, for either MiCs or MaCs, should lead to the largest BG improvements with rising M , compared to the grouped or spread MTs, due to the particularly favourable situation of such MT, with responses anyway differing between MiCs and MaCs. In fact, by observing the BGs relative to MT_1 (Figure 8.5 and Figure 8.6), one confirms that such is so, comparing to the BGs obtained with grouped or spread MTs (Figure 8.1 and Figure 8.3). Due to the advantageous position of such separate MT, the increase in the number of antennas results in better suppression, still depending on the *whole*-DCIR allowance, i.e., differing between MiCs and MaCs. Anyhow, for such MT_1 , the corresponding BG dependence with M is largest in the MiC situations, compared to the MaC ones, for either Se_A or Se_B scenarios, as Table 8.1 shows, by indicating the respective BG variation between $M = 2$ and $M = 20$, ΔBG . Again, it is visible how the larger richness of the MiC channel responses allows for the performance improvements to be larger, as the angular resolution of the array improves by increasing M . Therefore, one can say that there is more to gain from using more array elements in MiC situations, compared to MaC ones, even in the case of such favoured MT.

Sc #	Δ BG	Sc #	Δ BG
4u_mc_Se_A	11.8	4u_mc_Se_B	9.5
4u_Mc_Se_A	5.4	4u_Mc_Se_B	6.6
8u_mc_Se_A	17.2	8u_mc_Se_B	13.7
8u_Mc_Se_A	15.5	8u_Mc_Se_B	9.9
16u_mc_Se_A	12.6	16u_mc_Se_B	12.9
16u_Mc_Se_A	9.0	16u_Mc_Se_B	6.7

Table 8.1 – BG improvements, between using 20 and 2 array elements, for MiC and MaC Se_A and Se_B scenarios, MT₁.

Finally, in a most practical system-wise perspective, these results indicate that, in the perspective of UL beamforming, there is a larger SINR benefit in increasing the number of BS array elements in the MiC, compared to the MaC, divergences reaching as much as 5 dB.

8.2.4 Number of Active Links

The change in L affects the angular and temporal density of arriving signals, while maintaining the AoA and ToA spreads of each of the active links. In this way, the *whole*-DCIR is loaded with more single link DCIRs, therefore contributing to lower SINRs and lower BGs. Through the Figure 8.2 and Figure 8.4 examples, it has already been seen that the array SINRs are visibly dependent on the number of users, with SINRs decreasing with increasing L , its values keeping above the single element SINR values in the case of MiC scenarios, and the inability to improve SINRs in the case of MaC is clear, even for low L .

Another issue is the increase in BGs registered from $L = 4$ to 8, in most MiCs and MaCs scenario cases, previously analysed and justified by the worse code correlation properties found for $L = 4$ (described in Section 6.3). Confirming that these results apply to both MiCs and MaCs simulations, such can be seen as a further indication of its reasonable independence from the channel, in fact rooting from the dependence on the common referential codes.

Anyhow, the focus is on BG dependencies, measuring the interference suppression capacity over considering a single element antenna, as function of L and of the propagation scenario characteristics.

In the case of CSt #Lu_mc_Mc_Gr, and accounting for the past descriptions, BG dependence with L is not significant in the MaC situation. The grouped MaC situation is so critical, not making the discerning of each link possible, that it is inherently the least dependent on the number of links. As Figure 8.7 (b) shows, from 4 to 16 MTs, BGs gradually decrease towards 0 dB. For MiCs, the variations are greater, not only concerning the BG increases from 4 to 8 MTs, but also the reductions from 8 to 16, Figure 8.7 (a). By spreading MTs, in CSt #Lu_mc_Mc_Sp, as Figure 8.8 exemplifies, the dependencies are seen to be similar, between MiCs and MaCs, though the latter may involve

relatively larger variations. Anyhow these differences are not considered of relevance, again being anyway justified by the larger channel richness in MiCs, providing lower dependence on the NDesI variations due to L , and on the worse code correlation properties that has been found for $L = 4$. However, it is in the case of the separate MT_1 , in CSt #Lu_mc_Mc_Se_A, that these factors more clearly show their roles, MiC and MaC responses differing more significantly. Figure 8.9 exemplifies so, MT_1 BGs presenting variations larger than 10 dB in MaCs, whereas these reach close to 5 dB for MiCs, as a function of L . For MaCs, both the worse correlation code properties, for $L = 4$, and the increase in NDesI power from considering 8 to 16 MTs, result in larger BG degradations, since the involved channel properties allow for less freedom in the location of lobes and nulls. Concerning the grouped MTs, in such scenarios, the results are close to the CSt #Lu_mc_Mc_Gr cases.

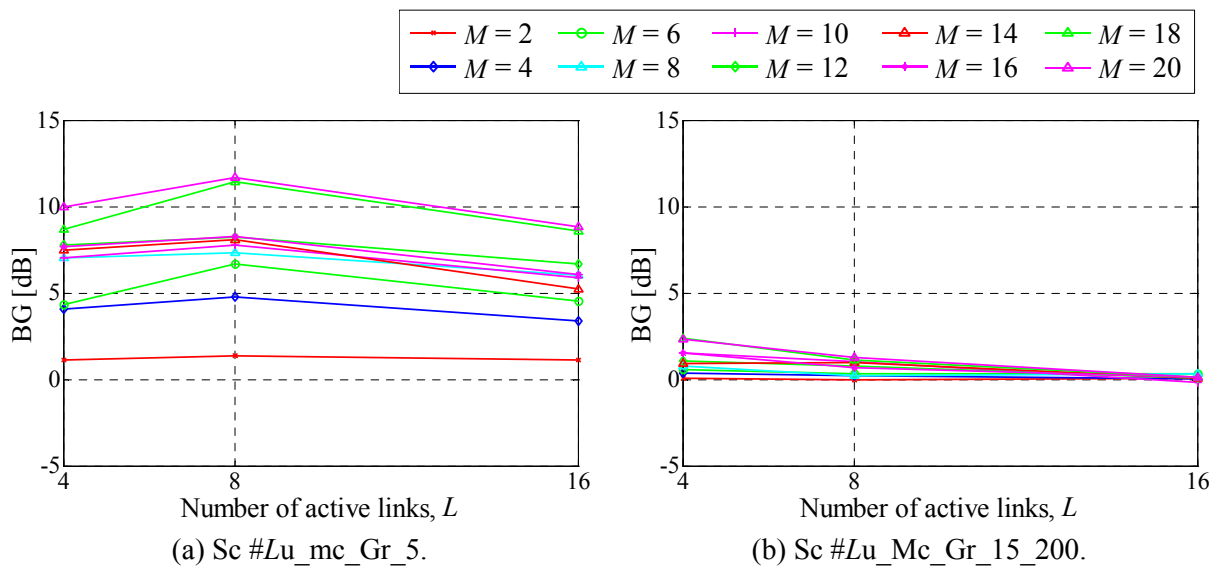


Figure 8.7 – BG, function of L , for several values of M , CSt #Lu_mc_Mc_Gr.

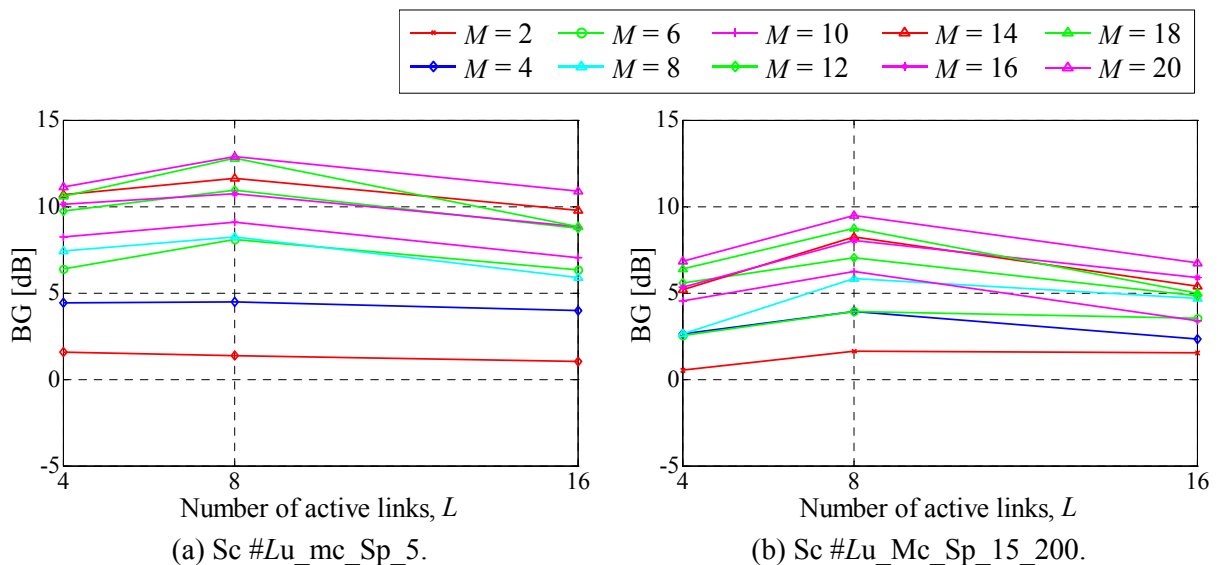


Figure 8.8 – BG, function of L , for several values of M , CSt #Lu_mc_Mc_Sp.

To finalise, one concludes that in MiC situations, in general, the BG dependency with L involves variations not as significant as those relative to MaC ones (if the MaC grouping does allow for any dependence, at all). The sort of MT positioning and angular displacement, as well as the reference code correlation properties, more strongly affect BGs in MaCs, compared to MiCs.

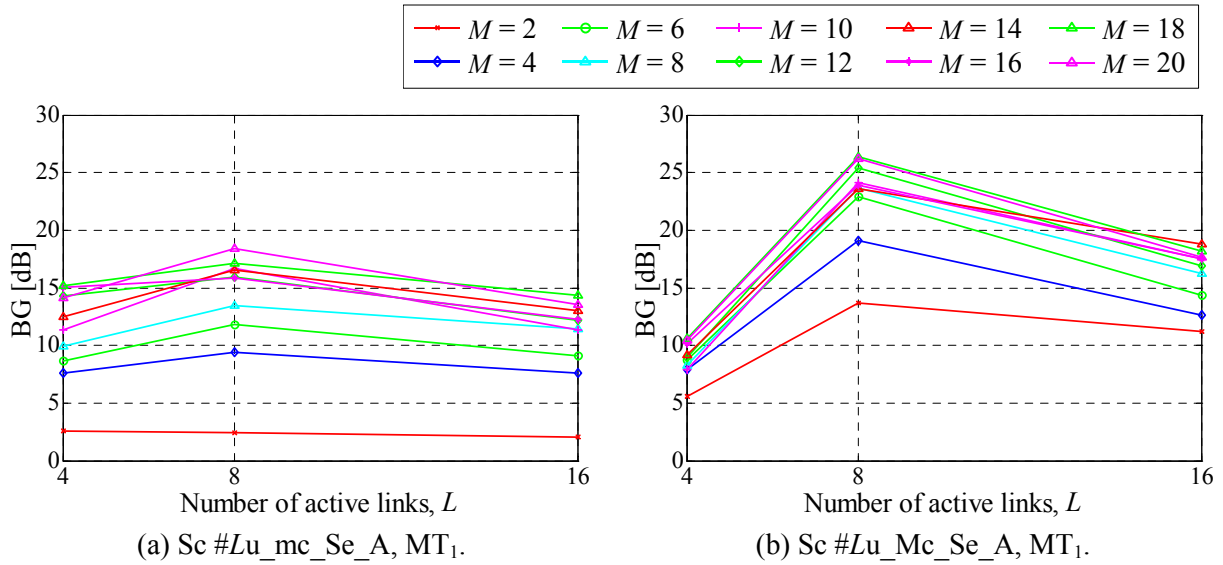


Figure 8.9 – BG, function of L , for several values of M , for MT₁ in CSt #Lu_mc_Mc_Se_A.

8.2.5 Correlation Matrix Components

Having characterised and compared the BG dependencies on MiC and MaC scenarios, it is also important to understand how the various involved powers depend on those scenarios, again in the perspective of comparing among the CSt scenarios. The correlation matrix components have been analysed for $M = 12$, and $L = 4$, for simplicity. For the explicit comparison of MiCs and MaCs, the same results will be used, being repeated for clarity in Figure 8.10, Figure 8.11 and Figure 8.12³⁶.

In the case of grouped MTs, Figure 8.10 presents many differences among the several power components, between MaCs and MiCs. Firstly, the $\mathbf{w}^H \mathbf{R} \mathbf{w}$ term is much closer to $N_s = 16$ (reaching 15.9) in the MiC case, but not for MaC (attaining 13.2, maximum), in agreement to viewing the MaC scenario as a more restrictive one, finally being reflected on the SINRs and BGs severe relative degradation. Secondly, the DesS power achieves much higher values in MiCs, compared to MaCs, also in conformity with the verification that the MaC situation involves a much poorer channel, making the extraction of DesS less efficient. Thirdly, the noise power achieves much higher values in the MaC situations, along optimisation, presenting a sudden increase after the 3rd iteration. Finally, it is seen that the delayed NDesI component, from the remaining MTs, $P_{>0}^{other}$, is larger in MaCs than in

³⁶ With smaller abscissa scale, cutting off cross-correlation negative contributions in favour of the real positive powers involved.

MiCs, being accompanied by a comparable decrease in the non-delayed NDesI term, from the remaining MTs, $P_{=0}^{other}$. Therefore, through these points, one verifies that the grouped MTs MaC situation is particularly affecting DesS and noise powers, NDesI powers not showing relevant changes in a whole, compared to the corresponding MiC scenario. Anyhow, keeping the study in Section 6.4 in mind, where for these MiC and MaC scenarios the significant iteration has been stated to be the 5th and 1st, respectively, the significant BGs are taken before the noise component acquires its greater importance, in the MaC case. Therefore, it is primarily due to the severe reduction in P_{DesS} that such MaC scenario delivers much lower BG values than in the comparative MiC one, anyhow³⁷.

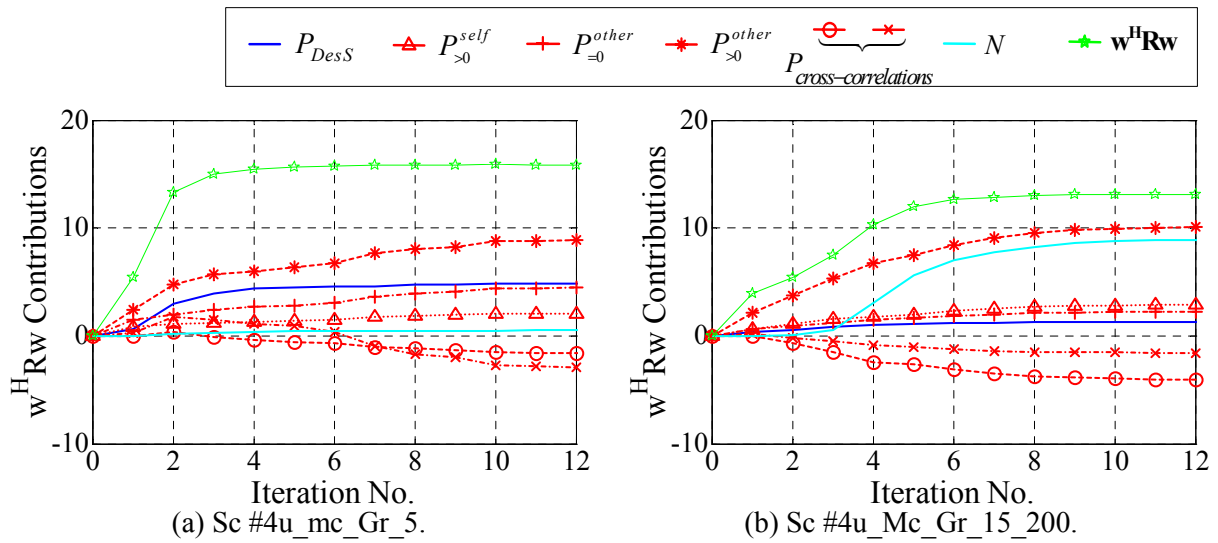


Figure 8.10 – Average power terms due to the composition of \mathbf{R} , for CSt #4u_mc_Mc_Gr, $M = 12$, $d_{MT} = 500$ m and 1 500 m, for MiCs and MaCs, respectively.

A similar, but less critical, effect is present in the CSt #4u_mc_Mc_Sp scenarios, where DesS power is also relatively smaller and the noise component larger in MaCs situation. As Figure 8.11 exemplifies, some NDesI power terms (the delayed terms, $P_{>0}^{other}$ and $P_{>0}^{self}$) are also larger in the MaC case. Hence, the conditions of MaC scenarios involve both higher NDesI and noise powers, with the decrease of P_{DesS} , compared to MiCs. The difficulties in both obtaining DesS power, and reducing interference, are also expressed by the lower values that the $\mathbf{w}^H \mathbf{R} \mathbf{w}$ term reaches in MaCs (up to 14.7, maximum), seeing that it reaches very close to 15.9, again for MiCs.

There is also the case of the single MT_1 , within CSt #4u_mc_Mc_Se_A scenarios, whose power terms are depicted in Figure 8.12, again revealing the larger beamforming difficulties expressed by the MaC conditions: the $\mathbf{w}^H \mathbf{R} \mathbf{w}$ term reaches 15.9 in the MiC case, but only 14.6 in the

³⁷ The noise term does influence the beamforming operation in the definition of the significant operation, therefore affecting BGs in a more indirect manner.

MaC one; the DesS term is lower, and the delayed NDesI and noise components are larger, in the MaC situation.

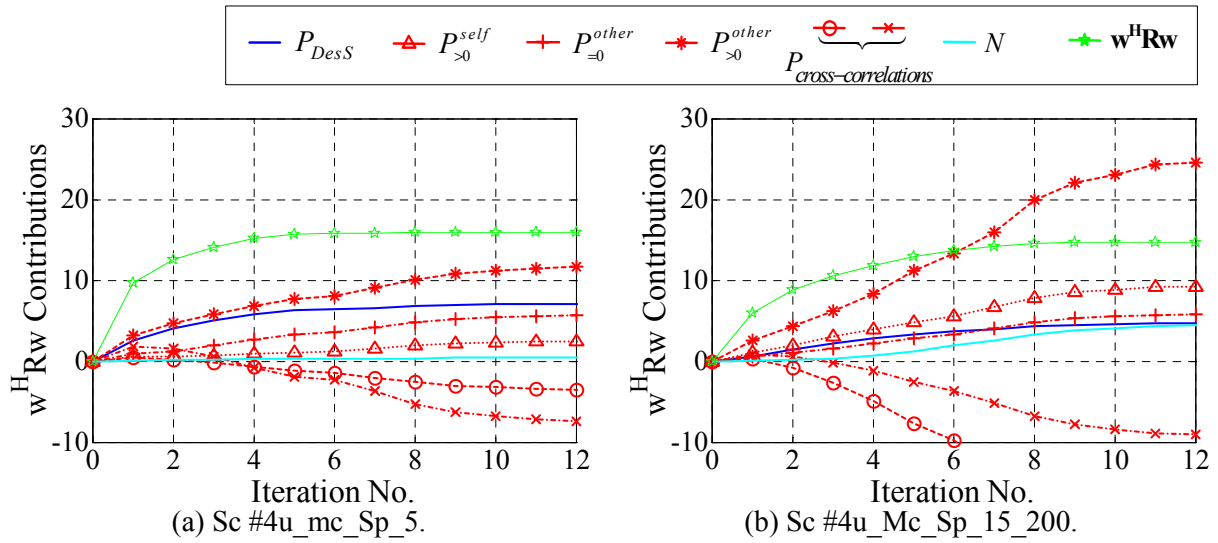


Figure 8.11 – Average power terms due to the composition of \mathbf{R} , for CS#4u_mc_Mc_Sp, $M = 12$, $d_{MT} = 500$ and $1\,500$ m, for MiCs and MaCs, respectively.

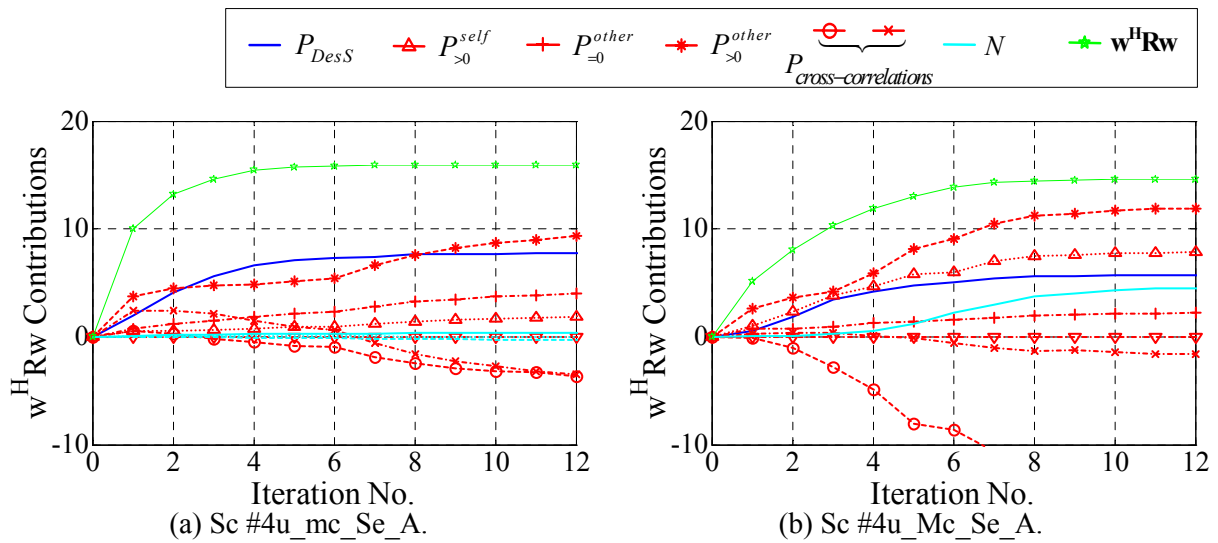


Figure 8.12 – Average power terms due to the composition of \mathbf{R} , for CS#4u_mc_Mc_Se_A, $M = 12$, MT_1 .

In order to more quantitatively be aware of the relative power values involved, Table 8.2 presents the relevant power levels for the examples of scenarios 4u_CSt_Gr, 4u_CSt_Sp and the case of MT_1 in 4u_CSt_Se_A: P_{DesS} powers, normalised to their maximum value amongst the three scenarios; the levels of $P_{>0}^{other}$ and N relative to P_{DesS} (notice that the values do not include the G_p CDMA processing gain, present in (5.14)). One sees that P_{DesS} values are highest for the single MT case, in the MiC Se_A scenario, as expected, reflecting the exceptional directional propagation

conditions at stake; these powers are also lowest for MaCs, compared to MiCs, especially in the Scs #Gr situations, being 13.19 dB below the best of these cases; also, among MiCs, P_{DesS} is lowest in the Scs #Gr situations, compared to the other two MiC scenarios, reaching 2.15 dB below the reference. As far as $P_{>0}^{other}$ and N are concerned, their attenuations generally exhibit the corresponding, but opposite, tendencies that P_{DesS} show, as function of the scenario, seeing that such attenuations are generally lower in the MaCs cases, relative to MiCs: $P_{>0}^{other}$ are less attenuated in respect to P_{DesS} in MaCs, for any of the CSt scenarios, and this attenuation is smallest for Scs #Gr situations; it is in the MiC Se_A case, the best case among all tabled ones, that P_{DesS} is highest compared to $P_{>0}^{other}$; concerning N , its values are lowest, in respect to P_{DesS} , for all MiC situations, reaching 20.78 dB below P_{DesS} in the MiC Sc #Sp case; the MaC Sc #Gr case also renders lowest noise relative levels, while the $P_{>0}^{other}$ contribution is anyway the highest; comparing the $P_{>0}^{other}$ and N levels, though the latter also exhibits close relation to the limitations imposed by the scenario, one sees that the interference component achieves greatest importance in the definition of the SINR, to which other involved interference components are further added (sub-Sections 7.2.7 and 7.3.7).

Scenario #		P_{DesS} [dB]	$P_{>0}^{other} - P_{DesS}$ [dB]	$N - P_{DesS}$ [dB]
4u_CSt_Gr	MiC	-2.15	1.42	-10.80
	MaC	-13.19	7.96	-14.40
4u_CSt_Sp	MiC	-1.16	1.51	-20.78
	MaC	-3.32	5.26	-4.31
4u_CSt_Se_A, MT ₁	MiC	0	-1.42	-13.96
	MaC	-1.71	2.30	-6.06

Table 8.2 – Values of the Power Components for MiC and MaC cases, for $M = 12$.

Conclusively, from the previous comparative display of BGs and the just presented results on the involved power terms, resulting from the decomposition of \mathbf{R} , the beamforming performance generally shows to be deteriorated in the MaC case, mostly due to the DesS power being lower. In this way, the lower richness that characterises the MaC scenarios reveals itself by primarily limiting the extraction of DesS power, a first indication of the larger beamforming difficulty, not being limited to the involved interference and noise power levels.

8.3 Relations to the MIMO Perspective

The aim of this work is not studying how a MIMO beamforming application is dependent on the propagation channel characteristics. From the start, the objective has been set to adopt a beamforming scheme, which from its simplicity would allow for the most generalising hypotheses and

conclusions, dealing only with fundamental propagation channel parameters. In this way, other than the physical limitations that rule the positioning of lobes and nulls of a radiation pattern, other modules of a transceiver chain have intentionally not been dealt with. Like this, as it has been expressed in Chapter 5, the dependencies on the performances of other processes are excluded, such as DF or tracking.

By having been able to resort to the fundamental physical aspects, which have been shown to limit beamforming in its simplest and plainest form, other sorts of issues may be naturally abridged. This is where links to MIMO result not only natural, but also necessary, in order to better base the importance of such presented hypotheses and conclusions. It must be understood that the henceforth consideration of MIMO is not only justified by the major research and technological trend that it is involving, but also explained by providing a better means of understanding, through confirming the wide coverage of the hereby adopted perspective, which would otherwise erroneously seem narrower. It is solely in that way that such incursion into the MIMO issue must be understood, thus, currently not going forth with any deep MIMO study³⁸.

Once more, it is stressed that such relation to MIMO is only possible through covering the physical level, only, i.e., establishing such relation independently of any encoding, interleaving, modulation, space-time coding, or any feedback modes, [HoTW03]. The matter is therefore kept at the physical, array pattern-shaping, level.

The hereby-presented definition of DCIR channel richness is based on a Single-Input-Single-Output (SISO) perspective, the angular and delay-spreads and densities that the DCIRs convey having been evaluated independently of any array or multiuser settings. On the other hand, if an array is considered at the BS, towards which the wideband directional propagation channel contributes with a more or less rich set of incoming signals, followed by resorting to a definition of channel richness to explain the results, then why not also evaluate the resulting correlation among array elements, its relations with the channel and with such parameter?

As it has been described in sub-Section 2.3.4, the MIMO implementation (depicted in Figure 2.5), requires that at least a certain uncorrelation exists among all M_{Tx} and M_{Rx} Tx and Rx antenna array elements, among the $M_{Tx} \cdot M_{Rx}$ available channels, where $h_{m_{Tx}, m_{Rx}}$ is the complex channel impulse response between the m_{Tx}^{th} Tx and the m_{Rx}^{th} Rx elements.

The consideration of total uncorrelation among array elements is a limit, best situation, in the sense of multipath diversity and MIMO. Nevertheless, seeing that the currently applied model assumes the planar wave NB assumption (Section 6.2), where AoAs of planar waves determine the phase differences among the elements of each array³⁹, a sufficiently rich multipath channel will

³⁸ E.g., clustering and the single-bounce assumption are very important issues, [Moli03a], [Moli03b].

³⁹ One must be aware that such may be a too tight an assumption, in the application to indoor scenarios.

inherently render enough uncorrelation within the BS Rx array elements. If this is understood in a MIMO perspective, it can also be understood in a Single-Input-Multiple-Output (SIMO) one, as it is shown in Figure 8.13, where a single element *array* antenna at the MT is at the Tx side, and the multi-element BS array at the Rx. This is, in fact, the perspective that is most directly conveyed in this work, additionally relating a definition of *channel richness* with the channel AoA and ToA spreads, in parallel with the fundamental beamforming evaluation.

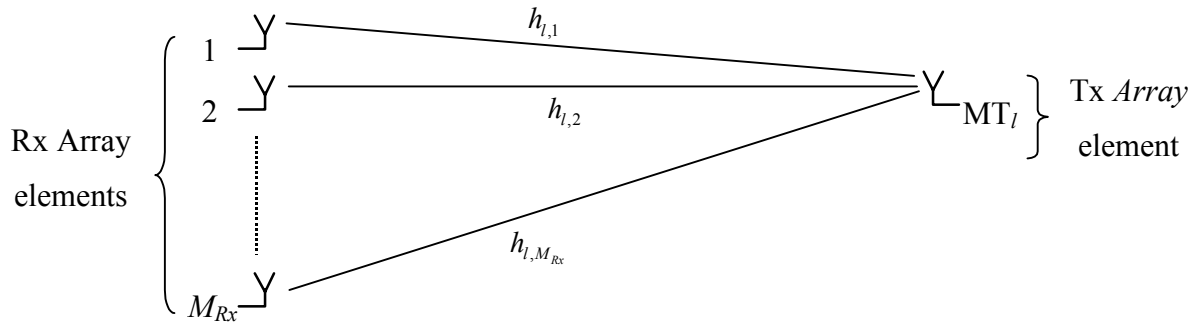


Figure 8.13 – The SIMO channel implementation perspective, between MT_l and M_{Rx} element BS array.

Following this reasoning further, consider the propagation scenarios where all L active MTs are grouped together, with the existing $h_{L,M_{Rx}}$ channel DCIRs solely differing on the fast-fading component between each l MT, due to the variation of the scattering coefficient phases. This is depicted in Figure 8.14, where the analogy to the MIMO scheme in Figure 2.5 is clear, having referred to the set of MTs as an *equivalent array*. Such MIMO-equivalent scenario therefore renders a total of $L \cdot M_{Rx}$ $h_{L,M_{Rx}}$ maximum independent fading available channels between both MT-equivalent *array* and the BS array.

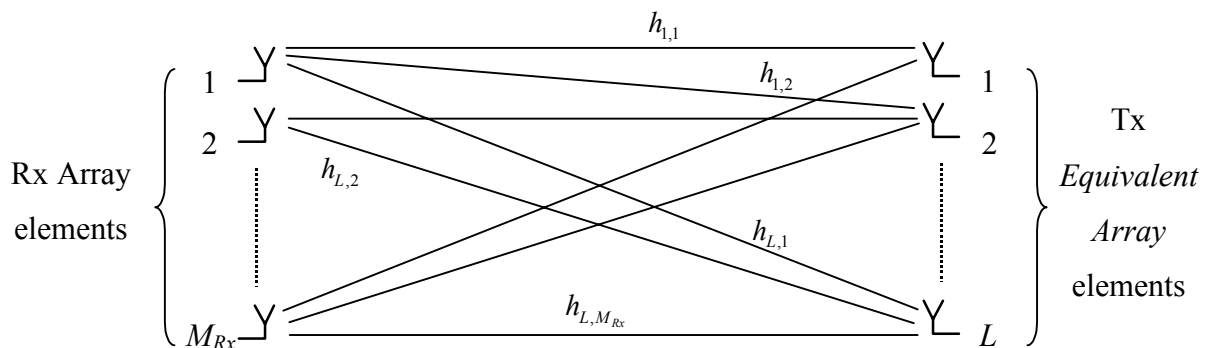


Figure 8.14 – The general MIMO channel implementation perspective, between L MTs and M_{Rx} element Rx array.

In this way, the channel matrix, \mathbf{H} , may be defined, where each entry $h_{l,m_{Rx}}$ corresponds to the complex channel response of the l^{th} transmitter to the m_{Rx}^{th} receiver, e.g., [SFGK00]:

$$\mathbf{H} = \begin{bmatrix} h_{1,1} & h_{1,2} & \cdots & h_{1,M} \\ h_{2,1} & h_{2,2} & \cdots & h_{2,M_{Rx}} \\ \vdots & \vdots & \ddots & \vdots \\ h_{L,1} & h_{L,2} & \cdots & h_{L,M_{Rx}} \end{bmatrix} \quad (8.1)$$

Therefore, having understood how a MIMO parallelism is possible, in the same way that it is known that the (un)correlation among array elements strongly depends on the angle-spreads involved and on the channel multipath richness, e.g., [SÖHM02], [XCHV02], [PAKM00], [FoGa98], such is also indirectly shown through this work, by another means, resorting to the evaluation of beamforming. Also, the inherent channel richness, in its several definition forms, the correlation matrices properties and the respective eigenspreads, must relate to the AoA and ToA spreads provided by the channel, i.e., further confirming their link to beamforming performance. Likewise, to further establish the bridge to the MIMO point of view, at the physical level, it is important to show how the presently defined channel richness and spreads do relate to the respective array correlation matrices.

There are various correlation matrices that may be at stake, in the presented beamforming application and the referred MIMO analogy: the \mathbf{R} correlation matrix that has been defined and used in the CG beamforming processing problem (Chapter 5), the Tx and Rx array correlation matrices, \mathbf{R}_{Tx} and \mathbf{R}_{Rx} , and the MIMO correlation matrix, \mathbf{R}_{MIMO} , e.g., [HoTW03].

In the SIMO perspective, pictured in Figure 8.13, \mathbf{R}_{Rx} is defined as in (8.2), where $\rho_{i,j}^{Rx} = (\rho_{j,i}^{Rx})^*$ is the complex spatial correlation coefficient between Rx array elements i and j , e.g., [KSMP00], defined as usual by (8.3).

$$\mathbf{R}_{Rx} = \begin{bmatrix} \rho_{1,1}^{Rx} & \rho_{1,2}^{Rx} & \cdots & \rho_{1,M_{Rx}}^{Rx} \\ \rho_{2,1}^{Rx} & \rho_{2,2}^{Rx} & \cdots & \rho_{2,M_{Rx}}^{Rx} \\ \vdots & \vdots & \ddots & \vdots \\ \rho_{M_{Rx},1}^{Rx} & \rho_{M_{Rx},2}^{Rx} & \cdots & \rho_{M_{Rx},M_{Rx}}^{Rx} \end{bmatrix} \quad (8.2)$$

$$\rho_{a,b} = \langle a, b \rangle = \frac{E[ab] - E[a]E[b]}{\sqrt{(E[a^2] - E^2[a])(E[b^2] - E^2[b])}} \quad (8.3)$$

The elements of such matrix will reflect the multipath richness of the involved propagation channel. In this way, such matrix has been calculated for the several scenarios, for $M = 4$, for a single MT, at 0° to the considered ULA. The samples used to calculate the involved expectancies result from 100 spatial concretisations of the same scenario type, each of these being used to further generate 500 DCIRs that differ on the phases of the reflection coefficients of the concerned scatterers, i.e.,

accounting for fast-fading. Therefore, for each spatial concretisation, a correlation matrix \mathbf{R}_{Rx} is calculated, followed by averaging all the resulting 100 \mathbf{R}_{Rx} matrices together.

In this sense, and for this objective, the WDCM has again been used according to its statistical features, rendering an average \mathbf{R}_{Rx} correlation matrix. It is therefore important to evaluate how these matrices do depend on the MiCs or MaCs channels, also as a function of d_{MT} and r . Namely, the obtained 1st, 2nd and 3rd diagonal correlation coefficient magnitudes have been calculated for the scenarios indicated in Table 4.10, averaging among the respective diagonal elements. These are shown in Table 8.3 (with two-digit precision), together with the respective standard deviation (with three-digit precision), these exhibiting very low relative values.

Cell Type	Physical Parameters		Magnitude Mean Standard Deviation		
	d_{MT} [m]	r [m]	1 st Diagonal	2 nd Diagonal	3 rd Diagonal
MiC	50	-	0.03 0.004	0.18 0.002	0.06 0
	500		0.29 0.004	0.07 0.007	0.01 0
	1 000		0.59 0.002	0.22 0.002	0.07 0
MaC	1 500	50	1.00 0	0.99 0	0.99 0
	1 000	200	0.95 0	0.82 0.001	0.63 0
	1 500	200	0.98 0	0.91 0	0.82 0
	2 000	200	0.99 0	0.95 0	0.90 0
	1 500	400	0.92 0	0.70 0.002	0.42 0

Table 8.3 – Mean and standard deviation of the 1st, 2nd and 3rd diagonal magnitude values of matrix \mathbf{R}_{Rx} , involved in several MiCs and MaCs scenarios.

Also, to further view from where these values have been extracted, and exemplify the type of matrices obtained, (8.4) and (8.5) present the magnitude of the correlation coefficients (shown in the form of matrices of the magnitudes, $\mathbf{R}_{Rx|}$), for particular concretisations of Sc #4u_mc_5 and Sc #4u_Mc_15_200, respectively. Through these examples, one also sees how the variations are lower amongst the values within each diagonal in the MiC case.

$$\mathbf{R}_{Rx|} = \begin{bmatrix} 1.00 & 0.27 & 0.15 & 0.15 \\ 0.27 & 1.00 & 0.31 & 0.07 \\ 0.15 & 0.31 & 1.00 & 0.37 \\ 0.15 & 0.07 & 0.37 & 1.00 \end{bmatrix} \quad (8.4)$$

$$\mathbf{R}_{Rx|} = \begin{bmatrix} 1.00 & 0.98 & 0.92 & 0.83 \\ 0.98 & 1.00 & 0.98 & 0.92 \\ 0.92 & 0.98 & 1.00 & 0.98 \\ 0.83 & 0.92 & 0.98 & 1.00 \end{bmatrix} \quad (8.5)$$

Focusing on the Table 8.3 1st diagonal results, as these provide indication of the correlation between direct-vicinity neighbour elements, one sees that the correlation coefficient magnitude values are higher for the scenarios that involve lower angle-spreads (Table 4.8 and Table 4.9). This is the expected, and well-known result, regarding angle-spread solely. Nevertheless, the fact that the spatial correlation coefficient does not take the temporal domain into account leads to apparent incongruences in their relation to the hereby defined and characterised densities and channel richness variations. For example, analysing Table 8.3 concerning the dependence with d_{MT} , one sees that the MiCs correlation coefficients show to increase with increasing d_{MT} . That seems to indicate lower multipath channel richness, as opposed to the ω_{DCIR} values that have been shown to increase (Table 4.10). Therefore, the tendency of the Table 8.3 correlation coefficient values do not reflect the effects of the temporal domain, due to the NB assumptions that have been put forward to calculate such coefficients, from the start, at the antenna array level: firstly, the array is assumed sufficiently small, so as not to consider signal delay among its elements; for this, the signal variations between each pair of array elements solely result from the phase differences due to each AoA in respect to the array geometry and positioning, i.e., such definition of \mathbf{R}_{Rx} does account only for the angular domain; as a result, Table 8.3 is consistent only with the angular domain spreads. As a further indication in favour of this reasoning, one sees that the discrepancy among channel richness and the correlation coefficients, as regards their dependence with d_{MT} , is in fact only present among the MiC cases, where the angle-spreads are larger, i.e., where the inter-element delays are largest and the lack of such temporal domain consideration results more evident. It is possible that an extended WB definition of the correlation coefficient should render better and more complete agreement, for MiCs. On the other hand, the tendencies of the MaC results, presented in Table 4.10 and Table 8.3, as function of either d_{MT} or r , are in total agreement with each other.

Anyhow, focusing on the comparison between MaCs and MiCs propagation channel conditions, Table 8.3 anyway very clearly shows how the latter channels are richer than the former ones, involving lower coefficients. In this way, these still reflect the relative differences in the degree of richness that MaCs and MiCs propagation channel scenarios have been shown to involve.

Finally, it has not only been shown how the hereby defined *channel richness* does relate to the known definition of Tx and Rx correlation matrices, but also its completeness has been confirmed, regarding the involvement of both the angular and temporal domains. By doing so, the strength of the simplicity of the definition of such channel parameter comes about, once more.

As it has been understood, the analogy of the current multiuser scenario implementations to MIMO, at the baseband physical array level only, can be easily envisaged. Such subsequent analysis could be done in several ways, either through the evaluation of both the Tx and Rx spatial correlation matrices, or through the channel matrix, \mathbf{H} , given by (8.1).

Notice that the hereby-mentioned \mathbf{H} matrix would be considered fixed during the assumed static/stationary period, having considered a time-flat channel. Another matter is the WB or NB representation of the MIMO channel (a matter that was summarily covered in sub-Section 2.3.4). Since a wideband channel is required, then a frequency selective, wideband representation of the channel matrix would be required, $\mathbf{H}(\tau)$. This representation will then be constituted by several frequency-flat, NB channel matrices, $\mathbf{H}(\tau_n)$, defined at the corresponding temporal bin, τ_n :

$$\mathbf{H}(\tau) = \sum_{n=1}^{N_s} \mathbf{H}(\tau_n) \delta(\tau - \tau_n) , \quad (8.6)$$

where the number of significant delays has been assumed equal to the number of samples, N_s . Going forth with a complete wideband MIMO channel, extending the study from considering inter-cluster delays (as it is stated in Chapter 4) to account for intra-cluster ones, therefore, making use of and analysing its richness in a wider sense, (8.6) will result in a larger summation. The number of samples will be much greater than the number of inter-cluster ToA hereby considered. In [DGVC03], it is described how the MGBSBCM and EM may be extended in that way, with the MIMO objective in mind.

For such study, on the one hand, one would need to understand better that at the Tx side, that is, at the equivalent MT L -sized array side, the spatial correlation matrix would be calculated, since the current application assumes that fast-fading is present among each MT_l pair, i.e., among each element l of the equivalent array (Figure 8.14). This means that additional uncorrelation is introduced within such array, and therefore among the involved $L \cdot M_{Rx}$ channels. Secondly, one must keep in mind that at the Tx side, the respective AoDs would need to be accounted for, in order to calculate the respective \mathbf{R}_{Tx} matrix. The current model application, [MaCo01], and the subsequent double directional version further directed towards the MIMO perspective, [DGVC03], do allow for such, but this study has not been pursued since, as it has been explained, this has not been its aim.

Lastly, by obtaining the \mathbf{H} matrix for each considered propagation scenario, including their multiuser characteristics as a function of the number of MTs and their angular positioning, it would be very interesting to evaluate how the corresponding eigenstatistics behave as function of the scenario. Taking the matter further, in the light of the previous section and in the perspective of this work, such properties could be related to the hereby-defined channel richness, involving both the temporal and angular domains at the physical level, also as functions of the scenario.

8.4 Summary and Conclusions

Having defined comparative scenario sets, among those implemented for MiCs and MaCs, a common set of fundamental scenario characteristics has been chosen and varied, on which the comparative analysis has been based – MT grouping and angular displacement, BS-MT distance, the

number of array elements and the number of active links. The comparative scenario sets present a reasonably wide variety of situations, from which important general conclusions have been extracted.

The *channel richness* parameter, as well as the *angular* and *temporal densities* of arriving signals, are found to be particularly important in the comparison of the selected MiC and MaC scenarios. The relationships of these parameters to beamforming performance have been fundamentally justified, complying to the logic in their definitions.

MT grouping and displacement most strongly affect beamforming performance in ways that significantly differ between MiC and MaC scenarios, in consistence with the differing channel richness, an order of magnitude higher for MiCs than for MaCs: the grouping of MTs leads to critically degraded BGs, in the MaCs case, near 0 dB (almost independent of any other parameter), while MiC scenarios always lead to positive average BGs (also being determined by the other parameters); the spreading of MTs leads to the improvement of MaC BGs, BGs being anyhow lower than the compared MiC scenarios; due to the larger inherent channel richness, the beamformer dependence does not heavily depend on the MT displacement in the MiCs case, as opposed to the MaCs one.

The performance dependencies with distance also differ, though not being as relevant as the discrepancies due to grouping, again in agreement with the channel richness opposite tendencies: BG dependencies on distance are also opposite between MiCs and MaCs. Regarding the sensitivity to the variation of the number of array elements, again the channel richness helps to understand that, for all scenarios, there is a larger benefit from increasing the number of array elements for MiCs, compared to that obtained for MaC situations. Similarly, concerning the dependency with the number of active MTs, MiC situations involve BG that are not as significantly sensitive compared to those in MaCs, again justifying so with the larger robustness and channel richness that MiCs entail.

Further consolidating these conclusions, the significant powers involved have been analysed, namely, P_{DesS} , $P_{>0}^{other}$ and N . It has been confirmed that, between MiCs and MaCs, P_{DesS} is particularly degraded in the latter situations, independent of MT grouping, again reflecting the larger beamforming difficulties. $P_{>0}^{other}$ and N also present the corresponding expected tendencies.

Besides the specific conclusions that make part of this chapter, the way of reasoning behind the reach for results is most important: firstly, the defined *channel richness* has been used to understand the fundamental factors behind the performance divergences towards MiCs and MaCs, such influences being understood to be most independent of the beamforming algorithm and the nevertheless limited number of propagation scenarios, to the necessary extent; secondly, by having established the bridge to SIMO and MIMO channel characterisation, it has been shown how the reasoning of combining the notion of *channel richness* and the beamforming application does cover general fundamental matters, providing further indication that one is dealing with the background ruling physical issues; thirdly, the simple but relevant analysis of the BS Rx array spatial correlation

coefficients has shown how these depend on the scenarios, presenting coherent relationships, while justifying the discrepancies through the same fundamental parameters.

Through this reasoning and logical arguments, one verifies that it is in the channel's own physical characteristics that the hypotheses have found their confirmation, and such simplicity and independence on other implementation specific factors have been possible since the algorithm application has resorted to the two domains available – the temporal and angular. Having dealt with such physical characterisation in this manner, one further fundamentals that more complex spatial adaptive schemes will also be subject to the same wideband directional constraints presented by the propagation channel and scenarios.

In a more practical-directed perspective, it is important to conclude that the added value of using SAs, spatial filtering and beamforming in particular, may be critical in MaCs, so as not to even possibly justify their implementation in those environments. Knowing that complex technologies are often applied to only later prove that their use is not necessary upon most channel conditions, e.g., channel equalisation being prepared for excess delays that are too large and unlikely in GSM, these conclusions render particular significance. In order not to exceed in the generalisation, one can definitely state that either more complex adaptive schemes, or the combination of several techniques are required in MaC environments, in order to make most efficient use of the channel spatial content. For example, the hard handover between MiCs and MaCs within a hierarchical cell structure may account for that, hading-over from a MaC without SAs to a MiC with these, according to capacity demands. Even in the case that particularly significant isolated clusters exist, outside the circular region around each MT, it is very unlikely that MTs close together will not share most of the clusters in the MaC. For these arguments, not only should spatial filtering applications involve lower costs in MiCs, but also render smaller dynamic range and larger interference suppression gains (also keeping in mind that it is in MiCs that larger capacities are demanded for, compared to MaCs). Additionally, if one envisages that the involvement of richer multipath content in MiCs is not only limited to the horizontal plane but is very much extendable to the whole spatial domain, and understanding that MaCs again may contribute much less in that manner, then larger divergences should be further expected.

In these senses, another step towards understanding and evaluating the physical roots behind the general dependence of adaptive antenna solutions on the complex mobile propagation channel has been sought for. Accordingly, these conclusions call for the careful analysis of what their implications are in future MBSs, following in the next chapter.

9 Towards Future Mobile Broadband Systems

(...) and be not faithless, but believing. (...) blessed are they who have not seen, and have believed.

— in *Holy Bible*, John, 20:27-29, Saint John the Apostle (unknown-101)

9.1 Introduction – Defining Perspective and Motivation

With the objective of evaluating the impact and contributions from the present study, in the perspectives of the present and future adaptive array transceiver related issues and mobile operational environments, this chapter exposes what fields are thought to be most directly involved, and what the extrapolated implications of the conclusions reached in the previous chapters may be. In order to do so, it is important to establish the relevant issues involved with wideband and the so-called 3rd and 4th generations (3G and 4G) of MBSs that are presently evolving and being envisaged. The perspective of such outline must, therefore, be understood to being limited to dealing with the major contributions from the present work. While covering the areas of propagation channel characterisation, adaptive array implementation, scenario and system embedding, involved in the previous chapters, the current purposes also demand for their more explicit and directed account.

The referred reasoning evolves from firstly focusing on the description of the major evolution trends that 3G, namely International Mobile Telecommunications after 2000 (IMT-2000)/UMTS, and further 4G systems are supposedly implying. Then, hypotheses are put forward, concerning the channel-, scenario-, array- and system-wise perspectives, extrapolating the implications of the hereby-presented results towards such visions. As it is understood, by doing such, one is in parallel pointing at areas towards which such work can evolve in the future, openly accepting that those have not been the centre objectives of the present study. On the other hand, it is hereby explicitly assumed that the final objective of this chapter is to establish bridges to such prominent fields that, as the text will show, are involving many parties. Though extrapolation hypotheses are presented separately, in many

cases they are inherently intertwined, justifying the conclusion of this approach with exposing such joint relations.

9.2 Future Wideband Mobile Systems Focus

9.2.1 Evolution Trends – A Literature Review

The investigation and discussion on *what*, *how* and *when* mobile wireless technologies beyond 3G will emerge are flourishing amongst the industry, financial institutions, universities, governments and international organisations, technical associations, through conferences, journals, books, and so on. A vision put forward by [WWRF01] is that the future will intake a worldwide market combining ubiquitous access to both Internet and general personal computing, resulting in a model different from that which has characterised past and present mobile communications generations. In [BeBT02], the vast term *next-generation wireless*, or *NextG*, or *4Gmobile* in [Lu02], involves the definition of “*Beyond 3G*” in the International Telecommunication Union (ITU) and Wireless World Research Forum (WWRF) views, also *4G* in the perspectives of the publications from the Institute of Electrical and Electronics Engineers (IEEE) and WWRF, and of technologies related to Wireless Personal, Local and Metropolitan Area Networks (WPAN, WLAN and WMAN) and use of wireless Internet. In this sense, one realises that not only the perspectives are numerous but also there are different ways to term such visions. For that, still keeping in mind such variety of perspectives, but in order to simplify the reading, terms such as *NextG*, or *4Gmobile*, or *Beyond-3G* will all be hereby referred as simply *4G*.

In 4G, a wide range of data rates must be readily available for the user, according to his/her demands, within multi-cell, multi-user, multi-standard and multi-network scenarios. A *transversal* communication model is forecasted to exist, involving a new whole architecture, services and applications, with several access technologies being combined to form a common complementing platform, covering cellular mobile, broadband wireless access, wide area broadcast, wireless LANs and PANs, and wired systems, [Wang01], [BeBT02], [Lu02]. For such, radio resources and services will require their intelligent and efficient management. Possible areas of future development range from, [LuZu02], [BeBT02], [Lu02], [BGQS01]:

- network-related technologies, such as all-Internet Protocol (IP), security, billing, user deployment, mobile ad-hoc and adaptive networks, new and dynamic multiple access schemes;
- application-related technologies, e.g., covering coding and compression dynamic variable-rate codecs, *intelligent* mobile terminal man-machine interfaces, highly functional display devices, streaming data related technologies, transparent interfacing to users and services, a variety of user-definable access and service options and inter-machine communication;

- advanced wireless access, covering dynamic Quality-of-Service (QoS) control, IP mobility control, link adaptation, among others;
- efficient spectrum use, involving smart spectrum assignment, interference and fading mitigation techniques, high-density multi-tier cellular structures, advanced adaptive transceiver technologies, adaptive high-efficiency multi-level modulation, dynamic multiple-access management techniques;
- advanced terminal technologies, either at the mobile terminal or at the base station, such as wearable terminal technology, Software-Defined Radio (SDR), multi-standard terminals, broadband wireless transceiver, highly functional display devices, next-generation semiconductor devices and power amplifiers, and equipment flexibility towards network and standard upgrading.

Such a *transversal* or *horizontal* architecture, in the sense of being an integration of several standards in a multi-network, providing *ultraconnectivity*, or a *Converged Broadband Wireless Core*, in the sense of involving seamless connectivity and transparency in network and service provider interfaces, establishes a *paradigm change*, as [BeBT02], [WWRf01] and [Lu02] envisage. The *classic* approach, as in cases of most of the previous generations, would firstly focus on higher data rates with new frequency bands for a world standard, as opposed to the primary objectives of firstly providing the user with connectivity, transparency and services on demand, [BGQS01].

In a more confined, and somewhat more evolutionary perspective, the convergence of very near future IMT-2000/UMTS and other wireless communication applications is forecast to cover the next several years, seeing that at their current onset those are being separately deployed and upgraded by operators, being subject to various types of constraints. Though such growth, having shown to be imposed by economical, political and technology trends (not the mention the related social implications), may take directions that to some may be surprising (e.g., HIPERLAN/2 being overridden by the IEEE 802.11 market, [Luce02]), it is predicted to be gradual and continuous towards the development of a whole mobile and personal communications system, [LuZu02]. In fact, this sort of general encompassing vision is also reported by [Lu02] as fitting the view of current IMT-2000/UMTS.

On the one hand, the numerous delays in the IMT-2000/UMTS deployment have shown that several of the last years' IMT-2000/UMTS growth predictions are not longer valid. On the other, its implementation is being indirectly pushed forward by other wireless systems and markets, e.g., IEEE 802.11, already providing data rates of up to 10 Mb/s, [KeVS02]. Therefore, the gradual growth is currently potentially evolving towards such integration in a whole. Presently, already, the perspective for IMT-2000 is that existing wireless systems should be complementary, not replacing others, further rendering the longer term view that 4G will involve several air interfaces, not unify nor be a replacement, so that there is accessibility to a *horizontal* set of wireless communication systems, adaptively using that/those which provide the most adequate service, [KeVS02], [Wang01], [Lu02].

Truly, though, high capacity and high bandwidth WLAN systems, e.g., IEEE 802.11 standards, are already in the market, being seen by such market as competing technologies. Nevertheless, the fact that these are only able to provide the capacities and bandwidths for limited service areas and low terminal velocities should decide the complementarity towards other wideband systems, such as HIPERLAN, HIPERLAN/2, or wireless mobile Asynchronous Transfer Mode (ATM), [Smul02], [Wang01].

Additionally, digital broadcasting, in the forms of Digital Video Broadcast (DVB) and Digital Audio Broadcast (DAB), is already being implemented throughout, being able to provide a variety of asymmetric multimedia services, [KeVS02]. Actual actions on the combination of IP-based data casting with GSM and Terrestrial DVB is another sign that these may also complementary converge to the overall 4G communications system, not as a competing communications system.

Through this reasoning, the door is open, the market allowing for such, towards a complementary implementation of several wireless communications systems, covering several frequency bands, propagation scenarios and mobility conditions.

As parts of this new *horizontal* perspective, being obligatory means to achieve so, multiple means of adaptation will be required: Dynamic Spectrum Allocation (DSA) and use, together with spectrum sharing, will make the optimisation of such resource in the frequency, geographical and temporal domain possible; service and application adaptation are required, to guarantee the provision of the desired services with the suitable QoS; an application discovery and application layer must be included, dealing with the regulation of communication radio and channel resources and the finding of applications that may be on offer, with channel adaptive source coding and data rates according to the offered channel capacity and user needs; Adaptive Resource Management (ARM) must be applied, aware of the several layer capabilities and states, deciding and controlling multi-layer activities so as to optimise QoS, general throughput, resource and power uses. Approaching the layers below the Network one, towards the Link, Radio, Medium Access Control (MAC), and Physical layers, the ARM in 4G provides and manages DSA among a set of access points and terminals, also dynamically controlling and allocating multiple access schemes to define a “soft” channel, dynamically managing modulation and coding for each soft channel, [BeBT02].

Following this, adaptation and dynamics at several levels seem to be major ruling forces that will accompany the new wireless communication systems in its transversal extension.

Apart from requiring an enormous endeavour by the intervening parties, such as governments, industry and markets, the technological efforts are also large and involve many of the beforehand listed issues, e.g., highly adaptive modulation and coding, multi-dimensional and composite multiple access techniques and DSA. Regarding the technologies behind such flexible implementations, SDR, in its smart and cognitive radio forms, is a fundamental platform, either at the baseband or at the RF levels. Its main advantages are the great flexibility in the programming of several wireless standards, rendering the dynamics required without changes in transceiver hardware, and rapid overall

deployment. The perspective of downloading a new air interface is a current and demanding objective, throughout the SDR field intervening parties, [Wang01], [BeBT02], [Lu02]. A related issue, also in the sense of convergence, is the implementation and use of multi-standard terminals. The IST-FLOWS project, e.g., [EHRC02], [Evan03], and the [KMRV01] contribution exemplify and describe actions in that field.

Multi-standard integration is, therefore, another fundamental objective in the construction of a 4G system.

A high performance physical layer will need to be at work, in order to provide 50-100 Mb/s or even up to 1 Gb/s, [BeBT02], [Lu02], [HoTW03], meaning that the channel coherence bandwidths will be highly overpassed. For this, CDMA will not suffice, other multiple access and modulation techniques appearing as more robust and even simpler alternatives. In this field, MC-CDMA, as one of the several multiple access schemes being envisaged for 4G, delivers good results to oppose multipath fading (besides frequency use efficiency). Orthogonal Frequency-Division Multiple Access (OFDM) forms, including MC-OFDM, allow for better exploitation of larger number of resolvable multipaths, besides adaptive frequency channel control and inherent frequency diversity. Additionally, adaptability to varying interference conditions is aided by the inherent subcarrier formation. Though one advantage of using OFDM is the low system complexity, guaranteeing subcarrier orthogonality, it may be particularly sensitive to synchronisation errors and amplifier/mixer non-linearities. The MC combination of OFDM and CDMA eases such problems, also leading to the improvement of NB interference (though not necessarily ending up with capacities higher than those obtained with single-carrier CDMA, [Wang01]). Such OFDM/CDMA combination leads to robustness in very *bad multipath*⁴⁰ conditions, delivering comparatively high bit rate and large capacity, [Lu02], [ChYS01]. Frequency hopping OFDM is also reported to being a preferred alternative, [BGQS01], and MC-CDMA using complementary codes is described to being particularly suited for spectrum efficiency, MAI and multipath mitigation, [ChYS01].

Multiple access schemes that involve new modulation types are, therefore, another strong field of development towards the most efficient implementation of future mobile systems.

Finally, SAs or adaptive transceiver structures will undoubtedly play a major role in the overall deployment of the hereby mentioned generally envisaged trends and objectives, rendering a most efficient spectrum use, already at the physical level. Exploiting the spatial domain delivers adaptation and dynamics at that level, further optimising integration of several standards in a terminal, with the combination of several multiple access schemes, including SDMA. In the far end, the complementary implementation of several wireless communications systems will surely involve several types of adaptive array solutions. The management of the spatial domain, a resource

⁴⁰ It must be kept in mind that characterising a channel to be *bad* in terms of multipath can be very relative, as in fact also this study shows.

inherently shared in mobile and cellular communication systems, will not only be required by several standards themselves but will further help in the their physical intertwined deployment.

With multi-antenna transmission and reception schemes, larger variety of diversity techniques may be applied to provide robustness against fading. On the other hand, the exploitation of multipath is also possible, turning it into an advantageous channel property. Additionally, several interference reduction methods may also be implemented, being based on beamforming DoA estimation, space-time modulation or multi-user detection schemes. Other advantages are the lower transmitter power levels per transmit antenna, and the inclusion of a new dimension for rate and power management. On the whole, higher system capacity may be provided. By resorting to MIMO for 4G systems, data rates of up to 100 Mb/s and 1 Gb/s, requiring 100 MHz bandwidth, are being predicted to be possible in wide-area high-mobility and local-area low mobility scenarios, respectively, provided the right coding and modulation are applied. Furthermore, the application of MIMO is also being extended towards WLAN, DAB, and DVB-Terrestrial systems, [HoTW03].

To conclude, one must be aware that, for all of these visions and trends to become a reality, or at least to progress in such directions, involving enormous increases in rate and spectrum efficiency, the wideband and directional propagation channel characterisation is mandatory. The application of WDCMs must accompany the technological growth of all physical level techniques. In a wireless environment that is thought to provide *ultraconnectivity*, with the shape of a *Converged Broadband Wireless Core*, with the need for transparency and adaptability in the wide sense, such knowledge of the propagation channel is even more demanding, covering a large spectrum to encompass several standards and the propagation scenarios that are applicable to each or several of such standards.

9.2.2 Intercepting Scopes from the Present Work

From the aforementioned rough listing of panoply of areas, present and forecast effort trends, the far-end scope of this work truly ends-up in aiming at the most efficient use and sharing of spectrum and space, with inherent adaptation at the physical level. It is within such shared resources, allocated among several mobile terminal users, that a certain interference mitigation scheme is studied, such as the presented beamforming application. Additionally, such requires the knowledge of the propagation channel, in its directional and wideband perspectives, in order to most effectively allow for the spatial and temporal discrimination of desired and non-desired sources, while sharing the same spectrum, temporal and spatial domains⁴¹.

In order to further view how the contributions of the presented work intercept the mentioned areas and trends that characterise wideband future mobile systems, it is important to explicitly state

⁴¹ The additional issues of frequency or temporal correlation are also of particular relevance, e.g., in MC-CDMA, though these matters have not been hereby intentionally studied.

what those contributing outputs are, covering the wideband and directional channel characterisation and adaptive array fields.

In a simple enumerative manner, if it is plausible enough to separate these from each other, especially in a study that particularly aims at treating them jointly, the propagation channel and scenario oriented outputs are the following:

- the work demonstrates the joint application of adaptive beamforming with a WDCM, clearly showing that the definition of such WDCM is not a secondary issue, but a primary one, in the simulation and testing of spatial adaptive techniques;
- by employing a propagation scenario perspective, the multi-user and WDCM conditions have been varied, accounting for the variation of several scenario parameters, in order to finally evaluate the fundamental dependencies that the generation of an user-specific optimised pattern exhibits, in the sense of interference reduction;
- the work presents insight towards the temporal and angular channel characterisation that strongly relates to the beamforming performance, namely, resorting to the definition of *angular* and *temporal densities*, and *channel richness*;
- by such characterisation, the performance has been analysed for MiC and MaC scenarios, either individually or comparatively.

In parallel, the contributions in the point of view of the adaptive array scheme presented are also listed below:

- while the correlation among array elements has been considered to be total, regarding the effect of each arriving planar wave, the operation of the applied beamforming strategy is shown to be highly determined by the channel multipath richness, i.e., inherent spatial uncorrelation existing among elements, independent of any diversity scheme. In this sense, it is also shown that, also in the perspective of beamforming, further exploration of the spatial domain must pass through the exploitation of such richness;
- the nature of the channel and the multi-user environment, the subsequent temporal and angular dispersions, may lead to an OD problem, where the MMSE does not necessarily lead to maximum SINR, such depending on the nature of the reference signals and the temporal and directional characteristics of the channel;
- due to the loss of temporal and spatial orthogonality of each links' incoming signals, the non-blind implementation has been shown to highly depend on the nature of the reference signals involved.

Judging by the issues just outlined, though many of the related problems and solutions have been promptly put forward at the end of the corresponding chapters, the ground is hereby set for the exploitation of hypotheses that such matters are seen to endeavour, in the prospect of the presented MBSs trends. Such hypotheses have been divided into channel-, scenario-, array- and system-oriented issues, some inevitably being intertwined.

9.3 Extrapolating Hypotheses

9.3.1 Propagation Channel Oriented Hypotheses

As it has been mentioned in parallel to the definition and evaluation of the temporal and angular densities and channel richness, accounting for all L links' contributions, within the *whole*-DCIR, may allow for the extension of those parameters to a multi-user channel characterisation of the same type. Additionally, due to the use of multi-antenna transceiver structures, at both the BS and the MT sides, the characterisation of the channel is required to be not only directional, but also *double*-directional, [StMB01]. This means that, besides characterising the channel at one side, as it has been done in the presented study, one needs to extend such study to relating the directional features between both Tx and Rx sides.

Such extensions, always in the wideband perspective, can be looked upon in different, yet complementary, ways.

By accounting for all L links, the *whole* temporal and angular densities may be defined accounting for the *whole* delay and angle-spreads, i.e., corresponding to all the involved DCIRs, the total scattering area involved. Nevertheless, additional parameters would need to be introduced, such as the spreads of each *single*-DCIR and the amount of superposition among these. Judging from the hereby-presented results, only in that way may a closer relation between propagation channel characterisation, within a complete multi-user scenario setting, and interference suppression beamforming performance be established.

In the same manner that this research has evolved, beamforming may be considered at the MT, further evaluating how it depends on the involved channel directional and wideband properties, regarding angular and temporal densities, and channel richness. In that way, not only can co-channel interference mitigation among MTs be evaluated, but also the inherent channel richness may allow for the further exploitation of the whole set of available scattering in between BS and MT. For example, the generation of most orthogonal pattern solutions at the MT array tends to making use of disjoint groups of clusters between MT and BS, further resulting in more independent *single*-DCIRs incoming at the BS array.

The directional properties of the channel at both the Tx and Rx sides may be further related between each other, regarding the aforementioned evaluation. In this sense, the double-directional channel properties, for the MiC and MaC situations, would result in deeper knowledge of the channel and subsequent most complete channel modelling.

By considering a multi-element transceiver at both the Tx and Rx sides, the path towards MIMO channel characterisation is further pursued, in either a single- or multi-user perspectives. In that way, a double-directional wideband channel model would also render the MIMO characterisation of the channel. Therefore, reasoning that the evolution of the mobile technologies will demand for the

most complete system- and link-level evaluation platforms, the double-directionality properties of the channel need to be addressed by future research.

Additionally, if today's channel modelling trend is sometimes simplistically focused on the capacity curves that MIMO modelling involve, the remaining channel knowledge will undoubtedly be always required concerning both the wideband and directional domains. From slow- and fast-fading WB characterisation, e.g., [CaCo03], to angular and temporal dispersion and multipath richness, future work needs to be undertaken.

In fact, the current evolution and efforts towards MIMO and multi-antenna transceiver structures is seen as a boost towards the acknowledgement by the processing-level community that making use of channel characterisation and modelling definitely needs to be part of their work. If in the last few years it has not been so, even with the onset of IMT-2000/UMTS and related research and development projects, one envisages that such issue will be very much solved. The 3GPP output on the definition of a SCM for MIMO simulations, [3GPP03], is not only a sign of a difficult convergence among the involved partners, but also a sign of such understanding. Furthermore, one envisages that the multi-user scenarios will also require being of strong concern in related research and development.

In these senses, the work hereby presented not only deals with such matters, calling upon their relevance, but further renders future development and pressing contributions.

9.3.2 Scenario Oriented Hypotheses

As it has already been mentioned, accounting for multi-antenna structures at the MT side requires the introduction of new multi-user propagation scenarios, in order to consider co-channel interference at the MT level and to fully make use of the channel richness potential. This sort of approach may be complex, requiring the intricate use of a WDCM that introduces several DCIRs among all MTs. Doing so will be possible while making use of the simplicity that the semi-statistical nature of the hereby used model involves.

In addition, keeping in mind that indoor or outdoor pico-cellular environments will cover user hotspots, possibly requiring large data rates, possibly highly asymmetrical traffic, smaller cell scenarios, then a new model scattering area will need to be accounted for, i.e., new scenarios. Therefore, in these highly rich multipath situations, MT-BS links will most probably make use of a large number of common sets of scatterers, resulting in many common ToAs and AoAs. As this study has concluded, the implied high DCIR channel richness and angular dispersion that will characterise each link will render better beamforming or other spatial techniques performance, as well as larger robustness towards the then most probable MT grouping. Anyhow, such sort of study needs to be put forward.

Still on the matter of extending the scenarios to other interference situations, especially thinking on the just mentioned pico-cell environments, the evaluation of inter-cell interference and its

reduction reaches particular importance, not only at the MT but also the BS levels. In this way, work also needs to be undertaken in that sense.

Anyhow, one must understand that the physical constraints and relations that have been brought up in this work will inevitably rule all the previously new scenarios, i.e., one not expecting to reach contradicting results. The application to other scenarios would therefore be seen as a complementary means to further generalise the conclusions presented here. By doing so, the type of cell layout and planning that is forecast to be at hand when using smart spatial techniques will most probably account for the involved scenario channel richness, angular and temporal densities or spreads. Therefore, one also envisages the contribution of this research at the level of cellular planning, through this scenario-based view.

9.3.3 Array Oriented Hypotheses

Having addressed the importance of considering other scenarios, involving other interference sources and higher level planning issues, while envisaging beamforming at the MT side, then the matters of array structures and configurations naturally come about.

Firstly, for lower frequency systems such as IMT-2000/UMTS ones, the number of array elements will inherently be small at the MT side. Considering the pico- or micro-cellular situations, where most of the MTs may be carried by people standing or sitting outside any means of transport, the terminal may be as large as a laptop⁴². Therefore a maximum of four elements can be considered for a planar array, but in many terminals no more than one element may be possible. In addition, though this limitation may be solved for higher frequency 4G systems, the user body will always contribute to the obstruction of the pattern, heavily conditioning the shape of such pattern. This actually means that some sort of large body-imposed sectorisation will be most probably happening at the MT side, therefore reducing the spatial freedom to make the most of the surrounding channel richness. On the other hand, due to the reasonably random orientation that the user-terminal pair may take, the several MTs present in a scenario will most probably have their smart radiating patterns towards disjoint groups of clusters, i.e., rendering more independent beamforming at the MT and BS sides, among active links, resulting in better overall interference mitigation.

There is no doubt that an adaptive configuration at the MT will be better than the monopole, and that such physical implementation may be highly limited. Nevertheless, the previous paragraph (and this study, itself) shows that such matter does require attention and study.

To add more, still regarding beamforming at the MT side, planar beamformer structures may be particularly useful in richer scenarios, indoor pico-cells, in particular. Though one would reach the same conclusions as those presented in this work, as far as the physical level constraints are

⁴² It is true that MTs will be placed in vehicles, naturally being able to involve much larger arrays, but the personal-held terminals should be in larger numbers.

concerned, the formation of 3D-adaptive array patterns would further enhance the capability for the array to make use of the available channel richness (not to mention the MT user obstruction matter).

Concerning the processing side of the array problem, one must keep aware that more complex and richer channels are even more demanding for DF adaptive array methods. Furthermore, DF followed by the resulting beamforming may inherently limit the consideration of multipath in a large scale, i.e., possibly contributing to losing the inherent channel richness and the total angular span occupied by DesSs, which one has seen to be very important. In the case of MIMO implementations, which deliberately exploit such multipath richness, one may argue that the correlation matrix eigenvector-based beamforming leads to array patterns that may not fully make use of the directional nature of the channel, being limited to generating a single beam pattern for each of the orthogonal and non-interfering parallel available $\min\{M_{Tx}, M_{Rx}\}$ channels, [HoTW03]. Furthermore, with the inclusion of multiple MT interference sources, one believes that such solution may not be the ideal in terms of interference suppression.

In this sense, and again bringing up the high probability of large densities of MTs, while beamforming may exist at both the MT and BS sides, more robust adaptive solutions should not be left behind, not discarding the control by reference-based algorithms. Since the study of MIMO implementations has not been deepened, one has hereby shown that there can be a critical and constructive view towards some of the present trends in the research and development of MIMO techniques. Such means that this further renders space for future work, again joining the physical wideband and directional characteristics of the propagation channel, the processing, the system-wise points-of-view, while viewing the matter in the form of multi-user interference scenarios.

Concerning the higher-level issue of planning the location of Access Points (APs) or BSs, the type of array structures that may be best applicable is another matter, as function of the involving environment. For example, there may be no reason to place other than a BS non-adaptive ULA in a MaC, where spatial filtering may be so limited and the discrimination of signals in elevation may be relatively irrelevant. On the other hand, planar adaptive BS arrays may be very adequate to indoor, or general pico-cellular situations. In this sense, radio planning is forecast to further include the evaluation and decision making towards the type of adaptive or non-adaptive arrays that BSs should include.

9.3.4 System Oriented Hypotheses

At the system level, the issues such as larger involved frequencies and smaller cells have direct impact on the propagation channel richness that may, or not, be available for future adaptive multiple antenna schemes.

The increase in the operating frequency, in the MT density, or in data rates, tends towards the implementation of smaller cells. For example, cell radii may reach 20 to 30 m, in 4G systems, [Wang01]. Though this matter has already been addressed, such reduction in size is in this case seen

as a consequence of several system parameters, such as operating frequency and demanded vs. available capacity. Therefore, the consequences in the available channel richness will tend to be reduced due to reduction in the total scattering area. Once again, keeping in mind that such sort of cell scenarios will most probably imply large AoA spreads, therefore, still rendering large freedom in the location of lobes and nulls, such reduction in the scattering area may not reach enough importance in the reduction of channel richness. Adding to this, as it has also been mentioned, inter-cell interference will need to be accounted for, though free-space attenuation will be larger or the involved transmitted powers will be lower.

Another related matter that is seen as a system-level one is how sectorisation and BS location will also affect the use of such channel richness. Most probably, in the case that the BS is in a pico-cellular environment, itself being within the scattering area, the involved relatively wide angle-spreads will again possibly make larger beamforming freedom available. Notice that, even more than in the MiC situation, the BS will most probably be embedded within the scatterers and MTs very close vicinity. Furthermore, not having any sectorisation will allow for such freedom to be maximised.

Finally, again the matter of radio planning is raised, once more seeing to be strongly subject to the adaptive spatial techniques vs. channel richness, and vs. the multi-user scenario binomials.

9.4 Summary and Conclusions

Summarily going through the major trends in mobile wireless communications, it has been put forward that *untraconnectivity* will be a value that will make part of the mobile wireless paradigm. For that, the *complementarity* among several wireless communications systems will be possible, most probably, after reaching industry, market and customer habit overall maturity, someday. Thus, *complementarity* will, or should, be another factor in the game of wireless evolution, resulting in that *adaptation* and *dynamics* at several levels will be necessary. Gradually going towards physical layer issues, these tendencies involve efforts in the sense of implementing multi-standard integration, new multiple access schemes, and smart multi-antenna implementations. At the basis of all of these highly demanding prospects, the knowledge and modelling of the wideband and directional propagation channel is proven to be necessary.

Having organised ideas in respect to the most probable and overall evolution perspective, the outputs of this work have been explicitly enumerated, covering contributions related to both propagation channel and scenario characterisation, and adaptive processing issues.

After doing so, hypotheses have been put forward, directed towards the propagation channel characterisation, scenarios, array schemes and system oriented matters. These are named as *hypotheses*, since they consist of extrapolations of the usefulness of this work towards the current and predicted mobile wireless future. Inherently, such ideas serve as follow-ons from the current work,

i.e., serving as both a morphological closure of this work and as the opening of several possible doors towards any progression.

Finally, apart from the more specific fields and matters that one has concluded to be most directly at stake, it has been shown that this study's contributions most directly relate to general mobile planning, by several means. For example, it is understood that future planning with SA solutions should take into account the morphological complexity of the scenarios at stake, since larger channel richness renders largest potential gain in their use. Knowing that, in general, this sort of scenarios coincide with user hotspots, with high user densities and relatively large traffic data, then the planner will better decide on resorting to more or less demanding and expensive adaptive array solutions, depending on such channel and scenario richness. In that sense, through the text, the reader is finally led to directly understand the practical implications that such hypotheses involve, once again, serving as another way to rightly envision doors towards future and necessary research.

10 Final Conclusions

Now this is not the end. It is not even the beginning of the end.

But it is, perhaps, the end of the beginning.

— Winston Churchill (1874-1965)

The aim of this work has been, from the start, to focus on the wideband directional propagation channel characteristics, and understanding which and how these fundamentally condition the spatial interference suppression capacity in SAs. Keeping well in mind that such objective can be too vast, a pragmatic posture has been adopted: by resorting to a semi-statistical and geometric WDCM, statistically valid propagation scenarios have been generated, and the analysis is therefore developed through simulation work; by resorting to simulation, through the model or the adaptive scheme, it is on the one hand faced naturally that reality is only slightly approximated, but on the other, simulation has allowed for the generation of multiple wideband directional propagation and multi-user scenario conditions; finally, by being able to build upon a consistent study workbench, the statistical simulations have developed in a controlled way, being able to generate independent channel and scenario concretisations, of similar nature, rendering statistical value.

Still on the pragmatic approach to the matter, adaptive beamforming has been chosen to deliver the necessary conclusions. That is so, since the focus is directed towards the basic physical, angular and temporal, properties of the channel, or scenario, and beamforming inherently and simply deals with the generation of a desired array pattern, i.e., placing lobes and nulls and shaping the overall response of the array towards a certain channel. By doing so, with the objective of minimising interference, the implemented adaptive beamforming has been used as a tool, therefore, to reflect the ways that the channel constrains its operation. In order to achieve that, beamforming is simple enough not to involve other physical effects and constraints that would be undoubtedly make part of more complex adaptive problems or structures.

Regarding the implemented algorithm, the resort to a reference-based one is again justified by the need not to involve other parameters, which not only could make the analysis more complex but also detract from the fundamental channel physical issues that have been hereby dealt with. It has

been shown that the results would be similar, though probably more difficult to characterise, to those obtained with another reference-based algorithm (the RLS). For that, and for the fundamental level and simplicity of the approach, it is argued that the results achieve a reasonable independency from the applied algorithm.

Adding to the model-scenario-beamforming strategy, a system-directed approach has helped this study to keep close to the current UMTS developments and specifications, only at the levels directly concerned, as well as naturally allowing for its projection towards future MBSs. This system-directed approach has undoubtedly further conveyed a practical view of the fundamental matter behind this study.

Being more specific, it is important to go through each chapter's most relevant conclusions, so as to grasp the overall contribution from this study.

Chapter 2, Laying Foundations and Background – Channel Models, and Chapter 3, Laying Foundations and Background – Adaptive Beamforming, establish the necessary channel modelling and adaptive beamforming strategies, from among the universe of WDCMs and beamforming applications.

In a MBSs perspective, for the study of adaptive beamforming, it is concluded that the implemented model should render the following: statistical value, enabling some generalisation of results; completeness, including all the major power contributing effects that determine relevant distributions in angle and delay, e.g., the clustering effect; flexibility, concerning their applicability to several environments, being macro-, micro-, or pico-cells, while maintaining the same fundamental modelling nature; implementation practicality and low complexity, enabling its practical use together with other simulation blocks such as a beamforming antenna array.

The need for the applied beamformer to work in the spatio-temporal domain has been confirmed, to fully make use of the signals transmitted and received, in future MBSs. With the current developments in electronics, it is most likely that issues such as accuracy, sensitivity to environmental effects, decalibration and weights phase errors will be dealt with, allowing the wide use of fully adaptive arrays. Similarly, making use of all available system resources to achieve best convergence rate and accuracy, all explicit sources of temporal or angular referential acquisition should be used to their maximum extent. In the case of UMTS and future MBSs, CDMA is inherently favourable to using adaptive techniques, in that sense, readily providing temporal referential sources. For the current study's needs, it is concluded that the applied algorithm should render stability, low convergence error and complexity. For its application, the channel should be considered stationary or static during a defined period, supporting the application of a sample-by-sample or a block-sample algorithm in such terms.

In Chapter 4, Implementation – the Channel and Scenarios, the applied model is defined – the MGBSBEM and CM – being a wideband cluster model, statistical in its nature, involving relatively low processing complexity, backed by some measurement campaigns, and flexible enough for future

extensions and use within propagation scenarios. Such model versions also apply to both micro- and macro-cellular situations, maintaining its fundamental nature. The implemented propagation scenarios pose differing wideband and directional multi-user interference situations, for both MiCs and MaCs. Their parallel conception is proven to be fundamental in the later comparison among performances towards MiC and MaC scenarios.

Directly related to angle- and delay-spreads, the definitions of temporal and angular densities, and DCIR channel richness parameters have been justified by logically affecting beamforming performance: larger ToA spreads imply larger NDesI powers, whilst larger AoA spreads are expected to lead to higher beamforming freedom in the location of lobes and nulls; larger temporal densities of arriving signals imply better correlation properties among all links' signals, tending to improve beamforming performance, whereas larger angular densities entail worse angular separation from among DesS and NDesI, rendering worse performance; the defined DCIR channel richness reflects these opposite effects in the temporal and angular domains. It is shown that those parameters render a direct physical level characterisation, also relating to important literature parameters of the kind, concluding that: σ_ϕ spreads decrease with increasing d_{MT} and such relative dependencies are of the same order, independent of the angle-spread definitions; for MiCs, the involved σ_ϕ values are one order of magnitude larger than those of MaCs, again independently of the spread definitions; for MaCs, the variation of σ_τ with d_{MT} is insignificant, whereas in the case of MiCs σ_τ varies by a factor around 4, for that expecting larger implications in the sensitivity to temporal discrimination in MiCs; though the delay-spreads involved with the implemented MiC and MaC scenarios may be of similar order, the angular ones vary substantially, not only between MiCs and MaCs, but also within each of those cases; compared to MaCs, the larger number of MiC scatterers implies a larger independency among the present DCIRs, resulting in a richer variety of uncorrelated arriving signals among the active links, i.e., larger multipath richness; the values of ω_{DCIR} are one order of magnitude greater in MiCs than MaCs, and the variations of ω_{DCIR} as functions of d_{MT} are inverse of the MaCs ones; in the MaC case, incoming signals are more concentrated in angle, but generally less in time, compared to MiCs; within the presented MaC cases, the effect of r in the densities is more evident than that of d_{MT} , whereas ω_{DCIR} varies more significantly with d_{MT} than with r ; for the MiC cases, the variations of densities with d_{MT} are much larger, compared to those of MaCs.

In both temporal and angular domains, the ways that the physical channel properties affect performance strongly root from the beamforming freedom that the channel or scenario allow for, i.e., from the involved multipath richness, which through those parameters is shown to differ among MiCs and MaCs.

Chapter 5, Implementation – the Adaptive Problem, covers the definition of the algorithm, and all the structure, inputs and outputs that its application involves. The CG algorithm is implemented and applied, in its block-sample form, using UMTS-specific codes, more directly

focusing on UMTS. Nevertheless, the adaptive application is shown to be neither system- nor algorithm-restrictive, since the conclusions drawn deal with physical fundamental and general aspects that involve the channel properties and the formation of an array pattern that minimises the relative level of NDesI power. The matter is viewed in the simplest way, seeing that the analysed dependencies on the channel/scenario properties prevail, the variations of SINR or BG due to changes in the array pattern lobe levels, positions and widths resulting from changes in the channel conditions in consistent physical senses.

It is understood that several NDesI powers are involved in the adaptive algorithm, developing on multi-user and wideband perspectives. The *self* and *other* MTs powers are differentiated from each other, as well as the non-delayed and delayed contributions become explicitly clear. Additionally, the applied PC process is described, showing its efficiency, though being applied independently from beamforming.

It is concluded that, from between the two possible types of averaging, PI and TI, the latter ones are the most important, involving the independent generation of DCIRs in both the temporal and angular domains. Anyhow, PI averaging is shown to allow the study of beamforming robustness against fast-fading. Already, the corresponding results show that the applied beamforming problem, by itself, is particularly sensitive to fast-fading. Anyhow, the statistical analysis of the obtained BGs confirms the general acceptance of the NH, confirming the general independency among the involved concretisations, and the Log-Normal distribution of the involved BG average values. For this, it is verified that the relatively large standard deviations obtained do not pose any threat to the independency of the obtained data, the study rendering statistical value.

In Chapter 6, Set-Up Analysis, a deep analysis of the problem is presented, at several levels. It has been verified that the system application is *wideband*, the applied channel model is *wideband*, the beamforming process is *wideband*, and that the array *narrowband assumption* is very valid. Concerning the application towards the TDD or the FDD mode, it is verified that the nature and correlation properties of the involved reference codes do vary between the two modes, and that these do not present ideal correlation properties. It is justified why the beamforming implementation may lead to SINR and BG values that are better for FDD than for TDD, also leading to different evolutions along optimisation. Anyhow, and most important, the beamforming performance dependencies on the implemented scenarios do not significantly vary with the considered duplex mode.

The MMSE and BG OD problem is described, justified and dealt with. It is shown that the OD does not root from the applied algorithm(s) themselves, but from the nature of the reference codes vs. the channel, and the way that those references are input. The *significant iteration* is defined as that at which SINR or BG maxima are most frequent, for each scenario, independent of being either MiC or MaC situations. The reasons for such root from the overall consistence in the obtained results, respecting logical fundamental relationships, anyway being also founded on other issues described in other chapters or sections. The presented practical solutions to the problem apply at either BS or at

MT levels. These cover the improvement of the algorithm application by: including a simple SINR control procedure; jointly linking all L independent beamformers through controlling orthogonality among the L weight vectors; making use of longer references, involving longer code lengths; extending the code references to their delayed versions; adding spatial diversity schemes; or considering additional beamforming at the MT, to selectively convey signals through AoA disjoint directions towards the BS. These methods have also been presented in the light of improving overall interference suppression capacity. Along the analysis of the OD problem, the extreme importance of the angular domain already arises, seeing that it is another factor strongly affecting SINR and BG evolutions, besides the temporal one.

Both RLS and CG implementations lead to agreeing beamforming dependencies on the WDCM characteristics, though the sample-by-sample RLS implementation achieves worse performances, compared to the block-sample CG. Regarding the OD, the RLS also exhibits non-monotonic evolutions in SINR or BG, in agreement to having previously justified such problem with the loss of arriving signals' orthogonality, i.e., independently of the applied algorithm. These results provide additional degree of confidence on the evaluation of beamforming performance. Both algorithms' general dependency on MiC or MaC scenarios is also clear, the RLS implementation being particularly sensitive in the grouped MT MaC case. Along iterations, the RLS and CG implementations do differ, the former exhibiting larger variations along iterations and among links' respective results. In this way, the CG most often converges to final values much faster than the RLS. By this, the CG shows to be comparatively more suitable for the analysis purposes carried out in this study.

Concerning complexity, the number of flops required by the RLS and block-sample CG implementations has been found to be approximated by second order polynomials, function of the number of antennas. The number of operations involved in each iteration is proportional to the number of active links, for both the CG or RLS applications. The RLS requires much less flops per iteration than the CG block-sample counterpart. The fact that the CG requires the calculation of a correlation matrix and a desired vector is partially counteracted by the need for several RLS iterations, ending up with complexities that do not significantly differ, in a whole, in a multi-user realistic mobile environment.

It is clearly expressed that undoubtedly many other algorithms could be applied and compared, further analysing how their behaviour would depend on the channel characteristics. Anyhow, the CG algorithm is capable of rendering fast and stable convergences in terms of SINR and BG. Its block-sample nature reflects the beamforming dependencies on the channel, while also not involving significantly large mathematical complexity.

Chapter 7, Beamforming in Micro- and Macro-cell Scenarios, presents performance results as a function of the several MiC and MaC scenarios.

For all scenarios, there is a large number of correlated and closely correlated arriving signals, due to multipath and several interfering sources, having important impact on the beamforming performance dependencies on channel/scenario parameters.

For MiC cases, it is both their AoA and ToA spreads that strongly affect beamforming gain, ToA spreads conditioning the BG much strongly over the former, leading to BG degradation for shorter BS-MT distances. From 50 to 1 000 m, BG may degrade by up to 5 dB, among the tested grouped MT scenarios, being particularly worse for 50 m BS-MT distance. By angularly spreading MTs, the BG dependency with d_{MT} becomes more visible, for lower number of array elements, especially in the case of larger distances, for which the sharing of AoAs among links is more reduced.

Higher number of elements has helped to confirm the dependencies with BS-MT distance, also verifying that the increase in M leads to an asymptotical evolution of BG. This *saturation* effect is justified by the increasingly uncorrelated signals that higher M implies, among array elements. Also, the WDCM implementation introduces a finite angular resolution, which for larger M may become gradually insufficient. These tests also show that for $M > L_T$, i.e., with apparently enough DoF to angularly discriminate the several temporally orthogonal sources, BG does not show any particular increase, therefore, again reflecting the importance of the angular domain issues that are involved in the multi-user WDCM scenarios.

In the case that MTs are angularly spread, BGs show increases relative to the cases where those are grouped, but these improvements are very limited by the relatively wide angle-spreads. Such is an expected tendency, since large AoA spreads imply large sharing of AoAs even if MTs are angularly scattered. For 1 000 m BS-MT distance, BG improvements reach 4 dB, whereas for 50 m, these are up to 2.3 dB. A single MT placed angularly separate from the remaining ones renders BGs of up to at least 5.6 to 9.0 dB above the BG values of the grouped cases. It is also concluded that the way the remaining MTs are angularly located is not significantly relevant to the definition of any of the beamformers' performances, again due to the wide angle-spreads at stake. Anyhow, all BG variations with MT spreading follow the expected logic, in the sense of sharing more or less AoAs among DesS and NDesI.

Besides the displacement in angle, the scenarios where a single MT is separate from the remaining grouped ones along the same street-confined axis have further confirmed the reasoning behind hypotheses and analyses. A group of MTs closer to the BS functions as clutter to a farther MT, due to both larger AoA and ToA spreads, leading to the subsequent degradation of BGs among all active MTs. Again, BGs corresponding to MTs within such group lead to lower values, relative to the single MT, for almost all of the tested scenarios.

Regarding the dependence with the number of active MTs, having 16 MTs leads to worse performances, as expected. Nevertheless, having from 4 to 8 MTs, BGs do not substantially vary, in fact even increasing in some cases. This is justified by the differing trends that single element and

array SINRs follow. Anyhow, BGs show relatively small sensitivity, among the tested scenarios, to the number of active MTs.

DesS and NDesI powers are affected in different manners by varying the sector width, depending on the sector widths and on the type of WB angle-spreads. It is generally confirmed that lowering sector widths implies lowering of beamforming freedom to place lobes and nulls in closer vicinity, towards DesS or NDesI signals, since the available channel AoA spreads are reduced, leading to lower BG.

Finishing the MiC analysis, the evaluation of the relative values of DesS, NDesI and noise powers have confirmed all of the previously gathered conclusions, also verifying that the delayed power from remaining MTs, $P_{>0}^{other}$, in the perspective of each single MT, is the most important NDesI component, taking larger relative values and being the most sensitive one to the scenario conditions. The DesS power, P_{DesS} , shows to be much less sensitive to those. These most significant power components follow the tendencies determined by the larger or lower freedom that the scenario presents to the beamformer.

In the MaCs case, it is the AoA spreads that play the most important part in determining beamforming performance. The MT distribution has a very strong impact on the beamforming performance, ruling the effects of all the remaining varied parameters: grouped MTs suffer from the limiting situation where all AoAs and ToAs are shared, leading to BGs close to 0 dB, independent of the number of array elements or any other scenario parameter; angularly spread MTs lead to BG that vary with the remaining parameters, always leading to positive values; the single separate MT leads to the highest BG values, possibly reaching 35 dB.

The dependence with MT-BS distance is not significant, among the tested MaC scenarios, though a tendency for BGs to decrease with increasing MT-BS distance has been registered. Anyhow, these are only significant in the case that MTs are spread, for larger number of array elements. From 1 000 to 2 000 m, values may vary by 4 dB. Since the variation of distance only involves significant angle-spread changes, the results again indicate how the beamforming may depend on such. By increasing the AoA spread, for the same ToA one, the beamformer may make use of more angular freedom in order to place lobes and nulls more effectively.

As regards scattering circle radius, the general tendency is for BGs to degrade for larger radii. It does not have any effect in the case that MTs are grouped together, unlike in the spread or in the separate MTs cases. The variations at stake vary from 3.8 to 8.6 dB, depending on the scenario situation, the highest variations corresponding to the single separate MT case. The effect of involving a larger scattering area is two fold: if MTs are spread, the larger are the chances of AoAs from differing MTs for superimposing, leading to lower BGs, for larger radii; on the other hand, the larger radii involve larger delayed NDesI power components, also incoming from a wider angular sector, meaning that most probably more undesired lobes will be directed towards such NDesI sources.

The dependence on the number of array elements is also a strong function of the distributing of MTs, in MaCs. BGs increase with M in a manner very close to linear, but again showing an asymptotical evolution, justified by spatial correlation and finite angular resolution issues. As in the MiC case, the relation of the number of orthogonal arriving codes to the number of array elements does not, by itself, determine the beamforming capabilities.

Regarding the dependence on the density of clusters and the average number of scatterers, again the effects vary according to MT positioning, in MaCs: no relevant changes are registered for grouped or spread MTs, unlike the single MT case, where larger number of incoming rays lead to lower BGs; the effects of these are more significant, as the scattering circle radius is reduced.

The dependence on the number of active links, in MaCs, is once more determined by how MTs are distributed: grouped together MTs do not exhibit particular dependencies, due to the inherently limited beamforming capacity; if MTs are angularly spread, BG results have shown to be best for 8 MTs, having clarified that such is due to the asymptotical reduction in the single antenna SINR, compared to the almost linear reduction of the beamformer's output SINR, from 4 to 16 users; in the case of the single separate MT, especially in the case of a well localised group of MTs at a different angle, its BGs and SINRs in fact increase from 4 to 8 MTs, while 16 terminals may not necessarily lead to lower BG or SINR results compared to the 4 MTs case. Such situation results from the cross-correlation nature of the reference codes involved, being worse in the case of 4 MTs.

The MaC involved power components confirm the reasoning behind the justification of the verified performance trends, as in the MiC cases. The $P_{>0}^{other}$ power is the most significant one, but P_{DesS} and N powers also show to considerably vary with the scenario. In the cases where a single MT is angularly separate from remaining ones, P_{DesS} values reach considerably high values in respect to the remaining components.

The fact that the MT positioning and distribution most strongly affect the beamforming performance, in MaCs, and the several dependencies on the varied parameters very clearly show the importance of not only considering a directional model by itself, for both the MiCs or MaCs cases, but also of applying such model in a multi-target implementation scenario perspective. The role of the angular domain not only plays a part among each active link, but also mostly determines how the multi-target scenarios affect beamforming performance, strongly establishing the available freedom that the channel presents to the beamformer.

Chapter 8, Beamforming Performance in Micro- vs. Macro-cell WDCM Scenarios, shows that the comparative scenario sets present a reasonably wide and significant variety of situations. The channel richness parameter, as well as the angular and temporal densities of arriving signals, are found to be particularly important in the comparison of the selected MiC and MaC scenarios. The relationships of these parameters to beamforming performance are further justified, complying with the logic and coherence in their definitions.

By directly going forth with the MiCs vs. MaCs comparison, it is concluded that MT grouping and displacement most strongly affect beamforming performance in ways that significantly differ between MiC and MaC scenarios, in consistence with the differing channel richness, an order of magnitude higher for MiCs than for MaCs: the grouping of MTs leads to critically degraded BGs, in the MaCs case, near 0 dB (almost independent of any other parameter), while MiC scenarios always lead to positive average BGs (also being determined by the other parameters); the spreading of MTs leads to the improvement of MaC BGs, BGs being anyhow lower than the compared MiC scenarios; due to the larger inherent channel richness, the beamformer dependence does not heavily depend on the MT displacement in the MiCs case, as opposed to the MaCs one.

The performance dependencies with distance also differ, though not being as relevant as the discrepancies due to grouping, again in agreement with the channel richness opposite tendencies: BG dependencies on distance are also opposite between MiCs and MaCs. Regarding the sensitivity to the variation of the number of array elements, the channel richness helps to understand that, for all scenarios, there is a larger benefit from increasing the number of array elements for MiCs, compared to that obtained for MaC situations. Similarly, concerning the dependency with the number of active MTs, MiC situations involve BG that are not as significantly sensitive compared to those in MaCs, again justifying so with the larger robustness and channel richness that MiCs entail.

The significant powers involved have been compared, namely, P_{DesS} , $P_{>0}^{other}$ and N . It has been confirmed that, between MiCs and MaCs, P_{DesS} is particularly degraded in the latter situations, independent of MT grouping, again reflecting the larger beamforming difficulties. $P_{>0}^{other}$ and N also present the corresponding expected tendencies.

It is in that chapter that the validity of the overall reasoning is confirmed: firstly, the defined channel richness is used to understand the fundamental factors behind the performance divergences towards MiCs and MaCs, such influences being understood to be most independent of the beamforming algorithm and the nevertheless limited number of propagation scenarios, to the necessary extent; secondly, by having established the bridge to SIMO and MIMO channel characterisation, it is shown how the reasoning of combining the notion of *channel richness* and the beamforming application does cover general fundamental matters, providing further indication that one is dealing with the background ruling physical issues; thirdly, the simple but relevant analysis of the BS Rx array spatial correlation coefficients has shown how these depend on the scenarios, presenting coherent relationships, while justifying the discrepancies through the same fundamental parameters.

It is in the channel's own physical characteristics that the hypotheses have found their confirmation, and such simplicity and independence on other implementation specific factors have been possible since the algorithm application has resorted to the two domains available – the temporal and angular ones. Having dealt with such physical characterisation in this manner, it is further

concluded that more complex spatial adaptive filtering schemes will also be subject to the same wideband directional constraints presented by the propagation channel and scenarios.

In a more practical-directed perspective, it is concluded that the added value of using SAs, spatial filtering and beamforming in particular, may be critical in MaCs, so as not to even possibly justify their implementation in those environments. Not exceeding in the generalisation, one can definitely state that either more complex adaptive schemes, or the combination of several techniques are required in MaC environments, in order to make most efficient use of the poorer channel spatial content. Even in the case that particularly significant isolated clusters exist, outside the circular region around each MT, it is very unlikely that MTs close together will not share most of the clusters in the MaC. For these arguments, not only should spatial filtering applications involve lower costs in MiCs, but also render smaller dynamic range and larger interference suppression gains.

Finally, Chapter 9, Towards Future Mobile Broadband Systems, establishes the direct bridge from the extracted results towards future MBSs. It is concluded that *untraconnectivity* rules the mobile wireless paradigm. The *complementarity* among several wireless communications systems will be possible, being another factor in the game of wireless evolution, resulting in that *adaptation* and *dynamics* will be necessary at several levels. These tendencies involve efforts in the sense of implementing multi-standard integration, new multiple access schemes, and smart multi-antenna implementations. At the basis of all of these highly demanding prospects, the knowledge and modelling of the wideband and directional propagation channel is very much necessary.

Hypotheses on the implications of this study's contributions are put forward, directed towards the propagation channel characterisation, scenarios, array schemes and system-oriented matters. These consist of extrapolations of the usefulness of this work towards the current and predicted mobile wireless future. Inherently, such ideas serve as follow-ons from the current research.

It is also shown that this study's contributions most directly relate to general mobile planning, by several means. For example, it is understood that future planning with SA solutions should take into account the morphological complexity of the scenarios at stake, since larger channel richness renders largest potential gain in their use. Knowing that, in general, this sort of scenarios coincide with user hotspots, with high user densities and relatively large traffic data, then the planner will better decide on resorting to more or less demanding and expensive adaptive array solutions, depending on such channel and scenario richness. The reader is finally led to directly understand the practical implications that such hypotheses involve, once again, serving as another way to rightly envision doors towards future and necessary research.

The increasingly challenging wideband mobile systems require an increasingly demanding usage of the channel, this dependence having major consequences at several levels. This study further shows that only by knowing the propagation channel better can those systems truly make use of larger capacities. Wideband mobile systems inherently have a resource that is still available, which needs to be evermore explored, even in most dense urban areas, where such resource seems less available – the

spatial domain. But then again, it is in the most urban dense areas that the channel is richer, having been shown in this work that this richness in fact allows for the exploitation of such domain.

Where *space* seems less available for us to physically be and move in, among the dense urban areas, with many and varied streets, several crossroads, a multitude of buildings, plazas, buses, cars, people, lighting posts, bus stops, etc, that's where *space* is most available for smart antennas to perform best in wideband mobile communication systems. We are fortunate, since those are the sort of places where we communicate and simultaneously move the most.

11 References

*Employ your time in improving yourself by other men's writings,
so that you shall gain easily what others have laboured hard for.*

— Socrates (470-399 BCE)

- [3GPP03] 3GPP, *Spatial Channel Model for Multiple-Input Multiple Output Simulations (Release 6)*, Technical Specification Group Radio Access Network, Technical Report TR 25.996 V 1.0.0(2003-05), Sophia Antipolis, France, May 2003, <http://www.3gpp.org>.
- [AFRV00] Agelet,F.A., Formella,A., Rábanos,J.M.H., Vicente,F.I. and Fontán,F.P., “Efficient Ray-tracing Acceleration Techniques for Radio Propagation Modeling”, *IEEE Transactions on Vehicular Technology*, Vol. 49, No. 6, Nov. 2000, pp. 2089-2104.
- [AFWP86] Adachi,F., Feeney,M.T., Williamson,A.G. and Parsons,J.D. “Crosscorrelation between the envelopes of 900 MHz signals received at a mobile radio base station site”, *IEE Proceedings - Radar, Sonar and Navigation*, Vol. 133, No. 6, Oct. 1986, pp. 506-512.
- [AMSM02] Asplund,H., Molisch,A.F., Steinbauer,M. and Mehta,N., “Clustering of scatterers in mobile radio channels - Evaluation and modeling in the COST 259 Directional Channel Model”, in *Proc. of ICC 2002 – International Conference on Communications*, New York, NY, USA, Apr. 2002.
- [ApCB00] Apolinário,J.A., de Campos,M.L.R. and Bernal,C.P., “The Constrained Conjugate Gradient Algorithm”, *IEEE Signal Processing Letters*, Vol. 7, No. 12, Dec. 2000, pp. 351-354.
- [ApCh76] Applebaum,S.P. and Chapman,D.J., “Adaptive Arrays in Main Beam Constraints”, *Special Issue on Adaptive Antennas, IEEE Transactions on Antennas and Propagation*, Vol. AP-24, No. 5, Sep. 1976, pp. 650-662.

- [Appl76] Applebaum,S.P., “Adaptive Arrays”, *Special Issue on Adaptive Antennas, IEEE Transactions on Antennas and Propagation*, Vol. AP-24, No. 5, Sep. 1976, pp. 585-598.
- [Aszt96] Asztély,D., *On Antenna Arrays in Mobile Communication Systems: Fast Fading and GSM Base Station Receiver Algorithms*, Ph.D. Thesis, Royal Institute of Technology, Stockholm, Sweden, Mar. 1996.
- [Bagh99] Baghaie,R., “Systolic Implementation of Sample-by-Sample Conjugate Gradient Algorithm”, in *Proc. of FINSIG '99 - IEEE Finish Signal Processing Symposium*, Oulu, Finland, May 1999.
- [BeBT02] Berezdivin,R., Breinig,R. and Topp,R., “Next-Generation Wireless Communications Concepts and Technologies”, *IEEE Communications Magazine*, Vol. 30, No. 3, Mar. 2002, pp. 108-116.
- [BeVö01] Bengtsson,M. and Völcker,B., “On the Estimation of Azimuth Distributions and Azimuth Spectra”, in *Proc. of VTC'01 Fall – 54th IEEE Vehicular Technology Conference*, Atlantic City, NJ, USA, Oct. 2001.
- [BeYO01] Bengtsson,M., Yu,K. and Ottersten,B., *Single and Dual Multi-Sensor Channel Characterisation – Analysis and Models, Stochastic Models*, IST-SATURN project, Deliverable 523, Part 1, Ver. 2.0, EC-IST Office, Brussels, Belgium, Nov. 2001, <http://www.ist-saturn.org/>.
- [BGQS01] Bria,A., Gessler,F., Queseth,O., Stridh,R., Unbehaun,M., Wu,J., Zander,J. and Flament,M., “4th-Generation Wireless Infrastructures: Scenarios and Research Challenges”, *IEEE Personal Communications Magazine*, Vol. 39, No. 12, Dec. 2001, pp. 25-31.
- [BIKM96] Blanz,J.J., Klein,A. and Mohr,W., “Measurement-Based Parameter Adaptation Of wideband Spatial Mobile Radio Channel Models”, in *Proc. ISSSTA '96 – 4th IEEE International Symposium on Spread Spectrum Techniques & Applications*, Mainz, Germany, Set. 1996.
- [BoSc03] Boche,H. and Schubert,M., “Optimal Multi-User Interference Balancing Using Transmit Beamforming”, *Wireless Personal Communications*, Vol. 26, No. 4, Sep. 2003, pp. 305-324.
- [BrUN01] Brunner,C., Utschick,W. and Nossek,J.A., “Exploiting the Short-Term and Long-Term Channel Properties in Space and Time: Eigenbeamforming Concepts for the BS in WCDMA”, *European Transactions on Telecommunications*, Vol. 12, No. 5, Sep./Oct. 2001, pp. 365-378.

- [BuLo61] Butler,J. and Lowe,R., “Beamforming Matrix Simplifies Design of Electronically Scanned Antennas ”, *Electronic Design*, No. 9, Apr. 1961, pp. 170-173.
- [CaCo03] Cardoso,F.D. and Correia,L.M., “Fading Depth Dependence on System Bandwidth in Mobile Communications - An Analytical Approximation”, *IEEE Transactions on Vehicular Technology*, Vol. 52, No. 3, May 2003, pp. 587-594.
- [Carl86] Carlson,A.B., *Communication Systems*, McGraw Hill, Singapore, 1986.
- [CCIC02] Choi,S., Choi,J., Im,H.-J. and Choi,B., “A Novel Adaptive Beamforming Algorithm for Antenna Array CDMA Systems with Strong Interferers”, *IEEE Transactions on Vehicular Technology*, Vol. 51, No. 5, Sep. 2002, pp. 808-816.
- [ChKi92] Choi,S. and Kim,D.H., “Adaptive Antenna Array Utilising the Conjugate Gradient Method for Compensation of Multipath Fading in a Land Mobile Communication”, in *Proc. of VTC'92 – 42nd IEEE Vehicular Technology Conference*, Denver, CO, USA, May 1992.
- [ChLa99] Charpentier,E. and Laurin,J., “An Implementation of a Direction-Finding Antenna for Mobile Communications Using a Neural Network”, *IEEE Transactions on Antennas and Propagation*, Vol. 47, No. 7, July 1999, pp. 1152-1159.
- [ChLH97] Choi,S., Lee,Y.U. and Hirasawa,K., “Real-time Design of a Smart Antenna System Utilising a Modified Conjugate Gradient Method for CDMA-based Mobile Communications”, in *Proc. of VTC'97 – 47th IEEE Vehicular Technology Conference*, Phoenix, AZ, USA, May 1997.
- [Chry00] Chryssomallis,M., “Smart Antennas”, *IEEE Antennas & Propagation Magazine*, Vol. 42, No. 3, June 2000, pp. 129-136.
- [CHSK76] Compton,R.T., Huff,R.J., Swarner,W.G. and Ksienski,A.A., “Adaptive Arrays for Communication systems: An Overview of Research at the Ohio State University”, *Special Issue on Adaptive Antennas, IEEE Transactions on Antennas and Propagation*, Vol. AP-24, No. 5, Sep. 1976, pp. 599-607.
- [ChSS99] Choi,S., Shim,D. and Sarkar,T.K., “A Comparison of Tracking-Beam Arrays and Switching-Beam Arrays Operating in a CDMA Mobile Communications Channel”, *IEEE Antennas & Propagation Magazine*, Vol. 41, No. 6, Dec. 1999, pp. 10-22.
- [ChWi00] Chang,S.P. and Willson,A.W., “Analysis of Conjugate Gradient Algorithms for Adaptive Filtering”, *IEEE Transactions on Signal Processing*, Vol. 48, No. 2, Feb. 2000, pp. 409-418.

- [ChWi95] Chang,S.P. and Willson,A.W., “Adaptive Filtering Using Modified Conjugate Gradient”, in *Proc. of the 38th Midwest Symposium on Circuits and Systems*, Rio de Janeiro, Brazil, Aug. 1995.
- [ChYC92] Chang,P., Yang,W. and Chan,K., “A Neural Network Approach to MVDR Beamforming Problem”, *IEEE Transactions on Antennas and Propagation*, Vol. 40, No. 3, Mar. 1992, pp. 313-322.
- [ChYS01] Chen,H.-H., Yeh,J.-F. and Suehiro,N., “A Multicarrier CDMA Architecture Based on Orthogonal Complementary Codes for New Generations of Wideband Wireless Communications”, *IEEE Communications Magazine*, Vol. 39, No. 10, Oct. 2001, pp. 126-35.
- [Coll85] Collin,R.E., *Antennas and Radiowave Propagation*, McGraw Hill, Singapore, 1985.
- [Comp88] Compton,R.T., “The Bandwidth Performance of a Two-Element Adaptive Array with Tapped Delay-Line Processing”, *IEEE Transactions on Antennas and Propagation*, Vol. 36, No. 1, Jan. 1988, pp. 5-14.
- [Corr01] Correia,L.M. (ed.), *Wireless Flexible Personalised Communications – COST 259 Final Report*, John Wiley & Sons, Chichester, UK, 2001.
- [DaCo99] Damosso,E. and Correia,L.M. (eds.), *Digital mobile radio towards future generation systems – COST 231 Final Report*, COST Secretariat, EC, Brussels, Belgium, 1999.
- [DGVC03] Debbah,M., Gil,J.M., Venes,J., Cardoso,F., Marques,G. and Correia,L.M., *Final report on channel models*, IST-FLOWS project, Deliverable D13, EC-IST Office, Brussels, Belgium, Sep. 2003, <http://www.flows-ist.org>.
- [DLPR01] Degli-Esposti,V., Lombardi,G., Passerini,C. and Riva,G., “Wide-Band Measurement and Ray-Tracing Simulation of the 1900 MHz Indoor Propagation Channel: Comparison Criteria and Results”, *IEEE Transactions on Antennas and Propagation*, Vol. 49, No. 7, July 2001, pp. 1111-1113.
- [ECSR98] Ertel,R.B., Cardieri,P., Sowerby,K.W., Rappaport,T.S. and Reed,J.H., “Overview of Spatial Channel Models for Antenna Array Communication Systems”, *IEEE Personal Communications Magazine*, Vol. 5, No. 1, Feb. 1998, pp. 10-22.
- [EHRC02] Evans,D., Hunt,B., Raynes,D.L., Correia,L.M., Hofstetter,H., Burr,A., Rohling,H., Lehmann,G., Williams,R. and Lehne,P.-H., “FLOWS – Flexible Convergence of Wireless Standards and Services”, in *Proc. of ICT’2002 – International Conference on Telecommunications*, Beijing, China, June 2002.

- [ETSI00] ETSI, Universal Mobile Telecommunications System (UMTS); *Spreading and Modulation (TDD)*, Technical Specification TS 125 223 V3.4.0 (2000-09), (3GPP TS 25.223 version 3.4.0), Sophia Antipolis, France, June 2002, <http://www.etsi.org>.
- [ETSI01a] ETSI, *Universal Mobile Telecommunications System (UMTS): UTRA (UE) TDD; Radio Transmission and reception*, Technical Specification TS 125 102 V4.3.0 (2001-12), (3GPP TS 25.102 version 4.3.0 Release 4), Sophia Antipolis, France, Dec. 2001, <http://www.etsi.org>.
- [ETSI01b] ETSI, *Universal Mobile Telecommunications System (UMTS): UTRA (BS) TDD; Radio Transmission and reception*, Technical Specification TS 125 105 V4.3.0 (2001-12), (3GPP TS 25.105 version 4.3.0 Release 4), Sophia Antipolis, France, Dec. 2001, <http://www.etsi.org>.
- [ETSI01c] ETSI, *Universal Mobile Telecommunications System (UMTS): Physical layer - General description*, Technical Specification TS 125 201 V4.1.0 (2001-12), (3GPP TS 25.201 version 4.1.0 Release 4), Sophia Antipolis, France, Dec. 2001, <http://www.etsi.org>.
- [ETSI01d] ETSI, *Universal Mobile Telecommunications System (UMTS): Spreading and Modulation (FDD)*, Technical Specification TS 125 213 V4.2.0 (2001-12), (3GPP TS 25.213 version 4.2.0), Sophia Antipolis, France, Dec. 2001, <http://www.etsi.org>.
- [ETSI02a] ETSI, *Universal Mobile Telecommunications System (UMTS): Physical channels and mapping of transport channels onto physical channels (TDD)*, Technical Specification TS 125 221 V5.2.0 (2002-09), (3GPP TS 25.221 version 5.2.0 Release 5), Sophia Antipolis, France, Sep. 2002, <http://www.etsi.org>.
- [ETSI02b] ETSI, *Universal Mobile Telecommunications System (UMTS): Deployment Aspects*, Technical Specification TS 125 943 V5.1.0 (2002-06), (3GPP TS 25.943 version 5.1.0 Release 5), Sophia Antipolis, France, June 2002, <http://www.etsi.org>.
- [ETSI93] ETSI, *Radio Transmission and Reception (GSM 05.05)*, TC SMG, Rec. GSM 05.05 v3.16.0, Sophia Antipolis, France, Apr. 1993, <http://www.etsi.org>.
- [ETSI96] ETSI, *Digital cellular telecommunications system (Phase 2); Radio transmission and reception*, ETS 300 577, Sophia Antipolis, France, 1996, <http://www.etsi.org>.
- [ETSI97] ETSI, *Universal Mobile Telecommunications System (UMTS): Selection procedures for the choice of radio transmission technologies of UMTS*, Technical Report TR 101 112 v3.1.0, Sophia Antipolis, France, 1997, <http://www.etsi.org>.
- [ETSI98] ETSI, *Evaluation Report for ETSI UMTS Terrestrial Radio Access (UTRA) ITU-R RTT Candidate*, SMG2, Sophia-Antipolis, France, Sep. 1998, <http://www.etsi.org>.

- [Evan03] Evans,D., “Standards Convergence”, in *Proc. of International Symposium on Advanced Radio Technologies*, Boulder, CO, USA, Mar. 2003, <http://www.its.bldrdoc.gov/meetings/art/art03/slides03/speakers03.html>.
- [Fail89] Faili,M. (ed.), COST 207, *Digital Land Mobile Radio Communications*, Final Report, COST Telecom Secretariat, EC, Brussels, Belgium, 1989.
- [FoGa98] Foschini,G.J. and Gans,M.J., “On Limits of Wireless Communications in a Fading Environment when Using Multiple Antennas”, *Wireless Personal Communications*, Vol. 6, No. 3, Mar. 1998, pp. 311-335.
- [Fosc96] Foschini,G.J., “Layered Space-Time Architecture for Wireless Communication in a Fading Environment When Using Multi-Element Antennas”, *Bell Labs Technical Journal*, Vol. 1, No. 2, Autumn 1996, pp. 41-59.
- [FSMH02] Fügen,T., Sommerkorn,G., Maurer,J., Hampicke,D., Wiesbeck,W. and Thomä,R., “MIMO Capacities for Different Antenna Arrangements Based on Double Directional Wide-Band Channel Measurements”, in *Proc. of PIMRC’2002 – 13th IEEE International Symposium in Personal, Indoor and Mobile Radio Communications*, Lisbon, Portugal, Sep. 2002.
- [Fuhl97] Fuhl,J., *Smart Antennas for Second and Third Generation Mobile Communications Systems*, Ph.D. Thesis, Technical University of Vienna, Vienna, Austria, Mar. 1997.
- [FuKS01] Furukawa,H., Kamio,Y. and Sasaoka,H., “Cochannel Interference Reduction and Path-Diversity Reception Technique Using CMA Adaptive Array Antenna in Digital Land Mobile Communications”, *IEEE Transactions on Vehicular Technology*, Vol. 50, No. 2, Mar. 2001, pp. 605-616.
- [FuMB98] Fuhl,J., Molisch,A.F. and Bonek,E., “Unified Channel Model for Mobile Radio Systems with Smart Antennas”, *IEE Proceedings - Radar, Sonar and Navigation*, Vol. 145, No. 1, Feb. 1998, pp. 32-41.
- [GiCo01a] Gil,J.M. and Correia,L.M., “An Implementation of Beamforming Adaptive Algorithms to Particular Mobile Propagation Conditions in UMTS”, in *Proc. of ConfTele 2001 – 3rd Conference on Telecommunications*, Figueira da Foz, Portugal, Apr. 2001.
- [GiCo01b] Gil,J.M. and Correia,L.M., “Combining Directional Channel Modelling with Beamforming Adaptive Antennas for UMTS”, in *Proc. of PIMRC’2001 – 12th IEEE International Symposium on Personal, Indoor and Mobile Radio Communications*, San Diego, CA, USA, Sep. 2001.

- [GiCo02a] Gil,J.M. and Correia,L.M., “Dependence of Adaptive Beamforming Performance on Directional Channel Modelled Micro-Cell Scenarios”, in *Proc. of PIMRC’2002 – 13th IEEE International Symposium on Personal, Indoor and Mobile Radio Communications*, Lisbon, Portugal, Sep. 2002.
- [GiCo02b] Gil,J.M. and Correia,L.M., “Impact of Wideband Directional Propagation Channel Characteristics on Adaptive Beamforming”, *IEICE Transactions on Communications*, Vol. E85-B, No. 12, Dec. 2002, pp. 1640-7.
- [GiCo03a] Gil,J.M. and Correia,L.M., “Impact of UMTS Macro-Cell Scenarios Directional Characteristics on Adaptive Beamforming Performance”, in *Proc. of IST-MWCS’2003 – IST Mobile and Wireless Communications Summit 2003*, Aveiro, Portugal, June 2003.
- [GiCo03b] Gil,J.M. and Correia,L.M., “The MMSE vs. Beamforming Gain Optima Discrepancy in Adaptive Beamforming Applied to Directional Channel Scenarios”, in *Proc. of ConfTele 2003 – 4th Conference on Telecommunications*, Aveiro, Portugal, June 2003.
- [GiCo03c] Gil,J.M. and Correia,L.M., “Adaptive Beamforming Dependencies on Wideband and Directional Propagation Characteristics in Micro- and Macro-Cell UMTS Scenarios”, in *Proc. of PIMRC’2003 – 14th IEEE International Symposium on Personal, Indoor and Mobile Radio Communications*, Beijing, China, Sep. 2003.
- [GiCo03d] Gil,J.M. and Correia,L.M., “Comparing Adaptive Beamforming in Micro- and Macro-Cells”, submitted to *IEEE Transactions on Vehicular Technology*, June 2003.
- [GiCo03e] Gil,J.M. and Correia,L.M., “Adaptive Beamforming Performance in Micro- and Macro-Cell Propagation Scenarios”, submitted as a contribution to a book entitled *Adaptive Antenna Array Techniques*, being edited by Dr. Sathish Chandran, Springer-Verlag, Heidelberg, Germany, June 2003.
- [GiCo03f] Gil,J.M. and Correia,L.M., “Fundamental Wideband and Directional Channel Parameters Ruling Adaptive Beamforming Performance in Micro- and Macro-Cells”, accepted to *VTC’04 Spring – 59th IEEE Vehicular Technology Conference*, Milan, Italy, May 2004.
- [GiMC01] Gil,J.M., Mendez,J.L. and Correia,L.M., “Comparison of Recursive Least Squares and Conjugate Gradient Applied to Adaptive Beamforming in UMTS”, in *Proc. of IST-MCS2001 – IST Mobile Communications Summit 2001*, Barcelona, Spain, Sep. 2001.
- [GoCo94] Gonçalves,N.C. and Correia,L.M., “Propagation Model for Urban Micro-Cellular Systems at the UHF Band”, in *Proc. of PIMRC’98 – 9th IEEE International Symposium on Personal, Indoor and Mobile Radio Communications*, Boston, MA, USA, Sep. 1998.

- [Goda97] Godara,L.C., “Application of antenna Arrays to Mobile Communications, Part II: Beam-forming and Direction-of-Arrival Considerations”, *Proc. of the IEEE*, Vol. 85, No. 8, Aug. 1997, pp. 1193-1245.
- [GoLo96] Golub,G.H. and Loan,C.F. Van, *Matrix Computations*, The John Hopkins University Press, Baltimore, MD, USA, 1996.
- [GrMa99] Grigat,M. and Martin,U., *Description of the modelling method*, IST-METAMORP project, Public Report C-2/1, EC-IST Office, Brussels, Belgium, Feb. 1999, <http://www.nt.tuwien.ac.at/mobile/en/>.
- [Hata80] Hata,M., “Empirical Formula for Propagation Loss in Land Mobile Radio Services”, *IEEE Transactions on Vehicular Technology*, Vol. VT-29, No. 3, Aug. 1980, pp. 317-325.
- [Hayk96] Haykin,S., *Adaptive Filter Theory*, Prentice Hall, Upper Saddle River, NJ, USA, 1996.
- [HeBF97] Hedergott,R., Bernhard,U.P. and Fleury,B.H., “Stochastic Radio Channel Model for Advanced Indoor Mobile Communication Systems”, in *Proc. of PIMRC'97 – 8th IEEE International Symposium on Personal, Indoor and Mobile Radio Communications*, Helsinki, Finland, Sep. 1997.
- [HeBK99] Hernández,R.I., Baghaie,R. and Kettunen,K., “Implementation of Gram-Schmidt Conjugate Direction and Conjugate Gradient Algorithms”, in *Proc. of FINSIG'99 - IEEE Finish Signal Processing Symposium*, Oulu, Finland, May 1999.
- [Hera00] Hérault,L., “*Project Presentation Report*”, IST-ASILUM project, Deliverable D0.2, EC-IST Office, Brussels, Belgium, Apr. 2000, <http://www.nari.ee.ethz.ch/~asilum/>.
- [HoSA98] Ho,M.-J., Stüber,G.L. and Austin,M.D., “Performance of Switched-Beam Smart Antennas for Cellular Radio Systems”, *IEEE Transactions on Vehicular Technology*, Vol. 47, No. 1, Feb. 1998, pp. 10-19.
- [HoTo00] Holma,H. and Toskala,A., *WDCMA for UMTS*, John Wiley & Sons, Chichester, UK, 2000.
- [HoTW03] Hottinen,A., Tirkkonen,O. and Wichman,R., *Multi-antenna Transceiver Techniques for 3G and Beyond*, John Wiley & Sons, Chichester, UK, 2003.
- [Howe76] Howells,P., “Explorations in Fixed and Adaptive Resolution at GE and SURC”, *Special Issue on Adaptive Antennas, IEEE Transactions on Antennas and Propagation*, Vol. AP-24, No. 5, Sep. 1976, pp. 575-584.

- [Hugl02] Hugl,K., *Spatial Channel Characteristics for Adaptive Antenna Downlink Transmission*, Ph.D. Thesis, Technical University of Vienna, Vienna, Austria, Jan. 2002.
- [HuLK82] Hufford,G.A., Longley,A.G and Kissick,W.A., *A Guide to the Use of the ITS Irregular Terrain Model in the Area Prediction Mode*, National Telecommunications and Information Administration (NTIA) Report 82-100, Boulder, CO, USA, Apr.1982.
- [ITRS02] *International Technology Roadmap for Semiconductors, 2002 Update*, 2002, <http://public.itrs.net/>.
- [ITUR95] ITU-R, *Prediction Methods for the Terrestrial Land Mobile Service in the VHF and UHF Bands*, Recommendation P.529-2, Geneva, Switzerland, 1995.
- [Jake74] Jakes,W.C., *Microwave Mobile Communications*, IEEE Press, New York, NY, USA, 1974.
- [KaBa99] Karttunen,P. and Baghaie,R., “Conjugate Gradient Based Signal Subspace Mobile User Tracking”, in *Proc. of VTC'99 Spring – 49th IEEE Vehicular Technology Conference*, Houston, TX, USA, May 1999.
- [Kall02] Kalliola,K., *Experimental Analysis of Multidimensional Radio Channels*, Ph.D. Thesis, Helsinki University of Technology, Radio Laboratory, Helsinki, Finland, Feb. 2002.
- [KeVS02] Kellerer,W., Vögel,H.-J., and Steinberg,K.-E., “A Communication Gateway for Infrastructure-Independent 4G Wireless Access”, *IEEE Communications Magazine*, Vol. 30, No. 3, Mar. 2002, pp. 126-131.
- [KlMo96] Klein,A. and Mohr,W., “A Statistical Wideband Mobile Radio Channel Model Including the Direction of Arrival”, in *Proc. ISSSTA'96 – 4th IEEE International Symposium on Spread Spectrum Techniques & Applications*, Mainz, Germany, Sep. 1996.
- [KMJA00] Kermaol,J.P., Mogensen,P.E., Jensen,S.H., Andersen,J.B., Frederiksen,F., Sørensen,T.B. and Pedersen,K.I., “Experimental Investigation of Multipath Richness for Multi-Element Transmit and Receive Antenna Arrays”, in *Proc. of VTC'2000 Spring – 51st IEEE Vehicular Technology Conference*, Tokyo, Japan, May 2000.
- [KMRV01] Kalliokulju,J., Meche,P., Rinne,M.J., Vallström,J., Varshney,P., and Häggman,S.-G., “Radio Access Selection for Multistandard Terminals”, *IEEE Personal Communications Magazine*, Vol. 39, No. 10, Oct. 2001, pp. 116-24.
- [KrVi96] Krim,H. and Viberg,M., “Two Decades of Array Signal Processing Research”, *IEEE Signal Processing Magazine*, Vol. 13, No. 4, July 1996, pp. 67-94.

- [KSLK02] Kalliola,K., Sulonen,K., Laitinen,H., Kivekas,O., Krogerus,J. and Vainikainen,P., “Angular Power Distribution and Mean Effective Gain of Mobile Antenna in Different Propagation Environments”, *IEEE Transactions on Vehicular Technology*, Vol. 51, No. 5, Sep. 2002, pp. 823-838.
- [KSMP00] Kermoal,J.P., Schumacher,L., Mogensen,P.E. and Pedersen,K.I., “Experimental Investigation of Correlation Properties of MIMO Radio Channels for Indoor Picocell Scenarios”, in *Proc. of VTC 2000 Fall – 52nd IEEE Vehicular Technology Conference*, Boston, MA, USA, Sep. 2000.
- [KuRB00] Kuchar,A., Rossi,J.-P. and Bonek,E., “Directional Macro-Cell Channel Characterization in Urban Measurements”, *IEEE Transactions on Antennas and Propagation*, Vol. 48, No.2, Feb. 2000, pp. 137-146.
- [Kurz01] Kurzweil,R., *The Law of Accelerating Results*, Mar. 2001, <http://www.kurzweilai.net/articles/art0134.html?printable=1>.
- [KuTB02] Kuchar,A., Tangemann,M. and Bonek,E., “A Real-Time DOA-Based Smart Antenna Processor”, *IEEE Transactions on Vehicular Technology*, Vol. 51, No. 6, Nov. 2002, pp. 1279-1293.
- [Laih02] Laiho,J., *Radio Network Planning and Optimisation for WCDMA*, Ph.D. Thesis, Helsinki University of Technology, Radio Laboratory, Helsinki, Finland, July 2002.
- [Lasp02] Laspougeas,P., *Single and Dual Multi-Sensor Channel Characterisation – Analysis and Models*, IST-SATURN project, Deliverable 523, Part 2, EC-IST Office, Brussels, Belgium, Oct. 2001, <http://www.ist-saturn.org/>.
- [Laur00] Laurila,J., *Semi-Blind Detection of Co-Channel Signals in Mobile Communications*, Ph.D. Thesis, Technical University of Vienna, Vienna, Austria, Dec. 2003.
- [Lee82] Lee, W.C.Y., *Mobile Communications Engineering*, McGraw Hill, New York, NY, USA, 1982.
- [LeHo03] Lehne,P.H. and Hofstetter,H., *Documentation of the Measurement Campaign – Part 1: 2.1 GHz*, IST-FLOWS project, Deliverable D10, EC-IST Office, Brussels, Belgium, Apr. 2003, <http://www.flows-ist.org>.
- [LeMi98] Lee,J.S. and Miller,L.E., *CDMA Systems Engineering Handbook*, Artech House, Boston, MA, USA, 1998.
- [LiKo99] Liberti,J.C. and Koshy,B.J., “Spatial Channel Measurements and Modelling for Smart Antenna Systems”, in *Proc. of COST 259/260 Joint Workshop, Spatial Channel Models and Adaptive Antennas*, Vienna, Austria, Apr. 1999.

- [LiLi03] Li,H.-J. and Liu,T.-Y., “Comparison of Beamforming Techniques for W-CDMA Communications Systems”, *IEEE Transactions on Vehicular Technology*, Vol. 52, No. 4, July 2003, pp. 752-760.
- [LiLo96] Litva,J. and Lo,T.K., *Digital Beamforming in Wireless Communications*, Artech House, Norwood, MA, USA, 1996.
- [Lind95] Lindskog,E., “Making SMI-Beamforming Insensitive to the Sampling Timing for GSM Signals”, in *Proc. of PIMRC'95 - IEEE International Symposium on Personal, Indoor and Mobile Communications*, Toronto, Canada, Sep. 1995.
- [LiRa99] Liberti,J.C. and Rappaport,T.S., *Smart Antennas for Wireless Communications: IS-95 and Third Generation CDMA Applications*, Prentice Hall, Upper Saddle River, NJ, USA, 1999.
- [LKTH02] Laurila,J., Kalliola,K., Toeltsch,M., Hugl,K., Vainikainen,P., and Bonek,E., “Wide-band 3-D Characterization of Mobile Radio Channels in Urban Environment”, *IEEE Transactions on Antennas and Propagation*, Vol. 50, No. 2, Feb. 2002, pp. 233-243.
- [LoRi68] Longley,A.G. and Rice,P.L., *Prediction of Tropospheric Radio Transmission Loss Over Irregular Terrain: A Computer Method – 1968*, Dept. of Commerce, Environmental Science Services Admin. (ESSA) Technical Report ERL 79-ITS 67, USA, July 1968.
- [Lu02] Lu,W.W. (ed.), *Broadband Wireless Mobile 3G and Beyond*, John Wiley & Sons, Chichester, UK, 2002.
- [Luce02] Lucero,S., “WLAN Starts to Go Mainstream”, *Get Connected*, Vol. 32, Apr. 2002, pp. 1-2, <http://www.instat.com/>.
- [LuLL97] Lu,M., Lo,T. and Litva,J., “A Physical Spation-Temporal Model of Multipath Propagation Channels”, in *Proc. of VTC'97 – 47th IEEE Vehicular Technology Conference*, Phoenix, AZ, USA, May 1997.
- [LuZu02] Lu,W.W. and Zukerman,M., “High-Performance 4G Systems”, *IEEE Personal Communications Magazine*, Guest Editorial, Vol. 40, No. 9, Sep. 2002, pp. 122-123.
- [MAC03] Multiple Access Communications Ltd, *The Benefits of Adaptive Antennas on Mobile Handsets for 3G Systems*, Radiocommunications Agency, Final Report, ra1002/r/17/105/3, Feb. 2003, <http://www.radio.gov.uk/>.
- [MaCo01] Marques,M.G. and Correia,L.M., “A Wideband Directional Channel Model for UMTS Micro-cells”, in *Proc. of PIMRC'2001 – 12th IEEE International Symposium on Personal, Indoor and Mobile Radio Communications*, San Diego, CA, USA, Sep. 2001.

- [MaCo02] Marques,M.G. and Correia,L.M., *Coherence Time in a Macro-cell Type Environment*, COST 273, Temporary Document TD(02)095, Espoo, Finland, May 2002.
- [MaCo03] Marques,M.G. and Correia,L.M., “A Wideband Directional Channel Model for Mobile Communication Systems”, submitted as a contribution to a book entitled *Adaptive Antenna Array Techniques*, being edited by Dr. Sathish Chandran, Springer-Verlag, Heidelberg, Germany, June 2003.
- [MaGr96] Martin,U. and Grigat,M., “A Statistical Simulation Model for the Directional Mobile Radio Channel and its Configuration”, in *Proc. ISSSTA'96 – 4th IEEE International Symposium on Spread Spectrum Techniques & Applications*, Mainz, Germany, Sep. 1996.
- [Marq01] Marques,M.G., *A Wideband Directional Model for Micro-Cells in UMTS*, M.Sc. Thesis, Instituto Superior Técnico, Technical University of Lisbon, Lisbon, Portugal, 2001.
- [Math03] The Mathworks, *MATLAB – The Language of Technical Computing*, 2003, <http://www.mathworks.com/products/matlab/>.
- [Mend01] Mendez,J.L., *Adaptive Beamforming in UTRA-TDD Applying the Recursive Least Squares Algorithm*, Graduation Report, Instituto Superior Técnico, Technical University of Lisbon, Lisbon, Portugal, 2001.
- [MeSc98] Medbo,J. and Schramm,P., *Channel Models for HIPERLAN/2 in Different Indoor Scenarios*, EP BRAN 3ERI085B, ETSI, Sophia Antipolis, France, Mar. 1998.
- [MFGH99] Martin,U., Fuhl,J., Gaspard,I., Haardt,M., Kuchar,A., Math,C., Molisch,A.F. and Thomä,R., “Model Scenarios for Direction-Selective Adaptive Antennas in Cellular Mobile Communication Systems – Scanning the Literature”, *Wireless Personal Communications*, Vol. 11, No. 1, Oct. 1999, pp. 109-129.
- [Mill92] Miller,L.E., *Propagation Model Sensitivity Study*, J. S. Lee Associates, Inc., Report under contract DAAL02-89-C-0040, July, 1992.
- [MKLH99] Molisch,A.F., Kuchar,A., Laurila,J., Hugel,K. and Bonek,E., “Efficient implementation of a geometry-based directional model for mobile radio channels”, in *Proc. of VTC'99 Fall – 50th IEEE Vehicular Technology Conference*, Amsterdam, The Netherlands, Sep. 1999.
- [Moli03a] Molisch,A.F., “Effect of Far Scatterer Clusters in MIMO Outdoor Channel Models”, in *Proc. of VTC'03 Spring – 57th IEEE Vehicular Technology Conference*, Jeju, Korea, Apr. 2003.

- [Moli03b] Molisch,A.F., “A Generic Model for MIMO Wireless Propagation Channels in Macro- and Microcells”, to appear in *IEEE Transactions on Signal Processing*, May, 2003, <http://www.merl.com/papers/TR2003-42/>.
- [MoRu94] Montgomery,D.C. and Runger,G.C., *Applied Statistics and Probability for Engineers*, John Wiley & Sons, New York, NY, USA, 1994.
- [Mous97] Moustakides,G.V. “Study of the transient Phase of the Forgetting Factor RLS”, *IEEE Transactions on Signal Processing*, Vol. 45, No. 10, Oct. 1997, pp. 2468-2476.
- [MPEF97] Mogensen,P.E., Pedersen,K.I., Espensen,P.L. and Fleury,B.H., “Preliminary Measurement Results From an Adaptive Antenna Array Testbed for GSM/UMTS”, in *Proc. of VTC'97 – 47th IEEE Vehicular Technology Conference*, Phoenix, AZ, USA, May 1997.
- [MPFF99] Mogensen,P.E., Pedersen,K.I., Frederiksen,F. and Fleury,B.H., “Measurements, Channel Statistics and Performance of Adaptive Base Station Antennas”, in *Proc. of COST 259/260 Joint Workshop, Spatial Channel Models and Adaptive Antennas*, Vienna, Austria, Apr. 1999.
- [MPKZ00] Marques,M.G., Pamp,J., Kunisch,J. and Zollinger,E., *Wideband Directional Channel Model and Measurement Campaign*, IST-ASILUM project, Deliverable D2.1, EC-IST Office, Brussels, Belgium, Oct. 2000, <http://www.nari.ee.ethz.ch/~asilum/>.
- [MPKZ01] Marques,M.G., Pamp,J., Kunisch,J. and Zollinger,E., *WDCM and Measurement Campaign*, IST-ASILUM project, Deliverable D2.3, EC-IST Office, Brussels, Belgium, Oct. 2001, <http://www.nari.ee.ethz.ch/~asilum/>.
- [MZDE96] Mogensen,P.E., Zetterberg,P., Dam,H., Espensen,P.L., Larsen,S.L. and Olesen,K., *Algorithms and Antenna Array Recommendations*, ACTS-TSUNAMI II project, Technical Report A020/AUC/A12/DR/P/1/xx-D2.1.2, Aalborg University, Aalborg, Denmark, Sep. 1996.
- [Nagu96] Naguib,A.F., *Adaptive Antennas for CDMA Wireless Networks*, Ph.D. Thesis, Stanford University, Stanford, CA, USA, Aug. 1996.
- [NIST03] *NIST/SEMATECH e-Handbook of Statistical Methods*, 2003, <http://www.itl.nist.gov/div898/handbook/>.
- [NøAn94] Nørklit,O. and Andersen,J.B., “Mobile Radio Environments and Adaptive Arrays”, in *Proc. of PIMRC'94 – 5th IEEE International Symposium on Personal, Indoor and Mobile Radio Communications*, Den Haag, The Netherlands, Sep. 1994.

- [Olej02] Olejniczak,J., *Impact of the directional channel in adaptive beamforming for UMTS-FDD in micro-cells*, Graduation Project, Instituto Superior Técnico, Technical University of Lisbon, Lisbon, Portugal, 2002.
- [OOKF69] Okumura,Y., Ohmuri,E., Kawano,T. and Fukuda,K., “Field Strength and its Variability in VHF and UHF Land-Mobile Radio Service”, *Reviews of the Electrical Communications Laboratory*, Vol. 16, No. 9-10, Sep.-Oct. 1968, pp. 825-873.
- [OpSc75] Oppenheim,A.V. and Schafer,R.W., *Digital Signal Processing*, Prentice Hall, Englewood Cliffs, NJ, USA, 1975.
- [OSMS93] Ohgane,T., Shimura,T., Matsuzawa,N. and Sasaoka,H., “An Implementation of a CMA Adaptive Array for High Speed GMSK Transmission in Mobile Communications”, *IEEE Transactions on Vehicular Technology*, Vol. 42, No. 3, Aug. 1993, pp. 282-288.
- [Otte95] Ottersten,B., “Spatial Division Multiple Access (SDMA) in Wireless Communications”, in *Proc. of NRS-95, Nordic Radio Symposium’95*, Saltsjöbaden, Sweden, Apr. 1995.
- [PAKM00] Pedersen,K.I., Andersen,J.B, Kermaol,J.P. and Mogensen P., “A Stochastic Multiple-Input-Multiple-Output Radio Channel Model for Evaluation of Space-Time Coding Algorithms”, in *Proc. of VTC’00 Fall – IEEE Vehicular Technology Conference*, Boston, MA, USA, Sep. 2000.
- [PaPa97] Paulraj,A.J. and Papadias,C.B., “Space-Time Processing for Wireless Communications”, *IEEE Signal Processing Magazine*, Vol. 14, No. 6, Nov. 1997, pp. 49-83.
- [Pars96] Parsons,J.D., *The Mobile Propagation Channel*, John Wiley & Sons, Chichester, UK, 1996.
- [Pätz03] Pätzold,M., “On the Stationarity and Ergodicity of Fading Channel Simulators Basing on Rice’s Sum-of-Sinusoids”, in *Proc. of PIMRC’2003 – 14th IEEE International Symposium on Personal, Indoor and Mobile Radio Communications*, Beijing, China, Sep. 2003.
- [PéJi94] Pérez,V. and Jiménez,J. (eds.), *Final Propagation Model*, RACE-CoDiT project, Deliverable R2020/TDE/PS/DS/P/040/a1, EC – RACE Office, Brussels, Belgium, June 1994.
- [PeMF97] Pedersen,K.I., Mogensen,P.E. and Fleury,B.H., “Power Azimuth Spectrum in Outdoor Environments”, *IEE Electronics Letters*, Vol. 33, No. 18, Aug. 1997, pp. 1583-84.

- [PeMF98] Pedersen,K.I., Mogensen,P.E. and Fleury,B.H., “Spatial Channel Characteristics in Outdoor Environments and their Impact on BS Antenna System Performance”, in *Proc. of VTC’98 – 48th IEEE Vehicular Technology Conference*, Ottawa, Canada, May 1998.
- [Pers01] Persefoni,K., *Multiple Element Antenna Systems in an Indoor Environment*, Ph.D. Thesis, Stanford University, Stanford, CA, USA, Nov. 2001.
- [Petr97] Petrus,P., *Novel Adaptive Array Algorithms and Their Impact on Cellular System Capacity*, Ph.D. Thesis, Virginia Polytechnical Institute, Blacksburg, VA, USA, Mar. 1997
- [PiTs99] Piechocki,R.J. and Tsoulos,G.V., “Combined GWSSUS and GBSR Channel Model with Temporal Variations”, in *Proc. of COST 259/260 Joint Workshop, Spatial Channel Models and Adaptive Antennas*, Vienna, Austria, Apr. 1999.
- [PrEU99] Prögler,M., Evci,C. and Umehira,M., “Air Interface Access Schemes for Broadband Mobile Systems”, *IEEE Communications Magazine*, Vol. 37, No. 9, Sep. 1999, pp. 106-115.
- [RaPa95] Raleigh,G.G. and Paulraj,A., “Time Varying Vector Channel Estimation for Adaptive Spatial Equalization”, in *Proc. of IEEE GLOBECOM – Global Communications Conference*, Singapore, Nov. 1995.
- [Rapp02] Rappaport,T.S., *Wireless Communications: Principles and Practice*, 2nd ed., Prentice Hall, Upper Saddle River, NJ, USA, 2002.
- [RaRL99] Razavilar,J., Rashid-Farrokhi,F. and Liu,K.J.R., “Software Radio Architecture with Smart Antennas: A Tutorial on Algorithms and Complexity”, *IEEE Journal on Selected Areas in Communications*, Vol. 17, No. 4, Apr. 1999, pp. 662-676.
- [ReMa01] Reed,M. and Maucher,J., “*Intermediate Report on the Evaluation of the Different Algorithms in Terms of Link Performance*”, IST-ASILUM Project, Deliverable D4.2, EC-IST Office, Brussels, Belgium, May 2001, <http://www.nari.ee.ethz.ch/~asilum/>.
- [ReMB74] Reed,I.S., Mallett,J.D. and Brennan,L.E., “Rapid Convergence Rate in Adaptive Arrays”, *IEEE Transactions on Aerospace and Electronic Systems*, Vol. AES-10, No. 6, Nov. 1974, pp. 853-863.
- [SaVa87] Saleh,A.A.M. and Valenzuela,R.A., “A Statistical Model for Indoor Multipath Propagation”, *IEEE Journal of Selected Areas in Communications*, Vol. SAC-5, No. 2, Feb. 1987, pp. 128-37.

- [SaWi94] Salz,J. and Winters,J.H., “Effect of Fading Correlation on Adaptive Arrays in Digital Mobile Radio”, *IEEE Transactions on Vehicular Technology*, Vol. 43, No. 4, Nov. 1994, pp. 1049-57.
- [Saye02] Sayeed,A.M., “Deconstructing Multiantenna Fading Channels”, *IEEE Transactions on Signal Processing*, Vol. 50, No. 10, Oct. 2002, pp. 2563-2579.
- [Scia90] Sciandra,R.M., *TIREM/SEM Programmer’s Reference Manual*, Electromagnetic Compatability Analysis Center Report ECAC-CR-90-039, Annapolis, MD, USA, July 1990.
- [ScKM02] Schumacher,L., Kermoal,J. and Mogensen,P., *Channel Characterisation*, IST-METRA project, Deliverable 2, EC-IST Office, Brussels, Belgium, Oct. 2002, <http://www.ist-metra.org/>.
- [ScWi03] Schafer,T.M. and Wiesbeck,W., “Effective Modeling of Composite Walls in Hospitals for Ray-Optical Wave Propagation Simulations”, in *Proc. of VTC’03 Fall – 58th IEEE Vehicular Technology Conference*, Orlando, FL, USA, Oct. 2003.
- [SeRa94] Seidel,S.Y. and Rappaport,T.S., “Site-Specific Propagation Prediction for Wireless In-Building Personal Communication System Design”, *IEEE Transactions on Vehicular Technology*, Vol. 43, No. 4, Nov. 1994, pp. 879-891.
- [SFBP00] Silva,J.S., Arroyo-Fernández,B., Barani,B., Pereira,J. and Ikonomou,D., “Evolution Towards UMTS”, EC – DG XIII-B.4, July 2000, <http://www.de.infowin.org>.
- [SFGK00] Shiu,D.-S., Foschini,G.J., Gans,M.J. and Kahn,J.M., “Fading Effect and Its Effect on the Capacity of Multielement Antenna Systems”, *IEEE Transactions on Communications*, Vol. 48, No. 3, Mar. 2000, pp. 502-513.
- [Shew94] Shewchuk,J.R., *An Introduction to the Conjugate Gradient Method Without the Agonising Pain*, Internal Report, School of Computer Science, Carnegie Mellon University, Pittsburgh, PA, USA, Aug. 1994, <http://www.cs.cmu.edu/~jrs/jrspapers.html>.
- [SJBF99] Stege,M., Jelitto,J., Bronzel,M. and Fettweis,G., “A Space-Time Channel Model with Stochastic Fading Simulation”, in *Proc. of ITG-Fachtagung Intelligente Antennen*, Stuttgart, Germany, Apr. 1999.
- [SJJS00] Spencer,Q.H., Jeffs,B.D., Jensen,M.A. and Swindlehurst,A.L., “Modeling the Statistical Time and Angle of Arrival Characteristics of an Indoor Multipath Channel”, *IEEE Journal of Selected Areas in Communications*, Vol. 18, No. 3, Mar. 2000, pp. 347-360.

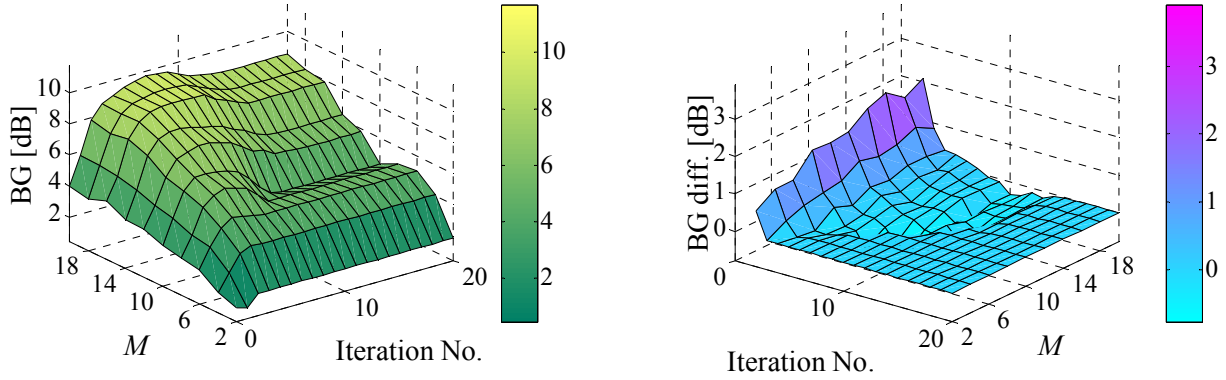
- [SLLL95] Sandhu,A., Lo,T., Leung,H. and Litva,J., “Hopfield Neurobeamformer for Spread Spectrum Communications”, in *Proc. of PIMRC'95 - IEEE International Symposium on Personal, Indoor and Mobile Communications*, Toronto, Canada, Sep. 1995.
- [Smul02] Smulders,P., “Exploiting the 60 GHz Band for Local Wireless Multimedia Access: Prospects and Future Directions”, *IEEE Personal Communications Magazine*, Vol. 40, No. 1, Jan. 2002, pp. 140-7.
- [SÖHM02] Steinbauer,M., Özcelik,H., Hofstetter,H., Mecklenbräuker,C.F. and Bonek,E., “How to Quantify Multipath Separation”, *IEICE Transactions on Communications*, Vol. E85-C, No. 3, Mar. 2002, pp. 552-557.
- [SoJD94] Sousa,E.S., Jovanovic,V.M. and Daigneault,C., “Delay Spread Measurements for the Digital Cellular Channel in Toronto”, *IEEE Transactions on Vehicular Technology*, Vol. 43, No. 4, Nov. 1994, pp. 837-47.
- [SRJJ97] Spencer,Q., Rice,M., Jeffs,B. and Jensen,M., “A Statistical Model for Angle of Arrival in Indoor Multipath Propagation”, in *Proc. of VTC'97 – 47th IEEE Vehicular Technology Conference*, Phoenix, AZ, USA, May 1997.
- [StCM94] Stapleton,S.P., Carbo,X. and McKeen,T., “Spatial Channel Simulator for Phased Arrays”, in *Proc. of VTC'94 – 44th IEEE Vehicular Technology Conference*, Stockholm, Sweden, June 1994.
- [StCM96] Stapleton,S.P., Carbo,X. and McKeen,T., “Tracking and Diversity for a Mobile Communications Base Station Array Antenna”, in *Proc. of VTC'96 – 46th IEEE Vehicular Technology Conference*, Atlanta, GA, USA, Apr. 1996.
- [Stee96] Steele,R., *Mobile Radio Communications*, IEEE Press, New York, NY, USA, 1996.
- [StMB01] Steinbauer,M., Molisch,A.F. and Bonek,E., “The Double Directional Radio Channel”, *IEEE Transactions on Antennas and Propagation*, Vol. 43, No. 4, Aug. 2001, pp. 51-63.
- [Stub96] Stuber,G.L., *Principles of Mobile Communications*, Kluwer Academic Publishers, Boston, MA, USA, 1996.
- [Svan01] Svantesson,T., “A Physical MIMO Radio Channel Model for Multi-Element Multi-Polarized Antenna Systems”, in *Proc. of VTC'01 Fall – 54th IEEE Vehicular Technology Conference*, Atlantic City, NJ, USA, Oct. 2001.
- [SvWa02] Svantesson,T. and Wallace,J., “On Signal Strength and Multipath Richness in Multi-Input Multi-Output Systems”, in *Proc. of RVK'02 - RadioVetenskap och Kommunikation*, Stockholm, Sweden, June 2002.

- [Szym02] Szymański,T., *Impact of the directional channel in adaptive beamforming for UMTS-FDD in macro-cells*, Graduation Project, Instituto Superior Técnico, Technical University of Lisbon, Lisbon, Portugal, 2002.
- [TI00] Texas Instruments, “TI DSP-based System-on-a-Chip Roadmap to Deliver 3 Trillion Instructions per second by 2010”, *Technology Innovations*, Vol. 2, Jan. 2000, http://www.ti.com/sc/docs/general/techinnovations/2000_01/index.htm.
- [TMCK97] Tanaka,T., Miura,R., Chiba,I. and Karasawa,Y., “Interference Cancellation Characteristics of a BSCMA Adaptive Array Antenna with a DFB Configuration”, *IEICE Transactions on Communications*, Vol. E80-B, No. 9, Sep. 1997, pp. 1363-1371.
- [ToFu00] Toda,T. and Fujii,M., “Implementation and Performance Evaluation of SMI Adaptive Array”, in *Proc. of VTC’00 Spring – 51st IEEE Vehicular Technology Conference*, Tokyo, Japan, May 2000.
- [TrOt95] Trump,T. and Ottersten,B., “Maximum Likelihood Estimation of Nominal Direction of Arrival and Angular Spread Using an Array of Sensors”, in *Proc. of COST 229 – Adaptive Systems, Intelligent Approaches, Massively Parallel Computing and Emergent Techniques in Signal Processing and Communications*, Vigo, Spain, Oct. 1995.
- [TsAP00] Tsoulos,G.V., Athanasiadou,G.E. and Pichocki,R.J., “Low-Complexity Smart Antenna Methods for Third-Generation W-CDMA Systems”, *IEEE Transactions on Vehicular Technology*, Vol. 49, No. 6, Nov. 2000, pp. 2382-2396.
- [TsAt02] Tsoulos,G.V. and Athanasiadou,G.E., “On the Application of Adaptive Antennas to Microcellular Environments: Radio Channel Characteristics and System Performance”, *IEEE Transactions on Vehicular Technology*, Vol. 51, No. 1, Jan. 2002, pp. 1-16.
- [Vaug88] Vaughan,R.G., “On Optimum Combining at the Mobile”, *IEEE Transactions on Vehicular Technology*, Vol. 37, No. 4, Nov. 1988, pp. 181-188.
- [VeBu88] Van Veen,B.D. and Buckley,K.M., “Beamforming: A Versatile Approach to Spatial Filtering”, *IEEE Acoustics, Speech and Signal Processing Magazine*, Vol. 5, No. 2, Apr. 1988, pp. 4-24.
- [Verd86] Verdú,S., “Minimum Probability of Error for Asynchronous Gaussian Multiple-Access Channels”, *IEEE Transactions on Information Theory*, Vol. IT-32, No. 1, Jan. 1986, pp. 85-96.

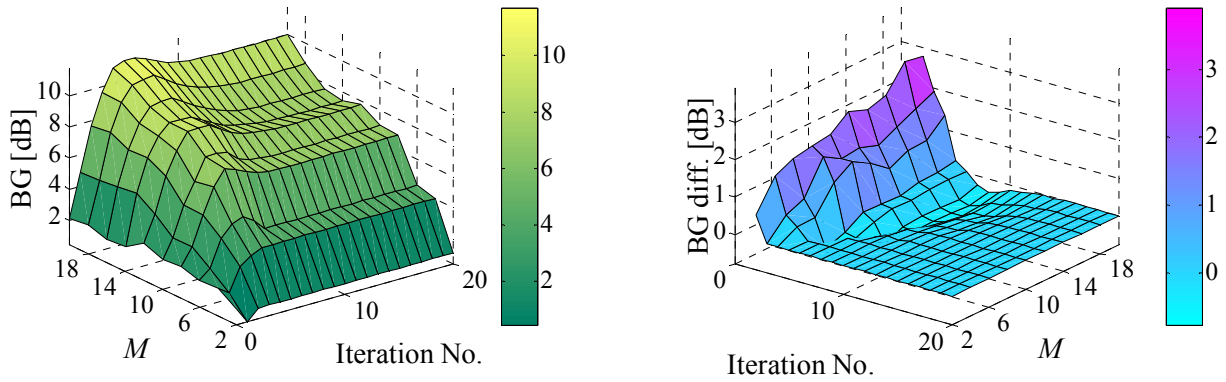
- [WaCr94] Wang,Y. and Cruz,J.R., “Adaptive Antenna Arrays for the Reverse Link of CDMA Cellular Communication Systems”, *IEE Electronics Letters*, Vol. 30, No. 13, June 1994, pp. 1017-1018.
- [Wang01] Wang,J., *Broadband Wireless Communications 3G, 4G and Wireless LAN*, Kluwer Academic Publishers, Norwell, MA, USA, 2001.
- [Weic03] Weichselberger,W., *Spatial Structure of Multiple Antenna Radio Channels – A Signal Processing Viewpoint*, Ph.D. Thesis, Technical University of Vienna, Vienna, Austria, Dec. 2003.
- [Weis82] Weissberger,M. *et al.*, *Radiowave Propagation: A Handbook of Practical Techniques for Computing Basic Transmission Loss and Field Strength*, IIT Research Institute Report to Electronic Compatability Analysis Center, Annapolis, MD, USA, Sep. 1982.
- [WiGa99] Winters,J.H. and Gans,M.J., “The Range Increase of Adaptive Versus Phased Arrays in Mobile Radio Systems”, *IEEE Transactions on Vehicular Technology*, Vol. 48, No. 2, Mar. 1999, pp. 353-362.
- [WiLe90] Widrow,B. and Lehr,M.A., “30 Years of Adaptive Neural Networks: Perceptron, Madaline and Backpropagation”, in *Proc. of the IEEE*, Vol. 78, No. 9, Sep. 1990, pp. 1415-1442.
- [Wint84] Winters,J.H., “Optimum Combining in Digital Mobile Radio with Co-Channel Interference”, *IEEE Transactions on Vehicular Technology*, Vol. VT-33, No. 3, Aug. 1984, pp. 144-155.
- [WiSt95] Widrow,B. and Stearns,S.D., *Adaptive Signal Processing*, Prentice Hall, Upper Saddle River, NJ, USA, 1995.
- [WJSJ03] Wallace,J.W., Jensen,M.A., Swindlehurst,A.L. and Jeffs,B.D., “Experimental Characterization of the MIMO Wireless Channel: Deta Acquisition and Analysis”, *IEEE Transactions on Wireless Communications*, Vol. 2, No. 2, Mar. 2003, pp. 335-343.
- [WÖHB03] Weichselberger,W., Özcelik,H., Herdin,M., Bonek,E., “A Novel Stochastic MIMO Model and its Physical Interpretation”, in *Proc. of WPMC'03 – International Symposium on Wireless Personal Multimedia Communications*, Yokosuka, Japan, Oct. 2003.
- [WuHa95] Wu,X. and Haimovich,A.M., “Adaptive Arrays for Increased Performance in Mobile Communications”, in *Proc. of PIMRC'95 - IEEE International Symposium on Personal, Indoor and Mobile Communications*, Toronto, Canada, Sep. 1995.

- [WWRF01] Wireless World Research Forum, *The Book of Visions 2001*, v. 1.0, Wireless World Research Forum, Dec. 2001, <http://www.wireless-world-research.org/>.
- [XCHV02] Xu,H., Chizik,H., Huang,H. and Valenzuela,R., “A Wave-based wideband MIMO Channel Modeling Technique”, in *Proc. of PIMRC’2002 – 13th IEEE International Symposium on Personal, Indoor, and Mobile Radio Communications*, Lisbon, Portugal, Sep. 2002.
- [YoCh01] Yonezawa,R. and Chiba,I., “A Combination of Two Adaptive Algorithms SMI and CMA”, *IEICE Transactions on Communications*, Vol. E84-B, No. 7, Jul. 2001, pp. 1768-1773.
- [YuOt02] Yu,K. and Ottersten,B., “Models for MIMO propagation channels: a review”, *Wireless Communications and Mobile Computing*, Vol. 2, No. 7, Nov. 2002, pp. 653-666.
- [ZeEM96] Zetterberg,P., Espensen,P.L. and Mogensen,P., “Propagation, Beamsteering and Uplink Combining Algorithms for Cellular Systems”, in *Proc. of ACTS Mobile Communications Summit*, Granada, Spain, Nov. 1996.
- [ZeEs96] Zetterberg,P. and Espensen,P.L., “A Downlink Beamsteering Technique for GSM/DCS1800/PCS1900”, in *Proc. of PIMRC’96 – IEEE International Symposium on Personal, Indoor and Mobile Radio Communications*, Taipei, Taiwan, Oct. 1996.
- [Zett96] Zetterberg,P., *The Propagation Models Used for Evaluation of Digital Beam Steering Techniques in the TSUNAMI (II) Project at Aalborg University*, Technical Report SB-9621, Center for PersonKommunikation, Aalborg University, Denmark, Aug. 1996.
- [Zett97] Zetterberg,P., *Mobile Cellular Communications with Base Station Antenna Arrays: Spectrum Efficiency, Algorithms and Propagation Models*, Ph.D. Thesis, Royal Institute of Technology, Stockholm, Sweden, Dec. 1997.
- [ZKVS03] Zhao,X, Kivinen,J., Vainikainen,P. and Skog,K., “Characterization of Doppler spectra for mobile communications at 5.3 GHz”, *IEEE Transactions on Vehicular Technology*, Vol. 52, No. 1, Jan. 2003, pp. 14-23.
- [ZoCG98] El Zooghby,A.H., Christodoulou,C.G. and Georgiopoulos,M., “Neural Network-Based Adaptive Beamforming for One- and Two-Dimensional Antenna Arrays”, *IEEE Transactions on Antennas and Propagation*, Vol. 46, No. 12, Dec. 1998, pp. 1891-1893.
- [ZoMa00] Zollinger,E. and Marques,M.G., *WDCM and Measurement Campaign*, IST-ASILUM project, Deliverable D2.1, EC-IST Office, Brussels, Belgium, Nov. 2000, <http://www.nari.ee.ethz.ch/~asilum/>.

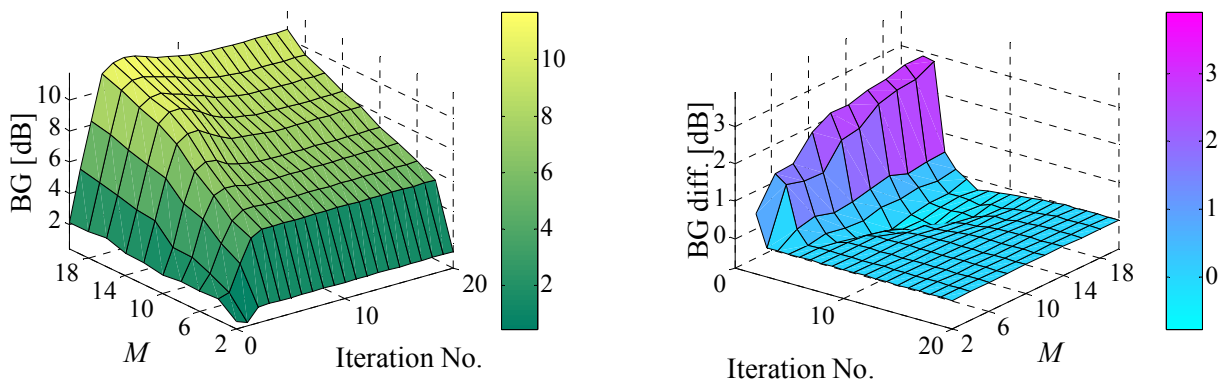
Annex A – Surface Plots – Micro-Cell Scenarios



(a) Sc #4u_mc_Gr_05.

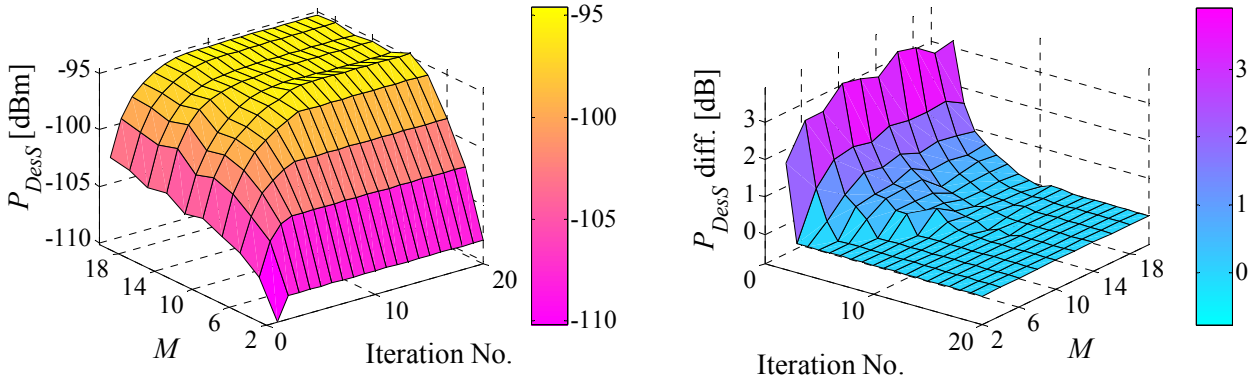


(b) Sc #4u_mc_Gr_5.

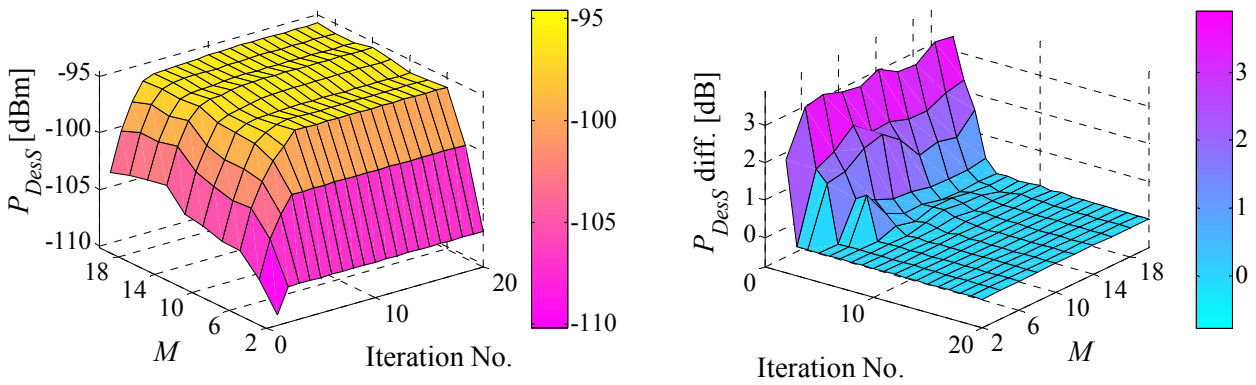


(c) Sc #4u_mc_Gr_10.

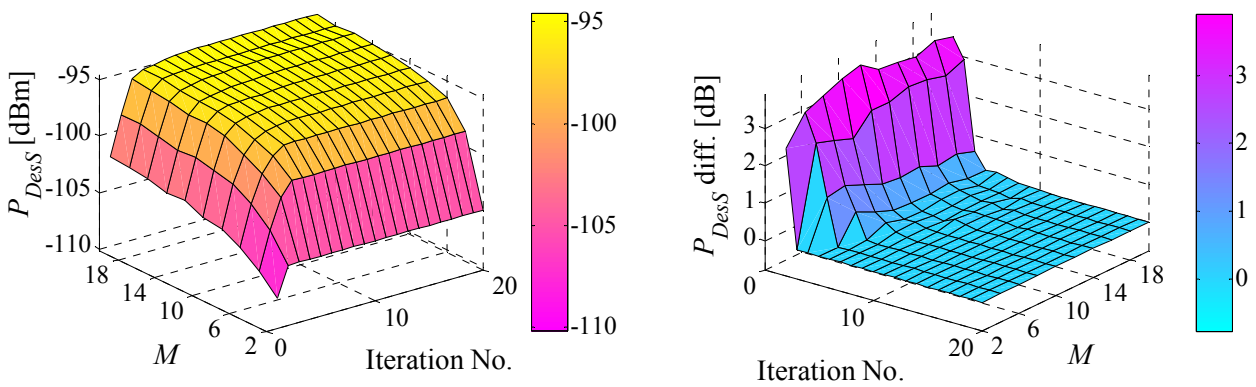
Figure A.1 – Average BG [dB] and differences (between consecutive iterations) along optimisation, for $L = 4$, function of d_{MT} , for several values of M .



(a) Sc #4u_mc_Gr_05.

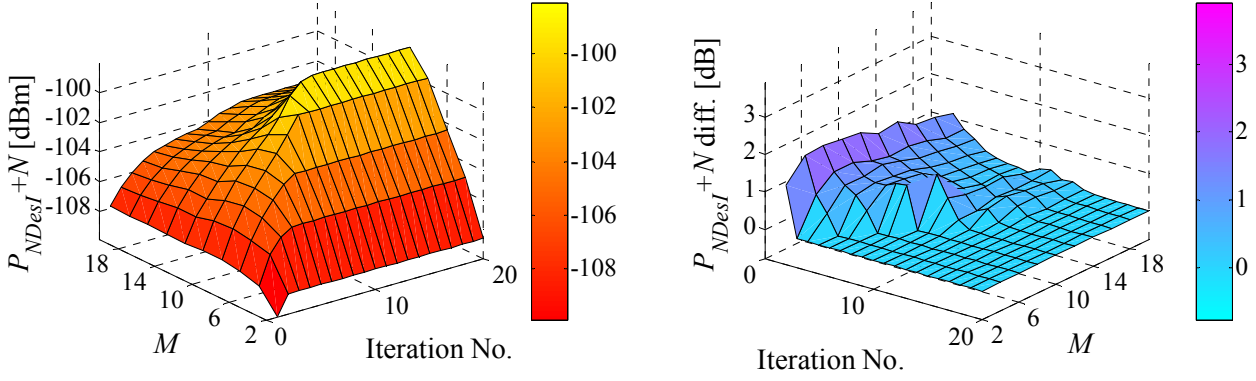


(b) Sc #4u_mc_Gr_5.

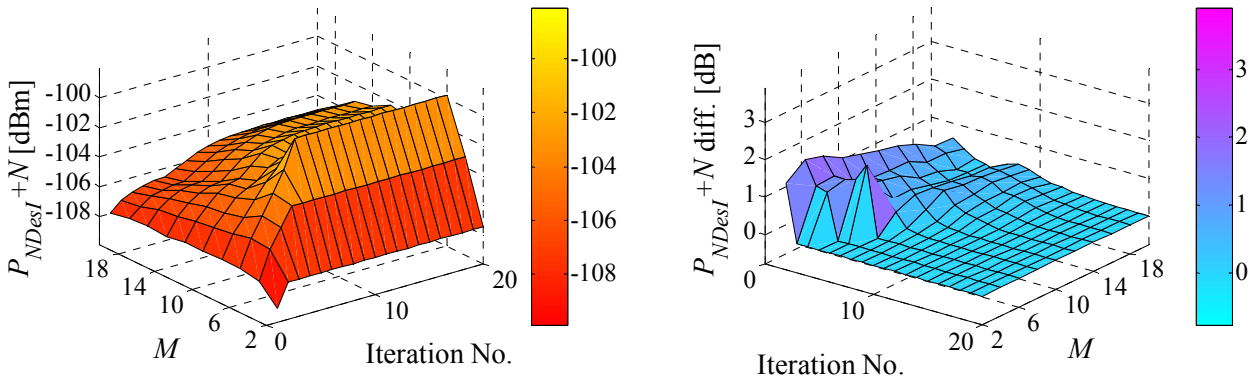


(c) Sc #4u_mc_Gr_10.

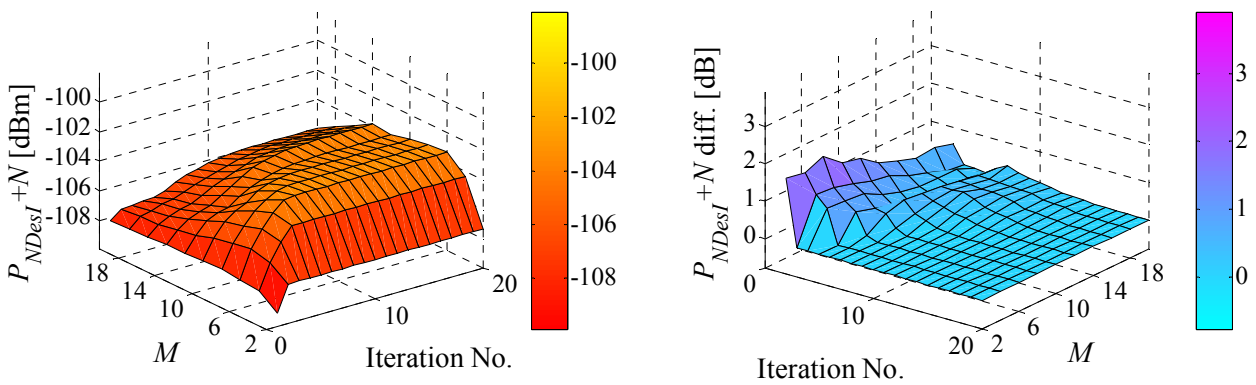
Figure A.2 – Average P_{DesS} [dBm] and differences along optimisation, for $L = 4$, function of d_{MT} , for several numbers of array elements.



(a) Sc #4u_mc_Gr_05.

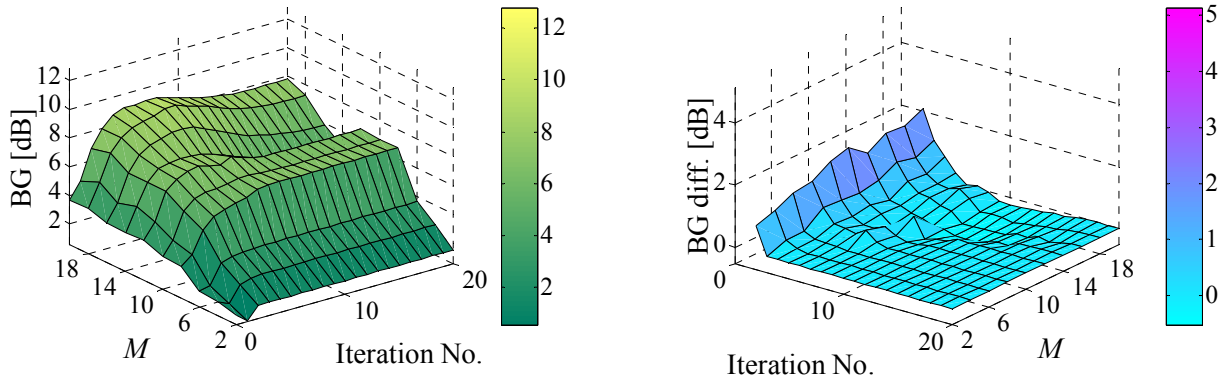


(b) Sc #4u_mc_Gr_5.

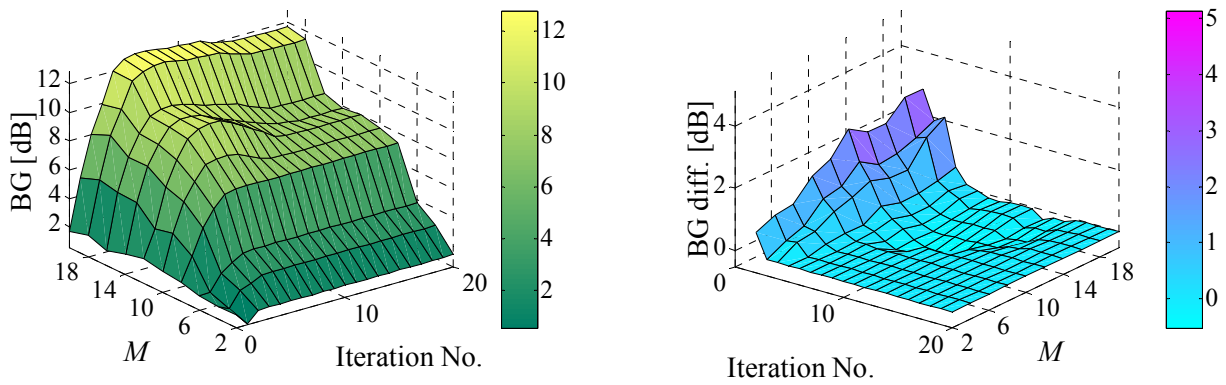


(c) Sc #4u_mc_Gr_10.

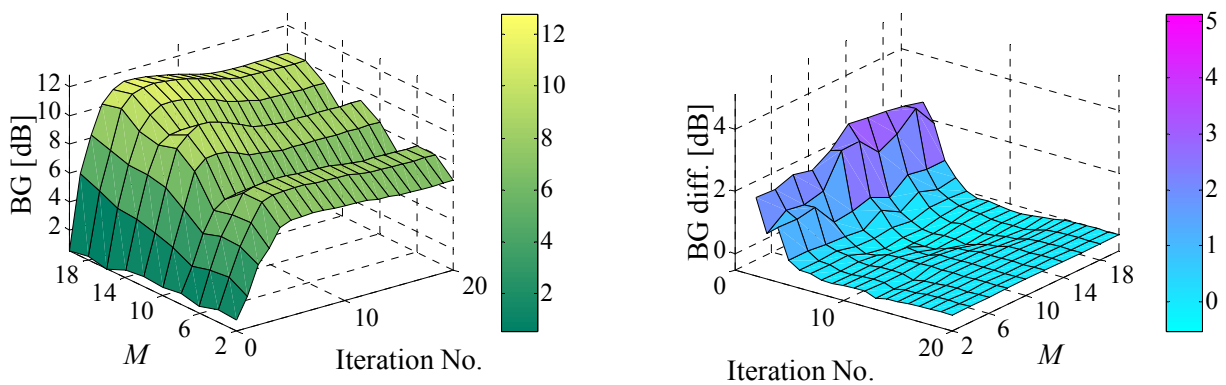
Figure A.3 – Average $P_{NDesI+N}$ [dBm] and differences along optimisation, for $L = 4$, function of d_{MT} , for several numbers of array elements.



(a) Sc #8u_mc_Gr_05.

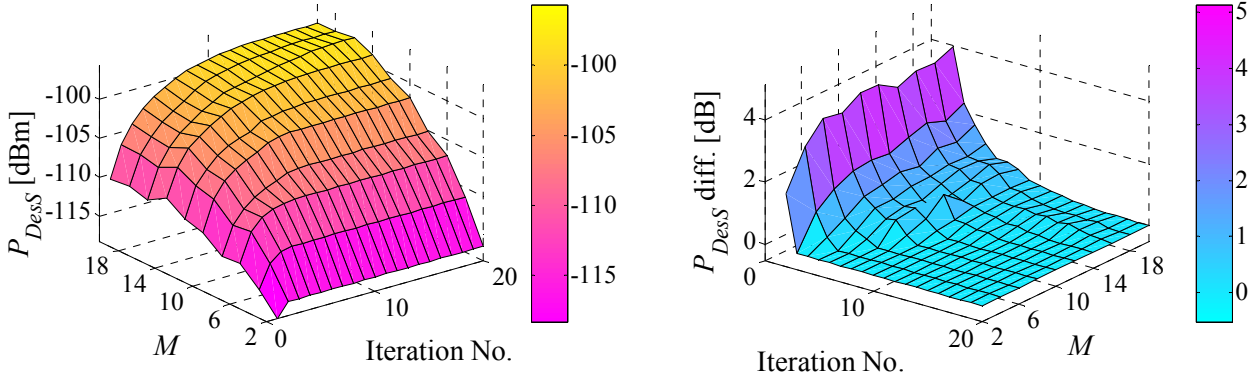


(b) Sc #8u_mc_Gr_5.

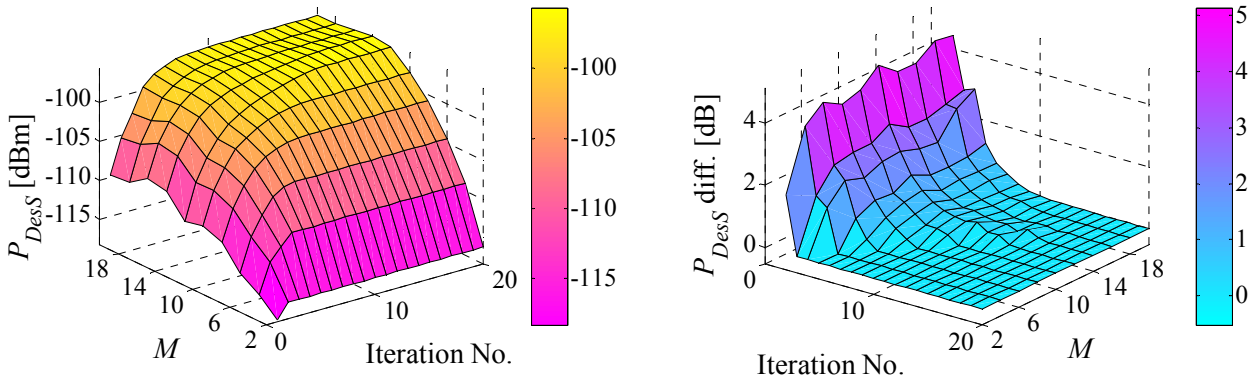


(c) Sc #8u_mc_Gr_10.

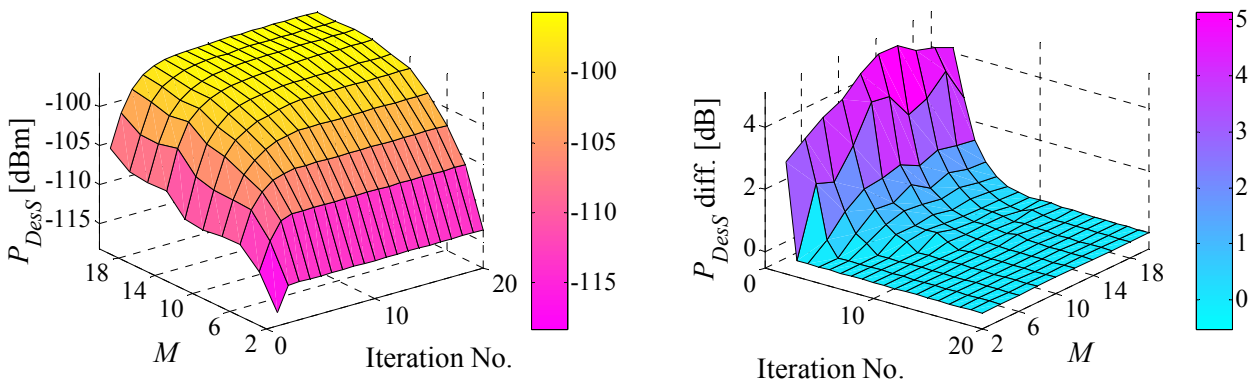
Figure A.4 – Average BG [dB] and differences along optimisation, for $L = 8$, function of d_{MT} , for several values of M .



(a) Sc #8u_mc_Gr_05.

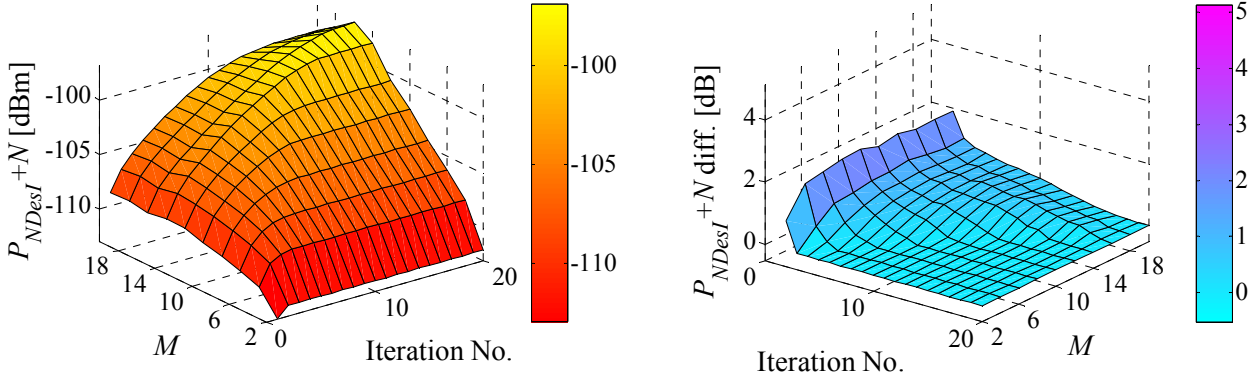


(b) Sc #8u_mc_Gr_5.

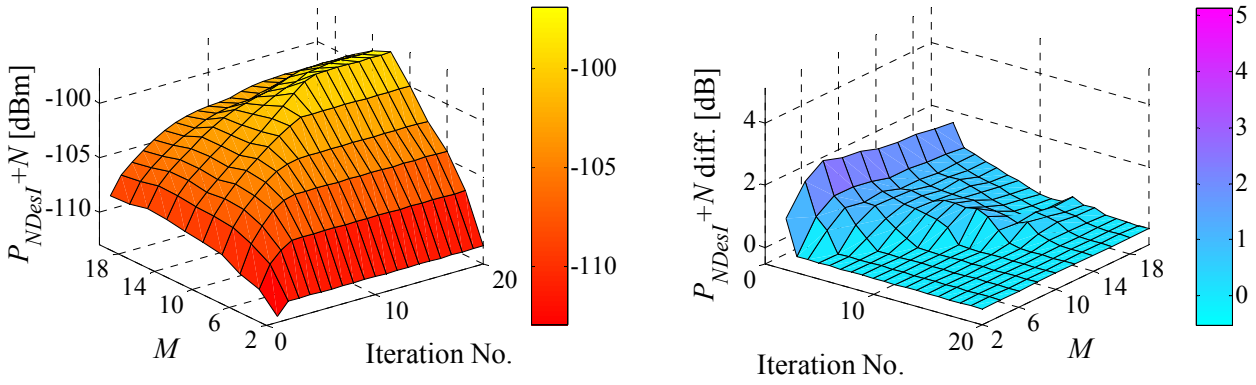


(c) Sc #8u_mc_Gr_10.

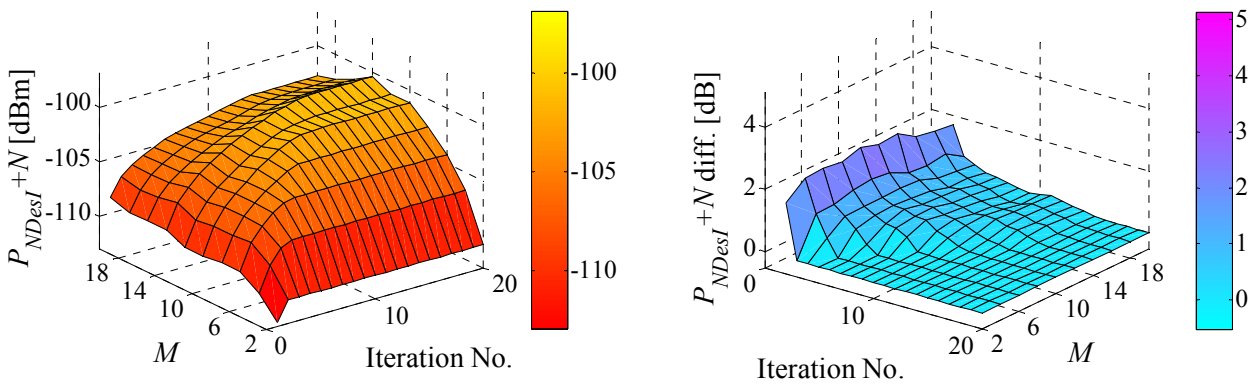
Figure A.5 – Average P_{DesS} [dBm] and differences along optimisation, for $L = 8$, function of d_{MT} , for several numbers of array elements.



(a) Sc #8u_mc_Gr_05.

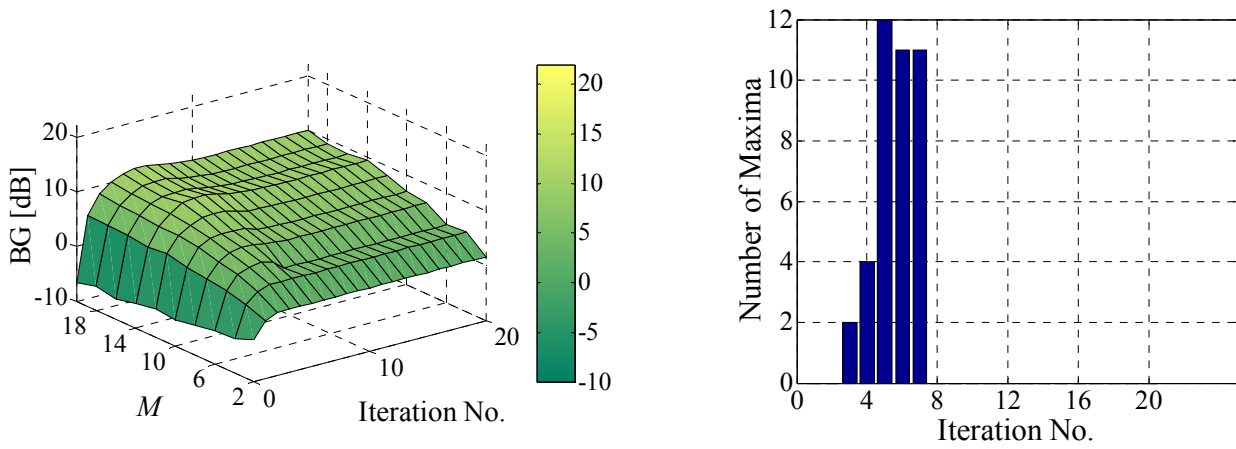


(b) Sc #8u_mc_Gr_5.

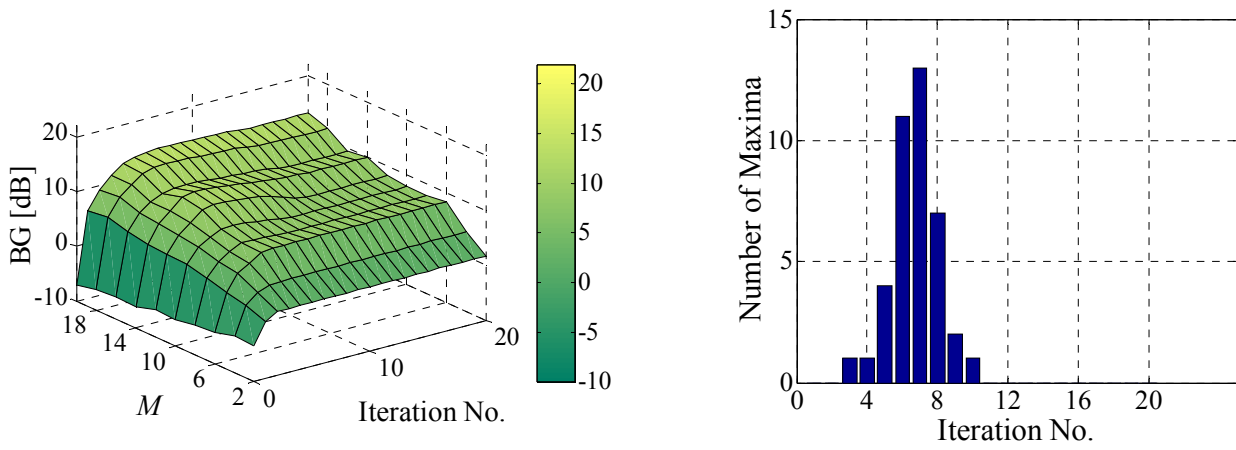


(c) Sc #8u_mc_Gr_10.

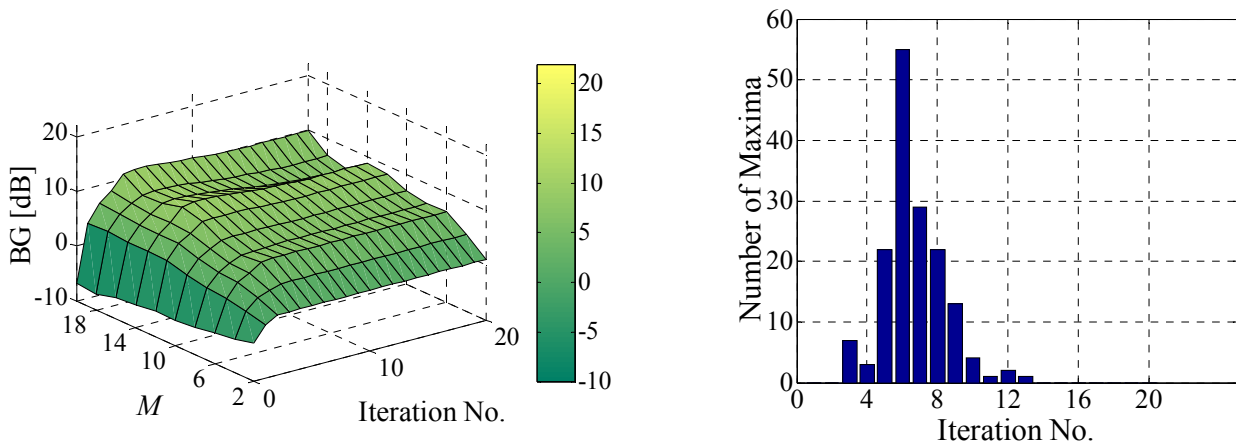
Figure A.6 – Average $P_{NDesI+N}$ [dBm] and differences along optimisation, for $L = 8$, function of d_{MT} , for several numbers of array elements.



(a) Sc #4u_mc_Sp_5.

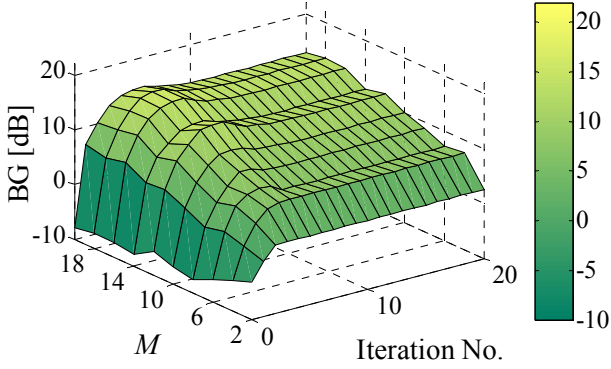


(b) Sc #8u_mc_Sp_5.

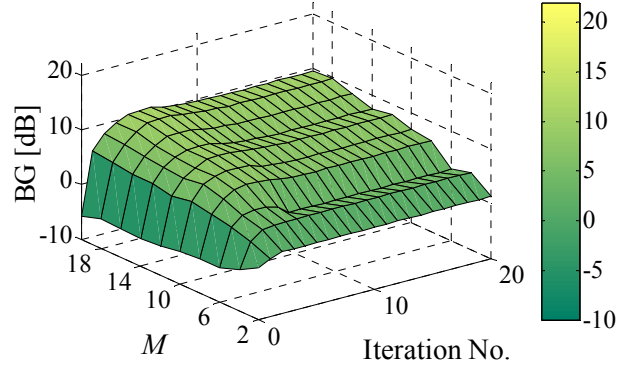


(c) Sc #16u_mc_Sp_5.

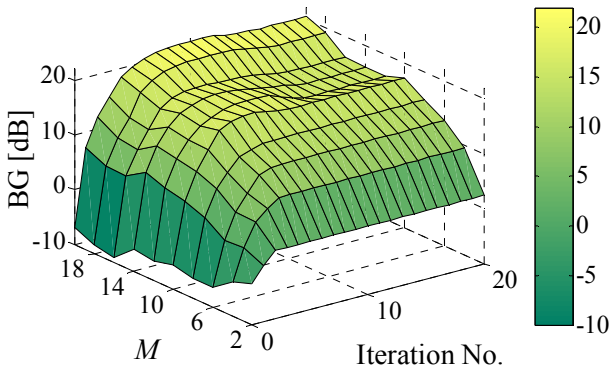
Figure A.7 – Average BG [dB] along optimisation, for Sc # L u_mc_Sp_5, function of L and M , and bar histograms of the maxima, function of the iteration number.



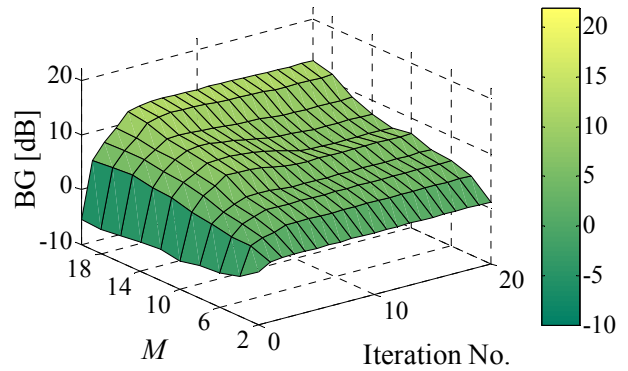
(a) MT₁, Sc #4u_mc_Se_A.



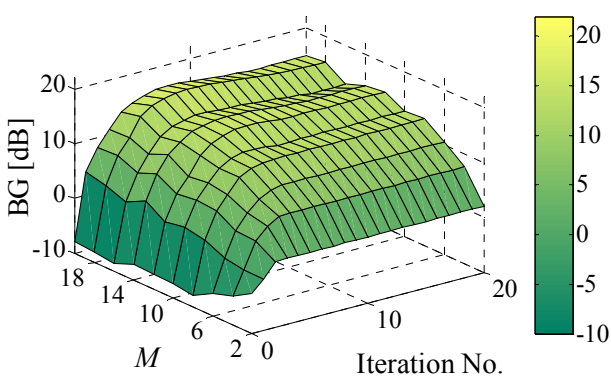
(b) MT Group, Sc #4u_mc_Se_A.



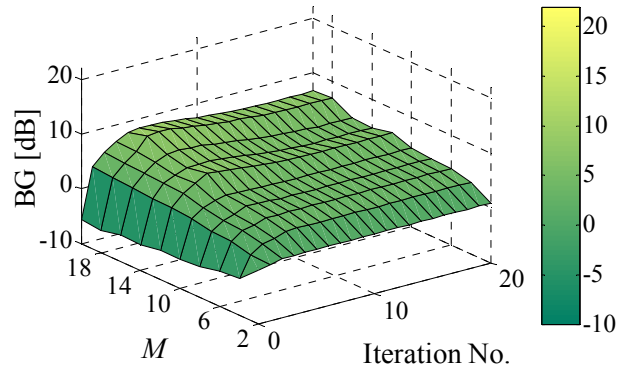
(c) MT₁, Sc #8u_mc_Se_A.



(d) MT Group, Sc #8u_mc_Se_A.

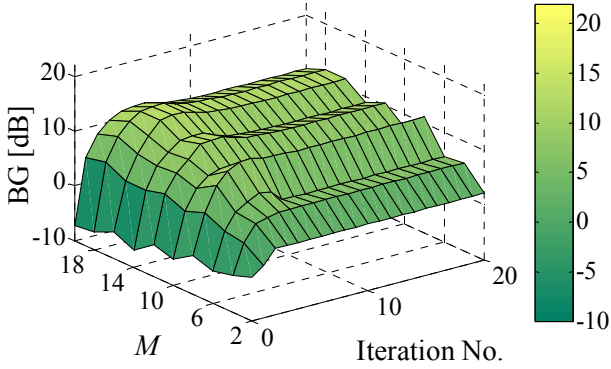


(e) MT₁, Sc #16u_mc_Se_A.

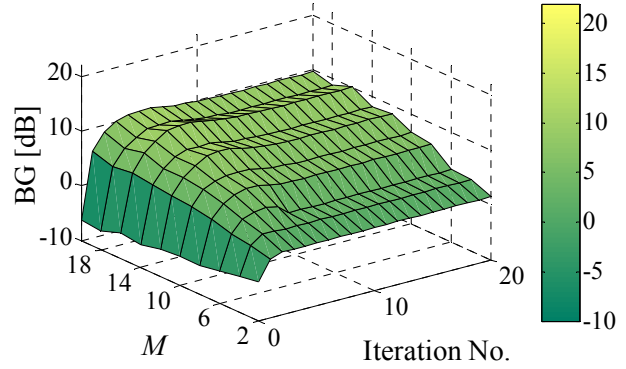


(f) MT Group, Sc #16u_mc_Se_A.

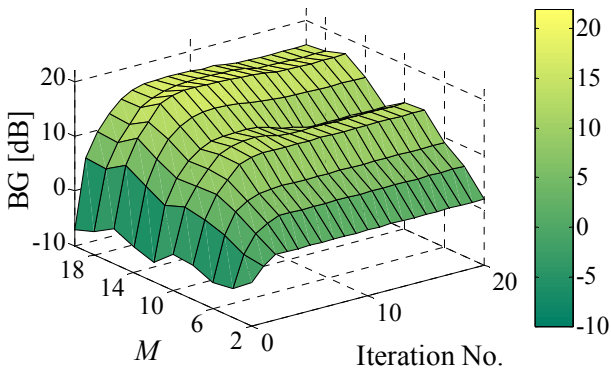
Figure A.8 – Average BG [dB] along optimisation, for Sc #Lu_mc_Se_A, function of L and M , for MT₁ and the MT group.



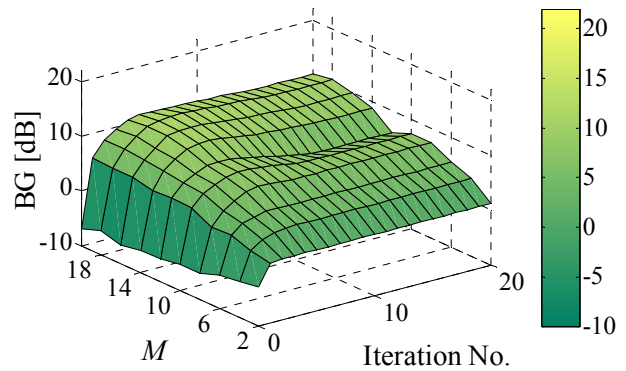
(a) MT_1 , Sc #4u_mc_Se_B.



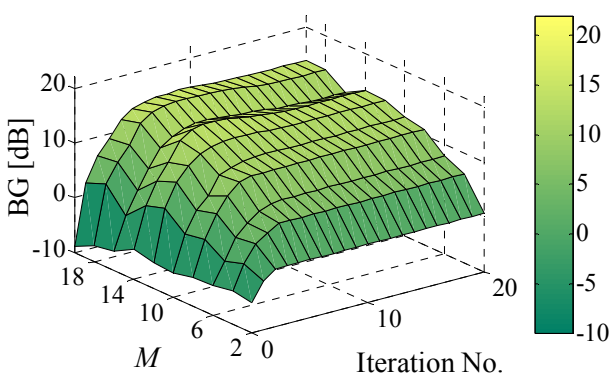
(b) MT Group, Sc #4u_mc_Se_B.



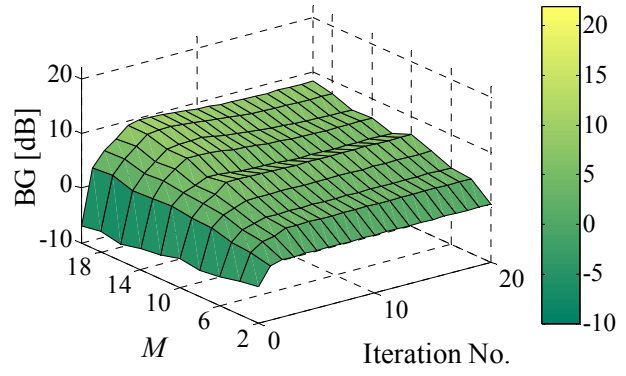
(c) MT_1 , Sc #8u_mc_Se_B.



(d) MT Group, Sc #8u_mc_Se_B.

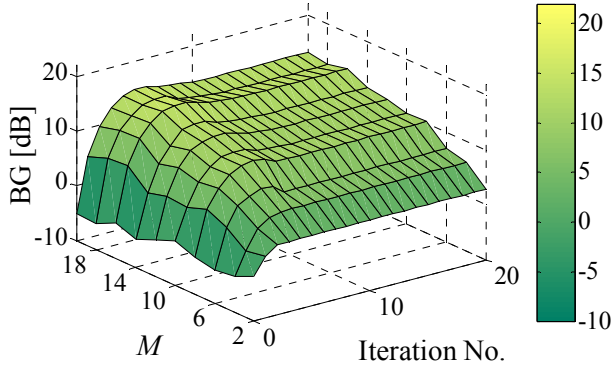


(e) MT_1 , Sc #16u_mc_Se_B.

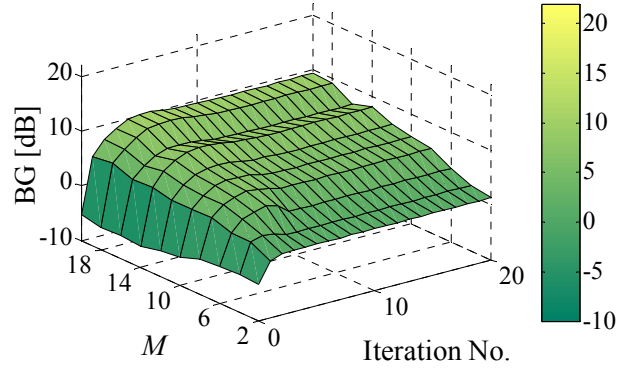


(f) MT Group, Sc #16u_mc_Se_B.

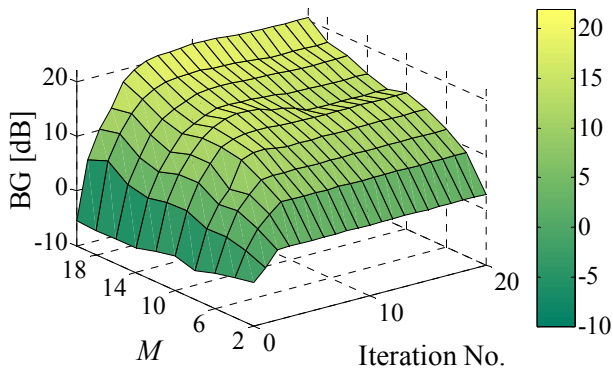
Figure A.9 – Average BG [dB] along optimisation, for Sc #Lu_mc_Se_B, function of L and M , for MT_1 and the MT group.



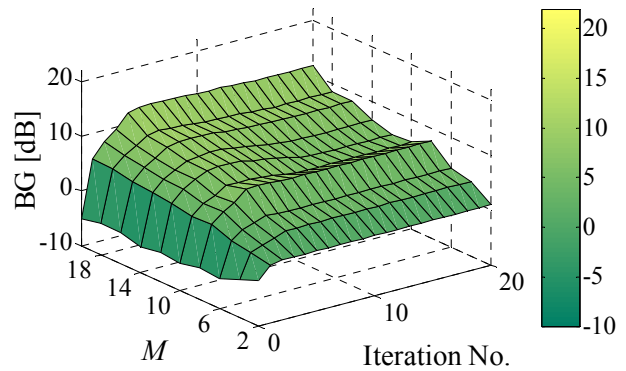
(a) MT_1 , Sc #4u_mc_Se_C.



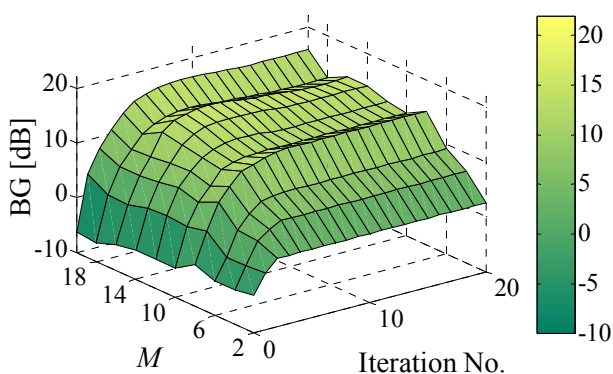
(b) MT Group, Sc #4u_mc_Se_C.



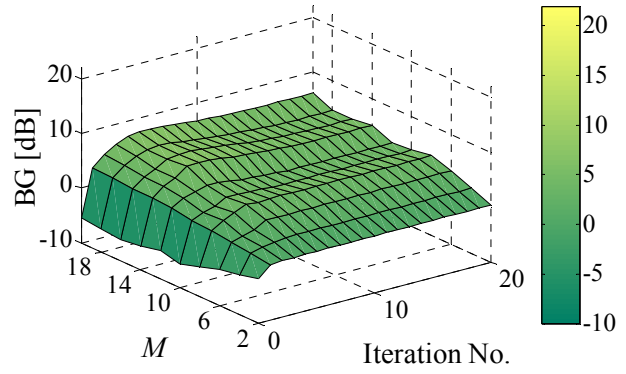
(c) MT_1 , Sc #8u_mc_Se_C.



(d) MT Group, Sc #8u_mc_Se_C.



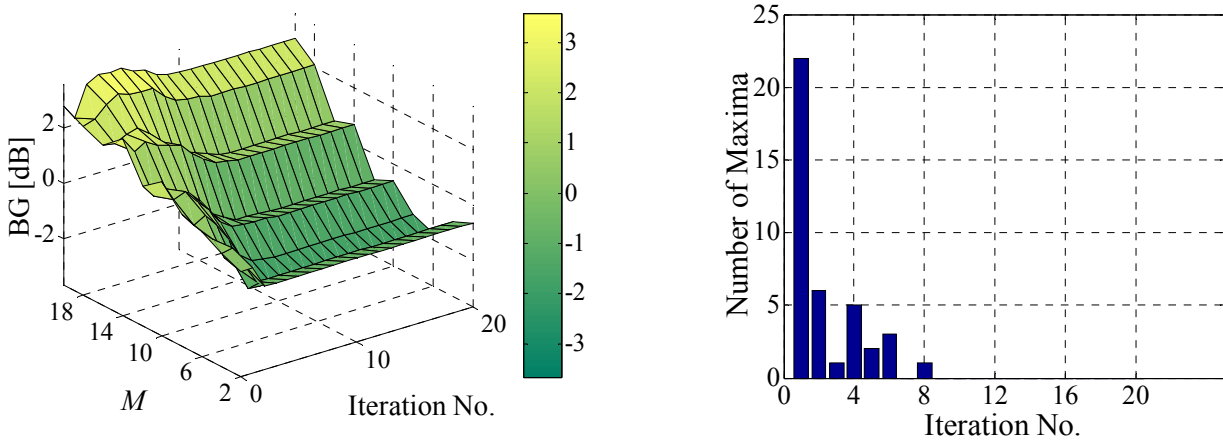
(e) MT_1 , Sc #16u_mc_Se_C.



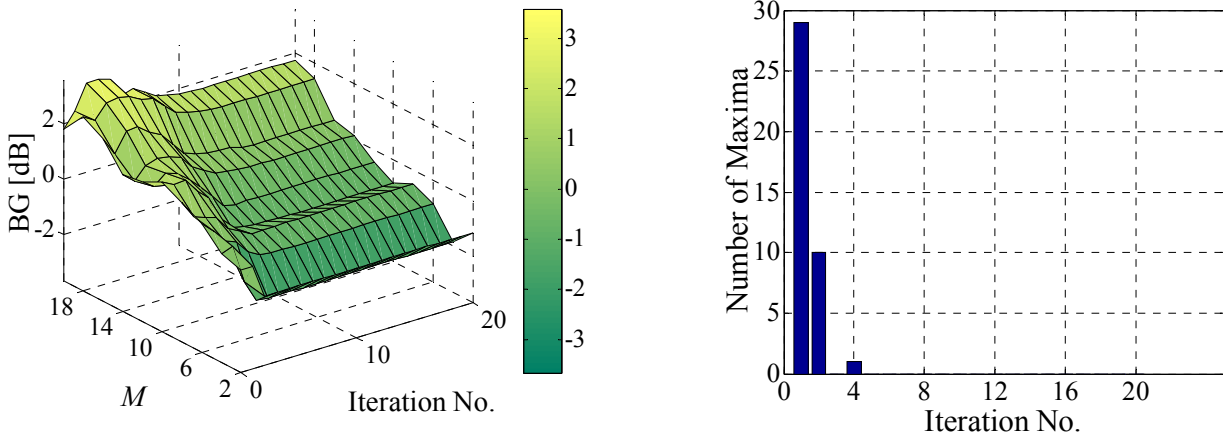
(f) MT Group, Sc #16u_mc_Se_C.

Figure A.10 – Average BG [dB] along optimisation, for Sc #Lu_mc_Se_C, function of L and M , for MT_1 and the MT group.

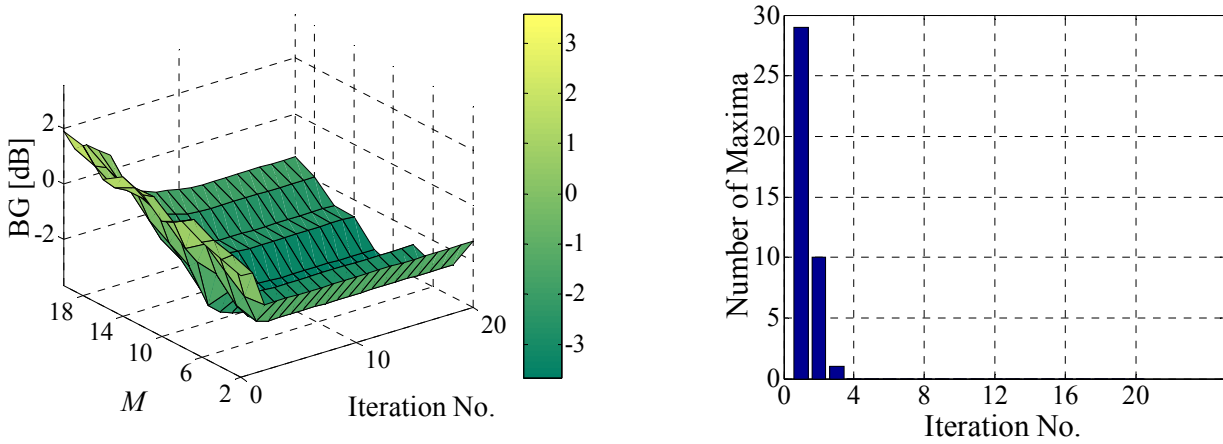
Annex B – Surface Plots – Macro-Cell Scenarios



(a) Sc #4u_Mc_Gr_10_200.

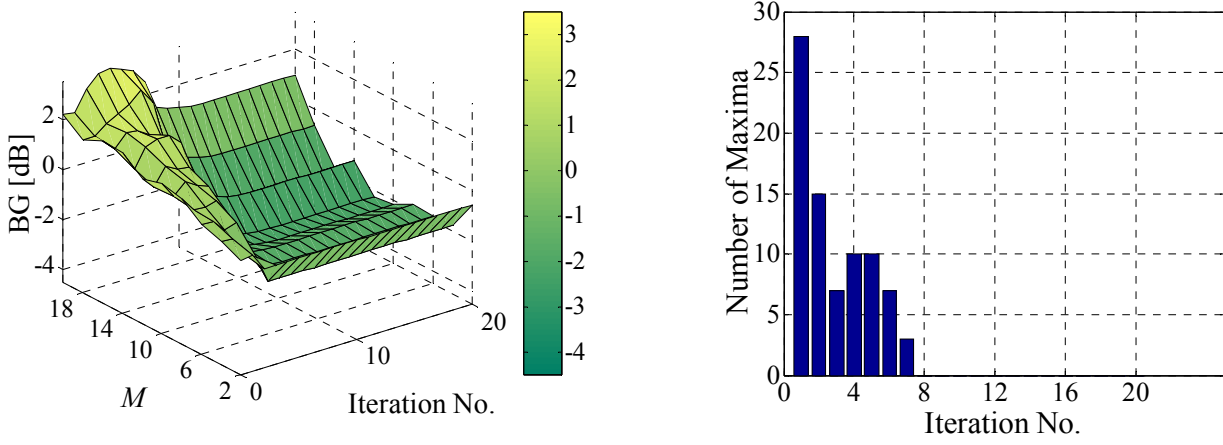


(b) Sc #4u_Mc_Gr_15_200.

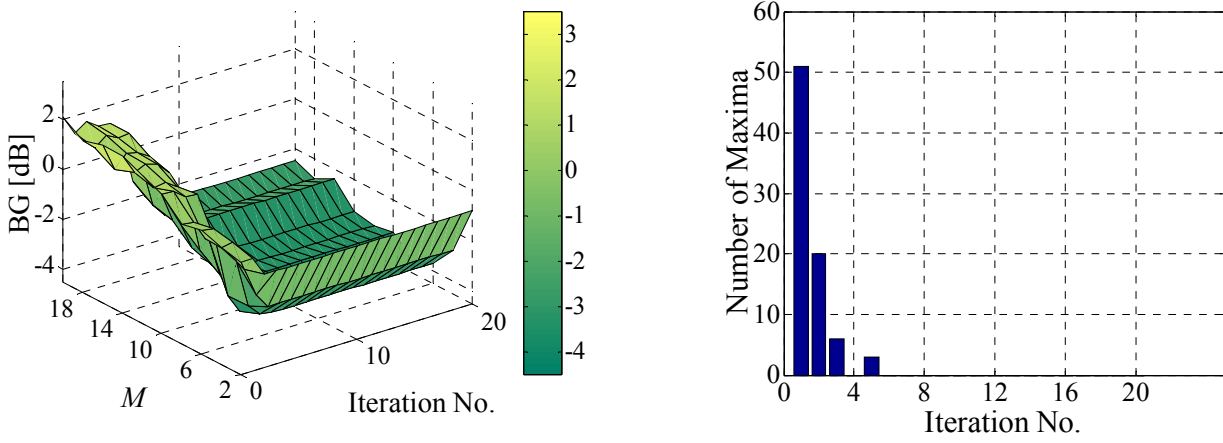


(c) Sc #4u_Mc_Gr_20_200.

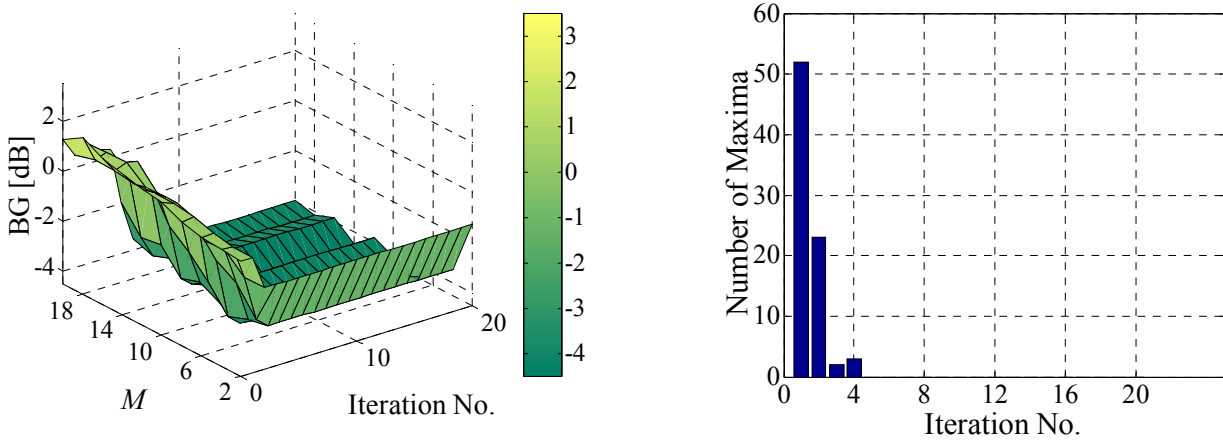
Figure B.1 – Average BG [dB] along optimisation, for Sc #4u_Mc_Gr_d_200, function of d_{MT} and M , and bar histograms of the maxima, function of the iteration number.



(a) Sc #8u_Mc_Gr_10_200.

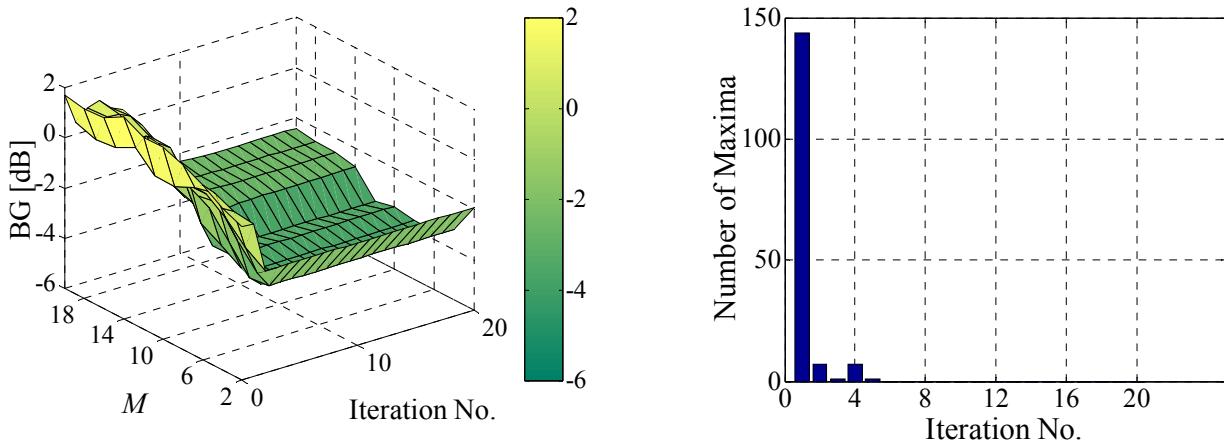


(b) Sc #8u_Mc_Gr_15_200.

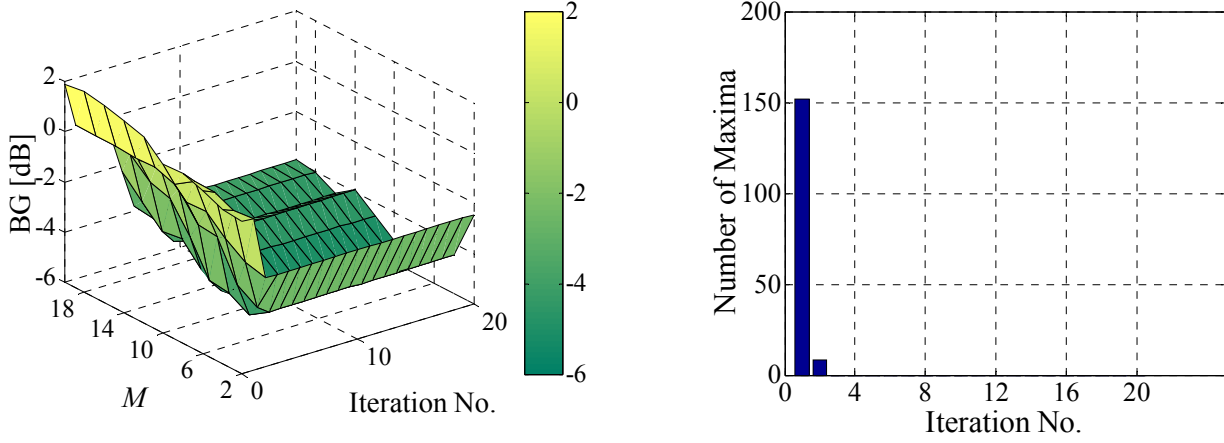


(c) Sc #8u_Mc_Gr_20_200.

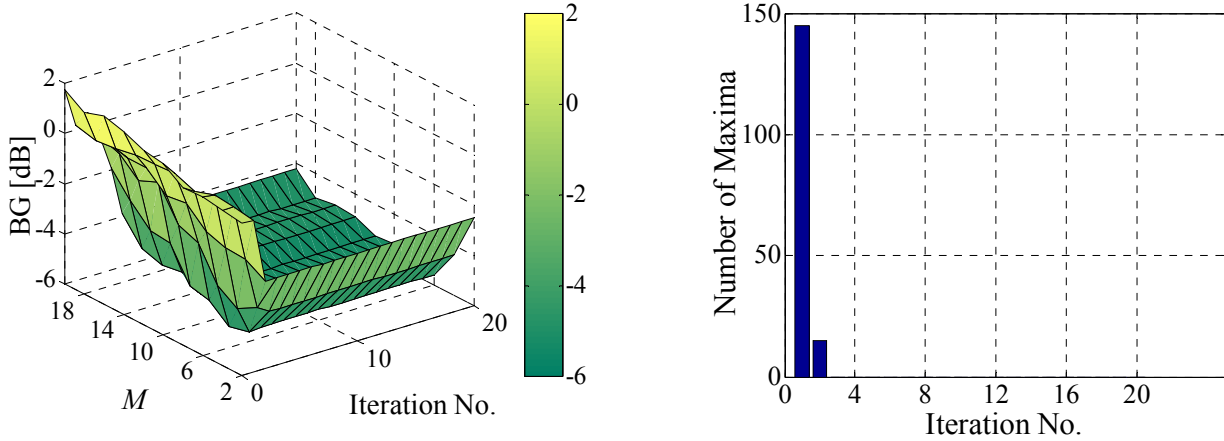
Figure B.2 – Average BG [dB] along optimisation, for Sc #8u_Mc_Gr_d_200, function of d_{MT} and M , and bar histograms of the maxima, function of the iteration number.



(a) Sc #16u_Mc_Gr_10_200.

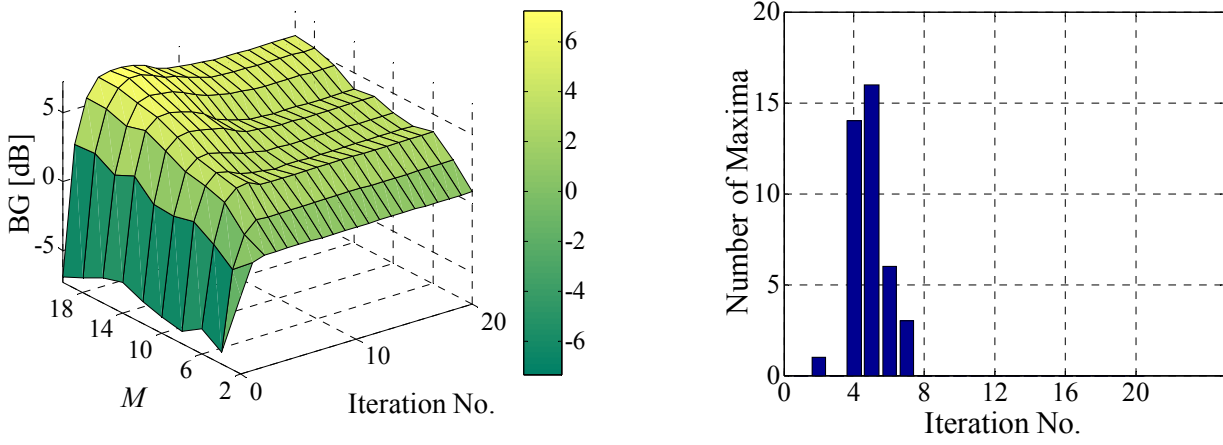


(b) Sc #16u_Mc_Gr_15_200.

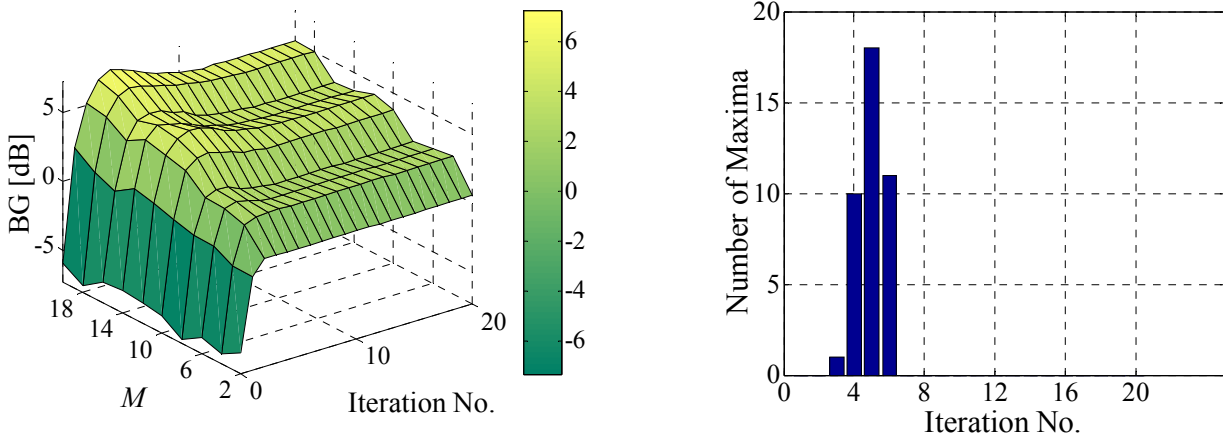


(c) Sc #16u_Mc_Gr_20_200.

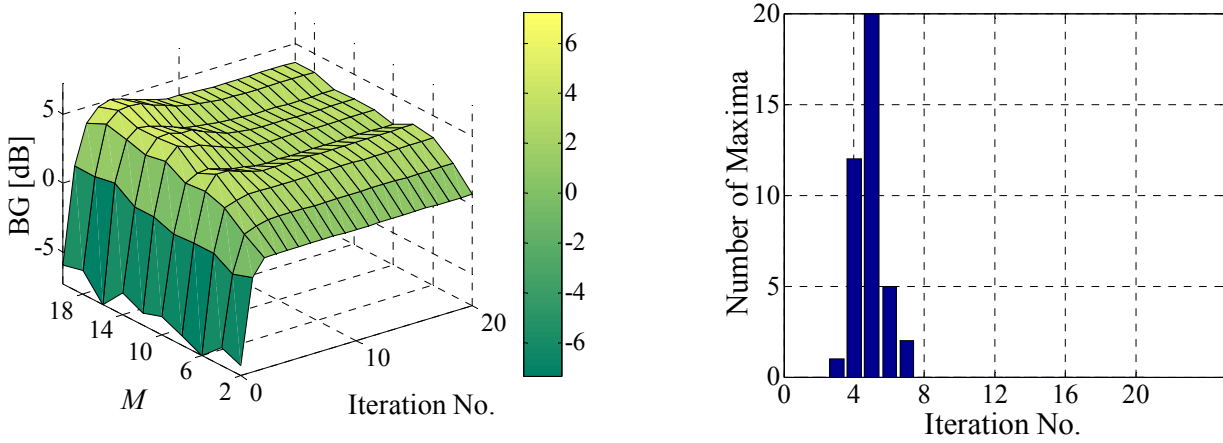
Figure B.3 – Average BG [dB] along optimisation, for Sc #16u_Mc_Gr_ d _200, function of d_{MT} and M , and bar histograms of the maxima, function of the iteration number.



(a) Sc #4u_Mc_Sp_10_200.

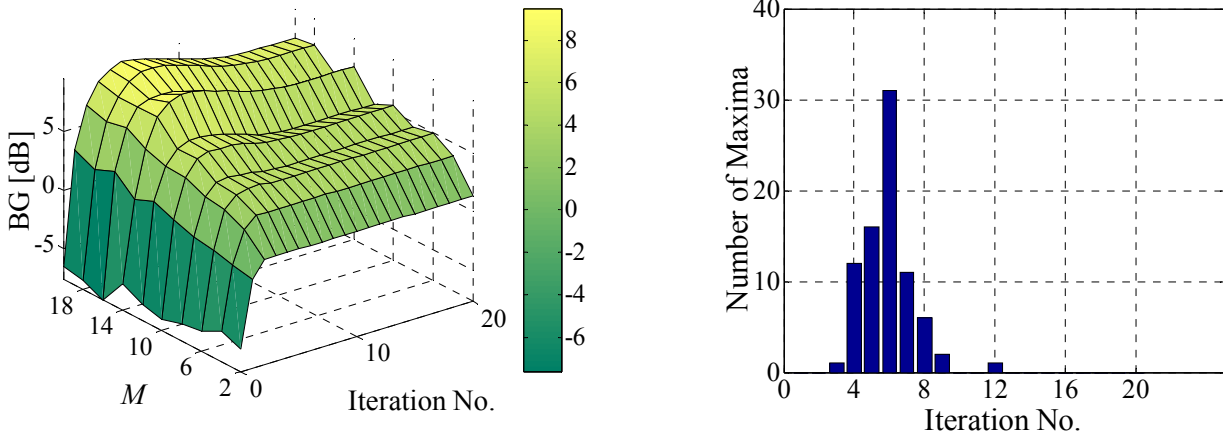


(b) Sc #4u_Mc_Sp_15_200.

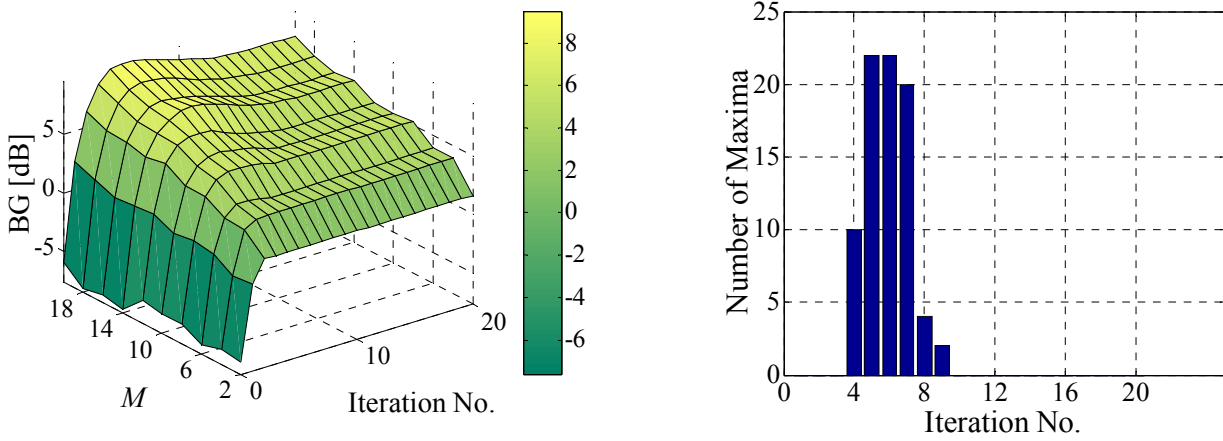


(c) Sc #4u_Mc_Sp_20_200.

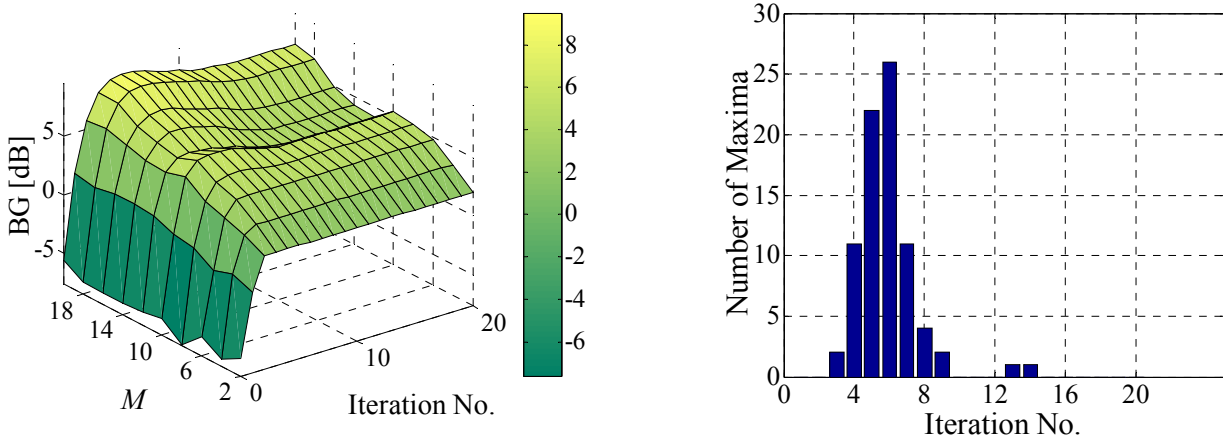
Figure B.4 – Average BG [dB] along optimisation, for Sc #4u_Mc_Sp_d_200, function of d_{MT} and M , and bar histograms of the maxima, function of the iteration number.



(a) Sc #8u_Mc_Sp_10_200.

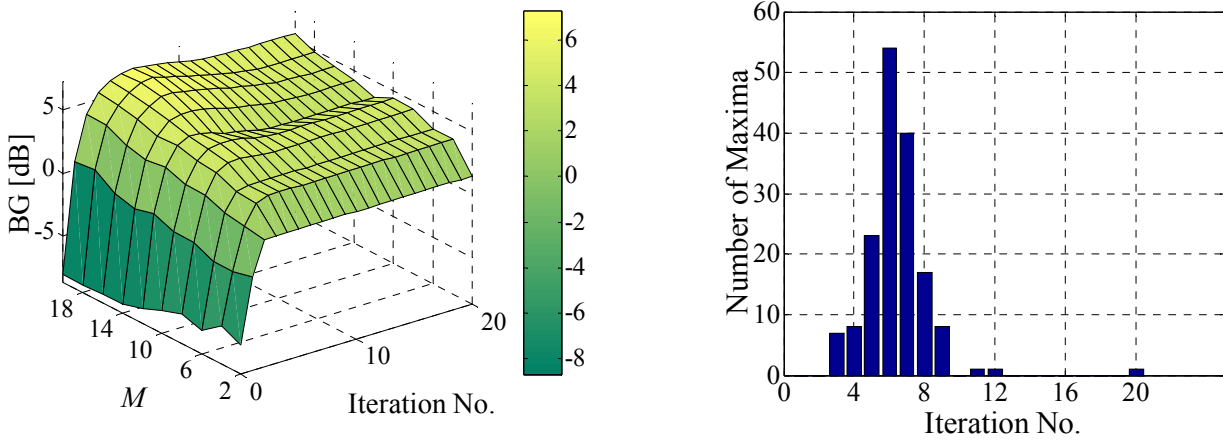


(b) Sc #8u_Mc_Sp_15_200.

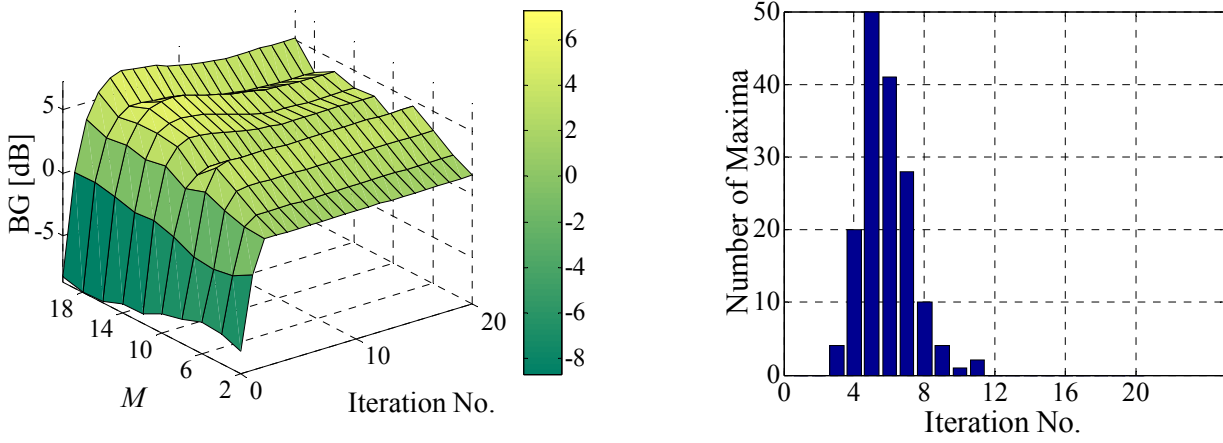


(c) Sc #8u_Mc_Sp_20_200.

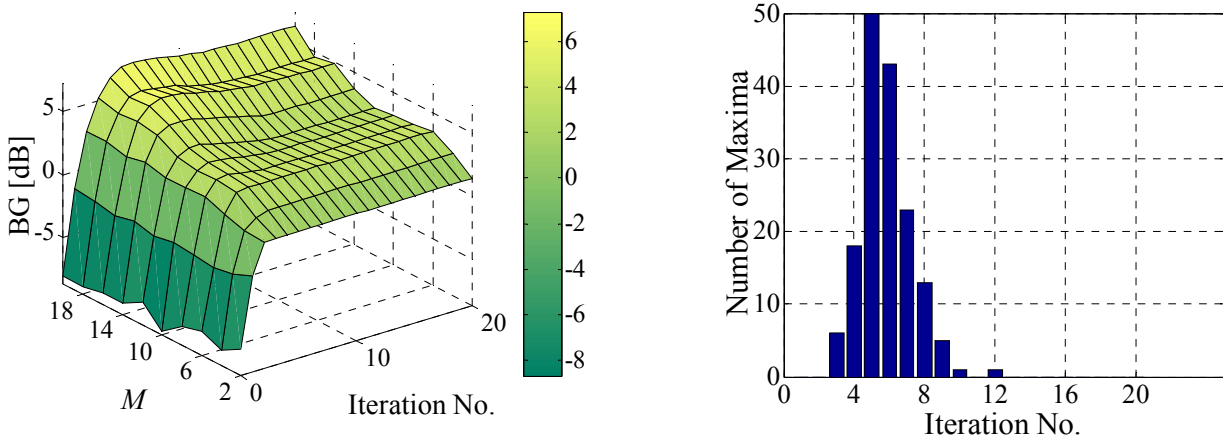
Figure B.5 – Average BG [dB] along optimisation, for Sc #8u_Mc_Sp_d_200, function of d_{MT} and M , and bar histograms of the maxima, function of the iteration number.



(a) Sc #16u_Mc_Sp_10_200.

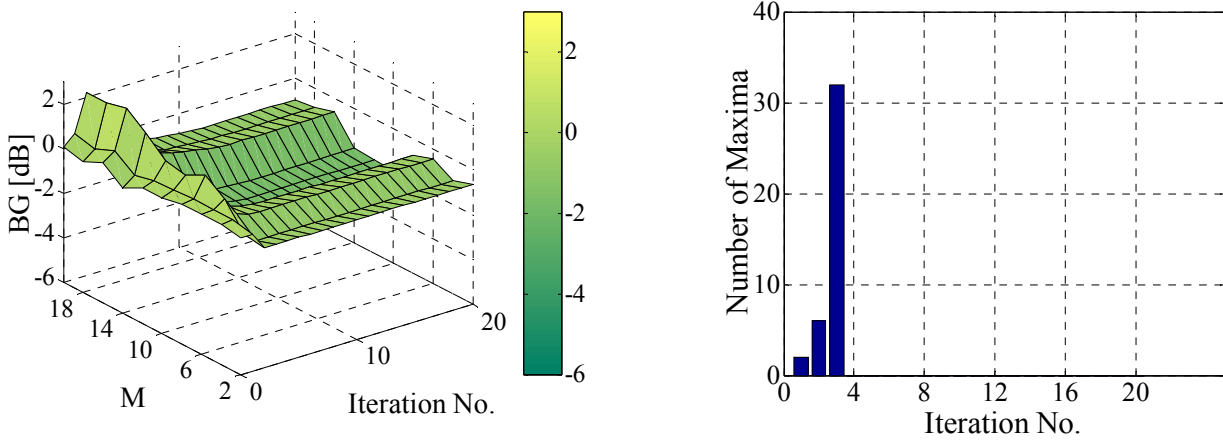


(b) Sc #16u_Mc_Sp_15_200.

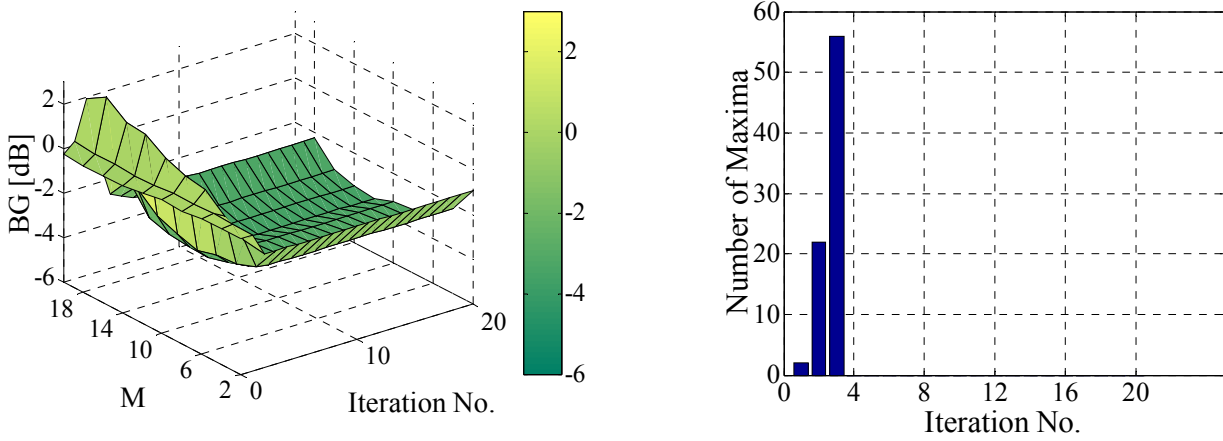


(c) Sc #16u_Mc_Sp_20_200.

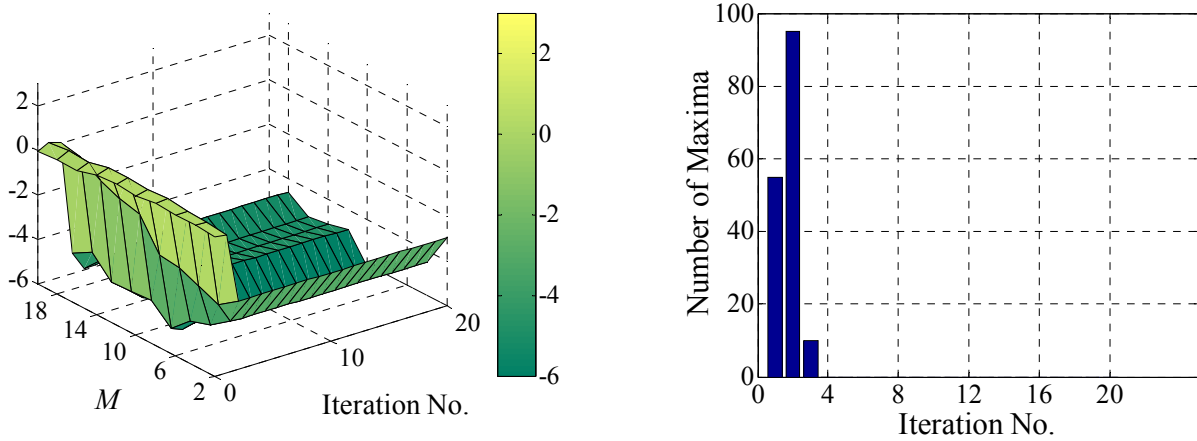
Figure B.6 – Average BG [dB] along optimisation, for Sc #16u_Mc_Sp_ d _200, function of d_{MT} and M , and bar histograms of the maxima, function of the iteration number.



(a) Sc #4u_Mc_Gr_15_50.

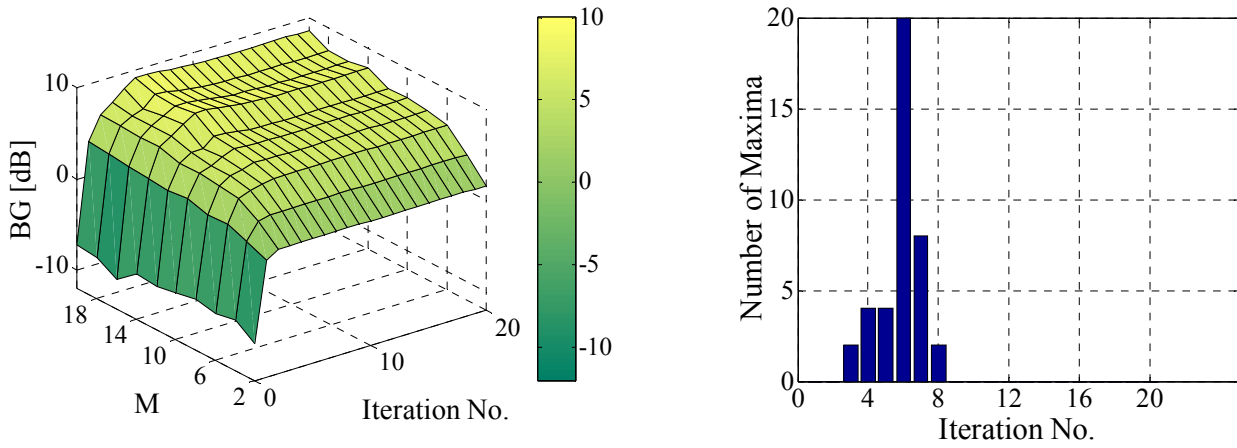


(b) Sc #8u_Mc_Gr_15_50.

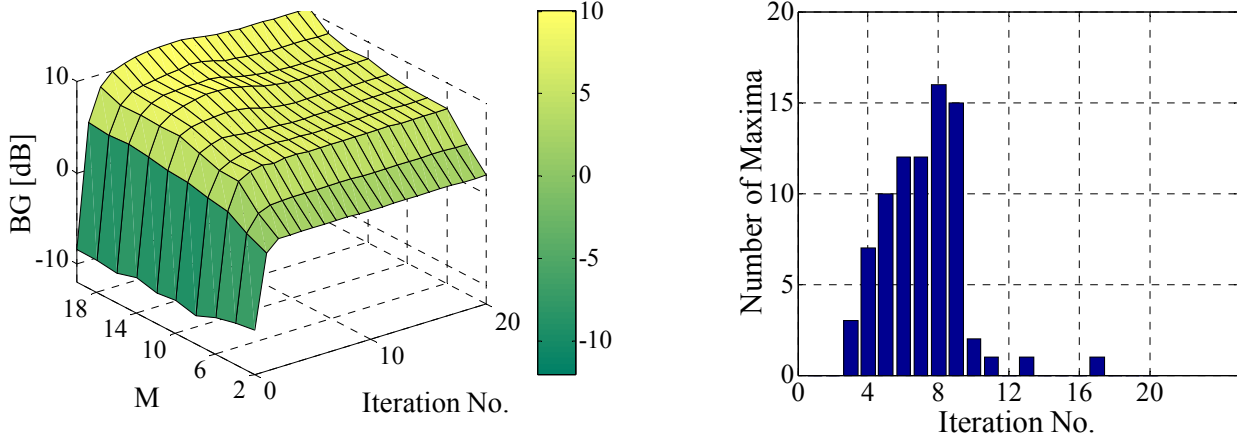


(c) Sc #16u_Mc_Gr_15_50.

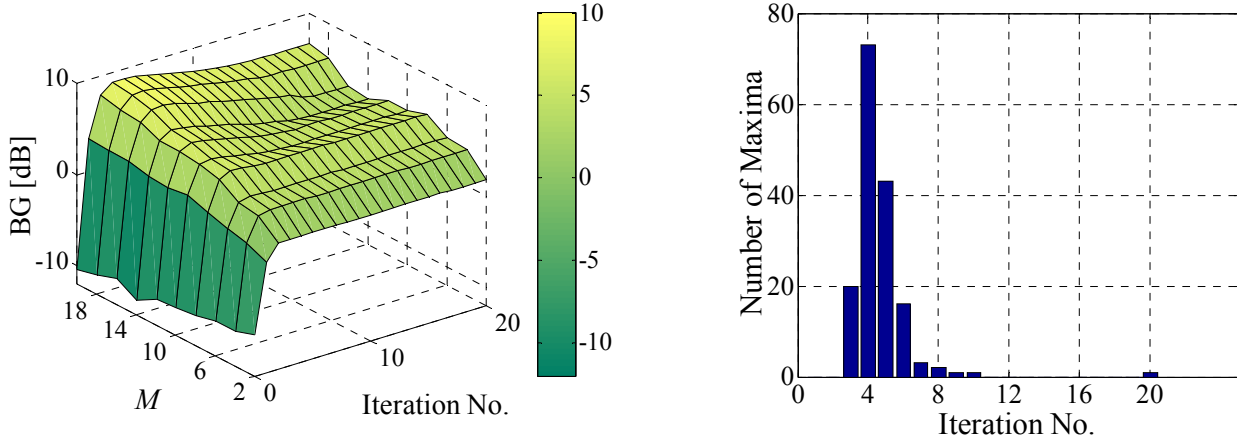
Figure B.7 – Average BG [dB] along optimisation, for Sc #Lu_Mc_Gr_15_50, function of L and M , and bar histograms of the maxima, function of the iteration number.



(a) Sc #4u_Mc_Sp_15_50.

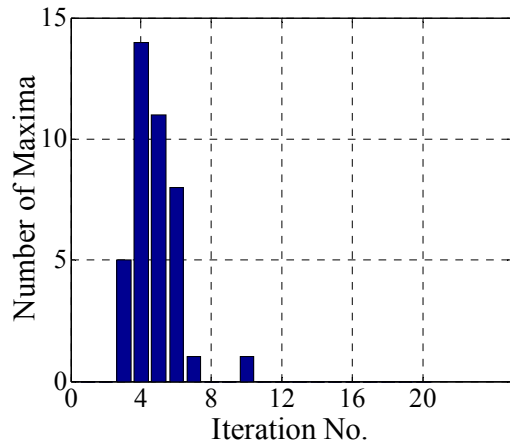
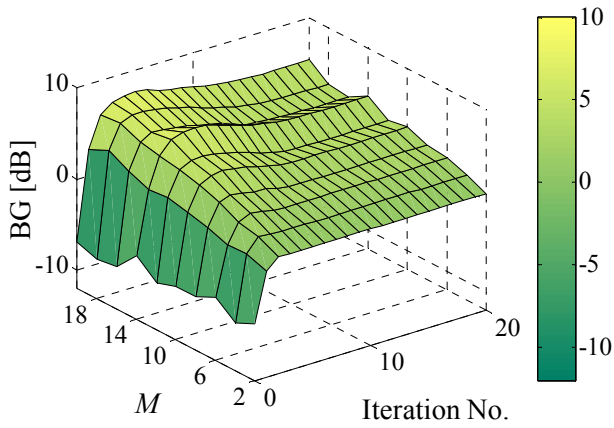


(b) Sc #8u_Mc_Sp_15_50.

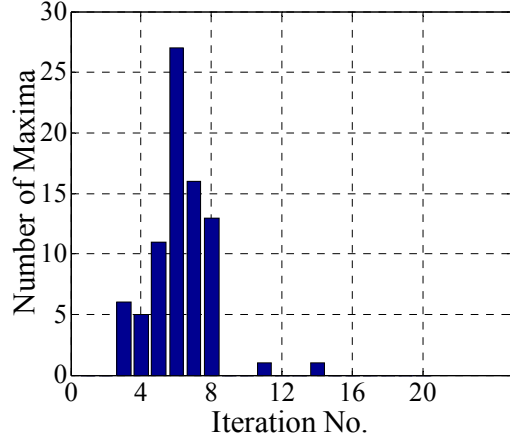
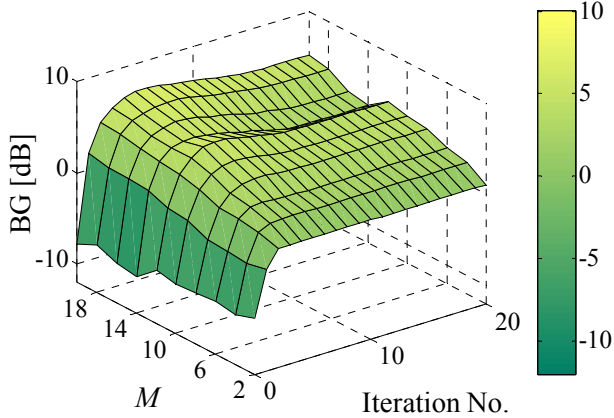


(c) Sc #16u_Mc_Sp_15_50.

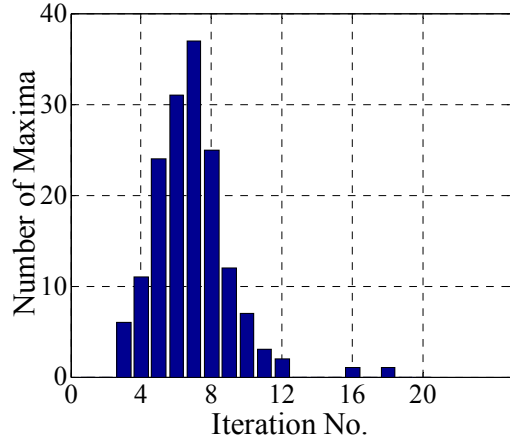
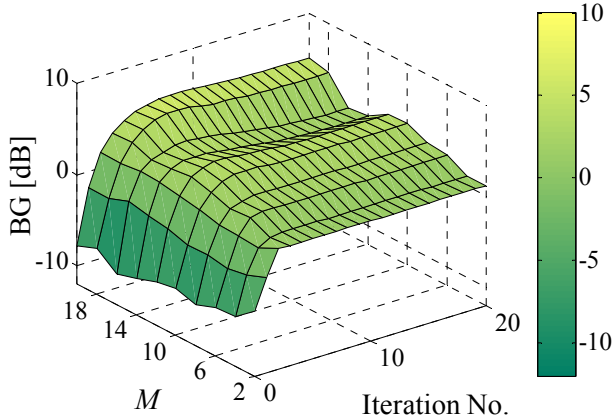
Figure B.8 – Average BG [dB] along optimisation, for Sc #Lu_Mc_Sp_15_50, function of L and M , and bar histograms of the maxima, function of the iteration number.



(a) Sc #4u_Mc_Sp_15_400.

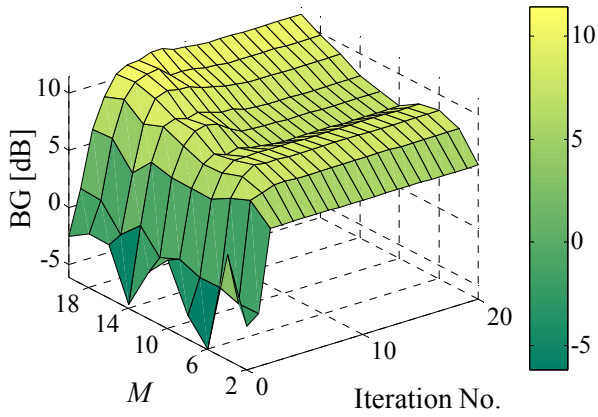


(b) Sc #8u_Mc_Sp_15_400.

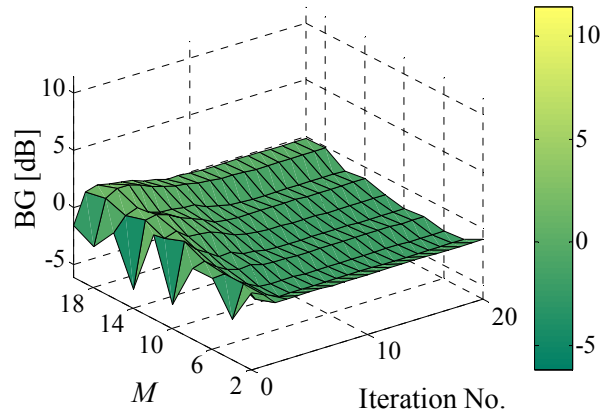


(a) Sc #4u_Mc_Sp_15_400.

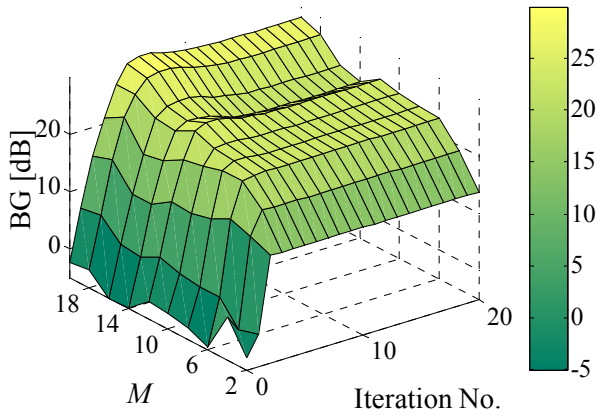
Figure B.9 – Average BG [dB] along optimisation, for Sc #Lu_Mc_Sp_15_400, function of L and M , and bar histograms of the maxima, function of the iteration number.



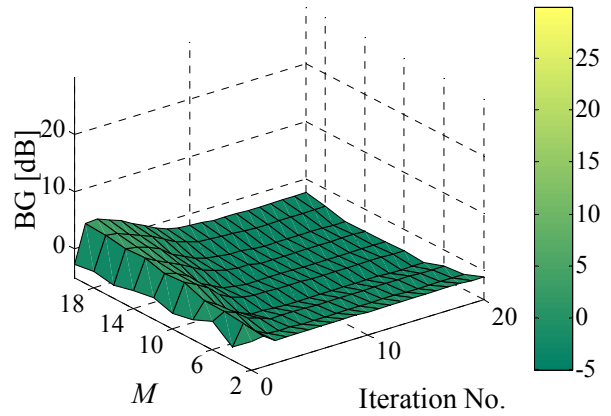
(a) MT_1 , Sc #4u_Mc_Se_A_200.



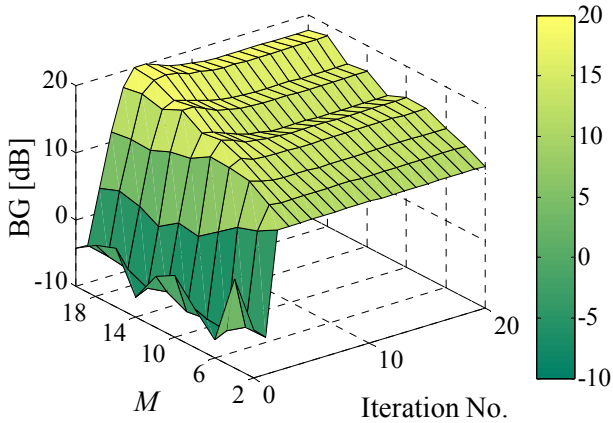
(b) MT Group, Sc #4u_Mc_Se_A_200.



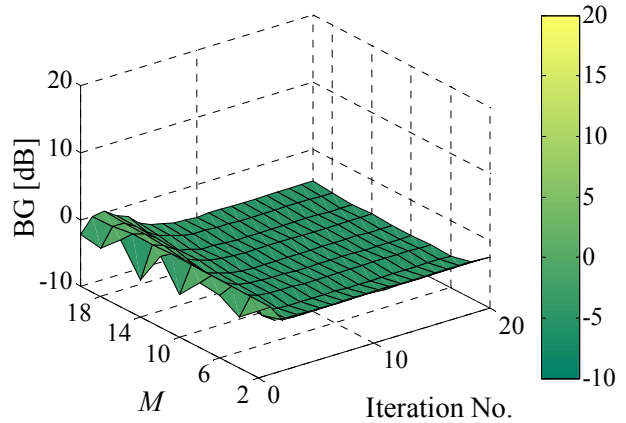
(c) MT_1 , Sc #8u_Mc_Se_A_200.



(d) MT Group, Sc #8u_Mc_Se_A_200.

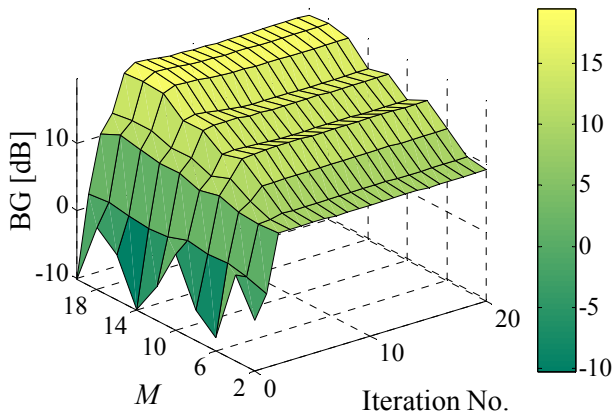


(e) MT_1 , Sc #16u_Mc_Se_A_200.

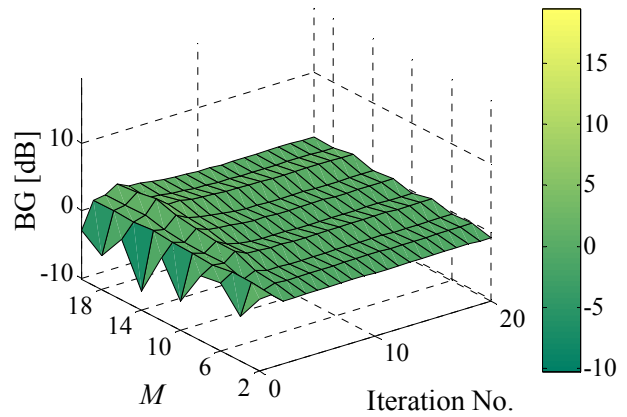


(f) MT Group, Sc #16u_Mc_Se_A_200.

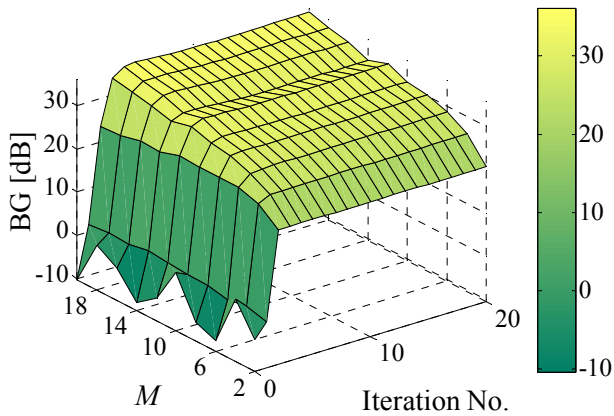
Figure B.10 – Average BG [dB] along optimisation, for Sc #Lu_Mc_Se_A_200, function of L and M , for MT_1 and the MT group.



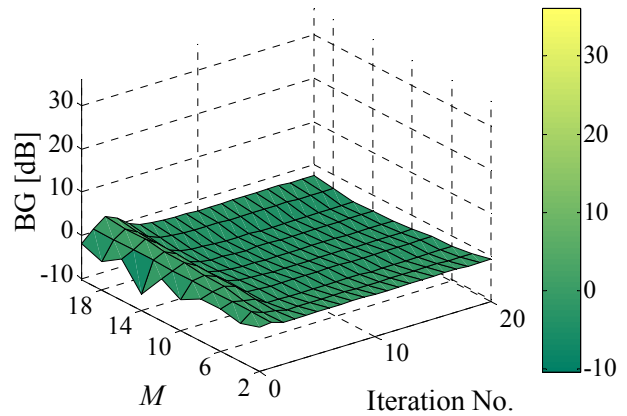
(a) MT_1 , Sc #4u_Mc_Se_A_50.



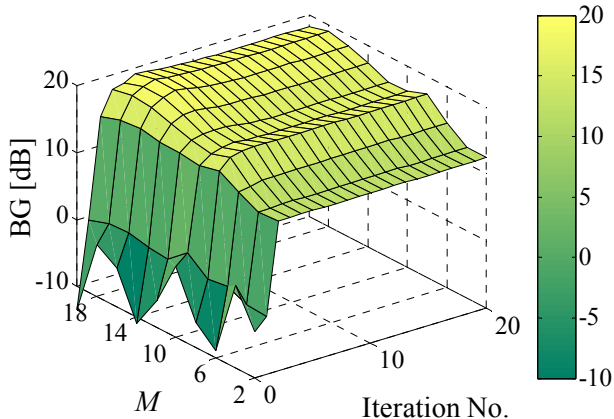
(b) MT Group, Sc #4u_Mc_Se_A_50.



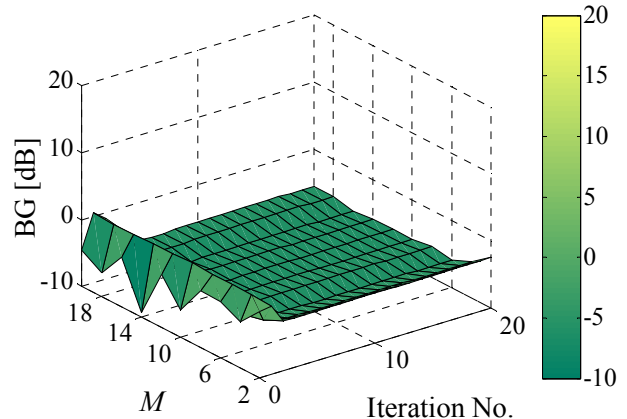
(c) MT_1 , Sc #8u_Mc_Se_A_50.



(d) MT Group, Sc #8u_Mc_Se_A_50.

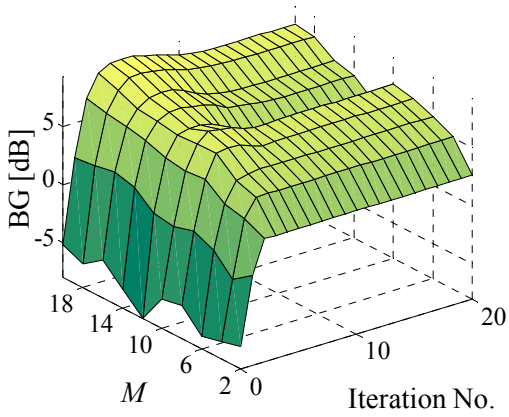


(e) MT_1 , Sc #16u_Mc_Se_A_50.

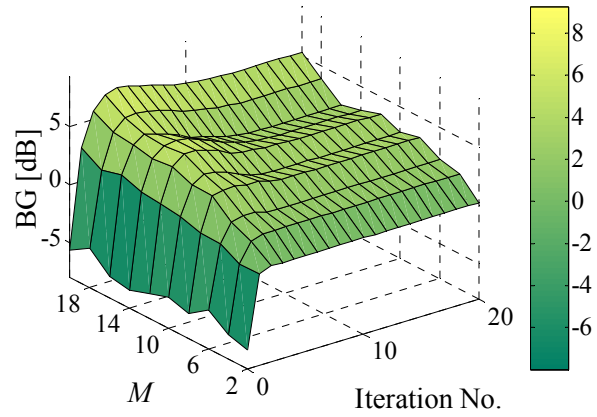


(f) MT Group, Sc #16u_Mc_Se_A_50.

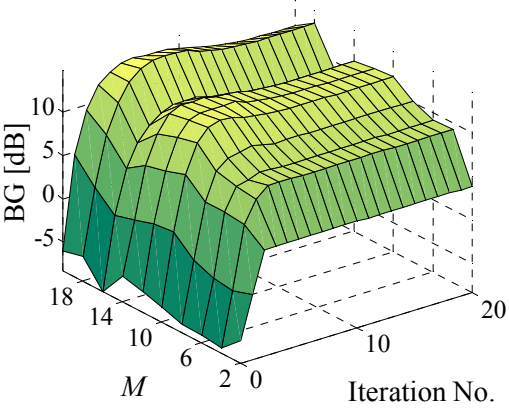
Figure B.11 – Average BG [dB] along optimisation, for Sc #Lu_Mc_Se_A_50, function of L and M , for MT_1 and the MT group.



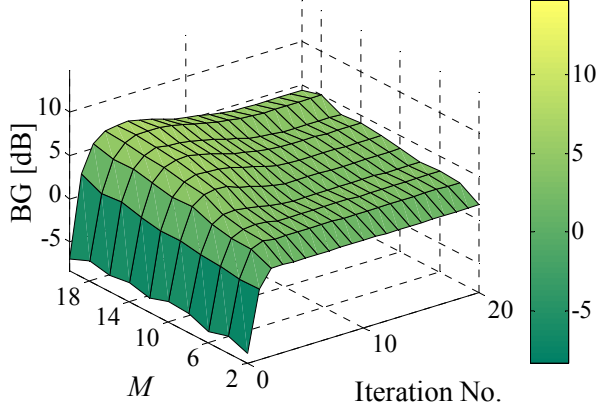
(a) MT₁, Sc #4u_Mc_Se_B_200.



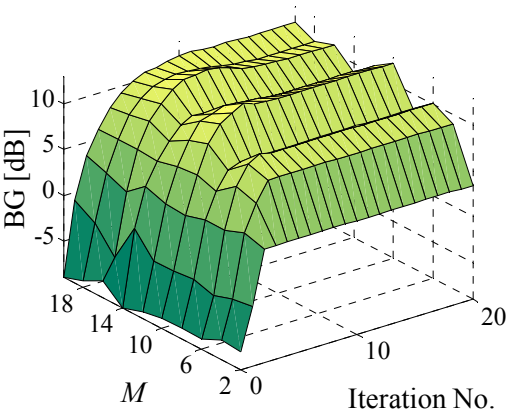
(b) MT Group, Sc #4u_Mc_Se_B_200.



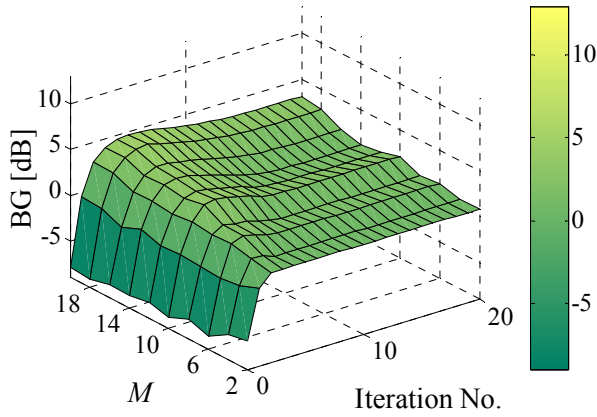
(c) MT₁, Sc #8u_Mc_Se_B_200.



(d) MT Group, Sc #8u_Mc_Se_B_200.

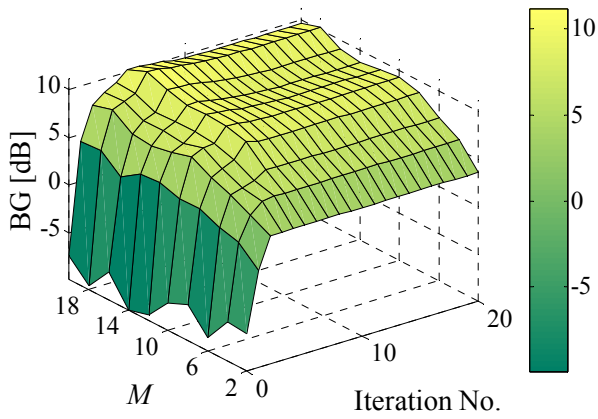


(e) MT₁, Sc #16u_Mc_Se_B_200.

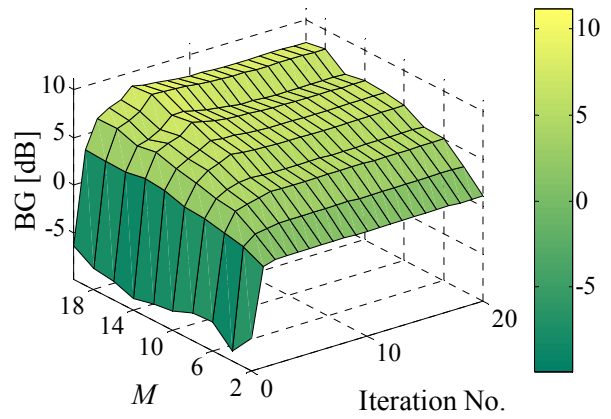


(f) MT Group, Sc #16u_Mc_Se_B_200.

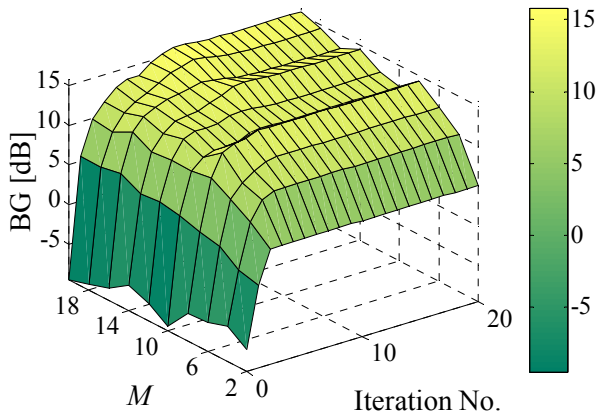
Figure B.12 – Average BG [dB] along optimisation, for Sc #Lu_Mc_Se_B_200, function of L and M , for MT₁ and the MT group.



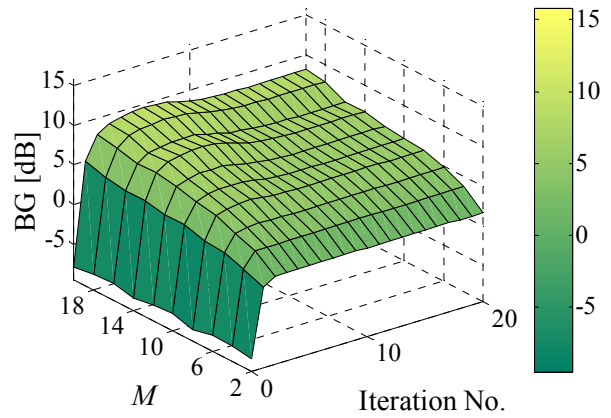
(a) MT_1 , Sc #4u_Mc_Se_B_50.



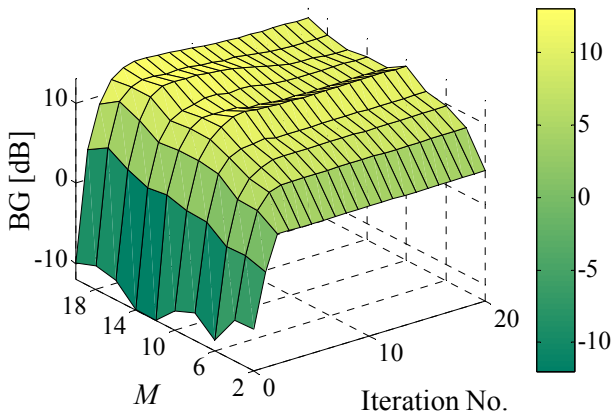
(b) MT Group, Sc #4u_Mc_Se_B_50.



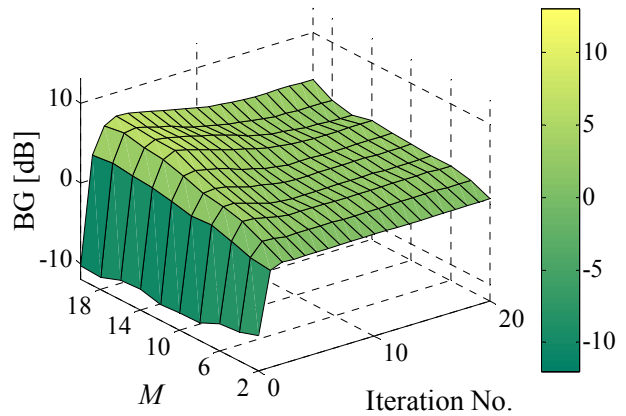
(c) MT_1 , Sc #8u_Mc_Se_B_50.



(d) MT Group, Sc #8u_Mc_Se_B_50.

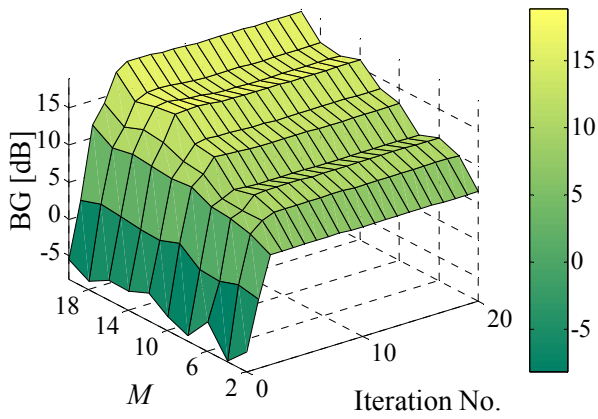


(e) MT_1 , Sc #16u_Mc_Se_B_50.

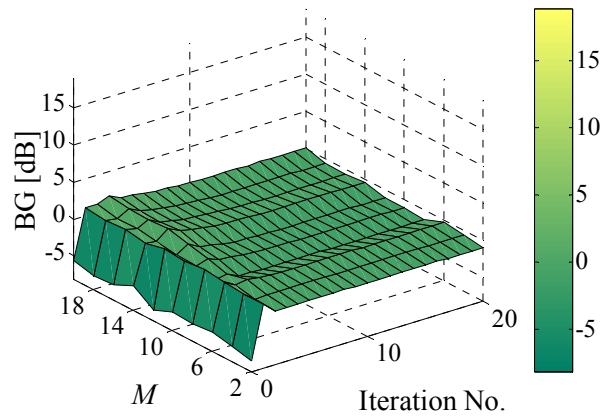


(f) MT Group, Sc #16u_Mc_Se_B_50.

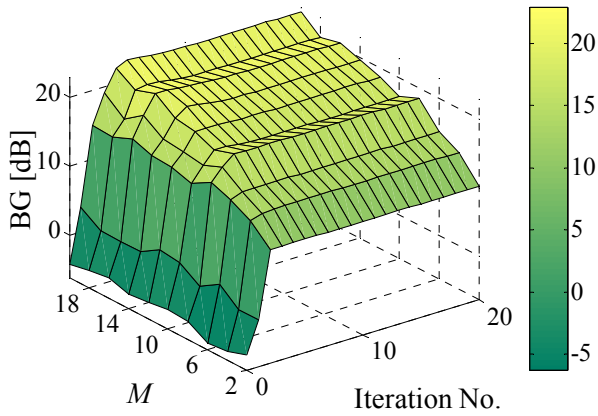
Figure B.13 – Average BG [dB] along optimisation, for Sc #Lu_Mc_Se_B_50, function of L and M , for MT_1 and the MT group.



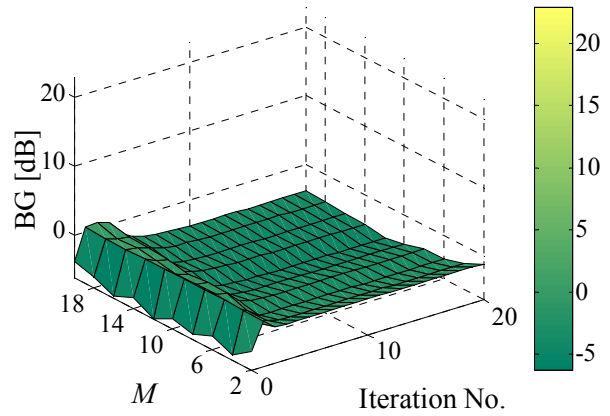
(a) MT_1 , Sc #4u_Mc_Se_C_50.



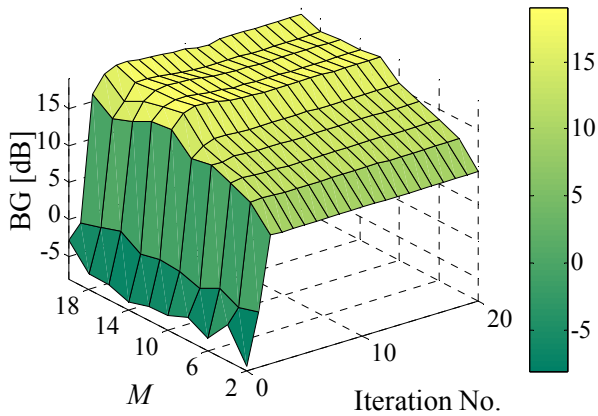
(b) MT Group, Sc #4u_Mc_Se_C_50.



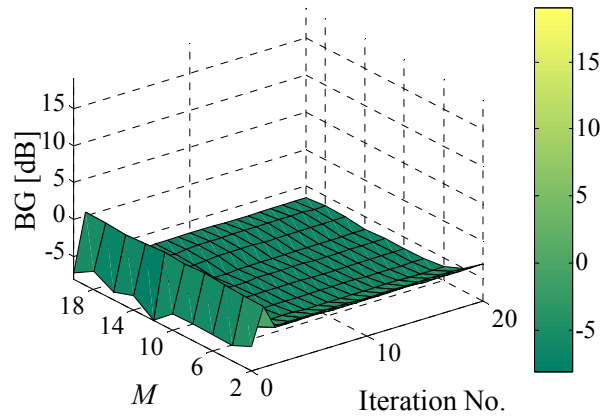
(c) MT_1 , Sc #8u_Mc_Se_C_50.



(d) MT Group, Sc #8u_Mc_Se_C_50.



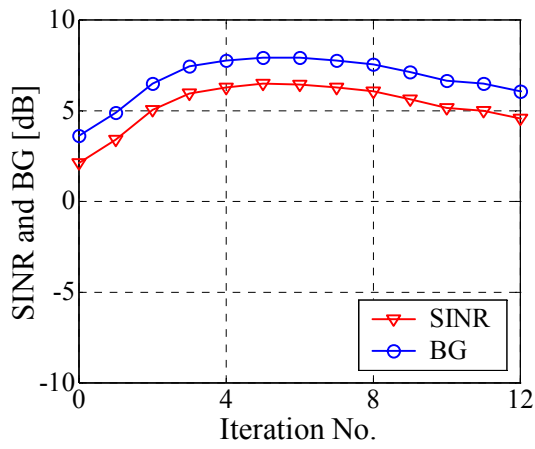
(e) MT_1 , Sc #16u_Mc_Se_C_50.



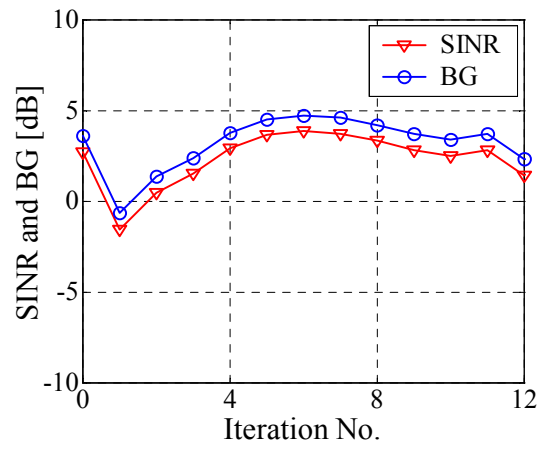
(f) MT Group, Sc #16u_Mc_Se_C_50.

Figure B.14 – Average BG [dB] along optimisation, for Sc #Lu_Mc_Se_C_50, function of L and M , for MT_1 and the MT group.

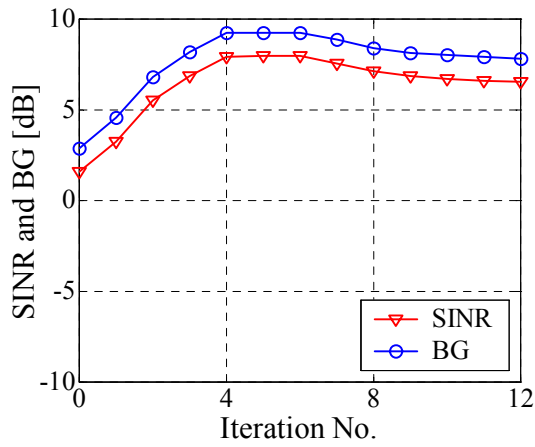
Annex C – CG vs. RLS Performance Plots



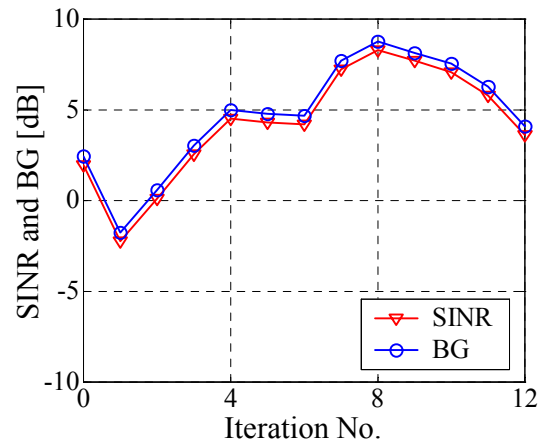
(a) CG, Sc #4u_mc_Gr_05.



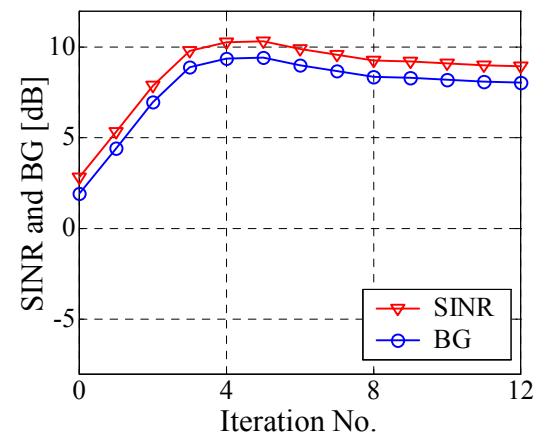
(b) RLS, Sc #4u_mc_Gr_05.



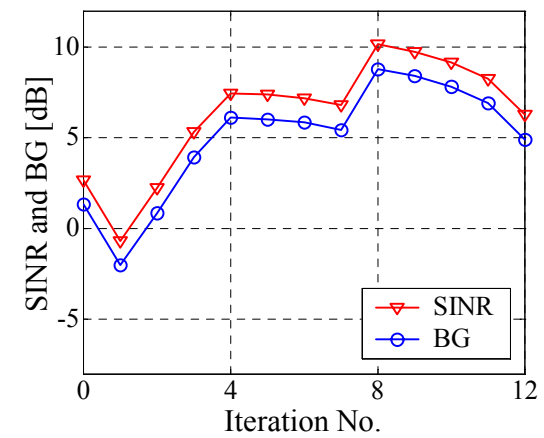
(c) CG, Sc #4u_mc_Gr_5.



(d) RLS, Sc #4u_mc_Gr_5.

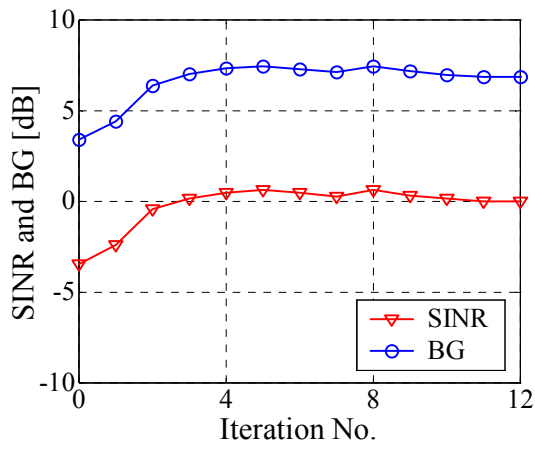


(e) CG, Sc #4u_mc_Gr_10.

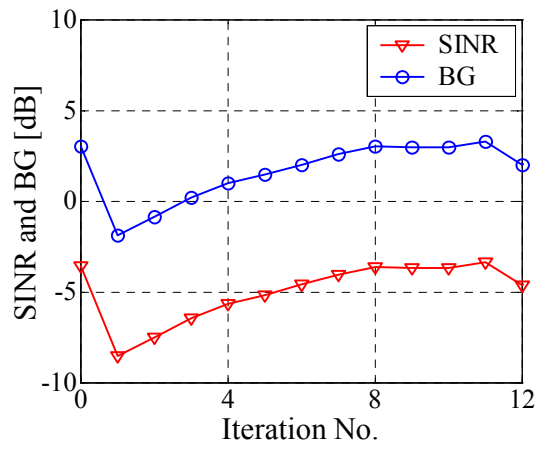


(f) RLS, Sc #4u_mc_Gr_10.

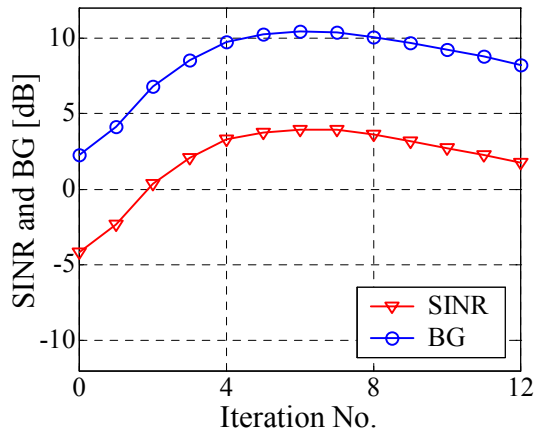
Figure C.1 – Average SINR and BG evolution along optimisation, for Sc #4u_mc_Gr_d, for $M = 12$, with the CG or the RLS.



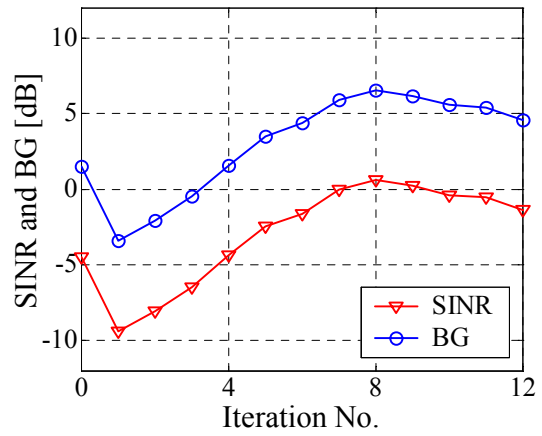
(a) CG, Sc #8u_mc_Gr_05.



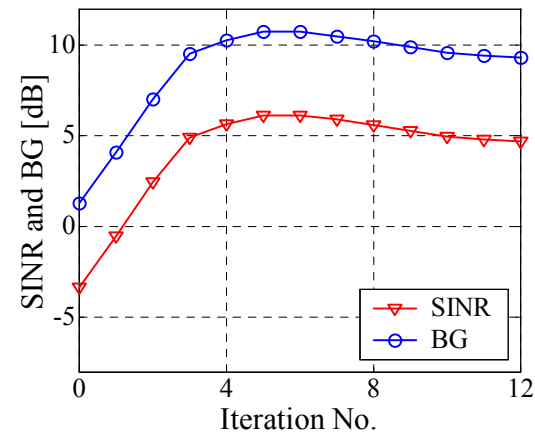
(b) RLS, Sc #8u_mc_Gr_05.



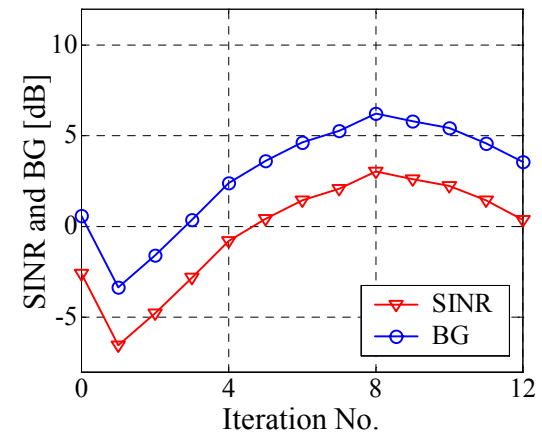
(c) CG, Sc #8u_mc_Gr_5.



(d) RLS, Sc #8u_mc_Gr_5.

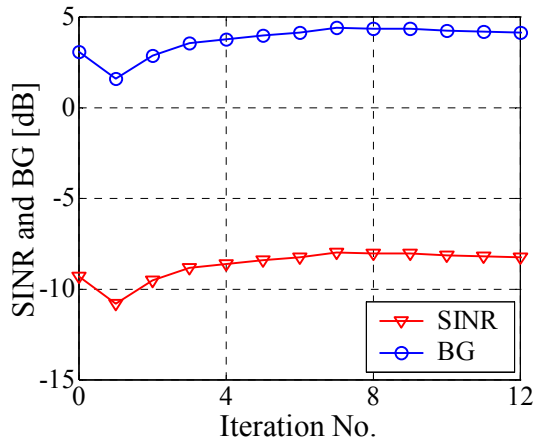


(e) CG, Sc #8u_mc_Gr_10.

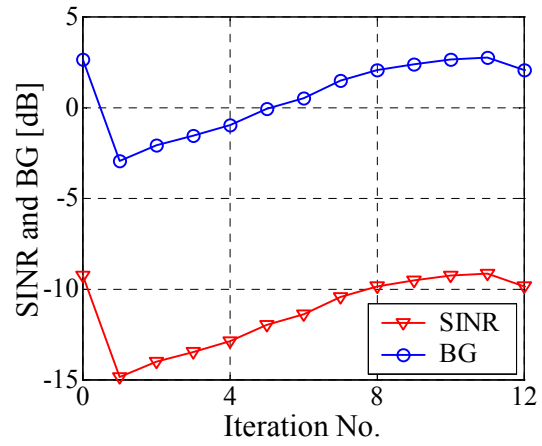


(f) RLS, Sc #8u_mc_Gr_10.

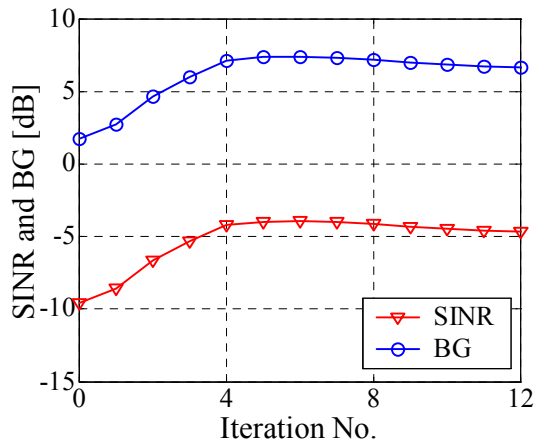
Figure C.2 – Average SINR and BG evolution along optimisation, for Sc #8u_mc_Gr_d, for $M = 12$, with the CG or the RLS.



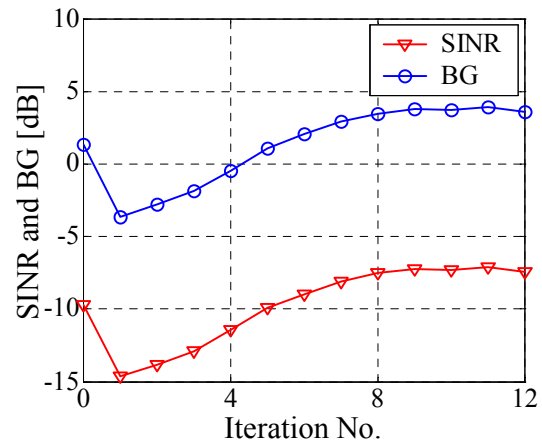
(a) CG, Sc #16u_mc_Gr_05.



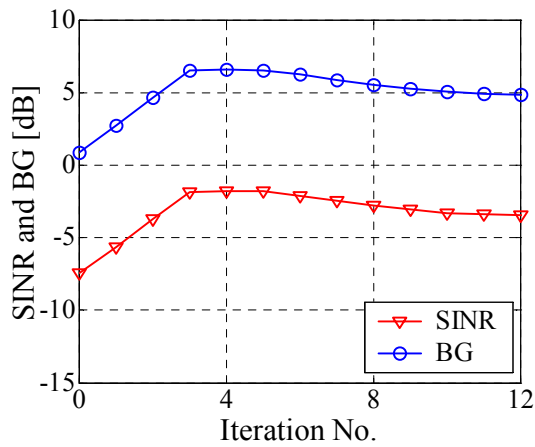
(b) RLS, Sc #16u_mc_Gr_05.



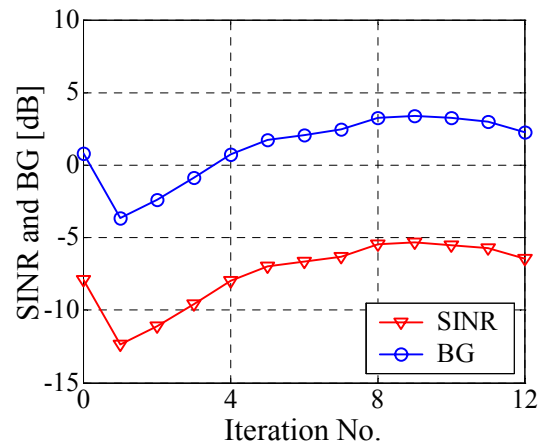
(c) CG, Sc #16u_mc_Gr_5.



(d) RLS, Sc #16u_mc_Gr_5.

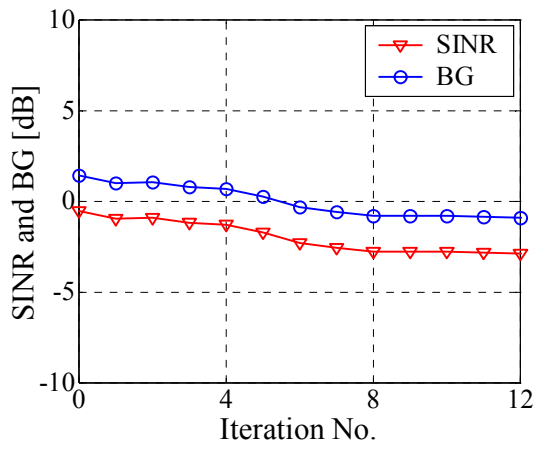


(e) CG, Sc #16u_mc_Gr_10.

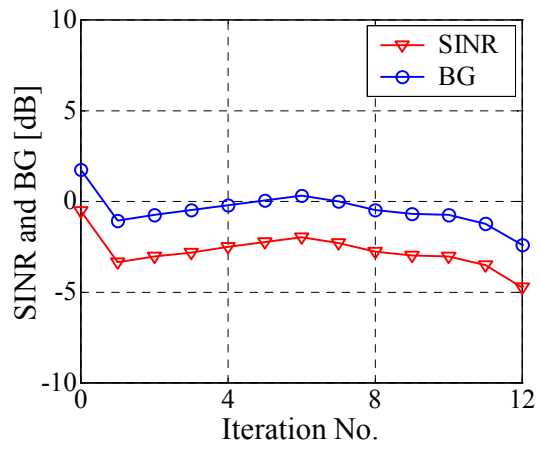


(f) RLS, Sc #16u_mc_Gr_10.

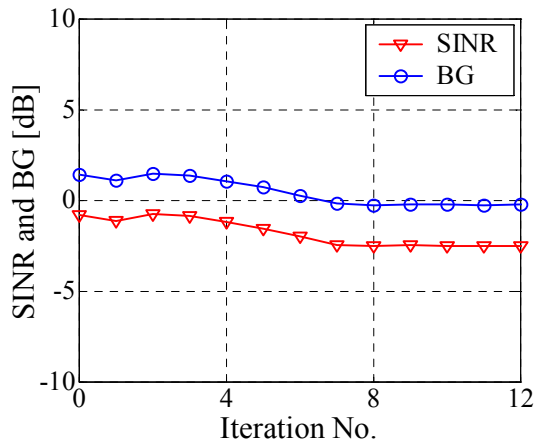
Figure C.3 – Average SINR and BG evolution along optimisation, for Sc #16u_mc_Gr_d, for $M = 12$, with the CG or the RLS.



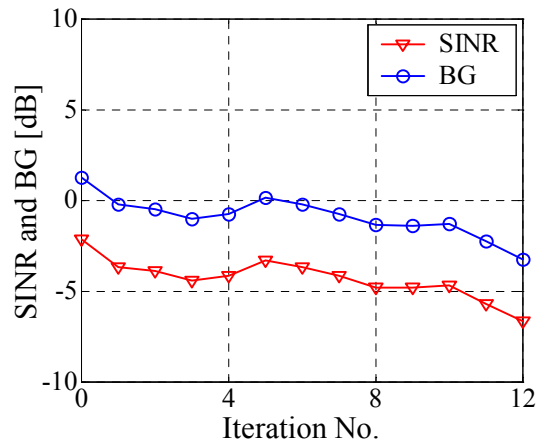
(a) CG, Sc #4u_Mc_Gr_10_200.



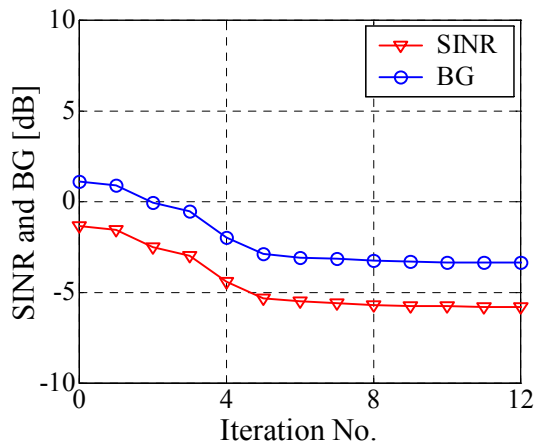
(b) RLS, Sc #4u_Mc_Gr_10_200.



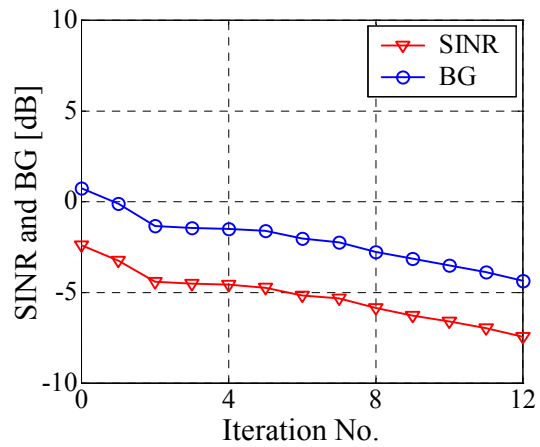
(c) CG, Sc #4u_Mc_Gr_15_200.



(d) RLS, Sc #4u_Mc_Gr_15_200.

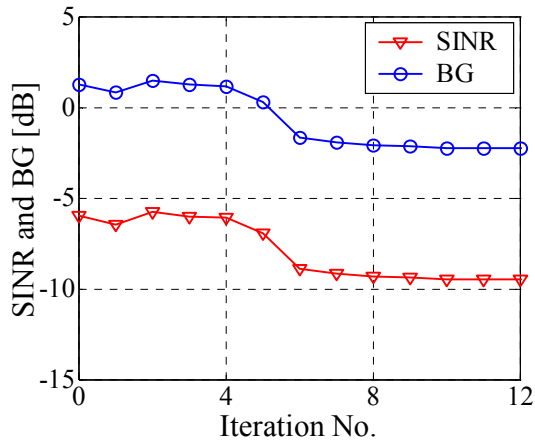


(e) CG, Sc #4u_Mc_Gr_20_200.

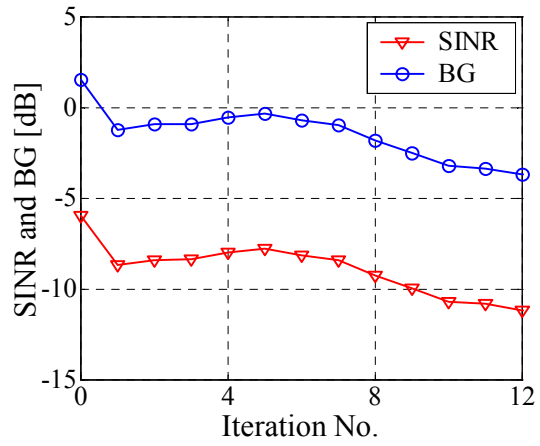


(f) RLS, Sc #4u_Mc_Gr_20_200.

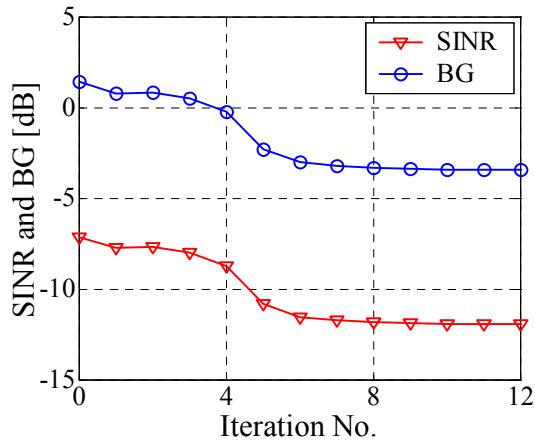
Figure C.4 – Average SINR and BG evolution along optimisation, for Sc #4u_Mc_Gr_d_200, for $M = 12$, with the CG or the RLS.



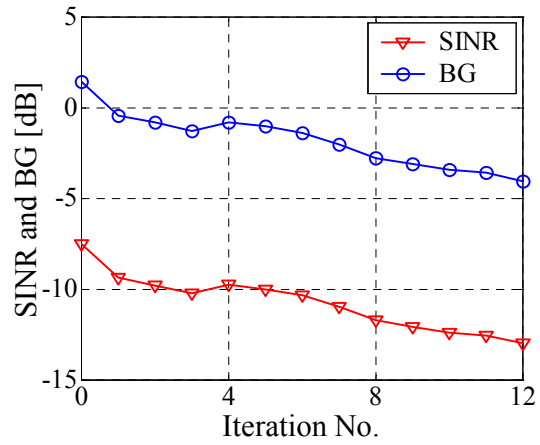
(a) CG, Sc #8u_Mc_Gr_10_200.



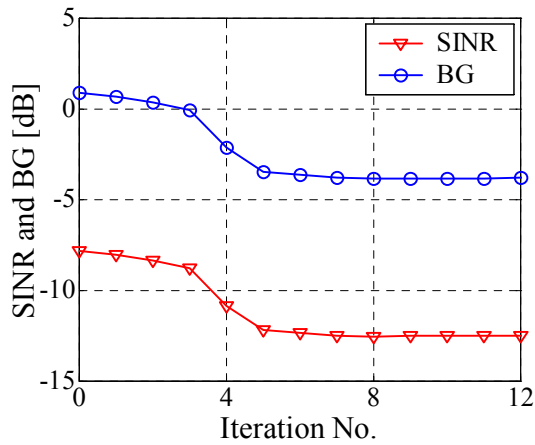
(b) RLS, Sc #8u_Mc_Gr_10_200.



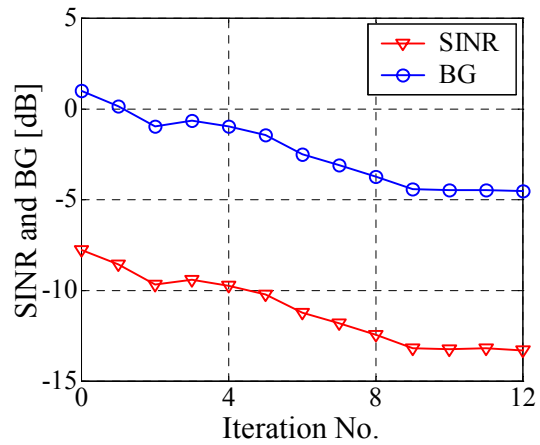
(c) CG, Sc #8u_Mc_Gr_15_200.



(d) RLS, Sc #8u_Mc_Gr_15_200.

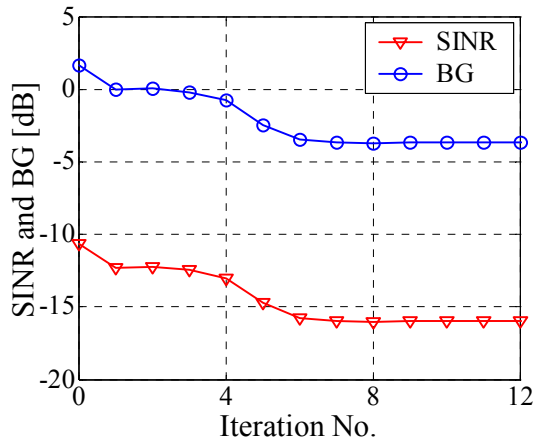


(e) CG, Sc #8u_Mc_Gr_20_200.

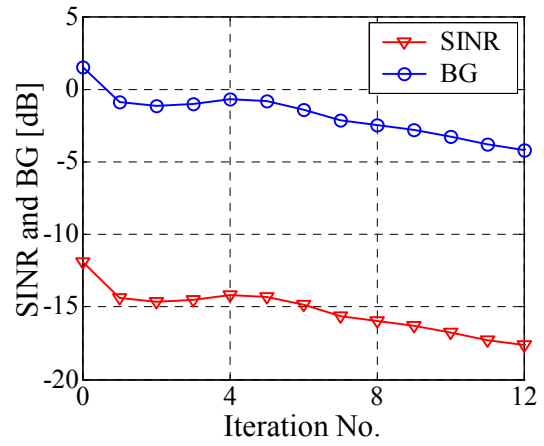


(f) RLS, Sc #8u_Mc_Gr_20_200.

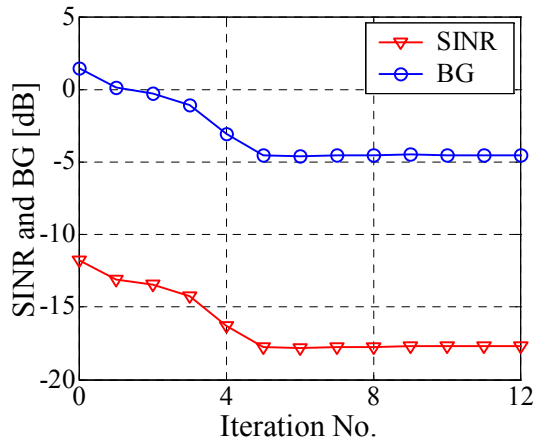
Figure C.5 – Average SINR and BG evolution along optimisation, for Sc #8u_Mc_Gr_d_200, for $M = 12$, with the CG or the RLS.



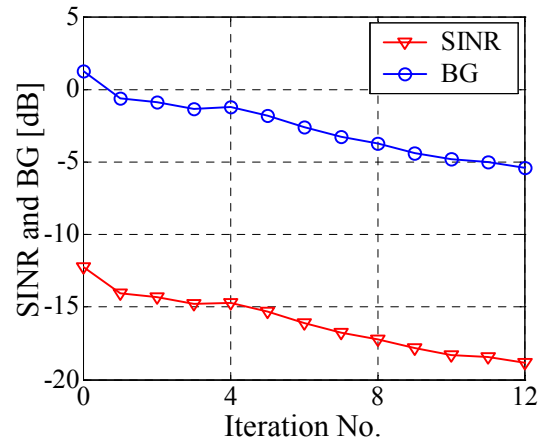
(a) CG, Sc #16u_Mc_Gr_10_200.



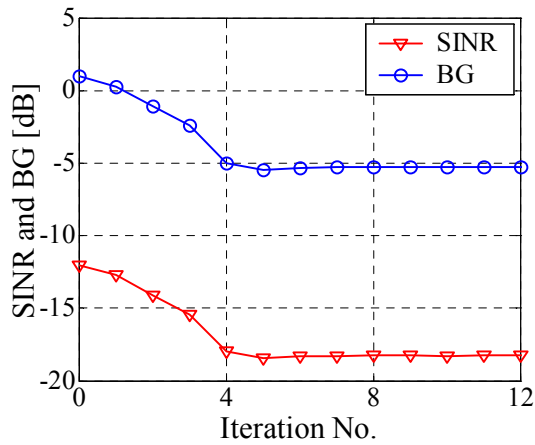
(b) RLS, Sc #16u_Mc_Gr_10_200.



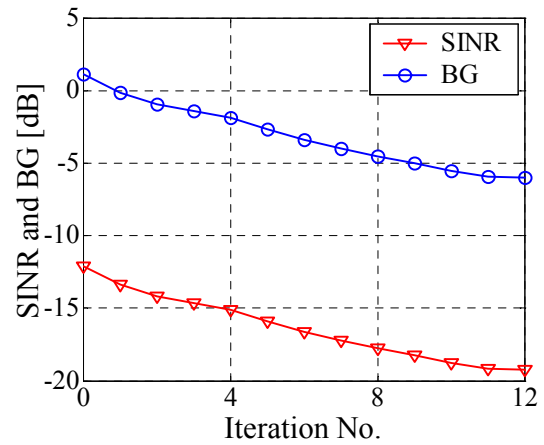
(c) CG, Sc #16u_Mc_Gr_15_200.



(d) RLS, Sc #16u_Mc_Gr_15_200.



(e) CG, Sc #16u_Mc_Gr_20_200.



(f) RLS, Sc #16u_Mc_Gr_20_200.

Figure C.6 – Average SINR and BG evolution along optimisation, for Sc #16u_Mc_Gr_d_200, for $M = 12$, with the CG or the RLS.

Was it worth while? It is worth while, all,

If the soul is not small.

Whoever means to sail beyond the Cape

Must double sorrow – no escape.

— in “Mar Portuguez”, *Mensagem*,

Fernando Pessoa (1888-1935), transl. Jonathan Griffin